















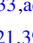



Averages of b -hadron, c -hadron, and τ -lepton properties as of summer 2016

Heavy Flavor Averaging Group (HFLAV): Y. Amhis^{1,a}, Sw. Banerjee^{2,b} , E. Ben-Haim^{3,c} , F. Bernlochner^{4,d}, A. Bozek^{5,e}, C. Bozzi^{6,f} , M. Chrzyszcz^{5,7,g} , J. Dingfelder^{4,h}, S. Duell⁴, M. Gersabeck^{8,i} , T. Gershon^{9,j} , D. Gerstel¹⁰, P. Goldenzweig^{11,k}, R. Harr¹², K. Hayasaka^{13,l}, H. Hayashii^{14,m}, M. Kenzie^{15,n} , T. Kuhr^{16,o} , O. Leroy^{10,p} , A. Lusiani^{17,18,q} , X. R. Lyu^{19,r} , K. Miyabayashi^{13,s} , P. Naik^{20,t} , T. Nanut^{21,u}, A. Oyanguren Campos^{22,v}, M. Patel²³, D. Pedrini^{24,w} , M. Petrić²⁵, M. Rama^{18,x} , M. Roney²⁶, M. Rotondo^{27,y} , O. Schneider^{28,z}, C. Schwanda^{29,aa}, A. J. Schwartz^{30,ab}, J. Serrano¹⁰, B. Shwartz^{31,32,ac}, R. Tesarek^{33,ad} , D. Tonelli^{18,ae}, K. Trabelsi^{34,35,af} , P. Urquijo³⁶, R. Van Kooten^{37,ag}, J. Yelton^{38,ah}, A. Zupanc^{21,39,ai}

- ¹ LAL, Université Paris-Sud, CNRS/IN2P3, Orsay, France
- ² University of Louisville, Louisville, KY, USA
- ³ LPNHE, Université Pierre et Marie Curie, Université Paris Diderot, CNRS/IN2P3, Paris, France
- ⁴ University of Bonn, Bonn, Germany
- ⁵ H. Niewodniczanski Institute of Nuclear Physics, Kraków, Poland
- ⁶ INFN, sezione di Ferrara, Ferrara, Italy
- ⁷ Physik-Institut, Universität Zürich, Zurich, Switzerland
- ⁸ School of Physics and Astronomy, University of Manchester, Manchester, UK
- ⁹ Department of Physics, University of Warwick, Coventry, UK
- ¹⁰ Aix Marseille Univ, CNRS/IN2P3, CPPM, Marseille, France
- ¹¹ Institut für Experimentelle Kernphysik, Karlsruher Institut für Technologie, Karlsruhe, Germany
- ¹² Wayne State University, Detroit, MI, USA
- ¹³ Niigata University, Niigata, Japan
- ¹⁴ Nara Women's University, Nara, Japan
- ¹⁵ Cavendish Laboratory, University of Cambridge, Cambridge, UK
- ¹⁶ Ludwig-Maximilians-University, Munich, Germany
- ¹⁷ Scuola Normale Superiore, Pisa, Italy
- ¹⁸ INFN, sezione di Pisa, Pisa, Italy
- ¹⁹ University of Chinese Academy of Sciences, Beijing, China
- ²⁰ H.H. Wills Physics Laboratory, University of Bristol, Bristol, UK
- ²¹ J. Stefan Institute, Ljubljana, Slovenia
- ²² Instituto de Física Corpuscular, Centro Mixto Universidad de Valencia-CSIC, Valencia, Spain
- ²³ Imperial College London, London, UK
- ²⁴ INFN, sezione di Milano-Bicocca, Milan, Italy
- ²⁵ European Organization for Nuclear Research (CERN), Geneva, Switzerland
- ²⁶ University of Victoria, Victoria, BC, Canada
- ²⁷ INFN, Laboratori Nazionali di Frascati, Frascati, Italy
- ²⁸ Institute of Physics, Ecole Polytechnique Fédérale de Lausanne (EPFL), Lausanne, Switzerland
- ²⁹ Institute of High Energy Physics, Vienna, Austria
- ³⁰ University of Cincinnati, Cincinnati, OH, USA
- ³¹ Budker Institute of Nuclear Physics (SB RAS), Novosibirsk, Russia
- ³² Novosibirsk State University, Novosibirsk, Russia
- ³³ Fermi National Accelerator Laboratory, Batavia, IL, USA
- ³⁴ High Energy Accelerator Research Organization (KEK), Tsukuba, Japan
- ³⁵ SOKENDAI (The Graduate University for Advanced Studies), Hayama, Japan
- ³⁶ School of Physics, University of Melbourne, Melbourne, VIC, Australia
- ³⁷ Indiana University, Bloomington, IN, USA
- ³⁸ University of Florida, Gainesville, FL, USA
- ³⁹ Faculty of Mathematics and Physics, University of Ljubljana, Ljubljana, Slovenia

Abstract This article reports world averages of measurements of b -hadron, c -hadron, and τ -lepton properties obtained by the Heavy Flavor Averaging Group using results available through summer 2016. For the averaging, common input parameters used in the various analyses are adjusted (rescaled) to common values, and known correlations are taken into account. The averages include branching fractions, lifetimes, neutral meson mixing parameters, CP violation parameters, parameters of semileptonic decays, and Cabibbo–Kobayashi–Maskawa matrix elements.

^a e-mail: yasmine.sara.amhis@cern.ch

^b e-mails: Swagato.Banerjee@cern.ch;
swagato.banerjee@louisville.edu

^c e-mail: benhaim@in2p3.fr

^d e-mail: florian.bernlochner@cern.ch

^e e-mail: bozek@belle2.ifj.edu.pl

^f e-mail: bozzi@fe.infn.it

^g e-mail: mchrzasz@cern.ch

^h e-mails: jochen.christian.dingfelder@cern.ch;
dingfelder@physik.uni-bonn.de

ⁱ e-mail: marco.gersabeck@manchester.ac.uk

^j e-mail: T.J.Gershon@warwick.ac.uk

^k e-mail: pablo.goldenzweig@kit.edu

^l e-mail: hayasaka@hepl.phys.nagoya-u.ac.jp

^m e-mail: hayashii@hepl.phys.nara-wu.ac.jp

ⁿ e-mail: matthew.william.kenzie@cern.ch

^o e-mail: thomas.kuhr@lmu.de

^p e-mail: olivier.leroy@in2p3.fr

^q e-mails: alberto.lusiani@cern.ch;
alberto.lusiani@pi.infn.it

^r e-mail: xiaorui@ucas.ac.cn

^s e-mail: miyabaya@cc.nara-wu.ac.jp

^t e-mail: paras.naik@bristol.ac.uk

^u e-mail: tara.nanut@ijs.si

^v e-mail: Arantza.Oyanguren@ific.uv.es

^w e-mail: daniele.pedrini@mib.infn.it

^x e-mail: matteo.rama@pi.infn.it

^y e-mail: marcello.rotondo@pd.infn.it

^z e-mail: Olivier.Schneider@epfl.ch

^{aa} e-mail: Christoph.Schwanda@oeaw.ac.at

^{ab} e-mail: alan.j.schwartz@uc.edu

^{ac} e-mail: shwartz@inp.nsk.ru

^{ad} e-mail: tesarek@fnal.gov

^{ae} e-mail: diego.tonelli@ts.infn.it

^{af} e-mails: karim.trabelsi@cern.ch;
karim.trabelsi@kek.jp

^{ag} e-mail: rvankoot@indiana.edu

^{ah} e-mails: john.martin.yelton@cern.ch;
yelton@phys.ufl.edu

^{ai} e-mail: anze.zupanc@ijs.si

Contents

1	Introduction	
2	Averaging methodology	
2.1	Treatment of correlated systematic uncertainties	
2.2	Treatment of non-Gaussian likelihood functions	
3	Production fractions, lifetimes and mixing parameters of b hadrons	
3.1	b -hadron production fractions	
3.1.1	b -hadron production fractions in $\Upsilon(4S)$ decays	
3.1.2	b -hadron production fractions in $\Upsilon(5S)$ decays	
3.1.3	b -hadron production fractions at high energy	
3.2	b -hadron lifetimes	
3.2.1	Lifetime measurements, uncertainties and correlations	
3.2.2	Inclusive b -hadron lifetimes	
3.2.3	B^0 and B^+ lifetimes and their ratio	
3.2.4	B_s^0 lifetimes	
3.2.5	B_c^+ lifetime	
3.2.6	Λ_b^0 and b -baryon lifetimes	
3.2.7	Summary and comparison with theoretical predictions	
3.3	Neutral B -meson mixing	
3.3.1	B^0 mixing parameters $\Delta\Gamma_d$ and Δm_d	
3.3.2	B_s^0 mixing parameters $\Delta\Gamma_s$ and Δm_s	
3.3.3	CP violation in B^0 and B_s^0 mixing	
3.3.4	Mixing-induced CP violation in B_s^0 decays	
4	Measurements related to unitarity triangle angles	
4.1	Introduction	
4.2	Notations	
4.2.1	CP asymmetries	
4.2.2	Time-dependent CP asymmetries in decays to CP eigenstates	
4.2.3	Time-dependent distributions with non-zero decay width difference	
4.2.4	Time-dependent CP asymmetries in decays to vector-vector final states	
4.2.5	Time-dependent asymmetries: self-conjugate multiparticle final states	
4.2.6	Time-dependent CP asymmetries in decays to non- CP eigenstates	
4.2.7	Asymmetries in $B \rightarrow D^{(*)}K^{(*)}$ decays	
4.3	Common inputs and error treatment	
4.4	Time-dependent asymmetries in $b \rightarrow c\bar{c}s$ transitions	

- 4.4.1 Time-dependent CP asymmetries in $b \rightarrow c\bar{c}s$ decays to CP eigenstates
- 4.4.2 Time-dependent transversity analysis of $B^0 \rightarrow J/\psi K^{*0}$ decays
- 4.4.3 Time-dependent CP asymmetries in $B^0 \rightarrow D^{*+}D^{*-}K_S^0$ decays
- 4.4.4 Time-dependent analysis of B_s^0 decays through the $b \rightarrow c\bar{c}s$ transition
- 4.5 Time-dependent CP asymmetries in colour-suppressed $b \rightarrow c\bar{u}d$ transitions
 - 4.5.1 Time-dependent CP asymmetries: $b \rightarrow c\bar{u}d$ decays to CP eigenstates
 - 4.5.2 Time-dependent Dalitz plot analyses of $b \rightarrow c\bar{u}d$ decays
- 4.6 Time-dependent CP asymmetries in $b \rightarrow c\bar{c}d$ transitions
 - 4.6.1 Time-dependent CP asymmetries in B_s^0 decays mediated by $b \rightarrow c\bar{c}d$ transitions
- 4.7 Time-dependent CP asymmetries in charmless $b \rightarrow q\bar{q}s$ transitions
 - 4.7.1 Time-dependent CP asymmetries: $b \rightarrow q\bar{q}s$ decays to CP eigenstates
 - 4.7.2 Time-dependent Dalitz plot analyses: $B^0 \rightarrow K^+K^-K^0$ and $B^0 \rightarrow \pi^+\pi^-K_S^0$
 - 4.7.3 Time-dependent analyses of $B^0 \rightarrow \phi K_S^0\pi^0$
 - 4.7.4 Time-dependent CP asymmetries in $B_s^0 \rightarrow K^+K^-$
 - 4.7.5 Time-dependent CP asymmetries in $B_s^0 \rightarrow \phi\phi$
- 4.8 Time-dependent CP asymmetries in $b \rightarrow q\bar{q}d$ transitions
- 4.9 Time-dependent asymmetries in $b \rightarrow s\gamma$ transitions
- 4.10 Time-dependent asymmetries in $b \rightarrow d\gamma$ transitions
- 4.11 Time-dependent CP asymmetries in $b \rightarrow u\bar{u}d$ transitions
 - 4.11.1 Constraints on $\alpha \equiv \phi_2$
- 4.12 Time-dependent CP asymmetries in $b \rightarrow c\bar{u}d/u\bar{c}d$ transitions
- 4.13 Time-dependent CP asymmetries in $b \rightarrow c\bar{u}s/u\bar{c}s$ transitions
 - 4.13.1 Time-dependent CP asymmetries in $B^0 \rightarrow D^{\mp}K_S^0\pi^{\pm}$
 - 4.13.2 Time-dependent CP asymmetries in $B_s^0 \rightarrow D_S^{\mp}K^{\pm}$
- 4.14 Rates and asymmetries in $B \rightarrow D^{(*)}K^{(*)}$ decays
 - 4.14.1 D decays to CP eigenstates
 - 4.14.2 D decays to quasi- CP eigenstates
 - 4.14.3 D decays to suppressed final states
 - 4.14.4 D decays to multiparticle self-conjugate final states (model-dependent analysis)
 - 4.14.5 D decays to multiparticle self-conjugate final states (model-independent analysis)
 - 4.14.6 D decays to multiparticle non-self-conjugate final states (model-independent analysis)
 - 4.14.7 Combinations of results on rates and asymmetries in $B \rightarrow D^{(*)}K^{(*)}$ decays to obtain constraints on $\gamma \equiv \phi_3$
- 5 Semileptonic B decays
 - 5.1 Exclusive CKM-favoured decays
 - 5.1.1 $\bar{B} \rightarrow D^*\ell^-\bar{\nu}_\ell$
 - 5.1.2 $\bar{B} \rightarrow D\ell^-\bar{\nu}_\ell$
 - 5.1.3 $\bar{B} \rightarrow D^{(*)}\pi\ell^-\bar{\nu}_\ell$
 - 5.1.4 $\bar{B} \rightarrow D^{**}\ell^-\bar{\nu}_\ell$
 - 5.2 Inclusive CKM-favored decays
 - 5.2.1 Global analysis of $\bar{B} \rightarrow X_c\ell^-\bar{\nu}_\ell$
 - 5.2.2 Analysis in the kinetic scheme
 - 5.2.3 Analysis in the 1S scheme
 - 5.3 Exclusive CKM-suppressed decays
 - 5.3.1 $B \rightarrow \pi l\nu$ branching fraction and q^2 spectrum
 - 5.3.2 $|V_{ub}|$ from $B \rightarrow \pi l\nu$
 - 5.3.3 Combined extraction of $|V_{ub}|$ and $|V_{cb}|$
 - 5.3.4 Other exclusive charmless semileptonic B decays
 - 5.4 Inclusive CKM-suppressed decays
 - 5.4.1 BLNP
 - 5.4.2 DGE
 - 5.4.3 GGOU
 - 5.4.4 ADFR
 - 5.4.5 BLL
 - 5.4.6 Summary
 - 5.5 $B \rightarrow D^{(*)}\tau\nu_\tau$ decays
- 6 Decays of b -hadrons into open or hidden charm hadrons
 - 6.1 Decays of \bar{B}^0 mesons
 - 6.1.1 Decays to a single open charm meson
 - 6.1.2 Decays to two open charm mesons
 - 6.1.3 Decays to charmonium states
 - 6.1.4 Decays to charm baryons
 - 6.1.5 Decays to other (XYZ) states
 - 6.2 Decays of B^- mesons
 - 6.2.1 Decays to a single open charm meson
 - 6.2.2 Decays to two open charm mesons
 - 6.2.3 Decays to charmonium states
 - 6.2.4 Decays to charm baryons
 - 6.2.5 Decays to other (XYZ) states
 - 6.3 Decays of admixtures of \bar{B}^0/B^- mesons

6.3.1	Decays to two open charm mesons	8.6.3	Comparison with other determinations of $ V_{cd} $ and $ V_{cs} $
6.3.2	Decays to charmonium states	8.6.4	Extraction of $D_{(s)}$ meson decay constants
6.3.3	Decays to other (XYZ) states	8.7	Hadronic decays of D_s mesons
6.4	Decays of \bar{B}_s^0 mesons	8.8	Two-body hadronic D^0 decays and final state radiation
6.4.1	Decays to a single open charm meson	8.8.1	Branching fraction corrections
6.4.2	Decays to two open charm mesons	8.8.2	Average branching fractions
6.4.3	Decays to charmonium states	8.9	Excited $D_{(s)}$ mesons
6.4.4	Decays to charm baryons	8.10	Λ_c^+ branching fractions
6.5	Decays of B_c^- mesons	8.11	Excited charm baryons
6.5.1	Decays to charmonium states	8.12	Rare and forbidden decays
6.5.2	Decays to a B meson	9	Tau lepton properties
6.6	Decays of b baryons	9.1	Branching fraction fit
6.6.1	Decays to a single open charm meson	9.1.1	Technical implementation of the fit procedure
6.6.2	Decays to charmonium states	9.1.2	Fit results
6.6.3	Decays to charm baryons	9.1.3	Changes with respect to the previous report
7	B decays to charmless final states	9.1.4	Differences between the HFLAV Spring 2017 fit and the PDG 2016 fit
7.1	Mesonic decays of B^0 and B^+ mesons	9.1.5	Branching ratio fit results and experimental inputs
7.2	Baryonic decays of B^+ and B^0 mesons	9.1.6	Correlation terms between basis branching fractions uncertainties
7.3	Decays of b baryons	9.1.7	Equality constraints
7.4	Decays of B_s^0 mesons	9.2	Tests of lepton universality
7.5	Radiative and leptonic decays of B^0 and B^+ mesons.	9.3	Universality improved $B(\tau \rightarrow e\nu\bar{\nu})$ and R_{had}
7.6	Charge asymmetries in b -hadron decays	9.4	$ V_{us} $ measurement
7.7	Polarization measurements in b -hadron decays	9.4.1	$ V_{us} $ from $B(\tau \rightarrow X_s\nu)$
7.8	Decays of B_c^+ mesons	9.4.2	$ V_{us} $ from $B(\tau \rightarrow K\nu)/B(\tau \rightarrow \pi\nu)$
8	Charm physics	9.4.3	$ V_{us} $ from τ summary
8.1	D^0 - \bar{D}^0 mixing and CP violation	9.5	Upper limits on τ lepton-flavour-violating branching fractions
8.1.1	Introduction	9.6	Combination of upper limits on τ lepton-flavour-violating branching fractions
8.1.2	Input observables	10	Summary
8.1.3	Fit results	References
8.1.4	Conclusions		
8.2	CP asymmetries		
8.3	T -odd asymmetries		
8.4	Interplay of direct and indirect CP violation		
8.5	Semileptonic decays		
8.5.1	Introduction		
8.5.2	$D \rightarrow P\ell\nu_\ell$ decays		
8.5.3	Form factor parameterizations		
8.5.4	Simple pole		
8.5.5	z expansion		
8.5.6	Three-pole formalism		
8.5.7	Experimental techniques and results		
8.5.8	Combined results for the $D \rightarrow K\ell\nu_\ell$ channel		
8.5.9	Combined results for the $D \rightarrow \pi\ell\nu_\ell$ channel		
8.5.10	V_{cs} and V_{cd} determination		
8.5.11	$D \rightarrow V\bar{\ell}\nu_\ell$ decays		
8.5.12	Form factor measurements		
8.6	Leptonic decays		
8.6.1	$D^+ \rightarrow \ell^+\nu_\ell$ decays and $ V_{cd} $		
8.6.2	$D_s^+ \rightarrow \ell^+\nu_\ell$ decays and $ V_{cs} $		

1 Introduction

Flavor dynamics plays an important role in elementary particle interactions. The accurate knowledge of properties of heavy flavor hadrons, especially b hadrons, plays an essential role for determining the elements of the Cabibbo–Kobayashi–Maskawa (CKM) quark-mixing matrix [1, 2]. The operation of the Belle and BABAR $e^+e^- B$ factory experiments led to a large increase in the size of available B -meson, D -hadron and τ -lepton samples, enabling dramatic improvement in the accuracies of related measurements. The CDF and D0 experiments at the Fermilab Tevatron have also

provided important results in heavy flavour physics, most notably in the B_s^0 sector. In the D -meson sector, the dedicated e^+e^- charm factory experiments CLEO-c and BESIII have made significant contributions. Run I of the CERN Large Hadron Collider delivered high luminosity, enabling the collection of even larger samples of b and c hadrons, and thus a further leap in precision in many areas, at the ATLAS, CMS, and (especially) LHCb experiments. With the LHC Run II ongoing, further improvements are keenly anticipated.

The Heavy Flavor Averaging Group (HFLAV)¹ was formed in 2002 to continue the activities of the LEP Heavy Flavor Steering Group [3]. This group was responsible for calculating averages of measurements of b -flavor related quantities. HFLAV has evolved since its inception and currently consists of seven subgroups:

- the “ B Lifetime and Oscillations” subgroup provides averages for b -hadron lifetimes, b -hadron fractions in $\Upsilon(4S)$ decay and pp or $p\bar{p}$ collisions, and various parameters governing $B^0-\bar{B}^0$ and $B_s^0-\bar{B}_s^0$ mixing;
- the “Unitarity Triangle Parameters” subgroup provides averages for parameters associated with time-dependent CP asymmetries and $B \rightarrow DK$ decays, and resulting determinations of the angles of the CKM unitarity triangle;
- the “Semileptonic B Decays” subgroup provides averages for inclusive and exclusive B -decay branching fractions, and subsequent determinations of the CKM matrix element magnitudes $|V_{cb}|$ and $|V_{ub}|$;
- the “ B to Charm Decays” subgroup provides averages of branching fractions for B decays to final states involving open charm or charmonium mesons;
- the “Rare Decays” subgroup provides averages of branching fractions and CP asymmetries for charmless, radiative, leptonic, and baryonic B -meson and b -baryon decays;
- the “Charm Physics” subgroup provides averages of numerous quantities in the charm sector, including branching fractions; properties of excited D^{**} and D_{sJ} mesons; properties of charm baryons; $D^0-\bar{D}^0$ mixing, CP , and T violation parameters; and D^+ and D_s^+ decay constants f_D and f_{D_s} .
- the “Tau Physics” subgroup provides averages for τ branching fractions using a global fit and elaborates the results to test lepton universality and to determine the CKM matrix element magnitude $|V_{us}|$; furthermore, it lists the τ lepton-flavor-violating upper limits and computes the combined upper limits.

¹ The group was originally known by the acronym “HFAG.” Following feedback from the community, this was changed to HFLAV in 2017.

Subgroups consist of representatives from experiments producing relevant results in that area, i.e., representatives from BABAR, Belle, BESIII, CDF, CLEO(c), D0, and LHCb.

This article is an update of the last HFLAV preprint, which used results available by summer 2014 [5]. Here we report world averages using results available by summer 2016. In some cases, important new results made available in the latter part of 2016 have been included, or there have been minor revisions in the averages since summer 2016. All plots carry a timestamp indicating when they were produced. In general, we use all publicly available results that are supported by written documentation, including preliminary results presented at conferences or workshops. However, we do not use preliminary results that remain unpublished for an extended period of time, or for which no publication is planned. Close contacts have been established between representatives from the experiments and members of subgroups that perform averaging to ensure that the data are prepared in a form suitable for combinations.

Section 2 describes the methodology used for calculating averages. In the averaging procedure, common input parameters used in the various analyses are adjusted (rescaled) to common values, and, where possible, known correlations are taken into account. Sections 3–9 present world average values from each of the subgroups listed above. A brief summary of the averages presented is given in Sect. 10. A complete listing of the averages and plots, including updates since this document was prepared, are also available on the HFLAV web site: <http://www.slac.stanford.edu/xorg/hflav>.

2 Averaging methodology

The main task of HFLAV is to combine independent but possibly correlated measurements of a parameter to obtain the world’s best estimate of that parameter’s value and uncertainty. These measurements are typically made by different experiments, or by the same experiment using different data sets, or sometimes by the same experiment using the same data but using different analysis methods. In this section, the general approach adopted by HFLAV is outlined. For some cases, somewhat simplified or more complex algorithms are used; these are noted in the corresponding sections.

Our methodology focuses on the problem of combining measurements obtained with different assumptions about external (or “nuisance”) parameters and with potentially correlated systematic uncertainties. It is important for any averaging procedure that the quantities measured by experiments be statistically well-behaved, which in this context means having a (one- or multi-dimensional) Gaussian likelihood function that is described by the central

value(s) \mathbf{x}_i and covariance matrix \mathbf{V}_i . In what follows we assume \mathbf{x} does not contain redundant information, i.e., if it contains n elements then n is the number of parameters being determined. A χ^2 statistic is constructed as

$$\chi^2(\mathbf{x}) = \sum_i^N (\mathbf{x}_i - \mathbf{x})^T \mathbf{V}_i^{-1} (\mathbf{x}_i - \mathbf{x}), \quad (1)$$

where the sum is over the N independent determinations of the quantities \mathbf{x} . These are typically from different experiments; possible correlations of the systematic uncertainties are discussed below. The results of the average are the central values $\hat{\mathbf{x}}$, which are the values of \mathbf{x} at the minimum of $\chi^2(\mathbf{x})$, and their covariance matrix

$$\hat{\mathbf{V}}^{-1} = \sum_i^N \mathbf{V}_i^{-1}. \quad (2)$$

We report the covariance matrices or the correlation matrices derived from the averages whenever possible. In some cases where the matrices are large, it is inconvenient to report them in this document; however, all results can be found on the HFLAV web pages.

The value of $\chi^2(\hat{\mathbf{x}})$ provides a measure of the consistency of the independent measurements of \mathbf{x} after accounting for the number of degrees of freedom (dof), which is the difference between the number of measurements and the number of fitted parameters: $N \cdot n - n$. The values of $\chi^2(\hat{\mathbf{x}})$ and dof are typically converted to a confidence level (C.L.) and reported together with the averages. In cases where $\chi^2/\text{dof} > 1$, we do not usually scale the resulting uncertainty, in contrast to what is done by the Particle Data Group [6]. Rather, we examine the systematic uncertainties of each measurement to better understand them. Unless we find systematic discrepancies among the measurements, we do not apply any additional correction to the calculated error. If special treatment is necessary to calculate an average, or if an approximation used in the calculation might not be sufficiently accurate (e.g., assuming Gaussian errors when the likelihood function exhibits non-Gaussian behavior), we include a warning message. Further modifications to the averaging procedures for non-Gaussian situations are discussed in Sect. 2.2.

For observables such as branching fractions, experiments typically report upper limits when the signal is not significant. Sometimes there is insufficient information available to combine upper limits on a parameter obtained by different experiments; in this case we usually report only the most restrictive upper limit. For branching fractions of lepton-flavor-violating decays of tau leptons, we calculate combined upper limits as discussed in Sect. 9.6.

2.1 Treatment of correlated systematic uncertainties

Consider two hypothetical measurements of a parameter x , which can be summarized as

$$\begin{aligned} x_1 &\pm \delta x_1 \pm \Delta x_{1,1} \pm \Delta x_{1,2} \dots \\ x_2 &\pm \delta x_2 \pm \Delta x_{2,1} \pm \Delta x_{2,2} \dots, \end{aligned}$$

where the δx_k are statistical uncertainties and the $\Delta x_{k,i}$ are contributions to the systematic uncertainty. The simplest approach is to combine statistical and systematic uncertainties in quadrature:

$$\begin{aligned} x_1 &\pm (\delta x_1 \oplus \Delta x_{1,1} \oplus \Delta x_{1,2} \oplus \dots) \\ x_2 &\pm (\delta x_2 \oplus \Delta x_{2,1} \oplus \Delta x_{2,2} \oplus \dots), \end{aligned}$$

and then perform a weighted average of x_1 and x_2 using their combined uncertainties, treating the measurements as independent. This approach suffers from two potential problems that we try to address. First, the values x_k may have been obtained using different assumptions for nuisance parameters; e.g., different values of the B^0 lifetime may have been used for different measurements of the oscillation frequency Δm_d . The second potential problem is that some systematic uncertainties may be correlated between measurements. For example, different measurements of Δm_d may depend on the same branching fraction used to model a common background.

The above two problems are related, as any quantity y_i upon which x_k depends gives a contribution $\Delta x_{k,i}$ to the systematic error that reflects the uncertainty Δy_i on y_i . We thus use the values of y_i and Δy_i assumed by each measurement in our averaging (we refer to these values as $y_{k,i}$ and $\Delta y_{k,i}$). To properly treat correlated systematic uncertainties among measurements requires decomposing the overall systematic uncertainties into correlated and uncorrelated components. As different measurements often quote different types of systematic uncertainties, achieving consistent definitions in order to properly treat correlations requires close coordination between HFLAV and the experiments. In some cases, a group of systematic uncertainties must be combined into a coarser description in order to obtain an average that is consistent among measurements. Systematic uncertainties that are uncorrelated with any other source of uncertainty are combined together with the statistical error, so that the only systematic uncertainties treated explicitly are those that are correlated with at least one other measurement via a consistently-defined external parameter y_i . When asymmetric statistical or systematic uncertainties are quoted by experiments, we symmetrize them since our combination method implicitly assumes Gaussian likelihoods (or parabolic log likelihoods) for each measurement.

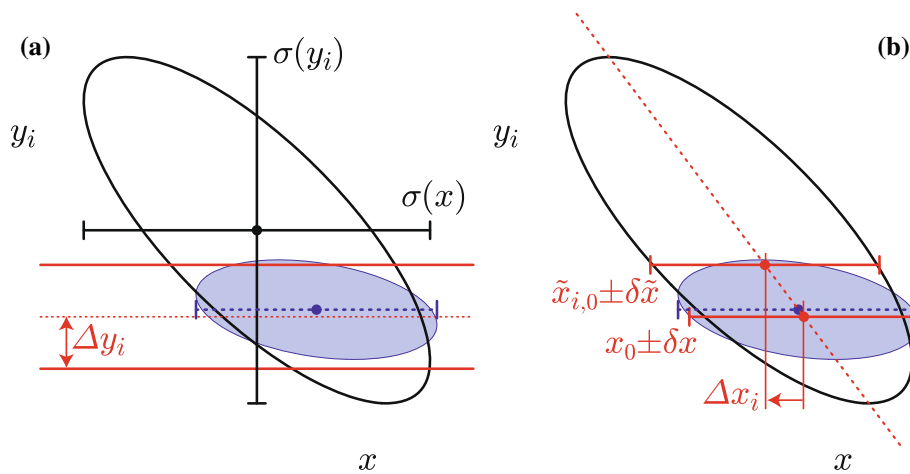


Fig. 1 Illustration of the possible dependence of a measured quantity x on a nuisance parameter y_i . The *left-hand plot a* compares the 68% confidence level contours of a hypothetical measurement's unconstrained (*large ellipse*) and constrained (*filled ellipse*) likelihoods, using the Gaussian constraint on y_i represented by the *horizontal band*. The *solid error bars* represent the statistical uncertainties $\sigma(x)$ and $\sigma(y_i)$ of the unconstrained likelihood. The *dashed error bar* shows the sta-

tistical error on x from a constrained simultaneous fit to x and y_i . The *right-hand plot b* illustrates the method described in the text of performing fits to x with y_i fixed at different values. The *dashed diagonal line* between these fit results has the slope $\rho(x, y_i)\sigma(y_i)/\sigma(x)$ in the limit of an unconstrained parabolic log likelihood. The result of the constrained simultaneous fit from **a** is shown as a *dashed error bar* on x

The fact that a measurement of x is sensitive to y_i indicates that, in principle, the data used to measure x could also be used for a simultaneous measurement of x and y_i . This is illustrated by the large contour in Fig. 1a. However, there often exists an external constraint Δy_i on y_i (represented by the horizontal band in Fig. 1a) that is more precise than the constraint $\sigma(y_i)$ from the x data alone. In this case one can perform a simultaneous fit to x and y_i , including the external constraint, and obtain the filled (x, y) contour and dashed one-dimensional estimate of x shown in Fig. 1a. For this procedure one usually takes the external constraint Δy_i to be Gaussian.

When the external constraints Δy_i are significantly more precise than the sensitivity $\sigma(y_i)$ of the data alone, the additional complexity of a constrained fit with extra free parameters may not be justified by the resulting increase in sensitivity. In this case the usual procedure is to perform a baseline fit with all y_i fixed to nominal values $y_{i,0}$, obtaining $x = x_0 \pm \delta x$. This baseline fit neglects the uncertainty due to Δy_i , but this error is subsequently recovered by repeating the fit separately for each external parameter y_i , with its value fixed to $y_i = y_{i,0} \pm \Delta y_i$. This gives the result $x = \tilde{x}_{0,i} \pm \delta \tilde{x}$ as illustrated in Fig. 1b. The shift in the central value $\Delta x_i = \tilde{x}_{0,i} - x_0$ is usually quoted as the systematic uncertainty due to the unknown value of y_i . If the unconstrained data can be represented by a Gaussian likelihood function, the shift will equal

$$\Delta x_i = \rho(x, y_i) \frac{\sigma(x)}{\sigma(y_i)} \Delta y_i, \tag{3}$$

where $\sigma(x)$ and $\rho(x, y_i)$ are the statistical uncertainty on x and the correlation between x and y_i in the unconstrained data, respectively. This procedure gives very similar results to that of the constrained fit with extra parameters: the central values x_0 agree to $\mathcal{O}(\Delta y_i/\sigma(y_i))^2$, and the uncertainties $\delta x \oplus \Delta x_i$ agree to $\mathcal{O}(\Delta y_i/\sigma(y_i))^4$.

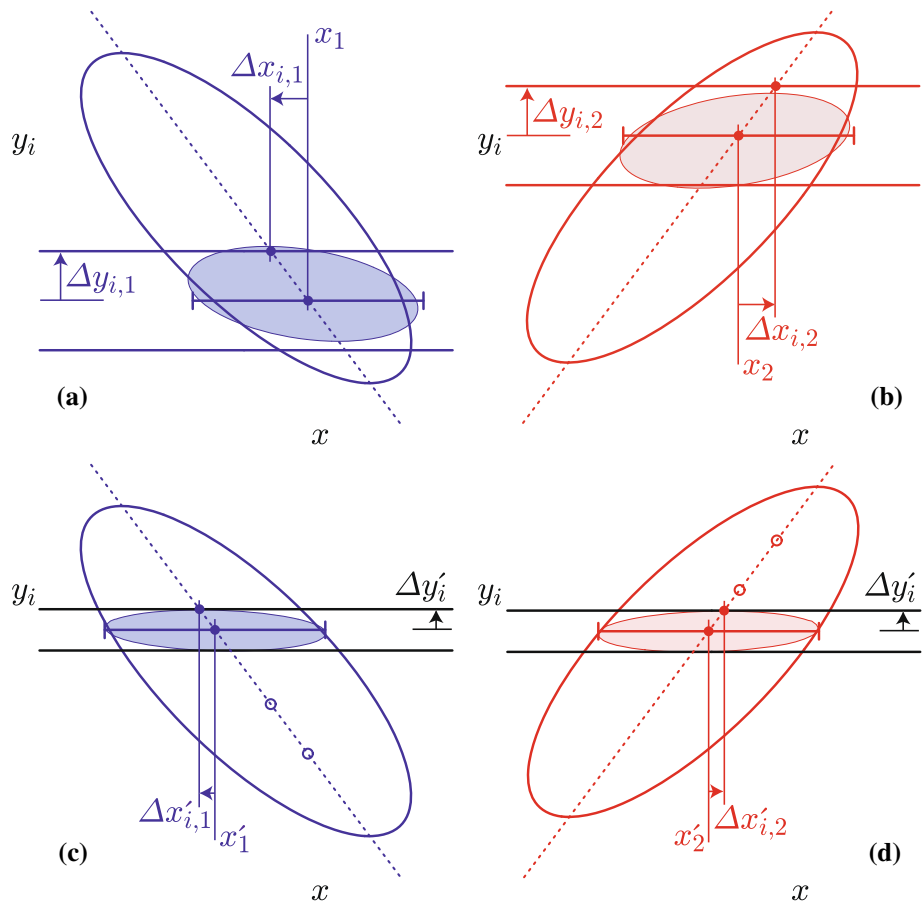
To combine two or more measurements that share systematic uncertainty due to the same external parameter(s) y_i , we try to perform a constrained simultaneous fit of all measurements to obtain values of x and y_i . When this is not practical, e.g. if we do not have sufficient information to reconstruct the likelihoods corresponding to each measurement, we perform the two-step approximate procedure described below.

Consider two statistically-independent measurements, $x_1 \pm (\delta x_1 \oplus \Delta x_{1,i})$ and $x_2 \pm (\delta x_2 \oplus \Delta x_{2,i})$, of the quantity x as shown in Fig. 2a, b. For simplicity we consider only one correlated systematic uncertainty for each external parameter y_i . As our knowledge of the y_i improves, the measurements of x will shift to different central values and uncertainties. The first step of our procedure is to adjust the values of each measurement to reflect the current best knowledge of the external parameters y'_i and their ranges $\Delta y'_i$, as illustrated in Fig. 2c, d. We adjust the central values x_k and correlated systematic uncertainties $\Delta x_{k,i}$ linearly for each measurement (indexed by k) and each external parameter (indexed by i):

$$x'_k = x_k + \sum_i \frac{\Delta x_{k,i}}{\Delta y_{k,i}} (y'_i - y_{k,i}) \tag{4}$$

$$\Delta x'_{k,i} = \Delta x_{k,i} \frac{\Delta y'_i}{\Delta y_{k,i}}. \tag{5}$$

Fig. 2 Illustration of the HFLAV combination procedure for correlated systematic uncertainties. *Upper plots a, b* show examples of two individual measurements to be combined. The large (filled) ellipses represent their unconstrained (constrained) likelihoods, while horizontal bands indicate the different assumptions about the value and uncertainty of y_i used by each measurement. The error bars show the results of the method described in the text for obtaining x by performing fits with y_i fixed to different values. *Lower plots c, d* illustrate the adjustments to accommodate updated and consistent knowledge of y_i . Open circles mark the central values of the unadjusted fits to x with y fixed; these determine the dashed line used to obtain the adjusted values



This procedure is exact in the limit that the unconstrained likelihood of each measurement is Gaussian.

The second step is to combine the adjusted measurements, $x'_k \pm (\delta x_k \oplus \Delta x'_{k,1} \oplus \Delta x'_{k,2} \oplus \dots)$ by constructing the goodness-of-fit statistic

$$\begin{aligned} \chi_{\text{comb}}^2(x, y_1, y_2, \dots) &\equiv \sum_k \frac{1}{\delta x_k^2} \times \left[x'_k - \left(x + \sum_i (y_i - y'_i) \frac{\Delta x'_{k,i}}{\Delta y'_i} \right) \right]^2 \\ &+ \sum_i \left(\frac{y_i - y'_i}{\Delta y'_i} \right)^2. \end{aligned} \tag{6}$$

We minimize this χ^2 to obtain the best values of x and y_i and their uncertainties, as shown in Fig. 3. Although this method determines new values for the y_i , we typically do not report them.

For comparison, the exact method we perform if the unconstrained likelihoods $\mathcal{L}_k(x, y_1, y_2, \dots)$ are available is to minimize the simultaneous likelihood

$$\mathcal{L}_{\text{comb}}(x, y_1, y_2, \dots) \equiv \prod_k \mathcal{L}_k(x, y_1, y_2, \dots) \prod_i \mathcal{L}_i(y_i), \tag{7}$$

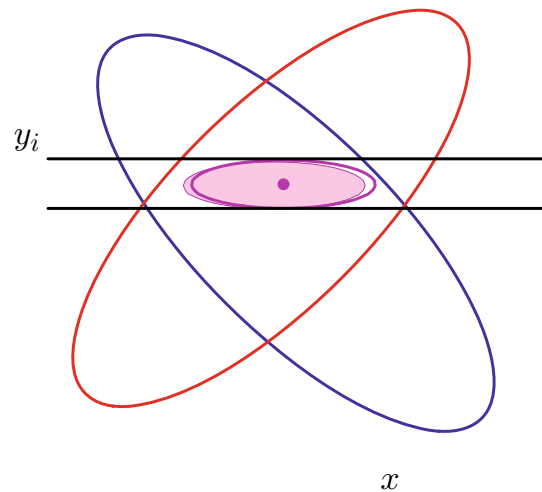


Fig. 3 Illustration of the combination of two hypothetical measurements of x using the method described in the text. The ellipses represent the unconstrained likelihoods of each measurement, and the horizontal band represents the latest knowledge about y_i that is used to adjust the individual measurements. The filled small ellipse shows the result of the exact method using $\mathcal{L}_{\text{comb}}$, and the hollow small ellipse and dot show the result of the approximate method using χ_{comb}^2

with an independent Gaussian constraint for each y_i :

$$\mathcal{L}_i(y_i) = \exp \left[-\frac{1}{2} \left(\frac{y_i - y'_i}{\Delta y'_i} \right)^2 \right]. \tag{8}$$

The results of this exact method agree with those of the approximate method when the \mathcal{L}_k are Gaussian and $\Delta y'_i \ll \sigma(y_i)$. If the likelihoods are non-Gaussian, experiments need to provide \mathcal{L}_k in order to perform a combination. If $\sigma(y_i) \approx \Delta y'_i$, experiments are encouraged to perform a simultaneous measurement of x and y_i so that their data will improve the world knowledge of y_i .

For averages where common sources of systematic uncertainty are important, central values and uncertainties are rescaled to a common set of input parameters following the prescription above. We use the most up-to-date values for common inputs, consistently across subgroups, taking values from within HFLAV or from the Particle Data Group when possible. The parameters and values used are listed in each subgroup section.

2.2 Treatment of non-Gaussian likelihood functions

For measurements with Gaussian errors, the usual estimator for the average of a set of measurements is obtained by minimizing

$$\chi^2(x) = \sum_k \frac{(x_k - x)^2}{\sigma_k^2}, \tag{9}$$

where x_k is the k th measured value of x and σ_k^2 is the variance of the distribution from which x_k was drawn. The value \hat{x} at minimum χ^2 is the estimate for the parameter x . The true σ_k are unknown but typically the error as assigned by the experiment σ_k^{raw} is used as an estimator for it. However, caution is advised when σ_k^{raw} depends on the measured value x_k . Examples of this are multiplicative systematic uncertainties such as those due to acceptance, or the \sqrt{N} dependence of Poisson statistics for which $x_k \propto N$ and $\sigma_k \propto \sqrt{N}$. Failing to account for this type of dependence when averaging leads to a biased average. Such biases can be avoided by minimizing

$$\chi^2(x) = \sum_k \frac{(x_k - x)^2}{\sigma_k^2(\hat{x})}, \tag{10}$$

where $\sigma_k(\hat{x})$ is the uncertainty on x_k that includes the dependence of the uncertainty on the value measured. As an example, consider the error due to acceptance for which $\sigma_k(\hat{x}) = (\hat{x}/x_k) \times \sigma_k^{\text{raw}}$. Inserting this into Eq. (10) leads to

$$\hat{x} = \frac{\sum_k x_k^3 / (\sigma_k^{\text{raw}})^2}{\sum_k x_k^2 / (\sigma_k^{\text{raw}})^2},$$

which is the correct behavior, i.e., weighting by the inverse square of the fractional uncertainty $\sigma_k^{\text{raw}}/x_k$. It is sometimes difficult to assess the dependence of σ_k^{raw} on \hat{x} from the errors quoted by the experiments.

Another issue that needs careful treatment is that of correlations among measurements, e.g., due to using the same decay model for intermediate states to calculate acceptances. A common practice is to set the correlation coefficient to unity to indicate full correlation. However, this is not necessarily conservative and can result in underestimated uncertainty on the average. The most conservative choice of correlation coefficient between two measurements i and j is that which maximizes the uncertainty on \hat{x} due to the pair of measurements,

$$\sigma_{\hat{x}(i,j)}^2 = \frac{\sigma_i^2 \sigma_j^2 (1 - \rho_{ij}^2)}{\sigma_i^2 + \sigma_j^2 - 2 \rho_{ij} \sigma_i \sigma_j}, \tag{11}$$

namely

$$\rho_{ij} = \min \left(\frac{\sigma_i}{\sigma_j}, \frac{\sigma_j}{\sigma_i} \right). \tag{12}$$

This corresponds to setting $\sigma_{\hat{x}(i,j)}^2 = \min(\sigma_i^2, \sigma_j^2)$. Setting $\rho_{ij} = 1$ when $\sigma_i \neq \sigma_j$ can lead to a significant underestimate of the uncertainty on \hat{x} , as can be seen from Eq. (11).

Finally, we carefully consider the various errors contributing to the overall uncertainty of an average. The covariance matrix describing the uncertainties of different measurements and their correlations is constructed, i.e., $\mathbf{V} = \mathbf{V}_{\text{stat}} + \mathbf{V}_{\text{sys}} + \mathbf{V}_{\text{theory}}$. If the measurements are from independent data samples, then \mathbf{V}_{stat} is diagonal, but \mathbf{V}_{sys} and $\mathbf{V}_{\text{theory}}$ may contain correlations. The variance on the average \hat{x} can be written

$$\begin{aligned} \sigma_{\hat{x}}^2 &= \frac{\sum_{i,j} \left(\mathbf{V}^{-1} \left[\mathbf{V}_{\text{stat}} + \mathbf{V}_{\text{sys}} + \mathbf{V}_{\text{theory}} \right] \mathbf{V}^{-1} \right)_{ij}}{\left(\sum_{i,j} \mathbf{V}_{ij}^{-1} \right)^2} \\ &= \sigma_{\text{stat}}^2 + \sigma_{\text{sys}}^2 + \sigma_{\text{th}}^2. \end{aligned} \tag{13}$$

This breakdown of uncertainties is used in certain cases, but usually only a single, total uncertainty is quoted for an average.

3 Production fractions, lifetimes and mixing parameters of b hadrons

Quantities such as b -hadron production fractions, b -hadron lifetimes, and neutral B -meson oscillation frequencies have been studied in the nineties at LEP and SLC (e^+e^- colliders at $\sqrt{s} = m_Z$) as well as at the first version of the Tevatron ($p\bar{p}$ collider at $\sqrt{s} = 1.8$ TeV). This was followed by precise measurements of the B^0 and B^+ mesons performed at the

asymmetric B factories, KEKB and PEP-II (e^+e^- colliders at $\sqrt{s} = m_{\Upsilon(4S)}$), as well as measurements related to the other b hadrons, in particular B_s^0 , B_c^+ and Λ_b^0 , performed at the upgraded Tevatron ($\sqrt{s} = 1.96$ TeV). Since a few years, the most precise measurements are coming from the LHC (pp collider at $\sqrt{s} = 7$ and 8 TeV), in particular the LHCb experiment.

In most cases, these basic quantities, although interesting by themselves, became necessary ingredients for the more refined measurements, such as those of decay-time dependent CP -violating asymmetries. It is therefore important that the best experimental values of these quantities continue to be kept up-to-date and improved.

In several cases, the averages presented in this section are needed and used as input for the results given in the subsequent sections. Within this section, some averages need the knowledge of other averages in a circular way. This coupling, which appears through the b -hadron fractions whenever inclusive or semi-exclusive measurements have to be considered, has been reduced drastically in the past several years with increasingly precise exclusive measurements becoming available and dominating practically all averages.

In addition to b -hadron fractions, lifetimes and oscillation frequencies, this section also deals with CP violation in the B^0 and B_s^0 mixing amplitudes, as well as the CP -violating phase $\phi_s^{c\bar{c}s} \simeq -2\beta_s$, which is the phase difference between the B_s^0 mixing amplitude and the $b \rightarrow c\bar{c}s$ decay amplitude. The angle β , which is the equivalent of β_s for the B^0 system, is discussed in Sect. 4.

Throughout this section published results that have been superseded by subsequent publications are ignored (i.e., excluded from the averages) and are only referred to if necessary.

3.1 b -hadron production fractions

We consider here the relative fractions of the different b -hadron species found in an unbiased sample of weakly decaying b hadrons produced under some specific conditions. The knowledge of these fractions is useful to characterize the signal composition in inclusive b -hadron analyses, to predict the background composition in exclusive analyses, or to convert (relative) observed rates into (relative) branching fraction measurements. We distinguish here the following three conditions: $\Upsilon(4S)$ decays, $\Upsilon(5S)$ decays, and high-energy collisions (including Z^0 decays).

3.1.1 b -hadron production fractions in $\Upsilon(4S)$ decays

Only pairs of the two lightest (charged and neutral) B mesons can be produced in $\Upsilon(4S)$ decays. Therefore only the follow-

ing two branching fractions must be considered:

$$f^{+-} = \Gamma(\Upsilon(4S) \rightarrow B^+ B^-) / \Gamma_{\text{tot}}(\Upsilon(4S)), \tag{14}$$

$$f^{00} = \Gamma(\Upsilon(4S) \rightarrow B^0 \bar{B}^0) / \Gamma_{\text{tot}}(\Upsilon(4S)). \tag{15}$$

In practice, most analyses measure their ratio

$$\begin{aligned} R^{+-/00} &= f^{+-} / f^{00} \\ &= \Gamma(\Upsilon(4S) \rightarrow B^+ B^-) / \Gamma(\Upsilon(4S) \rightarrow B^0 \bar{B}^0), \end{aligned} \tag{16}$$

which is easier to access experimentally. Since an inclusive (but separate) reconstruction of B^+ and B^0 is difficult, exclusive decay modes to specific final states f , $B^+ \rightarrow f^+$ and $B^0 \rightarrow f^0$, are usually considered to perform a measurement of $R^{+-/00}$, whenever they can be related by isospin symmetry (for example $B^+ \rightarrow J/\psi K^+$ and $B^0 \rightarrow J/\psi K^0$). Under the assumption that $\Gamma(B^+ \rightarrow f^+) = \Gamma(B^0 \rightarrow f^0)$, i.e., that isospin invariance holds in these B decays, the ratio of the number of reconstructed $B^+ \rightarrow f^+$ and $B^0 \rightarrow f^0$ mesons, after correcting for efficiency, is proportional to

$$\begin{aligned} \frac{f^{+-} \mathcal{B}(B^+ \rightarrow f^+)}{f^{00} \mathcal{B}(B^0 \rightarrow f^0)} &= \frac{f^{+-} \Gamma(B^+ \rightarrow f^+) \tau(B^+)}{f^{00} \Gamma(B^0 \rightarrow f^0) \tau(B^0)} \\ &= \frac{f^{+-} \tau(B^+)}{f^{00} \tau(B^0)}, \end{aligned} \tag{17}$$

where $\tau(B^+)$ and $\tau(B^0)$ are the B^+ and B^0 lifetimes respectively. Hence the primary quantity measured in these analyses is $R^{+-/00} \tau(B^+) / \tau(B^0)$, and the extraction of $R^{+-/00}$ with this method therefore requires the knowledge of the $\tau(B^+) / \tau(B^0)$ lifetime ratio.

The published measurements of $R^{+-/00}$ are listed in Table 1² together with the corresponding assumed values of $\tau(B^+) / \tau(B^0)$. All measurements are based on the above-mentioned method, except the one from Belle, which is a by-product of the B^0 mixing frequency analysis using dilepton events (but note that it also assumes isospin invariance, namely $\Gamma(B^+ \rightarrow \ell^+ X) = \Gamma(B^0 \rightarrow \ell^+ X)$). The latter is therefore treated in a slightly different manner in the following procedure used to combine these measurements:

- each published value of $R^{+-/00}$ from CLEO and BABAR is first converted back to the original measurement of $R^{+-/00} \tau(B^+) / \tau(B^0)$, using the value of the lifetime ratio assumed in the corresponding analysis;
- a simple weighted average of these original measurements of $R^{+-/00} \tau(B^+) / \tau(B^0)$ from CLEO and BABAR is then computed, assuming no statistical or systematic correlations between them;
- the weighted average of $R^{+-/00} \tau(B^+) / \tau(B^0)$ is converted into a value of $R^{+-/00}$, using the latest average of

² An old and imprecise measurement from CLEO [11] is not included in Table 1 nor in the average.

Table 1 Published measurements of the B^+/B^0 production ratio in $\Upsilon(4S)$ decays, together with their average (see text). Systematic uncertainties due to the imperfect knowledge of $\tau(B^+)/\tau(B^0)$ are included

Experiment, year	References	Decay modes or method	Published value of $R^{+-/00} = f^{+-}/f^{00}$	Assumed value of $\tau(B^+)/\tau(B^0)$
CLEO, 2001	[7]	$J/\psi K^{(*)}$	$1.04 \pm 0.07 \pm 0.04$	1.066 ± 0.024
CLEO, 2002	[8]	$D^* \ell \nu$	$1.058 \pm 0.084 \pm 0.136$	1.074 ± 0.028
Belle, 2003	[9]	Dilepton events	$1.01 \pm 0.03 \pm 0.09$	1.083 ± 0.017
BABAR, 2005	[10]	$(c\bar{c})K^{(*)}$	$1.06 \pm 0.02 \pm 0.03$	1.086 ± 0.017
Average			1.059 ± 0.027 (tot)	1.076 ± 0.004

the lifetime ratios, $\tau(B^+)/\tau(B^0) = 1.076 \pm 0.004$ (see Sect. 3.2.3);

- the Belle measurement of $R^{+-/00}$ is adjusted to the current values of $\tau(B^0) = 1.520 \pm 0.004$ ps and $\tau(B^+)/\tau(B^0) = 1.076 \pm 0.004$ (see Sect. 3.2.3), using the quoted systematic uncertainties due to these parameters;
- the combined value of $R^{+-/00}$ from CLEO and BABAR is averaged with the adjusted value of $R^{+-/00}$ from Belle, assuming a 100% correlation of the systematic uncertainty due to the limited knowledge on $\tau(B^+)/\tau(B^0)$; no other correlation is considered.

The resulting global average,

$$R^{+-/00} = \frac{f^{+-}}{f^{00}} = 1.059 \pm 0.027, \tag{18}$$

is consistent with equal production rate of charged and neutral B mesons, although only at the 2.2σ level.

On the other hand, the BABAR collaboration has performed a direct measurement of the f^{00} fraction using an original method, which neither relies on isospin symmetry nor requires the knowledge of $\tau(B^+)/\tau(B^0)$. Its analysis, based on a comparison between the number of events where a single $B^0 \rightarrow D^{*-} \ell^+ \nu$ decay could be reconstructed and the number of events where two such decays could be reconstructed, yields [12]

$$f^{00} = 0.487 \pm 0.010(\text{stat}) \pm 0.008(\text{syst}). \tag{19}$$

The two results of Eqs. (18) and (19) are of very different natures and completely independent of each other. Their product is equal to $f^{+-} = 0.516 \pm 0.019$, while another combination of them gives $f^{+-} + f^{00} = 1.003 \pm 0.029$, compatible with unity. Assuming³ $f^{+-} + f^{00} = 1$, also consistent with CLEO’s observation that the fraction of $\Upsilon(4S)$

decays to $B\bar{B}$ pairs is larger than 0.96 at 95% CL [16], the results of Eqs. (18) and (19) can be averaged (first converting Eq. (18) into a value of $f^{00} = 1/(R^{+-/00} + 1)$) to yield the following more precise estimates:

$$f^{00} = 0.486 \pm 0.006, \quad f^{+-} = 1 - f^{00} = 0.514 \pm 0.006, \\ \frac{f^{+-}}{f^{00}} = 1.058 \pm 0.024. \tag{20}$$

The latter ratio differs from one by 2.4σ .

3.1.2 b -hadron production fractions in $\Upsilon(5S)$ decays

Hadronic events produced in e^+e^- collisions at the $\Upsilon(5S)$ (also known as $\Upsilon(10860)$) energy can be classified into three categories: light-quark (u, d, s, c) continuum events, $b\bar{b}$ continuum events, and $\Upsilon(5S)$ events. The latter two cannot be distinguished and will be called $b\bar{b}$ events in the following. These $b\bar{b}$ events, which also include $b\bar{b}\gamma$ events because of possible initial-state radiation, can hadronize in different final states. We define $f_{u,d}^{\Upsilon(5S)}$ as the fraction of $b\bar{b}$ events with a pair of non-strange bottom mesons ($B\bar{B}, B\bar{B}^*, B^*\bar{B}, B^*\bar{B}^*, B\bar{B}\pi, B\bar{B}^*\pi, B^*\bar{B}\pi, B^*\bar{B}^*\pi$, and $B\bar{B}\pi\pi$ final states, where B denotes a B^0 or B^+ meson and \bar{B} denotes a \bar{B}^0 or B^- meson), $f_s^{\Upsilon(5S)}$ as the fraction of $b\bar{b}$ events with a pair of strange bottom mesons ($B_s^0\bar{B}_s^0, B_s^0\bar{B}_s^{*0}, B_s^{*0}\bar{B}_s^0$, and $B_s^{*0}\bar{B}_s^{*0}$ final states), and $f_B^{\Upsilon(5S)}$ as the fraction of $b\bar{b}$ events without any bottom meson in the final state. Note that the excited bottom-meson states decay via $B^* \rightarrow B\gamma$ and $B_s^{*0} \rightarrow B_s^0\gamma$. These fractions satisfy

$$f_{u,d}^{\Upsilon(5S)} + f_s^{\Upsilon(5S)} + f_B^{\Upsilon(5S)} = 1. \tag{21}$$

The CLEO and Belle collaborations have published measurements of several inclusive $\Upsilon(5S)$ branching fractions, $\mathcal{B}(\Upsilon(5S) \rightarrow D_s X)$, $\mathcal{B}(\Upsilon(5S) \rightarrow \phi X)$ and $\mathcal{B}(\Upsilon(5S) \rightarrow D^0 X)$, from which they extracted the model-dependent estimates of $f_s^{\Upsilon(5S)}$ reported in Table 2. This extraction was performed under the implicit assumption $f_B^{\Upsilon(5S)} = 0$, using the relation

³ A few non- $B\bar{B}$ decay modes of the $\Upsilon(4S)$ ($\Upsilon(1S)\pi^+\pi^-$, $\Upsilon(2S)\pi^+\pi^-$, $\Upsilon(1S)\eta$) have been observed with branching fractions of the order of 10^{-4} [13–15], corresponding to a partial width several times larger than that in the e^+e^- channel. However, this can still be neglected and the assumption $f^{+-} + f^{00} = 1$ remains valid in the present context of the determination of f^{+-} and f^{00} .

Table 2 Published measurements of $f_s^{\Upsilon(5S)}$, obtained assuming $f_B^{\Upsilon(5S)} = 0$ and quoted as in the original publications, except for the 2010 Belle measurement, which is quoted as $1 - f_{u,d}^{\Upsilon(5S)}$ with $f_{u,d}^{\Upsilon(5S)}$

from Ref. [17]. Our average of $f_s^{\Upsilon(5S)}$ assuming $f_B^{\Upsilon(5S)} = 0$, given on the penultimate line, does not include the most recent Belle result quoted on the last line (see footnote 4)

Experiment, year, dataset	Decay mode or method	Value of $f_s^{\Upsilon(5S)}$
CLEO, 2006, 0.42 fb ⁻¹ [18]	$\Upsilon(5S) \rightarrow D_s X$	$0.168 \pm 0.026^{+0.067}_{-0.034}$
	$\Upsilon(5S) \rightarrow \phi X$	$0.246 \pm 0.029^{+0.110}_{-0.053}$
	$\Upsilon(5S) \rightarrow B\bar{B}X$	$0.411 \pm 0.100 \pm 0.092$
	CLEO average of above 3	$0.21^{+0.06}_{-0.03}$
Belle, 2006, 1.86 fb ⁻¹ [19]	$\Upsilon(5S) \rightarrow D_s X$	$0.179 \pm 0.014 \pm 0.041$
	$\Upsilon(5S) \rightarrow D^0 X$	$0.181 \pm 0.036 \pm 0.075$
	Belle average of above 2	$0.180 \pm 0.013 \pm 0.032$
Belle, 2010, 23.6 fb ⁻¹ [17]	$\Upsilon(5S) \rightarrow B\bar{B}X$	$0.263 \pm 0.032 \pm 0.051^a$
Average of all above after adjustments to inputs of Table 3		0.215 ± 0.031
Belle, 2012, 121.4 fb ⁻¹ [20]	$\Upsilon(5S) \rightarrow D_s X, D^0 X$	0.172 ± 0.030

Table 3 External inputs on which the $f_s^{\Upsilon(5S)}$ averages are based

Branching fraction	Value	Explanation and reference
$\mathcal{B}(B \rightarrow D_s X) \times \mathcal{B}(D_s \rightarrow \phi\pi)$	0.00374 ± 0.00014	Derived from [6]
$\mathcal{B}(B_s^0 \rightarrow D_s X)$	0.92 ± 0.11	Model-dependent estimate [21]
$\mathcal{B}(D_s \rightarrow \phi\pi)$	0.045 ± 0.004	[6]
$\mathcal{B}(B \rightarrow D^0 X) \times \mathcal{B}(D^0 \rightarrow K\pi)$	0.0243 ± 0.0011	Derived from [6]
$\mathcal{B}(B_s^0 \rightarrow D^0 X)$	0.08 ± 0.07	Model-dependent estimate [19,21]
$\mathcal{B}(D^0 \rightarrow K\pi)$	0.0393 ± 0.0004	[6]
$\mathcal{B}(B \rightarrow \phi X)$	0.0343 ± 0.0012	[6]
$\mathcal{B}(B_s^0 \rightarrow \phi X)$	0.161 ± 0.024	Model-dependent estimate [18]

$$\frac{1}{2} \mathcal{B}(\Upsilon(5S) \rightarrow D_s X) = f_s^{\Upsilon(5S)} \times \mathcal{B}(B_s^0 \rightarrow D_s X) + \left(1 - f_s^{\Upsilon(5S)} - f_B^{\Upsilon(5S)}\right) \times \mathcal{B}(B \rightarrow D_s X), \quad (22)$$

and similar relations for $\mathcal{B}(\Upsilon(5S) \rightarrow D^0 X)$ and $\mathcal{B}(\Upsilon(5S) \rightarrow \phi X)$. In Table 2 we list also the values of $f_s^{\Upsilon(5S)}$ derived from measurements of $f_{u,d}^{\Upsilon(5S)} = \mathcal{B}(\Upsilon(5S) \rightarrow B\bar{B}X)$ [17,18], as well as our average value of $f_s^{\Upsilon(5S)}$, all obtained under the assumption $f_B^{\Upsilon(5S)} = 0$.

However, the assumption $f_B^{\Upsilon(5S)} = 0$ is known to be invalid since the observation of the following final states in e^+e^- collisions at the $\Upsilon(5S)$ energy: $\Upsilon(1S)\pi^+\pi^-$, $\Upsilon(2S)\pi^+\pi^-$, $\Upsilon(3S)\pi^+\pi^-$ and $\Upsilon(1S)K^+K^-$ [22,23], $h_b(1P)\pi^+\pi^-$ and $h_b(2P)\pi^+\pi^-$ [24], and more recently $\Upsilon(1S)\pi^0\pi^0$, $\Upsilon(2S)\pi^0\pi^0$ and $\Upsilon(3S)\pi^0\pi^0$ [25]. The sum of the measurements of the corresponding visible cross-sections, adding also the contributions of the unmeasured $\Upsilon(1S)K^0\bar{K}^0$, $h_b(1P)\pi^0\pi^0$ and $h_b(2P)\pi^0\pi^0$ final states assuming isospin conservation, amounts to

$$\sigma^{\text{vis}}(e^+e^- \rightarrow (b\bar{b})hh) = 13.2 \pm 1.4 \text{ pb},$$

for $(b\bar{b}) = \Upsilon(1S, 2S, 3S), h_b(1P, 2P)$ and $hh = \pi\pi, KK$.

We divide this by the $b\bar{b}$ production cross section, $\sigma(e^+e^- \rightarrow b\bar{b}X) = 337 \pm 15 \text{ pb}$, obtained as the average of the CLEO [21] and Belle [20]⁴ measurements, to obtain

$$\mathcal{B}(\Upsilon(5S) \rightarrow (b\bar{b})hh) = 0.039 \pm 0.004,$$

for $(b\bar{b}) = \Upsilon(1S, 2S, 3S), h_b(1P, 2P)$ and $hh = \pi\pi, KK$,

which is to be considered as a lower bound for $f_B^{\Upsilon(5S)}$.

Following the method described in Ref. [26], we perform a χ^2 fit of the original measurements of the $\Upsilon(5S)$ branching fractions of Refs. [17–19],⁴ using the inputs of Table 3, the relations of Eqs. (21) and (22) and the one-sided Gaussian constraint $f_B^{\Upsilon(5S)} \geq \mathcal{B}(\Upsilon(5S) \rightarrow (b\bar{b})hh)$, to simultaneously extract $f_{u,d}^{\Upsilon(5S)}$, $f_s^{\Upsilon(5S)}$ and $f_B^{\Upsilon(5S)}$. Taking all known correlations into account, the best fit values are

$$f_{u,d}^{\Upsilon(5S)} = 0.761^{+0.027}_{-0.042}, \quad (23)$$

⁴ Belle updated the analysis of Ref. [19] with the full $\Upsilon(5S)$ dataset. The resulting measurements of $\sigma(e^+e^- \rightarrow b\bar{b}X)$ and $f_s^{\Upsilon(5S)}$, which supersede those of Ref. [19], are quoted and used in Ref. [20]. However, no details are given. Because of the lack of relevant information, this measurement of $f_s^{\Upsilon(5S)}$ cannot be included in the averages presented here.

$$f_s^{\gamma(5S)} = 0.200^{+0.030}_{-0.031}, \tag{24}$$

$$f_B^{\gamma(5S)} = 0.039^{+0.050}_{-0.004}, \tag{25}$$

where the strongly asymmetric uncertainty on $f_B^{\gamma(5S)}$ is due to the one-sided constraint from the observed $(b\bar{b})hh$ decays. These results, together with their correlation, imply

$$f_s^{\gamma(5S)} / f_{u,d}^{\gamma(5S)} = 0.263^{+0.052}_{-0.044}, \tag{26}$$

in fair agreement with the results of a BABAR analysis [27], performed as a function of centre-of-mass energy.⁵

The production of B_s^0 mesons at the $\gamma(5S)$ is observed to be dominated by the $B_s^{*0} \bar{B}_s^{*0}$ channel, with $\sigma(e^+e^- \rightarrow B_s^{*0} \bar{B}_s^{*0}) / \sigma(e^+e^- \rightarrow B_s^{(*)0} \bar{B}_s^{(*)0}) = (87.0 \pm 1.7)\%$ [28, 29]. The proportions of the various production channels for non-strange B mesons have also been measured [17].

3.1.3 b -hadron production fractions at high energy

At high energy, all species of weakly decaying b hadrons may be produced, either directly or in strong and electromagnetic decays of excited b hadrons. It is often assumed that the fractions of these different species are the same in unbiased samples of high- p_T b jets originating from Z^0 decays, from $p\bar{p}$ collisions at the Tevatron, or from pp collisions at the LHC. This hypothesis is plausible under the condition that the square of the momentum transfer to the produced b quarks, Q^2 , is large compared with the square of the hadronization energy scale, $Q^2 \gg \Lambda_{\text{QCD}}^2$. On the other hand, there is no strong argument that the fractions at different machines should be strictly equal, so this assumption should be checked experimentally. The available data show that the fractions depend on the kinematics of the produced b hadron. A simple phenomenological model appears to agree with all data and indicates that the fractions are constant if the b hadron is produced with sufficiently high transverse momentum from any collider. Unless otherwise indicated, these fractions are assumed to be equal at all high-energy colliders until demonstrated otherwise by experiment. Both CDF and LHCb report a p_T dependence for Λ_b^0 production relative to B^+ and B^0 ; the number of Λ_b^0 baryons observed at low p_T is enhanced with respect to that seen at LEP's higher p_T . Therefore we present three sets of complete averages: one set including only measurements performed at LEP, a second set including only measurements performed at the Tevatron, a third set including measurements performed at LEP, Tevatron and LHC. The LHCb production fractions results by themselves are still incomplete, lacking measurements of the production of weakly-decaying baryons heavier than Λ_b^0 .

⁵ The results of Ref. [27] are not included in the average since no numerical value is given for $f_s^{\gamma(5S)} / f_{u,d}^{\gamma(5S)}$.

Contrary to what happens in the charm sector where the fractions of D^+ and D^0 are different, the relative amount of B^+ and B^0 is not affected by the electromagnetic decays of excited B^{*+} and B^{*0} states and strong decays of excited B^{**+} and B^{**0} states. Decays of the type $B_s^{*0} \rightarrow B^{(*)}K$ also contribute to the B^+ and B^0 rates, but with the same magnitude if mass effects can be neglected. We therefore assume equal production of B^+ and B^0 mesons. We also neglect the production of weakly decaying states made of several heavy quarks (like B_c^+ and doubly heavy baryons) which is known to be very small. Hence, for the purpose of determining the b -hadron fractions, we use the constraints

$$f_u = f_d \quad \text{and} \quad f_u + f_d + f_s + f_{\text{baryon}} = 1, \tag{27}$$

where f_u , f_d , f_s and f_{baryon} are the unbiased fractions of B^+ , B^0 , B_s^0 and b baryons, respectively.

We note that there are many measurements of the production cross-sections of different species of b hadrons. In principle these could be included in a global fit to determine the production fractions. We do not perform such a fit at the current time, and instead average only the explicit measurements of the production fractions.

The LEP experiments have measured $f_s \times \mathcal{B}(B_s^0 \rightarrow D_s^- \ell^+ \nu_\ell X)$ [30–32], $\mathcal{B}(b \rightarrow \Lambda_b^0) \times \mathcal{B}(\Lambda_b^0 \rightarrow \Lambda_c^+ \ell^- \bar{\nu}_\ell X)$ [33, 34] and $\mathcal{B}(b \rightarrow \Xi_b^-) \times \mathcal{B}(\Xi_b^- \rightarrow \Xi^- \ell^- \bar{\nu}_\ell X)$ [35, 36] from partially reconstructed final states including a lepton, f_{baryon} from protons identified in b events [37], and the production rate of charged b hadrons [38]. Ratios of b -hadron fractions have been measured by CDF using lepton+charm final states [39–41]⁶ and double semileptonic decays with $K^* \mu \mu$ and $\phi \mu \mu$ final states [42]. Measurements of the production of other heavy flavour baryons at the Tevatron are included in the determination of f_{baryon} [43–45]⁷ using the constraint

$$\begin{aligned} f_{\text{baryon}} &= f_{\Lambda_b^0} + f_{\Xi_b^0} + f_{\Xi_b^-} + f_{\Omega_b^-} \\ &= f_{\Lambda_b^0} \left(1 + 2 \frac{f_{\Xi_b^-}}{f_{\Lambda_b^0}} + \frac{f_{\Omega_b^-}}{f_{\Lambda_b^0}} \right), \end{aligned} \tag{28}$$

where isospin invariance is assumed in the production of Ξ_b^0 and Ξ_b^- . Other b baryons are expected to decay strongly or electromagnetically to those baryons listed. For the production measurements, both CDF and D0 reconstruct their b baryons exclusively to final states which include a J/ψ and a hyperon ($\Lambda_b^0 \rightarrow J/\psi \Lambda$, $\Xi_b^- \rightarrow J/\psi \Xi^-$ and $\Omega_b^- \rightarrow J/\psi \Omega^-$). We assume that the partial decay width of a b

⁶ CDF updated their measurement of $f_{\Lambda_b^0}/f_d$ [39] to account for a measured p_T dependence between exclusively reconstructed Λ_b^0 and B^0 [41].

⁷ D0 reports $f_{\Omega_b^-}/f_{\Xi_b^-}$. We use the CDF+D0 average of $f_{\Xi_b^-}/f_{\Lambda_b^0}$ to obtain $f_{\Omega_b^-}/f_{\Lambda_b^0}$ and then combine it with the CDF result.

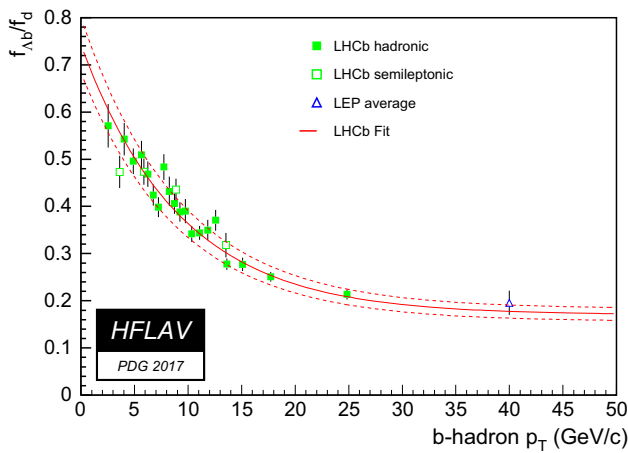


Fig. 4 Ratio of production fractions $f_{\Lambda_b^0}/f_d$ as a function of p_T of the b hadron from LHCb data for b hadrons decaying semileptonically [46] and fully reconstructed in hadronic decays [48]. The curve represents a fit to the LHCb hadronic data [48]. The computed LEP ratio is included at an approximate p_T in Z decays, but does not participate in any fit

baryon to a J/ψ and the corresponding hyperon is equal to the partial width of any other b baryon to a J/ψ and the corresponding hyperon. LHCb has also measured ratios of b -hadron fractions in charm+lepton final states [46] and in fully reconstructed hadronic two-body decays $B^0 \rightarrow D^-\pi^+$, $B_s^0 \rightarrow D_s^-\pi^+$ and $\Lambda_b^0 \rightarrow \Lambda_c^+\pi^-$ [47,48].

Both CDF and LHCb observe that the ratio $f_{\Lambda_b^0}/f_d$ depends on the p_T of the charm+lepton system [41,46].⁸ CDF chose to correct an older result to account for the p_T dependence. In a second result, CDF binned their data in p_T of the charm+electron system [40]. The more recent LHCb measurement using hadronic decays [48] obtains the scale for $R_{\Lambda_b^0} = f_{\Lambda_b^0}/f_d$ from their previous charm + lepton data [46]. The LHCb measurement using hadronic data also bins the same data in pseudorapidity (η) and sees a linear dependence of $R_{\Lambda_b^0}$. Since η is not entirely independent of p_T it is impossible to tell at this time whether this dependence is just an artifact of the p_T dependence. Figure 4 shows the ratio $R_{\Lambda_b^0}$ as a function of p_T for the b hadron, as measured by LHCb. LHCb fits their scaled hadronic data to obtain

$$R_{\Lambda_b^0} = (0.151 \pm 0.030) + \exp \left\{ - (0.57 \pm 0.11) - (0.095 \pm 0.016)[\text{GeV}/c]^{-1} \times p_T \right\}. \quad (29)$$

A value of $R_{\Lambda_b^0}$ is also calculated for LEP and placed at the approximate p_T for the charm+lepton system, but this value

⁸ CDF compares the p_T distribution of fully reconstructed $\Lambda_b^0 \rightarrow \Lambda_c^+\pi^-$ with $\bar{B}^0 \rightarrow D^+\pi^-$, which gives $f_{\Lambda_b^0}/f_d$ up to a scale factor. LHCb compares the p_T in the charm+lepton system between Λ_b^0 and B^0 and B^+ , giving $R_{\Lambda_b^0}/2 = f_{\Lambda_b^0}/(f_u + f_d) = f_{\Lambda_b^0}/2f_d$.

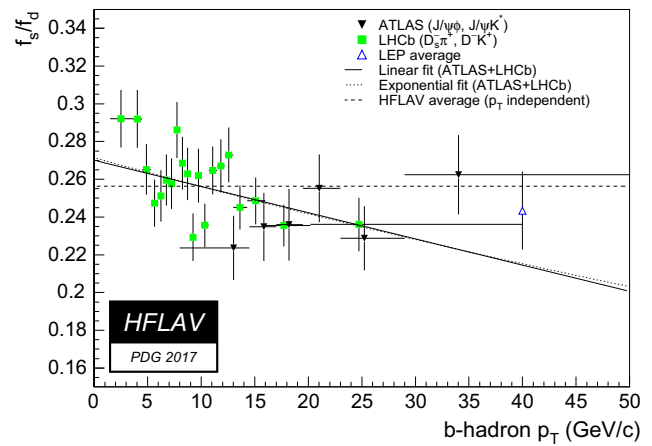


Fig. 5 Ratio of production fractions f_s/f_d as a function of p_T of the reconstructed b hadrons for the LHCb [47] and ATLAS [49] data. Note the suppressed zero for the vertical axis. The curves represent fits to the data: a linear fit (solid), and an exponential fit described in the text (dotted). The p_T independent value average of R_s (dashed) is shown for comparison. The computed LEP ratio is included at an approximate p_T in Z decays, but does not participate in any fit

does not participate in any fit.⁹ Because the two LHCb results for $R_{\Lambda_b^0}$ are not independent, we use only their semileptonic data for the averages. Note that the p_T dependence of $R_{\Lambda_b^0}$ combined with the constraint from Eq. (27) implies a compensating p_T dependence in one or more of the production fractions, f_u , f_d , or f_s .

LHCb and ATLAS have investigated the p_T dependence of f_s/f_d using fully reconstructed B_s^0 and B^0 decays. LHCb reported 3σ evidence that the ratio $R_s = f_s/f_d$ decreases with p_T using fully reconstructed B_s^0 and B^0 decays and theoretical predictions for branching ratios [47]. Data from the ATLAS experiment [49] using decays of B_s^0 and B^0 to J/ψ final states and using theoretical predictions for branching ratios [50] indicates that R_s is consistent with no p_T dependence. Figure 5 shows the ratio R_s as a function of p_T measured by LHCb and ATLAS. Two fits are performed. The first fit, using a linear parameterization, yields $R_s = (0.2701 \pm 0.0058) - (0.00139 \pm 0.00044)[\text{GeV}/c]^{-1} \times p_T$. A second fit, using a simple exponential, yields $R_s = \exp \{ (-1.304 \pm 0.024) - (0.0058 \pm 0.0019)[\text{GeV}/c]^{-1} \times p_T \}$. The two fits are nearly indistinguishable over the p_T range of the results, but the second gives a physical value for all p_T . R_s is also calculated for LEP and placed at the approximate p_T for the b hadron, though the LEP result doesn't participate in the fit. Our world average for R_s is also included in the figure for reference.

In order to combine or compare LHCb results with other experiments, the p_T -dependent $f_{\Lambda_b^0}/(f_u + f_d)$ is weighted by

⁹ The CDF semileptonic data would require significant corrections to obtain the p_T of the b hadron and be included on the same plot with the LHCb data. We do not have these corrections at this time.

Table 4 Comparison of average production fraction ratios from CDF [40,41] and LHCb [46]. The kinematic regime of the charm+lepton system reconstructed in each experiment is also shown

Quantity	CDF	LHCb
$f_s/(f_u + f_d)$	0.224 ± 0.057	0.134 ± 0.009
$f_{\Lambda_b^0}/(f_u + f_d)$	0.229 ± 0.062	0.240 ± 0.022
Average charm+lepton p_T	$\sim 13 \text{ GeV}/c$	$\sim 7 \text{ GeV}/c$
Pseudorapidity range	$-1 < \eta < 1$	$2 < \eta < 5$

the p_T spectrum.¹⁰ Table 4 compares the p_T -weighted LHCb data with comparable averages from CDF. The average CDF and LHCb data are in agreement despite the b hadrons being produced in different kinematic regimes.

Ignoring p_T dependence, all these published results have been adjusted to the latest branching fraction averages [6] and combined following the procedure and assumptions described in Ref. [3], to yield $f_u = f_d = 0.404 \pm 0.006$, $f_s = 0.102 \pm 0.005$ and $f_{\text{baryon}} = 0.090 \pm 0.012$ under the constraints of Eq. (27). Repeating the combinations for LEP and the Tevatron, we obtain $f_u = f_d = 0.412 \pm 0.008$, $f_s = 0.088 \pm 0.013$ and $f_{\text{baryon}} = 0.089 \pm 0.012$ when using the LEP data only, and $f_u = f_d = 0.340 \pm 0.021$, $f_s = 0.101 \pm 0.015$ and $f_{\text{baryon}} = 0.218 \pm 0.047$ when using the Tevatron data only. As noted previously, the LHCb data are insufficient to determine a complete set of b -hadron production fractions. The world averages (LEP, Tevatron and LHC) for the various fractions are presented here for comparison with previous averages. Significant differences exist between the LEP and Tevatron fractions, therefore use of the world averages should be taken with some care. For these combinations other external inputs are used, e.g., the branching ratios of B mesons to final states with a D or D^* in semileptonic decays, which are needed to evaluate the fraction of semileptonic B_s^0 decays with a D_s^- in the final state.

Time-integrated mixing analyses performed with lepton pairs from $b\bar{b}$ events produced at high-energy colliders measure the quantity

$$\bar{\chi} = f'_d \chi_d + f'_s \chi_s, \tag{30}$$

where f'_d and f'_s are the fractions of B^0 and B_s^0 hadrons in a sample of semileptonic b -hadron decays, and where χ_d and χ_s are the B^0 and B_s^0 time-integrated mixing probabilities. Assuming that all b hadrons have the same semileptonic decay width implies $f'_i = f_i R_i$, where $R_i = \tau_i/\tau_b$ is the ratio of the lifetime τ_i of species i to the average b -hadron

¹⁰ In practice the LHCb data are given in 14 bins in p_T and η with a full covariance matrix [46]. The weighted average is calculated as $D^T C^{-1} M/\sigma$, where $\sigma = D^T C^{-1} D$, M is a vector of measurements, C^{-1} is the inverse covariance matrix and D^T is the transpose of the design matrix (vector of 1's).

lifetime $\tau_b = \sum_i f_i \tau_i$. Hence measurements of the mixing probabilities $\bar{\chi}$, χ_d and χ_s can be used to improve our knowledge of f_u , f_d , f_s and f_{baryon} . In practice, the above relations yield another determination of f_s obtained from f_{baryon} and mixing information,

$$f_s = \frac{1}{R_s} \frac{(1+r)\bar{\chi} - (1 - f_{\text{baryon}} R_{\text{baryon}})\chi_d}{(1+r)\chi_s - \chi_d}, \tag{31}$$

where $r = R_u/R_d = \tau(B^+)/\tau(B^0)$.

The published measurements of $\bar{\chi}$ performed by the LEP experiments have been combined by the LEP Electroweak Working Group to yield $\bar{\chi} = 0.1259 \pm 0.0042$ [51].¹¹ This can be compared with the Tevatron average, $\bar{\chi} = 0.147 \pm 0.011$, obtained from D0 [52] and CDF [53]. The two averages deviate from each other by 1.8σ ; this could be an indication that the production fractions of b hadrons at the Z peak or at the Tevatron are not the same. We choose to combine these two results in a simple weighted average, assuming no correlations, and, following the PDG prescription, we multiply the combined uncertainty by 1.8to account for the discrepancy. Our world average is then $\bar{\chi} = 0.1284 \pm 0.0069$.

Introducing the $\bar{\chi}$ average in Eq. (31), together with our world average $\chi_d = 0.1860 \pm 0.0011$ [see Eq. (67) of Sect. 3.3.1], the assumption $\chi_s = 1/2$ [justified by Eq. (76) in Sect. 3.3.2], the best knowledge of the lifetimes (see Sect. 3.2) and the estimate of f_{baryon} given above, yields $f_s = 0.118 \pm 0.018$ (or $f_s = 0.111 \pm 0.011$ using only LEP data, or $f_s = 0.166 \pm 0.029$ using only Tevatron data), an estimate dominated by the mixing information. Taking into account all known correlations (including that introduced by f_{baryon}), this result is then combined with the set of fractions obtained from direct measurements (given above), to yield the improved estimates of Table 5, still under the constraints of Eq. (27). As can be seen, our knowledge on the mixing parameters reduces the uncertainty on f_s , quite substantially in the case of LEP data. It should be noted that the results are correlated, as indicated in Table 5.

3.2 b -hadron lifetimes

In the spectator model the decay of b hadrons H_b is governed entirely by the flavour changing $b \rightarrow Wq$ transition ($q = c, u$). For this very reason, lifetimes of all b hadrons are the same in the spectator approximation regardless of the (spectator) quark content of the H_b . In the early 1990's experiments became sophisticated enough to start seeing the differences of the lifetimes among various H_b

¹¹ We use the $\bar{\chi}$ average of Eq. 5.39 in Ref. [51], obtained from a 10-parameter global fit of all electroweak data where the asymmetry measurements have been excluded.

Table 5 Time-integrated mixing probability $\bar{\chi}$ (defined in Eq. (30)), and fractions of the different b -hadron species in an unbiased sample of weakly decaying b hadrons, obtained from both direct and mixing

measurements. The correlation coefficients between the fractions are also given. The last column includes measurements performed at LEP, Tevatron and LHC

Quantity		Z decays	Tevatron	LHCb [47]	All
Mixing probability	$\bar{\chi}$	0.1259 ± 0.0042	0.147 ± 0.011		0.1284 ± 0.0069
B^+ or B^0 fraction	$f_u = f_d$	0.407 ± 0.007	0.344 ± 0.021		0.404 ± 0.006
B_s^0 fraction	f_s	0.101 ± 0.008	0.115 ± 0.013		0.103 ± 0.005
b -baryon fraction	f_{baryon}	0.084 ± 0.011	0.196 ± 0.046		0.088 ± 0.012
B_s^0/B^0 ratio	f_s/f_d	0.249 ± 0.023	0.333 ± 0.041	0.256 ± 0.020^a	0.256 ± 0.013
$\rho(f_s, f_u) = \rho(f_s, f_d)$		-0.629	+0.153		-0.143
$\rho(f_{\text{baryon}}, f_u) = \rho(f_{\text{baryon}}, f_d)$		-0.822	-0.959		-0.921
$\rho(f_{\text{baryon}}, f_s)$		+0.074	-0.426		-0.254

^a This value has been updated with new inputs by LHCb to yield 0.259 ± 0.015 [54]

species. The first theoretical calculations of the spectator quark effects on H_b lifetime emerged only few years earlier [55].

Since then, such calculations are performed in the framework of the Heavy Quark Expansion (HQE) [55–57], using as most important assumption that of quark-hadron duality [58,59]. Since a few years, possible quark-hadron duality violating effects are severely constrained by experiments [60]. In these calculations, the total decay rate of an H_b is expressed as the sum of a series of expectation values of operators of increasing dimension, multiplied by the correspondingly higher powers of Λ_{QCD}/m_b :

$$\Gamma_{H_b} = |\text{CKM}|^2 \sum_n c_n \left(\frac{\Lambda_{\text{QCD}}}{m_b} \right)^n \langle H_b | O_n | H_b \rangle, \quad (32)$$

where $|\text{CKM}|^2$ is the relevant combination of CKM matrix elements. The coefficients c_n of this expansion, known as the Operator Product Expansion [61], can be calculated perturbatively. Hence, the HQE predicts Γ_{H_b} in the form of an expansion in both Λ_{QCD}/m_b and $\alpha_s(m_b)$. The precision of current experiments requires an expansion up to the next-to-leading order in QCD, i.e., the inclusion of corrections of the order of $\alpha_s(m_b)$ to the c_n terms. The non-perturbative parts of the calculation are grouped into the expectation values $\langle H_b | O_n | H_b \rangle$ of operators O_n . These can be calculated using lattice QCD or QCD sum rules, or can be related to other observables via the HQE. One may reasonably expect that powers of Λ_{QCD}/m_b provide enough suppression that only the first few terms of the sum in Eq. (32) matter.

Theoretical predictions are usually made for the ratios of the lifetimes (with $\tau(B^0)$ often chosen as the common denominator) rather than for the individual lifetimes, for this allows several uncertainties to cancel. The precision of the HQE calculations (see Refs. [62–67], and Refs. [68,69] for the latest updates) is in some instances already surpassed by

the measurements, e.g., in the case of $\tau(B^+)/\tau(B^0)$. More accurate predictions are now a matter of progress in the evaluation of the non-perturbative hadronic matrix elements, in particular using lattice QCD where significant advances were made in the last decade. However, the following important conclusions can be drawn from the HQE, even in its present state, which are in agreement with experimental observations:

- The heavier the mass of the heavy quark, the smaller is the variation in the lifetimes among different hadrons containing this quark, which is to say that as $m_b \rightarrow \infty$ we retrieve the spectator picture in which the lifetimes of all H_b states are the same. This is well illustrated by the fact that lifetimes are rather similar in the b sector, while they differ by large factors in the charm sector ($m_c < m_b$).
- The non-perturbative corrections arise only at the order of $\Lambda_{\text{QCD}}^2/m_b^2$, which translates into differences among H_b lifetimes of only a few percent.
- It is only the difference between meson and baryon lifetimes that appears at the $\Lambda_{\text{QCD}}^2/m_b^2$ level. The splitting of the meson lifetimes occurs at the $\Lambda_{\text{QCD}}^3/m_b^3$ level, yet it is enhanced by a phase space factor $16\pi^2$ with respect to the leading free b decay.

To ensure that certain sources of systematic uncertainty cancel, lifetime analyses are sometimes designed to measure ratios of lifetimes. However, because of the differences in decay topologies, abundance (or lack thereof) of decays of a certain kind, *etc.*, measurements of the individual lifetimes are also common. In the following section we review the most common types of lifetime measurements. This discussion is followed by the presentation of the averaging of the various lifetime measurements, each with a brief description of its particularities.

3.2.1 Lifetime measurements, uncertainties and correlations

In most cases, the lifetime of an H_b state is estimated from a flight distance measurement and a $\beta\gamma$ factor which is used to convert the geometrical distance into the proper decay time. Methods of accessing lifetime information can roughly be divided in the following five categories:

1. *Inclusive (flavour-blind) measurements.* These early measurements were aimed at extracting the lifetime from a mixture of b -hadron decays, without distinguishing the decaying species. Often the knowledge of the mixture composition was limited, which made these measurements experiment-specific. Also, these measurements had to rely on Monte Carlo simulation for estimating the $\beta\gamma$ factor, because the decaying hadrons are not fully reconstructed. These were usually the largest statistics b -hadron lifetime measurements accessible to a given experiment, and could therefore serve as an important performance benchmark.
2. *Measurements in semileptonic decays of a specific H_b .* The W boson from $b \rightarrow Wc$ produces a $\ell\nu_\ell$ pair ($\ell = e, \mu$) in about 21% of the cases. The electron or muon from such decays provides a clean and efficient trigger signature. The c quark from the $b \rightarrow Wc$ transition and the other quark(s) making up the decaying H_b combine into a charm hadron, which is reconstructed in one or more exclusive decay channels. Knowing what this charmed hadron is allows one to separate, at least statistically, different H_b species. The advantage of these measurements is in the sample size, which is usually larger than in the case of exclusively reconstructed H_b decays. Some of the main disadvantages are related to the difficulty of estimating the lepton+charm sample composition and to the Monte Carlo reliance for the momentum (and hence $\beta\gamma$ factor) estimate.
3. *Measurements in exclusively reconstructed hadronic decays.* These have the advantage of complete reconstruction of the decaying H_b state, which allows one to infer the decaying species as well as to perform precise measurement of the $\beta\gamma$ factor. Both lead to generally smaller systematic uncertainties than in the above two categories. The downsides are smaller branching ratios and larger combinatorial backgrounds, especially in $H_b \rightarrow H_c\pi(\pi\pi)$ and multi-body H_c decays, or in a hadron collider environment with non-trivial underlying event. Decays of the type $H_b \rightarrow J/\psi H_s$ are relatively clean and easy to trigger, due to the $J/\psi \rightarrow \ell^+\ell^-$ signature, but their branching fraction is only about 1%.

4. *Measurements at asymmetric B factories.* In the $\Upsilon(4S) \rightarrow B\bar{B}$ decay, the B mesons (B^+ or B^0) are essentially at rest in the $\Upsilon(4S)$ frame. This makes direct lifetime measurements impossible in experiments at symmetric colliders producing $\Upsilon(4S)$ at rest. At asymmetric B factories the $\Upsilon(4S)$ meson is boosted resulting in B and \bar{B} moving nearly parallel to each other with the same boost. The lifetime is inferred from the distance Δz separating the B and \bar{B} decay vertices along the beam axis and from the $\Upsilon(4S)$ boost known from the beam energies. This boost is equal to $\beta\gamma \approx 0.55$ (0.43) in the BABAR (Belle) experiment, resulting in an average B decay length of approximately 250 (190) μm .

In order to determine the charge of the B mesons in each event, one of them is fully reconstructed in a semileptonic or hadronic decay mode. The other B is typically not fully reconstructed, only the position of its decay vertex is determined from the remaining tracks in the event. These measurements benefit from large sample sizes, but suffer from poor proper time resolution, comparable to the B lifetime itself. This resolution is dominated by the uncertainty on the decay vertices, which is typically 50 (100) μm for a fully (partially) reconstructed B meson. With much larger samples in the future, the resolution and purity could be improved (and hence the systematics reduced) by fully reconstructing both B mesons in the event.

5. *Direct measurement of lifetime ratios.* This method, initially applied in the measurement of $\tau(B^+)/\tau(B^0)$, is now also used for other b -hadron species at the LHC. The ratio of the lifetimes is extracted from the proper time dependence of the ratio of the observed yields of two different b -hadron species, both reconstructed in decay modes with similar topologies. The advantage of this method is that subtle efficiency effects (partially) cancel in the ratio.

In some of the latest analyses, measurements of two (e.g., $\tau(B^+)$ and $\tau(B^+)/\tau(B^0)$) or three (e.g. $\tau(B^+)$, $\tau(B^+)/\tau(B^0)$, and Δm_d) quantities are combined. This introduces correlations among measurements. Another source of correlations among the measurements are the systematic effects, which could be common to an experiment or to an analysis technique across the experiments. When calculating the averages, such known correlations are taken into account.

3.2.2 Inclusive b -hadron lifetimes

The inclusive b -hadron lifetime is defined as $\tau_b = \sum_i f_i \tau_i$ where τ_i are the individual species lifetimes and f_i are the fractions of the various species present in an unbiased sample of weakly decaying b hadrons produced at a high-energy

Table 6 Measurements of average b -hadron lifetimes

Experiment	Method	Data set	τ_b (ps)	Refs.
ALEPH	Dipole	91	$1.511 \pm 0.022 \pm 0.078$	[70]
DELPHI	All track i.p. (2D)	91–92	$1.542 \pm 0.021 \pm 0.045$	[71] ^a
DELPHI	Sec. vtx	91–93	$1.582 \pm 0.011 \pm 0.027$	[72] ^a
DELPHI	Sec. vtx	94–95	$1.570 \pm 0.005 \pm 0.008$	[73]
L3	Sec. vtx + i.p.	91–94	$1.556 \pm 0.010 \pm 0.017$	[74] ^b
OPAL	Sec. vtx	91–94	$1.611 \pm 0.010 \pm 0.027$	[75]
SLD	Sec. vtx	93	$1.564 \pm 0.030 \pm 0.036$	[76]
Average set 1 (b vertex)			1.572 ± 0.009	
ALEPH	Lepton i.p. (3D)	91–93	$1.533 \pm 0.013 \pm 0.022$	[77]
L3	Lepton i.p. (2D)	91–94	$1.544 \pm 0.016 \pm 0.021$	[74] ^b
OPAL	Lepton i.p. (2D)	90–91	$1.523 \pm 0.034 \pm 0.038$	[78]
Average set 2 ($b \rightarrow \ell$)			1.537 ± 0.020	
CDF1	J/ψ vtx	92–95	$1.533 \pm 0.015^{+0.035}_{-0.031}$	[79]
Average set 3 ($b \rightarrow J/\psi$)			1.533 ± 0.036	

^a The combined DELPHI result quoted in [72] is $1.575 \pm 0.010 \pm 0.026$ ps

^b The combined L3 result quoted in [74] is $1.549 \pm 0.009 \pm 0.015$ ps

collider.¹² This quantity is certainly less fundamental than the lifetimes of the individual species, the latter being much more useful in comparisons of the measurements with the theoretical predictions. Nonetheless, we perform the averaging of the inclusive lifetime measurements for completeness and because they might be of interest as “technical numbers.”

In practice, an unbiased measurement of the inclusive lifetime is difficult to achieve, because it would imply an efficiency which is guaranteed to be the same across species. So most of the measurements are biased. In an attempt to group analyses that are expected to select the same mixture of b hadrons, the available results (given in Table 6) are divided into the following three sets:

1. measurements at LEP and SLD that include any b -hadron decay, based on topological reconstruction (secondary vertex or track impact parameters);
2. measurements at LEP based on the identification of a lepton from a b decay; and
3. measurements at hadron colliders based on inclusive $H_b \rightarrow J/\psi X$ reconstruction, where the J/ψ is fully reconstructed.

The measurements of the first set are generally considered as estimates of τ_b , although the efficiency to reconstruct a secondary vertex most probably depends, in an analysis-specific way, on the number of tracks coming from the vertex, thereby depending on the type of the H_b . Even though these

efficiency variations can in principle be accounted for using Monte Carlo simulations (which inevitably contain assumptions on branching fractions), the H_b mixture in that case can remain somewhat ill-defined and could be slightly different among analyses in this set.

On the contrary, the mixtures corresponding to the other two sets of measurements are better defined in the limit where the reconstruction and selection efficiency of a lepton or a J/ψ from an H_b does not depend on the decaying hadron type. These mixtures are given by the production fractions and the inclusive branching fractions for each H_b species to give a lepton or a J/ψ . In particular, under the assumption that all b hadrons have the same semileptonic decay width, the analyses of the second set should measure $\tau(b \rightarrow \ell) = (\sum_i f_i \tau_i^3) / (\sum_i f_i \tau_i^2)$ which is necessarily larger than τ_b if lifetime differences exist. Given the present knowledge on τ_i and f_i , $\tau(b \rightarrow \ell) - \tau_b$ is expected to be of the order of 0.003 ps. On the other hand, the third set measuring $\tau(b \rightarrow J/\psi)$ is expected to give an average smaller than τ_b because of the B_c^+ meson, which has a significantly larger probability to decay to a J/ψ than other b -hadron species.

Measurements by SLC and LEP experiments are subject to a number of common systematic uncertainties, such as those due to (lack of knowledge of) b and c fragmentation, b and c decay models, $\mathcal{B}(B \rightarrow \ell)$, $\mathcal{B}(B \rightarrow c \rightarrow \ell)$, $\mathcal{B}(c \rightarrow \ell)$, τ_c , and H_b decay multiplicity. In the averaging, these systematic uncertainties are assumed to be 100% correlated. The averages for the sets defined above (also given in Table 6) are

$$\tau(b \text{ vertex}) = 1.572 \pm 0.009 \text{ ps}, \tag{33}$$

$$\tau(b \rightarrow \ell) = 1.537 \pm 0.020 \text{ ps}, \tag{34}$$

¹² In principle such a quantity could be slightly different in Z decays, at the Tevatron or at the LHC, in case the fractions of b -hadron species are not exactly the same; see the discussion in Sect. 3.1.3.

Table 7 Measurements of the B^0 lifetime

Experiment	Method	Data set	$\tau(B^0)$ (ps)	Refs.
ALEPH	$D^{(*)}\ell$	91–95	$1.518 \pm 0.053 \pm 0.034$	[80]
ALEPH	Exclusive	91–94	$1.25^{+0.15}_{-0.13} \pm 0.05$	[81]
ALEPH	Partial rec. $\pi^+\pi^-$	91–94	$1.49^{+0.17+0.08}_{-0.15-0.06}$	[81]
DELPHI	$D^{(*)}\ell$	91–93	$1.61^{+0.14}_{-0.13} \pm 0.08$	[82]
DELPHI	Charge sec. vtx	91–93	$1.63 \pm 0.14 \pm 0.13$	[83]
DELPHI	Inclusive $D^*\ell$	91–93	$1.532 \pm 0.041 \pm 0.040$	[84]
DELPHI	Charge sec. vtx	94–95	$1.531 \pm 0.021 \pm 0.031$	[73]
L3	Charge sec. vtx	94–95	$1.52 \pm 0.06 \pm 0.04$	[85]
OPAL	$D^{(*)}\ell$	91–93	$1.53 \pm 0.12 \pm 0.08$	[86]
OPAL	Charge sec. vtx	93–95	$1.523 \pm 0.057 \pm 0.053$	[87]
OPAL	Inclusive $D^*\ell$	91–00	$1.541 \pm 0.028 \pm 0.023$	[88]
SLD	Charge sec. vtx ℓ	93–95	$1.56^{+0.14}_{-0.13} \pm 0.10$	[89] ^a
SLD	Charge sec. vtx	93–95	$1.66 \pm 0.08 \pm 0.08$	[89] ^a
CDF1	$D^{(*)}\ell$	92–95	$1.474 \pm 0.039^{+0.052}_{-0.051}$	[90]
CDF1	Excl. $J/\psi K^{*0}$	92–95	$1.497 \pm 0.073 \pm 0.032$	[91]
CDF2	Excl. $J/\psi K_S^0, J/\psi K^{*0}$	02–09	$1.507 \pm 0.010 \pm 0.008$	[92]
D0	Excl. $J/\psi K^{*0}$	03–07	$1.414 \pm 0.018 \pm 0.034$	[93]
D0	Excl. $J/\psi K_S^0$	02–11	$1.508 \pm 0.025 \pm 0.043$	[94]
D0	Inclusive $D^-\mu^+$	02–11	$1.534 \pm 0.019 \pm 0.021$	[95]
BABAR	Exclusive	99–00	$1.546 \pm 0.032 \pm 0.022$	[96]
BABAR	Inclusive $D^*\ell$	99–01	$1.529 \pm 0.012 \pm 0.029$	[97]
BABAR	Exclusive $D^*\ell$	99–02	$1.523^{+0.024}_{-0.023} \pm 0.022$	[98]
BABAR	Incl. $D^*\pi, D^*\rho$	99–01	$1.533 \pm 0.034 \pm 0.038$	[99]
BABAR	Inclusive $D^*\ell$	99–04	$1.504 \pm 0.013^{+0.018}_{-0.013}$	[100]
Belle	Exclusive	00–03	$1.534 \pm 0.008 \pm 0.010$	[101]
ATLAS	Excl. $J/\psi K_S^0$	2011	$1.509 \pm 0.012 \pm 0.018$	[102]
LHCb	Excl. $J/\psi K^{*0}$	2011	$1.524 \pm 0.006 \pm 0.004$	[103]
LHCb	Excl. $J/\psi K_S^0$	2011	$1.499 \pm 0.013 \pm 0.005$	[103]
LHCb	$K^+\pi^-$	2011	$1.524 \pm 0.011 \pm 0.004$	[104]
Average			1.520 ± 0.004	

^a The combined SLD result quoted in [89] is $1.64 \pm 0.08 \pm 0.08$ ps

$$\tau(b \rightarrow J/\psi) = 1.533 \pm 0.036 \text{ ps.} \tag{35}$$

The differences between these averages are consistent both with zero and with expectations within less than 2σ .

3.2.3 B^0 and B^+ lifetimes and their ratio

After a number of years of dominating these averages the LEP experiments yielded the scene to the asymmetric B factories and the Tevatron experiments. The B factories have been very successful in utilizing their potential – in only a few years of running, BABAR and, to a greater extent, Belle, have struck a balance between the statistical and the systematic uncertainties, with both being close to (or even better than) an impressive 1% level. In the mean-

while, CDF and D0 have emerged as significant contributors to the field as the Tevatron Run II data flowed in. Recently, the LHCb experiment reached a further step in precision, improving by a factor ~ 2 over the previous best measurements.

At the present time we are in an interesting position of having three sets of measurements (from LEP/SLC, B factories and Tevatron/LHC) that originate from different environments, are obtained using substantially different techniques and are precise enough for incisive comparison.

The averaging of $\tau(B^+)$, $\tau(B^0)$ and $\tau(B^+)/\tau(B^0)$ measurements is summarized in Tables 7, 8, and 9. For $\tau(B^+)/\tau(B^0)$ we average only the measurements of this quantity provided by experiments rather than using all available knowledge, which would have included, for example, $\tau(B^+)$

Table 8 Measurements of the B^+ lifetime

Experiment	Method	Data set	$\tau(B^+)$ (ps)	Refs.
ALEPH	$D^{(*)}\ell$	91–95	$1.648 \pm 0.049 \pm 0.035$	[80]
ALEPH	Exclusive	91–94	$1.58^{+0.21+0.04}_{-0.18-0.03}$	[81]
DELPHI	$D^{(*)}\ell$	91–93	$1.61 \pm 0.16 \pm 0.12$	[82] ^a
DELPHI	Charge sec. vtx	91–93	$1.72 \pm 0.08 \pm 0.06$	[83] ^a
DELPHI	Charge sec. vtx	94–95	$1.624 \pm 0.014 \pm 0.018$	[73]
L3	Charge sec. vtx	94–95	$1.66 \pm 0.06 \pm 0.03$	[85]
OPAL	$D^{(*)}\ell$	91–93	$1.52 \pm 0.14 \pm 0.09$	[86]
OPAL	Charge sec. vtx	93–95	$1.643 \pm 0.037 \pm 0.025$	[87]
SLD	Charge sec. vtx ℓ	93–95	$1.61^{+0.13}_{-0.12} \pm 0.07$	[89] ^b
SLD	Charge sec. vtx	93–95	$1.67 \pm 0.07 \pm 0.06$	[89] ^b
CDF1	$D^{(*)}\ell$	92–95	$1.637 \pm 0.058^{+0.045}_{-0.043}$	[90]
CDF1	Excl. $J/\psi K$	92–95	$1.636 \pm 0.058 \pm 0.025$	[91]
CDF2	Excl. $J/\psi K$	02–09	$1.639 \pm 0.009 \pm 0.009$	[92]
CDF2	Excl. $D^0\pi$	02–06	$1.663 \pm 0.023 \pm 0.015$	[105]
BABAR	Exclusive	99–00	$1.673 \pm 0.032 \pm 0.023$	[96]
Belle	Exclusive	00–03	$1.635 \pm 0.011 \pm 0.011$	[101]
LHCb	Excl. $J/\psi K$	2011	$1.637 \pm 0.004 \pm 0.003$	[103]
Average			1.638 ± 0.004	

^a The combined DELPHI result quoted in [83] is 1.70 ± 0.09 ps

^b The combined SLD result quoted in [89] is $1.66 \pm 0.06 \pm 0.05$ ps

Table 9 Measurements of the ratio $\tau(B^+)/\tau(B^0)$

Experiment	Method	Data set	Ratio $\tau(B^+)/\tau(B^0)$	Refs.
ALEPH	$D^{(*)}\ell$	91–95	$1.085 \pm 0.059 \pm 0.018$	[80]
ALEPH	Exclusive	91–94	$1.27^{+0.23+0.03}_{-0.19-0.02}$	[81]
DELPHI	$D^{(*)}\ell$	91–93	$1.00^{+0.17}_{-0.15} \pm 0.10$	[82]
DELPHI	Charge sec. vtx	91–93	$1.06^{+0.13}_{-0.11} \pm 0.10$	[83]
DELPHI	Charge sec. vtx	94–95	$1.060 \pm 0.021 \pm 0.024$	[73]
L3	Charge sec. vtx	94–95	$1.09 \pm 0.07 \pm 0.03$	[85]
OPAL	$D^{(*)}\ell$	91–93	$0.99 \pm 0.14^{+0.05}_{-0.04}$	[86]
OPAL	Charge sec. vtx	93–95	$1.079 \pm 0.064 \pm 0.041$	[87]
SLD	Charge sec. vtx ℓ	93–95	$1.03^{+0.16}_{-0.14} \pm 0.09$	[89] ^a
SLD	Charge sec. vtx	93–95	$1.01^{+0.09}_{-0.08} \pm 0.05$	[89] ^a
CDF1	$D^{(*)}\ell$	92–95	$1.110 \pm 0.056^{+0.033}_{-0.030}$	[90]
CDF1	Excl. $J/\psi K$	92–95	$1.093 \pm 0.066 \pm 0.028$	[91]
CDF2	Excl. $J/\psi K^{(*)}$	02–09	$1.088 \pm 0.009 \pm 0.004$	[92]
D0	$D^{*+}\mu D^0\mu$ ratio	02–04	$1.080 \pm 0.016 \pm 0.014$	[106]
BABAR	Exclusive	99–00	$1.082 \pm 0.026 \pm 0.012$	[96]
Belle	Exclusive	00–03	$1.066 \pm 0.008 \pm 0.008$	[101]
LHCb	Excl. $J/\psi K^{(*)}$	2011	$1.074 \pm 0.005 \pm 0.003$	[103]
Average			1.076 ± 0.004	

^a The combined SLD result quoted in [89] is $1.01 \pm 0.07 \pm 0.06$

and $\tau(B^0)$ measurements which did not contribute to any of the ratio measurements.

The following sources of correlated (within experiment/machine) systematic uncertainties have been considered:

- for SLC/LEP measurements – D^{**} branching ratio uncertainties [3], momentum estimation of b mesons from Z^0 decays (b -quark fragmentation parameter $\langle X_E \rangle = 0.702 \pm 0.008$ [3]), B_s^0 and b -baryon lifetimes (see Sects. 3.2.4, 3.2.6), and b -hadron fractions at high energy (see Table 5);
- for B -factory measurements – alignment, z scale, machine boost, sample composition (where applicable);
- for Tevatron/LHC measurements – alignment (separately within each experiment).

The resultant averages are:

$$\tau(B^0) = 1.520 \pm 0.004 \text{ ps}, \tag{36}$$

$$\tau(B^+) = 1.638 \pm 0.004 \text{ ps}, \tag{37}$$

$$\tau(B^+)/\tau(B^0) = 1.076 \pm 0.004. \tag{38}$$

3.2.4 B_s^0 lifetimes

Like neutral kaons, neutral B mesons contain short- and long-lived components, since the light (L) and heavy (H) eigenstates differ not only in their masses, but also in their total decay widths. Neglecting CP violation in $B_s^0 - \bar{B}_s^0$ mixing, which is expected to be very small [60, 107–110] (see also Sect. 3.3.3), the mass eigenstates are also CP eigenstates, with the light state being CP -even and the heavy state being CP -odd. While the decay width difference $\Delta\Gamma_d$ can be neglected in the B^0 system, the B_s^0 system exhibits a significant value of $\Delta\Gamma_s = \Gamma_{sL} - \Gamma_{sH}$, where Γ_{sL} and Γ_{sH} are the total decay widths of the light eigenstate B_{sL}^0 and the heavy eigenstate B_{sH}^0 , respectively. The sign of $\Delta\Gamma_s$ is known to be positive [111], i.e., B_{sH}^0 lives longer than B_{sL}^0 . Specific measurements of $\Delta\Gamma_s$ and $\Gamma_s = (\Gamma_{sL} + \Gamma_{sH})/2$ are explained and averaged in Sect. 3.3.2, but the results for $1/\Gamma_{sL} = 1/(\Gamma_s + \Delta\Gamma_s/2)$, $1/\Gamma_{sH} = 1/(\Gamma_s - \Delta\Gamma_s/2)$ and the mean B_s^0 lifetime, defined as $\tau(B_s^0) = 1/\Gamma_s$, are also quoted at the end of this section.

Many B_s^0 lifetime analyses, in particular the early ones performed before the non-zero value of $\Delta\Gamma_s$ was firmly established, ignore $\Delta\Gamma_s$ and fit the proper time distribution of a sample of B_s^0 candidates reconstructed in a certain final state f with a model assuming a single exponential function for the signal. We denote such effective lifetime measurements [112] as $\tau_{\text{single}}(B_s^0 \rightarrow f)$; their true values may lie *a priori* anywhere between $1/\Gamma_{sL}$ and $1/\Gamma_{sH}$, depending on the proportion of B_{sL}^0 and B_{sH}^0 in the final state f . More recent

determinations of effective lifetimes may be interpreted as measurements of the relative composition of B_{sL}^0 and B_{sH}^0 decaying to the final state f . Table 10 summarizes the effective lifetime measurements.

Averaging measurements of $\tau_{\text{single}}(B_s^0 \rightarrow f)$ over several final states f will yield a result corresponding to an ill-defined observable when the proportions of B_{sL}^0 and B_{sH}^0 differ. Therefore, the effective B_s^0 lifetime measurements are broken down into several categories and averaged separately.

- $B_s^0 \rightarrow D_s^\mp X$ decays include mostly flavour-specific decays but also decays with an unknown mixture of light and heavy components. Measurements performed with such inclusive states are no longer used in averages.
- *Decays to flavour-specific final states*, i.e., decays to final states f with decay amplitudes satisfying $A(B_s^0 \rightarrow f) \neq 0$, $A(\bar{B}_s^0 \rightarrow f) \neq 0$, $A(B_s^0 \rightarrow f) = 0$ and $A(\bar{B}_s^0 \rightarrow f) = 0$, have equal fractions of B_{sL}^0 and B_{sH}^0 at time zero. Their total untagged time-dependent decay rates $\Gamma_s(t)$ have a mean value $\int_0^\infty t\Gamma_s(t)dt / \int_0^\infty \Gamma_s(t)dt$, called the *flavour-specific lifetime*, equal to [131]

$$\begin{aligned} \tau_{\text{single}}(B_s^0 \rightarrow \text{flavour specific}) \\ = \frac{1/\Gamma_{sL}^2 + 1/\Gamma_{sH}^2}{1/\Gamma_{sL} + 1/\Gamma_{sH}} = \frac{1}{\Gamma_s} \frac{1 + \left(\frac{\Delta\Gamma_s}{2\Gamma_s}\right)^2}{1 - \left(\frac{\Delta\Gamma_s}{2\Gamma_s}\right)^2}. \end{aligned} \tag{39}$$

Because of the fast $B_s^0 - \bar{B}_s^0$ oscillations, possible biases of the flavour-specific lifetime due to a combination of B_s^0/\bar{B}_s^0 production asymmetry, CP violation in the decay amplitudes ($|A(B_s^0 \rightarrow f)| \neq |A(\bar{B}_s^0 \rightarrow \bar{f})|$), and CP violation in $B_s^0 - \bar{B}_s^0$ mixing ($|q_s/p_s| \neq 1$) are strongly suppressed, by a factor $\sim x_s^2$ (given in Eq. (75)). The B_s^0/\bar{B}_s^0 production asymmetry at LHCb and the CP asymmetry due to mixing have been measured to be compatible with zero with a precision below 3% [132] and 0.3% [see Eq. (83)], respectively. The corresponding effects on the flavour-specific lifetime, which therefore have a relative size of the order of 10^{-5} or smaller, can be neglected at the current level of experimental precision. Under the assumption of no production asymmetry and no CP violation in mixing, Eq. (39) is exact even for a flavour-specific decay with CP violation in the decay amplitudes. Hence any flavour-specific decay mode can be used to measure the flavour-specific lifetime.

The average of all flavour-specific B_s^0 lifetime measurements [95, 104, 116–122] is

$$\tau_{\text{single}}(B_s^0 \rightarrow \text{flavour specific}) = 1.516 \pm 0.014 \text{ ps}. \tag{40}$$

Table 10 Measurements of the effective B_s^0 lifetimes obtained from single exponential fits

Experiment	Final state f		Data set		$\tau_{\text{single}}(B_s^0 \rightarrow f)$ (ps)	Refs.
ALEPH	$D_s h$	Ill-defined	91–95		$1.47 \pm 0.14 \pm 0.08$	[113]
DELPHI	$D_s h$	Ill-defined	91–95		$1.53_{-0.15}^{+0.16} \pm 0.07$	[114]
OPAL	D_s incl.	Ill-defined	90–95		$1.72_{-0.19-0.17}^{+0.20+0.18}$	[115]
ALEPH	$D_s^- \ell^+$	Flavour-specific	91–95		$1.54_{-0.13}^{+0.14} \pm 0.04$	[116]
CDF1	$D_s^- \ell^+$	Flavour-specific	92–96		$1.36 \pm 0.09_{-0.05}^{+0.06}$	[117]
DELPHI	$D_s^- \ell^+$	Flavour-specific	92–95		$1.42_{-0.13}^{+0.14} \pm 0.03$	[118]
OPAL	$D_s^- \ell^+$	Flavour-specific	90–95		$1.50_{-0.15}^{+0.16} \pm 0.04$	[119]
D0	$D_s^- \mu^+ X$	Flavour-specific	Run II	10.4 fb^{-1}	$1.479 \pm 0.010 \pm 0.021$	[95]
CDF2	$D_s^- \pi^+(X)$	Flavour-specific	02–06	1.3 fb^{-1}	$1.518 \pm 0.041 \pm 0.027$	[120]
LHCb	$D_s^- D^+$	Flavour-specific	11–12	3 fb^{-1}	$1.52 \pm 0.15 \pm 0.01$	[121]
LHCb	$D_s^- \pi^+$	Flavour-specific	11	1 fb^{-1}	$1.535 \pm 0.015 \pm 0.014$	[122]
LHCb	$\pi^+ K^-$	Flavour-specific	11	1.0 fb^{-1}	$1.60 \pm 0.06 \pm 0.01$	[104]
Average of above 9 Flavour-specific lifetime measurements					1.516 ± 0.014	
CDF1	$J/\psi \phi$	CP even+odd	92–95		$1.34_{-0.19}^{+0.23} \pm 0.05$	[79]
D0	$J/\psi \phi$	CP even+odd	02–04		$1.444_{-0.090}^{+0.098} \pm 0.02$	[123]
LHCb	$J/\psi \phi$	CP even+odd	11	1 fb^{-1}	$1.480 \pm 0.011 \pm 0.005$	[103]
Average of above 3 $J/\psi \phi$ lifetime measurements					1.479 ± 0.012	
ALEPH	$D_s^{(*)+} D_s^{(*)-}$	mostly CP even	91–95		$1.27 \pm 0.33 \pm 0.08$	[124]
LHCb	$K^+ K^-$	CP -even	10	0.037 fb^{-1}	$1.440 \pm 0.096 \pm 0.009$	[125]
LHCb	$K^+ K^-$	CP -even	11	1.0 fb^{-1}	$1.407 \pm 0.016 \pm 0.007$	[104]
Average of above 2 $K^+ K^-$ lifetime measurements					1.408 ± 0.017	
LHCb	$D_s^+ D_s^-$	CP -even	11–12	3 fb^{-1}	$1.379 \pm 0.026 \pm 0.017$	[121]
LHCb	$J/\psi \eta$	CP -even	11–12	3 fb^{-1}	$1.479 \pm 0.034 \pm 0.011$	[126]
Average of above 2 measurements of $1/\Gamma_{sL}$					1.422 ± 0.023	
LHCb	$J/\psi K_S^0$	CP -odd	11	1.0 fb^{-1}	$1.75 \pm 0.12 \pm 0.07$	[127]
CDF2	$J/\psi f_0(980)$	CP -odd	02–08	3.8 fb^{-1}	$1.70_{-0.11}^{+0.12} \pm 0.03$	[128]
D0	$J/\psi f_0(980)$	CP -odd	Run II	10.4 fb^{-1}	$1.70 \pm 0.14 \pm 0.05$	[129]
LHCb	$J/\psi \pi^+ \pi^-$	CP -odd	11	1.0 fb^{-1}	$1.652 \pm 0.024 \pm 0.024$	[130]
Average of above 3 measurements of $1/\Gamma_{sH}$					1.658 ± 0.032	

- $B_s^0 \rightarrow J/\psi \phi$ decays contain a well-measured mixture of CP -even and CP -odd states. There are no known correlations between the existing $B_s^0 \rightarrow J/\psi \phi$ effective lifetime measurements; these are combined into the average $\tau_{\text{single}}(B_s^0 \rightarrow J/\psi \phi) = 1.479 \pm 0.012$ ps. A caveat is that different experimental acceptances may lead to different admixtures of the CP -even and CP -odd states, and simple fits to a single exponential may result in inherently different values of $\tau_{\text{single}}(B_s^0 \rightarrow J/\psi \phi)$. Analyses that separate the CP -even and CP -odd components in this decay through a full angular study, outlined in Sect. 3.3.2, provide directly precise measurements of $1/\Gamma_s$ and $\Delta\Gamma_s$ (see Table 21).
- Decays to CP eigenstates have also been measured, in the CP -even modes $B_s^0 \rightarrow D_s^{(*)+} D_s^{(*)-}$ by ALEPH [124], $B_s^0 \rightarrow K^+ K^-$ by LHCb [104, 125], $B_s^0 \rightarrow D_s^+ D_s^-$ by

LHCb [121] and $B_s^0 \rightarrow J/\psi \eta$ by LHCb [126], as well as in the CP -odd modes $B_s^0 \rightarrow J/\psi f_0(980)$ by CDF [128] and D0 [129], $B_s^0 \rightarrow J/\psi \pi^+ \pi^-$ by LHCb [130] and $B_s^0 \rightarrow J/\psi K_S^0$ by LHCb [127]. If these decays are dominated by a single weak phase and if CP violation can be neglected, then $\tau_{\text{single}}(B_s^0 \rightarrow CP\text{-even}) = 1/\Gamma_{sL}$ and $\tau_{\text{single}}(B_s^0 \rightarrow CP\text{-odd}) = 1/\Gamma_{sH}$ [see Eqs. (70) and (71) for approximate relations in presence of mixing-induced CP violation]. However, not all these modes can be considered as pure CP eigenstates: a small CP -odd component is most probably present in $B_s^0 \rightarrow D_s^{(*)+} D_s^{(*)-}$ decays. Furthermore the decays $B_s^0 \rightarrow K^+ K^-$ and $B_s^0 \rightarrow J/\psi K_S^0$ may suffer from direct CP violation due to interfering tree and loop amplitudes. The averages for the effective lifetimes obtained for decays to pure CP -even ($D_s^+ D_s^-$, $J/\psi \eta$) and CP -odd ($J/\psi f_0(980)$,

Table 11 Measurements of the B_c^+ lifetime

Experiment	Method	Data set		$\tau(B_c^+)$ (ps)	Refs.
CDF1	$J/\psi\ell$	92–95	0.11 fb ⁻¹	$0.46^{+0.18}_{-0.16} \pm 0.03$	[133]
CDF2	$J/\psi e$	02–04	0.36 fb ⁻¹	$0.463^{+0.073}_{-0.065} \pm 0.036$	[134]
D0	$J/\psi\mu$	02–06	1.3 fb ⁻¹	$0.448^{+0.038}_{-0.036} \pm 0.032$	[135]
CDF2	$J/\psi\pi$		6.7 fb ⁻¹	$0.452 \pm 0.048 \pm 0.027$	[136]
LHCb	$J/\psi\mu$	12	2 fb ⁻¹	$0.509 \pm 0.008 \pm 0.012$	[137]
LHCb	$J/\psi\pi$	11–12	3 fb ⁻¹	$0.5134 \pm 0.0110 \pm 0.0057$	[138]
Average				0.507 ± 0.009	

$J/\psi\pi^+\pi^-$ final states, where CP conservation can be assumed, are

$$\tau_{\text{single}}(B_s^0 \rightarrow CP\text{-even}) = 1.422 \pm 0.023 \text{ ps}, \quad (41)$$

$$\tau_{\text{single}}(B_s^0 \rightarrow CP\text{-odd}) = 1.658 \pm 0.032 \text{ ps}. \quad (42)$$

As described in Sect. 3.3.2, the effective lifetime averages of Eqs. (40), (41) and (42) are used as ingredients to improve the determination of $1/\Gamma_s$ and $\Delta\Gamma_s$ obtained from the full angular analyses of $B_s^0 \rightarrow J/\psi\phi$ and $B_s^0 \rightarrow J/\psi K^+K^-$ decays. The resulting world averages for the B_s^0 lifetimes are

$$\tau(B_{sL}^0) = \frac{1}{\Gamma_{sL}} = \frac{1}{\Gamma_s + \Delta\Gamma_s/2} = 1.413 \pm 0.006 \text{ ps}, \quad (43)$$

$$\tau(B_{sH}^0) = \frac{1}{\Gamma_{sH}} = \frac{1}{\Gamma_s - \Delta\Gamma_s/2} = 1.609 \pm 0.010 \text{ ps}, \quad (44)$$

$$\tau(B_s^0) = \frac{1}{\Gamma_s} = \frac{2}{\Gamma_{sL} + \Gamma_{sH}} = 1.505 \pm 0.005 \text{ ps}. \quad (45)$$

3.2.5 B_c^+ lifetime

Early measurements of the B_c^+ meson lifetime, from CDF [133,134] and D0 [135], use the semileptonic decay mode $B_c^+ \rightarrow J/\psi\ell^+\nu$ and are based on a simultaneous fit to the mass and lifetime using the vertex formed with the leptons from the decay of the J/ψ and the third lepton. Correction factors to estimate the boost due to the missing neutrino are used. Correlated systematic errors include the impact of the uncertainty of the B_c^+ p_T spectrum on the correction factors, the level of feed-down from $\psi(2S)$ decays, Monte Carlo modeling of the decay model varying from phase space to the ISGW model, and mass variations. With more statistics, CDF2 was able to perform the first B_c^+ lifetime based on fully reconstructed $B_c^+ \rightarrow J/\psi\pi^+$ decays [136], which does not suffer from a missing neutrino. Recent measurements from LHCb, both with $B_c^+ \rightarrow J/\psi\mu^+\nu$ [137] and $B_c^+ \rightarrow J/\psi\pi^+$ [138] decays, achieve the highest level of precision.

All the measurements are summarized in Table 11 and the world average, dominated by the LHCb measurements, is determined to be

$$\tau(B_c^+) = 0.507 \pm 0.009 \text{ ps}. \quad (46)$$

3.2.6 Λ_b^0 and b -baryon lifetimes

The first measurements of b -baryon lifetimes, performed at LEP, originate from two classes of partially reconstructed decays. In the first class, decays with an exclusively reconstructed Λ_c^+ baryon and a lepton of opposite charge are used. These products are more likely to occur in the decay of Λ_b^0 baryons. In the second class, more inclusive final states with a baryon (p , \bar{p} , Λ , or $\bar{\Lambda}$) and a lepton have been used, and these final states can generally arise from any b baryon. With the large b -hadron samples available at the Tevatron and the LHC, the most precise measurements of b baryons now come from fully reconstructed exclusive decays.

The following sources of correlated systematic uncertainties have been considered: experimental time resolution within a given experiment, b -quark fragmentation distribution into weakly decaying b baryons, Λ_b^0 polarisation, decay model, and evaluation of the b -baryon purity in the selected event samples. In computing the averages the central values of the masses are scaled to $M(\Lambda_b^0) = 5619.51 \pm 0.23 \text{ MeV}/c^2$ [6].

For measurements with partially reconstructed decays, the meaning of the decay model systematic uncertainties and the correlation of these uncertainties between measurements are not always clear. Uncertainties related to the decay model are dominated by assumptions on the fraction of n -body semileptonic decays. To be conservative, it is assumed that these are 100% correlated whenever given as an error. DELPHI varies the fraction of four-body decays from 0.0 to 0.3. In computing the average, the DELPHI result is corrected to a value of 0.2 ± 0.2 for this fraction. Furthermore the semileptonic decay results from LEP are corrected for a Λ_b^0 polar-

Table 12 Measurements of the b -baryon lifetimes

Experiment	Method	Data set	Lifetime (ps)	Refs.
ALEPH	$\Lambda\ell$	91–95	$1.20 \pm 0.08 \pm 0.06$	[34]
DELPHI	$\Lambda\ell\pi$ vtx	91–94	$1.16 \pm 0.20 \pm 0.08$	[139] ^b
DELPHI	$\Lambda\mu$ i.p.	91–94	$1.10^{+0.19}_{-0.17} \pm 0.09$	[140] ^b
DELPHI	$p\ell$	91–94	$1.19 \pm 0.14 \pm 0.07$	[139] ^b
OPAL	$\Lambda\ell$ i.p.	90–94	$1.21^{+0.15}_{-0.13} \pm 0.10$	[141] ^c
OPAL	$\Lambda\ell$ vtx	90–94	$1.15 \pm 0.12 \pm 0.06$	[141] ^c
ALEPH	$\Lambda_c^+\ell$	91–95	$1.18^{+0.13}_{-0.12} \pm 0.03$	[34] ^a
ALEPH	$\Lambda\ell^-\ell^+$	91–95	$1.30^{+0.26}_{-0.21} \pm 0.04$	[34] ^a
DELPHI	$\Lambda_c^+\ell$	91–94	$1.11^{+0.19}_{-0.18} \pm 0.05$	[139] ^b
OPAL	$\Lambda_c^+\ell, \Lambda\ell^-\ell^+$	90–95	$1.29^{+0.24}_{-0.22} \pm 0.06$	[119]
CDF1	$\Lambda_c^+\ell$	91–95	$1.32 \pm 0.15 \pm 0.07$	[142]
D0	$\Lambda_c^+\mu$	02–06	$1.290^{+0.119+0.087}_{-0.110-0.091}$	[143]
Average of above 6			$1.247^{+0.071}_{-0.069}$	
CDF2	$\Lambda_c^+\pi$	02–06	$1.401 \pm 0.046 \pm 0.035$	[144]
CDF2	$J/\psi\Lambda$	02–11	$1.565 \pm 0.035 \pm 0.020$	[145]
D0	$J/\psi\Lambda$	02–11	$1.303 \pm 0.075 \pm 0.035$	[94]
ATLAS	$J/\psi\Lambda$	2011	$1.449 \pm 0.036 \pm 0.017$	[102]
CMS	$J/\psi\Lambda$	2011	$1.503 \pm 0.052 \pm 0.031$	[146]
LHCb	$J/\psi\Lambda$	2011	$1.415 \pm 0.027 \pm 0.006$	[103]
LHCb	$J/\psi pK$ (w.r.t. B^0)	11–12	$1.479 \pm 0.009 \pm 0.010$	[147]
Average of above 7			Λ_b^0 lifetime = 1.470 ± 0.010	
ALEPH	$\Xi^-\ell^-X$	90–95	$1.35^{+0.37+0.15}_{-0.28-0.17}$	[35]
DELPHI	$\Xi^-\ell^-X$	91–93	$1.5^{+0.7}_{-0.4} \pm 0.3$	[148] ^d
DELPHI	$\Xi^-\ell^-X$	92–95	$1.45^{+0.55}_{-0.43} \pm 0.13$	[36] ^d
CDF2	$J/\psi\Xi^-$	02–11	$1.32 \pm 0.14 \pm 0.02$	[145]
LHCb	$J/\psi\Xi^-$	11–12	$1.55^{+0.10}_{-0.09} \pm 0.03$	[149]
LHCb	$\Xi_c^0\pi^-$ (w.r.t. Λ_b^0)	11–12	$1.599 \pm 0.041 \pm 0.022$	[150]
Average of above 3			Ξ_b^- lifetime = 1.571 ± 0.040	
LHCb	$\Xi_c^+\pi^-$ (w.r.t. Λ_b^0)	11–12	$1.477 \pm 0.026 \pm 0.019$	[151]
Average of above 1			Ξ_b^0 lifetime = 1.479 ± 0.031	
CDF2	$J/\psi\Omega^-$	02–11	$1.66^{+0.53}_{-0.40} \pm 0.02$	[145]
LHCb	$J/\psi\Omega^-$	11–12	$1.54^{+0.26}_{-0.21} \pm 0.05$	[149]
LHCb	$\Omega_c^0\pi^-$ (w.r.t. Ξ_b^-)	11–12	$1.78 \pm 0.26 \pm 0.05 \pm 0.06$	[152]
Average of above 3			Ω_b^- lifetime = $1.64^{+0.18}_{-0.17}$	

^a The combined ALEPH result quoted in [34] is 1.21 ± 0.11 ps
^b The combined DELPHI result quoted in [139] is $1.14 \pm 0.08 \pm 0.04$ ps
^c The combined OPAL result quoted in [141] is $1.16 \pm 0.11 \pm 0.06$ ps
^d The combined DELPHI result quoted in [36] is $1.48^{+0.40}_{-0.31} \pm 0.12$ ps

isation of $-0.45^{+0.19}_{-0.17}$ [3] and a b fragmentation parameter $\langle x_E \rangle_b = 0.702 \pm 0.008$ [51].

The list of all measurements are given in Table 12. We do not attempt to average measurements performed with $p\ell$ or $\Lambda\ell$ correlations, which select unknown mixtures of b baryons. Measurements performed with $\Lambda_c^+\ell$ or $\Lambda\ell^+\ell^-$ correlations can be assumed to correspond to semileptonic

Λ_b^0 decays. Their average ($1.247^{+0.071}_{-0.069}$ ps) is significantly different from the average using only measurements performed with exclusively reconstructed hadronic Λ_b^0 decays (1.470 ± 0.010 ps). The latter is much more precise and less prone to potential biases than the former. The discrepancy between the two averages is at the level of 3.1σ and assumed to be due to an experimental systematic effect in

the semileptonic measurements or to a rare statistical fluctuation. The best estimate of the Λ_b^0 lifetime is therefore taken as the average of the exclusive measurements only. The CDF $\Lambda_b^0 \rightarrow J/\psi \Lambda$ lifetime result [145] is larger than the average of all other exclusive measurements by 2.4σ . It is nonetheless kept in the average without adjustment of input errors. The world average Λ_b^0 lifetime is then

$$\tau(\Lambda_b^0) = 1.470 \pm 0.010 \text{ ps.} \tag{47}$$

For the strange b baryons, we do not include the measurements based on inclusive $\Xi^\mp \ell^\mp$ [35, 36, 148] final states, which consist of a mixture of Ξ_b^- and Ξ_b^0 baryons. Instead we only average results obtained with fully reconstructed Ξ_b^- , Ξ_b^0 and Ω_b^- baryons, and obtain

$$\tau(\Xi_b^-) = 1.571 \pm 0.040 \text{ ps,} \tag{48}$$

$$\tau(\Xi_b^0) = 1.479 \pm 0.031 \text{ ps,} \tag{49}$$

$$\tau(\Omega_b^-) = 1.64_{-0.17}^{+0.18} \text{ ps.} \tag{50}$$

It should be noted that several b -baryon lifetime measurements from LHCb [147, 150–152] were made with respect to the lifetime of another b hadron (i.e., the original measurement is that of a decay width difference). Before these measurements are included in the averages quoted above, we rescale them according to our latest lifetime average of that reference b hadron. This introduces correlations between our averages, in particular between the Ξ_b^- and Ξ_b^0 lifetimes. Taking this correlation into account leads to

$$\tau(\Xi_b^0)/\tau(\Xi_b^-) = 0.929 \pm 0.028. \tag{51}$$

3.2.7 Summary and comparison with theoretical predictions

Averages of lifetimes of specific b -hadron species are collected in Table 13. As described in the introduction to Sect. 3.2, the HQE can be employed to explain the hierarchy of $\tau(B_c^+) \ll \tau(\Lambda_b^0) < \tau(B_s^0) \approx \tau(B^0) < \tau(B^+)$, and used to predict the ratios between lifetimes. Recent predictions are compared to the measured lifetime ratios in Table 14.

The predictions of the ratio between the B^+ and B^0 lifetimes, 1.06 ± 0.02 [65, 66] or $1.04_{-0.01}^{+0.05} \pm 0.02 \pm 0.01$ [68, 69], are in good agreement with experiment.

The total widths of the B_s^0 and B^0 mesons are expected to be very close and differ by at most 1% [67–69, 153, 154]. This prediction is consistent with the experimental ratio $\tau(B_s^0)/\tau(B^0) = \Gamma_d/\Gamma_s$, which is smaller than 1 by $(1.0 \pm 0.4)\%$. The authors of Refs. [60, 107] predict $\tau(B_s^0)/\tau(B^0) = 1.00050 \pm 0.00108 \pm 0.0225 \times \delta$, where

Table 13 Summary of the lifetime averages for the different b -hadron species

b -Hadron species	Measured lifetime
B^+	$1.638 \pm 0.004 \text{ ps}$
B^0	$1.520 \pm 0.004 \text{ ps}$
B_s^0	$1/\Gamma_s = 1.505 \pm 0.005 \text{ ps}$
B_{sL}^0	$1/\Gamma_{sL} = 1.413 \pm 0.006 \text{ ps}$
B_{sH}^0	$1/\Gamma_{sH} = 1.609 \pm 0.010 \text{ ps}$
B_c^+	$0.507 \pm 0.009 \text{ ps}$
Λ_b^0	$1.470 \pm 0.010 \text{ ps}$
Ξ_b^-	$1.571 \pm 0.040 \text{ ps}$
Ξ_b^0	$1.479 \pm 0.031 \text{ ps}$
Ω_b^-	$1.64_{-0.17}^{+0.18}$

Table 14 Experimental averages of b -hadron lifetime ratios and Heavy-Quark Expansion (HQE) predictions [68, 69]

Lifetime ratio	Experimental average	HQE prediction
$\tau(B^+)/\tau(B^0)$	1.076 ± 0.004	$1.04_{-0.01}^{+0.05} \pm 0.02 \pm 0.01$
$\tau(B_s^0)/\tau(B^0)$	0.990 ± 0.004	1.001 ± 0.002
$\tau(\Lambda_b^0)/\tau(B^0)$	0.967 ± 0.007	0.935 ± 0.054
$\tau(\Xi_b^0)/\tau(\Xi_b^-)$	0.929 ± 0.028	0.95 ± 0.06

δ quantifies a possible breaking of the quark-hadron duality. In this context, they interpret the 2.5σ difference between theory and experiment as being due to either new physics or a sizable duality violation. The key message is that improved experimental precision on this ratio is very welcome.

The ratio $\tau(\Lambda_b^0)/\tau(B^0)$ has particularly been the source of theoretical scrutiny since earlier calculations using the HQE [55–57, 155] predicted a value larger than 0.90, almost 2σ above the world average at the time. Many predictions cluster around a most likely central value of 0.94 [159]. Calculations of this ratio that include higher-order effects predict a lower ratio between the Λ_b^0 and B^0 lifetimes [65–67] and reduce this difference. Since then the experimental average is now definitely settling at a value significantly larger than initially, in agreement with the latest theoretical predictions. A recent review [68, 69] concludes that the long-standing Λ_b^0 lifetime puzzle is resolved, with a nice agreement between the precise experimental determination of $\tau(\Lambda_b^0)/\tau(B^0)$ and the less precise HQE prediction which needs new lattice calculations. There is also good agreement for the $\tau(\Xi_b^0)/\tau(\Xi_b^-)$ ratio.

The lifetimes of the most abundant b -hadron species are now all known to sub-percent precision. Neglecting the contributions of the rarer species (B_c^+ meson and b baryons other than the Λ_b^0), one can compute the average b -hadron lifetime from the individual lifetimes and production fractions as

$$\tau_b = \frac{f_d \tau(B^0)^2 + f_u \tau(B^+)^2 + 0.5 f_s \tau(B_{sH}^0)^2 + 0.5 f_s \tau(B_{sL}^0)^2 + f_{\text{baryon}} \tau(\Lambda_b^0)^2}{f_d \tau(B^0) + f_u \tau(B^+) + 0.5 f_s \tau(B_{sH}^0) + 0.5 f_s \tau(B_{sL}^0) + f_{\text{baryon}} \tau(\Lambda_b^0)} \tag{52}$$

Using the lifetimes of Table 13 and the fractions in Z decays of Table 5, taking into account the correlations between the fractions (Table 5) as well as the correlation between $\tau(B_{sH})$ and $\tau(B_{sL})$ (-0.398), one obtains

$$\tau_b(Z) = 1.566 \pm 0.003 \text{ ps.} \tag{53}$$

This is in very good agreement with (and three times more precise than) the average of Eq. (33) for the inclusive measurements performed at LEP.

3.3 Neutral B -meson mixing

The $B^0 - \bar{B}^0$ and $B_s^0 - \bar{B}_s^0$ systems both exhibit the phenomenon of particle-antiparticle mixing. For each of them, there are two mass eigenstates which are linear combinations of the two flavour states, B_q^0 and \bar{B}_q^0 ,

$$|B_{qL}^0\rangle = p_q |B_q^0\rangle + q_q |\bar{B}_q^0\rangle, \tag{54}$$

$$|B_{qH}^0\rangle = p_q |B_q^0\rangle - q_q |\bar{B}_q^0\rangle, \tag{55}$$

where the subscript $q = d$ is used for the B_d^0 ($= B^0$) meson and $q = s$ for the B_s^0 meson. The heaviest (lightest) of these mass states is denoted B_{qH}^0 (B_{qL}^0), with mass m_{qH} (m_{qL}) and total decay width Γ_{qH} (Γ_{qL}). We define

$$\Delta m_q = m_{qH} - m_{qL}, \quad x_q = \Delta m_q / \Gamma_q, \tag{56}$$

$$\Delta \Gamma_q = \Gamma_{qL} - \Gamma_{qH}, \quad y_q = \Delta \Gamma_q / (2\Gamma_q), \tag{57}$$

where $\Gamma_q = (\Gamma_{qH} + \Gamma_{qL})/2 = 1/\bar{\tau}(B_q^0)$ is the average decay width. Δm_q is positive by definition, and $\Delta \Gamma_q$ is expected to be positive within the Standard Model.¹³

There are four different time-dependent probabilities describing the case of a neutral B meson produced as a flavour state and decaying without CP violation to a flavour-specific final state. If CPT is conserved (which will be assumed throughout), they can be written as

$$\begin{cases} \mathcal{P}(B_q^0 \rightarrow B_q^0) = \frac{1}{2} e^{-\Gamma_q t} \left[\cosh\left(\frac{1}{2} \Delta \Gamma_q t\right) + \cos\left(\Delta m_q t\right) \right] \\ \mathcal{P}(B_q^0 \rightarrow \bar{B}_q^0) = \frac{1}{2} e^{-\Gamma_q t} \left[\cosh\left(\frac{1}{2} \Delta \Gamma_q t\right) - \cos\left(\Delta m_q t\right) \right] |q_q/p_q|^2 \\ \mathcal{P}(\bar{B}_q^0 \rightarrow B_q^0) = \frac{1}{2} e^{-\Gamma_q t} \left[\cosh\left(\frac{1}{2} \Delta \Gamma_q t\right) - \cos\left(\Delta m_q t\right) \right] |p_q/q_q|^2 \\ \mathcal{P}(\bar{B}_q^0 \rightarrow \bar{B}_q^0) = \frac{1}{2} e^{-\Gamma_q t} \left[\cosh\left(\frac{1}{2} \Delta \Gamma_q t\right) + \cos\left(\Delta m_q t\right) \right] \end{cases} \tag{58}$$

¹³ For reasons of symmetry in Eqs. (56) and (57), $\Delta \Gamma$ is sometimes defined with the opposite sign. The definition adopted in Eq. (57) is the one used by most experimentalists and many phenomenologists in B physics.

where t is the proper time of the system (i.e., the time interval between the production and the decay in the rest frame of the B meson). At the B factories, only the proper-time difference Δt between the decays of the two neutral B mesons from the $\Upsilon(4S)$ can be determined, but, because the two B mesons evolve coherently (keeping opposite flavours as long as neither of them has decayed), the above formulae remain valid if t is replaced with Δt and the production flavour is replaced by the flavour at the time of the decay of the accompanying B meson in a flavour-specific state. As can be seen in the above expressions, the mixing probabilities depend on three mixing observables: Δm_q , $\Delta \Gamma_q$, and $|q_q/p_q|^2$, which signals CP violation in the mixing if $|q_q/p_q|^2 \neq 1$. Another (non independent) observable often used to characterize CP violation in the mixing is the so-called semileptonic asymmetry, defined as

$$\mathcal{A}_{\text{SL}}^q = \frac{|p_q/q_q|^2 - |q_q/p_q|^2}{|p_q/q_q|^2 + |q_q/p_q|^2}. \tag{59}$$

All mixing observables depend on two complex numbers, M_{12}^q and Γ_{12}^q , which are the off-diagonal elements of the mass and decay 2×2 matrices describing the evolution of the $B_q^0 - \bar{B}_q^0$ system. In the Standard Model the quantity $|\Gamma_{12}^q/M_{12}^q|$ is small, of the order of $(m_b/m_t)^2$ where m_b and m_t are the bottom and top quark masses. The following relations hold, to first order in $|\Gamma_{12}^q/M_{12}^q|$:

$$\Delta m_q = 2|M_{12}^q| \left[1 + \mathcal{O}\left(|\Gamma_{12}^q/M_{12}^q|^2\right) \right], \tag{60}$$

$$\Delta \Gamma_q = 2|\Gamma_{12}^q| \cos \phi_{12}^q \left[1 + \mathcal{O}\left(|\Gamma_{12}^q/M_{12}^q|^2\right) \right], \tag{61}$$

$$\begin{aligned} \mathcal{A}_{\text{SL}}^q &= \text{Im}\left(\Gamma_{12}^q/M_{12}^q\right) + \mathcal{O}\left(|\Gamma_{12}^q/M_{12}^q|^2\right) \\ &= \frac{\Delta \Gamma_q}{\Delta m_q} \tan \phi_{12}^q + \mathcal{O}\left(|\Gamma_{12}^q/M_{12}^q|^2\right), \end{aligned} \tag{62}$$

where

$$\phi_{12}^q = \arg\left(-M_{12}^q/\Gamma_{12}^q\right) \tag{63}$$

is the observable phase difference between $-M_{12}^q$ and Γ_{12}^q (often called the mixing phase). It should be noted that the theoretical predictions for Γ_{12}^q are based on the same HQE as the lifetime predictions.

In the next sections we review in turn the experimental knowledge on the B^0 decay-width and mass differences, the B_s^0 decay-width and mass differences, CP violation in B^0 and B_s^0 mixing, and mixing-induced CP violation in B_s^0 decays.

Table 15 Time-dependent measurements included in the Δm_d average. The results obtained from multi-dimensional fits involving also the B^0 (and B^+) lifetimes as free parameter(s) [98, 100, 101] have been con-

verted into one-dimensional measurements of Δm_d . All the measurements have then been adjusted to a common set of physics parameters before being combined

Experiment and Refs.	Method		Δm_d in ps^{-1}	
	Rec.	Tag	Before adjustment	After adjustment
ALEPH [163]	ℓ	Q_{jet}	$0.404 \pm 0.045 \pm 0.027$	
ALEPH [163]	ℓ	ℓ	$0.452 \pm 0.039 \pm 0.044$	
ALEPH [163]	Above two combined		$0.422 \pm 0.032 \pm 0.026$	$0.440 \pm 0.032^{+0.020}_{-0.019}$
ALEPH [163]	D^*	ℓ, Q_{jet}	$0.482 \pm 0.044 \pm 0.024$	$0.482 \pm 0.044 \pm 0.024$
DELPHI [164]	ℓ	Q_{jet}	$0.493 \pm 0.042 \pm 0.027$	$0.499 \pm 0.042 \pm 0.024$
DELPHI [164]	$\pi^* \ell$	Q_{jet}	$0.499 \pm 0.053 \pm 0.015$	$0.500 \pm 0.053 \pm 0.015$
DELPHI [164]	ℓ	ℓ	$0.480 \pm 0.040 \pm 0.051$	$0.495 \pm 0.040^{+0.042}_{-0.040}$
DELPHI [164]	D^*	Q_{jet}	$0.523 \pm 0.072 \pm 0.043$	$0.518 \pm 0.072 \pm 0.043$
DELPHI [165]	vtx	comb	$0.531 \pm 0.025 \pm 0.007$	$0.525 \pm 0.025 \pm 0.006$
L3 [166]	ℓ	ℓ	$0.458 \pm 0.046 \pm 0.032$	$0.466 \pm 0.046 \pm 0.028$
L3 [166]	ℓ	Q_{jet}	$0.427 \pm 0.044 \pm 0.044$	$0.439 \pm 0.044 \pm 0.042$
L3 [166]	ℓ	$\ell(\text{IP})$	$0.462 \pm 0.063 \pm 0.053$	$0.470 \pm 0.063 \pm 0.044$
OPAL [167]	ℓ	ℓ	$0.430 \pm 0.043^{+0.028}_{-0.030}$	$0.466 \pm 0.043^{+0.017}_{-0.016}$
OPAL [168]	ℓ	Q_{jet}	$0.444 \pm 0.029^{+0.020}_{-0.017}$	$0.481 \pm 0.029 \pm 0.013$
OPAL [169]	$D^* \ell$	Q_{jet}	$0.539 \pm 0.060 \pm 0.024$	$0.544 \pm 0.060 \pm 0.023$
OPAL [169]	D^*	ℓ	0.567 ± 0.089	$^{+0.029}_{-0.023} 0.572 \pm 0.089^{+0.028}_{-0.022}$
OPAL [88]	$\pi^* \ell$	Q_{jet}	$0.497 \pm 0.024 \pm 0.025$	$0.496 \pm 0.024 \pm 0.025$
CDF1 [170]	$D\ell$	SST	$0.471^{+0.078 +0.033}_{-0.068 -0.034}$	$0.470^{+0.078 +0.033}_{-0.068 -0.034}$
CDF1 [172]	μ	μ	$0.503 \pm 0.064 \pm 0.071$	$0.514 \pm 0.064^{+0.070}_{-0.069}$
CDF1 [173]	ℓ	ℓ, Q_{jet}	$0.500 \pm 0.052 \pm 0.043$	$0.546 \pm 0.052 \pm 0.036$
CDF1 [174]	$D^* \ell$	ℓ	$0.516 \pm 0.099^{+0.029}_{-0.035}$	$0.523 \pm 0.099^{+0.028}_{-0.035}$
D0 [175]	$D^{(*)} \mu$	OST	$0.506 \pm 0.020 \pm 0.016$	$0.506 \pm 0.020 \pm 0.016$
BABAR [176]	B^0	ℓ, K, NN	$0.516 \pm 0.016 \pm 0.010$	$0.521 \pm 0.016 \pm 0.008$
BABAR [178]	ℓ	ℓ	$0.493 \pm 0.012 \pm 0.009$	$0.487 \pm 0.012 \pm 0.006$
BABAR [98]	$D^* \ell \nu$	ℓ, K, NN	$0.492 \pm 0.018 \pm 0.014$	$0.493 \pm 0.018 \pm 0.013$
BABAR [100]	$D^* \ell \nu(\text{part})$	ℓ	$0.511 \pm 0.007 \pm 0.007$	$0.513 \pm 0.007 \pm 0.007$
Belle [101]	$B^0, D^* \ell \nu$	comb	$0.511 \pm 0.005 \pm 0.006$	$0.513 \pm 0.005 \pm 0.006$
Belle [179]	$D^* \pi(\text{part})$	ℓ	$0.509 \pm 0.017 \pm 0.020$	$0.513 \pm 0.017 \pm 0.019$
Belle [9]	ℓ	ℓ	$0.503 \pm 0.008 \pm 0.010$	$0.506 \pm 0.008 \pm 0.008$
LHCb [180]	B^0	OST	$0.499 \pm 0.032 \pm 0.003$	$0.499 \pm 0.032 \pm 0.003$
LHCb [181]	B^0	OST,SST	$0.5156 \pm 0.0051 \pm 0.0033$	$0.5156 \pm 0.0051 \pm 0.0033$
LHCb [182]	$D\mu$	OST,SST	$0.503 \pm 0.011 \pm 0.013$	$0.503 \pm 0.011 \pm 0.013$
LHCb [183]	$D^{(*)} \mu$	OST	$0.5050 \pm 0.0021 \pm 0.0010$	$0.5050 \pm 0.0021 \pm 0.0010$
World average (all above measurements included)				$0.5065 \pm 0.0016 \pm 0.0011$
– ALEPH, DELPHI, L3 and OPAL only				$0.493 \pm 0.011 \pm 0.009$
– CDF and D0 only				$0.509 \pm 0.017 \pm 0.013$
– BABAR and Belle only				$0.509 \pm 0.003 \pm 0.003$
– LHCb only				$0.5063 \pm 0.0019 \pm 0.0010$

3.3.1 B^0 mixing parameters $\Delta\Gamma_d$ and Δm_d

A large number of time-dependent $B^0-\bar{B}^0$ oscillation analyses have been performed in the past 20 years by the

ALEPH, DELPHI, L3, OPAL, CDF, D0, BABAR, Belle and LHCb collaborations. The corresponding measurements of Δm_d are summarized in Table 15. Although a variety of different techniques have been used, the individual

Δm_d results obtained at different colliders have remarkably similar precision. The systematic uncertainties are comparable to the statistical uncertainties; they are often dominated by sample composition, mistag probability, or b -hadron lifetime contributions. Before being combined, the measurements are adjusted on the basis of a common set of input values, including the averages of the b -hadron fractions and lifetimes given in this report (see Sects. 3.1, 3.2). Some measurements are statistically correlated. Systematic correlations arise both from common physics sources (fractions, lifetimes, branching ratios of b hadrons), and from purely experimental or algorithmic effects (efficiency, resolution, flavour tagging, background description). Combining all published measurements listed in Table 15 and accounting for all identified correlations as described in Ref. [3] yields $\Delta m_d = 0.5065 \pm 0.0016 \pm 0.0011 \text{ ps}^{-1}$.

On the other hand, ARGUS and CLEO have published measurements of the time-integrated mixing probability χ_d [184, 186, 187], which average to $\chi_d = 0.182 \pm 0.015$. Following Ref. [187], the decay width difference $\Delta\Gamma_d$ could in principle be extracted from the measured value of $\Gamma_d = 1/\tau(B^0)$ and the above averages for Δm_d and χ_d (provided that $\Delta\Gamma_d$ has a negligible impact on the Δm_d and $\tau(B^0)$ analyses that have assumed $\Delta\Gamma_d = 0$), using the relation

$$\chi_d = \frac{x_d^2 + y_d^2}{2(x_d^2 + 1)}. \quad (64)$$

However, direct time-dependent studies provide much stronger constraints: $|\Delta\Gamma_d|/\Gamma_d < 18\%$ at 95% CL from DELPHI [165], $-6.8\% < \text{sign}(\text{Re}\lambda_{CP})\Delta\Gamma_d/\Gamma_d < 8.4\%$ at 90% CL from BABAR [188], and $\text{sign}(\text{Re}\lambda_{CP})\Delta\Gamma_d/\Gamma_d = (1.7 \pm 1.8 \pm 1.1)\%$ [190] from Belle, where $\lambda_{CP} = (q_d/p_d)(\bar{A}_{CP}/A_{CP})$ is defined for a CP -even final state (the sensitivity to the overall sign of $\text{sign}(\text{Re}\lambda_{CP})\Delta\Gamma_d/\Gamma_d$ comes from the use of B^0 decays to CP final states). In addition LHCb has obtained $\Delta\Gamma_d/\Gamma_d = (-4.4 \pm 2.5 \pm 1.1)\%$ [103] by comparing measurements of the $B^0 \rightarrow J/\psi K^{*0}$ and $B^0 \rightarrow J/\psi K_S^0$ decays, following the method of Ref. [191]. More recently ATLAS has measured $\Delta\Gamma_d/\Gamma_d = (-0.1 \pm 1.1 \pm 0.9)\%$ [192] using a similar method. Assuming $\text{Re}\lambda_{CP} > 0$, as expected from the global fits of the Unitarity Triangle within the Standard Model [193], a combination of these five results (after adjusting the DELPHI and BABAR results to $1/\Gamma_d = \tau(B^0) = 1.520 \pm 0.004 \text{ ps}$) yields

$$\Delta\Gamma_d/\Gamma_d = -0.002 \pm 0.010, \quad (65)$$

an average consistent with zero and with the Standard Model prediction of $(3.97 \pm 0.90) \times 10^{-3}$ [107]. An independent result, $\Delta\Gamma_d/\Gamma_d = (0.50 \pm 1.38)\%$ [195], was obtained by the D0 collaboration from their measurements of the single

muon and same-sign dimuon charge asymmetries, under the interpretation that the observed asymmetries are due to CP violation in neutral B -meson mixing and interference. This indirect determination was called into question [196] and is therefore not included in the above average, as explained in Sect. 3.3.3 (see Footnote 17).

Assuming $\Delta\Gamma_d = 0$ and using $1/\Gamma_d = \tau(B^0) = 1.520 \pm 0.004 \text{ ps}$, the Δm_d and χ_d results are combined through Eq. (64) to yield the world average

$$\Delta m_d = 0.5064 \pm 0.0019 \text{ ps}^{-1}, \quad (66)$$

or, equivalently,

$$x_d = 0.770 \pm 0.004 \quad \text{and} \quad \chi_d = 0.1860 \pm 0.0011. \quad (67)$$

Figure 6 compares the Δm_d values obtained by the different experiments.

The B^0 mixing averages given in Eqs. (66) and (67) and the b -hadron fractions of Table 5 have been obtained in a fully consistent way, taking into account the fact that the fractions are computed using the χ_d value of Eq. (67) and that many individual measurements of Δm_d at high energy depend on the assumed values for the b -hadron fractions. Furthermore, this set of averages is consistent with the lifetime averages of Sect. 3.2.

3.3.2 B_s^0 mixing parameters $\Delta\Gamma_s$ and Δm_s

The best sensitivity to $\Delta\Gamma_s$ is currently achieved by the recent time-dependent measurements of the $B_s^0 \rightarrow J/\psi\phi$ (or more generally $B_s^0 \rightarrow (c\bar{c})K^+K^-$) decay rates performed at CDF [197], D0 [198], ATLAS [199, 200] CMS [201] and LHCb [202, 203], where the CP -even and CP -odd amplitudes are statistically separated through a full angular analysis. These studies use both untagged and tagged B_s^0 candidates and are optimized for the measurement of the CP -violating phase $\phi_s^{c\bar{c}s}$, defined later in Sect. 3.3.4. The LHCb collaboration analyzed the $B_s^0 \rightarrow J/\psi K^+K^-$ decay, considering that the K^+K^- system can be in a P -wave or S -wave state, and measured the dependence of the strong phase difference between the P -wave and S -wave amplitudes as a function of the K^+K^- invariant mass [111]. This allowed, for the first time, the unambiguous determination of the sign of $\Delta\Gamma_s$, which was found to be positive at the 4.7σ level. The following averages present only the $\Delta\Gamma_s > 0$ solutions.

The published results [197–203] are shown in Table 16. They are combined taking into account, in each analysis, the correlation between $\Delta\Gamma_s$ and Γ_s . The results, displayed as the red contours labelled “ $B_s^0 \rightarrow (c\bar{c})KK$ measurements” in the plots of Fig. 7, are given in the first column of numbers of Table 17.

An alternative approach, which is directly sensitive to first order in $\Delta\Gamma_s/\Gamma_s$, is to determine the effective life-

Fig. 6 The $B^0-\bar{B}^0$ oscillation frequency Δm_d as measured by the different experiments. The averages quoted for ALEPH, L3 and OPAL are taken from the original publications, while the ones for DELPHI, CDF, BABAR, Belle and LHCb are computed from the individual results listed in Table 15 without performing any adjustments. The time-integrated measurements of χ_d from the symmetric B factory experiments ARGUS and CLEO are converted to a Δm_d value using $\tau(B^0) = 1.520 \pm 0.004$ ps. The two global averages are obtained after adjustments of all the individual Δm_d results of Table 15 (see text)

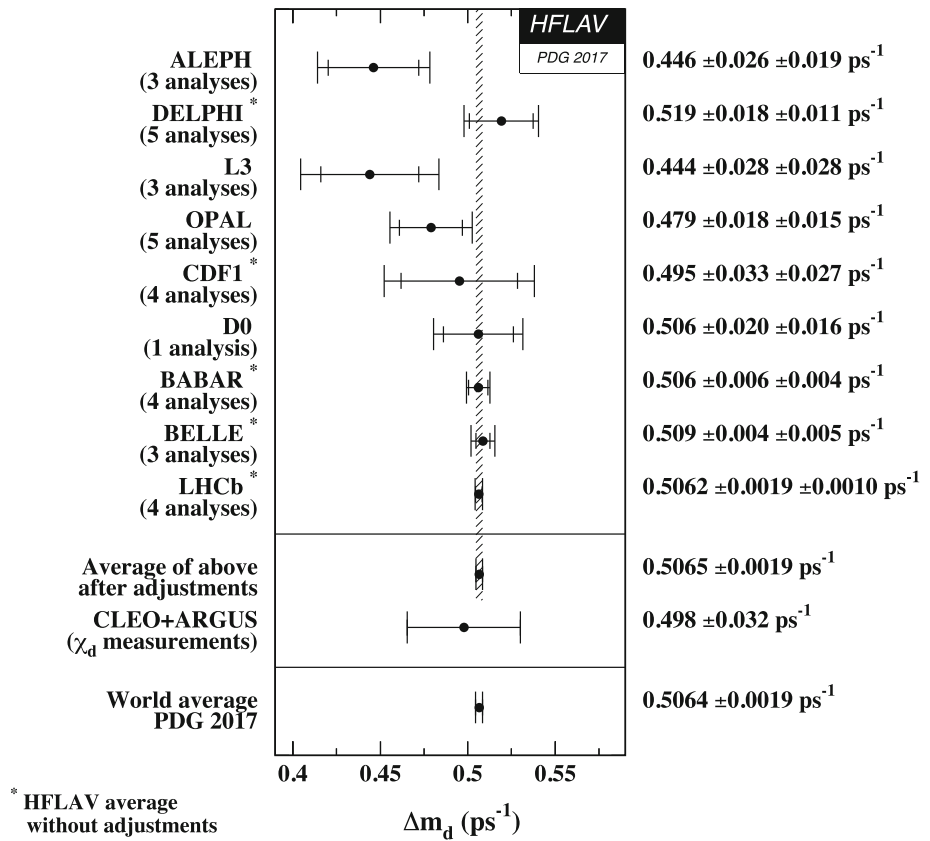


Table 16 Measurements of $\Delta\Gamma_s$ and Γ_s using $B_s^0 \rightarrow J/\psi\phi$, $B_s^0 \rightarrow J/\psi K^+K^-$ and $B_s^0 \rightarrow \psi(2S)\phi$ decays. Only the solution with $\Delta\Gamma_s > 0$ is shown, since the two-fold ambiguity has been resolved

in Ref. [111]. The first error is due to statistics, the second one to systematics. The last line gives our average

Exp.	Mode	Dataset	$\Delta\Gamma_s$ (ps ⁻¹)	Γ_s (ps ⁻¹)	Refs.
CDF	$J/\psi\phi$	9.6 fb ⁻¹	+0.068 ± 0.026 ± 0.009	0.654 ± 0.008 ± 0.004	[197]
D0	$J/\psi\phi$	8.0 fb ⁻¹	+0.163 ^{+0.065} _{-0.064}	0.693 ^{+0.018} _{-0.017}	[198]
ATLAS	$J/\psi\phi$	4.9 fb ⁻¹	+0.053 ± 0.021 ± 0.010	0.677 ± 0.007 ± 0.004	[199]
ATLAS	$J/\psi\phi$	14.3 fb ⁻¹	+0.101 ± 0.013 ± 0.007	0.676 ± 0.004 ± 0.004	[200]
ATLAS	Above 2 combined		+0.085 ± 0.011 ± 0.007	0.675 ± 0.003 ± 0.003	[200]
CMS	$J/\psi\phi$	19.7 fb ⁻¹	+0.095 ± 0.013 ± 0.007	0.6704 ± 0.0043 ± 0.0055	[201]
LHCb	$J/\psi K^+K^-$	3.0 fb ⁻¹	+0.0805 ± 0.0091 ± 0.0032	0.6603 ± 0.0027 ± 0.0015	[202]
LHCb	$\psi(2S)\phi$	3.0 fb ⁻¹	+0.066 ^{+0.041} _{-0.044} ± 0.007	0.668 ± 0.011 ± 0.006	[203]
All combined			+0.084 ± 0.007	0.6654 ± 0.0022	

time of untagged B_s^0 candidates decaying to pure CP eigenstates; we use here measurements with $B_s^0 \rightarrow D_s^+D_s^-$ [121], $B_s^0 \rightarrow J/\psi\eta$ [126], $B_s^0 \rightarrow J/\psi f_0(980)$ [128, 129] and $B_s^0 \rightarrow J/\psi\pi^+\pi^-$ [130] decays. The precise extraction of $1/\Gamma_s$ and $\Delta\Gamma_s$ from such measurements, discussed in detail in Ref. [112], requires additional information in the form of theoretical assumptions or external inputs on weak phases and hadronic parameters. If f designates a final state in which both B_s^0 and \bar{B}_s^0 can decay, the ratio of the effective B_s^0 life-

time decaying to f relative to the mean B_s^0 lifetime is [112]¹⁴

$$\frac{\tau_{\text{single}}(B_s^0 \rightarrow f)}{\tau(B_s^0)} = \frac{1}{1 - y_s^2} \left[\frac{1 - 2A_f^{\Delta\Gamma} y_s + y_s^2}{1 - A_f^{\Delta\Gamma} y_s} \right], \quad (68)$$

¹⁴ The definition of $A_f^{\Delta\Gamma}$ given in Eq. (69) has the sign opposite to that given in Ref. [112].

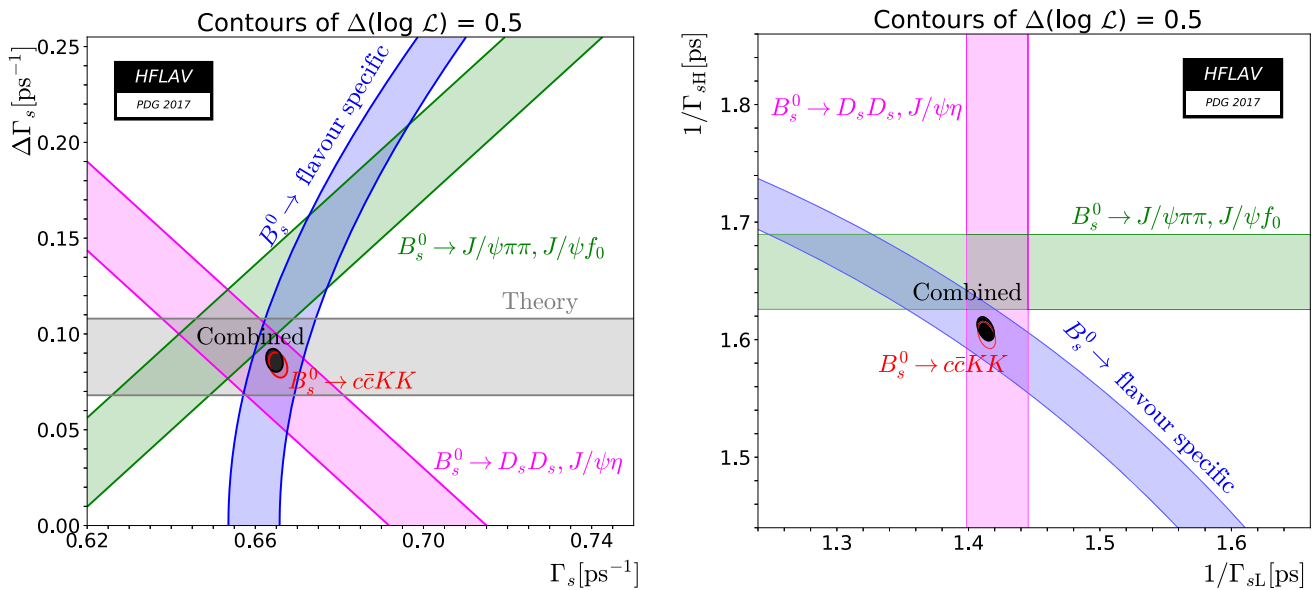


Fig. 7 Contours of $\Delta \ln L = 0.5$ (39% CL for the enclosed 2D regions, 68% CL for the bands) shown in the $(\Gamma_s, \Delta\Gamma_s)$ plane on the left and in the $(1/\Gamma_{sL}, 1/\Gamma_{sH})$ plane on the right. The average of all the $B_s^0 \rightarrow J/\psi\phi$, $B_s^0 \rightarrow J/\psi K^+K^-$ and $B_s^0 \rightarrow \psi(2S)\phi$ results is shown as the red contour, and the constraints given by the effective lifetime measurements of B_s^0 to flavour-specific, pure CP-odd and

pure CP-even final states are shown as the blue, green and purple bands, respectively. The average taking all constraints into account is shown as the grey-filled contour. The yellow band is a theory prediction $\Delta\Gamma_s = 0.088 \pm 0.020 \text{ ps}^{-1}$ [60, 107] that assumes no new physics in B_s^0 mixing

Table 17 Averages of $\Delta\Gamma_s$, Γ_s and related quantities, obtained from $B_s^0 \rightarrow J/\psi\phi$, $B_s^0 \rightarrow J/\psi K^+K^-$ and $B_s^0 \rightarrow \psi(2S)\phi$ alone (first column), adding the constraints from the effective lifetimes measured in pure CP modes $B_s^0 \rightarrow D_s^+D_s^-, J/\psi\eta$ and $B_s^0 \rightarrow$

$J/\psi f_0(980)$, $J/\psi\pi^+\pi^-$ (second column), and adding the constraint from the effective lifetime measured in flavour-specific modes $B_s^0 \rightarrow D_s^-\ell^+\nu X$, $D_s^-\pi^+$, $D_s^-D^+$ (third column, recommended world averages)

	$B_s^0 \rightarrow (c\bar{c})K^+K^-$ modes only (see Table 16)	$B_s^0 \rightarrow (c\bar{c})K^+K^-$ modes + pure CP modes	$B_s^0 \rightarrow (c\bar{c})K^+K^-$ modes + pure CP modes + flavour-specific modes
Γ_s	$0.6654 \pm 0.0022 \text{ ps}^{-1}$	$0.6645 \pm 0.0021 \text{ ps}^{-1}$	$0.6646 \pm 0.0020 \text{ ps}^{-1}$
$1/\Gamma_s$	$1.503 \pm 0.005 \text{ ps}$	$1.505 \pm 0.005 \text{ ps}$	$1.505 \pm 0.005 \text{ ps}$
$1/\Gamma_{sL}$	$1.414 \pm 0.007 \text{ ps}$	$1.413 \pm 0.006 \text{ ps}$	$1.413 \pm 0.006 \text{ ps}$
$1/\Gamma_{sH}$	$1.604 \pm 0.011 \text{ ps}$	$1.610 \pm 0.011 \text{ ps}$	$1.609 \pm 0.010 \text{ ps}$
$\Delta\Gamma_s$	$+0.084 \pm 0.007 \text{ ps}^{-1}$	$+0.086 \pm 0.006 \text{ ps}^{-1}$	$+0.086 \pm 0.006 \text{ ps}^{-1}$
$\Delta\Gamma_s/\Gamma_s$	$+0.126 \pm 0.010$	$+0.130 \pm 0.009$	$+0.130 \pm 0.009$
$\rho(\Gamma_s, \Delta\Gamma_s)$	-0.286	-0.267	-0.210

where

$$A_f^{\Delta\Gamma} = -\frac{2\text{Re}(\lambda_f)}{1 + |\lambda_f|^2}. \tag{69}$$

To include the measurements of the effective $B_s^0 \rightarrow D_s^+D_s^-$ (CP-even), $B_s^0 \rightarrow J/\psi f_0(980)$ (CP-odd) and $B_s^0 \rightarrow J/\psi\pi^+\pi^-$ (CP-odd) lifetimes as constraints in the $\Delta\Gamma_s$ fit,¹⁵ we neglect sub-leading penguin contributions and possible direct CP violation. Explicitly, in Eq. (69), we set

$A_{CP\text{-even}}^{\Delta\Gamma} = \cos\phi_s^{c\bar{c}s}$ and $A_{CP\text{-odd}}^{\Delta\Gamma} = -\cos\phi_s^{c\bar{c}s}$. Given the small value of $\phi_s^{c\bar{c}s}$, we have, to first order in y_s :

$$\tau_{\text{single}}(B_s^0 \rightarrow \text{CP-even}) \approx \frac{1}{\Gamma_{sL}} \left(1 + \frac{(\phi_s^{c\bar{c}s})^2 y_s}{2} \right), \tag{70}$$

$$\tau_{\text{single}}(B_s^0 \rightarrow \text{CP-odd}) \approx \frac{1}{\Gamma_{sH}} \left(1 - \frac{(\phi_s^{c\bar{c}s})^2 y_s}{2} \right). \tag{71}$$

The numerical inputs are taken from Eqs. (41) and (42) and the resulting averages, combined with the $B_s^0 \rightarrow J/\psi K^+K^-$ information, are indicated in the second column of numbers of Table 17. These averages assume $\phi_s^{c\bar{c}s} = 0$,

¹⁵ The effective lifetimes measured in $B_s^0 \rightarrow K^+K^-$ (mostly CP-even) and $B_s^0 \rightarrow J/\psi K_S^0$ (mostly CP-odd) are not used because we can not quantify the penguin contributions in those modes.

Table 18 Measurements of Δm_s

Experiment	Method	Data set		Δm_s (ps ⁻¹)	Refs.
CDF2	$D_s^{(*)-} \ell^+ \nu, D_s^{(*)-} \pi^+, D_s^- \rho^+$		1 fb ⁻¹	$17.77 \pm 0.10 \pm 0.07$	[218]
LHCb	$D_s^- \pi^+, D_s^- \pi^+ \pi^- \pi^+$	2010	0.034 fb ⁻¹	$17.63 \pm 0.11 \pm 0.02$	[219]
LHCb	$D_s^- \mu^+ X$	2011	1.0 fb ⁻¹	$17.93 \pm 0.22 \pm 0.15$	[182]
LHCb	$D_s^- \pi^+$	2011	1.0 fb ⁻¹	$17.768 \pm 0.023 \pm 0.006$	[220]
LHCb	$J/\psi K^+ K^-$	2011–2012	3.0 fb ⁻¹	$17.711^{+0.055}_{-0.057} \pm 0.011$	[202]
Average				$17.757 \pm 0.020 \pm 0.007$	

which is compatible with the $\phi_s^{c\bar{c}s}$ average presented in Sect. 3.3.4.

Information on $\Delta\Gamma_s$ can also be obtained from the study of the proper time distribution of untagged samples of flavour-specific B_s^0 decays [131], where the flavour (i.e., B_s^0 or \bar{B}_s^0) at the time of decay can be determined by the decay products. In such decays, e.g. semileptonic B_s^0 decays, there is an equal mix of the heavy and light mass eigenstates at time zero. The proper time distribution is then a superposition of two exponential functions with decay constants Γ_{sL} and Γ_{sH} . This provides sensitivity to both $1/\Gamma_s$ and $(\Delta\Gamma_s/\Gamma_s)^2$. Ignoring $\Delta\Gamma_s$ and fitting for a single exponential leads to an estimate of Γ_s with a relative bias proportional to $(\Delta\Gamma_s/\Gamma_s)^2$, as shown in Eq. (39). Including the constraint from the world-average flavour-specific B_s^0 lifetime, given in Eq. (40), leads to the results shown in the last column of Table 17. These world averages are displayed as the grey contours labelled ‘‘Combined’’ in the plots of Fig. 7. They correspond to the lifetime averages $1/\Gamma_s = 1.505 \pm 0.005$ ps, $1/\Gamma_{sL} = 1.413 \pm 0.006$ ps, $1/\Gamma_{sH} = 1.609 \pm 0.010$ ps, and to the decay-width difference

$$\begin{aligned} \Delta\Gamma_s &= +0.086 \pm 0.006 \text{ ps}^{-1} \quad \text{and} \\ \Delta\Gamma_s/\Gamma_s &= +0.130 \pm 0.009. \end{aligned} \tag{72}$$

The good agreement with the Standard Model prediction $\Delta\Gamma_s = 0.088 \pm 0.020 \text{ ps}^{-1}$ [60, 107] excludes significant quark-hadron duality violation in the HQE [204].

Estimates of $\Delta\Gamma_s/\Gamma_s$ obtained from measurements of the $B_s^0 \rightarrow D_s^{(*)+} D_s^{(*)-}$ branching fraction [124, 205–207] have not been used, since they are based on the questionable [208, 209] assumption that these decays account for all CP -even final states. The results of early lifetime analyses attempting to measure $\Delta\Gamma_s/\Gamma_s$ [79, 85, 114, 118] have not been used either.

The strength of B_s^0 mixing has been known to be large for more than 20 years. Indeed the time-integrated measurements of $\bar{\chi}$ (see Sect. 3.1.3), when compared to our knowledge of χ_d and the b -hadron fractions, indicated that χ_s should be close to its maximal possible value of 1/2. Many searches of the time dependence of this mixing were performed by

ALEPH [210], DELPHI [114, 118, 165, 211], OPAL [212, 213], SLD [214, 215], CDF (Run I) [216] and D0 [217] but did not have enough statistical power and proper time resolution to resolve the small period of the B_s^0 oscillations.

B_s^0 oscillations have been observed for the first time in 2006 by the CDF collaboration [218], based on samples of flavour-tagged hadronic and semileptonic B_s^0 decays (in flavour-specific final states), partially or fully reconstructed in 1 fb⁻¹ of data collected during Tevatron’s Run II. More recently the LHCb collaboration obtained the most precise results using fully reconstructed $B_s^0 \rightarrow D_s^- \pi^+$ and $B_s^0 \rightarrow D_s^- \pi^+ \pi^- \pi^+$ decays at the LHC [219, 220]. LHCb has also observed B_s^0 oscillations with $B_s^0 \rightarrow J/\psi K^+ K^-$ decays [202] and with semileptonic $B_s^0 \rightarrow D_s^- \mu^+ X$ decays [182]. The measurements of Δm_s are summarized in Table 18.

A simple average of the CDF and LHCb results, taking into account the correlated systematic uncertainties between the three LHCb measurements, yields

$$\begin{aligned} \Delta m_s &= 17.757 \pm 0.020 \pm 0.007 \text{ ps}^{-1} \\ &= 17.757 \pm 0.021 \text{ ps}^{-1} \end{aligned} \tag{73}$$

and is illustrated in Fig. 8. The Standard Model prediction $\Delta m_s = 18.3 \pm 2.7 \text{ ps}^{-1}$ [60, 107] is consistent with the experimental value, but has a much larger error dominated by the uncertainty on the hadronic matrix elements. The ratio $\Delta\Gamma_s/\Delta m_s$ can be predicted more accurately, 0.0048 ± 0.0008 [60, 107], and is in good agreement with the experimental determination of

$$\Delta\Gamma_s/\Delta m_s = 0.00486 \pm 0.00034. \tag{74}$$

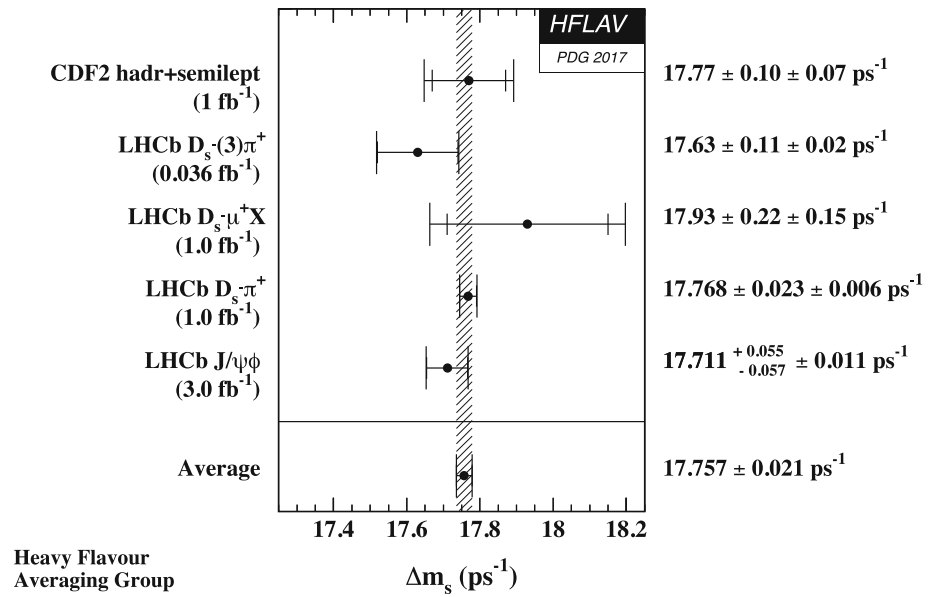
Multiplying the Δm_s result of Eq. (73) with the mean B_s^0 lifetime of Eq. (45), $1/\Gamma_s = 1.505 \pm 0.005$ ps, yields

$$x_s = 26.72 \pm 0.09. \tag{75}$$

With $2y_s = +0.130 \pm 0.009$ [see Eq. (72)] and under the assumption of no CP violation in B_s^0 mixing, this corresponds to

$$\chi_s = \frac{x_s^2 + y_s^2}{2(x_s^2 + 1)} = 0.499304 \pm 0.000005. \tag{76}$$

Fig. 8 Published measurements of Δm_s , together with their average



The ratio of the B^0 and B_s^0 oscillation frequencies, obtained from Eqs. (66) and (73),

$$\frac{\Delta m_d}{\Delta m_s} = 0.02852 \pm 0.00011, \tag{77}$$

can be used to extract the following magnitude of the ratio of CKM matrix elements,

$$\left| \frac{V_{td}}{V_{ts}} \right| = \xi \sqrt{\frac{\Delta m_d m(B_s^0)}{\Delta m_s m(B^0)}} = 0.2053 \pm 0.0004 \pm 0.0032, \tag{78}$$

where the first quoted error is from experimental uncertainties (with the masses $m(B_s^0)$ and $m(B^0)$ taken from Ref. [6]), and where the second quoted error is from theoretical uncertainties in the estimation of the SU(3) flavour-symmetry breaking factor $\xi = 1.206 \pm 0.018 \pm 0.006$, obtained from recent three-flavour lattice QCD calculations [221, 222]. Note that Eq. (78) assumes that Δm_s and Δm_d only receive Standard Model contributions.

3.3.3 CP violation in B^0 and B_s^0 mixing

Evidence for CP violation in B^0 mixing has been searched for, both with flavour-specific and inclusive B^0 decays, in samples where the initial flavour state is tagged. In the case of semileptonic (or other flavour-specific) decays, where the final state tag is also available, the asymmetry

$$\mathcal{A}_{\text{SL}}^d = \frac{N(\bar{B}^0(t) \rightarrow \ell^+ \nu_\ell X) - N(B^0(t) \rightarrow \ell^- \bar{\nu}_\ell X)}{N(\bar{B}^0(t) \rightarrow \ell^+ \nu_\ell X) + N(B^0(t) \rightarrow \ell^- \bar{\nu}_\ell X)} \tag{79}$$

has been measured, either in decay-time-integrated analyses at CLEO [187, 223], BABAR [224], CDF [225] and D0 [195],

or in decay-time-dependent analyses at OPAL [168], ALEPH [226], BABAR [188, 227, 228] and Belle [229]. Note that the asymmetry of time-dependent decay rates in Eq. (79) is related to $|q_d/p_d|$ through Eq. (59) and is therefore time-independent. In the inclusive case, also investigated and published by ALEPH [226] and OPAL [87], no final state tag is used, and the asymmetry [230, 231]

$$\frac{N(B^0(t) \rightarrow \text{all}) - N(\bar{B}^0(t) \rightarrow \text{all})}{N(B^0(t) \rightarrow \text{all}) + N(\bar{B}^0(t) \rightarrow \text{all})} \simeq \mathcal{A}_{\text{SL}}^d \left[\frac{\Delta m_d}{2\Gamma_d} \sin(\Delta m_d t) - \sin^2 \left(\frac{\Delta m_d t}{2} \right) \right] \tag{80}$$

must be measured as a function of the proper time to extract information on CP violation.

On the other hand, D0 [232] and LHCb [233] have studied the time-dependence of the charge asymmetry of $B^0 \rightarrow D^{(*)-} \mu^+ \nu_\mu X$ decays without tagging the initial state, which would be equal to

$$\frac{N(D^{(*)-} \mu^+ \nu_\mu X) - N(D^{(*)+} \mu^- \bar{\nu}_\mu X)}{N(D^{(*)-} \mu^+ \nu_\mu X) + N(D^{(*)+} \mu^- \bar{\nu}_\mu X)} = \mathcal{A}_{\text{SL}}^d \frac{1 - \cos(\Delta m_d t)}{2} \tag{81}$$

in absence of detection and production asymmetries.

Table 19 summarizes the different measurements¹⁶ of $\mathcal{A}_{\text{SL}}^d$ and $|q_d/p_d|$: in all cases asymmetries compatible with zero have been found, with a precision limited by the available statistics.

A simple average of all measurements performed at the B factories [187, 188, 223, 224, 227, 229] yields $\mathcal{A}_{\text{SL}}^d =$

¹⁶ A low-statistics result published by CDF using the Run I data [225] is not included in our averages, nor in Table 19.

Table 19 Measurements¹⁶ of CP violation in B^0 mixing and their average in terms of both \mathcal{A}_{SL}^d and $|q_d/p_d|$. The individual results are listed as quoted in the original publications, or converted¹⁸ to an \mathcal{A}_{SL}^d value.

When two errors are quoted, the first one is statistical and the second one systematic. The ALEPH and OPAL results assume no CP violation in B_s^0 mixing

Exp. and Refs.	Method	Measured \mathcal{A}_{SL}^d	Measured $ q_d/p_d $
CLEO [187]	Partial hadronic rec.	+0.017±0.070±0.014	
CLEO [223]	Dileptons	+0.013±0.050±0.005	
CLEO [223]	Average of above two	+0.014±0.041±0.006	
BABAR [188]	Full hadronic rec.	1.029 ± 0.013 ± 0.011	
BABAR [227]	Part. rec. $D^* X \ell \nu$	+0.0006±0.0017 ^{+0.0038} _{-0.0032}	0.99971±0.00084±0.00175
BABAR [224]	Dileptons	-0.0039±0.0035±0.0019	
Belle [229]	Dileptons	-0.0011 ± 0.0079 ± 0.0085	1.0005 ± 0.0040 ± 0.0043
Average of above 6 B -factory results		-0.0019 ± 0.0027 (tot)	1.0009 ± 0.0013 (tot)
D0 [232]	$B^0 \rightarrow D^{(*)-} \mu^+ \nu X$	+0.0068 ± 0.0045 ± 0.0014	
LHCb [233]	$B^0 \rightarrow D^{(*)-} \mu^+ \nu X$	-0.0002 ± 0.0019 ± 0.0030	
Average of above 8 pure B^0 results		+0.0001 ± 0.0020 (tot)	1.0000 ± 0.0010 (tot)
D0 [195]	Muons and dimuons	-0.0062±0.0043 (tot)	
Average of above 9 direct measurements		-0.0010 ± 0.0018 (tot)	1.0005 ± 0.0009 (tot)
OPAL [168]	Leptons	+0.008 ± 0.028 ± 0.012	
OPAL [87]	Inclusive (Eq. (80))	+0.005 ± 0.055 ± 0.013	
ALEPH [226]	Leptons	-0.037 ± 0.032 ± 0.007	
ALEPH [226]	Inclusive (Eq. (80))	+0.016 ± 0.034 ± 0.009	
ALEPH [226]	Average of above two	-0.013 ± 0.026 (tot)	
Average of above 13 results		-0.0010 ± 0.0018 (tot)	1.0005 ± 0.0009 (tot)
Best fit value from 2D combination of \mathcal{A}_{SL}^d and \mathcal{A}_{SL}^s results (see Eq. (82))		-0.0021 ± 0.0017 (tot)	1.0010 ± 0.0008 (tot)

-0.0019 ± 0.0027. Adding also the D0 [232] and LHCb [233] measurements obtained with reconstructed semileptonic B^0 decays yields $\mathcal{A}_{SL}^d = +0.0001 \pm 0.0020$. As discussed in more detail later in this section, the D0 analysis with single muons and like-sign dimuons [195] separates the B^0 and B_s^0 contributions by exploiting the dependence on the muon impact parameter cut; including the \mathcal{A}_{SL}^d result quoted by D0 in the average yields $\mathcal{A}_{SL}^d = -0.0010 \pm 0.0018$. All the other B^0 analyses performed at high energy, either at LEP or at the Tevatron, did not separate the contributions from the B^0 and B_s^0 mesons. Under the assumption of no CP violation in B_s^0 mixing ($\mathcal{A}_{SL}^s = 0$), a number of these early analyses [52, 87, 168, 226] quote a measurement of \mathcal{A}_{SL}^d or $|q_d/p_d|$ for the B^0 meson. However, these imprecise determinations no longer improve the world average of \mathcal{A}_{SL}^d . The latter assumption makes sense within the Standard Model, since \mathcal{A}_{SL}^s is predicted to be much smaller than \mathcal{A}_{SL}^d [60, 107], but may not be suitable in the presence of new physics.

The Tevatron experiments have measured linear combinations of \mathcal{A}_{SL}^d and \mathcal{A}_{SL}^s using inclusive semileptonic decays of b hadrons, $\mathcal{A}_{SL}^b = +0.0015 \pm 0.0038(\text{stat}) \pm 0.0020(\text{syst})$ [225] and $\mathcal{A}_{SL}^b = -0.00496 \pm 0.00153(\text{stat}) \pm 0.00072(\text{syst})$ [195], at CDF1 and D0 respectively. While the imprecise CDF1 result is compatible with no CP violation, the D0 result, obtained by measuring the single muon

and like-sign dimuon charge asymmetries, differs by 2.8 standard deviations from the Standard Model expectation of $\mathcal{A}_{SL}^{b,SM} = (-2.3 \pm 0.4) \times 10^{-4}$ [195, 208]. With a more sophisticated analysis in bins of the muon impact parameters, D0 conclude that the overall deviation of their measurements from the SM is at the level of 3.6σ . Interpreting the observed asymmetries in bins of the muon impact parameters in terms of CP violation in B -meson mixing and interference, and using the mixing parameters and the world b -hadron fractions of Ref. [234], the D0 collaboration extracts [195] values for \mathcal{A}_{SL}^d and \mathcal{A}_{SL}^s and their correlation coefficient,¹⁷ as shown in Table 20. However, the various contributions to the total quoted errors from this analysis and from the external inputs are not given, so the adjustment of these results to different

¹⁷ In each impact parameter bin i the measured same-sign dimuon asymmetry is interpreted as $A_i = K_i^s \mathcal{A}_{SL}^s + K_i^d \mathcal{A}_{SL}^d + \lambda K_i^{\text{int}} \Delta \Gamma_d / \Gamma_d$, where the factors K_i^s , K_i^d and K_i^{int} are obtained by D0 from Monte Carlo simulation. The D0 publication [195] assumes $\lambda = 1$, but it has been demonstrated subsequently that $\lambda \leq 0.49$ [196]. This particular point invalidates the $\Delta \Gamma_d / \Gamma_d$ result published by D0, but not the \mathcal{A}_{SL}^d and \mathcal{A}_{SL}^s results. As stated by D0, their \mathcal{A}_{SL}^d and \mathcal{A}_{SL}^s results assume the above expression for A_i , i.e. that the observed asymmetries are due to CP violation in B mixing. As long as this assumption is not shown to be wrong (or withdrawn by D0), we include the \mathcal{A}_{SL}^d and \mathcal{A}_{SL}^s results in our world average.

Table 20 Measurements of CP violation in B_s^0 and B^0 mixing, together with their correlations $\rho(\mathcal{A}_{SL}^s, \mathcal{A}_{SL}^d)$ and their two-dimensional average. Only total errors are quoted

Exp. and Refs.	Method	Measured \mathcal{A}_{SL}^s	Measured \mathcal{A}_{SL}^d	$\rho(\mathcal{A}_{SL}^s, \mathcal{A}_{SL}^d)$
<i>B</i> -factory average of Table 19			-0.0019±0.0027	
D0 [232,235]	$B_{(s)}^0 \rightarrow D_{(s)}^{(*)-} \mu^+ \nu X$	-0.0112 ± 0.0076	+0.0068 ± 0.0047	+0.
LHCb [233,236]	$B_{(s)}^0 \rightarrow D_{(s)}^{(*)-} \mu^+ \nu X$	+0.0039 ± 0.0033	-0.0002 ± 0.0036	+0.13
Average of above		+0.0016±0.0030	+0.0000±0.0019	+0.066
D0 [195]	Muons and dimuons	-0.0082 ± 0.0099	-0.0062 ± 0.0043	-0.61
Average of all above		-0.0006±0.0028	-0.0021±0.0017	-0.054

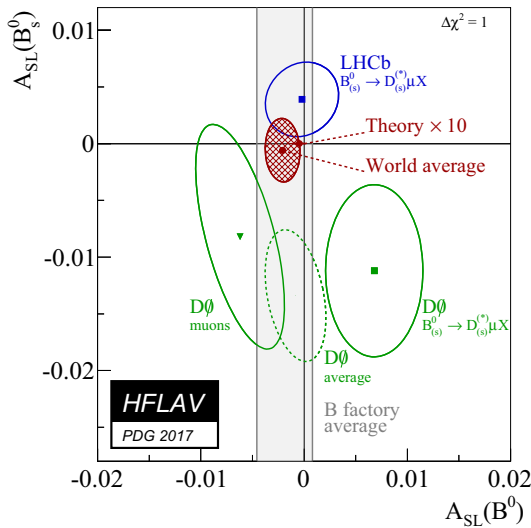


Fig. 9 Measurements of \mathcal{A}_{SL}^s and \mathcal{A}_{SL}^d listed in Table 20 (*B*-factory average as the grey band, D0 measurements as the green ellipses, LHCb measurements as the blue ellipse) together with their two-dimensional average (red hatched ellipse). The red point close to (0, 0) is the Standard Model prediction of Refs. [60,107] with error bars multiplied by 10. The prediction and the experimental world average deviate from each other by 0.5σ

or more recent values of the external inputs cannot (easily) be done.

Finally, direct determinations of \mathcal{A}_{SL}^s , also shown in Table 20, are obtained by D0 [235] and LHCb [236] from the time-integrated charge asymmetry of untagged $B_s^0 \rightarrow D_s^- \mu^+ \nu X$ decays.

Using a two-dimensional fit, all measurements of \mathcal{A}_{SL}^s and \mathcal{A}_{SL}^d obtained by D0 and LHCb are combined with the *B*-factory average of Table 19. Correlations are taken into account as shown in Table 20. The results, displayed graphically in Fig. 9, are

$$\mathcal{A}_{SL}^d = -0.0021 \pm 0.0017$$

$$\iff |q_d/p_d| = 1.0010 \pm 0.0008, \tag{82}$$

$$\mathcal{A}_{SL}^s = -0.0006 \pm 0.0028$$

$$\iff |q_s/p_s| = 1.0003 \pm 0.0014, \tag{83}$$

$$\rho(\mathcal{A}_{SL}^d, \mathcal{A}_{SL}^s) = -0.054, \tag{84}$$

where the relation between \mathcal{A}_{SL}^q and $|q_q/p_q|$ is given in Eq. (59).¹⁸ However, the fit χ^2 probability is only 4.5%. This is mostly due to an overall discrepancy between the D0 and LHCb averages at the level of 2.2σ . Since the assumptions underlying the inclusion of the D0 muon results in the average¹⁷ are somewhat controversial [237], we also provide in Table 20 an average excluding these results.

The above averages show no evidence of CP violation in B^0 or B_s^0 mixing. They deviate by 0.5σ from the very small predictions of the Standard Model (SM), $\mathcal{A}_{SL}^{d,SM} = -(4.7 \pm 0.6) \times 10^{-4}$ and $\mathcal{A}_{SL}^{s,SM} = +(2.22 \pm 0.27) \times 10^{-5}$ [60,107]. Given the current size of the experimental uncertainties, there is still significant room for a possible new physics contribution, in particular in the B_s^0 system. In this respect, the deviation of the D0 dimuon asymmetry [195] from expectation has generated a lot of excitement. However, the recent \mathcal{A}_{SL}^s and \mathcal{A}_{SL}^d results from LHCb are not precise enough yet to settle the issue. It was pointed out [238] that the D0 dimuon result can be reconciled with the SM expectations of \mathcal{A}_{SL}^s and \mathcal{A}_{SL}^d if there were non-SM sources of CP violation in the semileptonic decays of the *b* and *c* quarks. A recent Run 1 ATLAS study [239] of charge asymmetries in muon+jets $t\bar{t}$ events, in which a *b*-hadron decays semileptonically to a soft muon, yields results with limited statistical precision, compatible both with the D0 dimuon asymmetry and with the SM predictions. More experimental data, especially from Run 2 of LHC, is awaited eagerly.

At the more fundamental level, CP violation in B_s^0 mixing is caused by the weak phase difference ϕ_{12}^s defined in Eq. (63). The SM prediction for this phase is tiny [60,107],

$$\phi_{12}^{s,SM} = 0.0046 \pm 0.0012; \tag{85}$$

¹⁸ Early analyses and the PDG use the complex parameter $\epsilon_B = (p_q - q_q)/(p_q + q_q)$ for the B^0 ; if CP violation in the mixing is small, $\mathcal{A}_{SL}^d \cong 4\text{Re}(\epsilon_B)/(1 + |\epsilon_B|^2)$ and the average of Eq. (82) corresponds to $\text{Re}(\epsilon_B)/(1 + |\epsilon_B|^2) = -0.0005 \pm 0.0004$.

however, new physics in B_s^0 mixing could change this observed phase to

$$\phi_{12}^s = \phi_{12}^{s,SM} + \phi_{12}^{s,NP}. \tag{86}$$

Using Eq. (62), the current knowledge of \mathcal{A}_{SL}^s , $\Delta\Gamma_s$ and Δm_s , given in Eqs. (83), (72) and (73) respectively, yields an experimental determination of ϕ_{12}^s ,

$$\tan \phi_{12}^s = \mathcal{A}_{SL}^s \frac{\Delta m_s}{\Delta\Gamma_s} = -0.1 \pm 0.6, \tag{87}$$

which represents only a very weak constraint at present.

3.3.4 Mixing-induced CP violation in B_s^0 decays

CP violation induced by $B_s^0 - \bar{B}_s^0$ mixing has been a field of very active study and fast experimental progress in the past few years. The main observable is the CP-violating phase $\phi_s^{c\bar{c}s}$, defined as the weak phase difference between the $B_s^0 - \bar{B}_s^0$ mixing amplitude M_{12}^s and the $b \rightarrow c\bar{c}s$ decay amplitude.

The golden mode for such studies is $B_s^0 \rightarrow J/\psi\phi$, followed by $J/\psi \rightarrow \mu^+\mu^-$ and $\phi \rightarrow K^+K^-$, for which a full angular analysis of the decay products is performed to separate statistically the CP-even and CP-odd contributions in the final state. As already mentioned in Sect. 3.3.2, CDF [197], D0 [198], ATLAS [199,200], CMS [201] and LHCb [202,203] have used both untagged and tagged $B_s^0 \rightarrow J/\psi\phi$ (and more generally $B_s^0 \rightarrow (c\bar{c})K^+K^-$) events for the measurement of $\phi_s^{c\bar{c}s}$. LHCb [240] has used $B_s^0 \rightarrow J/\psi\pi^+\pi^-$ events, analyzed with a full amplitude model including several $\pi^+\pi^-$ resonances (e.g., $f_0(980)$), although the $J/\psi\pi^+\pi^-$ final state had already been shown to be almost CP pure with a CP-odd fraction larger than 0.977 at 95% CL [241]. In addition, LHCb has used the $B_s^0 \rightarrow D_s^+D_s^-$ channel [242] to measure $\phi_s^{c\bar{c}s}$.

All CDF, D0, ATLAS and CMS analyses provide two mirror solutions related by the transformation $(\Delta\Gamma_s, \phi_s^{c\bar{c}s}) \rightarrow (-\Delta\Gamma_s, \pi - \phi_s^{c\bar{c}s})$. However, the LHCb analysis of $B_s^0 \rightarrow J/\psi K^+K^-$ resolves this ambiguity and rules out the solution with negative $\Delta\Gamma_s$ [111], a result in agreement with the Standard Model expectation. Therefore, in what follows, we only consider the solution with $\Delta\Gamma_s > 0$.

We perform a combination of the CDF [197], D0 [198], ATLAS [199,200], CMS [201] and LHCb [202,203,240] results summarized in Table 21. This is done by adding the two-dimensional log profile-likelihood scans of $\Delta\Gamma_s$ and $\phi_s^{c\bar{c}s}$ from all $B_s^0 \rightarrow (c\bar{c})K^+K^-$ analyses and a one-dimensional log profile-likelihood of $\phi_s^{c\bar{c}s}$ from the $B_s^0 \rightarrow J/\psi\pi^+\pi^-$ and $B_s^0 \rightarrow D_s^+D_s^-$ analyses; the combined likelihood is then maximized with respect to $\Delta\Gamma_s$ and $\phi_s^{c\bar{c}s}$.

In the $B_s^0 \rightarrow J/\psi\phi$ and $B_s^0 \rightarrow J/\psi K^+K^-$ analyses, $\phi_s^{c\bar{c}s}$ and $\Delta\Gamma_s$ come from a simultaneous fit that determines also the B_s^0 lifetime, the polarisation amplitudes and strong phases. While the correlation between $\phi_s^{c\bar{c}s}$ and all other

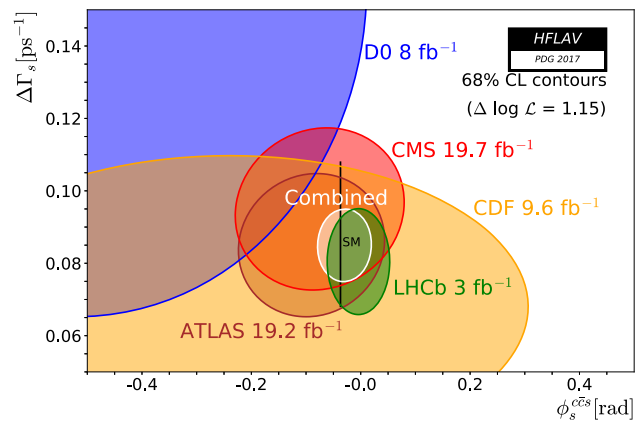


Fig. 10 68% CL regions in B_s^0 width difference $\Delta\Gamma_s$ and weak phase $\phi_s^{c\bar{c}s}$ obtained from individual and combined CDF [197], D0 [198], ATLAS [199,200], CMS [201] and LHCb [202,203,240,242] likelihoods of $B_s^0 \rightarrow J/\psi\phi$, $B_s^0 \rightarrow J/\psi K^+K^-$, $B_s^0 \rightarrow \psi(2S)\phi$, $B_s^0 \rightarrow J/\psi\pi^+\pi^-$ and $B_s^0 \rightarrow D_s^+D_s^-$ samples. The expectation within the Standard Model [60,107,193] is shown as the black rectangle

parameters is small, the correlations between $\Delta\Gamma_s$ and the polarisation amplitudes are sizable. However, since the various experiments use different conventions for the amplitudes and phases, a full combination including all correlations is not performed. Instead, our average only takes into account the correlation between $\phi_s^{c\bar{c}s}$ and $\Delta\Gamma_s$.

In the recent LHCb $B_s^0 \rightarrow J/\psi K^+K^-$ analysis [202], the $\phi_s^{c\bar{c}s}$ values are measured for the first time for each polarisation of the final state. Since those values are compatible within each other, we still use the unique value of $\phi_s^{c\bar{c}s}$ for our world average, corresponding to the one measured by the other-than-LHCb analyses. In the same analysis, the statistical correlation coefficient between $\phi_s^{c\bar{c}s}$ and $|\lambda|$ (which signals CP violation in the decay if different from unity) is measured to be very small (-0.02). We neglect this correlation in our average. Furthermore, the statistical correlation coefficient between $\phi_s^{c\bar{c}s}$ and $\Delta\Gamma_s$ is measured to be small (-0.08). When averaging LHCb results of $B_s^0 \rightarrow J/\psi K^+K^-$, $B_s^0 \rightarrow J/\psi\pi^+\pi^-$ and $B_s^0 \rightarrow D_s^+D_s^-$, we neglect this correlation coefficient (putting it to zero). Given the increasing experimental precision, we have also stopped using the two-dimensional $\Delta\Gamma_s - \phi_s^{c\bar{c}s}$ histograms provided by the CDF and D0 collaborations: we are now approximating those with two-dimensional Gaussian likelihoods.

We obtain the individual and combined contours shown in Fig. 10. Maximizing the likelihood, we find, as summarized in Table 21:

$$\Delta\Gamma_s = +0.085 \pm 0.007 \text{ ps}^{-1}, \tag{88}$$

$$\phi_s^{c\bar{c}s} = -0.030 \pm 0.033. \tag{89}$$

The above $\Delta\Gamma_s$ average is consistent, but highly correlated with the average of Eq. (72). Our final recommended average

Table 21 Direct experimental measurements of $\phi_s^{c\bar{c}s}$, $\Delta\Gamma_s$ and Γ_s using $B_s^0 \rightarrow J/\psi\phi$, $J/\psi K^+K^-$, $\psi(2S)\phi$, $J/\psi\pi^+\pi^-$ and $D_s^+D_s^-$ decays. Only the solution with $\Delta\Gamma_s > 0$ is shown, since the two-fold ambiguity

has been resolved in Ref. [111]. The first error is due to statistics, the second one to systematics. The last line gives our average

Exp.	Mode	Dataset	$\phi_s^{c\bar{c}s}$	$\Delta\Gamma_s$ (ps ⁻¹)	Refs.
CDF	$J/\psi\phi$	9.6 fb ⁻¹	[-0.60, +0.12], 68% CL	+0.068 ± 0.026 ± 0.009	[197]
D0	$J/\psi\phi$	8.0 fb ⁻¹	-0.55 ^{+0.38} _{-0.36}	+0.163 ^{+0.065} _{-0.064}	[198]
ATLAS	$J/\psi\phi$	4.9 fb ⁻¹	+0.12 ± 0.25 ± 0.05	+0.053 ± 0.021 ± 0.010	[199]
ATLAS	$J/\psi\phi$	14.3 fb ⁻¹	-0.110 ± 0.082 ± 0.042	+0.101 ± 0.013 ± 0.007	[200]
ATLAS	Above 2 combined		-0.090 ± 0.078 ± 0.041	+0.085 ± 0.011 ± 0.007	[200]
CMS	$J/\psi\phi$	19.7 fb ⁻¹	-0.075 ± 0.097 ± 0.031	+0.095 ± 0.013 ± 0.007	[201]
LHCb	$J/\psi K^+K^-$	3.0 fb ⁻¹	-0.058 ± 0.049 ± 0.006	+0.0805 ± 0.0091 ± 0.0032	[202]
LHCb	$J/\psi\pi^+\pi^-$	3.0 fb ⁻¹	+0.070 ± 0.068 ± 0.008	-	[240]
LHCb	Above 2 combined		-0.010 ± 0.039(tot)	-	[202]
LHCb	$\psi(2S)\phi$	3.0 fb ⁻¹	+0.23 ^{+0.29} _{-0.28} ± 0.02	+0.066 ^{+0.41} _{-0.44} ± 0.007	[203]
LHCb	$D_s^+D_s^-$	3.0 fb ⁻¹	+0.02 ± 0.17 ± 0.02	-	[242]
All combined			-0.030 ± 0.033	+0.085 ± 0.007	

for $\Delta\Gamma_s$ is the one of Eq. (72), which includes all available information on $\Delta\Gamma_s$.

In the Standard Model and ignoring sub-leading penguin contributions, $\phi_s^{c\bar{c}s}$ is expected to be equal to $-2\beta_s$, where $\beta_s = \arg[-(V_{ts}V_{tb}^*)/(V_{cs}V_{cb}^*)]$ is a phase analogous to the angle β of the usual CKM unitarity triangle (aside from a sign change). An indirect determination via global fits to experimental data gives [193]

$$(\phi_s^{c\bar{c}s})^{SM} = -2\beta_s = -0.0370 \pm 0.0006. \tag{90}$$

The average value of $\phi_s^{c\bar{c}s}$ from Eq. (89) is consistent with this Standard Model expectation.

From its measurements of time-dependent CP violation in $B_s^0 \rightarrow K^+K^-$ decays, the LHCb collaboration has determined the B_s^0 mixing phase to be $-2\beta_s = -0.12^{+0.14}_{-0.12}$ [243], assuming a U-spin relation (with up to 50% breaking effects) between the decay amplitudes of $B_s^0 \rightarrow K^+K^-$ and $B^0 \rightarrow \pi^+\pi^-$, and a value of the CKM angle γ of $(70.1 \pm 7.1)^\circ$. This determination is compatible with, and less precise than, the world average of $\phi_s^{c\bar{c}s}$ from Eq. (89).

New physics could contribute to $\phi_s^{c\bar{c}s}$. Assuming that new physics only enters in M_{12}^s (rather than in Γ_{12}^s), one can write [208,209]

$$\phi_s^{c\bar{c}s} = -2\beta_s + \phi_{12}^{s,NP}, \tag{91}$$

where the new physics phase $\phi_{12}^{s,NP}$ is the same as that appearing in Eq. (86). In this case

$$\phi_{12}^s = \phi_{12}^{s,SM} + 2\beta_s + \phi_s^{c\bar{c}s} = 0.012 \pm 0.033, \tag{92}$$

where the numerical estimation was performed with the values of Eqs. (85), (89) and (90). Keeping in mind the approximation and assumption mentioned above, this can serve as

a reference value to which the measurement of Eq. (87) can be compared.

4 Measurements related to unitarity triangle angles

The charge of the “CP(t) and Unitarity Triangle angles” group is to provide averages of measurements obtained from analyses of decay-time-dependent asymmetries, and other quantities that are related to the angles of the Unitarity Triangle (UT). In cases where considerable theoretical input is required to extract the fundamental quantities, no attempt to do so is made. However, straightforward interpretations of the averages are given, where possible.

In Sect. 4.1 a brief introduction to the relevant phenomenology is given. In Sect. 4.2 an attempt is made to clarify the various different notations in use. In Sect. 4.3 the common inputs to which experimental results are rescaled in the averaging procedure are listed. We also briefly introduce the treatment of experimental errors. In the remainder of this section, the experimental results and their averages are given, divided into subsections based on the underlying quark-level decays. All the measurements reported are quantities determined from decay-time-dependent analyses, with the exception of several in Sect. 4.14, which are related to the UT angle γ and are obtained from decay-time-integrated analyses. In the compilations of measurements, indications of the sizes of the data samples used by each experiment are given. For the $e^+e^- B\bar{B}$ factory experiments, this is quoted in terms of the number of $B\bar{B}$ pairs in the data sample, while the integrated luminosity is given for experiments at hadron colliders.

4.1 Introduction

The Standard Model Cabibbo–Kobayashi–Maskawa (CKM) quark mixing matrix V must be unitary. The CKM matrix has four free parameters and these are conventionally written by the product of three (complex) rotation matrices [244], where the rotations are characterised by the Euler mixing angles between the generations, θ_{12} , θ_{13} and θ_{23} , and one overall phase δ ,

$$\begin{aligned}
 V &= \begin{pmatrix} V_{ud} & V_{us} & V_{ub} \\ V_{cd} & V_{cs} & V_{cb} \\ V_{td} & V_{ts} & V_{tb} \end{pmatrix} \\
 &= \begin{pmatrix} c_{12}c_{13} & s_{12}c_{13} & s_{13}e^{-i\delta} \\ -s_{12}c_{23} - c_{12}s_{23}s_{13}e^{i\delta} & c_{12}c_{23} - s_{12}s_{23}s_{13}e^{i\delta} & s_{23}c_{13} \\ s_{12}s_{23} - c_{12}c_{23}s_{13}e^{i\delta} & -c_{12}s_{23} - s_{12}c_{23}s_{13}e^{i\delta} & c_{23}c_{13} \end{pmatrix} \quad (93)
 \end{aligned}$$

where $c_{ij} = \cos \theta_{ij}$, $s_{ij} = \sin \theta_{ij}$ for $i < j = 1, 2, 3$.

Following the observation of a hierarchy between the different matrix elements, the Wolfenstein parametrisation [245] is an expansion of V in terms of the four real parameters λ (the expansion parameter), A , ρ and η . Defining to all orders in λ [246]

$$\begin{aligned}
 s_{12} &\equiv \lambda, \\
 s_{23} &\equiv A\lambda^2, \\
 s_{13}e^{-i\delta} &\equiv A\lambda^3(\rho - i\eta), \quad (94)
 \end{aligned}$$

and inserting these into the representation of Eq. (93), unitarity of the CKM matrix is achieved to all orders. A Taylor expansion of V leads to the familiar approximation

$$\begin{aligned}
 V &= \begin{pmatrix} 1 - \lambda^2/2 & \lambda & A\lambda^3(\rho - i\eta) \\ -\lambda & 1 - \lambda^2/2 & A\lambda^2 \\ A\lambda^3(1 - \rho - i\eta) & -A\lambda^2 & 1 \end{pmatrix} \\
 &+ \mathcal{O}(\lambda^4). \quad (95)
 \end{aligned}$$

At order λ^5 , the obtained CKM matrix in this extended Wolfenstein parametrisation is:

$$\begin{aligned}
 V &= \begin{pmatrix} 1 - \frac{1}{2}\lambda^2 - \frac{1}{8}\lambda^4 & \lambda & A\lambda^3(\rho - i\eta) \\ -\lambda + \frac{1}{2}A^2\lambda^5 \left[1 - 2(\rho + i\eta) \right] & 1 - \frac{1}{2}\lambda^2 - \frac{1}{8}\lambda^4(1 + 4A^2)A\lambda^2 & \\ A\lambda^3 \left[1 - (1 - \frac{1}{2}\lambda^2)(\rho + i\eta) \right] & -A\lambda^2 + \frac{1}{2}A\lambda^4 \left[1 - 2(\rho + i\eta) \right] & 1 - \frac{1}{2}A^2\lambda^4 \end{pmatrix} + \mathcal{O}(\lambda^6). \quad (96)
 \end{aligned}$$

A non-zero value of η implies that the CKM matrix is not purely real in this, or any, parametrisation, and is the origin of

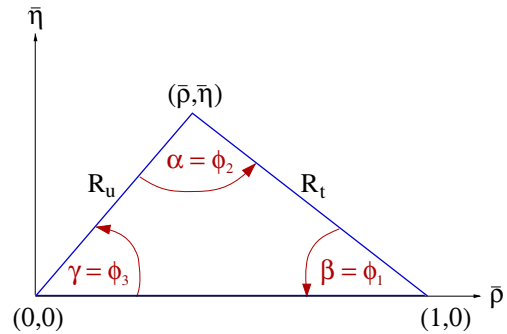


Fig. 11 The unitarity triangle

CP violation in the Standard Model. This is encapsulated in a parametrisation-invariant way through the Jarlskog parameter $J = \text{Im}(V_{us}V_{cb}V_{ub}^*V_{cs}^*)$ [247].

The unitarity relation $V^\dagger V = I$ results in a total of nine expressions, that can be written as $\sum_{i=u,c,t} V_{ij}^* V_{ik} = \delta_{jk}$, where δ_{jk} is the Kronecker symbol. Of the off-diagonal expressions ($j \neq k$), three can be transformed into the other three (under $j \leftrightarrow k$, corresponding to complex conjugation). This leaves three relations in which three complex numbers sum to zero, which therefore can be expressed as triangles in the complex plane, together with three relations in which the squares of the elements in each column of the CKM matrix sum to unity. Similar relations are obtained for the rows of the matrix from $VV^\dagger = I$, so there are in total six triangle relations and six sums to unity. More details about unitarity triangles can be found in Refs. [248–251].

One of the triangle relations,

$$V_{ud}V_{ub}^* + V_{cd}V_{cb}^* + V_{td}V_{tb}^* = 0, \quad (97)$$

is of particular importance to the B system, being specifically related to flavour-changing neutral-current $b \rightarrow d$ transitions. The three terms in Eq. (97) are of the same order, $\mathcal{O}(\lambda^3)$, and this relation is commonly known as the Unitarity Triangle. For presentational purposes, it is convenient to rescale the triangle by $(V_{cd}V_{cb}^*)^{-1}$, as shown in Fig. 11.

Two popular naming conventions for the UT angles exist in the literature:

$$\begin{aligned} \alpha \equiv \phi_2 &= \arg \left[-\frac{V_{td}V_{tb}^*}{V_{ud}V_{ub}^*} \right], \\ \beta \equiv \phi_1 &= \arg \left[-\frac{V_{cd}V_{cb}^*}{V_{td}V_{tb}^*} \right], \\ \gamma \equiv \phi_3 &= \arg \left[-\frac{V_{ud}V_{ub}^*}{V_{cd}V_{cb}^*} \right]. \end{aligned} \tag{98}$$

In this document the (α, β, γ) set is used. The sides R_u and R_t of the Unitarity Triangle (the third side being normalised to unity) are given by

$$\begin{aligned} R_u &= \left| \frac{V_{ud}V_{ub}^*}{V_{cd}V_{cb}^*} \right| = \sqrt{\bar{\rho}^2 + \bar{\eta}^2}, \\ R_t &= \left| \frac{V_{td}V_{tb}^*}{V_{cd}V_{cb}^*} \right| = \sqrt{(1 - \bar{\rho})^2 + \bar{\eta}^2}. \end{aligned} \tag{99}$$

where $\bar{\rho}$ and $\bar{\eta}$ define the apex of the Unitarity Triangle [246]

$$\begin{aligned} \bar{\rho} + i\bar{\eta} &\equiv -\frac{V_{ud}V_{ub}^*}{V_{cd}V_{cb}^*} \equiv 1 + \frac{V_{td}V_{tb}^*}{V_{cd}V_{cb}^*} \\ &= \frac{\sqrt{1 - \lambda^2}(\rho + i\eta)}{\sqrt{1 - A^2\lambda^4} + \sqrt{1 - \lambda^2}A^2\lambda^4(\rho + i\eta)}. \end{aligned} \tag{100}$$

The exact relation between (ρ, η) and $(\bar{\rho}, \bar{\eta})$ is

$$\rho + i\eta = \frac{\sqrt{1 - A^2\lambda^4}(\bar{\rho} + i\bar{\eta})}{\sqrt{1 - \lambda^2} \left[1 - A^2\lambda^4(\bar{\rho} + i\bar{\eta}) \right]}. \tag{101}$$

By expanding in powers of λ , several useful approximate expressions can be obtained, including

$$\begin{aligned} \bar{\rho} &= \rho \left(1 - \frac{1}{2}\lambda^2 \right) + \mathcal{O}(\lambda^4), \\ \bar{\eta} &= \eta \left(1 - \frac{1}{2}\lambda^2 \right) + \mathcal{O}(\lambda^4), \\ V_{td} &= A\lambda^3(1 - \bar{\rho} - i\bar{\eta}) + \mathcal{O}(\lambda^6). \end{aligned} \tag{102}$$

Recent world average values for the Wolfenstein parameters, evaluated using many of the measurements reported in this document, are [252]

$$\begin{aligned} A &= 0.8227^{+0.0066}_{-0.0136}, \quad \lambda = 0.22543^{+0.00042}_{-0.00031}, \\ \bar{\rho} &= 0.1504^{+0.0121}_{-0.0062}, \quad \bar{\eta} = 0.3540^{+0.0069}_{-0.0076}. \end{aligned} \tag{103}$$

The relevant unitarity triangle for the $b \rightarrow s$ transition is obtained by replacing $d \leftrightarrow s$ in Eq. (97). Definitions of the set of angles $(\alpha_s, \beta_s, \gamma_s)$ can be obtained using equivalent relations to those of Eq. (98). However, this gives a value of β_s that is negative in the Standard Model, so that the sign is usually flipped in the literature; this convention, i.e. $\beta_s = \arg \left[-(V_{ts}V_{tb}^*)/(V_{cs}V_{cb}^*) \right]$, is also followed here and in Sect. 3. Since the sides of the $b \rightarrow s$ unitarity triangle are

not all of the same order of λ , the triangle is squashed and $\beta_s \sim \lambda^2\eta$.

4.2 Notations

Several different notations for CP violation parameters are commonly used. This section reviews those found in the experimental literature, in the hope of reducing the potential for confusion, and to define the frame that is used for the averages.

In some cases, when B mesons decay into multibody final states via broad resonances (ρ, K^* , etc.), the experimental analyses ignore the effects of interference between the overlapping structures. This is referred to as the quasi-two-body (Q2B) approximation in the following.

4.2.1 CP asymmetries

The CP asymmetry is defined as the difference between the rate involving a b quark and that involving a \bar{b} quark, divided by the sum. For example, the partial rate (or charge) asymmetry for a charged B decay would be given as

$$\mathcal{A}_f \equiv \frac{\Gamma(B^- \rightarrow f) - \Gamma(B^+ \rightarrow \bar{f})}{\Gamma(B^- \rightarrow f) + \Gamma(B^+ \rightarrow \bar{f})}. \tag{104}$$

4.2.2 Time-dependent CP asymmetries in decays to CP eigenstates

If the amplitudes for B^0 and \bar{B}^0 to decay to a final state f , which is a CP eigenstate with eigenvalue η_f , are given by A_f and \bar{A}_f , respectively, then the decay distributions for neutral B mesons, with known (i.e. ‘‘tagged’’) flavour at time $\Delta t = 0$, are given by

$$\begin{aligned} \Gamma_{\bar{B}^0 \rightarrow f}(\Delta t) &= \frac{e^{-|\Delta t|/\tau(B^0)}}{4\tau(B^0)} \left[1 + \frac{2 \operatorname{Im}(\lambda_f)}{1 + |\lambda_f|^2} \sin(\Delta m \Delta t) \right. \\ &\quad \left. - \frac{1 - |\lambda_f|^2}{1 + |\lambda_f|^2} \cos(\Delta m \Delta t) \right], \end{aligned} \tag{105}$$

$$\begin{aligned} \Gamma_{B^0 \rightarrow f}(\Delta t) &= \frac{e^{-|\Delta t|/\tau(B^0)}}{4\tau(B^0)} \left[1 - \frac{2 \operatorname{Im}(\lambda_f)}{1 + |\lambda_f|^2} \sin(\Delta m \Delta t) \right. \\ &\quad \left. + \frac{1 - |\lambda_f|^2}{1 + |\lambda_f|^2} \cos(\Delta m \Delta t) \right]. \end{aligned} \tag{106}$$

Here $\lambda_f = \frac{q \bar{A}_f}{p A_f}$ contains terms related to $B^0 - \bar{B}^0$ mixing and to the decay amplitude (the eigenstates of the $B^0 - \bar{B}^0$ system with physical masses and lifetimes are $|B_{\pm}\rangle = p|B^0\rangle \pm q|\bar{B}^0\rangle$). This formulation assumes CPT invariance, and neglects possible lifetime differences between the two physical states (see Sect. 3.3 where the mass difference Δm is also defined) in the neutral B meson system. The case

where non-zero lifetime differences are taken into account is discussed in Sect. 4.2.3.

The notation and normalisation used in Eqs. (105) and (106) are relevant for the $e^+e^- B$ factory experiments. In this case, neutral B mesons are produced via the $e^+e^- \rightarrow \Upsilon(4S) \rightarrow B\bar{B}$ process, and the wavefunction of the produced $B\bar{B}$ pair evolves coherently until one meson decays. When one of the pair decays into a final state that tags its flavour, the flavour of the other at that instant is known. The evolution of the other neutral B meson is therefore described in terms of Δt , the difference between the decay times of the two mesons in the pair. At hadron collider experiments, t is usually used in place of Δt since the flavour tagging is done at production ($t = 0$); due to the nature of the production in hadron colliders (incoherent $b\bar{b}$ quark pair production with many additional associated particles), very different methods are used for tagging compared to those in e^+e^- experiments. Moreover, since negative values of t are not possible, the normalisation is such that $\int_0^{+\infty} (\Gamma_{\bar{B}^0 \rightarrow f}(t) + \Gamma_{B^0 \rightarrow f}(t)) dt = 1$, rather than $\int_{-\infty}^{+\infty} (\Gamma_{\bar{B}^0 \rightarrow f}(\Delta t) + \Gamma_{B^0 \rightarrow f}(\Delta t)) d(\Delta t) = 1$, as in Eqs. (105) and (106).

The time-dependent CP asymmetry, again defined as the difference between the rate involving a b quark and that involving a \bar{b} quark, is then given by

$$\begin{aligned} \mathcal{A}_f(\Delta t) &\equiv \frac{\Gamma_{\bar{B}^0 \rightarrow f}(\Delta t) - \Gamma_{B^0 \rightarrow f}(\Delta t)}{\Gamma_{\bar{B}^0 \rightarrow f}(\Delta t) + \Gamma_{B^0 \rightarrow f}(\Delta t)} \\ &= \frac{2 \operatorname{Im}(\lambda_f)}{1 + |\lambda_f|^2} \sin(\Delta m \Delta t) \\ &\quad - \frac{1 - |\lambda_f|^2}{1 + |\lambda_f|^2} \cos(\Delta m \Delta t). \end{aligned} \tag{107}$$

While the coefficient of the $\sin(\Delta m \Delta t)$ term in Eq. (107) is customarily¹⁹ denoted S_f :

$$S_f \equiv \frac{2 \operatorname{Im}(\lambda_f)}{1 + |\lambda_f|^2}, \tag{108}$$

different notations are in use for the coefficient of the $\cos(\Delta m \Delta t)$ term:

$$C_f \equiv -A_f \equiv \frac{1 - |\lambda_f|^2}{1 + |\lambda_f|^2}. \tag{109}$$

The C notation has been used by the BABAR collaboration (see e.g. Ref. [253]), and is also adopted in this document. The A notation has been used by the Belle collaboration (see e.g. Ref. [254]). When the final state is a CP eigenstate, the notation S_{CP} and C_{CP} is widely used, including in this document, instead of specifying the final state f . In

¹⁹ Occasionally one also finds Eq. (107) written as $\mathcal{A}_f(\Delta t) = A_f^{\text{mix}} \sin(\Delta m \Delta t) + A_f^{\text{dir}} \cos(\Delta m \Delta t)$, or similar.

addition, particularly when grouping together measurements with different final states mediated by the same quark-level transition, the S, C notation with a subscript indicating the transition is used.

Neglecting effects due to CP violation in mixing (by taking $|q/p| = 1$), if the decay amplitude contains terms with a single weak (i.e. CP violating) phase then $|\lambda_f| = 1$ and one finds $S_f = -\eta_f \sin(\phi_{\text{mix}} + \phi_{\text{dec}})$, $C_f = 0$, where $\phi_{\text{mix}} = \arg(q/p)$ and $\phi_{\text{dec}} = \arg(\bar{A}_f/A_f)$. Note that the $B^0-\bar{B}^0$ mixing phase ϕ_{mix} is approximately equal to 2β in the Standard Model (in the usual phase convention) [255, 256].

If amplitudes with different weak phases contribute to the decay, no clean interpretation of S_f is possible without further input. In this document, only the theoretically cleanest channels are interpreted as measurements of the weak phase (e.g. $b \rightarrow c\bar{c}s$ transitions for $\sin(2\beta)$), though even in these cases some care is necessary. In channels in which the second amplitude is expected to be suppressed, the concept of an effective weak phase difference is sometimes used, e.g. $\sin(2\beta^{\text{eff}})$ in $b \rightarrow q\bar{q}s$ transition.

If, in addition to having a weak phase difference, the decay amplitudes have different CP conserving strong phases, then $|\lambda_f| \neq 1$. Additional input is required for interpretation of the results. The coefficient of the cosine term becomes non-zero, indicating CP violation in decay.

Due to the fact that $\sin(\Delta m \Delta t)$ and $\cos(\Delta m \Delta t)$ are respectively odd and even functions of Δt , only small correlations (that can be induced by backgrounds, for example) between S_f and C_f are expected at an $e^+e^- B$ factory experiment, where the range of Δt is $-\infty < \Delta t < +\infty$. The situation is different for measurements at hadron collider experiments, where the range of the time variable is $0 < t < +\infty$, so that more sizable correlations can be expected. We include the correlations in the averages where available.

Frequently, we are interested in combining measurements governed by similar or identical short-distance physics, but with different final states (e.g., $B^0 \rightarrow J/\psi K_S^0$ and $B^0 \rightarrow J/\psi K_L^0$). In this case, we remove the dependence on the CP eigenvalue of the final state by quoting $-\eta S_f$. In cases where the final state is not a CP eigenstate but has an effective CP content (see below), the reported $-\eta S$ is corrected by the effective CP .

4.2.3 Time-dependent distributions with non-zero decay width difference

A complete analysis of the time-dependent decay rates of neutral B mesons must also take into account the difference in lifetimes, denoted $\Delta\Gamma$, between the mass eigenstates. This is particularly important in the B_s^0 system, since a non-

negligible value of $\Delta\Gamma_s$ has been established (see Sect. 3.3 for the latest experimental constraints). The formalism given here is therefore appropriate for measurements of B_s^0 decays to a CP eigenstate f as studied at hadron colliders, but appropriate modifications for B^0 mesons or for the e^+e^- environment are straightforward to make.

Neglecting CP violation in mixing, the relevant replacements for Eqs. (105) and (106) are [257]

$$\Gamma_{\bar{B}_s^0 \rightarrow f}(t) = \mathcal{N} \frac{e^{-t/\tau(B_s^0)}}{2\tau(B_s^0)} \left[\cosh\left(\frac{\Delta\Gamma_s t}{2}\right) + S_f \sin(\Delta m_s t) - C_f \cos(\Delta m_s t) + A_f^{\Delta\Gamma} \sinh\left(\frac{\Delta\Gamma_s t}{2}\right) \right], \tag{110}$$

and

$$\Gamma_{B_s^0 \rightarrow f}(t) = \mathcal{N} \frac{e^{-t/\tau(B_s^0)}}{2\tau(B_s^0)} \left[\cosh\left(\frac{\Delta\Gamma_s t}{2}\right) - S_f \sin(\Delta m_s t) + C_f \cos(\Delta m_s t) + A_f^{\Delta\Gamma} \sinh\left(\frac{\Delta\Gamma_s t}{2}\right) \right], \tag{111}$$

where S_f and C_f are as defined in Eqs. (108) and (109), respectively, $\tau(B_s^0) = 1/\Gamma_s$ is defined in Sect. 3.2.4, and the coefficient of the sinh term is²⁰

$$A_f^{\Delta\Gamma} = -\frac{2\text{Re}(\lambda_f)}{1 + |\lambda_f|^2}. \tag{112}$$

With the requirement $\int_0^{+\infty} [\Gamma_{\bar{B}_s^0 \rightarrow f}(t) + \Gamma_{B_s^0 \rightarrow f}(t)] dt = 1$, the normalisation factor is fixed to $\mathcal{N} = (1 - (\frac{\Delta\Gamma_s}{2\Gamma_s})^2) / (1 + \frac{A_f^{\Delta\Gamma} \Delta\Gamma_s}{2\Gamma_s})$.²¹

A time-dependent analysis of CP asymmetries in flavour-tagged B_s^0 decays to a CP eigenstate f can thus determine the parameters S_f , C_f and $A_f^{\Delta\Gamma}$. Note that, by definition,

$$(S_f)^2 + (C_f)^2 + (A_f^{\Delta\Gamma})^2 = 1, \tag{113}$$

and this constraint can be imposed or not in the fits. Since these parameters have sensitivity to both $\text{Im}(\lambda_f)$ and $\text{Re}(\lambda_f)$, alternative choices of parametrisation, including those directly involving CP violating phases (such as β_s), are possible. These can also be adopted for vector-vector final states.

²⁰ As ever, alternative and conflicting notations appear in the literature. One popular alternative notation for this parameter is $\mathcal{A}_{\Delta\Gamma}$. Particular care must be taken over the signs.

²¹ The prefactor of $\mathcal{N}/2\tau(B_s^0)$ in Eqs. (108) and (109) has been chosen so that $\mathcal{N} = 1$ in the limit $\Delta\Gamma_s = 0$. In the e^+e^- environment, where the range is $-\infty < \Delta t < \infty$, the prefactor should be $\mathcal{N}/4\tau(B_s^0)$ and $\mathcal{N} = 1 - (\frac{\Delta\Gamma_s}{2\Gamma_s})^2$.

The *untagged* time-dependent decay rate is given by

$$\Gamma_{\bar{B}_s^0 \rightarrow f}(t) + \Gamma_{B_s^0 \rightarrow f}(t) = \mathcal{N} \frac{e^{-t/\tau(B_s^0)}}{\tau(B_s^0)} \times \left[\cosh\left(\frac{\Delta\Gamma_s t}{2}\right) + A_f^{\Delta\Gamma} \sinh\left(\frac{\Delta\Gamma_s t}{2}\right) \right]. \tag{114}$$

Thus, an untagged time-dependent analysis can probe λ_f , through the dependence of $A_f^{\Delta\Gamma}$ on $\text{Re}(\lambda_f)$, when $\Delta\Gamma_s \neq 0$. This is equivalent to determining the “effective lifetime” [112], as discussed in Sect. 3.2.4. The analysis of flavour-tagged B_s^0 mesons is, of course, more sensitive.

The discussion in this and the previous section is relevant for decays to CP eigenstates. In the following sections, various cases of time-dependent CP asymmetries in decays to non- CP eigenstates are considered. For brevity, these will be given assuming that the decay width difference $\Delta\Gamma$ is negligible. Modifications similar to those described here can be made to take into account a non-zero decay width difference.

4.2.4 Time-dependent CP asymmetries in decays to vector-vector final states

Consider B decays to states consisting of two spin-1 particles, such as $J/\psi K^{*0} (\rightarrow K_S^0 \pi^0)$, $J/\psi \phi$, $D^{*+} D^{*-}$ and $\rho^+ \rho^-$, which are eigenstates of charge conjugation but not of parity.²² For such a system, there are three possible final states: in the helicity basis these can be written h_{-1}, h_0, h_{+1} . The h_0 state is an eigenstate of parity, and hence of CP , however CP transforms $h_{+1} \leftrightarrow h_{-1}$ (up to an unobservable phase). In the transversity basis, these states are transformed into $h_{\parallel} = (h_{+1} + h_{-1})/2$ and $h_{\perp} = (h_{+1} - h_{-1})/2$. In this basis all three states are CP eigenstates, and h_{\perp} has the opposite CP to the others.

The amplitude for decays to the transversity basis states are usually given by $A_{0,\perp,\parallel}$, with normalisation such that $|A_0|^2 + |A_{\perp}|^2 + |A_{\parallel}|^2 = 1$. Given the relation between the CP eigenvalues of the states, the effective CP content of the vector-vector state is known if $|A_{\perp}|^2$ is measured. An alternative strategy is to measure just the longitudinally polarised component, $|A_0|^2$ (sometimes denoted by f_{long}), which allows a limit to be set on the effective CP since $|A_{\perp}|^2 \leq |A_{\perp}|^2 + |A_{\parallel}|^2 = 1 - |A_0|^2$. The value of the effective CP content can be used to treat the decay with the same formalism as for CP eigenstates. The most complete treatment for neutral B decays to vector-vector final states is, however, time-dependent angular analysis (also known as time-dependent transversity analysis). In such an analysis, interference between CP -even and CP -odd states pro-

²² This is not true for all vector-vector final states, e.g., $D^{*\pm} \rho^{\mp}$ is clearly not an eigenstate of charge conjugation.

vides additional sensitivity to the weak and strong phases involved.

In most analyses of time-dependent CP asymmetries in decays to vector-vector final states carried out to date, an assumption has been made that each helicity (or transversity) amplitude has the same weak phase. This is a good approximation for decays that are dominated by amplitudes with a single weak phase, such as $B^0 \rightarrow J/\psi K^{*0}$, and is a reasonable approximation in any mode for which only very limited statistics are available. However, for modes that have contributions from amplitudes with different weak phases, the relative size of these contributions can be different for each helicity (or transversity) amplitude, and therefore the time-dependent CP asymmetry parameters can also differ. The most generic analysis, suitable for modes with sufficient statistics, allows for this effect; such an analysis has been carried out by LHCb for the $B^0 \rightarrow J/\psi \rho^0$ decay [258]. An intermediate analysis can allow different parameters for the CP -even and CP -odd components; such an analysis has been carried out by BABAR for the decay $B^0 \rightarrow D^{*+}D^{*-}$ [259]. The independent treatment of each helicity (or transversity) amplitude, as in the latest result on $B_s^0 \rightarrow J/\psi \phi$ [202] (discussed in Sect. 3), becomes increasingly important for high precision measurements.

4.2.5 Time-dependent asymmetries: self-conjugate multiparticle final states

Amplitudes for neutral B decays into self-conjugate multiparticle final states such as $\pi^+\pi^-\pi^0$, $K^+K^-K_S^0$, $\pi^+\pi^-K_S^0$, $J/\psi\pi^+\pi^-$ or $D\pi^0$ with $D \rightarrow K_S^0\pi^+\pi^-$ may be written in terms of CP -even and CP -odd amplitudes. As above, the interference between these terms provides additional sensitivity to the weak and strong phases involved in the decay, and the time-dependence depends on both the sine and cosine of the weak phase difference. In order to perform unbinned maximum likelihood fits, and thereby extract as much information as possible from the distributions, it is necessary to choose a model for the multiparticle decay, and therefore the results acquire some model dependence. In certain cases, model-independent methods are also possible, but the resulting need to bin the Dalitz plot leads to some loss of statistical precision. The number of observables depends on the final state (and on the model used); the key feature is that as long as there are regions where both CP -even and CP -odd amplitudes contribute, the interference terms will be sensitive to the cosine of the weak phase difference. Therefore, these measurements allow distinction between multiple solutions for, e.g., the two values of 2β from the measurement of $\sin(2\beta)$.

We now consider the various notations that have been used in experimental studies of time-dependent asymmetries in decays to self-conjugate multiparticle final states.

$$B^0 \rightarrow D^{(*)}h^0 \text{ with } D \rightarrow K_S^0\pi^+\pi^-$$

The states $D\pi^0$, $D^*\pi^0$, $D\eta$, $D^*\eta$, $D\omega$ are collectively denoted $D^{(*)}h^0$. When the D decay model is fixed, fits to the time-dependent decay distributions can be performed to extract the weak phase difference. However, it is experimentally advantageous to use the sine and cosine of this phase as fit parameters, since these behave as essentially independent parameters, with low correlations and (potentially) rather different uncertainties. A parameter representing CP violation in the B decay can be simultaneously determined. For consistency with other analyses, this could be chosen to be C_f , but could equally well be $|\lambda_f|$, or other possibilities.

Belle performed an analysis of these channels with $\sin(2\phi_1)$ and $\cos(2\phi_1)$ as free parameters [260]. BABAR has performed an analysis in which $|\lambda_f|$ was also determined [261]. Belle has in addition performed a model-independent analysis [262] using as input information about the average strong phase difference between symmetric bins of the Dalitz plot determined by CLEO-c [263].²³ The results of this analysis are measurements of $\sin(2\phi_1)$ and $\cos(2\phi_1)$.

$$B^0 \rightarrow D^{*+}D^{*-}K_S^0$$

The hadronic structure of the $B^0 \rightarrow D^{*+}D^{*-}K_S^0$ decay is not sufficiently well understood to perform a full time-dependent Dalitz plot analysis. Instead, following Ref. [264], BABAR [265] and Belle [266] divide the Dalitz plane in two regions: $m(D^{*+}K_S^0)^2 > m(D^{*-}K_S^0)^2$ ($\eta_y = +1$) and $m(D^{*+}K_S^0)^2 < m(D^{*-}K_S^0)^2$ ($\eta_y = -1$); and then fit to a decay time distribution with asymmetry given by

$$\begin{aligned} \mathcal{A}_f(\Delta t) = \eta_y \frac{J_c}{J_0} \cos(\Delta m \Delta t) - \left[\frac{2J_{s1}}{J_0} \sin(2\beta) \right. \\ \left. + \eta_y \frac{2J_{s2}}{J_0} \cos(2\beta) \right] \sin(\Delta m \Delta t). \end{aligned} \quad (115)$$

The fitted observables are $\frac{J_c}{J_0}$, $\frac{2J_{s1}}{J_0} \sin(2\beta)$ and $\frac{2J_{s2}}{J_0} \cos(2\beta)$, where the parameters J_0 , J_c , J_{s1} and J_{s2} are the integrals over the half Dalitz plane $m(D^{*+}K_S^0)^2 < m(D^{*-}K_S^0)^2$ of the functions $|a|^2 + |\bar{a}|^2$, $|a|^2 - |\bar{a}|^2$, $\text{Re}(\bar{a}a^*)$ and $\text{Im}(\bar{a}a^*)$ respectively, where a and \bar{a} are the decay amplitudes of $B^0 \rightarrow D^{*+}D^{*-}K_S^0$ and $\bar{B}^0 \rightarrow D^{*+}D^{*-}K_S^0$ respectively. The parameter J_{s2} (and hence J_{s2}/J_0) is predicted to be pos-

²³ The external input needed for this analysis is the same as in the model-independent analysis of $B^+ \rightarrow DK^+$ with $D \rightarrow K_S^0\pi^+\pi^-$, discussed in Sect. 4.14.5.

itive; assuming this prediction to be correct, it is possible to determine the sign of $\cos(2\beta)$.

$$B^0 \rightarrow J/\psi \pi^+ \pi^-$$

Amplitude analyses of $B^0 \rightarrow J/\psi \pi^+ \pi^-$ decays [258, 267] show large contributions from the $\rho(770)^0$ and $f_0(500)$ states, together with smaller contributions from higher resonances. Since modelling the $f_0(500)$ structure is challenging [268], it is difficult to determine reliably its associated CP violation parameters. Corresponding parameters for the $J/\psi \rho^0$ decay can, however, be determined. In the LHCb analysis [258], $2\beta^{\text{eff}}$ is determined from the fit; results are then converted into values for S_{CP} and C_{CP} to allow comparison with other modes. Here, the notation S_{CP} and C_{CP} denotes parameters obtained for the $J/\psi \rho^0$ final state accounting for the composition of CP -even and CP -odd amplitudes (while assuming that all amplitudes involve the same phases), so that no dilution occurs. Possible CP violation effects in the other amplitudes contributing to the Dalitz plot are treated as a source of systematic uncertainty.

Amplitude analyses have also been done for the $B_s^0 \rightarrow J/\psi \pi^+ \pi^-$ decay, where the final state is dominated by scalar resonances including the $f_0(980)$ [240, 241]. Time-dependent analyses of this B_s^0 decay allow a determination of $2\beta_s$, as discussed in Sect. 3.

$$B^0 \rightarrow K^+ K^- K^0$$

Studies of $B^0 \rightarrow K^+ K^- K^0$ [269–271] and of the related decay $B^+ \rightarrow K^+ K^- K^+$ [271–273], show that the decay is dominated by a large nonresonant contribution with significant components from the intermediate $K^+ K^-$ resonances $\phi(1020)$, $f_0(980)$, and other higher resonances, as well as a contribution from χ_{c0} .

The full time-dependent Dalitz plot analysis allows the complex amplitudes of each contributing term to be determined from data, including CP violation effects (i.e. allowing the complex amplitude for the B^0 decay to be independent from that for \bar{B}^0 decay), although one amplitude must be fixed to serve as a reference. There are several choices for parametrisation of the complex amplitudes (e.g. real and imaginary part, or magnitude and phase). Similarly, there are various approaches to include CP violation effects. Note that positive definite parameters such as magnitudes are disfavoured in certain circumstances (they inevitably lead to biases for small values). In order to compare results between analyses, it is useful for each experiment to present results in terms of the parameters that can be measured in a Q2B analysis (such as \mathcal{A}_f , S_f , C_f , $\sin(2\beta_f^{\text{eff}})$, $\cos(2\beta_f^{\text{eff}})$, etc.)

In the BABAR analysis of the $B^0 \rightarrow K^+ K^- K^0$ decay [271], the complex amplitude for each resonant contribution is written as

$$\begin{aligned} A_f &= c_f(1 + b_f)e^{i(\phi_f + \delta_f)}, \\ \bar{A}_f &= c_f(1 - b_f)e^{i(\phi_f - \delta_f)}, \end{aligned} \quad (116)$$

where b_f and δ_f introduce CP violation in the magnitude and phase respectively. Belle [270] use the same parametrisation but with a different notation for the parameters.²⁴ (The weak phase in B^0 – \bar{B}^0 mixing (2β) also appears in the full formula for the time-dependent decay distribution.) The Q2B parameter of CP violation in decay is directly related to b_f ,

$$\mathcal{A}_f = \frac{-2b_f}{1 + b_f^2} \approx C_f, \quad (117)$$

and the mixing-induced CP violation parameter can be used to obtain $\sin(2\beta_f^{\text{eff}})$,

$$-\eta_f S_f \approx \frac{1 - b_f^2}{1 + b_f^2} \sin(2\beta_f^{\text{eff}}), \quad (118)$$

where the approximations are exact in the case that $|q/p| = 1$.

Both BABAR [271] and Belle [270] present results for c_f and ϕ_f , for each resonant contribution, and in addition present results for \mathcal{A}_f and β_f^{eff} for $\phi(1020)K^0$, $f_0(980)K^0$ and for the remainder of the contributions to the $K^+ K^- K^0$ Dalitz plot combined. BABAR also present results for the Q2B parameter S_f for these channels. The models used to describe the resonant structure of the Dalitz plot differ, however. Both analyses suffer from symmetries in the likelihood that lead to multiple solutions, from which we select only one for averaging.

$$B^0 \rightarrow \pi^+ \pi^- K_S^0$$

Studies of $B^0 \rightarrow \pi^+ \pi^- K_S^0$ [274, 275] and of the related decay $B^+ \rightarrow \pi^+ \pi^- K^+$ [272, 276–278] show that the decay is dominated by components from intermediate resonances in the $K\pi$ ($K^*(892)$, $K_0^*(1430)$) and $\pi\pi$ ($\rho(770)$, $f_0(980)$, $f_2(1270)$) spectra, together with a poorly understood scalar structure that peaks near $m(\pi\pi) \sim 1300$ MeV/ c^2 and is denoted f_X ²⁵ and a large nonresonant component. There is also a contribution from the χ_{c0} state.

The full time-dependent Dalitz plot analysis allows the complex amplitudes of each contributing term to be determined from data, including CP violation effects. In

²⁴ $(c, b, \phi, \delta) \leftrightarrow (a, c, b, d)$. See Eq. (120).

²⁵ The f_X component may originate from either the $f_0(1370)$ or $f_0(1500)$ resonances, or from interference between those or other states and nonresonant amplitudes in this region.

the BABAR analysis [274], the magnitude and phase of each component (for both B^0 and \bar{B}^0 decays) are measured relative to $B^0 \rightarrow f_0(980)K_S^0$, using the following parametrisation

$$A_f = |A_f|e^{i \arg(A_f)} \quad \bar{A}_f = |\bar{A}_f|e^{i \arg(\bar{A}_f)}. \tag{119}$$

In the Belle analysis [275], the $B^0 \rightarrow K^{*+}\pi^-$ amplitude is chosen as the reference, and the amplitudes are parametrised as

$$A_f = a_f(1 + c_f)e^{i(b_f+d_f)} \quad \bar{A}_f = a_f(1 - c_f)e^{i(b_f-d_f)}. \tag{120}$$

In both cases, the results are translated into Q2B parameters such as $2\beta_f^{\text{eff}}$, S_f , C_f for each CP eigenstate f , and parameters of CP violation in decay for each flavour-specific state. Relative phase differences between resonant terms are also extracted.

$$B^0 \rightarrow \pi^+\pi^-\pi^0$$

The $B^0 \rightarrow \pi^+\pi^-\pi^0$ decay is dominated by intermediate ρ resonances. Though it is possible, as above, to determine directly the complex amplitudes for each component, an alternative approach [279,280] has been used by both BABAR [281,282] and Belle [283,284]. The amplitudes for B^0 and \bar{B}^0 decays to $\pi^+\pi^-\pi^0$ are written as

$$\begin{aligned} A_{3\pi} &= f_+A_+ + f_-A_- + f_0A_0, \\ \bar{A}_{3\pi} &= f_+\bar{A}_+ + f_-\bar{A}_- + f_0\bar{A}_0, \end{aligned} \tag{121}$$

respectively. The symbols A_+ , A_- and A_0 represent the complex decay amplitudes for $B^0 \rightarrow \rho^+\pi^-$, $B^0 \rightarrow \rho^-\pi^+$ and $B^0 \rightarrow \rho^0\pi^0$ while \bar{A}_+ , \bar{A}_- and \bar{A}_0 represent those for $\bar{B}^0 \rightarrow \rho^+\pi^-$, $\bar{B}^0 \rightarrow \rho^-\pi^+$ and $\bar{B}^0 \rightarrow \rho^0\pi^0$ respectively. The terms f_+ , f_- and f_0 incorporate kinematic and dynamical factors and depend on the Dalitz plot coordinates. The full time-dependent decay distribution can then be written in terms of 27 free parameters, one for each coefficient of the form factor bilinears, as listed in Table 22. These parameters are sometimes referred to as ‘‘the U s and I s’’, and can be expressed in terms of A_+ , A_- , A_0 , \bar{A}_+ , \bar{A}_- and \bar{A}_0 . If the full set of parameters is determined, together with their correlations, other parameters, such as weak and strong phases, parameters of CP violation in decay, etc., can be subsequently extracted. Note that one of the parameters (typically U_+^+) is often fixed to unity to provide a reference; this does not affect the analysis.

4.2.6 Time-dependent CP asymmetries in decays to non- CP eigenstates

Consider a non- CP eigenstate f , and its conjugate \bar{f} . For neutral B decays to these final states, there are four ampli-

Table 22 Definitions of the U and I coefficients. Modified from Ref. [281]

Parameter	Description
U_+^+	Coefficient of $ f_+ ^2$
U_0^+	Coefficient of $ f_0 ^2$
U_-^+	Coefficient of $ f_- ^2$
U_0^-	Coefficient of $ f_0 ^2 \cos(\Delta m \Delta t)$
U_-^-	Coefficient of $ f_- ^2 \cos(\Delta m \Delta t)$
U_+^-	Coefficient of $ f_+ ^2 \cos(\Delta m \Delta t)$
I_0	Coefficient of $ f_0 ^2 \sin(\Delta m \Delta t)$
I_-	Coefficient of $ f_- ^2 \sin(\Delta m \Delta t)$
I_+	Coefficient of $ f_+ ^2 \sin(\Delta m \Delta t)$
$U_{+-}^{+, \text{Im}}$	Coefficient of $\text{Im}[f_+ f_-^*]$
$U_{+-}^{+, \text{Re}}$	Coefficient of $\text{Re}[f_+ f_-^*]$
$U_{+-}^{-, \text{Im}}$	Coefficient of $\text{Im}[f_+ f_-^*] \cos(\Delta m \Delta t)$
$U_{+-}^{-, \text{Re}}$	Coefficient of $\text{Re}[f_+ f_-^*] \cos(\Delta m \Delta t)$
I_{+-}^{Im}	Coefficient of $\text{Im}[f_+ f_-^*] \sin(\Delta m \Delta t)$
I_{+-}^{Re}	Coefficient of $\text{Re}[f_+ f_-^*] \sin(\Delta m \Delta t)$
$U_{+0}^{+, \text{Im}}$	Coefficient of $\text{Im}[f_+ f_0^*]$
$U_{+0}^{+, \text{Re}}$	Coefficient of $\text{Re}[f_+ f_0^*]$
$U_{+0}^{-, \text{Im}}$	Coefficient of $\text{Im}[f_+ f_0^*] \cos(\Delta m \Delta t)$
$U_{+0}^{-, \text{Re}}$	Coefficient of $\text{Re}[f_+ f_0^*] \cos(\Delta m \Delta t)$
I_{+0}^{Im}	Coefficient of $\text{Im}[f_+ f_0^*] \sin(\Delta m \Delta t)$
I_{+0}^{Re}	Coefficient of $\text{Re}[f_+ f_0^*] \sin(\Delta m \Delta t)$
$U_{-0}^{+, \text{Im}}$	Coefficient of $\text{Im}[f_- f_0^*]$
$U_{-0}^{+, \text{Re}}$	Coefficient of $\text{Re}[f_- f_0^*]$
$U_{-0}^{-, \text{Im}}$	Coefficient of $\text{Im}[f_- f_0^*] \cos(\Delta m \Delta t)$
$U_{-0}^{-, \text{Re}}$	Coefficient of $\text{Re}[f_- f_0^*] \cos(\Delta m \Delta t)$
I_{-0}^{Im}	Coefficient of $\text{Im}[f_- f_0^*] \sin(\Delta m \Delta t)$
I_{-0}^{Re}	Coefficient of $\text{Re}[f_- f_0^*] \sin(\Delta m \Delta t)$

tudes to consider: those for B^0 to decay to f and \bar{f} (A_f and $A_{\bar{f}}$, respectively), and the equivalents for \bar{B}^0 (\bar{A}_f and $\bar{A}_{\bar{f}}$). If CP is conserved in the decay, then $A_f = \bar{A}_{\bar{f}}$ and $A_{\bar{f}} = \bar{A}_f$.

The time-dependent decay distributions can be written in many different ways. Here, we follow Sect. 4.2.2 and define $\lambda_f = \frac{q}{p} \frac{\bar{A}_f}{A_f}$ and $\lambda_{\bar{f}} = \frac{q}{p} \frac{\bar{A}_{\bar{f}}}{A_{\bar{f}}}$. The time-dependent CP asymmetries that are sensitive to mixing-induced CP violation effects then follow Eq. (107):

$$\begin{aligned} A_f(\Delta t) &\equiv \frac{\Gamma_{\bar{B}^0 \rightarrow f}(\Delta t) - \Gamma_{B^0 \rightarrow f}(\Delta t)}{\Gamma_{\bar{B}^0 \rightarrow f}(\Delta t) + \Gamma_{B^0 \rightarrow f}(\Delta t)} \\ &= S_f \sin(\Delta m \Delta t) - C_f \cos(\Delta m \Delta t), \end{aligned} \tag{122}$$

$$\begin{aligned} A_{\bar{f}}(\Delta t) &\equiv \frac{\Gamma_{\bar{B}^0 \rightarrow \bar{f}}(\Delta t) - \Gamma_{B^0 \rightarrow \bar{f}}(\Delta t)}{\Gamma_{\bar{B}^0 \rightarrow \bar{f}}(\Delta t) + \Gamma_{B^0 \rightarrow \bar{f}}(\Delta t)} \\ &= S_{\bar{f}} \sin(\Delta m \Delta t) - C_{\bar{f}} \cos(\Delta m \Delta t), \end{aligned} \tag{123}$$

with the definitions of the parameters $C_f, S_f, C_{\bar{f}}$ and $S_{\bar{f}}$, following Eqs. (108) and (109).

The time-dependent decay rates are given by

$$\Gamma_{B^0 \rightarrow f}(\Delta t) = \frac{e^{-|\Delta t|/\tau(B^0)}}{8\tau(B^0)}(1 + \langle \mathcal{A}_{f\bar{f}} \rangle) \times \left[1 + S_f \sin(\Delta m \Delta t) - C_f \cos(\Delta m \Delta t) \right], \tag{124}$$

$$\Gamma_{B^0 \rightarrow \bar{f}}(\Delta t) = \frac{e^{-|\Delta t|/\tau(B^0)}}{8\tau(B^0)}(1 + \langle \mathcal{A}_{f\bar{f}} \rangle) \times \left[1 - S_f \sin(\Delta m \Delta t) + C_f \cos(\Delta m \Delta t) \right], \tag{125}$$

$$\Gamma_{\bar{B}^0 \rightarrow f}(\Delta t) = \frac{e^{-|\Delta t|/\tau(B^0)}}{8\tau(B^0)}(1 - \langle \mathcal{A}_{f\bar{f}} \rangle) \times \left[1 + S_{\bar{f}} \sin(\Delta m \Delta t) - C_{\bar{f}} \cos(\Delta m \Delta t) \right], \tag{126}$$

$$\Gamma_{\bar{B}^0 \rightarrow \bar{f}}(\Delta t) = \frac{e^{-|\Delta t|/\tau(B^0)}}{8\tau(B^0)}(1 - \langle \mathcal{A}_{f\bar{f}} \rangle) \times \left[1 - S_{\bar{f}} \sin(\Delta m \Delta t) + C_{\bar{f}} \cos(\Delta m \Delta t) \right], \tag{127}$$

where the time-independent parameter $\langle \mathcal{A}_{f\bar{f}} \rangle$ represents an overall asymmetry in the production of the f and \bar{f} final states,²⁶

$$\langle \mathcal{A}_{f\bar{f}} \rangle = \frac{\left(|A_f|^2 + |\bar{A}_f|^2 \right) - \left(|A_{\bar{f}}|^2 + |\bar{A}_{\bar{f}}|^2 \right)}{\left(|A_f|^2 + |\bar{A}_f|^2 \right) + \left(|A_{\bar{f}}|^2 + |\bar{A}_{\bar{f}}|^2 \right)}. \tag{128}$$

Assuming $|q/p| = 1$, i.e. absence of CP violation in mixing, the parameters C_f and $C_{\bar{f}}$ can also be written in terms of the decay amplitudes as follows:

$$C_f = \frac{|A_f|^2 - |\bar{A}_f|^2}{|A_f|^2 + |\bar{A}_f|^2} \quad \text{and} \quad C_{\bar{f}} = \frac{|A_{\bar{f}}|^2 - |\bar{A}_{\bar{f}}|^2}{|A_{\bar{f}}|^2 + |\bar{A}_{\bar{f}}|^2}, \tag{129}$$

giving asymmetries in the decay amplitudes of B^0 and \bar{B}^0 to the final states f and \bar{f} respectively. In this notation, the conditions for absence of CP violation in decay are $\langle \mathcal{A}_{f\bar{f}} \rangle = 0$ and $C_f = -C_{\bar{f}}$. Note that C_f and $C_{\bar{f}}$ are typically non-zero; e.g., for a flavour-specific final state, $\bar{A}_f = A_{\bar{f}} = 0$

($A_f = \bar{A}_{\bar{f}} = 0$), they take the values $C_f = -C_{\bar{f}} = 1$ ($C_f = -C_{\bar{f}} = -1$).

The coefficients of the sine terms contain information about the weak phase. In the case that each decay amplitude contains only a single weak phase (i.e., no CP violation in decay as well as none in mixing), these terms can be written as

$$S_f = \frac{-2|A_f||\bar{A}_f| \sin(\phi_{\text{mix}} + \phi_{\text{dec}} - \delta_f)}{|A_f|^2 + |\bar{A}_f|^2} \quad \text{and} \quad S_{\bar{f}} = \frac{-2|A_{\bar{f}}||\bar{A}_{\bar{f}}| \sin(\phi_{\text{mix}} + \phi_{\text{dec}} + \delta_f)}{|A_{\bar{f}}|^2 + |\bar{A}_{\bar{f}}|^2}, \tag{130}$$

where δ_f is the strong phase difference between the decay amplitudes. If there is no CP violation, the condition $S_f = -S_{\bar{f}}$ holds. If decay amplitudes with different weak and strong phases contribute, no clean interpretation of S_f and $S_{\bar{f}}$ is possible.

The conditions for CP invariance $C_f = -C_{\bar{f}}$ and $S_f = -S_{\bar{f}}$ motivate a rotation of the parameters:

$$S_{f\bar{f}} = \frac{S_f + S_{\bar{f}}}{2}, \quad \Delta S_{f\bar{f}} = \frac{S_f - S_{\bar{f}}}{2} \\ C_{f\bar{f}} = \frac{C_f + C_{\bar{f}}}{2}, \quad \Delta C_{f\bar{f}} = \frac{C_f - C_{\bar{f}}}{2}. \tag{131}$$

With these parameters, the CP invariance conditions become $S_{f\bar{f}} = 0$ and $C_{f\bar{f}} = 0$. The parameter $\Delta C_{f\bar{f}}$ gives a measure of the ‘‘flavour-specificity’’ of the decay: $\Delta C_{f\bar{f}} = \pm 1$ corresponds to a completely flavour-specific decay, in which no interference between decays with and without mixing can occur, while $\Delta C_{f\bar{f}} = 0$ results in maximum sensitivity to mixing-induced CP violation. The parameter $\Delta S_{f\bar{f}}$ is related to the strong phase difference between the decay amplitudes of the B^0 meson to the f and to \bar{f} final states. We note that the observables of Eq. (131) exhibit experimental correlations (typically of $\sim 20\%$, depending on the tagging purity, and other effects) between $S_{f\bar{f}}$ and $\Delta S_{f\bar{f}}$, and between $C_{f\bar{f}}$ and $\Delta C_{f\bar{f}}$. On the other hand, the final state specific observables of Eqs. (124)–(127) tend to have low correlations.

Alternatively, if we recall that the CP invariance conditions at the decay amplitude level are $A_f = \bar{A}_{\bar{f}}$ and $A_{\bar{f}} = \bar{A}_f$, we are led to consider the parameters [252]

$$\mathcal{A}_{f\bar{f}} = \frac{|\bar{A}_{\bar{f}}|^2 - |A_f|^2}{|\bar{A}_{\bar{f}}|^2 + |A_f|^2} \quad \text{and} \quad \mathcal{A}_{\bar{f}f} = \frac{|\bar{A}_f|^2 - |A_{\bar{f}}|^2}{|\bar{A}_f|^2 + |A_{\bar{f}}|^2}. \tag{132}$$

These are sometimes considered more physically intuitive parameters since they characterise CP violation in decay in decays with particular topologies. For example, in the case of $B^0 \rightarrow \rho^\pm \pi^\mp$ (choosing $f = \rho^+ \pi^-$ and $\bar{f} = \rho^- \pi^+$), $\mathcal{A}_{f\bar{f}}$ (also denoted $\mathcal{A}_{\rho\pi}^{+-}$) parametrises CP violation in decays in

²⁶ This parameter is often denoted \mathcal{A}_f (or \mathcal{A}_{CP}), but here we avoid this notation to prevent confusion with the time-dependent CP asymmetry.

which the produced ρ meson does not contain the spectator quark, while $\mathcal{A}_{\bar{f}f}$ (also denoted $\mathcal{A}_{\rho\pi^+}$) parametrises CP violation in decays in which it does. Note that we have again followed the sign convention that the asymmetry is the difference between the rate involving a b quark and that involving a \bar{b} quark, cf. Eq. (104). Of course, these parameters are not independent of the other sets of parameters given above, and can be written

$$\begin{aligned} \mathcal{A}_{f\bar{f}} &= -\frac{\langle \mathcal{A}_{f\bar{f}} \rangle + C_{f\bar{f}} + \langle \mathcal{A}_{f\bar{f}} \rangle \Delta C_{f\bar{f}}}{1 + \Delta C_{f\bar{f}} + \langle \mathcal{A}_{f\bar{f}} \rangle C_{f\bar{f}}} \quad \text{and} \\ \mathcal{A}_{\bar{f}f} &= \frac{-\langle \mathcal{A}_{f\bar{f}} \rangle + C_{f\bar{f}} + \langle \mathcal{A}_{f\bar{f}} \rangle \Delta C_{f\bar{f}}}{-1 + \Delta C_{f\bar{f}} + \langle \mathcal{A}_{f\bar{f}} \rangle C_{f\bar{f}}}. \end{aligned} \tag{133}$$

They usually exhibit strong correlations.

We now consider the various notations used in experimental studies of time-dependent CP asymmetries in decays to non- CP eigenstates.

$$B^0 \rightarrow D^{*\pm} D^\mp$$

The $(\langle \mathcal{A}_{f\bar{f}} \rangle, C_f, S_f, C_{\bar{f}}, S_{\bar{f}})$ set of parameters was used in early publications by both BABAR [285] and Belle [286] (albeit with slightly different notations) in the $D^{*\pm} D^\mp$ system ($f = D^{*+} D^-$, $\bar{f} = D^{*-} D^+$). In their most recent paper on this topic Belle [287] instead used the parametrisation $(A_{D^*D}, S_{D^*D}, \Delta S_{D^*D}, C_{D^*D}, \Delta C_{D^*D})$, while BABAR [259] give results in both sets of parameters. We therefore use the $(A_{D^*D}, S_{D^*D}, \Delta S_{D^*D}, C_{D^*D}, \Delta C_{D^*D})$ set.

$$B^0 \rightarrow \rho^\pm \pi^\mp$$

In the $\rho^\pm \pi^\mp$ system, the $(\langle \mathcal{A}_{f\bar{f}} \rangle, C_{f\bar{f}}, S_{f\bar{f}}, \Delta C_{f\bar{f}}, \Delta S_{f\bar{f}})$ set of parameters has been used originally by BABAR [288] and Belle [289], in the Q2B approximation; the exact names²⁷ used in this case are $(\mathcal{A}_{CP}^{\rho\pi}, C_{\rho\pi}, S_{\rho\pi}, \Delta C_{\rho\pi}, \Delta S_{\rho\pi})$, and these names are also used in this document.

Since $\rho^\pm \pi^\mp$ is reconstructed in the final state $\pi^+ \pi^- \pi^0$, the interference between the ρ resonances can provide additional information about the phases (see Sect. 4.2.5). Both BABAR [281] and Belle [283, 284] have performed time-dependent Dalitz plot analyses, from which the weak phase α is directly extracted. In such an analysis, the measured Q2B parameters are also naturally corrected for interference effects.

$$B^0 \rightarrow D^\mp \pi^\pm, D^{*\mp} \pi^\pm, D^\mp \rho^\pm$$

Time-dependent CP analyses have also been performed for the final states $D^\mp \pi^\pm$, $D^{*\mp} \pi^\pm$ and $D^\mp \rho^\pm$. In these theoretically clean cases, no penguin contributions are possible, so there is no CP violation in decay. Furthermore, due

to the smallness of the ratio of the magnitudes of the suppressed ($b \rightarrow u$) and favoured ($b \rightarrow c$) amplitudes (denoted R_f), to a very good approximation, $C_f = -C_{\bar{f}} = 1$ (using $f = D^{(*)-} h^+$, $\bar{f} = D^{(*)+} h^-$, $h = \pi, \rho$), and the coefficients of the sine terms are given by

$$\begin{aligned} S_f &= -2R_f \sin(\phi_{\text{mix}} + \phi_{\text{dec}} - \delta_f) \quad \text{and} \\ S_{\bar{f}} &= -2R_f \sin(\phi_{\text{mix}} + \phi_{\text{dec}} + \delta_f). \end{aligned} \tag{134}$$

Thus weak phase information can be cleanly obtained from measurements of S_f and $S_{\bar{f}}$, although external information on at least one of R_f or δ_f is necessary. (Note that $\phi_{\text{mix}} + \phi_{\text{dec}} = 2\beta + \gamma \equiv 2\phi_1 + \phi_3$ for all the decay modes in question, while R_f and δ_f depend on the decay mode.)

Again, different notations have been used in the literature. BABAR [290, 291] defines the time-dependent probability function by

$$\begin{aligned} f^\pm(\eta, \Delta t) &= \frac{e^{-|\Delta t|/\tau}}{4\tau} \\ &\times \left[1 \mp S_\zeta \sin(\Delta m \Delta t) \mp \eta C_\zeta \cos(\Delta m \Delta t) \right], \end{aligned} \tag{135}$$

where the upper (lower) sign corresponds to the tagging meson being a B^0 (\bar{B}^0). The parameters η and ζ take the values $+1$ and $+(-1$ and $-)$ when the final state is, e.g., $D^- \pi^+$ ($D^+ \pi^-$). However, in the fit, the substitutions $C_\zeta = 1$ and $S_\zeta = a \mp \eta b_i - \eta c_i$ are made, where the subscript i denotes tagging category. Neglecting b terms,

$$\begin{aligned} S_+ &= a - c \quad \text{and} \quad S_- = a + c \Leftrightarrow \\ a &= (S_+ + S_-)/2 \quad \text{and} \\ c &= (S_- - S_+)/2, \end{aligned} \tag{136}$$

in analogy to the parameters of Eq. (131). These are motivated by the possibility of CP violation on the tag side [292], which is absent for semileptonic B decays (mostly lepton tags). The parameter a is not affected by tag side CP violation. The parameter b only depends on tag side CP violation parameters and is not directly useful for determining UT angles. A clean interpretation of the c parameter is only possible for lepton-tagged events, so the BABAR measurements report c measured with those events only.

The parameters used by Belle in the analysis using partially reconstructed B decays [293], are similar to the S_ζ parameters defined above. However, in the Belle convention, a tagging B^0 corresponds to a $+$ sign in front of the sine coefficient; furthermore the correspondence between the super/subscript and the final state is opposite, so that S_\pm (BABAR) = $-S^\mp$ (Belle). In this analysis, only lepton tags are used, so there is no effect from tag side CP violation. In the Belle analysis using fully reconstructed B decays [294],

²⁷ BABAR has used the notations $A_{CP}^{\rho\pi}$ [288] and $\mathcal{A}_{\rho\pi}$ [281] in place of $\mathcal{A}_{CP}^{\rho\pi}$.

Table 23 Conversion between the various notations used for CP violation parameters in the $D^\pm \pi^\mp$, $D^{*\pm} \pi^\mp$ and $D^\pm \rho^\mp$ systems. The b_i terms used by BABAR have been neglected. Recall that $(\alpha, \beta, \gamma) \equiv (\phi_2, \phi_1, \phi_3)$

	BABAR	Belle partial rec.	Belle full rec.
$S_{D^+\pi^-}$	$-S_- = -(a + c_i)$	–	$2R_{D\pi} \sin(2\phi_1 + \phi_3 + \delta_{D\pi})$
$S_{D^-\pi^+}$	$-S_+ = -(a - c_i)$	–	$2R_{D\pi} \sin(2\phi_1 + \phi_3 - \delta_{D\pi})$
$S_{D^{*+}\pi^-}$	$-S_- = -(a + c_i)$	S^+	$-2R_{D^*\pi} \sin(2\phi_1 + \phi_3 + \delta_{D^*\pi})$
$S_{D^{*-}\pi^+}$	$-S_+ = -(a - c_i)$	S^-	$-2R_{D^*\pi} \sin(2\phi_1 + \phi_3 - \delta_{D^*\pi})$
$S_{D^+\rho^-}$	$-S_- = -(a + c_i)$	–	–
$S_{D^-\rho^+}$	$-S_+ = -(a - c_i)$	–	–

Table 24 Translations used to convert the parameters measured by Belle to the parameters used for averaging in this document. The angular momentum factor L is -1 for $D^*\pi$ and $+1$ for $D\pi$. Recall that $(\alpha, \beta, \gamma) \equiv (\phi_2, \phi_1, \phi_3)$

	$D^*\pi$ partial rec.	$D^{(*)}\pi$ full rec.
a	$-(S^+ + S^-)$	$\frac{1}{2}(-1)^{L+1} \left(2R_{D^{(*)}\pi} \sin(2\phi_1 + \phi_3 + \delta_{D^{(*)}\pi}) + 2R_{D^{(*)}\pi} \sin(2\phi_1 + \phi_3 - \delta_{D^{(*)}\pi}) \right)$
c	$-(S^+ - S^-)$	$\frac{1}{2}(-1)^{L+1} \left(2R_{D^{(*)}\pi} \sin(2\phi_1 + \phi_3 + \delta_{D^{(*)}\pi}) - 2R_{D^{(*)}\pi} \sin(2\phi_1 + \phi_3 - \delta_{D^{(*)}\pi}) \right)$

this effect is measured and taken into account using $D^*\ell\nu$ decays; in neither Belle analysis are the a , b and c parameters used. In the latter case, the measured parameters are $2R_{D^{(*)}\pi} \sin(2\phi_1 + \phi_3 \pm \delta_{D^{(*)}\pi})$; the definition is such that S^\pm (Belle) = $-2R_{D^*\pi} \sin(2\phi_1 + \phi_3 \pm \delta_{D^*\pi})$. However, the definition includes an angular momentum factor $(-1)^L$ [295], and so for the results in the $D\pi$ system, there is an additional factor of -1 in the conversion.

Explicitly, the conversion then reads as given in Table 23, where we have neglected the b_i terms used by BABAR (which are zero in the absence of tag side CP violation). For the averages in this document, we use the a and c parameters, and give the explicit translations used in Table 24. It is to be fervently hoped that the experiments will converge on a common notation in future.

$$B_s^0 \rightarrow D_s^\mp K^\pm$$

The phenomenology of $B_s^0 \rightarrow D_s^\mp K^\pm$ decays is similar to that for $B^0 \rightarrow D^\mp \pi^\pm$, with some important caveats. The two amplitudes $b \rightarrow u$ and $b \rightarrow c$ amplitudes have the same level of Cabibbo-suppression (i.e. are of the same order in λ) though the former is suppressed by $\sqrt{\rho^2 + \eta^2}$. The large value of the ratio R of their magnitudes allows it to be determined from data, as the deviation of C_f and $C_{\bar{f}}$ from unity (in magnitude) can be observed. Moreover, the non-zero value of $\Delta\Gamma_s$ allows the determination of additional terms, $A_f^{\Delta\Gamma}$ and $A_{\bar{f}}^{\Delta\Gamma}$ (see Sect. 4.2.3), that break ambiguities in the solutions for $\phi_{\text{mix}} + \phi_{\text{dec}}$, which for $B_s^0 \rightarrow D_s^\mp K^\pm$ decays is equal to $\gamma - 2\beta_s$.

LHCb [296] has performed such an analysis with $B_s^0 \rightarrow D_s^\mp K^\pm$ decays. The absence of CP violation in decay is

assumed, and the parameters that are determined from the fit are labelled C , $A^{\Delta\Gamma}$, $\bar{A}^{\Delta\Gamma}$, S , \bar{S} . These are trivially related to the definitions used in this section.

Time-dependent asymmetries in radiative B decays

As a special case of decays to non- CP eigenstates, let us consider radiative B decays. Here, the emitted photon has a distinct helicity, which is in principle observable, but in practice is not usually measured. Thus the measured time-dependent decay rates for B^0 decays are given by [297,298]

$$\begin{aligned} \Gamma_{\bar{B}^0 \rightarrow X\gamma}(\Delta t) &= \Gamma_{\bar{B}^0 \rightarrow X\gamma_L}(\Delta t) + \Gamma_{\bar{B}^0 \rightarrow X\gamma_R}(\Delta t) \\ &= \frac{e^{-|\Delta t|/\tau(B^0)}}{4\tau(B^0)} [1 + (S_L + S_R) \times \sin(\Delta m \Delta t) \\ &\quad - (C_L + C_R) \cos(\Delta m \Delta t)], \end{aligned} \tag{137}$$

$$\begin{aligned} \Gamma_{B^0 \rightarrow X\gamma}(\Delta t) &= \Gamma_{B^0 \rightarrow X\gamma_L}(\Delta t) + \Gamma_{B^0 \rightarrow X\gamma_R}(\Delta t) \\ &= \frac{e^{-|\Delta t|/\tau(B^0)}}{4\tau(B^0)} \left[1 - (S_L + S_R) \times \sin(\Delta m \Delta t) \right. \\ &\quad \left. + (C_L + C_R) \cos(\Delta m \Delta t) \right], \end{aligned} \tag{138}$$

where in place of the subscripts f and \bar{f} we have used L and R to indicate the photon helicity. In order for interference between decays with and without B^0 - \bar{B}^0 mixing to occur, the X system must not be flavour-specific, e.g., in case of $B^0 \rightarrow K^{*0}\gamma$, the final state must be $K_S^0\pi^0\gamma$. The sign of the sine term depends on the C eigenvalue of the X system. At leading order, the photons from $b \rightarrow q\gamma$ ($\bar{b} \rightarrow \bar{q}\gamma$) are predominantly left (right) polarised, with

corrections of order of m_q/m_b , thus interference effects are suppressed. Higher-order effects can lead to corrections of order Λ_{QCD}/m_b [299,300], though explicit calculations indicate that such corrections may be small for exclusive final states [301,302]. The predicted smallness of the S terms in the Standard Model results in sensitivity to new physics contributions.

The formalism discussed above is valid for any radiative decay to a final state where the hadronic system is an eigenstate of C . In addition to $K_S^0\pi^0\gamma$, experiments have presented results using B^0 decays to $K_S^0\eta\gamma$, $K_S^0\rho^0\gamma$ and $K_S^0\phi\gamma$. For the case of the $K_S^0\rho^0\gamma$ final state, particular care is needed, as due to the non-negligible width of the ρ^0 meson, decays selected as $B^0 \rightarrow K_S^0\rho^0\gamma$ can include a significant contribution from $K^{*\pm}\pi^\mp\gamma$ decays, which are flavour-specific and do not have the same oscillation phenomenology. It is therefore necessary to correct the fitted asymmetry parameter for a ‘‘dilution factor’’.

In the case of radiative B_s^0 decays, the time-dependent decay rates of Eqs. (137) and (138) must be modified, in a similar way as discussed in Sect. 4.2.3, to account for the non-zero value of $\Delta\Gamma_s$. Thus, for decays such as $B_s^0 \rightarrow \phi\gamma$, there is an additional observable, $A_{\phi\gamma}^{\Delta\Gamma}$, which can be determined from an untagged effective lifetime measurement [303].

4.2.7 Asymmetries in $B \rightarrow D^{(*)}K^{(*)}$ decays

CP asymmetries in $B \rightarrow D^{(*)}K^{(*)}$ decays are sensitive to γ . The neutral $D^{(*)}$ meson produced is an admixture of $D^{(*)0}$ (produced by a $b \rightarrow c$ transition) and $\bar{D}^{(*)0}$ (produced by a colour-suppressed $b \rightarrow u$ transition) states. If the final state is chosen so that both $D^{(*)0}$ and $\bar{D}^{(*)0}$ can contribute, the two amplitudes interfere, and the resulting observables are sensitive to γ , the relative weak phase between the two B decay amplitudes [304]. Various methods have been proposed to exploit this interference, including those where the neutral D meson is reconstructed as a CP eigenstate (GLW) [305,306], in a suppressed final state (ADS) [307,308], or in a self-conjugate three-body final state, such as $K_S^0\pi^+\pi^-$ (GGSZ or Dalitz) [309,310]. It should be emphasised that while each method differs in the choice of D decay, they are all sensitive to the same parameters of the B decay, and can be considered as variations of the same technique.

Consider the case of $B^\mp \rightarrow DK^\mp$, with D decaying to a final state f , which is accessible from both D^0 and \bar{D}^0 . We can write the decay rates for B^- and B^+ (Γ_\mp), the charge averaged rate [$\Gamma = (\Gamma_- + \Gamma_+)/2$] and the charge asymmetry ($A = (\Gamma_- - \Gamma_+)/(\Gamma_- + \Gamma_+)$), see Eq. (104)] as

$$\Gamma_\mp \propto r_B^2 + r_D^2 + 2r_B r_D \cos(\delta_B + \delta_D \mp \gamma), \tag{139}$$

$$\Gamma \propto r_B^2 + r_D^2 + 2r_B r_D \cos(\delta_B + \delta_D) \cos(\gamma), \tag{140}$$

$$A = \frac{2r_B r_D \sin(\delta_B + \delta_D) \sin(\gamma)}{r_B^2 + r_D^2 + 2r_B r_D \cos(\delta_B + \delta_D) \cos(\gamma)}, \tag{141}$$

where the ratio of B decay amplitudes²⁸ is usually defined to be less than one,

$$r_B = \left| \frac{A(B^- \rightarrow \bar{D}^0 K^-)}{A(B^- \rightarrow D^0 K^-)} \right| = \left| \frac{A(B^+ \rightarrow D^0 K^+)}{A(B^+ \rightarrow \bar{D}^0 K^+)} \right|, \tag{142}$$

and the ratio of D decay amplitudes is correspondingly defined by

$$r_D = \left| \frac{A(D^0 \rightarrow f)}{A(\bar{D}^0 \rightarrow f)} \right|. \tag{143}$$

The relation between B^- and B^+ amplitudes given in Eq. (142) is a result of their being only one weak phase contributing to each amplitude in the Standard Model, which is the source of the theoretical cleanliness of this approach to measure γ [311]. The strong phase differences between the B and D decay amplitudes are given by δ_B and δ_D , respectively. The values of r_D and δ_D depend on the final state f : for the GLW analysis, $r_D = 1$ and δ_D is trivial (either zero or π); for other modes, values of r_D and δ_D are not trivial and for multi-body final states they vary across the phase space. This can be quantified either by an explicit D decay amplitude model or by model-independent information. In the case that the multi-body final state is treated inclusively, the formalism is modified by the inclusion of a coherence factor, usually denoted κ , while r_D and δ_D become effectively parameters corresponding to amplitude-weighted averages across the phase space.

Note that, for given values of r_B and r_D , the maximum size of A (at $\sin(\delta_B + \delta_D) = 1$) is $2r_B r_D \sin(\gamma)/(r_B^2 + r_D^2)$. Thus even for D decay modes with small r_D , large asymmetries, and hence sensitivity to γ , may occur for B decay modes with similar values of r_B . For this reason, the ADS analysis of the decay $B^\mp \rightarrow D\pi^\mp$ is also of interest.

The expressions of Eqs. (139)–(143) are for a specific point in phase space, and therefore are relevant where both B and D decays are to two-body final states. Additional coherence factors enter the expressions when the B decay is to a multibody final state (further discussion of multibody D decays can be found below). In particular, experiments have studied $B^+ \rightarrow DK^*(892)^+$, $B^0 \rightarrow DK^*(892)^0$ and $B^+ \rightarrow DK^+\pi^+\pi^-$ decays. Considering, for concreteness, the $B \rightarrow DK^*(892)$ case, the non-negligible width of the $K^*(892)$ resonance implies that contributions from other

²⁸ Note that here we use the notation r_B to denote the ratio of B decay amplitudes, whereas in Sect. 4.2.6 we used, e.g., $R_{D\pi}$, for a rather similar quantity. The reason is that here we need to be concerned also with D decay amplitudes, and so it is convenient to use the subscript to denote the decaying particle. Hopefully, using r in place of R will reduce the potential for confusion.

$B \rightarrow DK\pi$ decays can pass the selection requirements. Their effect on the Q2B analysis can be accounted for with a coherence factor [312], usually denoted κ , which tends to unity in the limit that the $K^*(892)$ resonance is the only signal amplitude contributing in the selected region of phase space. In this case, the hadronic parameters r_B and δ_B become effectively weighted averages across the selected phase space of the magnitude ratio and relative strong phase between the CKM-suppressed and -favoured amplitudes; these effective parameters are denoted \bar{r}_B and $\bar{\delta}_B$ (the notations r_S, δ_S and $r_{\bar{S}}, \delta_{\bar{S}}$ are also found in the literature). An alternative, and in certain cases more advantageous, approach is Dalitz plot analysis of the full $B \rightarrow DK\pi$ phase space [313,314].

$B \rightarrow D^{(*)}K^{(*)}$ with $D \rightarrow CP$ eigenstate decays

In the GLW analysis, the measured quantities are the partial rate asymmetry and the charge averaged rate, which are measured both for CP -even and CP -odd D decays. The latter is defined as

$$R_{CP} = \frac{2\Gamma(B^+ \rightarrow D_{CP}K^+)}{\Gamma(B^+ \rightarrow \bar{D}^0K^+)}. \tag{144}$$

It is experimentally convenient to measure R_{CP} using a double ratio,

$$R_{CP} = \frac{\Gamma(B^+ \rightarrow D_{CP}K^+) / \Gamma(B^+ \rightarrow \bar{D}^0K^+)}{\Gamma(B^+ \rightarrow D_{CP}\pi^+) / \Gamma(B^+ \rightarrow \bar{D}^0\pi^+)} \tag{145}$$

that is normalised both to the rate for the favoured $\bar{D}^0 \rightarrow K^+\pi^-$ decay, and to the equivalent quantities for $B^+ \rightarrow D\pi^+$ decays (charge conjugate processes are implicitly included in Eqs. (144) and (145)). In this way the constant of proportionality drops out of Eq. (140). Equation (145) is exact in the limit that the contribution of the $b \rightarrow u$ decay amplitude to $B^+ \rightarrow D\pi^+$ vanishes and when the flavour-specific rates $\Gamma(B^+ \rightarrow \bar{D}^0h^+)$ ($h = \pi, K$) are determined using appropriately flavour-specific D decays. In reality, the decay $D \rightarrow K\pi$ is used, leading to a small source of systematic uncertainty. The CP asymmetry is defined as

$$A_{CP} = \frac{\Gamma(B^- \rightarrow D_{CP}K^-) - \Gamma(B^+ \rightarrow D_{CP}K^+)}{\Gamma(B^- \rightarrow D_{CP}K^-) + \Gamma(B^+ \rightarrow D_{CP}K^+)}. \tag{146}$$

$B \rightarrow D^{(*)}K^{(*)}$ with $D \rightarrow$ non- CP eigenstate two-body decays

For the ADS analysis, based on a suppressed $D \rightarrow f$ decay, the measured quantities are again the partial rate asymmetry, and the charge averaged rate. In this case it is sufficient to measure the rate in a single ratio (normalised to the favoured $D \rightarrow \bar{f}$ decay) since potential systematic uncer-

tainties related to detection cancel naturally; the observed quantity is then

$$R_{ADS} = \frac{\Gamma(B^- \rightarrow [f]_D K^-) + \Gamma(B^+ \rightarrow [\bar{f}]_D K^+)}{\Gamma(B^- \rightarrow [\bar{f}]_D K^-) + \Gamma(B^+ \rightarrow [f]_D K^+)}, \tag{147}$$

where the inclusion of charge-conjugate modes has been made explicit. The CP asymmetry is defined as

$$A_{ADS} = \frac{\Gamma(B^- \rightarrow [f]_D K^-) - \Gamma(B^+ \rightarrow [f]_D K^+)}{\Gamma(B^- \rightarrow [f]_D K^-) + \Gamma(B^+ \rightarrow [f]_D K^+)}. \tag{148}$$

Since the uncertainty of A_{ADS} depends on the central value of R_{ADS} , for some statistical treatments it is preferable to use an alternative pair of parameters [315]

$$\begin{aligned} R_- &= \frac{\Gamma(B^- \rightarrow [f]_D K^-)}{\Gamma(B^- \rightarrow [\bar{f}]_D K^-)} \\ R_+ &= \frac{\Gamma(B^+ \rightarrow [\bar{f}]_D K^+)}{\Gamma(B^+ \rightarrow [f]_D K^+)}, \end{aligned} \tag{149}$$

where there is no implied inclusion of charge-conjugate processes. These parameters are statistically uncorrelated but may be affected by common sources of systematic uncertainty. We use the (R_{ADS}, A_{ADS}) set in our compilation where available.

In the ADS analysis, there are two additional unknowns (r_D and δ_D) compared to the GLW case. However, the value of r_D can be measured using decays of D mesons of known flavour, and δ_D can be measured from interference effects in decays of quantum-correlated $D\bar{D}$ pairs produced at the $\psi(3770)$ resonance. More generally, one needs access to two different linear admixtures of D^0 and \bar{D}^0 states in order to determine the relative phase: one such sample can be flavour tagged D mesons, which are available in abundant quantities in many experiments; the other can be CP -tagged D mesons from $\psi(3770)$ decays or could be mixed D mesons (or could be the combination of D^0 and \bar{D}^0 that is found in $B \rightarrow DK$ decays). In fact, the most precise information on both r_D and δ_D currently comes from global fits on charm mixing parameters, as discussed in Sect. 8.1.

The relation of A_{ADS} to the underlying parameters given in Eq. (141) and Table 25 is exact for a two-body D decay. For multibody decays, a similar formalism can be used with the introduction of a coherence factor [316]. This is most appropriate for doubly-Cabibbo-suppressed decays to non-self-conjugate final states, but can also be modified for use with singly-Cabibbo-suppressed decays [317]. For multibody self-conjugate final states, such as $K_S^0\pi^+\pi^-$, a Dalitz plot analysis (discussed below) is often more appropriate. However, in certain cases where the final state can be approximated as a CP eigenstate, a modified version of the GLW formalism can be used [318]. In such cases the observables

are denoted $A_{q\text{GLW}}$ and $R_{q\text{GLW}}$ to indicate that the final state is not a pure CP eigenstate.

$B \rightarrow D^{(*)}K^{(*)}$ with $D \rightarrow$ multibody final state decays

In the Dalitz plot (or GGSZ) analysis of D decays to multibody self-conjugate final states, once a model is assumed for the D decay, which gives the values of r_D and δ_D across the Dalitz plot, it is possible to perform a simultaneous fit to the B^+ and B^- samples and directly extract γ , r_B and δ_B . However, the uncertainties on the phases depend approximately inversely on r_B . Furthermore, r_B is positive definite and therefore tends to be overestimated (unless $\sigma(r_B) \ll r_B$), which leads to an underestimation of the uncertainty on γ that must be corrected statistically. An alternative approach is to extract from the data the ‘‘Cartesian’’ variables

$$(x_{\pm}, y_{\pm}) = (\text{Re}(r_B e^{i(\delta_B \pm \gamma)}), \text{Im}(r_B e^{i(\delta_B \pm \gamma)})) \\ = (r_B \cos(\delta_B \pm \gamma), r_B \sin(\delta_B \pm \gamma)). \tag{150}$$

These variables tend to be statistically well-behaved, and are therefore appropriate for combination of results. The pairs of variables (x_{\pm}, y_{\pm}) can be extracted from independent fits of the B^{\pm} data samples.

The assumption of a model for the D decay leads to a non-negligible, and hard to quantify, source of uncertainty. To obviate this, it is possible to use instead a model-independent approach, in which the Dalitz plot (or, more generally, the phase space) is binned [309, 319, 320]. In this case, hadronic parameters describing the average strong phase difference in each bin between the suppressed and favoured decay amplitudes enter the equations. These parameters can be determined from interference effects in decays of quantum-correlated $D\bar{D}$ pairs produced at the $\psi(3770)$ resonance. Measurements of such parameters have been made for various different hadronic D decays by CLEO-c and BESIII.

If a multibody decay is dominated by one CP state, there will be additional sensitivity to γ in the numbers of events in the B^{\pm} data samples. This can be taken into account in various ways. One possibility is to perform a GLW-like analysis, as mentioned above. An alternative approach proceeds by defining $z_{\pm} = x_{\pm} + iy_{\pm}$ and $x_0 = -\int \text{Re}[f(s_1, s_2)f^*(s_2, s_1)]ds_1ds_2$, where s_1, s_2 are the coordinates of invariant mass squared that define the Dalitz plot and f is the complex amplitude for D decay as a function of the Dalitz plot coordinates.²⁹ The fitted parameters $(\rho^{\pm}, \theta^{\pm})$ are then defined by

$$\rho^{\pm} e^{i\theta^{\pm}} = z_{\pm} - x_0. \tag{151}$$

²⁹ The x_0 parameter gives a model-dependent measure of the net CP content of the final state [318, 321]. It is closely related to the c_i parameters of the model dependent Dalitz plot analysis [309, 319, 320], and the coherence factor of inclusive ADS-type analyses [316], integrated over the entire Dalitz plot.

Table 25 Summary of relations between measured and physical parameters in GLW, ADS and Dalitz analyses of $B \rightarrow D^{(*)}K^{(*)}$ decays

GLW analysis	
$R_{CP\pm}$	$1 + r_B^2 \pm 2r_B \cos(\delta_B) \cos(\gamma)$
$A_{CP\pm}$	$\pm 2r_B \sin(\delta_B) \sin(\gamma)/R_{CP\pm}$
ADS analysis	
R_{ADS}	$r_B^2 + r_D^2 + 2r_B r_D \cos(\delta_B + \delta_D) \cos(\gamma)$
A_{ADS}	$2r_B r_D \sin(\delta_B + \delta_D) \sin(\gamma)/R_{\text{ADS}}$
GGSZ Dalitz analysis ($D \rightarrow K_S^0 \pi^+ \pi^-$)	
x_{\pm}	$r_B \cos(\delta_B \pm \gamma)$
y_{\pm}	$r_B \sin(\delta_B \pm \gamma)$
Dalitz analysis ($D \rightarrow \pi^+ \pi^- \pi^0$)	
ρ^{\pm}	$ z_{\pm} - x_0 $
θ^{\pm}	$\tan^{-1}(\text{Im}(z_{\pm})/(\text{Re}(z_{\pm}) - x_0))$

Table 26 Common inputs used in calculating the averages

$\tau(B^0)$ (ps)	1.520 ± 0.004
Δm_d (ps ⁻¹)	0.5064 ± 0.0019
$\Delta\Gamma_d/\Gamma_d$	-0.002 ± 0.010
$ A_{\perp} ^2(J/\psi K^*)$	0.209 ± 0.006

Note that the yields of B^{\pm} decays are proportional to $1 + (\rho^{\pm})^2 - (x_0)^2$. This choice of variables has been used by BABAR in the analysis of $B^+ \rightarrow DK^+$ with $D \rightarrow \pi^+ \pi^- \pi^0$ [322]; for this D decay, and with the assumed amplitude model, a value of $x_0 = 0.850$ is obtained.

The relations between the measured quantities and the underlying parameters are summarised in Table 25. It must be emphasised that the hadronic factors r_B and δ_B are different, in general, for each B decay mode.

4.3 Common inputs and error treatment

The common inputs used for rescaling are listed in Table 26. The B^0 lifetime ($\tau(B^0)$), mixing parameter (Δm_d) and relative width difference ($\Delta\Gamma_d/\Gamma_d$) averages are provided by the HFLAV Lifetimes and Oscillations subgroup (Sect. 3). The fraction of the perpendicularly polarised component ($|A_{\perp}|^2$) in $B \rightarrow J/\psi K^*(892)$ decays, which determines the CP composition in these decays, is averaged from results by BABAR [323], Belle [324], CDF [325], D0 [93] and LHCb [326]. See also the HFLAV B to Charm Decay Parameters subgroup (Sect. 6).

At present, we only rescale to a common set of input parameters for modes with reasonably small statistical errors ($b \rightarrow c\bar{c}s$ transitions of B^0 mesons). Correlated systematic errors are taken into account in these modes as well. For all other modes, the effect of such a procedure is currently negligible.

Table 27 Results and averages for $S_{b \rightarrow c\bar{c}s}$ and $C_{b \rightarrow c\bar{c}s}$. The result marked (*) uses “hadronic and previously unused muonic decays of the J/ψ ”. We neglect a small possible correlation of this result with the main BABAR result [331] that could be caused by reprocessing of the data

Experiment	Sample size	$-\eta S_{b \rightarrow c\bar{c}s}$	$C_{b \rightarrow c\bar{c}s}$
BABAR [331]	$N(B\bar{B}) = 465\text{M}$	$0.687 \pm 0.028 \pm 0.012$	$0.024 \pm 0.020 \pm 0.016$
BABAR $\chi_{c0} K_S^0$ [274]	$N(B\bar{B}) = 383\text{M}$	$0.69 \pm 0.52 \pm 0.04 \pm 0.07$	$-0.29^{+0.53}_{-0.44} \pm 0.03 \pm 0.05$
BABAR $J/\psi K_S^0$ (*) [332]	$N(B\bar{B}) = 88\text{M}$	$1.56 \pm 0.42 \pm 0.21$	–
Belle [333]	$N(B\bar{B}) = 772\text{M}$	$0.667 \pm 0.023 \pm 0.012$	$-0.006 \pm 0.016 \pm 0.012$
<i>B</i> factory average		0.679 ± 0.020	0.005 ± 0.017
Confidence level		0.28 (1.2 σ)	0.47 (0.5 σ)
ALEPH [334]	$N(Z \rightarrow \text{hadrons}) = 4\text{M}$	$0.84^{+0.82}_{-1.04} \pm 0.16$	–
OPAL [335]	$N(Z \rightarrow \text{hadrons}) = 4.4\text{M}$	$3.2^{+1.8}_{-2.0} \pm 0.5$	–
CDF [336]	$\int \mathcal{L} dt = 110 \text{ pb}^{-1}$	$0.79^{+0.41}_{-0.44}$	–
LHCb [337]	$\int \mathcal{L} dt = 3 \text{ fb}^{-1}$	$0.731 \pm 0.035 \pm 0.020$	$-0.038 \pm 0.032 \pm 0.005$
Belle $\Upsilon(5S)$ [338]	$\int \mathcal{L} dt = 121 \text{ fb}^{-1}$	$0.57 \pm 0.58 \pm 0.06$	–
Average		0.691 ± 0.017	-0.004 ± 0.015

As explained in Sect. 1, we do not apply a rescaling factor on the error of an average that has $\chi^2/\text{dof} > 1$ (unlike the procedure currently used by the PDG [327]). We provide a confidence level of the fit so that one can know the consistency of the measurements included in the average, and attach comments in case some care needs to be taken in the interpretation. Note that, in general, results obtained from data samples with low statistics will exhibit some non-Gaussian behaviour. We average measurements with asymmetric errors using the PDG [327] prescription. In cases where several measurements are correlated (e.g. S_f and C_f in measurements of time-dependent CP violation in B decays to a particular CP eigenstate) we take these into account in the averaging procedure if the uncertainties are sufficiently Gaussian. For measurements where one error is given, it represents the total error, where statistical and systematic uncertainties have been added in quadrature. If two errors are given, the first is statistical and the second systematic. If more than two errors are given, the origin of the additional uncertainty will be explained in the text.

4.4 Time-dependent asymmetries in $b \rightarrow c\bar{c}s$ transitions

4.4.1 Time-dependent CP asymmetries in $b \rightarrow c\bar{c}s$ decays to CP eigenstates

In the Standard Model, the time-dependent parameters for B^0 decays governed by $b \rightarrow c\bar{c}s$ transitions are predicted to be $S_{b \rightarrow c\bar{c}s} = -\eta \sin(2\beta)$ and $C_{b \rightarrow c\bar{c}s} = 0$ to very good accuracy. Deviations from this relation are currently limited to the level of $\lesssim 1^\circ$ on 2β [328–330]. The averages for $-\eta S_{b \rightarrow c\bar{c}s}$ and $C_{b \rightarrow c\bar{c}s}$ are provided in Table 27. The averages for $-\eta S_{b \rightarrow c\bar{c}s}$ are shown in Fig. 12.

Both BABAR and Belle have used the $\eta = -1$ modes $J/\psi K_S^0$, $\psi(2S) K_S^0$, $\chi_{c1} K_S^0$ and $\eta_c K_S^0$, as well as $J/\psi K_L^0$, which has $\eta = +1$ and $J/\psi K^{*0}(892)$, which is found to have η close to $+1$ based on the measurement of $|A_\perp|$ (see Sect. 4.3). The most recent Belle result does not use $\eta_c K_S^0$ or $J/\psi K^{*0}(892)$ decays.³⁰ ALEPH, OPAL, CDF and LHCb have used only the $J/\psi K_S^0$ final state. BABAR has also determined the CP violation parameters of the $B^0 \rightarrow \chi_{c0} K_S^0$ decay from the time-dependent Dalitz plot analysis of the $B^0 \rightarrow \pi^+ \pi^- K_S^0$ mode (see Sect. 4.7.2). In addition, Belle has performed a measurement with data accumulated at the $\Upsilon(5S)$ resonance, using the $J/\psi K_S^0$ final state – this involves a different flavour tagging method compared to the measurements performed with data accumulated at the $\Upsilon(4S)$ resonance. A breakdown of results in each charmonium-kaon final state is given in Table 28.

It should be noted that, while the uncertainty in the average for $-\eta S_{b \rightarrow c\bar{c}s}$ is still limited by statistics, the precision for $C_{b \rightarrow c\bar{c}s}$ is close to being dominated by the systematic uncertainty, particularly for measurements from the e^+e^- B factory experiments. This occurs due to the possible effect of tag side interference [292] on the $C_{b \rightarrow c\bar{c}s}$ measurement, an effect which is correlated between different $e^+e^- \rightarrow \Upsilon(4S) \rightarrow B\bar{B}$ experiments. Understanding of this effect may continue to improve in future, allowing the uncertainty to reduce.

From the average for $-\eta S_{b \rightarrow c\bar{c}s}$ above, we obtain the following solutions for β (in $[0, \pi]$):

$$\beta = (21.9 \pm 0.7)^\circ \quad \text{or} \quad \beta = (68.1 \pm 0.7)^\circ. \quad (152)$$

³⁰ Previous analyses from Belle did include these channels [101], but it is not possible to obtain separate results for those modes from the published information.

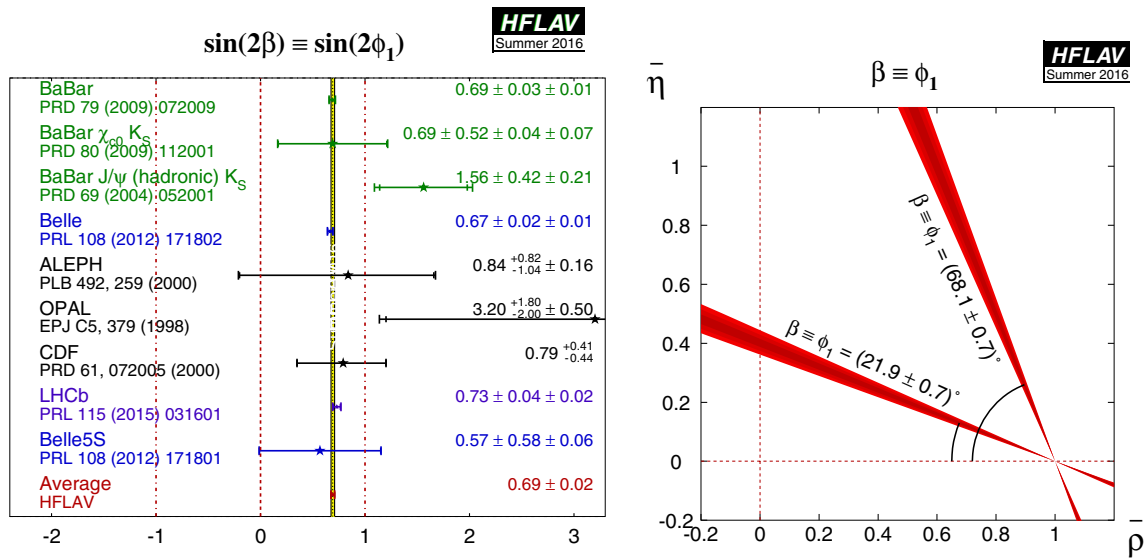


Fig. 12 (Left) Average of measurements of $S_{b \rightarrow c\bar{c}s}$, interpreted as $\sin(2\beta)$. (Right) Constraints on the $(\bar{\rho}, \bar{\eta})$ plane, obtained from the average of $-\eta S_{b \rightarrow c\bar{c}s}$ and Eq. (152). Note that the solution with the smaller (larger) value of β has $\cos(2\beta) > 0$ (< 0)

Table 28 Breakdown of B factory results on $S_{b \rightarrow c\bar{c}s}$ and $C_{b \rightarrow c\bar{c}s}$

Mode	$N(B\bar{B})$	$-\eta S_{b \rightarrow c\bar{c}s}$	$C_{b \rightarrow c\bar{c}s}$
BABAR			
$J/\psi K_S^0$ [331]	465M	$0.657 \pm 0.036 \pm 0.012$	$0.026 \pm 0.025 \pm 0.016$
$J/\psi K_L^0$ [331]	465M	$0.694 \pm 0.061 \pm 0.031$	$-0.033 \pm 0.050 \pm 0.027$
$J/\psi K^0$ [331]	465M	$0.666 \pm 0.031 \pm 0.013$	$0.016 \pm 0.023 \pm 0.018$
$\psi(2S) K_S^0$ [331]	465M	$0.897 \pm 0.100 \pm 0.036$	$0.089 \pm 0.076 \pm 0.020$
$\chi_{c1} K_S^0$ [331]	465M	$0.614 \pm 0.160 \pm 0.040$	$0.129 \pm 0.109 \pm 0.025$
$\eta_c K_S^0$ [331]	465M	$0.925 \pm 0.160 \pm 0.057$	$0.080 \pm 0.124 \pm 0.029$
$J/\psi K^{*0}(892)$ [331]	465M	$0.601 \pm 0.239 \pm 0.087$	$0.025 \pm 0.083 \pm 0.054$
All [331]	465M	$0.687 \pm 0.028 \pm 0.012$	$0.024 \pm 0.020 \pm 0.016$
Belle			
$J/\psi K_S^0$ [333]	772M	$0.670 \pm 0.029 \pm 0.013$	$0.015 \pm 0.021^{+0.023}_{-0.045}$
$J/\psi K_L^0$ [333]	772M	$0.642 \pm 0.047 \pm 0.021$	$-0.019 \pm 0.026^{+0.041}_{-0.017}$
$\psi(2S) K_S^0$ [333]	772M	$0.738 \pm 0.079 \pm 0.036$	$-0.104 \pm 0.055^{+0.027}_{-0.047}$
$\chi_{c1} K_S^0$ [333]	772M	$0.640 \pm 0.117 \pm 0.040$	$0.017 \pm 0.083^{+0.026}_{-0.046}$
All [333]	772M	$0.667 \pm 0.023 \pm 0.012$	$-0.006 \pm 0.016 \pm 0.012$
Averages			
$J/\psi K_S^0$		0.665 ± 0.024	0.024 ± 0.026
$J/\psi K_L^0$		0.663 ± 0.041	-0.023 ± 0.030
$\psi(2S) K_S^0$		0.807 ± 0.067	-0.009 ± 0.055
$\chi_{c1} K_S^0$		0.632 ± 0.099	0.066 ± 0.074

In radians, these values are $\beta = (0.382 \pm 0.012)$, $\beta = (1.189 \pm 0.012)$.

This result gives a precise constraint on the $(\bar{\rho}, \bar{\eta})$ plane, as shown in Fig. 12. The measurement is in remarkable agreement with other constraints from CP conserving quantities,

and with CP violation in the kaon system, in the form of the parameter ϵ_K . Such comparisons have been performed by various phenomenological groups, such as CKMfitter [252] and UFit [339] (see also Refs. [340,341]).

Table 29 Averages from $B^0 \rightarrow J/\psi K^{*0}$ transversity analyses

Experiment	$N(B\bar{B})$	$\sin 2\beta$	$\cos 2\beta$	Correlation
BABAR [345]	88M	$-0.10 \pm 0.57 \pm 0.14$	$3.32^{+0.76}_{-0.96} \pm 0.27$	-0.37
Belle [324]	275M	$0.24 \pm 0.31 \pm 0.05$	$0.56 \pm 0.79 \pm 0.11$	0.22
Average		0.16 ± 0.28	1.64 ± 0.62	Uncorrelated averages
Confidence level		0.61 (0.5 σ)	0.03 (2.2 σ)	

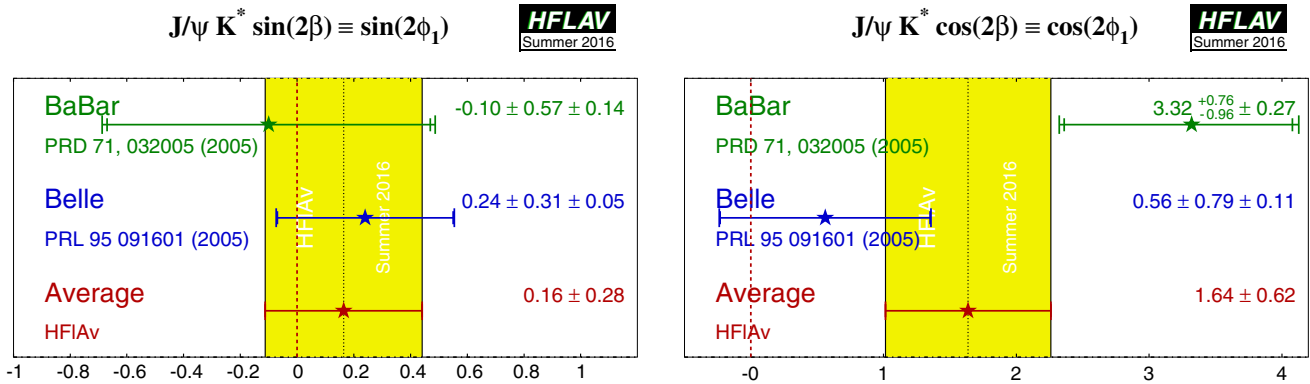


Fig. 13 Averages of (left) $\sin(2\beta) \equiv \sin(2\phi_1)$ and (right) $\cos(2\beta) \equiv \cos(2\phi_1)$ from time-dependent analyses of $B^0 \rightarrow J/\psi K^{*0}$ decays

4.4.2 Time-dependent transversity analysis of $B^0 \rightarrow J/\psi K^{*0}$ decays

B meson decays to the vector-vector final state $J/\psi K^{*0}$ are also mediated by the $b \rightarrow c\bar{c}s$ transition. When a final state that is not flavour-specific ($K^{*0} \rightarrow K_S^0\pi^0$) is used, a time-dependent transversity analysis can be performed allowing sensitivity to both $\sin(2\beta)$ and $\cos(2\beta)$ [342]. Such analyses have been performed by both B factory experiments. In principle, the strong phases between the transversity amplitudes are not uniquely determined by such an analysis, leading to a discrete ambiguity in the sign of $\cos(2\beta)$. The BABAR collaboration resolves this ambiguity using the known variation [343] of the P-wave phase (fast) relative to the S-wave phase (slow) with the invariant mass of the $K\pi$ system in the vicinity of the $K^*(892)$ resonance. The result is in agreement with the prediction from s quark helicity conservation, and corresponds to Solution II defined by Suzuki [344]. We include only the solutions consistent with this phase variation in Table 29 and Fig. 13.

At present the results are dominated by large and non-Gaussian statistical errors, and exhibit significant correlations. We perform uncorrelated averages, the interpretation of which has to be done with the greatest care. Nonetheless, it is clear that $\cos(2\beta) > 0$ is preferred by the experimental data in $J/\psi K^{*0}$ (for example, BABAR [345] find a confidence level for $\cos(2\beta) > 0$ of 89%).

4.4.3 Time-dependent CP asymmetries in $B^0 \rightarrow D^{*+}D^{*-}K_S^0$ decays

Both BABAR [265] and Belle [266] have performed time-dependent analyses of the $B^0 \rightarrow D^{*+}D^{*-}K_S^0$ decay, to obtain information on the sign of $\cos(2\beta)$. More information can be found in Sect. 4.2.5. The results are given in Table 30, and shown in Fig. 14.

From the above result and the assumption that $J_{S2} > 0$, BABAR infer that $\cos(2\beta) > 0$ at the 94% confidence level [265].

4.4.4 Time-dependent analysis of B_S^0 decays through the $b \rightarrow c\bar{c}s$ transition

As described in Sect. 4.2.3, time-dependent analysis of decays such as $B_S^0 \rightarrow J/\psi\phi$ probes the CP violating phase of $B_S^0-\bar{B}_S^0$ oscillations, ϕ_s .³¹ The combination of results on $B_S^0 \rightarrow J/\psi\phi$ decays, including also results from $B_S^0 \rightarrow J/\psi\pi^+\pi^-$ and $B_S^0 \rightarrow D_s^+D_s^-$ decays, is performed by the HFLAV Lifetimes and Oscillations subgroup, see Sect. 3.

³¹ We use ϕ_s here to denote the same quantity labelled $\phi_s^{c\bar{c}s}$ in Sect. 3. It should not be confused with the parameter $\phi_{12} \equiv \arg[-M_{12}/\Gamma_{12}]$, which historically was also often referred to as ϕ_s .

Table 30 Results from time-dependent analysis of $B^0 \rightarrow D^{*+} D^{*-} K_S^0$

Experiment	$N(B\bar{B})$	J_c/J_0	$\frac{2J_{s1}}{J_0} \sin(2\beta)$	$\frac{2J_{s2}}{J_0} \cos(2\beta)$
BABAR [265]	230M	$0.76 \pm 0.18 \pm 0.07$	$0.10 \pm 0.24 \pm 0.06$	$0.38 \pm 0.24 \pm 0.05$
Belle [266]	449M	$0.60^{+0.25}_{-0.28} \pm 0.08$	$-0.17 \pm 0.42 \pm 0.09$	$-0.23^{+0.43}_{-0.41} \pm 0.13$
Average		0.71 ± 0.16	0.03 ± 0.21	0.24 ± 0.22
Confidence level		0.63 (0.5 σ)	0.59 (0.5 σ)	0.23 (1.2 σ)

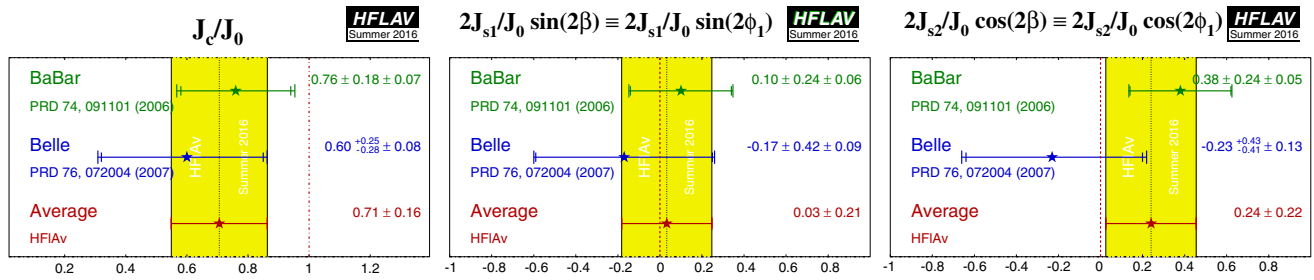


Fig. 14 Averages of (left) (J_c/J_0) , (middle) $(2J_{s1}/J_0) \sin(2\beta)$ and (right) $(2J_{s2}/J_0) \cos(2\beta)$ from time-dependent analyses of $B^0 \rightarrow D^{*+} D^{*-} K_S^0$ decays

Table 31 Results from analyses of $B^0 \rightarrow D^{(*)} h^0$, $D \rightarrow CP$ eigenstates decays

Experiment	$N(B\bar{B})$	S_{CP}	C_{CP}	Correlation
BABAR and Belle [349]	1243M	$0.66 \pm 0.10 \pm 0.06$	$-0.02 \pm 0.07 \pm 0.03$	-0.05

4.5 Time-dependent CP asymmetries in colour-suppressed $b \rightarrow c\bar{u}d$ transitions

4.5.1 Time-dependent CP asymmetries: $b \rightarrow c\bar{u}d$ decays to CP eigenstates

Decays of B mesons to final states such as $D\pi^0$ are governed by $b \rightarrow c\bar{u}d$ transitions. If the final state is a CP eigenstate, e.g. $D_{CP}\pi^0$, the usual time-dependence formulae are recovered, with the sine coefficient sensitive to $\sin(2\beta)$. Since there is no penguin contribution to these decays, there is even less associated theoretical uncertainty than for $b \rightarrow c\bar{c}s$ decays such as $B \rightarrow J/\psi K_S^0$. Such measurements therefore allow to test the Standard Model prediction that the CP violation parameters in $b \rightarrow c\bar{u}d$ transitions are the same as those in $b \rightarrow c\bar{c}s$ [346]. Although there is an additional contribution from CKM suppressed $b \rightarrow u\bar{c}d$ amplitudes, which have a different weak phase compared to the leading $b \rightarrow c\bar{u}d$ transition, the effect is small and can be taken into account in the analysis [347, 348].

Results are available from a joint analysis of BABAR and Belle data [349]. The following CP-even final states are included: $D\pi^0$ and $D\eta$ with $D \rightarrow K_S^0\pi^0$ and $D \rightarrow K_S^0\omega$; $D\omega$ with $D \rightarrow K_S^0\pi^0$; $D^*\pi^0$ and $D^*\eta$ with $D^* \rightarrow D\pi^0$

and $D \rightarrow K^+K^-$. The following CP-odd final states are included: $D\pi^0$, $D\eta$ and $D\omega$ with $D \rightarrow K^+K^-$, $D^*\pi^0$ and $D^*\eta$ with $D^* \rightarrow D\pi^0$ and $D \rightarrow K_S^0\pi^0$. All $B^0 \rightarrow D^{(*)}h^0$ decays are analysed together, taking into account the different CP factors (denoted $D_{CP}^{(*)}h^0$). The results are summarised in Table 31.

4.5.2 Time-dependent Dalitz plot analyses of $b \rightarrow c\bar{u}d$ decays

When multibody D decays, such as $D \rightarrow K_S^0\pi^+\pi^-$ are used, a time-dependent analysis of the Dalitz plot of the neutral D decay allows for a direct determination of the weak phase 2β . (Equivalently, both $\sin(2\beta)$ and $\cos(2\beta)$ can be measured.) This information can be used to resolve the ambiguity in the measurement of 2β from $\sin(2\beta)$ [350].

Results of such analyses are available from both Belle [260] and BABAR [261]. The decays $B \rightarrow D\pi^0$, $B \rightarrow D\eta$, $B \rightarrow D\omega$, $B \rightarrow D^*\pi^0$ and $B \rightarrow D^*\eta$ are used. (This collection of states is denoted by $D^{(*)}h^0$.) The daughter decays are $D^* \rightarrow D\pi^0$ and $D \rightarrow K_S^0\pi^+\pi^-$. The results are given in Table 32, and shown in Fig. 15. Note that BABAR quote uncertainties due to the D decay model separately from other

Table 32 Averages from $B^0 \rightarrow D^{(*)}h^0, D \rightarrow K_S^0\pi^+\pi^-$ analyses

Experiment	$N(B\bar{B})$	$\sin 2\beta$	$\cos 2\beta$	$ \lambda $
Model dependent				
BABAR [261]	383M	$0.29 \pm 0.34 \pm 0.03 \pm 0.05$	$0.42 \pm 0.49 \pm 0.09 \pm 0.13$	$1.01 \pm 0.08 \pm 0.02$
Belle [260]	386M	$0.78 \pm 0.44 \pm 0.22$	$1.87^{+0.40+0.22}_{-0.53-0.32}$	–
Average		0.45 ± 0.28	1.01 ± 0.40	1.01 ± 0.08
Confidence level		$0.59 (0.5\sigma)$	$0.12 (1.6\sigma)$	–
Model independent				
Belle [262]	772M	$0.43 \pm 0.27 \pm 0.08$	$1.06 \pm 0.33^{+0.21}_{-0.15}$	–

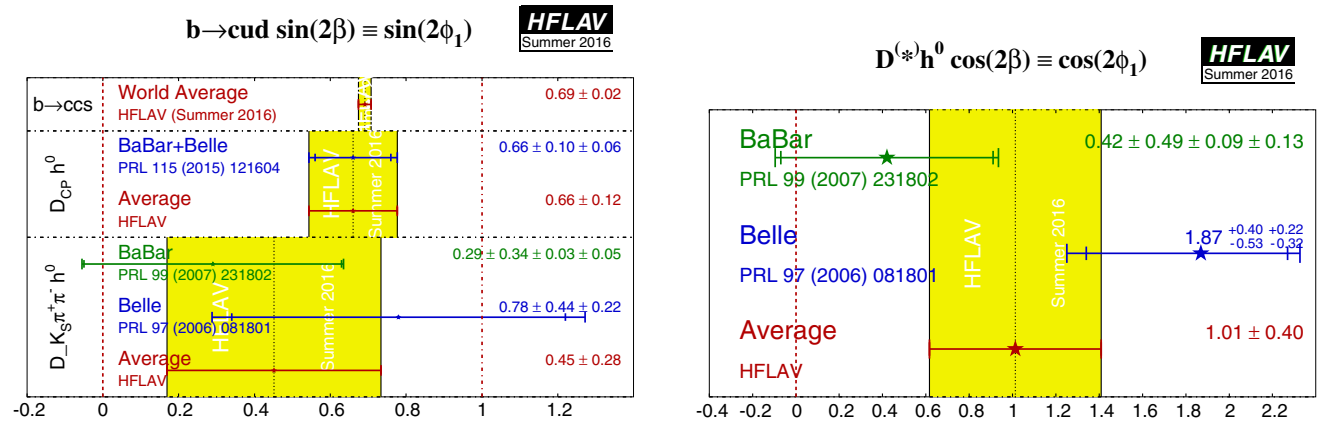


Fig. 15 Averages of (left) $\sin(2\beta)$ and (right) $\cos(2\beta)$ measured in colour-suppressed $b \rightarrow c\bar{u}d$ transitions

systematic errors as a third source of uncertainty, while Belle do not.

Again, it is clear that the data prefer $\cos(2\beta) > 0$. Indeed, Belle [260] determine the sign of $\cos(2\phi_1)$ to be positive at 98.3% confidence level, while BABAR [261] favour the solution of β with $\cos(2\beta) > 0$ at 87% confidence level. Note, however, that the Belle measurement has strongly non-Gaussian behaviour. Therefore, we perform uncorrelated averages, from which any interpretation has to be done with the greatest care.

A model-independent time-dependent analysis of $B^0 \rightarrow D^{(*)}h^0$ decays, with $D \rightarrow K_S^0\pi^+\pi^-$, has been performed by Belle [262]. The decays $B^0 \rightarrow D\pi^0, B^0 \rightarrow D\eta, B^0 \rightarrow D\eta', B^0 \rightarrow D\omega, B^0 \rightarrow D^*\pi^0$ and $B^0 \rightarrow D^*\eta$ are used. The results are also included in Table 32. From these results, Belle disfavour the solution with the value of $\sin(2\phi_1)$ from $b \rightarrow c\bar{c}s$ transitions but a negative value for $\cos(2\phi_1)$, at 5.1σ significance. The solution with the $b \rightarrow c\bar{c}s$ value of $\sin(2\phi_1)$ and positive $\cos(2\phi_1)$ is consistent with the data at the level of 1.3σ . Note that due to the strong statistical and systematic correlations, model-dependent results and model-independent results from the same experiment cannot be combined.

4.6 Time-dependent CP asymmetries in $b \rightarrow c\bar{c}d$ transitions

The transition $b \rightarrow c\bar{c}d$ can occur via either a $b \rightarrow c$ tree or a $b \rightarrow d$ penguin amplitude. The flavour changing neutral current $b \rightarrow d$ penguin can be mediated by any up-type quark in the loop, and hence the amplitude can be written as

$$A_{b \rightarrow d} = F_u V_{ub} V_{ud}^* + F_c V_{cb} V_{cd}^* + F_t V_{tb} V_{td}^* = (F_u - F_c) V_{ub} V_{ud}^* + (F_t - F_c) V_{tb} V_{td}^*, \quad (153)$$

where $F_{u,c,t}$ describe all factors except CKM suppression entering each quark loop diagram. In the last line, both terms are $\mathcal{O}(\lambda^3)$, so it can be seen that the $b \rightarrow d$ penguin amplitude contains terms with different weak phases at the same order of CKM suppression.

In the above, we have chosen to eliminate the F_c term using unitarity. However, we could equally well write

$$A_{b \rightarrow d} = (F_u - F_t) V_{ub} V_{ud}^* + (F_c - F_t) V_{cb} V_{cd}^* = (F_c - F_u) V_{cb} V_{cd}^* + (F_t - F_u) V_{tb} V_{td}^*. \quad (154)$$

Since the $b \rightarrow c\bar{c}d$ tree amplitude has the weak phase of $V_{cb} V_{cd}^*$, either of the above expressions allow the penguin amplitude to be decomposed into a part with weak phase the

Table 33 Averages for the $b \rightarrow c\bar{c}d$ modes, $B^0 \rightarrow J/\psi\pi^0$ and D^+D^-

Experiment	Sample size	S_{CP}	C_{CP}	Correlation
$J/\psi\pi^0$				
BABAR [353]	$N(B\bar{B}) = 466\text{M}$	$-1.23 \pm 0.21 \pm 0.04$	$-0.20 \pm 0.19 \pm 0.03$	0.20
Belle [354]	$N(B\bar{B}) = 535\text{M}$	$-0.65 \pm 0.21 \pm 0.05$	$-0.08 \pm 0.16 \pm 0.05$	-0.10
Average		-0.93 ± 0.15	-0.10 ± 0.13	0.04
Confidence level		0.15 (1.4 σ)		
D^+D^-				
BABAR [259]	$N(B\bar{B}) = 467\text{M}$	$-0.65 \pm 0.36 \pm 0.05$	$-0.07 \pm 0.23 \pm 0.03$	-0.01
Belle [287]	$N(B\bar{B}) = 772\text{M}$	$-1.06^{+0.21}_{-0.14} \pm 0.08$	$-0.43 \pm 0.16 \pm 0.05$	-0.12
LHCb [355]	$\int \mathcal{L} dt = 3\text{fb}^{-1}$	$-0.54^{+0.17}_{-0.16} \pm 0.05$	$0.26^{+0.18}_{-0.17} \pm 0.02$	0.48
Average		-0.84 ± 0.12	-0.13 ± 0.10	0.18
Confidence level		0.027 (2.2 σ)		

Table 34 Averages for the $b \rightarrow c\bar{c}d$ modes, $J/\psi\rho^0$, $D^{*+}D^{*-}$ and $D^{*\pm}D^\mp$

Experiment	$N(B\bar{B})$	S_{CP}	C_{CP}	R_\perp		
$J/\psi\rho^0$						
LHCb [258]	3fb^{-1}	$-0.66^{+0.13+0.09}_{-0.12-0.03}$	$-0.06 \pm 0.06^{+0.02}_{-0.01}$	0.198 ± 0.017		
$D^{*+}D^{*-}$						
BABAR [259]	467M	$-0.70 \pm 0.16 \pm 0.03$	$0.05 \pm 0.09 \pm 0.02$	0.17 ± 0.03		
BABAR part. rec. [356]	471M	$-0.49 \pm 0.18 \pm 0.07 \pm 0.04$	$0.15 \pm 0.09 \pm 0.04$	-		
Belle [352]	772M	$-0.79 \pm 0.13 \pm 0.03$	$-0.15 \pm 0.08 \pm 0.02$	$0.14 \pm 0.02 \pm 0.01$		
Average		-0.71 ± 0.09	-0.01 ± 0.05	0.15 ± 0.02		
Confidence level			0.72 (0.4 σ)			
Experiment	$N(B\bar{B})$	S_{CP+}	C_{CP+}	S_{CP-}	C_{CP-}	R_\perp
$D^{*+}D^{*-}$						
BABAR [259]	467M	$-0.76 \pm 0.16 \pm 0.04$	$0.02 \pm 0.12 \pm 0.02$	$-1.81 \pm 0.71 \pm 0.16$	$0.41 \pm 0.50 \pm 0.08$	0.15 ± 0.03
Experiment	$N(B\bar{B})$	S	C	ΔS	ΔC	\mathcal{A}
$D^{*\pm}D^\mp$						
BABAR [259]	467M	$-0.68 \pm 0.15 \pm 0.04$	$0.04 \pm 0.12 \pm 0.03$	$0.05 \pm 0.15 \pm 0.02$	$0.04 \pm 0.12 \pm 0.03$	$0.01 \pm 0.05 \pm 0.01$
Belle [287]	772M	$-0.78 \pm 0.15 \pm 0.05$	$-0.01 \pm 0.11 \pm 0.04$	$-0.13 \pm 0.15 \pm 0.04$	$0.12 \pm 0.11 \pm 0.03$	$0.06 \pm 0.05 \pm 0.02$
Average		-0.73 ± 0.11	0.01 ± 0.09	-0.04 ± 0.11	0.08 ± 0.08	0.03 ± 0.04
Confidence level		0.65 (0.5 σ)	0.77 (0.3 σ)	0.41 (0.8 σ)	0.63 (0.5 σ)	0.48 (0.7 σ)

same as the tree amplitude and another part with a different weak phase, which can be chosen to be either β or γ . The choice of parametrisation cannot, of course, affect the physics [351]. In any case, if the tree amplitude dominates, there is little sensitivity to any phase other than that from $B^0-\bar{B}^0$ mixing.

The $b \rightarrow c\bar{c}d$ transitions can be investigated with studies of various different final states. Results are available from both BABAR and Belle using the final states $J/\psi\pi^0$, D^+D^- , $D^{*+}D^{*-}$ and $D^{*\pm}D^\mp$, and from LHCb using the final states $J/\psi\rho^0$ and D^+D^- ; the averages of these results are given in Tables 33 and 34. The results using the CP eigenstate

($\eta = +1$) modes $J/\psi\pi^0$ and D^+D^- are shown in Fig. 16 and Fig. 17 respectively, with two-dimensional constraints shown in Fig. 18.

Results for the vector-vector mode $J/\psi\rho^0$ are obtained from a full time-dependent amplitude analysis of $B^0 \rightarrow J/\psi\pi^+\pi^-$ decays. LHCb [258] find a $J/\psi\rho^0$ fit fraction of $65.6 \pm 1.9\%$ and a longitudinal polarisation fraction of $56.7 \pm 1.8\%$ (uncertainties are statistical only; both results are consistent with those from a time-integrated amplitude analysis [267] where systematic uncertainties were also evaluated). Fits are performed to obtain $2\beta^{\text{eff}}$ in the cases that all transversity amplitudes are assumed to have

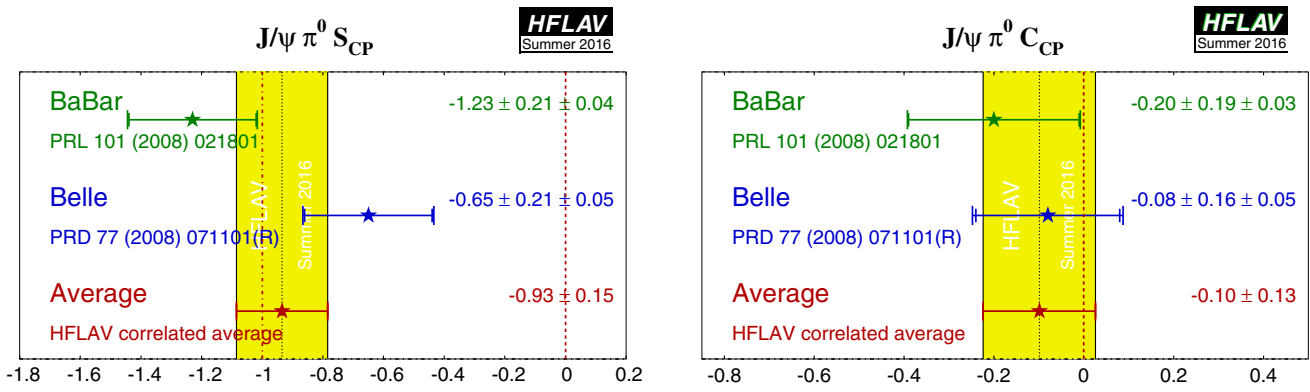


Fig. 16 Averages of (left) $S_{b \rightarrow c\bar{c}d}$ and (right) $C_{b \rightarrow c\bar{c}d}$ for the mode $B^0 \rightarrow J/\psi\pi^0$

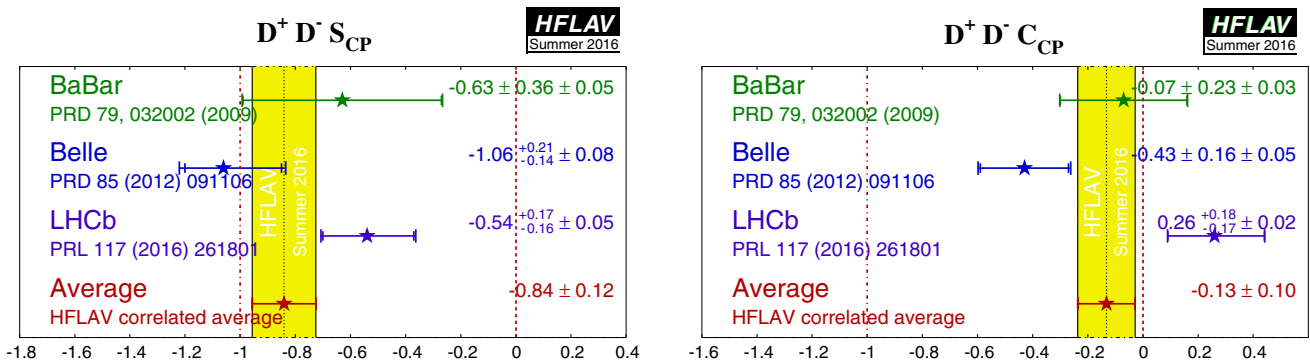


Fig. 17 Averages of (left) $S_{b \rightarrow c\bar{c}d}$ and (right) $C_{b \rightarrow c\bar{c}d}$ for the mode $B^0 \rightarrow D^+D^-$

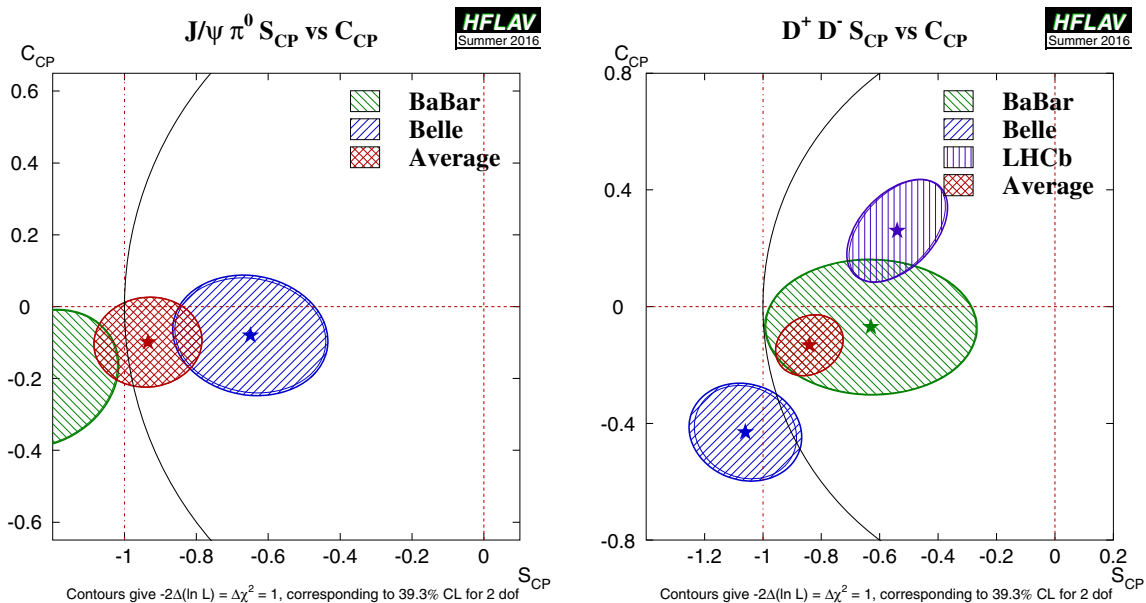


Fig. 18 Averages of two $b \rightarrow c\bar{c}d$ dominated channels, for which correlated averages are performed, in the S_{CP} vs. C_{CP} plane. (Left) $B^0 \rightarrow J/\psi\pi^0$ and (right) $B^0 \rightarrow D^+D^-$

the same CP violation parameter. A separate fit is performed allowing different parameters. The results in the former case are presented in terms of S_{CP} and C_{CP} in Table 34.

The vector-vector mode $D^{*+}D^{*-}$ is found to be dominated by the CP -even longitudinally polarised component; BABAR measures a CP -odd fraction of $0.158 \pm 0.028 \pm 0.006$ [259] while Belle measures a CP -odd fraction of

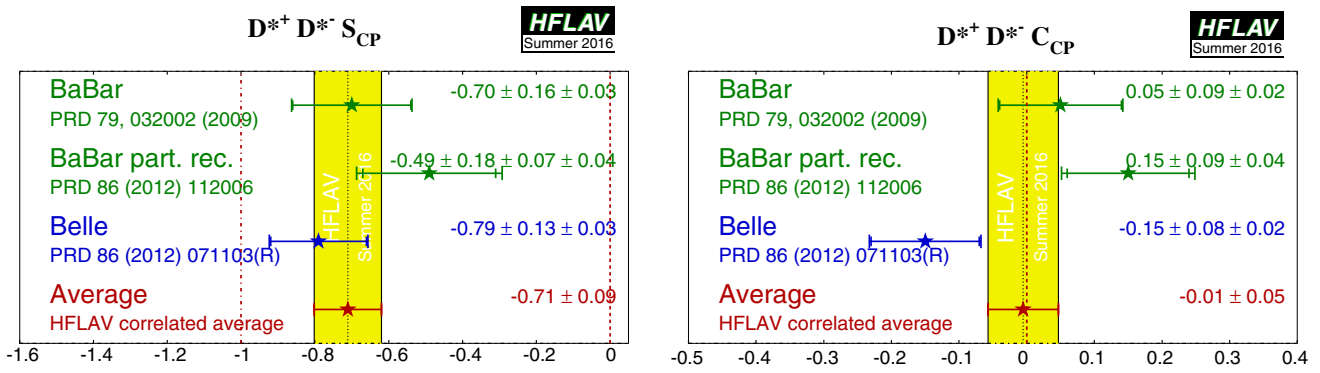


Fig. 19 Averages of (left) $S_{b \rightarrow c \bar{c} d}$ and (right) $C_{b \rightarrow c \bar{c} d}$ for the mode $B^0 \rightarrow D^{*+} D^{*-}$

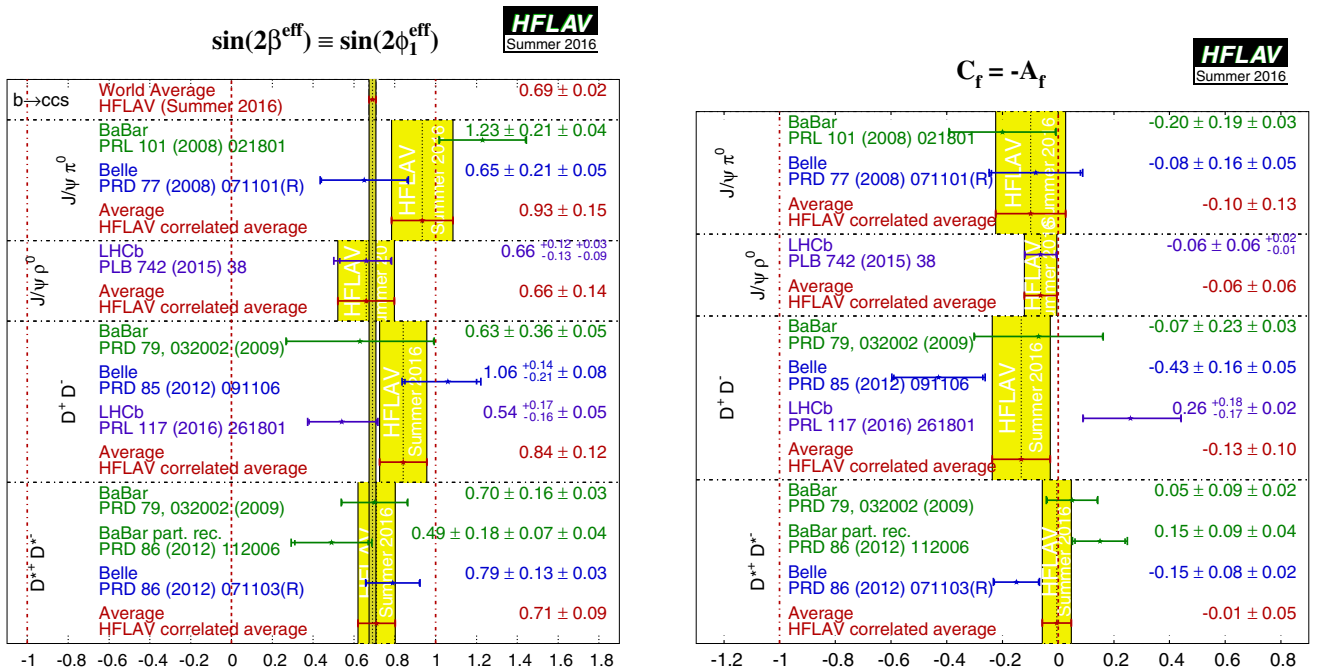


Fig. 20 Averages of (left) $-\eta S_{b \rightarrow c \bar{c} d}$ interpreted as $\sin(2\beta^{\text{eff}})$ and (right) $C_{b \rightarrow c \bar{c} d}$. The $-\eta S_{b \rightarrow c \bar{c} d}$ figure compares the results to the world average for $-\eta S_{b \rightarrow c \bar{c} s}$ (see Sect. 4.4.1)

$0.138 \pm 0.024 \pm 0.006$ [352]. These values, listed as R_{\perp} , are included in the averages, which ensures that the correlations are taken into account.³² BABAR has also performed an additional fit in which the CP -even and CP -odd components are allowed to have different CP violation parameters S and C . These results are included in Table 34. Results using $D^{*+} D^{*-}$ are shown in Fig. 19.

As discussed in Sect. 4.2.6, the most recent papers on the non- CP eigenstate mode $D^{* \pm} D^{\mp}$ use the $(A, S, \Delta S, C, \Delta C)$ set of parameters, and we therefore perform the averages with this choice.

In the absence of the penguin contribution (tree dominance), the time-dependent parameters would be given by $S_{b \rightarrow c \bar{c} d} = -\eta \sin(2\beta)$, $C_{b \rightarrow c \bar{c} d} = 0$, $S_{+-} = \sin(2\beta + \delta)$, $S_{-+} = \sin(2\beta - \delta)$, $C_{+-} = -C_{-+}$ and $\mathcal{A} = 0$, where δ is the strong phase difference between the $D^{*+} D^-$ and $D^{*-} D^+$ decay amplitudes. In the presence of the penguin contribution, there is no clean interpretation in terms of CKM parameters; however, direct CP violation may be observed through any of $C_{b \rightarrow c \bar{c} d} \neq 0$, $C_{+-} \neq -C_{-+}$ or $A_{+-} \neq 0$.

The averages for the $b \rightarrow c \bar{c} d$ modes are shown in Figs. 20 and 21. Results are consistent with tree dominance, and with the Standard Model, though the Belle results in $B^0 \rightarrow D^+ D^-$ [357] show an indication of CP violation in decay, and hence a non-zero penguin contribution. The average of $S_{b \rightarrow c \bar{c} d}$ in each of the $J/\psi \pi^0$, $D^+ D^-$ and $D^{*+} D^{*-}$

³² Note that the BABAR value given in Table 34 differs from the value quoted here, since that in the table is not corrected for efficiency.

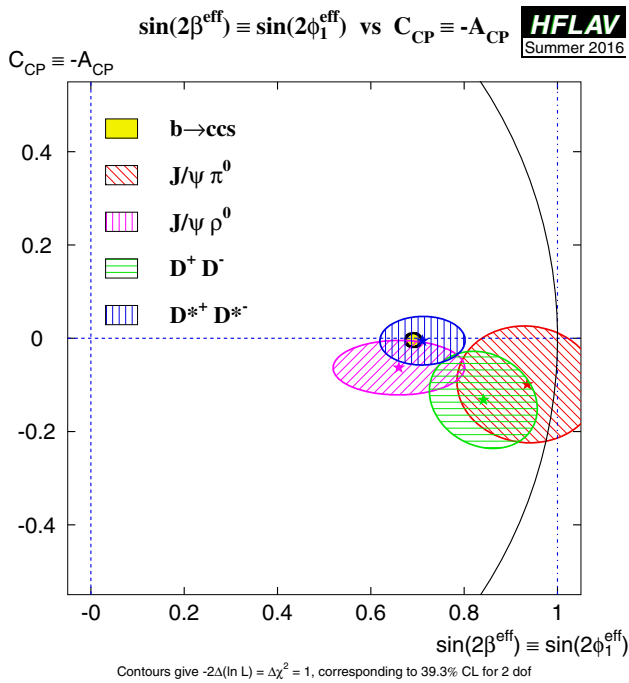


Fig. 21 Compilation of constraints in the $-\eta S_{b \rightarrow c\bar{c}d}$, interpreted as $\sin(2\beta^{\text{eff}})$, vs. $C_{b \rightarrow c\bar{c}d}$ plane

final states is more than 5σ from zero, corresponding to observations of CP violation in these decay channels. Possible non-Gaussian effects due to some of the inputs measurements being outside the physical region ($S_{CP}^2 + C_{CP}^2 \leq 1$) should, however, be borne in mind.

4.6.1 Time-dependent CP asymmetries in B_s^0 decays mediated by $b \rightarrow c\bar{c}d$ transitions

Time-dependent CP asymmetries in B_s^0 decays mediated by $b \rightarrow c\bar{c}d$ transitions provide a determination of $2\beta_s^{\text{eff}}$ where possible effects from penguin amplitudes may cause a shift from the value of $2\beta_s$ seen in $b \rightarrow c\bar{c}s$ transitions. Results in the $b \rightarrow c\bar{c}d$ case, with larger penguin effects, can be used together with flavour symmetries to derive limits on the possible size of penguin effects in the $b \rightarrow c\bar{c}s$ transitions [358, 359].

The parameters have been measured in $B_s^0 \rightarrow J/\psi K_S^0$ decays by LHCb, as summarised in Table 35. The results supersede an earlier measurement of the effective lifetime, which is directly related to $A^{\Delta\Gamma}$, in the same mode [127], which is discussed in Sect. 3.

4.7 Time-dependent CP asymmetries in charmless $b \rightarrow q\bar{q}s$ transitions

Similarly to Eq. (153), the $b \rightarrow s$ penguin amplitude can be written as

$$A_{b \rightarrow s} = F_u V_{ub} V_{us}^* + F_c V_{cb} V_{cs}^* + F_t V_{tb} V_{ts}^* = (F_u - F_c) V_{ub} V_{us}^* + (F_t - F_c) V_{tb} V_{ts}^*, \quad (155)$$

using the unitarity of the CKM matrix to eliminate the F_c term. In this case, the first term in the last line is $\mathcal{O}(\lambda^4)$ while the second is $\mathcal{O}(\lambda^2)$. Therefore, in the Standard Model, this amplitude is dominated by $V_{tb} V_{ts}^*$, and to within a few degrees ($|\delta\beta^{\text{eff}}| \equiv |\beta^{\text{eff}} - \beta| \lesssim 2^\circ$ for $\beta \approx 20^\circ$) the time-dependent parameters can be written³³ $S_{b \rightarrow q\bar{q}s} \approx -\eta \sin(2\beta)$, $C_{b \rightarrow q\bar{q}s} \approx 0$, assuming $b \rightarrow s$ penguin contributions only ($q = u, d, s$).

Due to the suppression of the Standard Model amplitude, contributions of additional diagrams from physics beyond the Standard Model, with heavy virtual particles in the penguin loops, may have observable effects. In general, these contributions will affect the values of $S_{b \rightarrow q\bar{q}s}$ and $C_{b \rightarrow q\bar{q}s}$. A discrepancy between the values of $S_{b \rightarrow c\bar{c}s}$ and $S_{b \rightarrow q\bar{q}s}$ can therefore provide a clean indication of new physics [346, 361–363].

However, there is an additional consideration to take into account. The above argument assumes that only the $b \rightarrow s$ penguin contributes to the $b \rightarrow q\bar{q}s$ transition. For $q = s$ this is a good assumption, which neglects only rescattering effects. However, for $q = u$ there is a colour-suppressed $b \rightarrow u$ tree diagram (of order $\mathcal{O}(\lambda^4)$), which has a different weak (and possibly strong) phase. In the case $q = d$, any light neutral meson that is formed from $d\bar{d}$ also has a $u\bar{u}$ component, and so again there is “tree pollution”. The B^0 decays to $\pi^0 K_S^0, \rho^0 K_S^0$ and ωK_S^0 belong to this category. The mesons ϕ, f_0 and η' are expected to have predominant $s\bar{s}$ composition, which reduces the relative size of the possible tree pollution. If the inclusive decay $B^0 \rightarrow K^+ K^- K^0$ (excluding ϕK^0) is dominated by a nonresonant three-body transition, an Okubo–Zweig–Iizuka-suppressed [364–366] tree-level diagram can occur through insertion of an $s\bar{s}$ pair. The corresponding penguin-type transition proceeds via insertion of a $u\bar{u}$ pair, which is expected to be favoured over the $s\bar{s}$ insertion by fragmentation models. Neglecting rescattering, the final state $K^0 \bar{K}^0 K^0$ (reconstructed as $K_S^0 K_S^0 K_S^0$) has no tree pollution [367]. Various estimates, using different theoretical approaches, of the values of $\Delta S = S_{b \rightarrow q\bar{q}s} - S_{b \rightarrow c\bar{c}s}$ exist in the literature [368–381]. In general, there is agreement that the modes $\phi K^0, \eta' K^0$ and $K^0 \bar{K}^0 K^0$ are the cleanest, with values of $|\Delta S|$ at or below the few percent level (ΔS is usually predicted to be positive). Nonetheless, the uncertainty is sufficient that interpretation is given in terms of $\sin(2\beta^{\text{eff}})$.

³³ The presence of a small ($\mathcal{O}(\lambda^2)$) weak phase in the dominant amplitude of the s penguin decays introduces a phase shift given by $S_{b \rightarrow q\bar{q}s} = -\eta \sin(2\beta)(1 + \Delta)$. Using the CKMfitter results for the Wolfenstein parameters [252], one finds $\Delta \simeq 0.033$, which corresponds to a shift of 2β of $+2.1^\circ$. Nonperturbative contributions can alter this result.

Table 35 Measurements of CP violation parameters from $B^0 \rightarrow J/\psi K_S^0$

Experiment	$\int \mathcal{L} dt$	S_{CP}	C_{CP}	$A^{\Delta\Gamma}$
LHCb [360]	3 fb^{-1}	$0.49^{+0.77}_{-0.65} \pm 0.06$	$-0.28 \pm 0.41 \pm 0.08$	$-0.08 \pm 0.40 \pm 0.08$

4.7.1 Time-dependent CP asymmetries: $b \rightarrow q\bar{q}s$ decays to CP eigenstates

The averages for $-\eta S_{b \rightarrow q\bar{q}s}$ and $C_{b \rightarrow q\bar{q}s}$ can be found in Tables 36 and 37, and are shown in Figs. 22, 23 and 24. Results from both BABAR and Belle are averaged for the modes $\eta'K^0$ (K^0 indicates that both K_S^0 and K_L^0 are used) $K_S^0 K_S^0 K_S^0, \pi^0 K_S^0$ and ωK_S^0 .³⁴ Results on ϕK_S^0 and $K^+ K^- K_S^0$ (implicitly excluding ϕK_S^0 and $f_0 K_S^0$) are taken from time-dependent Dalitz plot analyses of $K^+ K^- K_S^0$; results on $\rho^0 K_S^0, f_2 K_S^0, f_X K_S^0$ and $\pi^+ \pi^- K_S^0$ nonresonant are taken from time-dependent Dalitz plot analyses of $\pi^+ \pi^- K_S^0$ (see Sect. 4.7.2). The results on $f_0 K_S^0$ are from combinations of both Dalitz plot analyses. BABAR has also presented results with the final states $\pi^0 \pi^0 K_S^0$ and $\phi K_S^0 \pi^0$.

Of these final states, $\phi K_S^0, \eta' K_S^0, \pi^0 K_S^0, \rho^0 K_S^0, \omega K_S^0$ and $f_0 K_L^0$ have CP eigenvalue $\eta = -1$, while $\phi K_L^0, \eta' K_L^0, K_S^0 K_S^0 K_S^0, f_0 K_S^0, f_2 K_S^0, f_X K_S^0, \pi^0 \pi^0 K_S^0$ and $\pi^+ \pi^- K_S^0$ nonresonant have $\eta = +1$. The final state $K^+ K^- K_S^0$ (with ϕK_S^0 and $f_0 K_S^0$ implicitly excluded) is not a CP eigenstate, but the CP -content can be absorbed in the amplitude analysis to allow the determination of a single effective S parameter. (In earlier analyses of the $K^+ K^- K^0$ final state, its CP composition was determined using an isospin argument [383] and a moments analysis [384].) Throughout this section, $f_0 \equiv f_0(980)$ and $f_2 \equiv f_2(1270)$. Details of the assumed lineshapes of these states, and of the f_X (which is taken to have even spin), can be found in the relevant experimental papers [270, 271, 274, 275].

The final state $\phi K_S^0 \pi^0$ is also not a CP eigenstate but its CP -composition can be determined from an angular analysis. Since the parameters are common to the $B^0 \rightarrow \phi K_S^0 \pi^0$ and $B^0 \rightarrow \phi K^+ \pi^-$ decays (because only $K\pi$ resonances contribute), BABAR perform a simultaneous analysis of the two final states [391] (see Sect. 4.7.3).

It must be noted that Q2B parameters extracted from Dalitz plot analyses are constrained to lie within the physical boundary ($S_{CP}^2 + C_{CP}^2 < 1$) and consequently the obtained errors are highly non-Gaussian when the central value is close to the boundary. This is particularly evident in the BABAR results for $B^0 \rightarrow f_0 K^0$ with $f_0 \rightarrow \pi^+ \pi^-$ [274]. These results must be treated with extreme caution.

As explained above, each of the modes listed in Tables 36 and 37 has potentially different subleading contributions within the Standard Model, and thus each may have a different value of $-\eta S_{b \rightarrow q\bar{q}s}$. Therefore, there is no strong motivation to make a combined average over the different modes. We refer to such an average as a “naïve s -penguin average”. It is naïve not only because the theoretical uncertainties are neglected, but also since possible correlations of systematic effects between different modes are not included. In spite of these caveats there remains interest in the value of this quantity and therefore it is given here: $\langle -\eta S_{b \rightarrow q\bar{q}s} \rangle = 0.655 \pm 0.032$, with confidence level 0.77 (0.3 σ). This value is in agreement with the average $-\eta S_{b \rightarrow c\bar{c}s}$ given in Sect. 4.4.1. (The average for $C_{b \rightarrow q\bar{q}s}$ is $\langle C_{b \rightarrow q\bar{q}s} \rangle = -0.006 \pm 0.026$ with confidence level 0.53 (0.6 σ).)

From Table 36 it may be noted that the averages for $-\eta S_{b \rightarrow q\bar{q}s}$ in $\phi K_S^0, \eta' K^0, f_0 K_S^0$ and $K^+ K^- K_S^0$ are all now more than 5 σ away from zero, so that CP violation in these modes can be considered well established. There is no evidence (above 2 σ) for CP violation in any $b \rightarrow q\bar{q}s$ decay.

4.7.2 Time-dependent Dalitz plot analyses:

$$B^0 \rightarrow K^+ K^- K^0 \text{ and } B^0 \rightarrow \pi^+ \pi^- K_S^0$$

As mentioned in Sect. 4.2.5 and above, both BABAR and Belle have performed time-dependent Dalitz plot analysis of $B^0 \rightarrow K^+ K^- K^0$ and $B^0 \rightarrow \pi^+ \pi^- K_S^0$ decays. The results are summarised in Tables 38 and 39. Averages for the $B^0 \rightarrow f_0 K_S^0$ decay, which contributes to both Dalitz plots, are shown in Fig. 25. Results are presented in terms of the effective weak phase (from mixing and decay) difference β^{eff} and the parameter of CP violation in decay \mathcal{A} ($\mathcal{A} = -C$) for each of the resonant contributions. Note that Dalitz plot analyses, including all those included in these averages, often suffer from ambiguous solutions – we quote the results corresponding to those presented as solution 1 in all cases. Results on flavour specific amplitudes that may contribute to these Dalitz plots (such as $K^{*+} \pi^-$) are averaged by the HFLAV Rare Decays subgroup (Sect. 7).

For the $B^0 \rightarrow K^+ K^- K^0$ decay, both BABAR and Belle measure the CP violation parameters for the $\phi K^0, f_0 K^0$ and “other $K^+ K^- K^0$ ” amplitudes, where the latter includes all remaining resonant and nonresonant contributions to the charmless three-body decay. For the $B^0 \rightarrow \pi^+ \pi^- K_S^0$ decay, BABAR reports CP violation parameters for all of the CP

³⁴ Belle [382] include the $\pi^0 K_L^0$ final state together with $\pi^0 K_S^0$ in order to improve the constraint on the parameter of CP violation in decay; these events cannot be used for time-dependent analysis.

Table 36 Averages of $-\eta S_{b \rightarrow q\bar{q}s}$ and $C_{b \rightarrow q\bar{q}s}$. Where a third source of uncertainty is given, it is due to model uncertainties arising in Dalitz plot analyses

Experiment	$N(B\bar{B})$	$-\eta S_{b \rightarrow q\bar{q}s}$	$C_{b \rightarrow q\bar{q}s}$	Correlation
ϕK^0				
BABAR [271]	470M	$0.66 \pm 0.17 \pm 0.07$	$0.05 \pm 0.18 \pm 0.05$	–
Belle [270]	657M	$0.90^{+0.09}_{-0.19}$	$-0.04 \pm 0.20 \pm 0.10 \pm 0.02$	–
Average		$0.74^{+0.11}_{-0.13}$	0.01 ± 0.14	Uncorrelated averages
$\eta' K^0$				
BABAR [385]	467M	$0.57 \pm 0.08 \pm 0.02$	$-0.08 \pm 0.06 \pm 0.02$	0.03
Belle [386]	772M	$0.68 \pm 0.07 \pm 0.03$	$-0.03 \pm 0.05 \pm 0.03$	0.03
Average		0.63 ± 0.06	-0.05 ± 0.04	0.02
Confidence level		0.53 (0.6 σ)		
$K_S^0 K_S^0 K_S^0$				
BABAR [387]	468M	$0.94^{+0.21}_{-0.24} \pm 0.06$	$-0.17 \pm 0.18 \pm 0.04$	0.16
Belle [388]	535M	$0.30 \pm 0.32 \pm 0.08$	$-0.31 \pm 0.20 \pm 0.07$	–
Average		0.72 ± 0.19	-0.24 ± 0.14	0.09
Confidence level		0.26 (1.1 σ)		
$\pi^0 K^0$				
BABAR [385]	467M	$0.55 \pm 0.20 \pm 0.03$	$0.13 \pm 0.13 \pm 0.03$	0.06
Belle [382]	657M	$0.67 \pm 0.31 \pm 0.08$	$-0.14 \pm 0.13 \pm 0.06$	-0.04
Average		0.57 ± 0.17	0.01 ± 0.10	0.02
Confidence level		0.37 (0.9 σ)		
$\rho^0 K_S^0$				
BABAR [274]	383M	$0.35^{+0.26}_{-0.31} \pm 0.06 \pm 0.03$	$-0.05 \pm 0.26 \pm 0.10 \pm 0.03$	–
Belle [275]	657M	$0.64^{+0.19}_{-0.25} \pm 0.09 \pm 0.10$	$-0.03^{+0.24}_{-0.23} \pm 0.11 \pm 0.10$	–
Average		$0.54^{+0.18}_{-0.21}$	-0.06 ± 0.20	Uncorrelated averages
ωK_S^0				
BABAR [385]	467M	$0.55^{+0.26}_{-0.29} \pm 0.02$	$-0.52^{+0.22}_{-0.20} \pm 0.03$	0.03
Belle [389]	772M	$0.91 \pm 0.32 \pm 0.05$	$0.36 \pm 0.19 \pm 0.05$	-0.00
Average		0.71 ± 0.21	-0.04 ± 0.14	0.01
Confidence level		0.007 (2.7 σ)		
$f_0 K^0$				
BABAR [271,274]	–	$0.74^{+0.12}_{-0.15}$	0.15 ± 0.16	–
Belle [270,275]	–	$0.63^{+0.16}_{-0.19}$	0.13 ± 0.17	–
Average		$0.69^{+0.10}_{-0.12}$	0.14 ± 0.12	Uncorrelated averages
$f_2 K_S^0$				
BABAR [274]	383M	$0.48 \pm 0.52 \pm 0.06 \pm 0.10$	$0.28^{+0.35}_{-0.40} \pm 0.08 \pm 0.07$	–
$f_X K_S^0$				
BABAR [274]	383M	$0.20 \pm 0.52 \pm 0.07 \pm 0.07$	$0.13^{+0.33}_{-0.35} \pm 0.04 \pm 0.09$	–

eigenstate components in the Dalitz plot model ($\rho^0 K_S^0$, $f_0 K_S^0$, $f_2 K_S^0$, $f_X K_S^0$ and nonresonant decays; see Sect. 4.2.5), while Belle reports the CP violation parameters for only the $\rho^0 K_S^0$ and $f_0 K_S^0$ amplitudes, although the used Dalitz plot model is rather similar.

4.7.3 Time-dependent analyses of $B^0 \rightarrow \phi K_S^0 \pi^0$

The final state in the decay $B^0 \rightarrow \phi K_S^0 \pi^0$ is a mixture of CP -even and CP -odd amplitudes. However, since only ϕK^{*0} resonant states contribute (in particular, $\phi K^{*0}(892)$, $\phi K_0^{*0}(1430)$ and $\phi K_2^{*0}(1430)$ are seen), the composition

Table 37 Averages of $-\eta S_{b \rightarrow q\bar{q}s}$ and $C_{b \rightarrow q\bar{q}s}$ (continued). Where a third source of uncertainty is given, it is due to model uncertainties arising in Dalitz plot analyses

Experiment	$N(B\bar{B})$	$-\eta S_{b \rightarrow q\bar{q}s}$	$C_{b \rightarrow q\bar{q}s}$	Correlation
$\pi^0 \pi^0 K_S^0$				
BABAR [390]	227M	$-0.72 \pm 0.71 \pm 0.08$	$0.23 \pm 0.52 \pm 0.13$	-0.02
$\phi K_S^0 \pi^0$				
BABAR [391]	465M	$0.97^{+0.03}_{-0.52}$	$-0.20 \pm 0.14 \pm 0.06$	-
$\pi^+ \pi^- K_S^0$ nonresonant				
BABAR [274]	383M	$0.01 \pm 0.31 \pm 0.05 \pm 0.09$	$0.01 \pm 0.25 \pm 0.06 \pm 0.05$	-
$K^+ K^- K^0$				
BABAR [271]	470M	$0.65 \pm 0.12 \pm 0.03$	$0.02 \pm 0.09 \pm 0.03$	-
Belle [270]	657M	$0.76^{+0.14}_{-0.18}$	$0.14 \pm 0.11 \pm 0.08 \pm 0.03$	-
Average		$0.68^{+0.09}_{-0.10}$	0.06 ± 0.08	Uncorrelated averages

can be determined from the analysis of $B \rightarrow \phi K^+ \pi^-$ decays, assuming only that the ratio of branching fractions $\mathcal{B}(K^{*0} \rightarrow K_S^0 \pi^0) / \mathcal{B}(K^{*0} \rightarrow K^+ \pi^-)$ is the same for each excited kaon state.

BABAR [391] has performed a simultaneous analysis of $B^0 \rightarrow \phi K_S^0 \pi^0$ and $B^0 \rightarrow \phi K^+ \pi^-$ decays that is time-dependent for the former mode and time-integrated for the latter. Such an analysis allows, in principle, all parameters of the $B^0 \rightarrow \phi K^{*0}$ system to be determined, including mixing-induced CP violation effects. The latter is determined to be $\Delta\phi_{00} = 0.28 \pm 0.42 \pm 0.04$, where $\Delta\phi_{00}$ is half the weak phase difference between B^0 and \bar{B}^0 decays to the ϕK_0^{*0} (1430) final state. As discussed above, this can also be presented in terms of the Q2B parameter $\sin(2\beta_{00}^{\text{eff}}) = \sin(2\beta + 2\Delta\phi_{00}) = 0.97^{+0.03}_{-0.52}$. The highly asymmetric uncertainty arises due to the conversion from the phase to the sine of the phase, and the proximity of the physical boundary.

Similar $\sin(2\beta^{\text{eff}})$ parameters can be defined for each of the helicity amplitudes for both ϕK^{*0} (892) and ϕK_2^{*0} (1430). However, the relative phases between these decays are constrained due to the nature of the simultaneous analysis of $B^0 \rightarrow \phi K_S^0 \pi^0$ and $B^0 \rightarrow \phi K^+ \pi^-$, decays and therefore these measurements are highly correlated. Instead of quoting all these results, BABAR provide an illustration of their measurements with the following differences:

$$\sin(2\beta - 2\Delta\delta_{01}) - \sin(2\beta) = -0.42^{+0.26}_{-0.34}, \tag{156}$$

$$\sin(2\beta - 2\Delta\phi_{\parallel 1}) - \sin(2\beta) = -0.32^{+0.22}_{-0.30}, \tag{157}$$

$$\sin(2\beta - 2\Delta\phi_{\perp 1}) - \sin(2\beta) = -0.30^{+0.23}_{-0.32}, \tag{158}$$

$$\sin(2\beta - 2\Delta\phi_{\perp 1}) - \sin(2\beta - 2\Delta\phi_{\parallel 1}) = 0.02 \pm 0.23, \tag{159}$$

$$\sin(2\beta - 2\Delta\delta_{02}) - \sin(2\beta) = -0.10^{+0.18}_{-0.29}, \tag{160}$$

where the first subscript indicates the helicity amplitude and the second indicates the spin of the kaon resonance. For the

complete definitions of the $\Delta\delta$ and $\Delta\phi$ parameters, please refer to the BABAR paper [391].

Parameters of CP violation in decay for each of the contributing helicity amplitudes can also be measured. Again, these are determined from a simultaneous fit of $B^0 \rightarrow \phi K_S^0 \pi^0$ and $B^0 \rightarrow \phi K^+ \pi^-$ decays, with the precision being dominated by the statistics of the latter mode. Measurements of CP violation in decay, obtained from decay-time-integrated analyses, are tabulated by the HFLAV Rare Decays subgroup (Sect. 7).

4.7.4 Time-dependent CP asymmetries in $B_s^0 \rightarrow K^+ K^-$

The decay $B_s^0 \rightarrow K^+ K^-$ involves a $b \rightarrow u\bar{u}s$ transition, and hence has both penguin and tree contributions. Both mixing-induced and CP violation in decay effects may arise, and additional input is needed to disentangle the contributions and determine γ and β_s^{eff} . For example, the observables in $B^0 \rightarrow \pi^+ \pi^-$ can be related using U-spin, as proposed in Refs. [392,393].

The observables are $A_{\text{mix}} = S_{CP}$, $A_{\text{dir}} = -C_{CP}$, and $A_{\Delta\Gamma}$. They can all be treated as free parameters, but are physically constrained to satisfy $A_{\text{mix}}^2 + A_{\text{dir}}^2 + A_{\Delta\Gamma}^2 = 1$. Note that the untagged decay distribution, from which an ‘‘effective lifetime’’ can be measured, retains sensitivity to $A_{\Delta\Gamma}$; measurements of the $B_s^0 \rightarrow K^+ K^-$ effective lifetime have been made by LHCb [104,125]. Compilations and averages of effective lifetimes are performed by the HFLAV Lifetimes and Oscillations subgroup, see Sect. 3.

The observables in $B_s^0 \rightarrow K^+ K^-$ have been measured by LHCb [394], who do not impose the constraint mentioned above to eliminate $A_{\Delta\Gamma}$. The results are shown in Table 40, and correspond to evidence for CP violation both in the interference between mixing and decay, and in the $B_s^0 \rightarrow K^+ K^-$ decay.

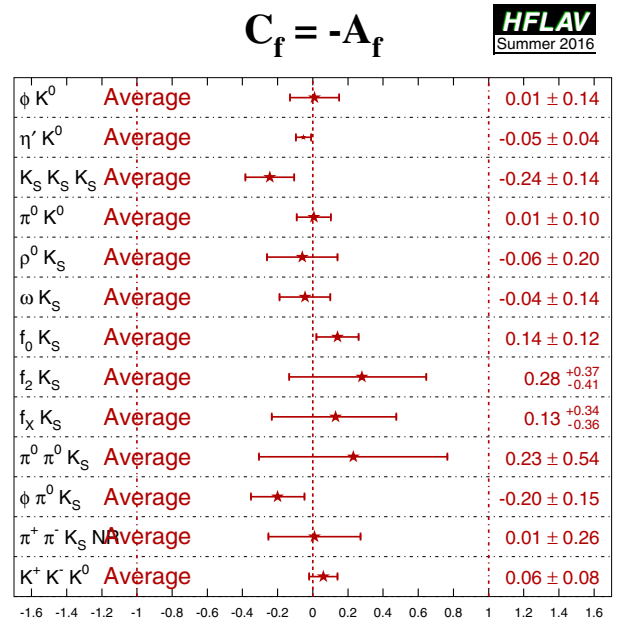
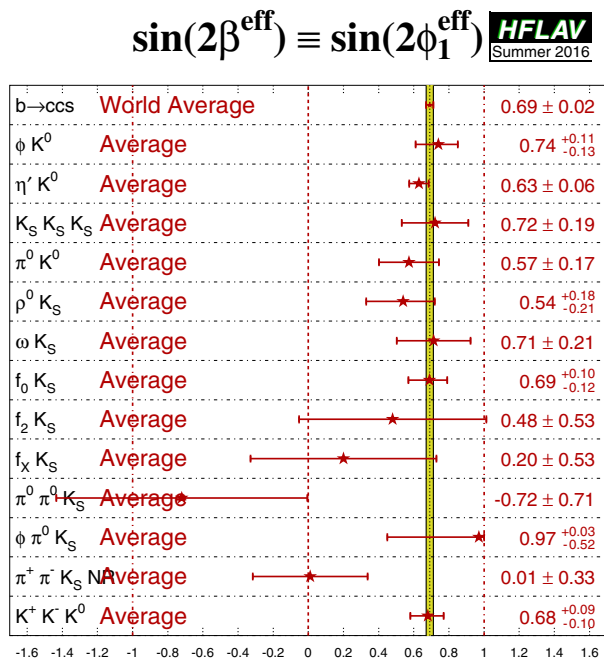
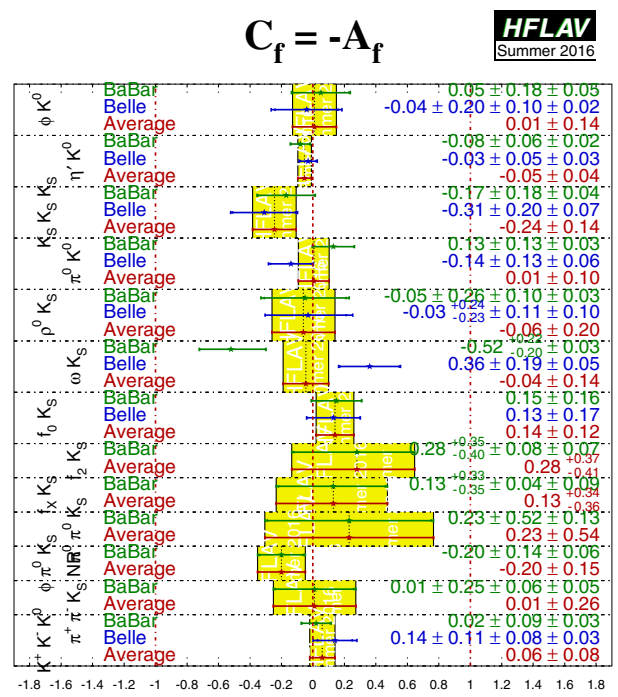
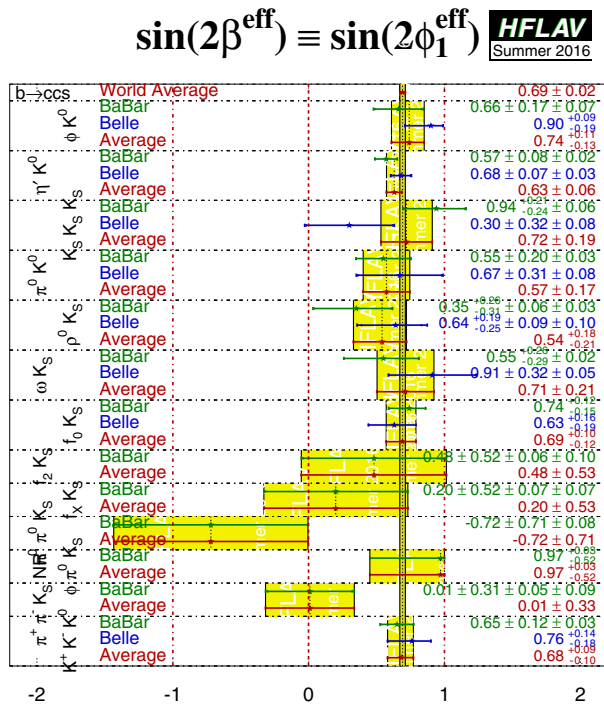


Fig. 22 (Top) Averages of (left) $-\eta S_{b \rightarrow q\bar{q}s}$, interpreted as $\sin(2\beta^{\text{eff}})$ and (right) $C_{b \rightarrow q\bar{q}s}$. The $-\eta S_{b \rightarrow q\bar{q}s}$ figure compares the results to the world average for $-\eta S_{b \rightarrow c\bar{c}s}$ (see Sect. 4.4.1). (Bottom) Same, but only

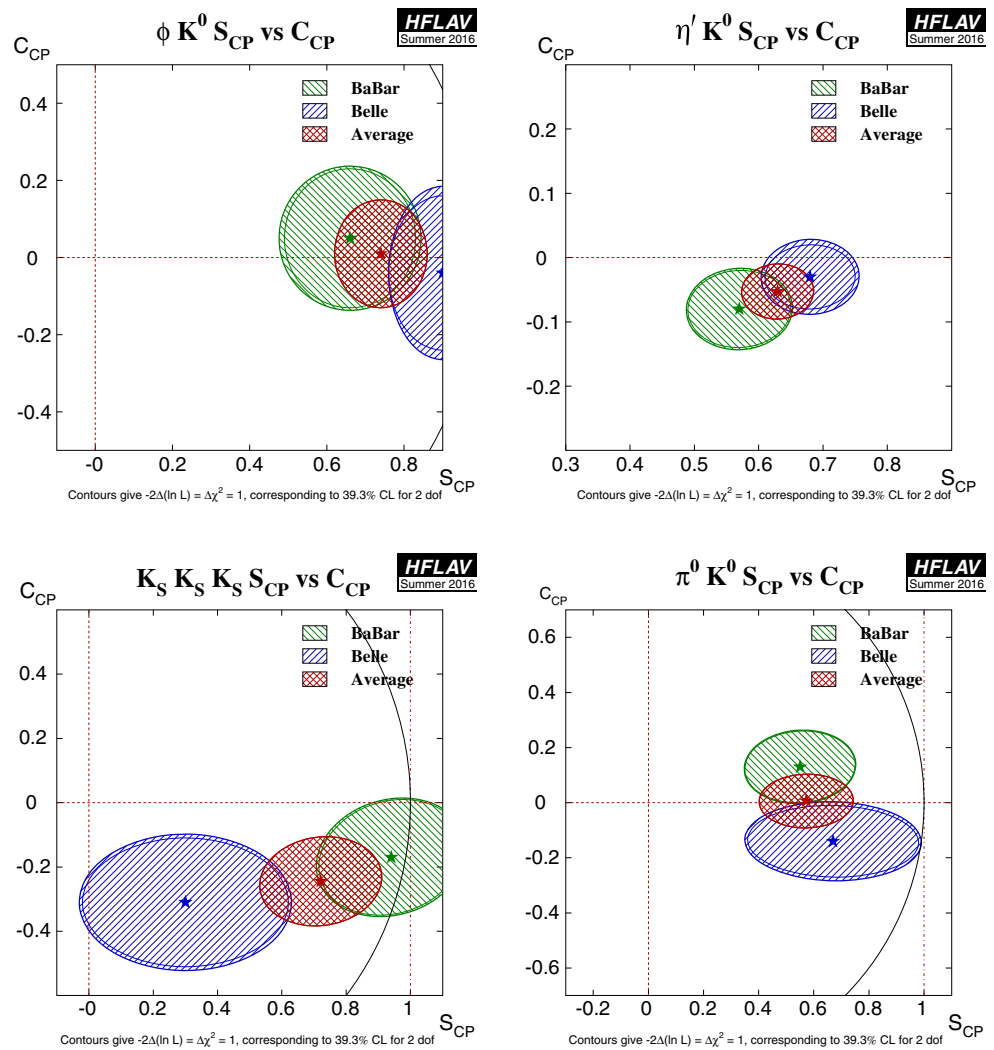
averages for each mode are shown. More figures are available from the HFLAV web pages

Interpretations of an earlier set of results [395], in terms of constraints on γ and $2\beta_s$, have been separately published by LHCb [243].

4.7.5 Time-dependent CP asymmetries in $B_s^0 \rightarrow \phi\phi$

The decay $B_s^0 \rightarrow \phi\phi$ involves a $b \rightarrow s\bar{s}s$ transition, and hence is a “pure penguin” mode (in the limit that the ϕ meson

Fig. 23 Averages of four $b \rightarrow q\bar{q}s$ dominated channels, for which correlated averages are performed, in the S_{CP} vs. C_{CP} plane, where S_{CP} has been corrected by the CP eigenvalue to give $\sin(2\beta^{\text{eff}})$. (Top left) $B^0 \rightarrow \phi K^0$, (top right) $B^0 \rightarrow \eta' K^0$, (bottom left) $B^0 \rightarrow K_S^0 K_S^0 K_S^0$, (bottom right) $B^0 \rightarrow \pi^0 K_S^0$. More figures are available from the HFLAV web pages



is considered a pure $s\bar{s}$ state). Since the mixing phase and the decay phase are expected to cancel in the Standard Model, the prediction for the phase from the interference of mixing and decay is predicted to be $\phi_s(\phi\phi) = 0$ with low uncertainty [396]. Due to the vector-vector nature of the final state, angular analysis is needed to separate the CP -even and CP -odd contributions. Such an analysis also makes it possible to fit directly for $\phi_s(\phi\phi)$.

A constraint on $\phi_s(\phi\phi)$ has been obtained by LHCb using 3.0 fb^{-1} of data [397]. The result is $\phi_s(\phi\phi) = -0.17 \pm 0.15 \pm 0.03 \text{ rad}$ where the first uncertainty is statistical and the second is systematic.

4.8 Time-dependent CP asymmetries in $b \rightarrow q\bar{q}d$ transitions

Decays such as $B^0 \rightarrow K_S^0 K_S^0$ are pure $b \rightarrow q\bar{q}d$ penguin transitions. As shown in Eq. (153), this diagram has different contributing weak phases, and therefore the observables are

sensitive to their difference (which can be chosen to be either β or γ). Note that if the contribution with the top quark in the loop dominates, the weak phase from the decay amplitudes should cancel that from mixing, so that no CP violation (neither mixing-induced nor in decay) occurs. Non-zero contributions from loops with intermediate up and charm quarks can result in both types of effect (as usual, a strong phase difference is required for CP violation in decay to occur).

Both BABAR [398] and Belle [399] have performed time-dependent analyses of $B^0 \rightarrow K_S^0 K_S^0$ decays. The results are given in Table 41 and shown in Fig. 26.

4.9 Time-dependent asymmetries in $b \rightarrow s\gamma$ transitions

The radiative decays $b \rightarrow s\gamma$ produce photons which are highly polarised in the Standard Model. The decays $B^0 \rightarrow F\gamma$ and $\bar{B}^0 \rightarrow F\gamma$ produce photons with opposite helicities, and since the polarisation is, in principle, observable, these

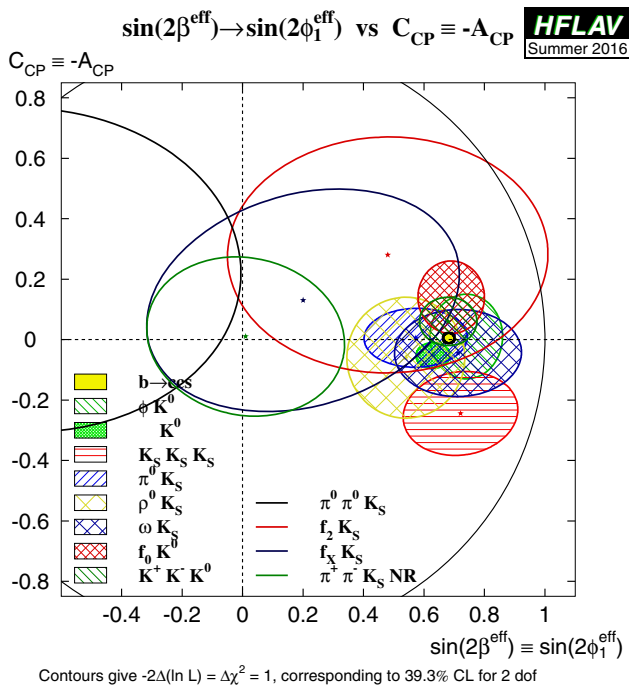


Fig. 24 Compilation of constraints in the $-\eta S_{b \rightarrow q\bar{q}s}$, interpreted as $\sin(2\beta^{\text{eff}})$, vs. $C_{b \rightarrow q\bar{q}s}$ plane

final states cannot interfere. The finite mass of the s quark introduces small corrections to the limit of maximum polarisation, but any large mixing-induced CP violation would be a signal for new physics. Since a single weak phase dominates the $b \rightarrow s\gamma$ transition in the Standard Model, the cosine term is also expected to be small.

Atwood et al. [298] have shown that an inclusive analysis of $K_S^0\pi^0\gamma$ can be performed, since the properties of the decay amplitudes are independent of the angular momentum of the $K_S^0\pi^0$ system. However, if non-dipole operators contribute significantly to the amplitudes, then the Standard Model mixing-induced CP violation could be larger than the naïve expectation $S \simeq -2(m_s/m_b) \sin(2\beta)$ [299,300]. In this case, the CP parameters may vary over the $K_S^0\pi^0\gamma$ Dalitz plot, for example as a function of the $K_S^0\pi^0$ invariant mass.

With the above in mind, we quote two averages: one for $K^*(892)$ candidates only, and the other one for the inclusive $K_S^0\pi^0\gamma$ decay (including the $K^*(892)$). If the Standard Model dipole operator is dominant, both should give the same quantities (the latter naturally with smaller statistical error). If not, care needs to be taken in interpretation of the inclusive parameters, while the results on the $K^*(892)$ resonance remain relatively clean. Results from BABAR and Belle are used for both averages; both experiments use the invariant mass range $0.60 < M_{K_S^0\pi^0} < 1.80 \text{ GeV}/c^2$ in the inclusive analysis.

Table 38 Results from time-dependent Dalitz plot analyses of the $B^0 \rightarrow K^+K^-K_S^0$ decay. Correlations (not shown) are taken into account in the average

Experiment	$N(B\bar{B})$	ϕK_S^0		$f_0 K_S^0$		$K^+K^-K_S^0$	
		$\beta^{\text{eff}} (^\circ)$	\mathcal{A}	$\beta^{\text{eff}} (^\circ)$	\mathcal{A}	$\beta^{\text{eff}} (^\circ)$	\mathcal{A}
BABAR [271]	470M	$21 \pm 6 \pm 2$	$-0.05 \pm 0.18 \pm 0.05$	$18 \pm 6 \pm 4$	$-0.28 \pm 0.24 \pm 0.09$	$20.3 \pm 4.3 \pm 1.2$	$-0.02 \pm 0.09 \pm 0.03$
Belle [270]	657M	$32.2 \pm 9.0 \pm 2.6 \pm 1.4$	$0.04 \pm 0.20 \pm 0.10 \pm 0.02$	$31.3 \pm 9.0 \pm 3.4 \pm 4.0$	$-0.30 \pm 0.29 \pm 0.11 \pm 0.09$	$24.9 \pm 6.4 \pm 2.1 \pm 2.5$	$-0.14 \pm 0.11 \pm 0.08 \pm 0.03$
Average		24 ± 5	-0.01 ± 0.14	22 ± 6	-0.29 ± 0.20	21.6 ± 3.7	-0.06 ± 0.08
Confidence level							$0.93 (0.1\sigma)$

Table 39 Results from time-dependent Dalitz plot analysis of the $B^0 \rightarrow \pi^+\pi^-K_S^0$ decay. Correlations (not shown) are taken into account in the average

Experiment	$N(B\bar{B})$	$\rho^0 K_S^0$		$f_0 K_S^0$	
		β^{eff}	\mathcal{A}	β^{eff}	\mathcal{A}
BABAR [274]	383M	(10.2 ± 8.9 ± 3.0 ± 1.9)°	0.05 ± 0.26 ± 0.10 ± 0.03	(36.0 ± 9.8 ± 2.1 ± 2.1)°	-0.08 ± 0.19 ± 0.03 ± 0.04
Belle [275]	657M	(20.0 ^{+8.6} _{-8.5} ± 3.2 ± 3.5)°	0.03 ^{+0.23} _{-0.24} ± 0.11 ± 0.10	(12.7 ^{+6.9} _{-6.5} ± 2.8 ± 3.3)°	-0.06 ± 0.17 ± 0.07 ± 0.09
Average		16.4 ± 6.8	0.06 ± 0.20	20.6 ± 6.2	-0.07 ± 0.14
Confidence level			0.39 (0.9σ)		
Experiment	$N(B\bar{B})$	$f_2 K_S^0$		$f_X K_S^0$	
		β^{eff}	\mathcal{A}	β^{eff}	\mathcal{A}
BABAR [274]	383M	(14.9 ± 17.9 ± 3.1 ± 5.2)°	-0.28 ^{+0.40} _{-0.35} ± 0.08 ± 0.07	(5.8 ± 15.2 ± 2.2 ± 2.3)°	-0.13 ^{+0.35} _{-0.33} ± 0.04 ± 0.09
Experiment	$N(B\bar{B})$	$B^0 \rightarrow \pi^+\pi^-K_S^0$ nonresonant		$\chi_{c0} K_S^0$	
		β^{eff}	\mathcal{A}	β^{eff}	\mathcal{A}
BABAR [274]	383M	(0.4 ± 8.8 ± 1.9 ± 3.8)°	-0.01 ± 0.25 ± 0.06 ± 0.05	(23.2 ± 22.4 ± 2.3 ± 4.2)°	0.29 ^{+0.44} _{-0.53} ± 0.03 ± 0.05

In addition to the $K_S^0\pi^0\gamma$ decay, both BABAR and Belle have presented results using the $K_S^0\rho\gamma$ mode, while BABAR (Belle) has in addition presented results using the $K_S^0\eta\gamma$ ($K_S^0\phi\gamma$) channel. For the $K_S^0\rho\gamma$ case, due to the non-negligible width of the ρ^0 meson, decays selected as $B^0 \rightarrow K_S^0\rho^0\gamma$ can include a significant contribution from $K^{*\pm}\pi^\mp\gamma$ decays, which are flavour-specific and do not have the same oscillation phenomenology. Both BABAR and Belle measure S_{eff} for all B decay candidates with the ρ^0 selection being $0.6 < m(\pi^+\pi^-) < 0.9 \text{ GeV}/c^2$, obtaining 0.14 ± 0.25 ^{+0.04}_{-0.03} (BABAR) and 0.09 ± 0.27 ^{+0.04}_{-0.07} (Belle). These values are then corrected for a ‘‘dilution factor’’, that is evaluated with different methods in the two experiments: BABAR [400,401] obtains a dilution factor of -0.78 ^{+0.19}_{-0.17} while Belle [402] obtains $+0.83$ ^{+0.19}_{-0.03}. Until the discrepancy between these values is understood, the average of the results should be treated with caution.

The results are given in Table 42, and shown in Figs. 27 and 28. No significant CP violation results are seen; the results are consistent with the Standard Model and with other measurements in the $b \rightarrow s\gamma$ system (see Sect. 7).

A similar analysis can be performed for radiative B_S^0 decays to, for example, the $\phi\gamma$ final state. As for other observables determined with self-conjugate final states produced in B_S^0 decays, the effective lifetime also provides sensitivity, and can be determined without tagging the initial flavour of the decaying meson. The LHCb collaboration has determined the associated parameter $A_{\Delta\Gamma}(\phi\gamma) = -0.98$ ^{+0.46}_{-0.52}^{+0.23}_{-0.20} [407].

4.10 Time-dependent asymmetries in $b \rightarrow d\gamma$ transitions

The formalism for the radiative decays $b \rightarrow d\gamma$ is much the same as that for $b \rightarrow s\gamma$ discussed above. Assuming dominance of the top quark in the loop, the weak phase in decay should cancel with that from mixing, so that the mixing-induced CP violation parameter S_{CP} should be very small. Corrections due to the finite light quark mass are smaller compared to $b \rightarrow s\gamma$, since $m_d < m_s$, but QCD corrections of $\mathcal{O}(A_{\text{QCD}}/m_b)$ may be sizable [299]. Large CP violation effects could be seen through a non-zero value of $C_{b \rightarrow d\gamma}$ since the top loop is not the only contribution.

Results using the mode $B^0 \rightarrow \rho^0\gamma$ are available from Belle and are given in Table 43.

4.11 Time-dependent CP asymmetries in $b \rightarrow u\bar{u}d$ transitions

The $b \rightarrow u\bar{u}d$ transition can be mediated by either a $b \rightarrow u$ tree amplitude or a $b \rightarrow d$ penguin amplitude. These transitions can be investigated using the time dependence of B^0 decays to final states containing light mesons. Results are

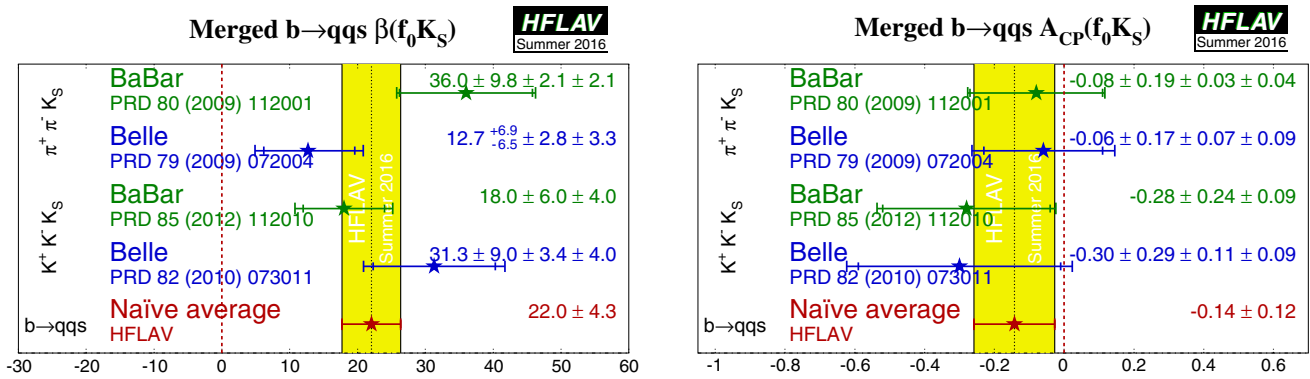


Fig. 25 Averages of (left) $\beta_1^{\text{eff}} \equiv \phi_1^{\text{eff}}$ and (right) A_{CP} for the $B^0 \rightarrow f_0 K_S^0$ decay including measurements from Dalitz plot analyses of both $B^0 \rightarrow K^+ K^- K_S^0$ and $B^0 \rightarrow \pi^+ \pi^- K_S^0$

Table 40 Results from time-dependent analysis of the $B_s^0 \rightarrow K^+ K^-$ decay

Experiment	Sample size	S_{CP}	C_{CP}	$A^{\Delta\Gamma}$
LHCb [394]	$\int \mathcal{L} dt = 3.0 \text{ fb}^{-1}$	$0.22 \pm 0.06 \pm 0.02$	$0.24 \pm 0.06 \pm 0.02$	$-0.75 \pm 0.07 \pm 0.11$

Table 41 Results for $B^0 \rightarrow K_S^0 K_S^0$

Experiment	$N(B\bar{B})$	S_{CP}	C_{CP}	Correlation
BABAR [398]	350M	$-1.28^{+0.80}_{-0.73} {}^{+0.11}_{-0.16}$	$-0.40 \pm 0.41 \pm 0.06$	-0.32
Belle [399]	657M	$-0.38^{+0.69}_{-0.77} \pm 0.09$	$0.38 \pm 0.38 \pm 0.05$	0.48
Average		-1.08 ± 0.49	-0.06 ± 0.26	0.14
Confidence level		0.29 (1.1 σ)		

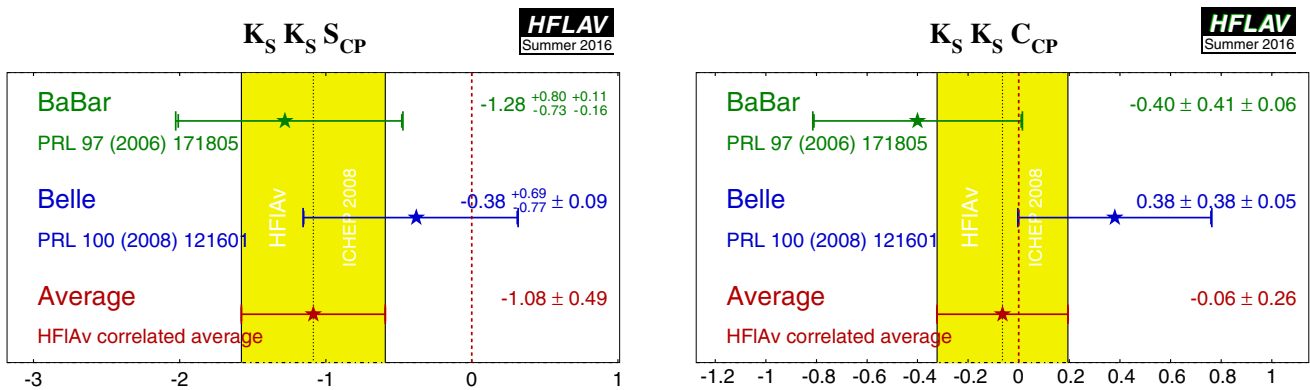


Fig. 26 Averages of (left) S_{CP} and (right) C_{CP} for the mode $B^0 \rightarrow K_S^0 K_S^0$

available from both BABAR and Belle for the CP eigenstate ($\eta = +1$) $\pi^+ \pi^-$ final state and for the vector-vector final state $\rho^+ \rho^-$, which is found to be dominated by the CP -even longitudinally polarised component (BABAR measures $f_{\text{long}} = 0.992 \pm 0.024 {}^{+0.026}_{-0.013}$ [409] while Belle measures $f_{\text{long}} = 0.988 \pm 0.012 \pm 0.023$ [410]). BABAR has also performed a time-dependent analysis of the vector-

vector final state $\rho^0 \rho^0$ [411], in which they measure $f_{\text{long}} = 0.70 \pm 0.14 \pm 0.05$; Belle measure a smaller branching fraction than BABAR for $B^0 \rightarrow \rho^0 \rho^0$ [412] with corresponding signal yields too small to perform a time-dependent analysis; for the longitudinal polarisation they measure $f_{\text{long}} = 0.21 {}^{+0.18}_{-0.22} \pm 0.13$. LHCb has measured the branching fraction and longitudinal polarisation for $B^0 \rightarrow \rho^0 \rho^0$, and for

Table 42 Averages for $b \rightarrow s\gamma$ modes

Experiment	$N(B\bar{B})$	$S_{CP}(b \rightarrow s\gamma)$	$C_{CP}(b \rightarrow s\gamma)$	Correlation
$K^*(892)\gamma$				
BABAR [403]	467M	$-0.03 \pm 0.29 \pm 0.03$	$-0.14 \pm 0.16 \pm 0.03$	0.05
Belle [404]	535M	$-0.32^{+0.36}_{-0.33} \pm 0.05$	$0.20 \pm 0.24 \pm 0.05$	0.08
Average		-0.16 ± 0.22	-0.04 ± 0.14	0.06
Confidence level		0.40 (0.9 σ)		
$K_S^0\pi^0\gamma$ (including $K^*(892)\gamma$)				
BABAR [403]	467M	$-0.17 \pm 0.26 \pm 0.03$	$-0.19 \pm 0.14 \pm 0.03$	0.04
Belle [404]	535M	$-0.10 \pm 0.31 \pm 0.07$	$0.20 \pm 0.20 \pm 0.06$	0.08
Average		-0.15 ± 0.20	-0.07 ± 0.12	0.05
Confidence level		0.30 (1.0 σ)		
$K_S^0\eta\gamma$				
BABAR [405]	465M	$-0.18^{+0.49}_{-0.46} \pm 0.12$	$-0.32^{+0.40}_{-0.39} \pm 0.07$	-0.17
$K_S^0\rho^0\gamma$				
BABAR [401]	471M	$-0.18 \pm 0.32^{+0.06}_{-0.05}$	$-0.39 \pm 0.20^{+0.03}_{-0.02}$	-0.09
Belle [402]	657M	$0.11 \pm 0.33^{+0.05}_{-0.09}$	$-0.05 \pm 0.18 \pm 0.06$	0.04
Average		-0.06 ± 0.23	-0.22 ± 0.14	-0.02
Confidence level		0.38 (0.9 σ)		
$K_S^0\phi\gamma$				
Belle [406]	772M	$0.74^{+0.72+0.10}_{-1.05-0.24}$	$-0.35 \pm 0.58^{+0.10}_{-0.23}$	-

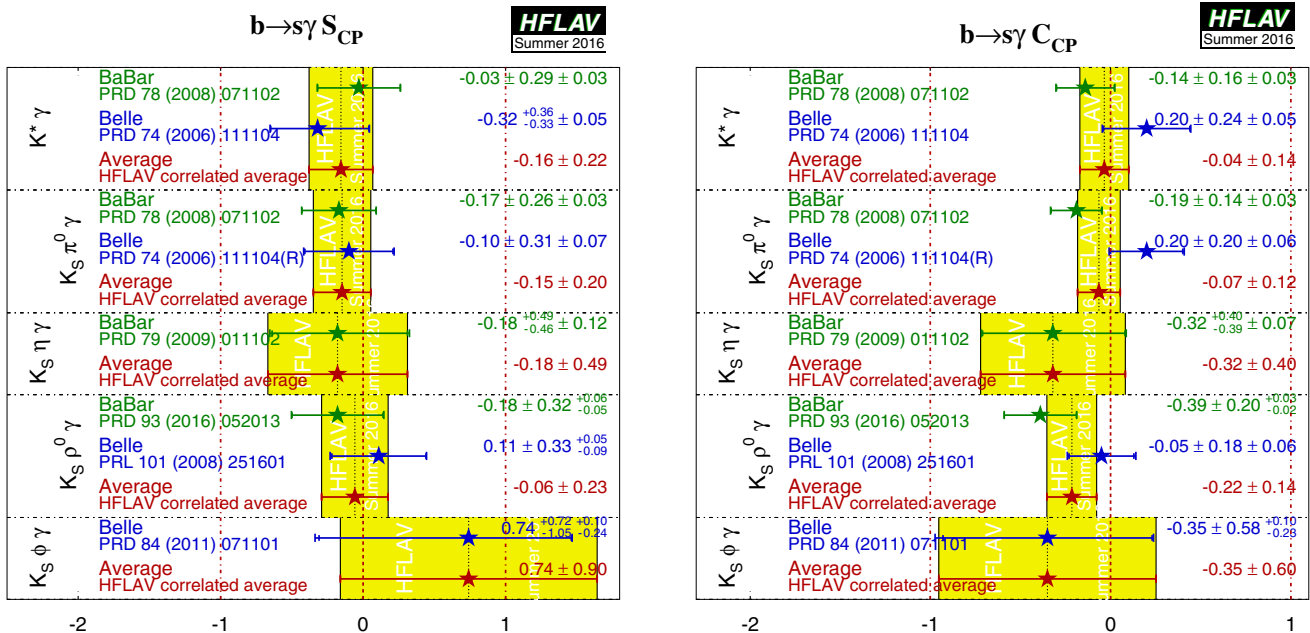


Fig. 27 Averages of (left) $S_{b \rightarrow s\gamma}$ and (right) $C_{b \rightarrow s\gamma}$. Recall that the data for $K^*\gamma$ is a subset of that for $K_S^0\pi^0\gamma$

the latter finds $f_{\text{long}} = 0.745^{+0.048}_{-0.058} \pm 0.034$ [413], but has not yet performed a time-dependent analysis of this decay. The Belle measurement for f_{long} is thus in some tension with the other results. BABAR has furthermore performed a time-

dependent analysis of the $B^0 \rightarrow a_1^\pm \pi^\mp$ decay [414]; further experimental input for the extraction of α from this channel is reported in a later publication [415].

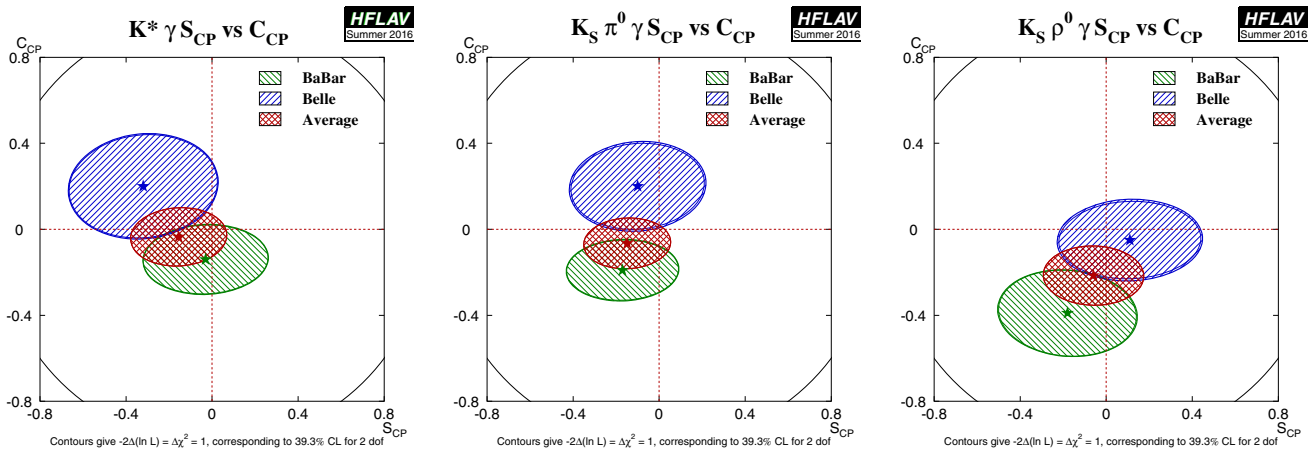


Fig. 28 Averages of three $b \rightarrow s\gamma$ dominated channels, for which correlated averages are performed, in the S_{CP} vs. C_{CP} plane. (Left) $B^0 \rightarrow K^*\gamma$, (middle) $B^0 \rightarrow K_S^0\pi^0\gamma$ (including $K^*\gamma$), (right) $B^0 \rightarrow K_S^0\rho^0\gamma$

Table 43 Averages for $B^0 \rightarrow \rho^0\gamma$

Experiment	$N(B\bar{B})$	S_{CP}	C_{CP}	Correlation
Belle [408]	657M	$-0.83 \pm 0.65 \pm 0.18$	$0.44 \pm 0.49 \pm 0.14$	-0.08

Results, and averages, of time-dependent CP violation parameters in $b \rightarrow u\bar{u}d$ transitions are listed in Table 44. The averages for $\pi^+\pi^-$ are shown in Fig. 29, and those for $\rho^+\rho^-$ are shown in Fig. 30, with the averages in the S_{CP} vs. C_{CP} plane shown in Fig. 31 and averages of CP violation parameters in $B^0 \rightarrow a_1^\pm\pi^\mp$ decay shown in Fig. 32.

If the penguin contribution is negligible, the time-dependent parameters for $B^0 \rightarrow \pi^+\pi^-$ and $B^0 \rightarrow \rho^+\rho^-$ are given by $S_{b \rightarrow u\bar{u}d} = \eta \sin(2\alpha)$ and $C_{b \rightarrow u\bar{u}d} = 0$. In the presence of the penguin contribution, CP violation in decay may arise, and there is no straightforward interpretation of $S_{b \rightarrow u\bar{u}d}$ and $C_{b \rightarrow u\bar{u}d}$. An isospin analysis [419] can be used to disentangle the contributions and extract α .

For the non- CP eigenstate $\rho^\pm\pi^\mp$, both BABAR [281] and Belle [283,284] have performed time-dependent Dalitz plot analyses of the $\pi^+\pi^-\pi^0$ final state [279]; such analyses allow direct measurements of the phases. Both experiments have measured the U and I parameters discussed in Sect. 4.2.5 and defined in Table 22. We have performed a full correlated average of these parameters, the results of which are summarised in Fig. 33.

Both experiments have also extracted the Q2B parameters. We have performed a full correlated average of these parameters, which is equivalent to determining the values from the averaged U and I parameters. The results are given in Table 45.³⁵ Averages of the $B^0 \rightarrow \rho^0\pi^0$ Q2B parameters are shown in Figs. 34 and 35.

³⁵ The $B^0 \rightarrow \rho^\pm\pi^\mp$ Q2B parameters are comparable to the parameters used for $B^0 \rightarrow a_1^\pm\pi^\mp$ decays, reported in Table 44. For the

With the notation described in Sect. 4.2 (Eq. (131)), the time-dependent parameters for the Q2B $B^0 \rightarrow \rho^\pm\pi^\mp$ analysis are, neglecting penguin contributions, given by

$$\begin{aligned}
 S_{\rho\pi} &= \sqrt{1 - \left(\frac{\Delta C}{2}\right)^2} \sin(2\alpha) \cos(\delta) \\
 \Delta S_{\rho\pi} &= \sqrt{1 - \left(\frac{\Delta C}{2}\right)^2} \cos(2\alpha) \sin(\delta)
 \end{aligned}
 \tag{161}$$

and $C_{\rho\pi} = \mathcal{A}_{CP}^{\rho\pi} = 0$, where $\delta = \arg(A_{-+}A_{+-}^*)$ is the strong phase difference between the $\rho^-\pi^+$ and $\rho^+\pi^-$ decay amplitudes. In the presence of the penguin contribution, there is no straightforward interpretation of the Q2B observables in the $B^0 \rightarrow \rho^\pm\pi^\mp$ system in terms of CKM parameters. However, CP violation in decay may arise, resulting in either or both of $C_{\rho\pi} \neq 0$ and $\mathcal{A}_{CP}^{\rho\pi} \neq 0$. Equivalently, CP violation in decay may be seen by either of the decay-type-specific observables $\mathcal{A}_{\rho\pi}^{+-}$ and $\mathcal{A}_{\rho\pi}^{-+}$, defined in Eq. (132), deviating from zero. Results and averages for these parameters are also given in Table 45. Averages of CP violation parameters in $B^0 \rightarrow \rho^\pm\pi^\mp$ decays are shown in Fig. 36, both in $\mathcal{A}_{CP}^{\rho\pi}$ vs. $C_{\rho\pi}$ space and in $\mathcal{A}_{\rho\pi}^{-+}$ vs. $\mathcal{A}_{\rho\pi}^{+-}$ space.

The averages for $S_{b \rightarrow u\bar{u}d}$ and $C_{b \rightarrow u\bar{u}d}$ in $B^0 \rightarrow \pi^+\pi^-$ decays are both more than 5σ away from zero, suggesting that both mixing-induced and CP violation in decay are well-established in this channel. The discrepancy between

Footnote 35 continued

$B^0 \rightarrow a_1^\pm\pi^\mp$ case there has not yet been a full amplitude analysis of $B^0 \rightarrow \pi^+\pi^-\pi^+\pi^-$ and therefore only the Q2B parameters are available.

Table 44 Averages for $b \rightarrow u\bar{u}d$ modes

Experiment	Sample size	S_{CP}	C_{CP}	Correlation		
$\pi^+\pi^-$						
BABAR [416]	$N(B\bar{B}) = 467\text{M}$	$-0.68 \pm 0.10 \pm 0.03$	$-0.25 \pm 0.08 \pm 0.02$	-0.06		
Belle [417]	$N(B\bar{B}) = 772\text{M}$	$-0.64 \pm 0.08 \pm 0.03$	$-0.33 \pm 0.06 \pm 0.03$	-0.10		
Average		-0.68 ± 0.04	-0.27 ± 0.04	0.14		
Confidence level		$0.88 (0.2\sigma)$				
$\rho^+\rho^-$						
BABAR [409]	$N(B\bar{B}) = 387\text{M}$	$-0.17 \pm 0.20^{+0.05}_{-0.06}$	$0.01 \pm 0.15 \pm 0.06$	-0.04		
Belle [410]	$N(B\bar{B}) = 772\text{M}$	$-0.13 \pm 0.15 \pm 0.05$	$0.00 \pm 0.10 \pm 0.06$	-0.02		
Average		-0.14 ± 0.13	0.00 ± 0.09	-0.02		
Confidence level		$0.99 (0.02\sigma)$				
$\rho^0\rho^0$						
BABAR [411]	$N(B\bar{B}) = 465\text{M}$	$0.3 \pm 0.7 \pm 0.2$	$0.2 \pm 0.8 \pm 0.3$	-0.04		
Experiment	$N(B\bar{B})$	$A_{CP}^{a_1\pi}$	$C_{a_1\pi}$	$S_{a_1\pi}$	$\Delta C_{a_1\pi}$	$\Delta S_{a_1\pi}$
$a_1^\pm\pi^\mp$						
BABAR [414]	384M	$-0.07 \pm 0.07 \pm 0.02$	$-0.10 \pm 0.15 \pm 0.09$	$0.37 \pm 0.21 \pm 0.07$	$0.26 \pm 0.15 \pm 0.07$	$-0.14 \pm 0.21 \pm 0.06$
Belle [418]	772M	$-0.06 \pm 0.05 \pm 0.07$	$-0.01 \pm 0.11 \pm 0.09$	$-0.51 \pm 0.14 \pm 0.08$	$0.54 \pm 0.11 \pm 0.07$	$-0.09 \pm 0.14 \pm 0.06$
Average		-0.06 ± 0.06	-0.05 ± 0.11	-0.20 ± 0.13	0.43 ± 0.10	-0.10 ± 0.12
Confidence level				$0.03 (2.1\sigma)$		
Experiment	$N(B\bar{B})$	$\mathcal{A}_{a_1\pi}^{-+}$	$\mathcal{A}_{a_1\pi}^{+-}$	Correlation		
BABAR [414]	384M	$0.07 \pm 0.21 \pm 0.15$	$0.15 \pm 0.15 \pm 0.07$	0.63		
Belle [418]	772M	$-0.04 \pm 0.26 \pm 0.19$	$0.07 \pm 0.08 \pm 0.10$	0.61		
Average		0.02 ± 0.20	0.10 ± 0.10	0.38		
Confidence level			$0.92 (0.1\sigma)$			

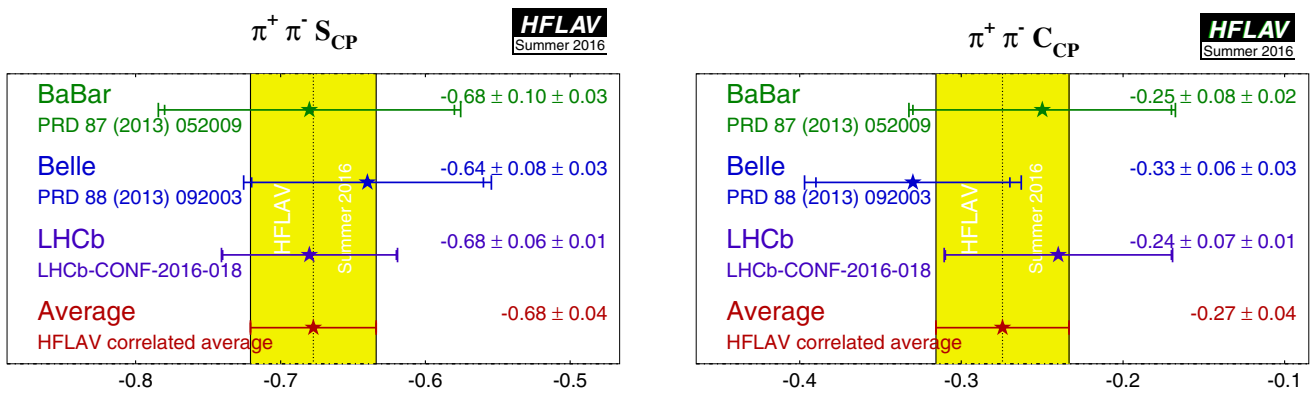


Fig. 29 Averages of (left) S_{CP} and (right) C_{CP} for the mode $B^0 \rightarrow \pi^+\pi^-$

results from BABAR and Belle that used to exist in this channel (see, for example, Ref. [420]) is no longer apparent, and the results from LHCb are also fully consistent with other measurements. Some difference is, however, seen between the BABAR and Belle measurements in the $a_1^\pm\pi^\mp$ system. The confidence level of the five-dimensional aver-

age is 0.03, which corresponds to a 2.1σ discrepancy. As seen in Table 44, this discrepancy is primarily in the values of $S_{a_1\pi}$, and is not evident in the $\mathcal{A}_{a_1\pi}^{-+}$ vs. $\mathcal{A}_{a_1\pi}^{+-}$ projection shown in Fig. 32. Since there is no evidence of systematic problems in either analysis, we do not rescale the errors of the averages.

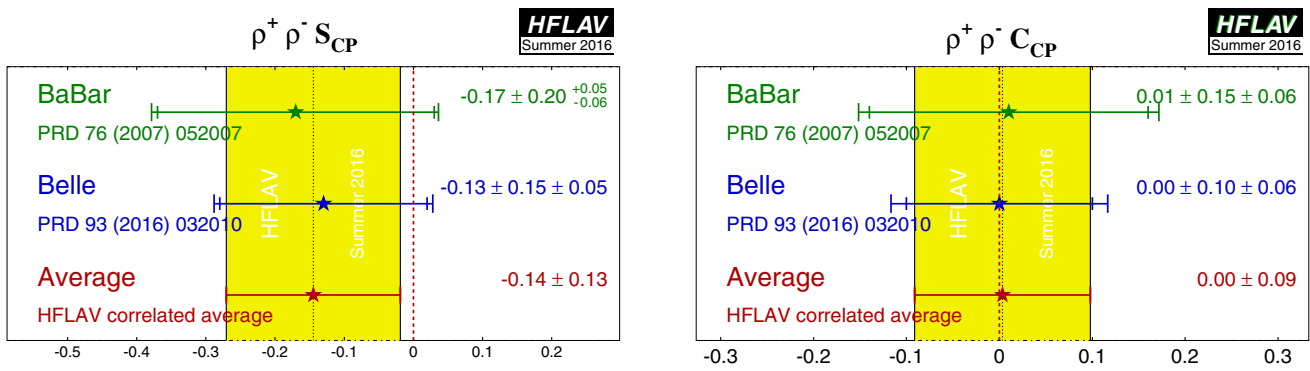


Fig. 30 Averages of (left) S_{CP} and (right) C_{CP} for the mode $B^0 \rightarrow \rho^+ \rho^-$

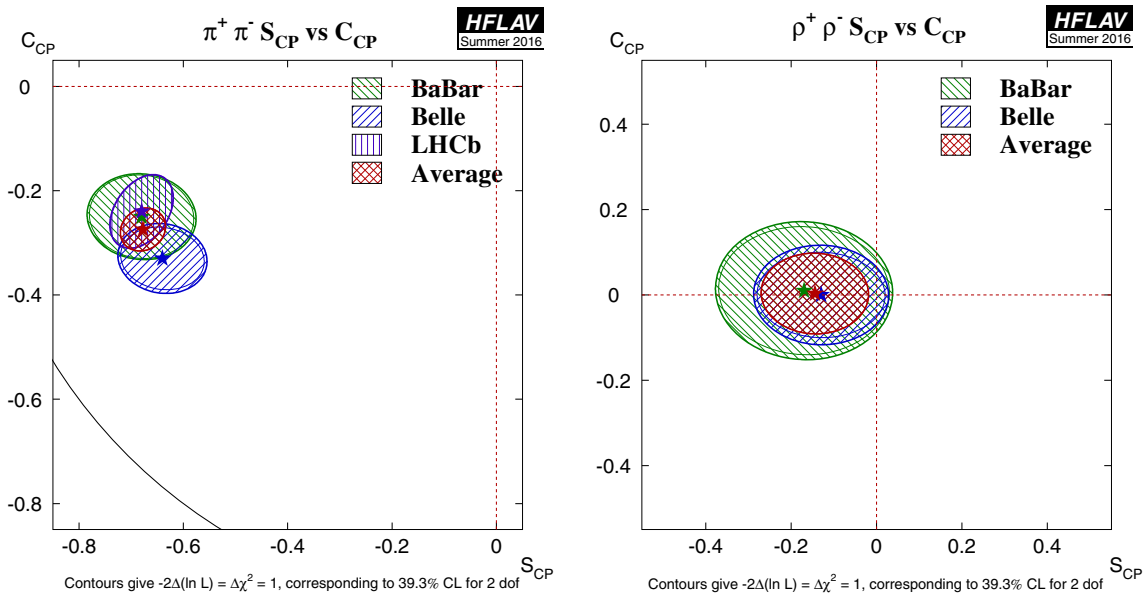


Fig. 31 Averages of $b \rightarrow u\bar{d}$ dominated channels, for which correlated averages are performed, in the S_{CP} vs. C_{CP} plane. (Left) $B^0 \rightarrow \pi^+ \pi^-$ and (right) $B^0 \rightarrow \rho^+ \rho^-$

In $B^0 \rightarrow \rho^\pm \pi^\mp$ decays, both experiments see an indication of CP violation in the $\mathcal{A}_{CP}^{\rho\pi}$ parameter (as seen in Fig. 36). The average is more than 3σ from zero, providing evidence of direct CP violation in this channel. In $B^0 \rightarrow \rho^+ \rho^-$ decays there is no evidence for CP violation, either mixing-induced or in decay. The absence of evidence of penguin contributions in this mode leads to strong constraints on $\alpha \equiv \phi_2$.

4.11.1 Constraints on $\alpha \equiv \phi_2$

The precision of the measured CP violation parameters in $b \rightarrow u\bar{d}$ transitions allows constraints to be set on the UT angle $\alpha \equiv \phi_2$. Constraints have been obtained with various methods:

- Both BABAR [416] and Belle [417] have performed isospin analyses in the $\pi\pi$ system. Belle exclude $23.8^\circ < \phi_2 < 66.8^\circ$ at 68% CL while BABAR give a confidence

level interpretation for α , and constrain $\alpha \in [71^\circ, 109^\circ]$ at 68% CL. Values in the range $[23^\circ, 67^\circ]$ are excluded at 90% CL. In both cases, only solutions in 0° – 180° are quoted.

- Both experiments have also performed isospin analyses in the $\rho\rho$ system. The most recent result from BABAR is given in an update of the measurements of the $B^+ \rightarrow \rho^+ \rho^0$ decay [421], and sets the constraint $\alpha = (92.4^{+6.0}_{-6.5})^\circ$. The most recent result from Belle is given in their paper on time-dependent CP violation parameters in $B^0 \rightarrow \rho^+ \rho^-$ decays, and sets the constraint $\phi_2 = (93.7 \pm 10.6)^\circ$ [410].
- The time-dependent Dalitz plot analysis of the $B^0 \rightarrow \pi^+ \pi^- \pi^0$ decay allows a determination of α without input from any other channels. BABAR [282] present a scan, but not an interval, for α , since their studies indicate that the scan is not statistically robust and cannot be interpreted as $1 - \text{CL}$. Belle [283, 284] has obtained a con-

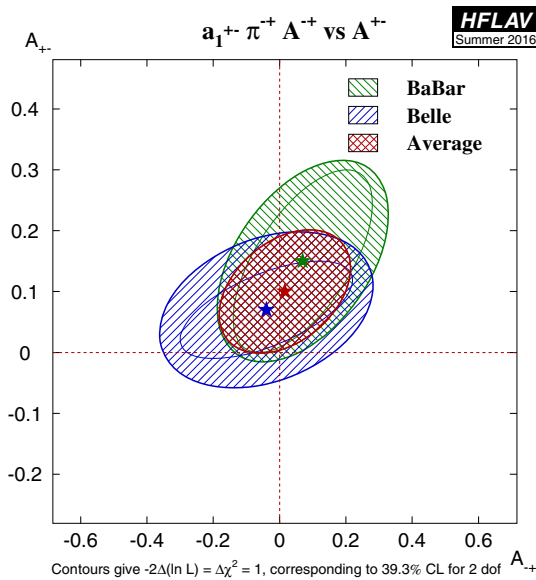


Fig. 32 Averages of CP violation parameters in $B^0 \rightarrow a_1^\pm \pi^\mp$ in $\mathcal{A}_{a_1\pi}^\pm$ space

straint on α using additional information from the SU(2) partners of $B \rightarrow \rho\pi$, which can be used to constrain α via an isospin pentagon relation [422]. With this analysis, Belle obtains the constraint $\phi_2 = (83^{+12}_{-23})^\circ$ (where the errors correspond to 1σ , i.e. 68.3% confidence level).

- The results from BABAR on $B^0 \rightarrow a_1^\pm \pi^\mp$ [414] can be combined with results from modes related by

flavour symmetries ($a_1 K$ and $K_1\pi$) [423]. This has been done by BABAR [415], resulting in the constraint $\alpha = (79 \pm 7 \pm 11)^\circ$, where the first uncertainty is from the analysis of $B^0 \rightarrow a_1^\pm \pi^\mp$ that obtains α^{eff} , and the second is due to the constraint on $|\alpha^{\text{eff}} - \alpha|$. This approach gives a result with several ambiguous solutions; that consistent with other determinations of α and with global fits to the CKM matrix parameters is quoted here.

- The CKMfitter [252] and UFit [339] groups use the measurements from Belle and BABAR given above with other branching fractions and CP asymmetries in $B \rightarrow \pi\pi, \rho\pi$ and $\rho\rho$ modes, to perform isospin analyses for each system, and to obtain combined constraints on α .
- The BABAR and Belle collaborations have combined their results on $B \rightarrow \pi\pi, \pi\pi\pi^0$ and $\rho\rho$ decays to obtain [424]

$$\alpha \equiv \phi_2 = (88 \pm 5)^\circ. \tag{162}$$

The above solution is that consistent with the Standard Model (an ambiguous solution shifted by 180° exists). The strongest constraint currently comes from the $B \rightarrow \rho\rho$ system. The inclusion of results from $B^0 \rightarrow a_1^\pm \pi^\mp$ does not significantly affect the average.

Note that methods based on isospin symmetry make extensive use of measurements of branching fractions and CP asymmetries, as averaged by the HFLAV Rare Decays sub-

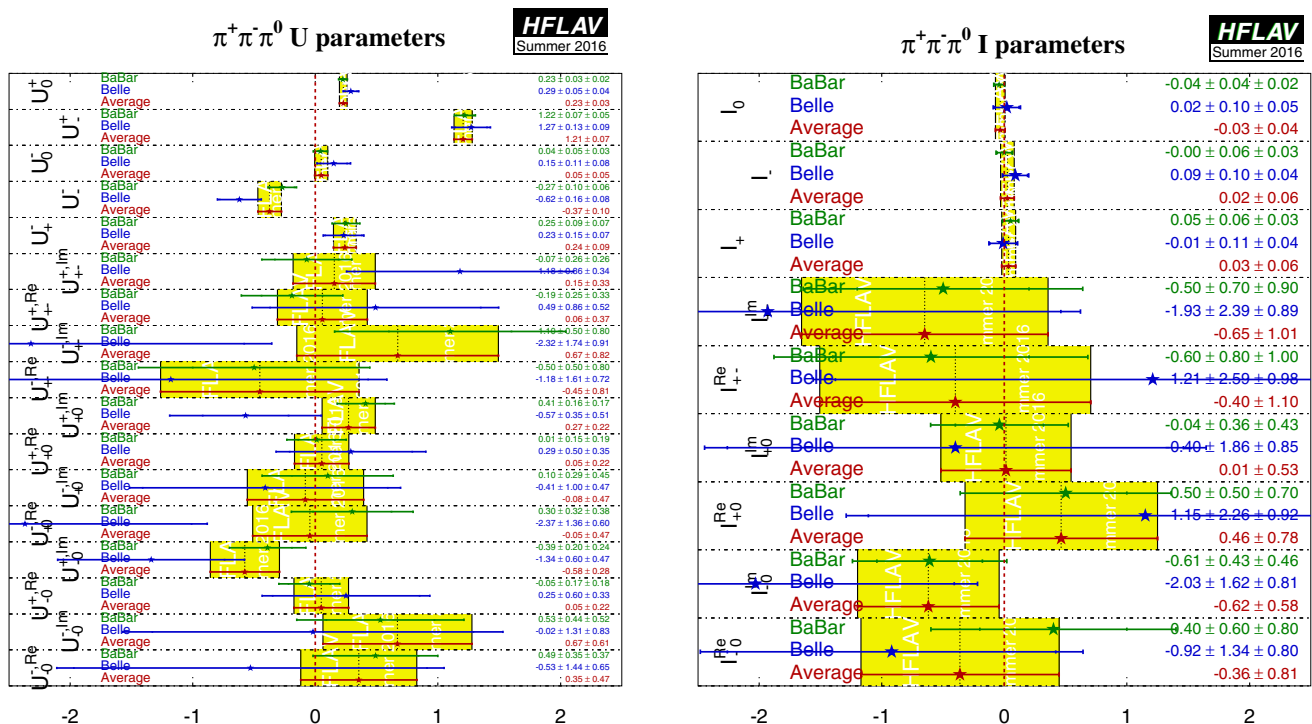


Fig. 33 Summary of the U and I parameters measured in the time-dependent $B^0 \rightarrow \pi^+\pi^-\pi^0$ Dalitz plot analysis

Table 45 Averages of quasi-two-body parameters extracted from time-dependent Dalitz plot analysis of $B^0 \rightarrow \pi^+\pi^-\pi^0$

Experiment	$N(B\bar{B})$	$\mathcal{A}_{CP}^{\rho\pi}$	$C_{\rho\pi}$	$S_{\rho\pi}$	$\Delta C_{\rho\pi}$	$\Delta S_{\rho\pi}$
BABAR [282]	471M	$-0.10 \pm 0.03 \pm 0.02$	$0.02 \pm 0.06 \pm 0.04$	$0.05 \pm 0.08 \pm 0.03$	$0.23 \pm 0.06 \pm 0.05$	$0.05 \pm 0.08 \pm 0.04$
Belle [283,284]	449M	$-0.12 \pm 0.05 \pm 0.04$	$-0.13 \pm 0.09 \pm 0.05$	$0.06 \pm 0.13 \pm 0.05$	$0.36 \pm 0.10 \pm 0.05$	$-0.08 \pm 0.13 \pm 0.05$
Average		-0.11 ± 0.03	-0.03 ± 0.06	0.06 ± 0.07	0.27 ± 0.06	0.01 ± 0.08
Confidence level				0.63 (0.5 σ)		

Experiment	$N(B\bar{B})$	$\mathcal{A}_{\rho\pi}^{+-}$	$\mathcal{A}_{\rho\pi}^{+-}$	Correlation
BABAR [282]	471M	$-0.12 \pm 0.08^{+0.04}_{-0.05}$	$0.09^{+0.05}_{-0.06} \pm 0.04$	0.55
Belle [283,284]	449M	$0.08 \pm 0.16 \pm 0.11$	$0.21 \pm 0.08 \pm 0.04$	0.47
Average		-0.08 ± 0.08	0.13 ± 0.05	0.37
Confidence level		0.47 (0.7 σ)		

Experiment	$N(B\bar{B})$	$C_{\rho^0\pi^0}$	$S_{\rho^0\pi^0}$	Correlation
BABAR [282]	471M	$0.19 \pm 0.23 \pm 0.15$	$-0.37 \pm 0.34 \pm 0.20$	0.00
Belle [283,284]	449M	$0.49 \pm 0.36 \pm 0.28$	$0.17 \pm 0.57 \pm 0.35$	0.08
Average		0.27 ± 0.24	-0.23 ± 0.34	0.02
Confidence level		0.68 (0.4 σ)		

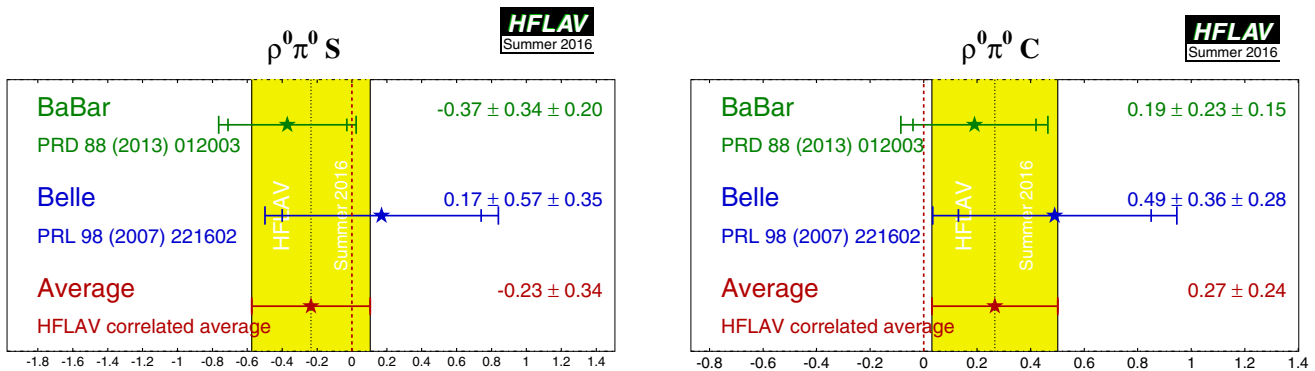


Fig. 34 Averages of (left) $S_{b \rightarrow u\bar{u}d}$ and (right) $C_{b \rightarrow u\bar{u}d}$ for the mode $B^0 \rightarrow \rho^0\pi^0$

group (Sect. 7). Note also that each method suffers from discrete ambiguities in the solutions. The model assumption in the $B^0 \rightarrow \pi^+\pi^-\pi^0$ analysis helps resolve some of the multiple solutions, and results in a single preferred value for α in $[0, \pi]$. All the above measurements correspond to the choice that is in agreement with the global CKM fit.

At present we make no attempt to provide an HFLAV average for $\alpha \equiv \phi_2$. More details on procedures to calculate a best fit value for α can be found in Refs. [252,339].

4.12 Time-dependent CP asymmetries in $b \rightarrow c\bar{u}d/u\bar{c}d$ transitions

Non-CP eigenstates such as $D^\mp\pi^\pm$, $D^{*\mp}\pi^\pm$ and $D^\mp\rho^\pm$ can be produced in decays of B^0 mesons either via Cabibbo

favoured ($b \rightarrow c$) or doubly Cabibbo suppressed ($b \rightarrow u$) tree amplitudes. Since no penguin contribution is possible, these modes are theoretically clean. The ratio of the magnitudes of the suppressed and favoured amplitudes, R , is sufficiently small (predicted to be about 0.02), that $\mathcal{O}(R^2)$ terms can be neglected, and the sine terms give sensitivity to the combination of UT angles $2\beta + \gamma$.

As described in Sect. 4.2.6, the averages are given in terms of the parameters a and c of Eq. (136). CP violation would appear as $a \neq 0$. Results are available from both BABAR and Belle in the modes $D^\mp\pi^\pm$ and $D^{*\mp}\pi^\pm$; for the latter mode both experiments have used both full and partial reconstruction techniques. Results are also available from BABAR using $D^\mp\rho^\pm$. These results, and their averages, are listed in Table 46, and are shown in Fig. 37. The constraints in c vs.

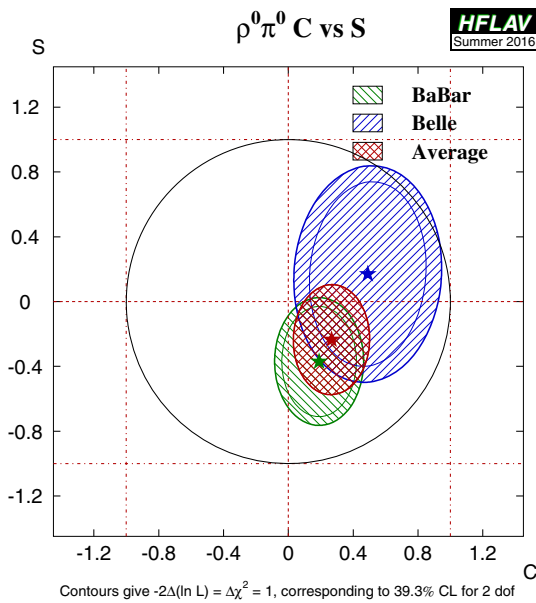


Fig. 35 Averages of $b \rightarrow u\bar{u}d$ dominated channels, for the mode $B^0 \rightarrow \rho^0\pi^0$ in the S_{CP} vs. C_{CP} plane

a space for the $D\pi$ and $D^*\pi$ modes are shown in Fig. 38. It is notable that the average value of a from $D^*\pi$ is more than 3σ from zero, providing evidence of CP violation in this channel.

For each mode, $D\pi$, $D^*\pi$ and $D\rho$, there are two measurements (a and c , or S^+ and S^-) that depend on three unknowns (R , δ and $2\beta + \gamma$), of which two are different for each decay mode. Therefore, there is not enough information to solve directly for $2\beta + \gamma$. However, for each choice of R and $2\beta + \gamma$, one can find the value of δ that allows a and

c to be closest to their measured values, and calculate the separation in terms of numbers of standard deviations. (We currently neglect experimental correlations in this analysis.) These values of $N(\sigma)_{\min}$ can then be displayed as a function of R and $2\beta + \gamma$ (and can trivially be converted to confidence levels). These plots are given for the $D\pi$ and $D^*\pi$ modes in Fig. 38; the uncertainties in the $D\rho$ mode are currently too large to give any meaningful constraint.

The constraints can be tightened if one is willing to use theoretical input on the values of R and/or δ . One popular choice is the use of $SU(3)$ symmetry to obtain R by relating the suppressed decay mode to B decays involving D_s mesons. More details can be found in Refs. [295, 425–428].

4.13 Time-dependent CP asymmetries in $b \rightarrow c\bar{u}s/u\bar{c}s$ transitions

4.13.1 Time-dependent CP asymmetries in $B^0 \rightarrow D^\mp K_S^0 \pi^\pm$

Time-dependent analyses of transitions such as $B^0 \rightarrow D^\mp K_S^0 \pi^\pm$ can be used to probe $\sin(2\beta + \gamma)$ in a similar way to that discussed above (Sect. 4.12). Since the final state contains three particles, a Dalitz plot analysis is necessary to maximise the sensitivity. BABAR [429] has carried out such an analysis. They obtain $2\beta + \gamma = (83 \pm 53 \pm 20)^\circ$ (with an ambiguity $2\beta + \gamma \leftrightarrow 2\beta + \gamma + \pi$) assuming the ratio of the $b \rightarrow u$ and $b \rightarrow c$ amplitude to be constant across the Dalitz plot at 0.3.

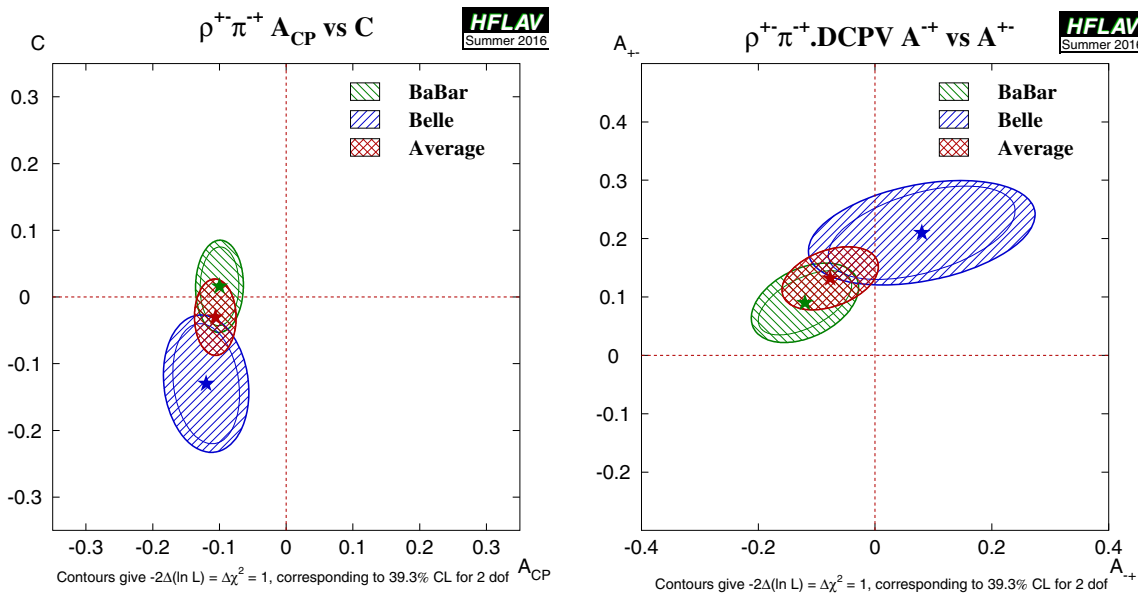


Fig. 36 CP violation in $B^0 \rightarrow \rho^\pm \pi^\mp$ decays. (Left) $A_{CP}^{\rho\pi}$ vs. $C_{\rho\pi}$ space, (right) $A_{\rho\pi}^-$ vs. $A_{\rho\pi}^+$ space

Table 46 Averages for $b \rightarrow \bar{c}u\bar{d}/u\bar{c}d$ modes

Experiment	$N(B\bar{B})$	a	c
$D^\mp\pi^\pm$			
BABAR (full rec.) [290]	232M	$-0.010 \pm 0.023 \pm 0.007$	$-0.033 \pm 0.042 \pm 0.012$
Belle (full rec.) [294]	386M	$-0.050 \pm 0.021 \pm 0.012$	$-0.019 \pm 0.021 \pm 0.012$
Average		-0.030 ± 0.017	-0.022 ± 0.021
Confidence level		0.24 (1.2 σ)	0.78 (0.3 σ)
$D^{*\mp}\pi^\pm$			
BABAR (full rec.) [290]	232M	$-0.040 \pm 0.023 \pm 0.010$	$0.049 \pm 0.042 \pm 0.015$
BABAR (partial rec.) [291]	232M	$-0.034 \pm 0.014 \pm 0.009$	$-0.019 \pm 0.022 \pm 0.013$
Belle (full rec.) [294]	386M	$-0.039 \pm 0.020 \pm 0.013$	$-0.011 \pm 0.020 \pm 0.013$
Belle (partial rec.) [293]	657M	$-0.046 \pm 0.013 \pm 0.015$	$-0.015 \pm 0.013 \pm 0.015$
Average		-0.039 ± 0.010	-0.010 ± 0.013
Confidence level		0.97 (0.03 σ)	0.59 (0.6 σ)
$D^\mp\rho^\pm$			
BABAR (full rec.) [290]	232M	$-0.024 \pm 0.031 \pm 0.009$	$-0.098 \pm 0.055 \pm 0.018$

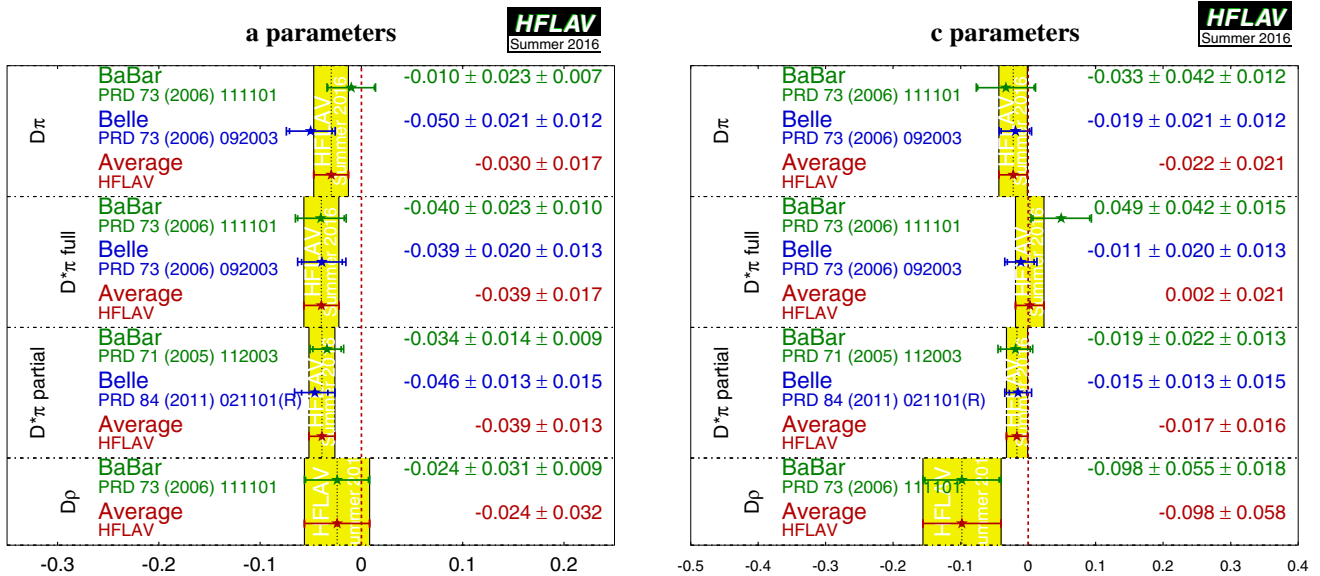


Fig. 37 Averages for $b \rightarrow \bar{c}u\bar{d}/u\bar{c}d$ modes

4.13.2 Time-dependent CP asymmetries in $B_s^0 \rightarrow D_s^\mp K^\pm$

Time-dependent analysis of $B_s^0 \rightarrow D_s^\mp K^\pm$ decays can be used to determine $\gamma - 2\beta_s$ [430,431]. Compared to the situation for $B^0 \rightarrow D^{(*)\mp}\pi^\pm$ decays discussed in Sect. 4.12, the larger value of the ratio R of the magnitudes of the suppressed and favoured amplitudes allows it to be determined from the data. Moreover, the non-zero value of $\Delta\Gamma_s$ allows the determination of additional terms, labelled $A^{\Delta\Gamma}$ and $\bar{A}^{\Delta\Gamma}$, that break ambiguities in the solutions for $\gamma - 2\beta_s$.

LHCb [296,432] has measured the time-dependent CP violation parameters in $B_s^0 \rightarrow D_s^\mp K^\pm$ decays, using

3.0 fb^{-1} of data. The results are given in Table 47, and correspond to 3.6σ evidence for CP violation in the interference between mixing and $B_s^0 \rightarrow D_s^\mp K^\pm$ decays. From these results, and a constraint on $2\beta_s$ from independent LHCb measurements [202], LHCb determine $\gamma = (127_{-22}^{+17})^\circ$, $\delta_{D_s K} = (358_{-16}^{+15})^\circ$ and $R_{D_s K} = 0.37_{-0.09}^{+0.10}$.

4.14 Rates and asymmetries in $B \rightarrow D^{(*)}K^{(*)}$ decays

As explained in Sect. 4.2.7, rates and asymmetries in $B^+ \rightarrow D^{(*)}K^{(*)+}$ decays are sensitive to γ , and have negligible the-

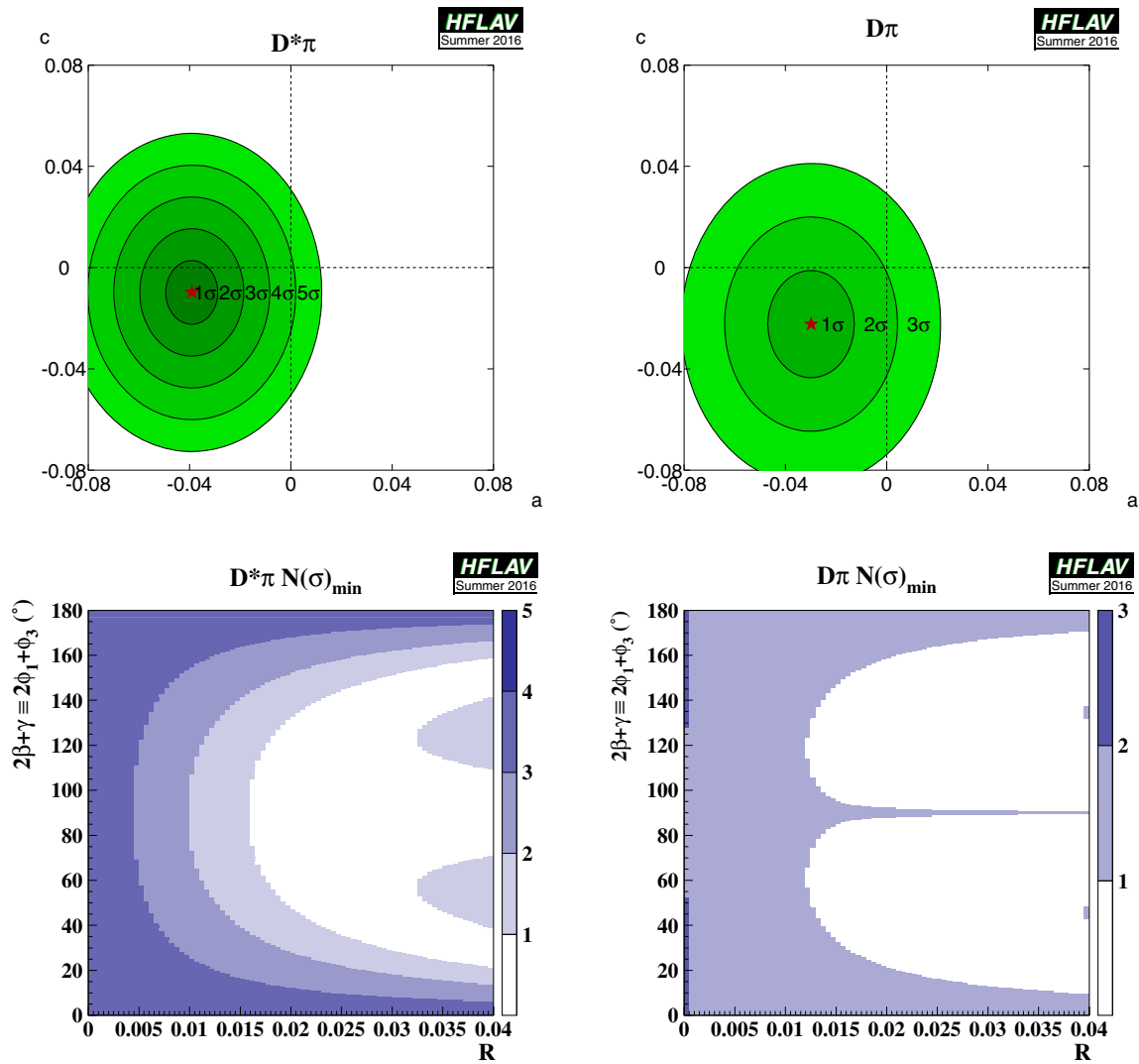


Fig. 38 Results from $b \rightarrow \bar{c}u\bar{d}/u\bar{c}d$ modes. (Top) Constraints in c vs. a space. (Bottom) Constraints in $2\beta + \gamma$ vs. R space. (Left) $D^*\pi$ and (right) $D\pi$ modes

Table 47 Results for $B_s^0 \rightarrow D_s^\mp K^\pm$

Experiment	$\int \mathcal{L} dt$	C	$A^{\Delta\Gamma}$	$\bar{A}^{\Delta\Gamma}$	S	\bar{S}
LHCb [432]	3 fb^{-1}	$0.74 \pm 0.14 \pm 0.05$	$0.40 \pm 0.28 \pm 0.12$	$0.31 \pm 0.27 \pm 0.11$	$-0.52 \pm 0.20 \pm 0.07$	$-0.50 \pm 0.20 \pm 0.07$

oretical uncertainty [311]. Various methods using different $D^{(*)}$ final states have been used.

4.14.1 D decays to CP eigenstates

Results are available from BABAR, Belle, CDF and LHCb on GLW analyses in the decay mode $B^+ \rightarrow DK^+$. All experiments use the CP -even D decay final states K^+K^- and $\pi^+\pi^-$; BABAR and Belle in addition use the CP -odd decay modes $K_S^0\pi^0$, $K_S^0\omega$ and $K_S^0\phi$, though care is taken to avoid statistical overlap with the $K_S^0K^+K^-$ sample used for Dalitz plot analyses (see Sect. 4.14.4). BABAR and Belle also

have results in the decay mode $B^+ \rightarrow D^*K^+$, using both the $D^* \rightarrow D\pi^0$ decay, which gives $CP(D^*) = CP(D)$, and the $D^* \rightarrow D\gamma$ decays, which gives $CP(D^*) = -CP(D)$. In addition, BABAR and LHCb have results in the decay mode $B^+ \rightarrow DK^{*+}$, and LHCb has results in the decay mode $B^+ \rightarrow DK^+\pi^+\pi^-$. The results and averages are given in Table 48 and shown in Fig. 39.

LHCb has performed a GLW analysis using the $B^0 \rightarrow DK^{*0}$ decay with the CP -even $D \rightarrow K^+K^-$ and $D \rightarrow \pi^+\pi^-$ channels [441]. The results are presented separately to allow for possible CP violation effects in the charm decays, which are, however, known to be small.

Table 48 Averages from GLW analyses of $b \rightarrow c\bar{u}s/u\bar{c}s$ modes. The sample size is given in terms of number of $B\bar{B}$ pairs, $N(B\bar{B})$, for the e^+e^- B factory experiments BABAR and Belle, and in terms of integrated luminosity, $\int \mathcal{L} dt$, for the hadron collider experiments CDF and LHCb

Experiment	Sample size	A_{CP+}	A_{CP-}	R_{CP+}	R_{CP-}
$D_{CP}K^+$					
BABAR [433]	467M	$0.25 \pm 0.06 \pm 0.02$	$-0.09 \pm 0.07 \pm 0.02$	$1.18 \pm 0.09 \pm 0.05$	$1.07 \pm 0.08 \pm 0.04$
Belle [434]	275M	$0.06 \pm 0.14 \pm 0.05$	$-0.12 \pm 0.14 \pm 0.05$	$1.13 \pm 0.16 \pm 0.08$	$1.17 \pm 0.14 \pm 0.14$
CDF [435]	1 fb^{-1}	$0.39 \pm 0.17 \pm 0.04$	–	$1.30 \pm 0.24 \pm 0.12$	–
LHCb KK [436]	3 fb^{-1}	$0.087 \pm 0.020 \pm 0.008$	–	$0.968 \pm 0.022 \pm 0.021$	–
LHCb $\pi\pi$ [436]	3 fb^{-1}	$0.128 \pm 0.037 \pm 0.012$	–	$1.002 \pm 0.040 \pm 0.026$	–
LHCb average [436]	3 fb^{-1}	$0.097 \pm 0.018 \pm 0.009$	–	$0.978 \pm 0.019 \pm 0.018$	–
Average		0.111 ± 0.018	-0.10 ± 0.07	0.995 ± 0.025	1.09 ± 0.08
Confidence level		$0.063 (1.9\sigma)$	$0.86 (0.2\sigma)$	$0.21 (1.3\sigma)$	$0.65 (0.5\sigma)$
$D_{CP}^*K^+$					
BABAR [437]	383M	$-0.11 \pm 0.09 \pm 0.01$	$0.06 \pm 0.10 \pm 0.02$	$1.31 \pm 0.13 \pm 0.03$	$1.09 \pm 0.12 \pm 0.04$
Belle [434]	275M	$-0.20 \pm 0.22 \pm 0.04$	$0.13 \pm 0.30 \pm 0.08$	$1.41 \pm 0.25 \pm 0.06$	$1.15 \pm 0.31 \pm 0.12$
Average		-0.12 ± 0.07	0.13 ± 0.07	1.25 ± 0.09	1.06 ± 0.09
Confidence level		$0.82 (0.2\sigma)$	$0.29 (1.1\sigma)$	$0.52 (0.6\sigma)$	$0.74 (0.3\sigma)$
$D_{CP}K^{*+}$					
BABAR [438]	379M	$0.09 \pm 0.13 \pm 0.06$	$-0.23 \pm 0.21 \pm 0.07$	$2.17 \pm 0.35 \pm 0.09$	$1.03 \pm 0.27 \pm 0.13$
LHCb KK [439]	4 fb^{-1}	$0.12 \pm 0.08 \pm 0.01$	–	$1.31 \pm 0.11 \pm 0.05$	–
LHCb $\pi\pi$ [439]	4 fb^{-1}	$0.08 \pm 0.16 \pm 0.02$	–	$0.98 \pm 0.17 \pm 0.04$	–
LHCb average [439]	4 fb^{-1}	0.11 ± 0.07	–	1.21 ± 0.10	–
Average		0.11 ± 0.06	-0.23 ± 0.22	1.27 ± 0.10	1.03 ± 0.30
Confidence level		$0.97 (0.04\sigma)$		$0.01 (2.6\sigma)$	
$D_{CP}K^+\pi^+\pi^-$					
LHCb KK [440]	3 fb^{-1}	$-0.045 \pm 0.064 \pm 0.011$	–	$1.043 \pm 0.069 \pm 0.034$	–
LHCb $\pi\pi$ [440]	3 fb^{-1}	$-0.054 \pm 0.101 \pm 0.011$	–	$1.035 \pm 0.108 \pm 0.038$	–
LHCb average [440]	3 fb^{-1}	-0.048 ± 0.055	–	1.040 ± 0.064	–

The results are given in Table 49 where an average is also reported.

As pointed out in Refs. [313,314], a Dalitz plot analysis of $B^0 \rightarrow DK^+\pi^-$ decays provides more sensitivity to $\gamma \equiv \phi_3$ than the quasi-two-body DK^{*0} approach. The analysis provides direct sensitivity to the hadronic parameters r_B and δ_B associated with the $B^0 \rightarrow DK^{*0}$ decay amplitudes, rather than effective hadronic parameters averaged over the K^{*0} selection window as in the quasi-two-body case.

Such an analysis has been performed by LHCb. A simultaneous fit is performed to the $B^0 \rightarrow DK^+\pi^-$ Dalitz plots with the neutral D meson reconstructed in the $K^+\pi^-$, K^+K^- and $\pi^+\pi^-$ final states. The reported results in Table 50 are for the Cartesian parameters, defined in Eq. (150) associated with the $B^0 \rightarrow DK^*(892)^0$ decay. Note that, since the measurements use overlapping data samples, these results cannot be combined with the LHCb results for GLW observables in $B^0 \rightarrow DK^*(892)^0$ decays reported in Table 49.

LHCb use these results to obtain confidence levels for γ , $r_B(DK^{*0})$ and $\delta_B(DK^{*0})$. In addition, results are reported for the hadronic parameters needed to relate these results to quasi-two-body measurements of $B^0 \rightarrow DK^*(892)^0$ decays, where a selection window of $m(K^+\pi^-)$ within $50 \text{ MeV}/c^2$ of the pole mass and helicity angle satisfying $|\cos(\theta_{K^{*0}})| > 0.4$ is assumed. These parameters are the coherence factor κ , the ratio of quasi-two-body and amplitude level r_B values, $\bar{R}_B = \bar{r}_B/r_B$, and the difference between quasi-two-body and amplitude level δ_B values, $\Delta\bar{\delta}_B = \bar{\delta}_B - \delta_B$. LHCb [442] obtain

$$\begin{aligned}
 \gamma &= 0.958^{+0.005+0.002}_{-0.010-0.045}, \\
 \bar{R}_B &= 1.02^{+0.03}_{-0.01} \pm 0.06, \\
 \Delta\bar{\delta}_B &= 0.02^{+0.03}_{-0.02} \pm 0.11.
 \end{aligned}
 \tag{163}$$

4.14.2 D decays to quasi-CP eigenstates

As discussed in Sect. 4.2.7, if a multibody neutral D meson decay can be shown to be dominated by one CP eigenstate,

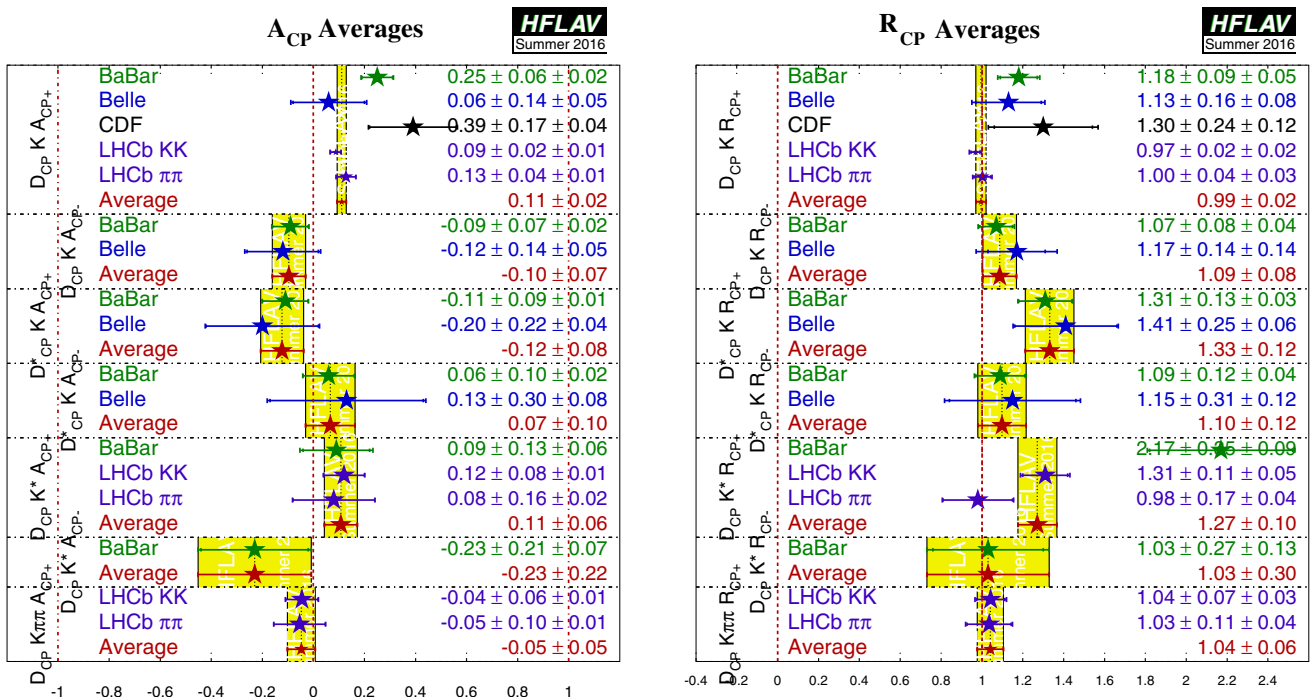


Fig. 39 Averages of A_{CP} and R_{CP} from GLW analyses

Table 49 Results from GLW analysis of $B^0 \rightarrow DK^{*0}$

Experiment	Sample size	A_{CP+}	R_{CP+}
LHCb KK [441]	$\int \mathcal{L} dt = 3 \text{ fb}^{-1}$	$-0.20 \pm 0.15 \pm 0.02$	$1.05^{+0.17}_{-0.15} \pm 0.04$
LHCb $\pi\pi$ [441]	$\int \mathcal{L} dt = 3 \text{ fb}^{-1}$	$-0.09 \pm 0.22 \pm 0.02$	$1.21^{+0.28}_{-0.25} \pm 0.05$
Average		-0.16 ± 0.12	1.10 ± 0.14

Table 50 Results from Dalitz plot analysis of $B^0 \rightarrow DK^+\pi^-$ decays with $D \rightarrow K^+K^-$ and $\pi^+\pi^-$

Experiment	$\int \mathcal{L} dt$	x_+	y_+	x_-	y_-
LHCb [442]	3 fb^{-1}	$0.04 \pm 0.16 \pm 0.11$	$-0.47 \pm 0.28 \pm 0.22$	$-0.02 \pm 0.13 \pm 0.14$	$-0.35 \pm 0.26 \pm 0.41$

Table 51 Averages from GLW-like analyses of $b \rightarrow c\bar{u}s/\bar{u}\bar{c}s$ modes

Experiment	Sample size	A_{qGLW}	R_{qGLW}
$D_{\pi^+\pi^-\pi^0}K^+$			
LHCb [444]	$\int \mathcal{L} dt = 3 \text{ fb}^{-1}$	$0.05 \pm 0.09 \pm 0.01$	$0.98 \pm 0.11 \pm 0.05$
BABAR [322]	$N(B\bar{B}) = 324\text{M}$	$-0.02 \pm 0.15 \pm 0.03$	–
Average		0.03 ± 0.08	0.98 ± 0.12
Confidence level		$0.68 (0.4\sigma)$	–
$D_{K^+K^-\pi^0}K^+$			
LHCb [444]	$\int \mathcal{L} dt = 3 \text{ fb}^{-1}$	$0.30 \pm 0.20 \pm 0.02$	$0.95 \pm 0.22 \pm 0.04$
$D_{\pi^+\pi^-\pi^+\pi^-}K^+$			
LHCb [436]	$\int \mathcal{L} dt = 3 \text{ fb}^{-1}$	$0.10 \pm 0.03 \pm 0.02$	$0.97 \pm 0.04 \pm 0.02$

it can be used in a “GLW-like” (sometimes called “quasi-GLW”) analysis [318]. The same observables R_{CP} , A_{CP} as for the GLW case are measured, but an additional factor

of $(2F_+ - 1)$, where F_+ is the fractional CP -even content, enters the expressions relating these observables to $\gamma \equiv \phi_3$. The F_+ factors have been measured using CLEO-c data to

Table 52 Averages from ADS analyses of $b \rightarrow c\bar{u}s/u\bar{c}s$ modes

Experiment	Sample size	A_{ADS}	R_{ADS}
$DK^+, D \rightarrow K^-\pi^+$			
BABAR [445]	$N(B\bar{B}) = 467\text{M}$	$-0.86 \pm 0.47^{+0.12}_{-0.16}$	$0.011 \pm 0.006 \pm 0.002$
Belle [446]	$N(B\bar{B}) = 772\text{M}$	$-0.39^{+0.26+0.04}_{-0.28-0.03}$	$0.0163^{+0.0044+0.0007}_{-0.0041-0.0013}$
CDF [447]	$\int \mathcal{L} dt = 7 \text{ fb}^{-1}$	$-0.82 \pm 0.44 \pm 0.09$	$0.0220 \pm 0.0086 \pm 0.0026$
LHCb [436]	$\int \mathcal{L} dt = 3 \text{ fb}^{-1}$	$-0.403 \pm 0.056 \pm 0.011$	$0.0188 \pm 0.0011 \pm 0.0010$
Average		-0.415 ± 0.055	0.0183 ± 0.0014
Confidence level		$0.64 (0.5\sigma)$	$0.61 (0.5\sigma)$
$DK^+, D \rightarrow K^-\pi^+\pi^0$			
BABAR [448]	474M	–	$0.0091^{+0.0082+0.0014}_{-0.0076-0.0037}$
Belle [449]	772M	$0.41 \pm 0.30 \pm 0.05$	$0.0198 \pm 0.0062 \pm 0.0024$
LHCb [444]	$\int \mathcal{L} dt = 3 \text{ fb}^{-1}$	$-0.20 \pm 0.27 \pm 0.03$	$0.0140 \pm 0.0047 \pm 0.0019$
Average		0.07 ± 0.20	0.0148 ± 0.0036
Confidence level		$0.13 (1.5\sigma)$	$0.59 (0.5\sigma)$
$DK^+, D \rightarrow K^-\pi^+\pi^+\pi^-$			
LHCb [436]	$\int \mathcal{L} dt = 3 \text{ fb}^{-1}$	$-0.313 \pm 0.102 \pm 0.038$	$0.0140 \pm 0.0015 \pm 0.0006$
$D^*K^+, D^* \rightarrow D\pi^0, D \rightarrow K^-\pi^+$			
BABAR [445]	$N(B\bar{B}) = 467\text{M}$	$0.77 \pm 0.35 \pm 0.12$	$0.018 \pm 0.009 \pm 0.004$
$D^*K^+, D^* \rightarrow D\gamma, D \rightarrow K^-\pi^+$			
BABAR [445]	$N(B\bar{B}) = 467\text{M}$	$0.36 \pm 0.94^{+0.25}_{-0.41}$	$0.013 \pm 0.014 \pm 0.008$
$DK^{*+}, D \rightarrow K^-\pi^+, K^{*+} \rightarrow K_S^0\pi^+$			
BABAR [438]	$N(B\bar{B}) = 379\text{M}$	$-0.34 \pm 0.43 \pm 0.16$	$0.066 \pm 0.031 \pm 0.010$
LHCb [439]	$\int \mathcal{L} dt = 4 \text{ fb}^{-1}$	–	0.003 ± 0.004
Average		-0.34 ± 0.46	0.004 ± 0.004
Confidence level		–	$0.06 (1.9\sigma)$
$DK^+\pi^+\pi^-, D \rightarrow K^-\pi^+$			
LHCb [440]	$\int \mathcal{L} dt = 3 \text{ fb}^{-1}$	$-0.32^{+0.27}_{-0.34}$	$0.0082^{+0.0038}_{-0.0030}$

be $F_+(\pi^+\pi^-\pi^0) = 0.973 \pm 0.017$, $F_+(K^+K^-\pi^0) = 0.732 \pm 0.055$, $F_+(\pi^+\pi^-\pi^+\pi^-) = 0.737 \pm 0.028$ [443].

The GLW-like observables for $D \rightarrow \pi^+\pi^-\pi^0$, $K^+K^-\pi^0$ and $D \rightarrow \pi^+\pi^-\pi^+\pi^-$ have been measured by LHCb. The A_{qGLW} observable for $D \rightarrow \pi^+\pi^-\pi^0$ was measured in an earlier analysis by BABAR, from which additional observables, discussed in Sect. 4.2.7 and reported in Table 55 below, were reported. The results are given in Table 51.

4.14.3 D decays to suppressed final states

For ADS analyses, all of BABAR, Belle, CDF and LHCb have studied the modes $B^+ \rightarrow DK^+$ and $B^+ \rightarrow D\pi^+$. BABAR has also analysed the $B^+ \rightarrow D^*K^+$ mode. There is an effective shift of π in the strong phase difference between the cases that the D^* is reconstructed as $D\pi^0$ and $D\gamma$ [315], therefore these modes are studied separately. In addition, BABAR has studied the $B^+ \rightarrow DK^{*+}$ mode,

where K^{*+} is reconstructed as $K_S^0\pi^+$, and LHCb has studied the $B^+ \rightarrow DK^+\pi^+\pi^-$ mode. In all the above cases the suppressed decay $D \rightarrow K^-\pi^+$ has been used. BABAR, Belle and LHCb also have results using $B^+ \rightarrow DK^+$ with $D \rightarrow K^-\pi^+\pi^0$, while LHCb has results using $B^+ \rightarrow DK^+$ with $D \rightarrow K^-\pi^+\pi^+\pi^-$. The results and averages are given in Table 52 and shown in Fig. 40.

Similar phenomenology as for $B \rightarrow DK$ decays holds for $B \rightarrow D\pi$ decays, though in this case the interference is between $b \rightarrow c\bar{u}d$ and $b \rightarrow u\bar{c}d$ transitions, and the ratio of suppressed to favoured amplitudes is expected to be much smaller, $\mathcal{O}(1\%)$. For most D meson final states this implies that the interference effect is too small to be of interest, but in the case of ADS analysis it is possible that effects due to γ may be observable. Accordingly, the experiments now measure the corresponding observables in the $D\pi$ final states. The results and averages are given in Table 53 and shown in Fig. 41.

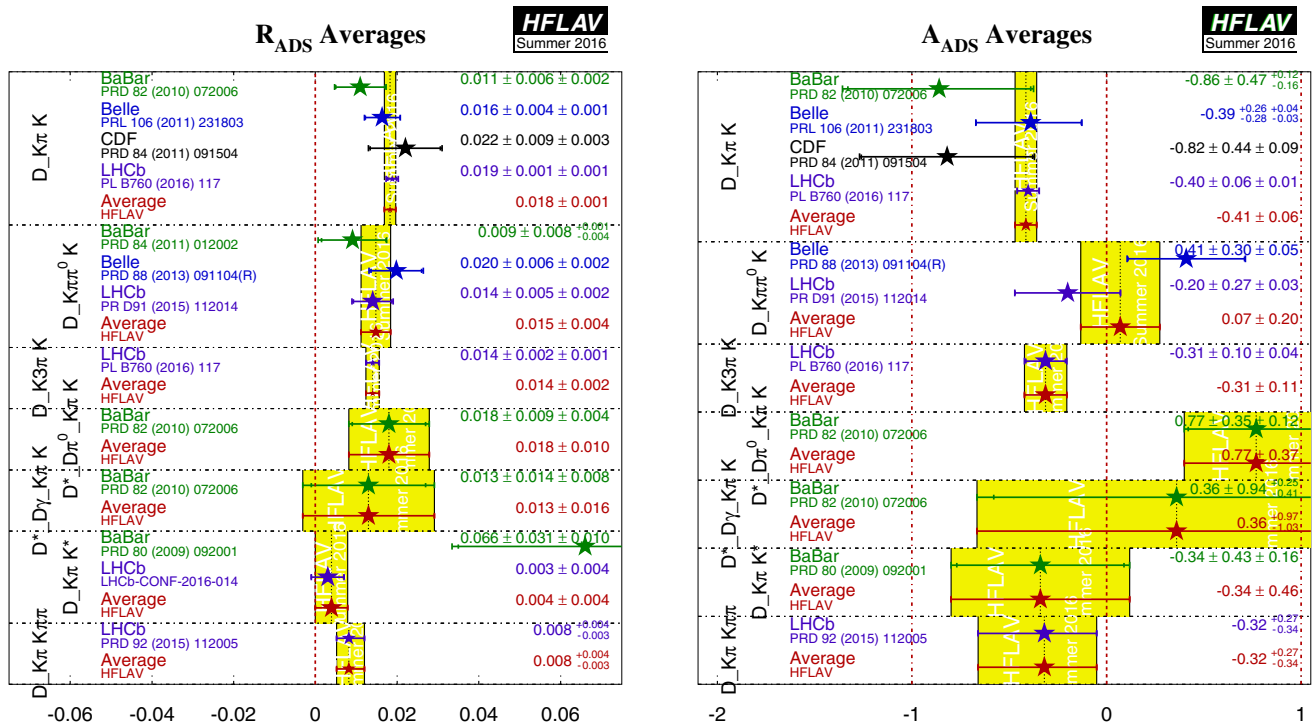


Fig. 40 Averages of R_{ADS} and A_{ADS} for $B \rightarrow D^{(*)}K^{(*)}$ decays

Table 53 Averages from ADS analyses of $b \rightarrow c\bar{u}d/u\bar{c}d$ modes

Experiment	Sample size	A_{ADS}	R_{ADS}
<i>Dπ⁺, D → K⁻π⁺</i>			
BABAR [445]	$N(B\bar{B}) = 467M$	$0.03 \pm 0.17 \pm 0.04$	$0.0033 \pm 0.0006 \pm 0.0004$
Belle [446]	$N(B\bar{B}) = 772M$	$-0.04 \pm 0.11^{+0.02}_{-0.01}$	$0.00328^{+0.00038+0.00012}_{-0.00036-0.00018}$
CDF [447]	$\int \mathcal{L} dt = 7 \text{ fb}^{-1}$	$0.13 \pm 0.25 \pm 0.02$	$0.0028 \pm 0.0007 \pm 0.0004$
LHCb [436]	$\int \mathcal{L} dt = 3 \text{ fb}^{-1}$	$0.100 \pm 0.031 \pm 0.009$	$0.00360 \pm 0.00012 \pm 0.00009$
Average		0.088 ± 0.030	0.00353 ± 0.00014
Confidence level		$0.66 (0.4\sigma)$	$0.68 (0.4\sigma)$
<i>Dπ⁺, D → K⁻π⁺π⁰</i>			
Belle [449]	772M	$0.16 \pm 0.27^{+0.03}_{-0.04}$	$0.00189 \pm 0.00054^{+0.00022}_{-0.00025}$
LHCb [444]	$\int \mathcal{L} dt = 3 \text{ fb}^{-1}$	$0.44 \pm 0.19 \pm 0.01$	$0.00235 \pm 0.00049 \pm 0.00004$
Average		0.35 ± 0.16	0.00216 ± 0.00038
Confidence level		$0.40 (0.8\sigma)$	$0.55 (0.6\sigma)$
<i>Dπ⁺, D → K⁻π⁺π⁺π⁻</i>			
LHCb [436]	$\int \mathcal{L} dt = 3 \text{ fb}^{-1}$	$0.023 \pm 0.048 \pm 0.005$	$0.00377 \pm 0.00018 \pm 0.00006$
<i>D*π⁺, D* → Dπ⁰, D → K⁻π⁺</i>			
BABAR [445]	467M	$-0.09 \pm 0.27 \pm 0.05$	$0.0032 \pm 0.0009 \pm 0.0008$
<i>D*π⁺, D* → Dγ, D → K⁻π⁺</i>			
BABAR [445]	467M	$-0.65 \pm 0.55 \pm 0.22$	$0.0027 \pm 0.0014 \pm 0.0022$
<i>Dπ⁺π⁺π⁻, D → K⁻π⁺</i>			
LHCb [440]	$\int \mathcal{L} dt = 3 \text{ fb}^{-1}$	-0.003 ± 0.090	0.00427 ± 0.00043

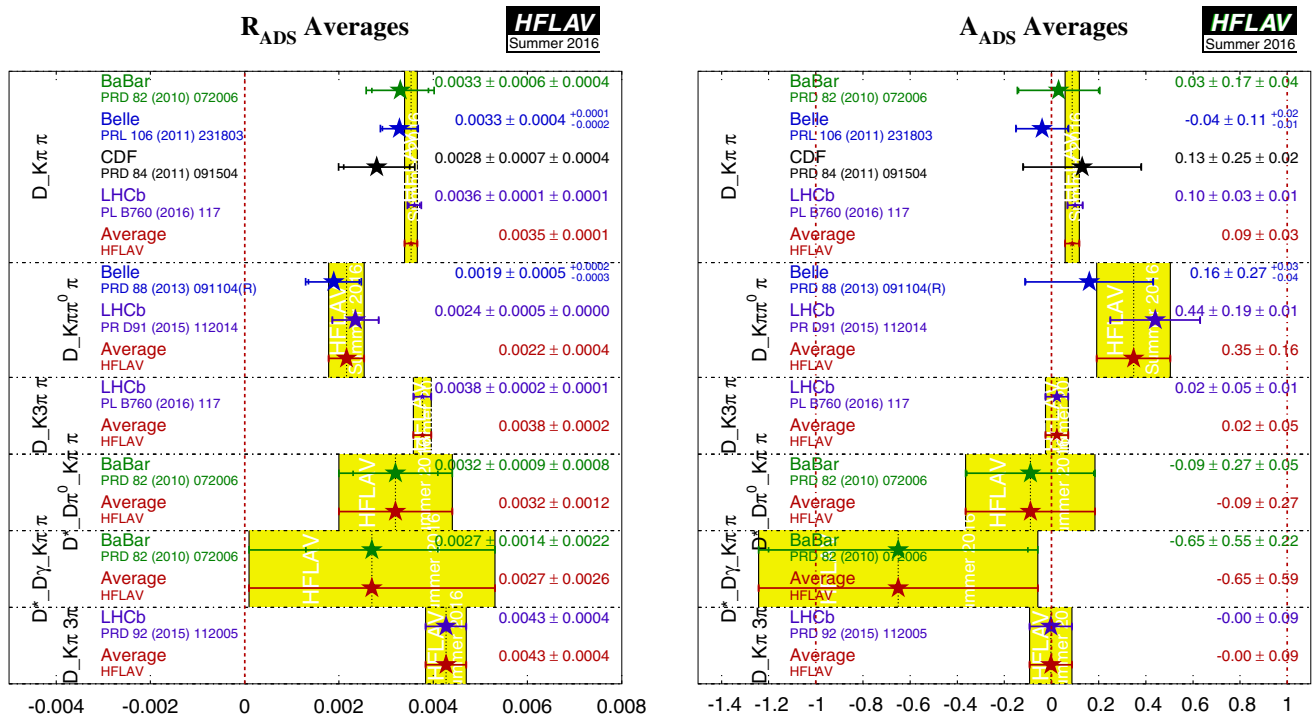


Fig. 41 Averages of R_{ADS} and A_{ADS} for $B \rightarrow D^{(*)}\pi$ decays

Table 54 Results from ADS analysis of $B^0 \rightarrow DK^{*0}, D \rightarrow K^-\pi^+$

Experiment	Sample size	R_+	R_-
LHCb [441]	$\int \mathcal{L} dt = 3\text{fb}^{-1}$	$0.06 \pm 0.03 \pm 0.01$	$0.06 \pm 0.03 \pm 0.01$

BABAR, Belle and LHCb have also presented results from a similar analysis method with self-tagging neutral B decays: $B^0 \rightarrow DK^{*0}$ with $D \rightarrow K^-\pi^+$ (all), $D \rightarrow K^-\pi^+\pi^0$ and $D \rightarrow K^-\pi^+\pi^+\pi^-$ (BABAR only). All these results are obtained with the $K^{*0} \rightarrow K^+\pi^-$ decay. Effects due to the natural width of the K^{*0} are handled using the parametrisation suggested by Gronau [312].

The following 95% CL limits are set by BABAR [450]:

$$R_{ADS}(K\pi) < 0.244 \quad R_{ADS}(K\pi\pi^0) < 0.181$$

$$R_{ADS}(K\pi\pi\pi) < 0.391, \tag{164}$$

while Belle [451] obtain

$$R_{ADS}(K\pi) < 0.16. \tag{165}$$

The results from LHCb, which are presented in terms of the parameters R_+ and R_- instead of R_{ADS} and A_{ADS} , are given in Table 54.

Combining the results and using additional input from CLEO-c [452,453] a limit on the ratio between the $b \rightarrow u$ and $b \rightarrow c$ amplitudes of $\bar{r}_B(DK^{*0}) \in [0.07, 0.41]$ at 95% CL limit is set by BABAR. Belle set a limit of $\bar{r}_B < 0.4$ at 95% CL. LHCb take input from Sect. 8 and obtain $\bar{r}_B = 0.240^{+0.055}_{-0.048}$ (different from zero with 2.7σ significance).

4.14.4 D decays to multiparticle self-conjugate final states (model-dependent analysis)

For the model-dependent Dalitz plot analysis, both BABAR and Belle have studied the modes $B^+ \rightarrow DK^+$, $B^+ \rightarrow D^*K^+$ and $B^+ \rightarrow DK^{*+}$. For $B^+ \rightarrow D^*K^+$, both experiments have used both D^* decay modes, $D^* \rightarrow D\pi^0$ and $D^* \rightarrow D\gamma$, taking the effective shift in the strong phase difference into account.³⁶ In all cases the decay $D \rightarrow K_S^0\pi^+\pi^-$ has been used. BABAR also used the decay $D \rightarrow K_S^0K^+K^-$. LHCb has also studied $B^+ \rightarrow DK^+$ decays with $D \rightarrow K_S^0\pi^+\pi^-$. BABAR has also performed an analysis of $B^+ \rightarrow DK^+$ with $D \rightarrow \pi^+\pi^-\pi^0$. Results and averages are given in Table 55, and shown in Figs. 42 and 43. The third error on each measurement is due to D decay model uncertainty.

³⁶ Belle [454] quote separate results for $B^+ \rightarrow D^*K^+$ with $D^* \rightarrow D\pi^0$ and $D^* \rightarrow D\gamma$. The results quoted in Table 55 are from our average, performed using the statistical correlations provided, and neglecting all systematic correlations; model uncertainties are not included. The first uncertainty on the quoted results is combined statistical and systematic, the second is the model error (taken from the Belle results on $B^+ \rightarrow D^*K^+$ with $D^* \rightarrow D\pi^0$).

Table 55 Averages from model-dependent Dalitz plot analyses of $b \rightarrow \bar{c}is/uc\bar{s}$ modes. Note that the uncertainties assigned to the averages do not include model errors

Experiment	Sample size	x_+	y_+	x_-	y_-
$DK^+, D \rightarrow K_S^0 \pi^+ \pi^-$					
BABAR [455]	$N(B\bar{B}) = 468M$	$-0.103 \pm 0.037 \pm 0.006 \pm 0.007$	$-0.021 \pm 0.048 \pm 0.004 \pm 0.009$	$0.060 \pm 0.039 \pm 0.007 \pm 0.006$	$0.062 \pm 0.045 \pm 0.004 \pm 0.006$
Belle [454]	$N(B\bar{B}) = 657M$	$-0.107 \pm 0.043 \pm 0.011 \pm 0.055$	$-0.067 \pm 0.059 \pm 0.018 \pm 0.063$	$0.105 \pm 0.047 \pm 0.011 \pm 0.064$	$0.177 \pm 0.060 \pm 0.018 \pm 0.054$
LHCb [456]	$\int \mathcal{L} dt = 1\text{fb}^{-1}$	$-0.084 \pm 0.045 \pm 0.009 \pm 0.005$	$-0.032 \pm 0.048^{+0.010}_{-0.009} \pm 0.008$	$0.027 \pm 0.044^{+0.010}_{-0.008} \pm 0.001$	$0.013 \pm 0.048^{+0.009}_{-0.007} \pm 0.003$
Average		-0.098 ± 0.024	-0.036 ± 0.030	0.070 ± 0.025	0.075 ± 0.029
Confidence level					
$D^* K^+, D^* \rightarrow D\pi^0$ or $D\gamma, D \rightarrow K_S^0 \pi^+ \pi^-$					
BABAR [455]	$N(B\bar{B}) = 468M$	$0.147 \pm 0.053 \pm 0.017 \pm 0.003$	$-0.032 \pm 0.077 \pm 0.008 \pm 0.006$	$-0.104 \pm 0.051 \pm 0.019 \pm 0.002$	$-0.052 \pm 0.063 \pm 0.009 \pm 0.007$
Belle [454]	$N(B\bar{B}) = 657M$	$0.100 \pm 0.074 \pm 0.081$	$0.155 \pm 0.101 \pm 0.063$	$-0.023 \pm 0.112 \pm 0.090$	$-0.252 \pm 0.112 \pm 0.049$
Average		0.132 ± 0.044	0.037 ± 0.061	-0.081 ± 0.049	-0.107 ± 0.055
Confidence level					
$DK^{*+}, D \rightarrow K_S^0 \pi^+ \pi^-$					
BABAR [455]	$N(B\bar{B}) = 468M$	$-0.151 \pm 0.083 \pm 0.029 \pm 0.006$	$0.045 \pm 0.106 \pm 0.036 \pm 0.008$	$0.075 \pm 0.096 \pm 0.029 \pm 0.007$	$0.127 \pm 0.095 \pm 0.027 \pm 0.006$
Belle [457]	$N(B\bar{B}) = 386M$	$-0.105^{+0.177}_{-0.167} \pm 0.006 \pm 0.088$	$-0.004^{+0.164}_{-0.156} \pm 0.013 \pm 0.095$	$-0.784^{+0.249}_{-0.295} \pm 0.029 \pm 0.097$	$-0.281^{+0.440}_{-0.335} \pm 0.046 \pm 0.086$
Average		-0.152 ± 0.077	0.024 ± 0.091	-0.043 ± 0.094	0.091 ± 0.096
Confidence level					
$DK^{*0}, D \rightarrow K_S^0 \pi^+ \pi^-, K^{*0} \rightarrow K^+ \pi^-$					
LHCb [458]	$\int \mathcal{L} dt = 3\text{fb}^{-1}$	$0.05 \pm 0.24 \pm 0.04 \pm 0.01$	$-0.65^{+0.24}_{-0.23} \pm 0.08 \pm 0.01$	$-0.15 \pm 0.14 \pm 0.03 \pm 0.01$	$0.25 \pm 0.15 \pm 0.06 \pm 0.01$
Experiment $N(B\bar{B})$					
$DK^+, D \rightarrow \pi^+ \pi^- \pi^0$		ρ^+	θ^+	ρ^-	θ^-
BABAR [322]	324M	$0.75 \pm 0.11 \pm 0.04$	$147 \pm 23 \pm 1$	$0.72 \pm 0.11 \pm 0.04$	$173 \pm 42 \pm 2$

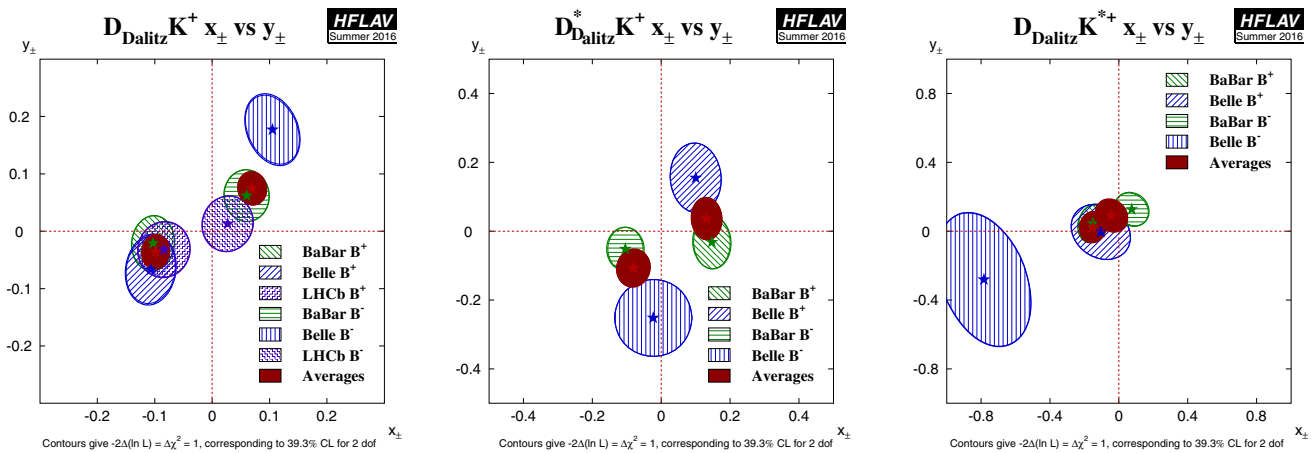


Fig. 42 Contours in the (x_{\pm}, y_{\pm}) from model-dependent analysis of $B^+ \rightarrow D^{(*)}K^{(*)+}$, $D \rightarrow K_S^0 h^+ h^-$ ($h = \pi, K$). (Left) $B^+ \rightarrow DK^+$, (middle) $B^+ \rightarrow D^*K^+$, (right) $B^+ \rightarrow DK^{*+}$. Note that the uncertainties assigned to the averages given in these plots do not include model errors

The parameters measured in the analyses are explained in Sect. 4.2.7. All experiments measure the Cartesian variables, defined in Eq. (150), and perform frequentist statistical procedures, to convert these into measurements of γ , r_B and δ_B . In the $B^+ \rightarrow DK^+$ with $D \rightarrow \pi^+ \pi^- \pi^0$ analysis, the parameters $(\rho^{\pm}, \theta^{\pm})$ are used instead.

Both experiments reconstruct K^{*+} as $K_S^0 \pi^+$, but the treatment of possible nonresonant $K_S^0 \pi^+$ differs: Belle assign an additional model uncertainty, while BABAR use a parametrisation suggested by Gronau [312]. The parameters r_B and δ_B are replaced with effective parameters $\kappa \bar{r}_B$ and $\bar{\delta}_B$; no attempt is made to extract the true hadronic parameters of the $B^+ \rightarrow DK^{*+}$ decay.

We perform averages using the following procedure, which is based on a set of reasonable, though imperfect, assumptions.

- It is assumed that effects due to the different D decay models used by the two experiments are negligible. Therefore, we do not rescale the results to a common model.
- It is further assumed that the model uncertainty is 100% correlated between experiments, and therefore this source of error is not used in the averaging procedure. (This approximation is compromised by the fact that the BABAR results include $D \rightarrow K_S^0 K^+ K^-$ decays in addition to $D \rightarrow K_S^0 \pi^+ \pi^-$.)
- We include in the average the effect of correlations within each experiment’s set of measurements.
- At present it is unclear how to assign an average model uncertainty. We have not attempted to do so. Our average includes only statistical and systematic errors. An unknown amount of model uncertainty should be added to the final error.

- We follow the suggestion of Gronau [312] in making the DK^* averages. Explicitly, we assume that the selection of $K^{*+} \rightarrow K_S^0 \pi^+$ is the same in both experiments (so that κ , \bar{r}_B and $\bar{\delta}_B$ are the same), and drop the additional source of model uncertainty assigned by Belle due to possible nonresonant decays.
- We do not consider common systematic errors, other than the D decay model.

Constraints on $\gamma \equiv \phi_3$

The measurements of (x_{\pm}, y_{\pm}) can be used to obtain constraints on $\gamma \equiv \phi_3$, as well as the hadronic parameters r_B and δ_B . BABAR [455], Belle [454,457] and LHCb [456] have all done so using a frequentist procedure (there are some differences in the details of the techniques used).

- BABAR obtain $\gamma = (68_{-14}^{+15} \pm 4 \pm 3)^\circ$ from DK^+ , D^*K^+ and DK^{*+} .
- Belle obtain $\phi_3 = (78_{-12}^{+11} \pm 4 \pm 9)^\circ$ from DK^+ and D^*K^+ .
- LHCb obtain $\gamma = (84_{-42}^{+49})^\circ$ from DK^+ using 1 fb^{-1} of data (a more precise result using 3 fb^{-1} and the model-independent method is reported below).
- The experiments also obtain values for the hadronic parameters as detailed in Table 56.
- In the BABAR analysis of $B^+ \rightarrow DK^+$ with $D \rightarrow \pi^+ \pi^- \pi^0$ decays [322], a constraint of $-30^\circ < \gamma < 76^\circ$ is obtained at the 68% confidence level.
- The results discussed here are included in the HFLAV combination to obtain a world average value for $\gamma \equiv \phi_3$, as discussed in Sect. 4.14.7.

BABAR and LHCb have performed a similar analysis using the self-tagging neutral B decay $B^0 \rightarrow DK^{*0}$ (with $K^{*0} \rightarrow K^+ \pi^-$). Effects due to the natural width of the

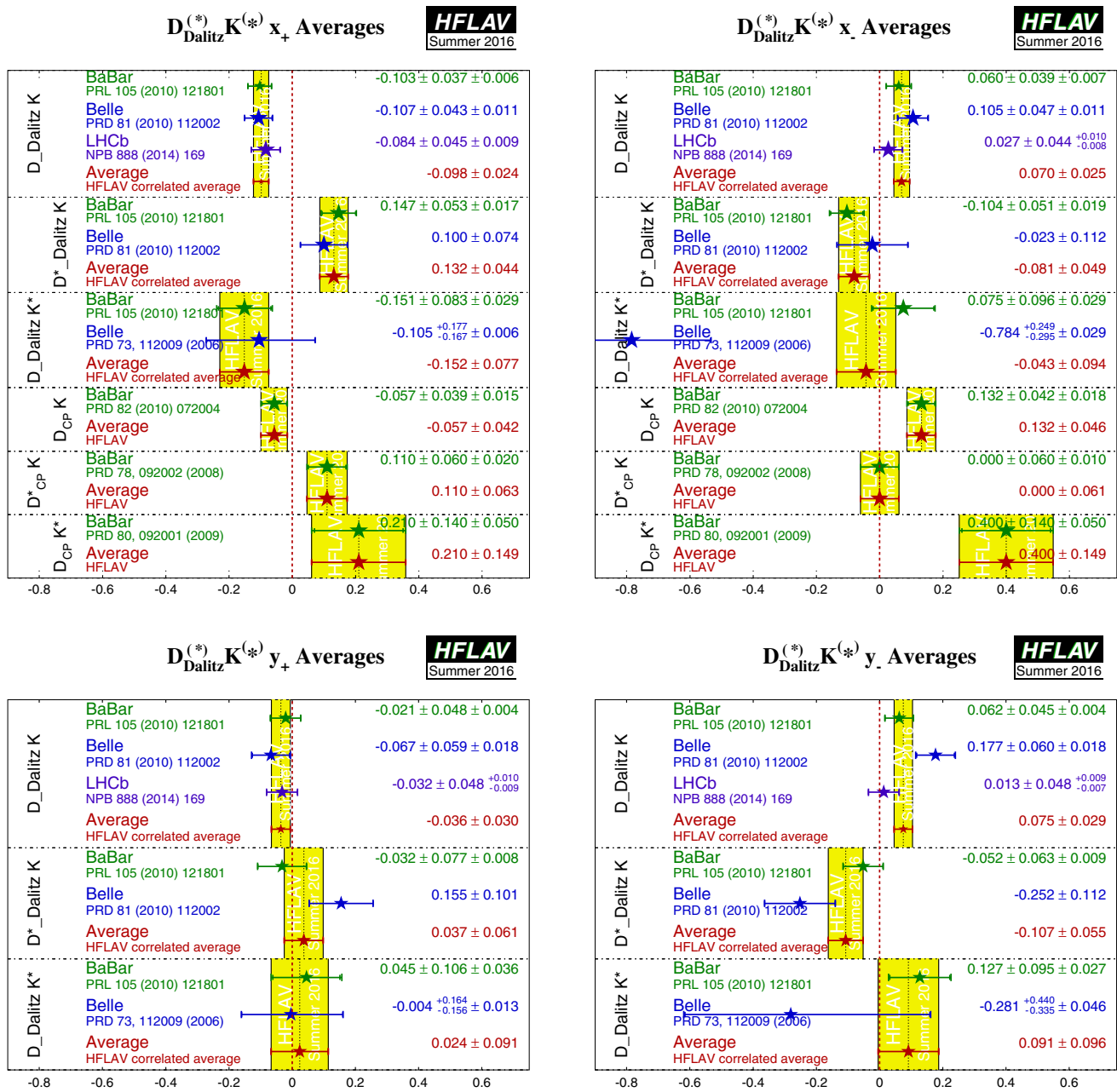


Fig. 43 Averages of (x_{\pm}, y_{\pm}) from model-dependent analyses of $B^+ \rightarrow D^{(*)}K^{(*)+}$ with $D \rightarrow K_S^0 h^+ h^-$ ($h = \pi, K$). (Top left) x_+ , (top right) x_- , (bottom left) y_+ , (bottom right) y_- . The top plots include

K^{*0} are handled using the parametrisation suggested by Gronau [312]. LHCb give results in terms of the Cartesian parameters, as shown in Table 55. BABAR [459] present results only in terms of γ and the hadronic parameters. The obtained constraints on $\gamma \equiv \phi_3$ are

- BABAR obtain $\gamma = (162 \pm 56)^\circ$
- LHCb obtain $\gamma = (80^{+21}_{-22})^\circ$
- Values for the hadronic parameters are given in Table 56.

constraints on x_{\pm} obtained from GLW analyses (see Sect. 4.14.1). Note that the uncertainties assigned to the averages given in these plots do not include model errors

4.14.5 D decays to multiparticle self-conjugate final states (model-independent analysis)

A model-independent approach to the analysis of $B^+ \rightarrow D^{(*)}K^+$ with multiparticle D decays was proposed by Giri, Grossman, Soffer and Zupan [309], and further developed by Bondar and Poluektov [319, 320]. The method relies on information on the average strong phase difference between D^0 and \bar{D}^0 decays in bins of Dalitz plot position that can be obtained from quantum-correlated $\psi(3770) \rightarrow D^0 \bar{D}^0$

Table 56 Summary of constraints on hadronic parameters from model-dependent analyses of $B^+ \rightarrow D^{(*)}K^{(*)+}$ and $B^0 \rightarrow DK^{*0}$ decays. Note the alternative parametrisation of the hadronic parameters used by BABAR in the DK^{*+} mode

	r_B	δ_B
In DK^+		
BABAR	$0.096 \pm 0.029 \pm 0.005 \pm 0.004$	$(119^{+19}_{-20} \pm 3 \pm 3)^\circ$
Belle	$0.160^{+0.040}_{-0.038} \pm 0.011^{+0.05}_{-0.010}$	$(138^{+13}_{-16} \pm 4 \pm 23)^\circ$
LHCb	0.06 ± 0.04	$(115^{+41}_{-51})^\circ$
In D^*K^+		
BABAR	$0.133^{+0.042}_{-0.039} \pm 0.014 \pm 0.003$	$(-82 \pm 21 \pm 5 \pm 3)^\circ$
Belle	$0.196^{+0.072}_{-0.069} \pm 0.012^{+0.062}_{-0.012}$	$(342^{+19}_{-21} \pm 3 \pm 23)^\circ$
	\bar{r}_B	$\bar{\delta}_B$
In DK^{*+}		
BABAR	$\kappa \bar{r}_B = 0.149^{+0.066}_{-0.062} \pm 0.026 \pm 0.006$	$(111 \pm 32 \pm 11 \pm 3)^\circ$
Belle	$0.56^{+0.22}_{-0.16} \pm 0.04 \pm 0.08$	$(243^{+20}_{-23} \pm 3 \pm 50)^\circ$
In DK^{*0}		
BABAR	<0.55 at 95% probability	$(62 \pm 57)^\circ$
LHCb	0.39 ± 0.13	$(197^{+24}_{-20})^\circ$

events. This information is measured in the form of parameters c_i and s_i that are the amplitude weighted averages of the cosine and sine of the strong phase difference in a Dalitz plot bin labelled by i , respectively. These quantities have been obtained for $D \rightarrow K_S^0 \pi^+ \pi^-$ (and $D \rightarrow K_S^0 K^+ K^-$) decays by CLEO-c [263,460].

Belle [461] and LHCb [462] have used the model-independent Dalitz plot analysis approach to study the mode $B^+ \rightarrow DK^+$. Both Belle [463] and LHCb [464] have also used this approach to study $B^0 \rightarrow DK^*(892)^0$ decays. In both cases, the experiments use $D \rightarrow K_S^0 \pi^+ \pi^-$ decays while LHCb has also included the $D \rightarrow K_S^0 K^+ K^-$ decay. The Cartesian variables (x_\pm, y_\pm) , defined in Eq. (150), are determined from the data. Note that due to the strong statistical and systematic correlations with the model-dependent results given in Sect. 4.14.4, these results cannot be combined.

The results and averages are given in Table 57, and shown in Fig. 44. Most results have three sets of errors, which are statistical, systematic, and uncertainty coming from the knowledge of c_i and s_i respectively. To perform the average, we remove the last uncertainty, which should be 100% correlated between the measurements. Since the size of the uncertainty from c_i and s_i is found to depend on the size of the $B \rightarrow DK$ data sample, we assign the LHCb uncertainties (which are mostly the smaller of the Belle and LHCb values) to the averaged result. This procedure should be conservative. In the LHCb $B^0 \rightarrow DK^*(892)^0$ results [464], the values of c_i and s_i are constrained to their measured values within uncertainties in the fit to data, and hence the effect is absorbed in their statistical uncertainties. The $B^0 \rightarrow DK^*(892)^0$ aver-

age is performed neglecting the model uncertainties on the Belle results.

Constraints on $\gamma \equiv \phi_3$

The measurements of (x_\pm, y_\pm) can be used to obtain constraints on γ , as well as the hadronic parameters r_B and δ_B . The experiments have done so using frequentist procedures (there are some differences in the details of the techniques used) (Table 58).

- From $B^+ \rightarrow DK^+$, Belle [461] obtain $\phi_3 = (77.3^{+15.1}_{-14.9} \pm 4.1 \pm 4.3)^\circ$.
- From $B^+ \rightarrow DK^+$, LHCb [462] obtain $\gamma = (62^{+15}_{-14})^\circ$.
- From $B^0 \rightarrow DK^*(892)^0$, LHCb [464] obtain $\gamma = (71 \pm 20)^\circ$.
- The experiments also obtain values for the hadronic parameters as detailed in Table 59.
- The results discussed here are included in the HFLAV combination to obtain a world average value for $\gamma \equiv \phi_3$, as discussed in Sect. 4.14.7.

4.14.6 D decays to multiparticle non-self-conjugate final states (model-independent analysis)

Following the original suggestion of Grossman, Ligeti and Soffer [317], decays of D mesons to $K_S^0 K^\pm \pi^\mp$ can be used in a similar approach to that discussed above to determine $\gamma \equiv \phi_3$. Since these decays are less abundant, the event samples available to date have not been sufficient for a fine binning of the Dalitz plots, but the analysis can be performed using only an overall coherence factor and related strong phase difference for the decay. These quantities have been

Table 57 Averages from model-independent Dalitz plot analyses of $b \rightarrow c\bar{u}s/u\bar{c}s$ modes

Experiment	Sample size	x_+	y_+	x_-	y_-
$DK^+, D \rightarrow K_S^0\pi^+\pi^-$					
Belle [461]	$N(B\bar{B}) = 772M$	$-0.110 \pm 0.043 \pm 0.014 \pm 0.007$	$-0.050^{+0.052}_{-0.055} \pm 0.011 \pm 0.007$	$0.095 \pm 0.045 \pm 0.014 \pm 0.010$	$0.137^{+0.053}_{-0.057} \pm 0.015 \pm 0.023$
LHCb [462]	$\int \mathcal{L} dt = 3fb^{-1}$	$-0.077 \pm 0.024 \pm 0.010 \pm 0.004$	$-0.022 \pm 0.025 \pm 0.004 \pm 0.010$	$0.025 \pm 0.025 \pm 0.010 \pm 0.005$	$0.075 \pm 0.029 \pm 0.005 \pm 0.014$
Average		$-0.085 \pm 0.023 \pm 0.04$	$-0.027 \pm 0.023 \pm 0.010$	$0.044 \pm 0.023 \pm 0.005$	$0.090 \pm 0.026 \pm 0.014$
Confidence level					
0.39 (0.9 σ)					
$DK^{*0}, D \rightarrow K_S^0\pi^+\pi^-$					
Belle [463]	$N(B\bar{B}) = 772M$	$0.1^{+0.7}_{-0.4} \pm 0.1$	$0.3^{+0.5}_{-0.8} \pm 0.1$	$0.4^{+1.0}_{-0.6} \pm 0.0$	$-0.6^{+0.8}_{-1.0} \pm 0.1$
LHCb [464]	$\int \mathcal{L} dt = 3fb^{-1}$	$0.05 \pm 0.35 \pm 0.02$	$-0.81 \pm 0.28 \pm 0.06$	$-0.31 \pm 0.20 \pm 0.04$	$0.31 \pm 0.21 \pm 0.05$
Average		0.10 ± 0.30	-0.63 ± 0.26	-0.27 ± 0.20	0.27 ± 0.21
Confidence level					
0.38 (0.9 σ)					

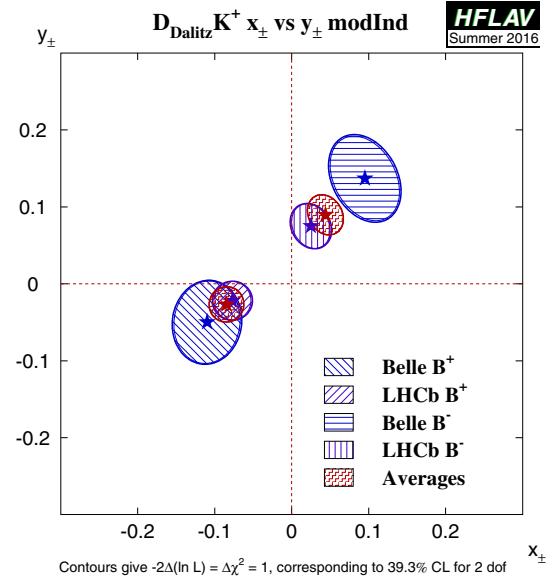


Fig. 44 Contours in the (x_{\pm}, y_{\pm}) plane from model-independent analysis of $B^+ \rightarrow DK^+$ with $D \rightarrow K_S^0 h^+ h^-$ ($h = \pi, K$)

determined by CLEO-c [466] both for the full Dalitz plots and in a restricted region $\pm 100 \text{ MeV}/c^2$ around the peak of the $K^*(892)^\pm$ resonance.

LHCb [465] has reported results of an analysis of $B^+ \rightarrow DK^+$ and $B^+ \rightarrow D\pi^+$ decays with $D \rightarrow K_S^0 K^\pm \pi^\mp$. The decays with different final states of the D meson are distinguished by the charge of the kaon from the decay of the D meson relative to the charge of the B meson, and are labelled “same sign” (SS) and “opposite sign” (OS). Six observables potentially sensitive to $\gamma \equiv \phi_3$ are measured: two ratios of rates for DK and $D\pi$ decays (one each for SS and OS) and four asymmetries (for DK and $D\pi$, SS and OS). This is done both for the full Dalitz plot of the D decay and for the $K^*(892)^\pm$ -dominated region (with the same boundaries as used by CLEO-c). Note that there is a significant overlap of events between the two samples. The results, shown in Table 58 do not yet have sufficient precision to set significant constraints on $\gamma \equiv \phi_3$.

4.14.7 Combinations of results on rates and asymmetries in $B \rightarrow D^{(*)}K^{(*)}$ decays to obtain constraints on $\gamma \equiv \phi_3$

BABAR and LHCb have both produced constraints on $\gamma \equiv \phi_3$ from combinations of their results on $B^+ \rightarrow DK^+$ and related processes. The experiments use a frequentist procedure (there are some differences in the details of the techniques used).

- BABAR [467] use results from DK, D^*K and DK^* modes with GLW, ADS and GGSZ analyses, to obtain $\gamma = (69^{+17}_{-16})^\circ$.

Table 58 Results from model-independent Dalitz plot analysis of $B^+ \rightarrow DK^+, D \rightarrow K_S^0 K^\pm \pi^\mp$

Experiment	$\int \mathcal{L} dt$	R_{SS}	R_{OS}	Ass. DK	Aos. DK	Ass. $D\pi$	Aos. $D\pi$
$D \rightarrow K_S^0 K^\pm \pi^\mp$ (whole Dalitz plot)							
LHCb [465]	3 fb^{-1}	$0.092 \pm 0.009 \pm 0.004$	$0.066 \pm 0.009 \pm 0.002$	$0.040 \pm 0.091 \pm 0.018$	$0.233 \pm 0.129 \pm 0.024$	$-0.025 \pm 0.024 \pm 0.010$	$-0.052 \pm 0.029 \pm 0.017$
$D \rightarrow K^{*(892)\pm} K^\mp$							
LHCb [465]	3 fb^{-1}	$0.084 \pm 0.011 \pm 0.003$	$0.056 \pm 0.013 \pm 0.002$	$0.026 \pm 0.109 \pm 0.029$	$0.336 \pm 0.208 \pm 0.026$	$-0.012 \pm 0.028 \pm 0.010$	$-0.054 \pm 0.043 \pm 0.017$

- LHCb [468] use results from the DK^+ mode with GLW, GLW-like, ADS, GGSZ ($K_S^0 h^+ h^-$) and GLS ($K_S^0 K^\pm \pi^\mp$) analyses, as well as DK^{*0} with GLW, ADS and GGSZ analyses, $DK^+ \pi^-$ GLW Dalitz plot analysis, $DK^+ \pi^- \pi^+$ with GLW and ADS analyses and $B_S^0 \rightarrow D_S^\mp K^\pm$ decays. The LHCb combination takes into account subleading effects due to charm mixing and CP violation [469]. The result is $\gamma = (72.2_{-7.3}^{+6.8})^\circ$.
- All the combinations use inputs determined from $\psi(3770) \rightarrow D^0 \bar{D}^0$ data samples (and/or from the HFLAV Charm Physics subgroup global fits on charm mixing parameters; see Sect. 8.1) to constrain the hadronic parameters in the charm system.
- Constraints are also obtained on the hadronic parameters involved in the decays. A summary of these is given in Table 60.
- The CKMfitter [252] and UTfit [339] groups perform similar combinations of all available results to obtain combined constraints on $\gamma \equiv \phi_3$.

Independently from the constraints on $\gamma \equiv \phi_3$ obtained by the experiments, the results summarised in Sect. 4.14 are statistically combined to produce world average constraints on $\gamma \equiv \phi_3$ and the hadronic parameters involved. The combination is performed with the GAMMACOMBO framework [470] and follows a frequentist procedure, similar to those used by the experiments [467, 468, 471].

The input measurements used in the combination are listed in Table 61. Individual measurements are used as inputs, rather than the averages presented in Sect. 4.14, in order to facilitate cross-checks and to ensure the most appropriate treatment of correlations. A combination based on our averages for each of the quantities measured by experiments gives consistent results.

All results from GLW and GLW-like analyses of $B^+ \rightarrow D^{(*)} K^{(*)+}$ modes, as listed in Tables 48 and 51, are used. All results from ADS analyses of $B^+ \rightarrow D^{(*)} K^{(*)+}$ as listed in Table 52 are also used. Regarding $B^0 \rightarrow DK^{*0}$ decays, the results of the $B^0 \rightarrow DK^+ \pi^-$ GLW-Dalitz analysis (Table 50) are included, as are the LHCb results of the ADS analysis of $B^0 \rightarrow DK^{*0}$ (Table 54). Concerning results of GGSZ analyses of $B^+ \rightarrow D^{(*)} K^{(*)+}$ with $D \rightarrow K_S^0 h^+ h^-$, the model-dependent results, as listed in Table 55, are used for the BABAR and Belle experiments, whilst the model-independent results, as listed in Table 57, are used for LHCb. This choice is made in order to maintain consistency of the approach across experiments whilst maximising the size of the samples used to obtain inputs for the combination. For GGSZ analyses of $B^0 \rightarrow DK^{*0}$ with $D \rightarrow K_S^0 h^+ h^-$ the model-independent result from LHCb (given in Table 57) is used for consistency with the treatment of the LHCb $B^+ \rightarrow DK^+$ GGSZ result; the model-

Table 59 Summary of constraints on hadronic parameters from model-independent analyses of $B^+ \rightarrow DK^+$ and $B^0 \rightarrow DK^{*0}$, $D \rightarrow K_S^0 h^+ h^-$ ($h = \pi, K$) decays

	$r_B(DK^+)$	$\delta_B(DK^+)$
Belle	0.145 ± 0.030 $\pm 0.010 \pm 0.011$	$(129.9 \pm 15.0$ $\pm 3.8 \pm 4.7)^\circ$
LHCb	$0.080^{+0.019}_{-0.021}$	$(134^{+14}_{-15})^\circ$
	$\bar{r}_B(DK^{*0})$	$\bar{\delta}_B(DK^{*0})$
Belle	<0.87 at 68% confidence level	
LHCb	0.56 ± 0.17	$(204^{+21}_{-20})^\circ$

independent result by Belle is also included. The result of the GLS analysis of $B^+ \rightarrow DK^+$ with $D \rightarrow K^{*\pm} K^\mp$ from LHCb (Table 58) are used. Finally, results from the time-dependent analysis of $B_s^0 \rightarrow D_s^\mp K^\pm$ from LHCb (Table 47) are used.

Several results with sensitivity to γ are not included in the combination. Results from time-dependent analyses of $B^0 \rightarrow D^{(*)\mp} \pi^\pm$ and $D^\mp \rho^\pm$ (Table 46) are not used as there are insufficient constraints on the associated hadronic parameters. Similarly, results from $B^0 \rightarrow D^\mp K_S^0 \pi^\pm$ (Sect. 4.13.1) are not used. Results from the LHCb $B^0 \rightarrow DK^{*0}$ GLW analysis (Table 49) are not used because of the statistical overlap with the GLW–Dalitz analysis which is used instead. Limits on ADS parameters reported in Sect. 4.14.3 are not used. Results on $B^+ \rightarrow D\pi^+$ decays, given in Table 53, are not used since the small value of $r_B(D\pi^+)$ means these channels have less sensitivity to γ and are more vulnerable to biases due to subleading effects [468]. Results from the BABAR Dalitz plot analysis of $B^+ \rightarrow DK^+$ with $D \rightarrow \pi^+ \pi^- \pi^0$ (given in Table 55) are not included due to their limited sensitivity. Results from the $B^+ \rightarrow DK^+$, $D \rightarrow K_S^0 \pi^+ \pi^-$ GGSZ model-dependent analysis by LHCb (given in Table 55), and of the model-independent analysis of the same decay by Belle (given in Table 57) are not included due to the statistical overlap with results from model-(in)dependent analyses of the same data.

Auxiliary inputs are used in the combination in order to constrain the D system parameters and subsequently improve the determination of $\gamma \equiv \phi_3$. These include the ratio of suppressed to favoured decay amplitudes and the strong phase difference for $D \rightarrow K^\pm \pi^\mp$ decays, taken from the HFLAV Charm Physics subgroup global fits (see Sect. 8). The amplitude ratios, strong phase differences and coherence factors of $D \rightarrow K^\pm \pi^\mp \pi^0$, $D \rightarrow K^\pm \pi^\mp \pi^+ \pi^-$ and $D \rightarrow K_S^0 K^\pm \pi^\pm$ decays are taken from CLEO-c and LHCb measurements [466,472,473]. The fraction of CP -even content for quasi-GLW $D \rightarrow \pi^+ \pi^- \pi^+ \pi^-$, $D \rightarrow K^+ K^- \pi^0$ and $D \rightarrow \pi^+ \pi^- \pi^0$ decays are taken

Table 60 Summary of constraints on hadronic parameters obtained from global combinations of results in $B^+ \rightarrow D^{(*)} K^{(*)+}$ and $B^0 \rightarrow DK^{*0}$ decays

	$r_B(DK^+)$	$\delta_B(DK^+)$
BABAR	$0.092^{+0.013}_{-0.012}$	$(105^{+16}_{-17})^\circ$
LHCb	0.1019 ± 0.0056	$(142.6^{+5.7}_{-6.6})^\circ$
	$r_B(DK^{*0})$	$\delta_B(DK^{*0})$
LHCb	$0.218^{+0.045}_{-0.047}$	$(189^{+23}_{-20})^\circ$

from CLEO-c measurements [443]. Constraints required to relate the hadronic parameters of the $B^0 \rightarrow DK^{*0}$ GLW–Dalitz analysis to the effective hadronic parameters of the quasi-two-body approaches are taken from LHCb measurements [442]. Finally, the value of $-2\beta_s$ is taken from the HFLAV Lifetimes and Oscillations subgroup (see Sect. 3); this is required to obtain sensitivity to $\gamma \equiv \phi_3$ from the time-dependent analysis of $B_s^0 \rightarrow D_s^\mp K^\pm$ decays. A summary of the auxiliary constraints is given in Table 62.

The following reasonable, although imperfect, assumptions are made when performing the averages.

- CP violation in $D \rightarrow K^+ K^-$ and $D \rightarrow \pi^+ \pi^-$ decays is assumed to be zero. The results of Sect. 8 anyhow suggest such effects to be negligible.
- The combination is potentially sensitive to subleading effects from D^0 – \bar{D}^0 mixing which is not accounted for [469,474,475]. The effect is expected to be small given that $r_B \gtrsim 0.1$ (for all included modes) whilst $r_D \approx 0.05$.
- All $B^+ \rightarrow DK^{*+}$ modes are treated as two-body decays. In other words any dilution caused by non- K^{*+} contributions in the selected regions of the $DK_S^0 \pi^+$ or $DK^+ \pi^0$ Dalitz plots is assumed to be negligible. As a check of this assumption, it was found that including a coherence factor for $B^+ \rightarrow DK^{*+}$ modes, $\kappa_B(DK^{*+}) = 0.9$, had negligible impact on the results.
- All of the inputs are assumed to be completely uncorrelated. Whilst this is true of the statistical uncertainties, it is not necessarily the case for systematic uncertainties. In particular, the model uncertainties for different model-dependent GGSZ analyses are fully correlated (when the same model is used) and similarly the model-independent GGSZ analyses have correlated systematic uncertainties originating from the knowledge of the strong phase variation across the Dalitz plot. The effect of including these correlations is estimated to be $<1^\circ$.

Table 61 List of measurements used in the γ combination

<i>B</i> decay	<i>D</i> decay	Method	Experiment	Refs.
$B^+ \rightarrow DK^+$	$D \rightarrow K^+K^-, D \rightarrow \pi^+\pi^-,$ $D \rightarrow K_S^0\pi^0, D \rightarrow K_S^0\omega, D \rightarrow K_S^0\phi$	GLW	BABAR	[433]
$B^+ \rightarrow DK^+$	$D \rightarrow K^+K^-, D \rightarrow \pi^+\pi^-,$ $D \rightarrow K_S^0\pi^0, D \rightarrow K_S^0\omega, D \rightarrow K_S^0\phi$	GLW	Belle	[434]
$B^+ \rightarrow DK^+$	$D \rightarrow K^+K^-, D \rightarrow \pi^+\pi^-$	GLW	CDF	[435]
$B^+ \rightarrow DK^+$	$D \rightarrow K^+K^-, D \rightarrow \pi^+\pi^-$	GLW	LHCb	[436]
$B^+ \rightarrow D^*K^+$	$D \rightarrow K^+K^-, D \rightarrow \pi^+\pi^-,$ $D \rightarrow K_S^0\pi^0, D \rightarrow K_S^0\omega, D \rightarrow K_S^0\phi$	GLW	BABAR	[437]
$D^* \rightarrow D\gamma (\pi^0)$	$D \rightarrow K^+K^-, D \rightarrow \pi^+\pi^-,$ $D \rightarrow K_S^0\pi^0, D \rightarrow K_S^0\omega, D \rightarrow K_S^0\phi$	GLW	Belle	[434]
$B^+ \rightarrow D^*K^+$	$D \rightarrow K^+K^-, D \rightarrow \pi^+\pi^-,$ $D \rightarrow K_S^0\pi^0, D \rightarrow K_S^0\omega, D \rightarrow K_S^0\phi$	GLW	BABAR	[438]
$B^+ \rightarrow DK^{*+}$	$D \rightarrow K^+K^-, D \rightarrow \pi^+\pi^-,$ $D \rightarrow K_S^0\pi^0, D \rightarrow K_S^0\omega, D \rightarrow K_S^0\phi$	GLW	LHCb	[439]
$B^+ \rightarrow DK^+\pi^+\pi^-$	$D \rightarrow K^+K^-, D \rightarrow \pi^+\pi^-$	GLW	LHCb	[440]
$B^+ \rightarrow DK^+$	$D \rightarrow \pi^+\pi^-\pi^0$	GLW-like	BABAR	[322]
$B^+ \rightarrow DK^+$	$D \rightarrow h^+h^-\pi^0$	GLW-like	LHCb	[444]
$B^+ \rightarrow DK^+$	$D \rightarrow \pi^+\pi^-\pi^+\pi^-$	GLW-like	LHCb	[436]
$B^+ \rightarrow DK^+$	$D \rightarrow K^\pm\pi^\mp$	ADS	BABAR	[445]
$B^+ \rightarrow DK^+$	$D \rightarrow K^\pm\pi^\mp$	ADS	Belle	[446]
$B^+ \rightarrow DK^+$	$D \rightarrow K^\pm\pi^\mp$	ADS	CDF	[447]
$B^+ \rightarrow DK^+$	$D \rightarrow K^\pm\pi^\mp$	ADS	LHCb	[436]
$B^+ \rightarrow DK^+$	$D \rightarrow K^\pm\pi^\mp\pi^0$	ADS	BABAR	[448]
$B^+ \rightarrow DK^+$	$D \rightarrow K^\pm\pi^\mp\pi^0$	ADS	Belle	[449]
$B^+ \rightarrow DK^+$	$D \rightarrow K^\pm\pi^\mp\pi^0$	ADS	LHCb	[444]
$B^+ \rightarrow DK^+$	$D \rightarrow K^\pm\pi^\mp\pi^+\pi^-$	ADS	LHCb	[436]
$B^+ \rightarrow D^*K^+$	$D \rightarrow K^\pm\pi^\mp$	ADS	BABAR	[445]
$D^* \rightarrow D\gamma$				
$B^+ \rightarrow D^*K^+$	$D \rightarrow K^\pm\pi^\mp$	ADS	BABAR	[445]
$D^* \rightarrow D\pi^0$				
$B^+ \rightarrow DK^{*+}$	$D \rightarrow K^\pm\pi^\mp$	ADS	BABAR	[438]
$B^+ \rightarrow DK^{*+}$	$D \rightarrow K^\pm\pi^\mp$	ADS	LHCb	[439]
$B^+ \rightarrow DK^+\pi^+\pi^-$	$D \rightarrow K^\pm\pi^\mp$	ADS	LHCb	[440]
$B^+ \rightarrow DK^+$	$D \rightarrow K_S^0\pi^+\pi^-$	GGSZ MD	BABAR	[455]
$B^+ \rightarrow DK^+$	$D \rightarrow K_S^0\pi^+\pi^-$	GGSZ MD	Belle	[454]
$B^+ \rightarrow D^*K^+$	$D \rightarrow K_S^0\pi^+\pi^-$	GGSZ MD	BABAR	[455]
$D^* \rightarrow D\gamma (\pi^0)$				
$B^+ \rightarrow D^*K^+$	$D \rightarrow K_S^0\pi^+\pi^-$	GGSZ MD	Belle	[454]
$D^* \rightarrow D\gamma (\pi^0)$				
$B^+ \rightarrow DK^{*+}$	$D \rightarrow K_S^0\pi^+\pi^-$	GGSZ MD	BABAR	[455]
$B^+ \rightarrow DK^{*+}$	$D \rightarrow K_S^0\pi^+\pi^-$	GGSZ MD	Belle	[457]
$B^+ \rightarrow DK^+$	$D \rightarrow K_S^0\pi^+\pi^-$	GGSZ MI	LHCb	[462]
$B^+ \rightarrow DK^+$	$D \rightarrow K_S^0K^+\pi^-$	GLS	LHCb	[465]
$B^0 \rightarrow DK^{*0}$	$D \rightarrow K^\pm\pi^\mp$	ADS	LHCb	[441]
$B^0 \rightarrow DK^+\pi^-$	$D \rightarrow h^+h^-$	GLW–Dalitz	LHCb	[442]
$B^0 \rightarrow DK^{*0}$	$D \rightarrow K_S^0h^+h^-$	GGSZ MI	Belle	[463]
$B^0 \rightarrow DK^{*0}$	$D \rightarrow K_S^0h^+h^-$	GGSZ MI	LHCb	[464]
$B_S^0 \rightarrow D_S^\mp K^\pm$	$D_S^+ \rightarrow h^+h^-\pi^+$	TD	LHCb	[432]

Table 62 List of the auxiliary inputs used in the combinations

Decay	Parameters	Source	Refs.
$D \rightarrow K^\pm \pi^\mp$	$r_D^{K\pi}, \delta_D^{K\pi}$	HFLAV	Sect. 8
$D \rightarrow K^\pm \pi^\mp \pi^+ \pi^-$	$\delta_D^{K3\pi}, \kappa_D^{K3\pi}, r_D^{K3\pi}$	CLEO+LHCb	[472]
$D \rightarrow \pi^+ \pi^- \pi^+ \pi^-$	$F_+(\pi^+ \pi^- \pi^+ \pi^-)$	CLEO	[443]
$D \rightarrow K^\pm \pi^\mp \pi^0$	$\delta_D^{K2\pi}, \kappa_D^{K2\pi}, r_D^{K2\pi}$	CLEO+LHCb	[472]
$D \rightarrow h^+ h^- \pi^0$	$F_+(\pi^+ \pi^- \pi^0), F_+(K^+ K^- \pi^0)$	CLEO	[443]
$D \rightarrow K_S^0 K^+ \pi^-$	$\delta_D^{K_S K\pi}, \kappa_D^{K_S K\pi}, r_D^{K_S K\pi}$ $r_D^{K_S K\pi}$	CLEO LHCb	[466] [473]
$B^0 \rightarrow DK^{*0}$	$\kappa_B(DK^{*0}), \bar{R}_B^{DK^{*0}}, \bar{\Delta}_B^{DK^{*0}}$	LHCb	[442]
$B_s^0 \rightarrow D_s^\mp K^\pm$	ϕ_s	HFLAV	Sect. 3

Table 63 Averages values obtained for the hadronic parameters in $B \rightarrow D^{(*)} K^{(*)}$ decays

Parameter	Value
$r_B(DK^+)$	0.104 ± 0.005
$r_B(D^* K^+)$	0.12 ± 0.02
$r_B(DK^{*+})$	0.05 ± 0.03
$r_B(DK^{*0})$	0.55 ± 0.16
$\delta_B(DK^+)$	$(137.7^{+5.1}_{-6.0})^\circ$
$\delta_B(D^* K^+)$	$(311^{+13}_{-17})^\circ$
$\delta_B(DK^{*+})$	$(108^{+33}_{-74})^\circ$
$\delta_B(DK^{*0})$	$(203^{+22}_{-20})^\circ$

Table 64 Averages of $\gamma \equiv \phi_3$ split by B meson decay mode

Decay mode	Value
$B_s^0 \rightarrow D_s^\mp K^\pm$	$(128^{+18}_{-22})^\circ$
$B^+ \rightarrow DK^{*+}$	$(33^{+30}_{-20})^\circ$
$B^+ \rightarrow D^* K^+$	$(64^{+18}_{-19})^\circ$
$B^0 \rightarrow DK^{*0}$	$(92^{+23}_{-21})^\circ$
$B^+ \rightarrow DK^+$	$(72.2^{+5.9}_{-7.0})^\circ$

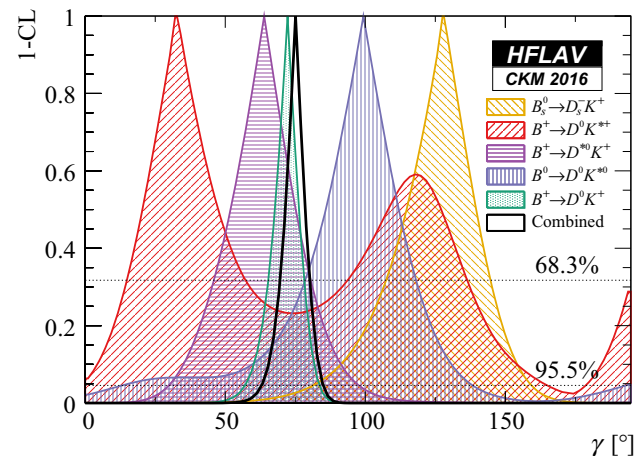


Fig. 45 World average of $\gamma \equiv \phi_3$, in terms of 1-CL, split by decay mode

Table 65 Averages of $\gamma \equiv \phi_3$ split by method. For GLW method only the solution nearest the combined average is shown

Method	Value
GLW	$(82.7^{+5.5}_{-6.9})^\circ$
ADS	$(72^{+12}_{-18})^\circ$
GGSZ	$(67.3^{+8.1}_{-7.8})^\circ$

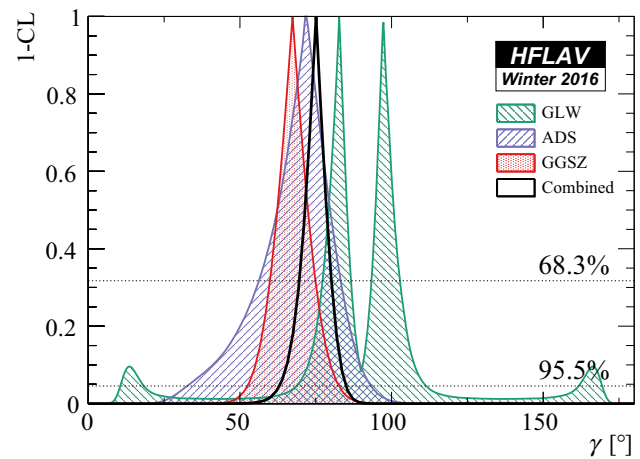


Fig. 46 World average of $\gamma \equiv \phi_3$, in terms of 1-CL, split by analysis method

In total, there are 116 observables and 33 free parameters. The combination has a χ^2 value of 95.5, which corresponds to a global p-value of 0.164. The obtained world average for the Unitarity Triangle angle $\gamma \equiv \phi_3$ is

$$\gamma \equiv \phi_3 = (74.0^{+5.8}_{-6.4})^\circ. \tag{166}$$

An ambiguous solution at $\gamma \equiv \phi_3 \rightarrow \gamma \equiv \phi_3 + \pi$ also exists. The results for the hadronic parameters are listed in Table 63. Results for input analyses as split by B meson decay mode are shown in Table 64 and Fig. 45. Results for

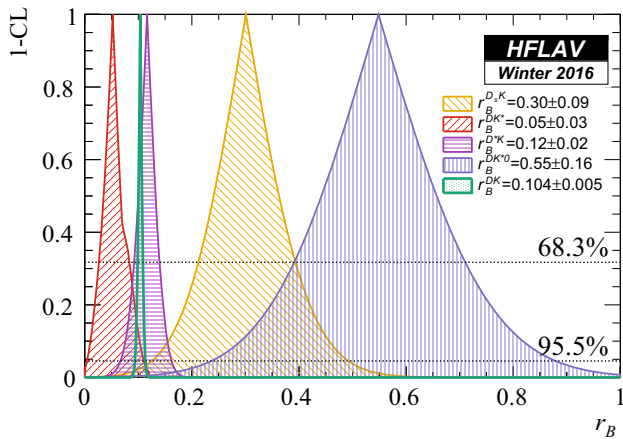


Fig. 47 World averages for the hadronic parameters r_B in the different decay modes, in terms of 1-CL

input analyses as split by the method are shown in Table 65 and Fig. 46. Results for the hadronic ratios, r_B , are shown in Fig. 47. A demonstration of how the various analyses contribute to the combination is shown in Fig. 48.

5 Semileptonic B decays

This section contains our averages for semileptonic B meson decays, i.e. decays of the type $B \rightarrow X \ell \nu_\ell$, where X refers to one or more hadrons, ℓ to a charged lepton and ν_ℓ to its associated neutrino. Unless otherwise stated, ℓ stands for an electron *or* a muon, lepton universality is assumed, and both charge conjugate states are combined. Some averages assume isospin symmetry, this will be explicitly mentioned at every instance.

Averages are presented separately for CKM favored $b \rightarrow c$ quark transitions and CKM suppressed $b \rightarrow u$ transitions. Among these transitions we distinguish *exclusive* decays involving a specific meson ($X = D, D^*, \pi, \rho, \dots$) from *inclusive* decay modes, i.e. the sum over all possible hadronic states, one or more mesons and baryons. Semileptonic decays proceed via first order weak interactions and are well described in the framework of the standard model (SM). Their decay rates are sensitive to the magnitude squared of the CKM elements V_{cb} and V_{ub} , and their determination is one of the primary goals for the study of these decays. Semileptonic

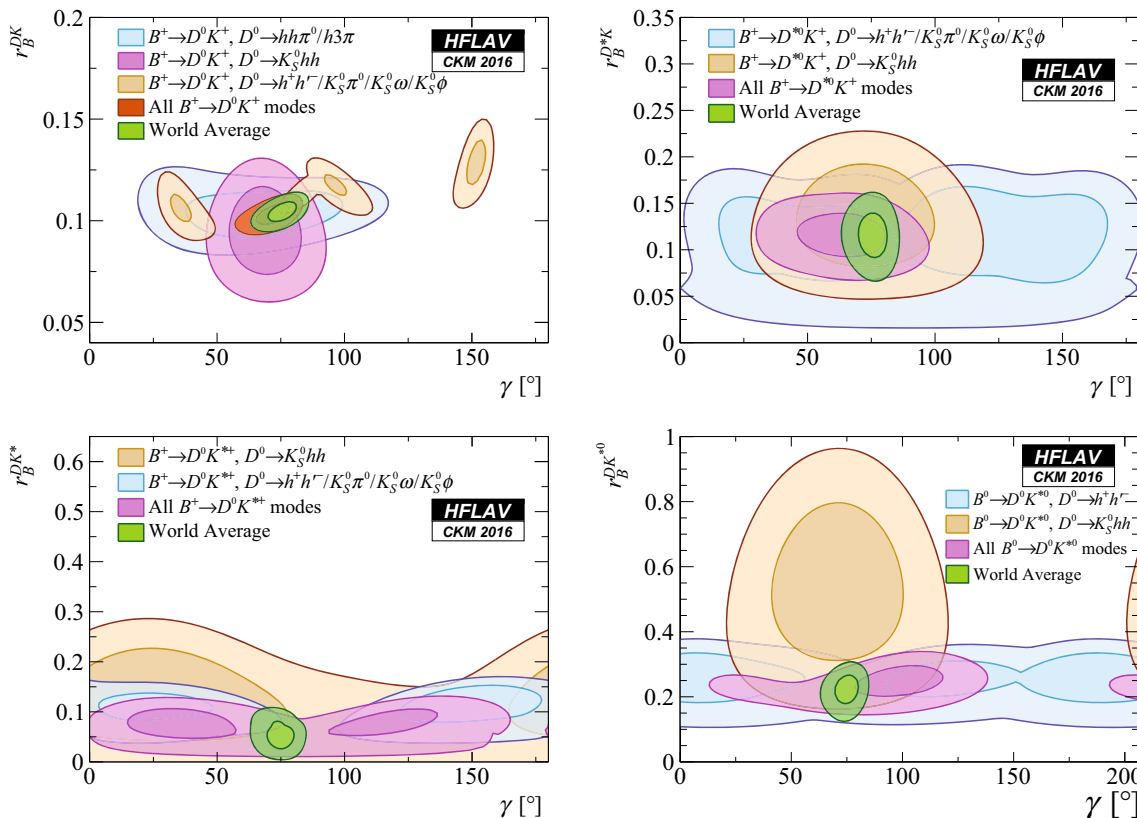


Fig. 48 Contributions to the combination from different input measurements, shown in the plane of the relevant r_B parameter *vs.* $\gamma \equiv \phi_3$. From left to right, top to bottom: $B^+ \rightarrow DK^+$, $B^+ \rightarrow D^*K^+$, $B^+ \rightarrow$

DK^{*+} and $B^0 \rightarrow DK^{*0}$. Contours show the two-dimensional 68 % and 95 % CL regions

decays involving the τ lepton might be sensitive to beyond SM processes because of the high τ mass, which might result in enhanced couplings to a hypothetical charged Higgs boson or leptoquarks.

The technique for obtaining the averages follows the general HFLAV procedure (Sect. 2) unless otherwise stated. More information on the averages, in particular on the common input parameters is available on the HFLAV semileptonic webpage.

5.1 Exclusive CKM-favoured decays

5.1.1 $\bar{B} \rightarrow D^* \ell^- \bar{\nu}_\ell$

The recoil variable w used to describe $\bar{B} \rightarrow D^* \ell^- \bar{\nu}_\ell$ decays is the product of the four-velocities of the initial and final state mesons, $w = v_B \cdot v_{D^*}$. The differential decay rate for massless fermions as a function of w is given by (see, e.g., [476])

$$\frac{d\Gamma(\bar{B} \rightarrow D^* \ell^- \bar{\nu}_\ell)}{dw} = \frac{G_F^2 m_{D^*}^3}{48\pi^3} (m_B - m_{D^*})^2 \times \chi(w) \eta_{EW}^2 \mathcal{F}^2(w) |V_{cb}|^2, \quad (167)$$

where G_F is Fermi's constant, m_B and m_{D^*} are the B and D^* meson masses, $\chi(w)$ is a known expression of w and η_{EW} is a small electroweak correction [477]. Some authors also include a long-distance EM radiation effect (Coulomb correction) in this factor. The form factor $\mathcal{F}(w)$ for the $\bar{B} \rightarrow D^* \ell^- \bar{\nu}_\ell$ decay contains three independent functions, $h_{A_1}(w)$, $R_1(w)$ and $R_2(w)$,

$$\chi(w) \mathcal{F}^2(w) = h_{A_1}^2(w) \sqrt{w^2 - 1} (w + 1)^2 \times \left\{ 2 \left[\frac{1 - 2wr + r^2}{(1 - r)^2} \right] \left[1 + R_1^2(w) \frac{w^2 - 1}{w + 1} \right] + \left[1 + (1 - R_2(w)) \frac{w - 1}{1 - r} \right]^2 \right\}, \quad (168)$$

where $r = m_{D^*}/m_B$.

To extract $|V_{cb}|$, the experimental analyses we consider in this section use the parametrization of these form factor functions by Caprini, Lellouch and Neubert (CLN) [478],

$$h_{A_1}(w) = h_{A_1}(1) [1 - 8\rho^2 z + (53\rho^2 - 15)z^2 - (231\rho^2 - 91)z^3], \quad (169)$$

$$R_1(w) = R_1(1) - 0.12(w - 1) + 0.05(w - 1)^2, \quad (170)$$

$$R_2(w) = R_2(1) + 0.11(w - 1) - 0.06(w - 1)^2, \quad (171)$$

where $z = (\sqrt{w + 1} - \sqrt{2})/(\sqrt{w + 1} + \sqrt{2})$. The form factor $\mathcal{F}(w)$ is thus described by the slope ρ^2 and the ratios $R_1(1)$ and $R_2(1)$.

We use the measurements of these form factor parameters shown in Table 66 and rescale them to the latest values of the input parameters (mainly branching fractions of charmed mesons) [479]. Most of the measurements in Table 66 are based on the decay $\bar{B}^0 \rightarrow D^{*+} \ell^- \bar{\nu}_\ell$. Some measurements [480,481] are sensitive also to the $B^- \rightarrow D^{*0} \ell^- \bar{\nu}_\ell$, and one measurement [482] is based on the decay $B^- \rightarrow D^{*0} \ell^- \bar{\nu}_\ell$. Isospin symmetry is assumed in this average. The earlier results for the LEP experiments and CLEO have significantly rescaled results, and significantly larger uncertainties than the recent measurements by the B-factories Belle and BABAR.

In the next step, we perform a four parameter fit of $\eta_{EW} \mathcal{F}(1) |V_{cb}|$, ρ^2 , $R_1(1)$ and $R_2(1)$ to the rescaled measurements, taking into account correlated statistical and systematic uncertainties. Only two measurements constrain all four parameters [483,484], the remaining measurements determine only the normalization $\eta_{EW} \mathcal{F}(1) |V_{cb}|$ and the slope ρ^2 . The result of the fit is

$$\eta_{EW} \mathcal{F}(1) |V_{cb}| = (35.61 \pm 0.43) \times 10^{-3}, \quad (172)$$

$$\rho^2 = 1.205 \pm 0.026, \quad (173)$$

$$R_1(1) = 1.404 \pm 0.032, \quad (174)$$

$$R_2(1) = 0.854 \pm 0.020, \quad (175)$$

and the correlation coefficients are

$$\rho_{\eta_{EW} \mathcal{F}(1) |V_{cb}|, \rho^2} = 0.338, \quad (176)$$

$$\rho_{\eta_{EW} \mathcal{F}(1) |V_{cb}|, R_1(1)} = -0.104, \quad (177)$$

$$\rho_{\eta_{EW} \mathcal{F}(1) |V_{cb}|, R_2(1)} = -0.071, \quad (178)$$

$$\rho_{\rho^2, R_1(1)} = 0.570, \quad (179)$$

$$\rho_{\rho^2, R_2(1)} = -0.810, \quad (180)$$

$$\rho_{R_1(1), R_2(1)} = -0.758. \quad (181)$$

The uncertainties and correlations quoted here include both statistical and systematic contributions. The χ^2 of the fit is 30.2 for 23 degrees of freedom, which corresponds to a confidence level of 14.4%. An illustration of this fit result is given in Fig. 49.

Using the latest update from the Fermilab Lattice and MILC Collaborations [489], the form factor normalization $\eta_{EW} \mathcal{F}(1)$ is

$$\eta_{EW} \mathcal{F}(1) = 0.912 \pm 0.014, \quad (182)$$

where $\eta_{EW} = 1.0066 \pm 0.0050$ has been used. The central value of this number corresponds to the electroweak correc-

Table 66 Measurements of the Caprini, Lellouch and Neubert (CLN) [478] form factor parameters in $\bar{B} \rightarrow D^* \ell^- \bar{\nu}_\ell$ before and after rescaling. Most analyses (except [483,484]) measure only $\eta_{EW} \mathcal{F}(1) |V_{cb}|$, and ρ^2 , so only these two parameters are shown here

Experiment	$\eta_{EW} \mathcal{F}(1) V_{cb} [10^{-3}]$ (rescaled) $\eta_{EW} \mathcal{F}(1) V_{cb} [10^{-3}]$ (published)	ρ^2 (rescaled) ρ^2 (published)
ALEPH [485]	$30.97 \pm 1.78_{\text{stat}} \pm 1.29_{\text{syst}}$ $31.9 \pm 1.8_{\text{stat}} \pm 1.9_{\text{syst}}$	$0.491 \pm 0.227_{\text{stat}} \pm 0.146_{\text{syst}}$ $0.37 \pm 0.26_{\text{stat}} \pm 0.14_{\text{syst}}$
CLEO [480]	$39.67 \pm 1.22_{\text{stat}} \pm 1.62_{\text{syst}}$ $43.1 \pm 1.3_{\text{stat}} \pm 1.8_{\text{syst}}$	$1.366 \pm 0.085_{\text{stat}} \pm 0.087_{\text{syst}}$ $1.61 \pm 0.09_{\text{stat}} \pm 0.21_{\text{syst}}$
OPAL excl [486]	$35.81 \pm 1.57_{\text{stat}} \pm 1.62_{\text{syst}}$ $36.8 \pm 1.6_{\text{stat}} \pm 2.0_{\text{syst}}$	$1.205 \pm 0.207_{\text{stat}} \pm 0.153_{\text{syst}}$ $1.31 \pm 0.21_{\text{stat}} \pm 0.16_{\text{syst}}$
OPAL partial reco [486]	$36.98 \pm 1.19_{\text{stat}} \pm 2.32_{\text{syst}}$ $37.5 \pm 1.2_{\text{stat}} \pm 2.5_{\text{syst}}$	$1.149 \pm 0.145_{\text{stat}} \pm 0.296_{\text{syst}}$ $1.12 \pm 0.14_{\text{stat}} \pm 0.29_{\text{syst}}$
DELPHI partial reco [487]	$35.15 \pm 1.39_{\text{stat}} \pm 2.30_{\text{syst}}$ $35.5 \pm 1.4_{\text{stat}}^{+2.3}_{-2.4} \text{syst}$	$1.168 \pm 0.126_{\text{stat}} \pm 0.381_{\text{syst}}$ $1.34 \pm 0.14_{\text{stat}}^{+0.24}_{-0.22} \text{syst}$
DELPHI excl [488]	$35.85 \pm 1.68_{\text{stat}} \pm 1.98_{\text{syst}}$ $39.2 \pm 1.8_{\text{stat}} \pm 2.3_{\text{syst}}$	$1.084 \pm 0.143_{\text{stat}} \pm 0.151_{\text{syst}}$ $1.32 \pm 0.15_{\text{stat}} \pm 0.33_{\text{syst}}$
Belle [483]	$34.39 \pm 0.17_{\text{stat}} \pm 1.01_{\text{syst}}$ $34.6 \pm 0.2_{\text{stat}} \pm 1.0_{\text{syst}}$	$1.213 \pm 0.034_{\text{stat}} \pm 0.008_{\text{syst}}$ $1.214 \pm 0.034_{\text{stat}} \pm 0.009_{\text{syst}}$
BABAR excl [484]	$33.59 \pm 0.29_{\text{stat}} \pm 1.03_{\text{syst}}$ $34.7 \pm 0.3_{\text{stat}} \pm 1.1_{\text{syst}}$	$1.184 \pm 0.048_{\text{stat}} \pm 0.029_{\text{syst}}$ $1.18 \pm 0.05_{\text{stat}} \pm 0.03_{\text{syst}}$
BABAR D^{*0} [482]	$34.96 \pm 0.58_{\text{stat}} \pm 1.32_{\text{syst}}$ $35.9 \pm 0.6_{\text{stat}} \pm 1.4_{\text{syst}}$	$1.126 \pm 0.058_{\text{stat}} \pm 0.055_{\text{syst}}$ $1.16 \pm 0.06_{\text{stat}} \pm 0.08_{\text{syst}}$
BABAR global fit [481]	$35.49 \pm 0.20_{\text{stat}} \pm 1.09_{\text{syst}}$ $35.7 \pm 0.2_{\text{stat}} \pm 1.2_{\text{syst}}$	$1.185 \pm 0.020_{\text{stat}} \pm 0.061_{\text{syst}}$ $1.21 \pm 0.02_{\text{stat}} \pm 0.07_{\text{syst}}$
Average	$35.61 \pm 0.11_{\text{stat}} \pm 0.41_{\text{syst}}$	$1.205 \pm 0.015_{\text{stat}} \pm 0.021_{\text{syst}}$

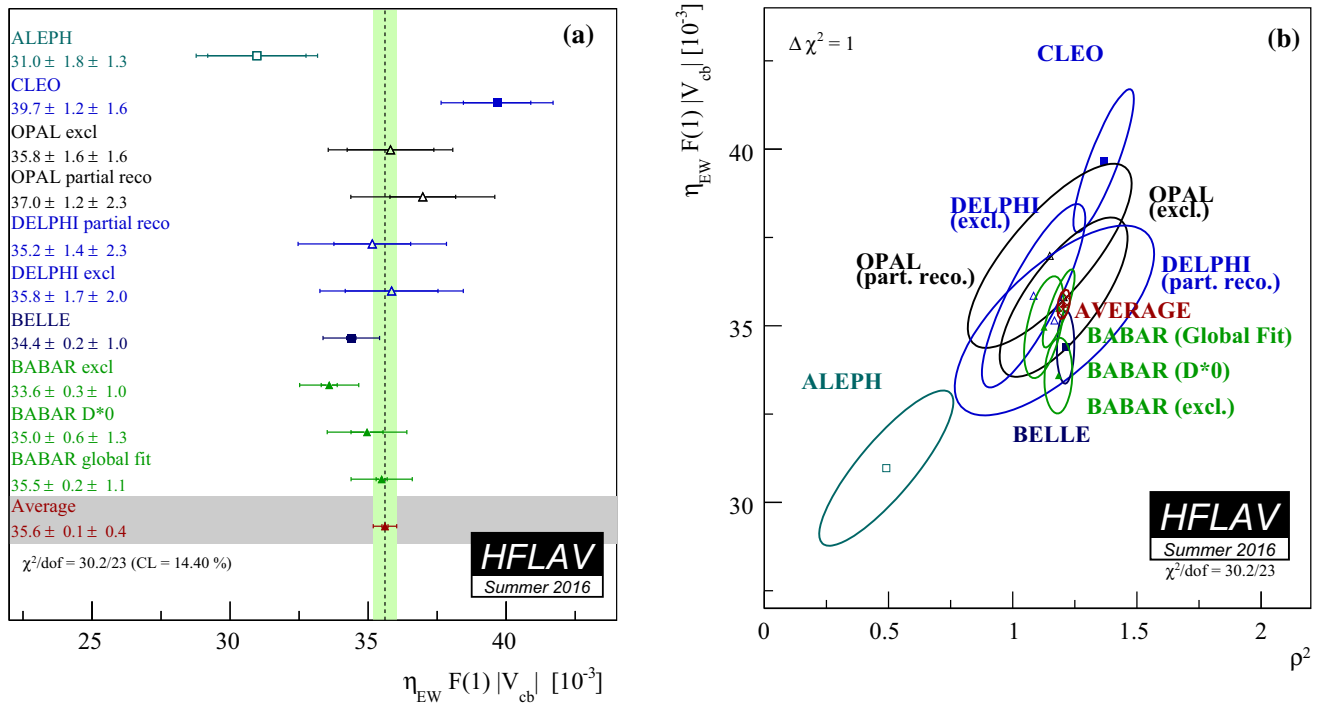


Fig. 49 Illustration of **a** the average and **b** the dependence of $\eta_{EW} \mathcal{F}(1) |V_{cb}|$ on ρ^2 . The error ellipses correspond to $\Delta\chi^2 = 1$ (CL = 39%)

Table 67 $\bar{B}^0 \rightarrow D^{*+} \ell^- \bar{\nu}_\ell$ branching fractions calculated from the rescaled CLN parameters in Table 66. For Ref. [482] the published value of $\mathcal{B}(B^- \rightarrow D^{*0} \ell^- \bar{\nu}_\ell)$ has been rescaled by the factor $\tau(B^0)/\tau(B^+)$ for comparison to the other measurements

Experiment	$\mathcal{B}(\bar{B}^0 \rightarrow D^{*+} \ell^- \bar{\nu}_\ell)$ [%] (calculated)	$\mathcal{B}(\bar{B}^0 \rightarrow D^{*+} \ell^- \bar{\nu}_\ell)$ [%] (published)
ALEPH [485]	$5.26 \pm 0.25_{\text{stat}} \pm 0.30_{\text{syst}}$	$5.53 \pm 0.26_{\text{stat}} \pm 0.52_{\text{syst}}$
CLEO [480]	$5.55 \pm 0.17_{\text{stat}} \pm 0.24_{\text{syst}}$	$6.09 \pm 0.19_{\text{stat}} \pm 0.40_{\text{syst}}$
OPAL excl [486]	$4.93 \pm 0.18_{\text{stat}} \pm 0.43_{\text{syst}}$	$5.11 \pm 0.19_{\text{stat}} \pm 0.49_{\text{syst}}$
OPAL partial reco [486]	$5.42 \pm 0.25_{\text{stat}} \pm 0.52_{\text{syst}}$	$5.92 \pm 0.27_{\text{stat}} \pm 0.68_{\text{syst}}$
DELPHI partial reco [487]	$4.85 \pm 0.13_{\text{stat}} \pm 0.72_{\text{syst}}$	$4.70 \pm 0.13_{\text{stat}}^{+0.36}_{-0.31 \text{ syst}}$
DELPHI excl [488]	$5.27 \pm 0.20_{\text{stat}} \pm 0.37_{\text{syst}}$	$5.90 \pm 0.22_{\text{stat}} \pm 0.50_{\text{syst}}$
Belle [483]	$4.51 \pm 0.03_{\text{stat}} \pm 0.26_{\text{syst}}$	$4.58 \pm 0.03_{\text{stat}} \pm 0.26_{\text{syst}}$
BABAR excl [484]	$4.45 \pm 0.04_{\text{stat}} \pm 0.26_{\text{syst}}$	$4.69 \pm 0.04_{\text{stat}} \pm 0.34_{\text{syst}}$
BABAR D^{*0} [482]	$4.90 \pm 0.07_{\text{stat}} \pm 0.34_{\text{syst}}$	$5.15 \pm 0.07_{\text{stat}} \pm 0.38_{\text{syst}}$
BABAR global fit [481]	$4.90 \pm 0.02_{\text{stat}} \pm 0.19_{\text{syst}}$	$5.00 \pm 0.02_{\text{stat}} \pm 0.19_{\text{syst}}$
Average	$4.88 \pm 0.01_{\text{stat}} \pm 0.10_{\text{syst}}$	$\chi^2/\text{dof} = 30.2/23$ (CL = 14.4%)

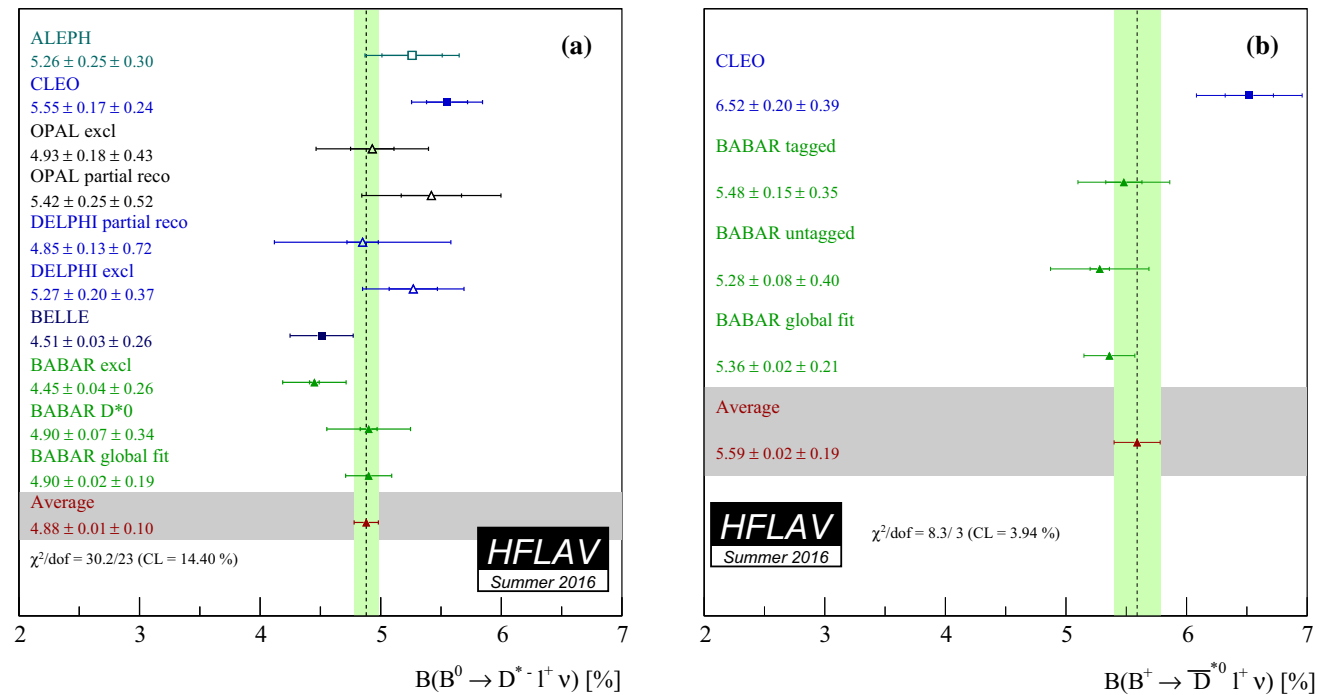


Fig. 50 Branching fractions of exclusive semileptonic B decays: **a** $\bar{B}^0 \rightarrow D^{*+} \ell^- \bar{\nu}_\ell$ (Table 67) and **b** $B^- \rightarrow D^{*0} \ell^- \bar{\nu}_\ell$ (Table 68)

tion only. The uncertainty has been increased to accommodate the Coulomb effect. Based on Eq. (172), this results in $|V_{cb}| = (39.05 \pm 0.47_{\text{exp}} \pm 0.58_{\text{th}}) \times 10^{-3}$, (183) where the first uncertainty is experimental and the second error is theoretical (lattice QCD calculation and electro-weak correction).

From each rescaled measurements in Table 66, we calculate the $\bar{B} \rightarrow D^{*} \ell^- \bar{\nu}_\ell$ form factor $\eta_{EW} \mathcal{F}(w)$ and, by numerical integration, the branching ratio of the decay

$\bar{B}^0 \rightarrow D^{*+} \ell^- \bar{\nu}_\ell$. For measurements that do not determine the parameters $R_1(1)$ and $R_2(1)$ we assume the average values given in Eqs. (174) and (175). The results are quoted in Table 67 and Fig. 50a. The branching ratio is

$$\mathcal{B}(\bar{B}^0 \rightarrow D^{*+} \ell^- \bar{\nu}_\ell) = (4.88 \pm 0.10)\% \tag{184}$$

We have also performed a one-dimensional average of measurements of the decay $B^- \rightarrow D^{*0} \ell^- \bar{\nu}_\ell$, which is shown in Table 68 and Fig. 50b. The result of this average, $(5.59 \pm 0.02 \pm 0.19)\%$, is consistent with the average including both

Table 68 Average of the $B^- \rightarrow D^{*0} \ell^- \bar{\nu}_\ell$ branching fraction measurements

Experiment	$\mathcal{B}(B^- \rightarrow D^{*0} \ell^- \bar{\nu}_\ell)$ [%] (rescaled)	$\mathcal{B}(B^- \rightarrow D^{*0} \ell^- \bar{\nu}_\ell)$ [%] (published)
CLEO [480]	$6.52 \pm 0.20_{\text{stat}} \pm 0.39_{\text{syst}}$	$6.50 \pm 0.20_{\text{stat}} \pm 0.43_{\text{syst}}$
BABARtagged [490]	$5.48 \pm 0.15_{\text{stat}} \pm 0.35_{\text{syst}}$	$5.83 \pm 0.15_{\text{stat}} \pm 0.30_{\text{syst}}$
BABAR [482]	$5.28 \pm 0.08_{\text{stat}} \pm 0.40_{\text{syst}}$	$5.56 \pm 0.08_{\text{stat}} \pm 0.41_{\text{syst}}$
BABAR [481]	$5.36 \pm 0.02_{\text{stat}} \pm 0.21_{\text{syst}}$	$5.40 \pm 0.02_{\text{stat}} \pm 0.21_{\text{syst}}$
Average	$5.59 \pm 0.02_{\text{stat}} \pm 0.19_{\text{syst}}$	$\chi^2/\text{dof} = 8.3/3$ (CL = 3.94%)

charge states given in Eq. (184) rescaled by the lifetime ratio $\tau(B^+)/\tau(B^0)$, $(5.26 \pm 0.11)\%$.

5.1.2 $\bar{B} \rightarrow D \ell^- \bar{\nu}_\ell$

The differential decay rate for massless fermions as a function of w (introduced in the previous section) is given by (see, e.g., [476])

$$\frac{\bar{B} \rightarrow D \ell^- \bar{\nu}_\ell}{dw} = \frac{G_F^2 m_D^3}{48\pi^3} (m_B + m_D)^2 (w^2 - 1)^{3/2} \times \eta_{\text{EW}}^2 \mathcal{G}^2(w) |V_{cb}|^2, \tag{185}$$

where G_F is Fermi’s constant, and m_B and m_D are the B and D meson masses. Again, η_{EW} is the electroweak correction introduced in the previous section. In contrast to $\bar{B} \rightarrow D^* \ell^- \bar{\nu}_\ell$, $\mathcal{G}(w)$ contains a single form-factor function $f_+(w)$,

$$\mathcal{G}^2(w) = \frac{4r}{(1+r)^2} f_+^2(w), \tag{186}$$

where $r = m_D/m_B$.

As for $\bar{B} \rightarrow D^* \ell^- \bar{\nu}_\ell$ decays, we adopt the prescription by Caprini, Lellouch and Neubert [478], which describes the shape and normalization of the measured decay distributions

in terms of two parameters: the normalization $\mathcal{G}(1)$ and the slope ρ^2 ,

$$\mathcal{G}(z) = \mathcal{G}(1) [1 - 8\rho^2 z + (51\rho^2 - 10)z^2 - (252\rho^2 - 84)z^3], \tag{187}$$

where $z = (\sqrt{w+1} - \sqrt{2})/(\sqrt{w+1} + \sqrt{2})$.

Table 69 shows experimental measurements of the two CLN parameters, which are corrected to match the latest values of the input parameters [479]. Both measurements of $\bar{B}^0 \rightarrow D^+ \ell^- \bar{\nu}_\ell$ and $B^- \rightarrow D^0 \ell^- \bar{\nu}_\ell$ are used and isospin symmetry is assumed in the analysis.

The form factor parameters are extracted by a two-parameter fit to the rescaled measurements of $\eta_{\text{EW}} \mathcal{G}(1) |V_{cb}|$ and ρ^2 taking into account correlated statistical and systematic uncertainties. The result of the fit is

$$\eta_{\text{EW}} \mathcal{G}(1) |V_{cb}| = (41.57 \pm 1.00) \times 10^{-3}, \tag{188}$$

$$\rho^2 = 1.128 \pm 0.033, \tag{189}$$

with a correlation of

$$\rho_{\eta_{\text{EW}} \mathcal{G}(1) |V_{cb}|, \rho^2} = 0.751. \tag{190}$$

The uncertainties and the correlation coefficient include both statistical and systematic contributions. The χ^2 of the fit is 4.7

Table 69 Measurements of the Caprini, Lellouch and Neubert (CLN) [478] form factor parameters in $\bar{B} \rightarrow D \ell^- \bar{\nu}_\ell$ before and after rescaling

Experiment	$\eta_{\text{EW}} \mathcal{G}(1) V_{cb} $ [10^{-3}] (rescaled)	ρ^2 (rescaled)
	$\eta_{\text{EW}} \mathcal{G}(1) V_{cb} $ [10^{-3}] (published)	ρ^2 (published)
ALEPH [485]	$36.67 \pm 10.05_{\text{stat}} \pm 7.33_{\text{syst}}$	$0.845 \pm 0.879_{\text{stat}} \pm 0.448_{\text{syst}}$
	$31.1 \pm 9.9_{\text{stat}} \pm 8.6_{\text{syst}}$	$0.70 \pm 0.98_{\text{stat}} \pm 0.50_{\text{syst}}$
CLEO [491]	$44.18 \pm 5.70_{\text{stat}} \pm 3.47_{\text{syst}}$	$1.270 \pm 0.215_{\text{stat}} \pm 0.121_{\text{syst}}$
	$44.8 \pm 6.1_{\text{stat}} \pm 3.7_{\text{syst}}$	$1.30 \pm 0.27_{\text{stat}} \pm 0.14_{\text{syst}}$
Belle [492]	$41.94 \pm 0.60_{\text{stat}} \pm 1.21_{\text{syst}}$	$1.090 \pm 0.036_{\text{stat}} \pm 0.019_{\text{syst}}$
	42.29 ± 1.37	1.09 ± 0.05
BABAR global fit [481]	$42.23 \pm 0.74_{\text{stat}} \pm 2.14_{\text{syst}}$	$1.186 \pm 0.035_{\text{stat}} \pm 0.062_{\text{syst}}$
	$43.1 \pm 0.8_{\text{stat}} \pm 2.3_{\text{syst}}$	$1.20 \pm 0.04_{\text{stat}} \pm 0.07_{\text{syst}}$
BABAR tagged [493]	$42.60 \pm 1.71_{\text{stat}} \pm 1.26_{\text{syst}}$	$1.200 \pm 0.088_{\text{stat}} \pm 0.043_{\text{syst}}$
	$42.3 \pm 1.9_{\text{stat}} \pm 1.0_{\text{syst}}$	$1.20 \pm 0.09_{\text{stat}} \pm 0.04_{\text{syst}}$
Average	$41.57 \pm 0.45_{\text{stat}} \pm 0.89_{\text{syst}}$	$1.128 \pm 0.024_{\text{stat}} \pm 0.023_{\text{syst}}$

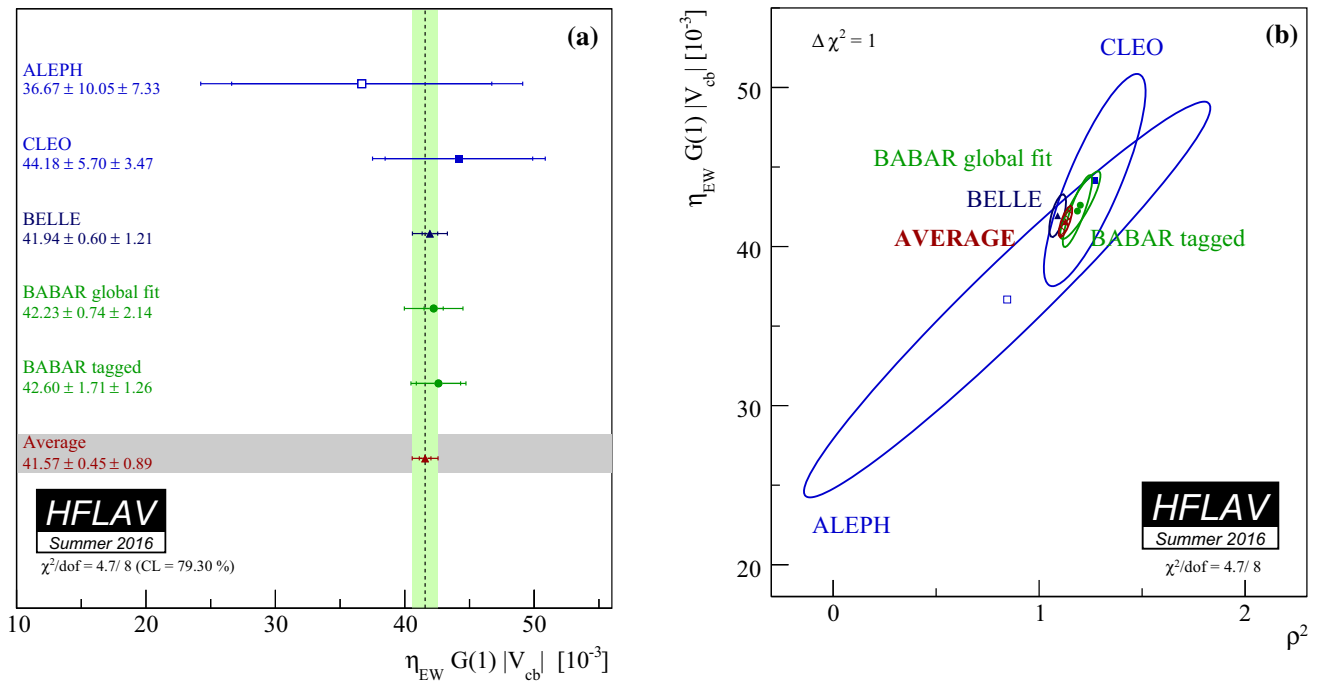


Fig. 51 Illustration of **a** the average and **b** dependence of $\eta_{EW} \mathcal{G}(w) |V_{cb}|$ on ρ^2 . The error ellipses correspond to $\Delta\chi^2 = 1$ (CL = 39%)

Table 70 $\bar{B}^0 \rightarrow D^+ \ell^- \bar{\nu}_\ell$ branching fractions calculated from the rescaled CLN parameters in Table 69, which are based on both charged and neutral B decays, combined under the assumption of isospin symmetry

Experiment	$\mathcal{B}(\bar{B}^0 \rightarrow D^+ \ell^- \bar{\nu}_\ell)$ [%] (calculated)	$\mathcal{B}(\bar{B}^0 \rightarrow D^+ \ell^- \bar{\nu}_\ell)$ [%] (published)
ALEPH [485]	$2.09 \pm 0.15_{\text{stat}} \pm 0.37_{\text{syst}}$	$2.35 \pm 0.20_{\text{stat}} \pm 0.44_{\text{syst}}$
CLEO [491]	$2.12 \pm 0.23_{\text{stat}} \pm 0.29_{\text{syst}}$	$2.20 \pm 0.16_{\text{stat}} \pm 0.19_{\text{syst}}$
Belle [492]	$2.24 \pm 0.03_{\text{stat}} \pm 0.11_{\text{syst}}$	$2.31 \pm 0.03_{\text{stat}} \pm 0.11_{\text{syst}}$
BABAR global fit [481]	$2.09 \pm 0.03_{\text{stat}} \pm 0.13_{\text{syst}}$	$2.34 \pm 0.03_{\text{stat}} \pm 0.13_{\text{syst}}$
BABAR tagged [493]	$2.10 \pm 0.07_{\text{stat}} \pm 0.08_{\text{syst}}$	$2.23 \pm 0.11_{\text{stat}} \pm 0.11_{\text{syst}}$
Average	$2.13 \pm 0.02_{\text{stat}} \pm 0.07_{\text{syst}}$	$\chi^2/\text{dof} = 4.7/8$ (CL = 79.3%)

for 8 degrees of freedom, which corresponds to a probability of 79.3%. An illustration of this fit result is given in Fig. 51.

The most recent lattice QCD result obtained for the form factor normalization is [494]

$$\mathcal{G}(1) = 1.0541 \pm 0.0083. \tag{191}$$

Using again $\eta_{EW} = 1.0066 \pm 0.0050$, we determine $|V_{cb}|$ from Eq. (188),

$$|V_{cb}| = (39.18 \pm 0.94_{\text{exp}} \pm 0.36_{\text{th}}) \times 10^{-3}, \tag{192}$$

where the first error is experimental and the second theoretical. This number is in excellent agreement with $|V_{cb}|$ obtained from $\bar{B} \rightarrow D^* \ell^- \bar{\nu}_\ell$ decays given in Eq. (183).

From each rescaled measurement in Table 69, we have calculated the $\bar{B} \rightarrow D \ell^- \bar{\nu}_\ell$ form factor $\mathcal{G}(w)$ and, by numerical integration, the branching ratio of the decay $\bar{B}^0 \rightarrow D^+ \ell^- \bar{\nu}_\ell$. The results are quoted in Table 70 and illustrated in Fig. 52.

The branching ratio for the average values of $\eta_{EW} \mathcal{G}(1) |V_{cb}|$ and ρ^2 is

$$\mathcal{B}(\bar{B}^0 \rightarrow D^+ \ell^- \bar{\nu}_\ell) = (2.13 \pm 0.07)\%. \tag{193}$$

We have also performed one-dimensional averages of measurements of $\bar{B}^0 \rightarrow D^+ \ell^- \bar{\nu}_\ell$ and $B^- \rightarrow D^0 \ell^- \bar{\nu}_\ell$ decays. The results are shown in Tables 71 and 72. The $\bar{B}^0 \rightarrow D^+ \ell^- \bar{\nu}_\ell$ average, $(2.20 \pm 0.04 \pm 0.09)\%$, is consistent with the result in Eq. (193), $(2.13 \pm 0.07)\%$. The $B^- \rightarrow D^0 \ell^- \bar{\nu}_\ell$ average, $(2.33 \pm 0.04 \pm 0.09)\%$, also compares well to the result in Eq. (193), rescaled by the lifetime ratio $\tau(B^-)/\tau(B^0)$, $(2.30 \pm 0.07)\%$.

5.1.3 $\bar{B} \rightarrow D^{(*)} \pi \ell^- \bar{\nu}_\ell$

The average inclusive branching fractions for $\bar{B} \rightarrow D^{(*)} \pi \ell^- \bar{\nu}_\ell$ decays, where no constraint is applied to the $D^{(*)} \pi$

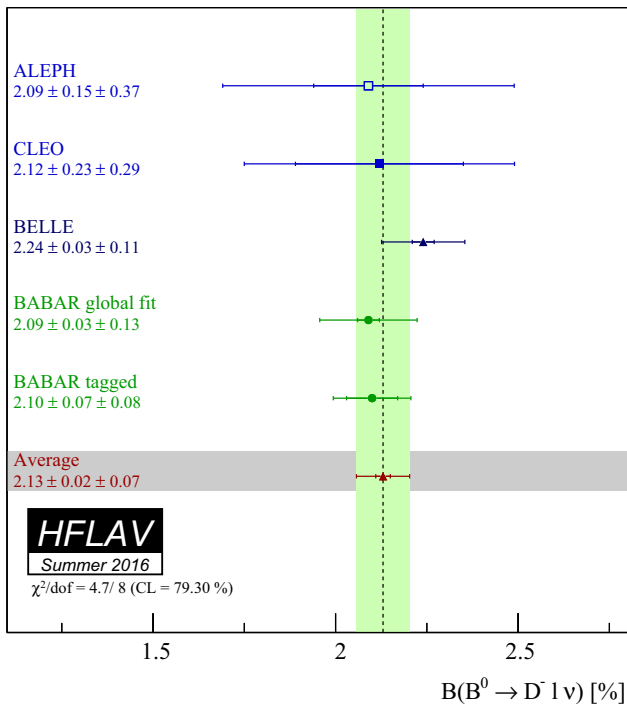


Fig. 52 Illustration of Table 70

system, are determined by the combination of the results provided in Table 73 for $\bar{B}^0 \rightarrow D^0 \pi^+ \ell^- \bar{\nu}_\ell$, $\bar{B}^0 \rightarrow D^{*0} \pi^+ \ell^- \bar{\nu}_\ell$, $B^- \rightarrow D^+ \pi^- \ell^- \bar{\nu}_\ell$, and $B^- \rightarrow D^{*+} \pi^- \ell^- \bar{\nu}_\ell$ decays. The measurements included in the average are scaled to a consistent set of input parameters and their uncertainties [479]. For both the BABAR and Belle results, the B semileptonic signal yields are extracted from a fit to the missing mass squared distribution for a sample of fully reconstructed $B\bar{B}$ events. Figure 53 shows the measurements and the resulting average for the four decay modes.

Table 71 Average of $\bar{B}^0 \rightarrow D^+ \ell^- \bar{\nu}_\ell$ branching fraction measurements

Experiment	$\mathcal{B}(\bar{B}^0 \rightarrow D^+ \ell^- \bar{\nu}_\ell)$ [%] (rescaled)	$\mathcal{B}(\bar{B}^0 \rightarrow D^+ \ell^- \bar{\nu}_\ell)$ [%] (published)
ALEPH [485]	$2.14 \pm 0.18_{\text{stat}} \pm 0.36_{\text{syst}}$	$2.35 \pm 0.20_{\text{stat}} \pm 0.44_{\text{syst}}$
CLEO [491]	$2.09 \pm 0.13_{\text{stat}} \pm 0.16_{\text{syst}}$	$2.20 \pm 0.16_{\text{stat}} \pm 0.19_{\text{syst}}$
Belle [492]	$2.30 \pm 0.04_{\text{stat}} \pm 0.12_{\text{syst}}$	$2.39 \pm 0.04_{\text{stat}} \pm 0.11_{\text{syst}}$
BABAR [490]	$2.08 \pm 0.11_{\text{stat}} \pm 0.14_{\text{syst}}$	$2.21 \pm 0.11_{\text{stat}} \pm 0.12_{\text{syst}}$
Average	$2.20 \pm 0.04_{\text{stat}} \pm 0.09_{\text{syst}}$	$\chi^2/\text{dof} = 1.7/3$ (CL = 63.9%)

Table 72 Average of $B^- \rightarrow D^0 \ell^- \bar{\nu}_\ell$ branching fraction measurements

Experiment	$\mathcal{B}(B^- \rightarrow D^0 \ell^- \bar{\nu}_\ell)$ [%] (rescaled)	$\mathcal{B}(B^- \rightarrow D^0 \ell^- \bar{\nu}_\ell)$ [%] (published)
CLEO [491]	$2.16 \pm 0.13_{\text{stat}} \pm 0.17_{\text{syst}}$	$2.32 \pm 0.17_{\text{stat}} \pm 0.20_{\text{syst}}$
BABAR [490]	$2.21 \pm 0.09_{\text{stat}} \pm 0.12_{\text{syst}}$	$2.33 \pm 0.09_{\text{stat}} \pm 0.09_{\text{syst}}$
Belle [492]	$2.48 \pm 0.04_{\text{stat}} \pm 0.12_{\text{syst}}$	$2.54 \pm 0.04_{\text{stat}} \pm 0.13_{\text{syst}}$
Average	$2.33 \pm 0.04_{\text{stat}} \pm 0.09_{\text{syst}}$	$\chi^2/\text{dof} = 2.8/2$ (CL = 25.2%)

5.1.4 $\bar{B} \rightarrow D^{**} \ell^- \bar{\nu}_\ell$

D^{**} mesons contain one charm quark and one light anti-quark with relative angular momentum $L = 1$. According to Heavy Quark Symmetry (HQS) [496], they form one doublet of states with angular momentum $j \equiv s_q + L = 3/2$ [$D_1(2420), D_2^*(2460)$] and another doublet with $j = 1/2$ [$D_0^*(2400), D_1'(2430)$], where s_q is the light quark spin. Parity and angular momentum conservation constrain the decays allowed for each state. The D_1 and D_2^* states decay via a D-wave to $D^* \pi$ and $D^{(*)} \pi$, respectively, and have small decay widths, while the D_0^* and D_1' states decay via an S-wave to $D \pi$ and $D^* \pi$ and are very broad. For the narrow states, the averages are determined by the combination of the results provided in Tables 74 and 75 for $\mathcal{B}(B^- \rightarrow D_1^0 \ell^- \bar{\nu}_\ell) \times \mathcal{B}(D_1^0 \rightarrow D^{*+} \pi^-)$ and $\mathcal{B}(B^- \rightarrow D_2^{*0} \ell^- \bar{\nu}_\ell) \times \mathcal{B}(D_2^{*0} \rightarrow D^{*+} \pi^-)$. For the broad states, the averages are determined by the combination of the results provided in Tables 76 and 77 for $\mathcal{B}(B^- \rightarrow D_1^{*0} \ell^- \bar{\nu}_\ell) \times \mathcal{B}(D_1^{*0} \rightarrow D^{*+} \pi^-)$ and $\mathcal{B}(B^- \rightarrow D_0^{*0} \ell^- \bar{\nu}_\ell) \times \mathcal{B}(D_0^{*0} \rightarrow D^+ \pi^-)$. The measurements are scaled to a consistent set of input parameters and their uncertainties [479].

For both the B-factory and the LEP and Tevatron results, the B semileptonic signal yields are extracted from a fit to the invariant mass distribution of the $D^{(*)+} \pi^-$ system. Apart for the CLEO, Belle and BABAR results, the other measurements are for the $\bar{B} \rightarrow D^{**} (D^{*+} \pi^-) X \ell^- \bar{\nu}_\ell$ final state and we assume that no particles are left in the X system. The BABAR tagged $\bar{B} \rightarrow D_2^{*0} \ell^- \bar{\nu}_\ell$ has been measured selecting $D_s^* \rightarrow D \pi$ final state and it has been translated in a result on $D_2^* \rightarrow D^* \pi$ decay mode, assuming $\mathcal{B}(D_2^* \rightarrow D \pi) / \mathcal{B}(D_2^* \rightarrow D^* \pi) = 1.54 \pm 0.15$ [327]. Figures 54 and 55 show the measurements and the resulting averages.

Table 73 Averages of the $B \rightarrow D^{(*)}\pi^-\ell^-\bar{\nu}_\ell$ branching fractions and individual results

Experiment	$\mathcal{B}(B^- \rightarrow D^+\pi^-\ell^-\bar{\nu}_\ell)[\%]$ (rescaled)	$\mathcal{B}(B^- \rightarrow D^+\pi^-\ell^-\bar{\nu}_\ell)[\%]$ (published)
Belle [495]	$0.42 \pm 0.04_{\text{stat}} \pm 0.05_{\text{syst}}$	$0.40 \pm 0.04_{\text{stat}} \pm 0.06_{\text{syst}}$
BABAR [490]	$0.40 \pm 0.06_{\text{stat}} \pm 0.03_{\text{syst}}$	$0.42 \pm 0.06_{\text{stat}} \pm 0.03_{\text{syst}}$
Average	0.41 ± 0.04	$\chi^2/\text{dof} = 0.073$ (CL = 78.9%)
Experiment	$\mathcal{B}(B^- \rightarrow D^{*+}\pi^-\ell^-\bar{\nu}_\ell)[\%]$ (rescaled)	$\mathcal{B}(B^- \rightarrow D^{*+}\pi^-\ell^-\bar{\nu}_\ell)[\%]$ (published)
Belle [495]	$0.68 \pm 0.08_{\text{stat}} \pm 0.07_{\text{syst}}$	$0.64 \pm 0.08_{\text{stat}} \pm 0.09_{\text{syst}}$
BABAR [490]	$0.57 \pm 0.05_{\text{stat}} \pm 0.04_{\text{syst}}$	$0.59 \pm 0.05_{\text{stat}} \pm 0.04_{\text{syst}}$
Average	0.60 ± 0.06	$\chi^2/\text{dof} = 0.778$ (CL = 37.9%)
Experiment	$\mathcal{B}(\bar{B}^0 \rightarrow D^0\pi^+\ell^-\bar{\nu}_\ell)[\%]$ (rescaled)	$\mathcal{B}(\bar{B}^0 \rightarrow D^0\pi^+\ell^-\bar{\nu}_\ell)[\%]$ (published)
Belle [495]	$0.43 \pm 0.07_{\text{stat}} \pm 0.05_{\text{syst}}$	$0.42 \pm 0.07_{\text{stat}} \pm 0.06_{\text{syst}}$
BABAR [490]	$0.40 \pm 0.08_{\text{stat}} \pm 0.03_{\text{syst}}$	$0.43 \pm 0.08_{\text{stat}} \pm 0.03_{\text{syst}}$
Average	0.42 ± 0.06	$\chi^2/\text{dof} = 0.061$ (CL = 80.5%)
Experiment	$\mathcal{B}(\bar{B}^0 \rightarrow D^{*0}\pi^+\ell^-\bar{\nu}_\ell)[\%]$ (rescaled)	$\mathcal{B}(\bar{B}^0 \rightarrow D^{*0}\pi^+\ell^-\bar{\nu}_\ell)[\%]$ (published)
Belle [495]	$0.58 \pm 0.21_{\text{stat}} \pm 0.07_{\text{syst}}$	$0.56 \pm 0.21_{\text{stat}} \pm 0.08_{\text{syst}}$
BABAR [490]	$0.46 \pm 0.08_{\text{stat}} \pm 0.04_{\text{syst}}$	$0.48 \pm 0.08_{\text{stat}} \pm 0.04_{\text{syst}}$
Average	0.47 ± 0.08	$\chi^2/\text{dof} = 0.262$ (CL = 60.9%)

5.2 Inclusive CKM-favored decays

5.2.1 Global analysis of $\bar{B} \rightarrow X_c\ell^-\bar{\nu}_\ell$

The semileptonic decay width $\Gamma(\bar{B} \rightarrow X_c\ell^-\bar{\nu}_\ell)$ has been calculated in the framework of the operator production expansion (OPE) [55–57]. The result is a double-expansion in Λ_{QCD}/m_b and α_s , which depends on a number of non-perturbative parameters. These parameters describe the dynamics of the b -quark inside the B hadron and can be measured using observables in $\bar{B} \rightarrow X_c\ell^-\bar{\nu}_\ell$ decays, such as the moments of the lepton energy and the hadronic mass spectrum.

Two renormalization schemes are commonly used to define the b -quark mass and other theoretical quantities: the kinetic [504–507] and the 1S [508] schemes. An independent set of theoretical expressions is available for each, with several non-perturbative parameters. The non-perturbative parameters in the kinetic scheme are: the quark masses m_b and m_c , μ_π^2 and μ_G^2 at $O(1/m_b^2)$, and ρ_D^3 and ρ_{LS}^3 at $O(1/m_b^3)$. In the 1S scheme, the parameters are: m_b , λ_1 at $O(1/m_b^2)$, and ρ_1 , τ_1 , τ_2 and τ_3 at $O(1/m_b^3)$. Note that the numerical values of the kinetic and 1S b -quark masses cannot be compared without converting one or the other, or both, to the same renormalization scheme.

We used two kinematic distributions for $\bar{B} \rightarrow X_c\ell^-\bar{\nu}_\ell$ decays, the hadron effective mass to derive moments $\langle M_X^n \rangle$ of order $n = 2, 4, 6$, and the charged lepton momentum to derive moments $\langle E_\ell^n \rangle$ of order $n = 0, 1, 2, 3$. Moments are determined for different values of E_{cut} , the lower limit on the minimum lepton momentum. The moments derived

from the same distributions with different value of E_{cut} are highly correlated. The list of measurements is given in Table 78. The only input is the average lifetime τ_B of neutral and charged B mesons, taken to be (1.579 ± 0.004) ps (Sect. 3).

In the kinetic and 1S schemes, the moments in $\bar{B} \rightarrow X_c\ell^-\bar{\nu}_\ell$ are not sufficient to determine the b -quark mass precisely. In the kinetic scheme analysis we constrain the c -quark mass (defined in the $\overline{\text{MS}}$ scheme) to the value of Ref. [515],

$$m_c^{\overline{\text{MS}}}(3 \text{ GeV}) = 0.986 \pm 0.013 \text{ GeV}. \tag{194}$$

In the 1S scheme analysis, the b -quark mass is constrained by measurements of the photon energy moments in $B \rightarrow X_s\gamma$ [516–519].

5.2.2 Analysis in the kinetic scheme

The fit relies on the calculations of the lepton energy and hadron mass moments in $\bar{B} \rightarrow X_c\ell^-\bar{\nu}_\ell$ decays described in Refs. [506,507] and closely follows the procedure of Ref. [520]. The analysis determines $|V_{cb}|$ and the six non-perturbative parameters mentioned above.

The detailed fit result and the matrix of the correlation coefficients is given in Table 79. The fit to the lepton energy and hadronic mass moments is shown in Figs. 56 and 57, respectively. The result in terms of the main parameters is

$$|V_{cb}| = (42.19 \pm 0.78) \times 10^{-3}, \tag{195}$$

$$m_b^{\text{kin}} = 4.554 \pm 0.018 \text{ GeV}, \tag{196}$$

$$\mu_\pi^2 = 0.464 \pm 0.076 \text{ GeV}^2, \tag{197}$$

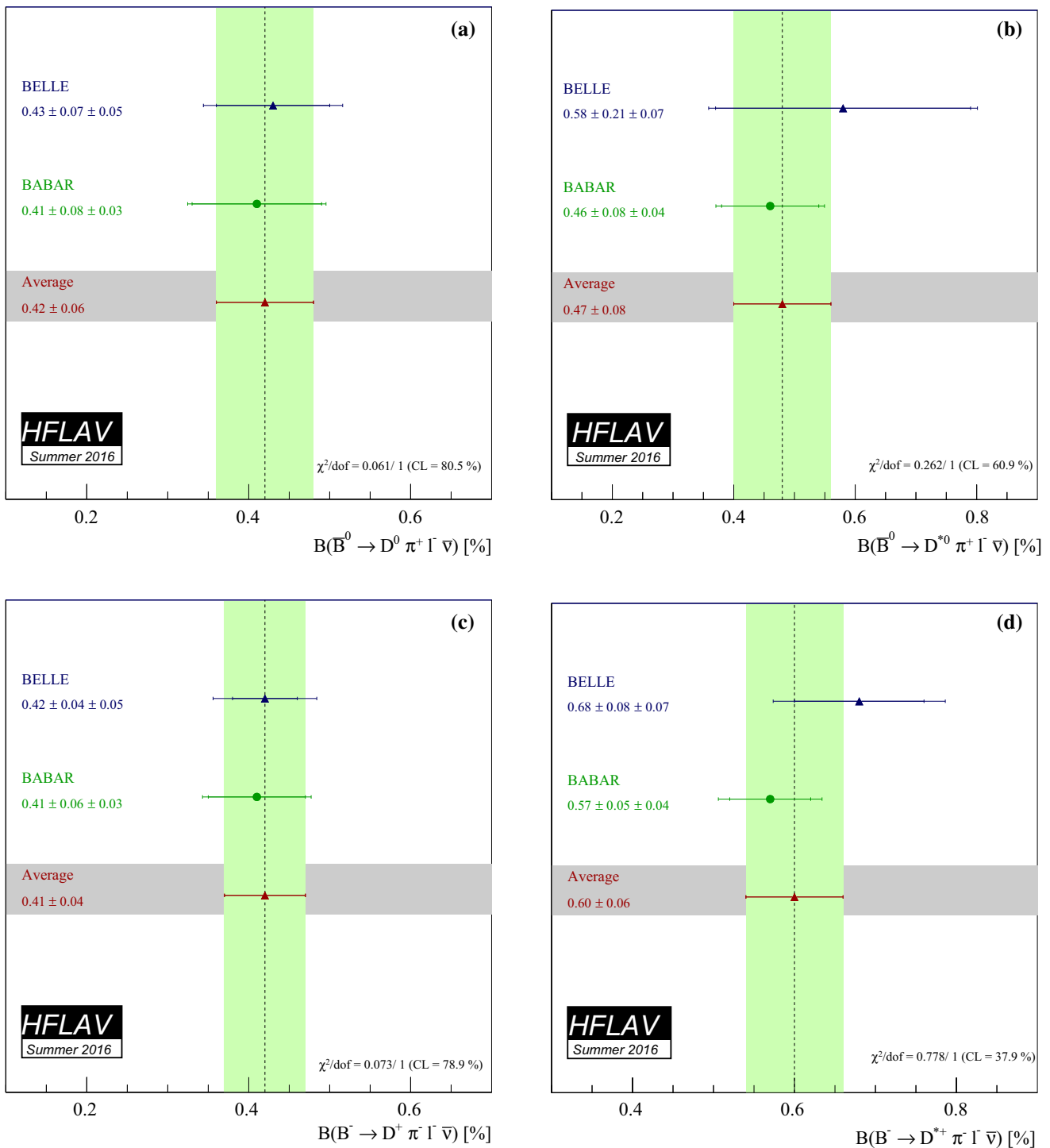


Fig. 53 Average branching fraction of exclusive semileptonic B decays **a** $\bar{B}^0 \rightarrow D^0 \pi^+ \ell^- \bar{\nu}_\ell$, **b** $\bar{B}^0 \rightarrow D^{*0} \pi^+ \ell^- \bar{\nu}_\ell$, **c** $B^- \rightarrow D^+ \pi^- \ell^- \bar{\nu}_\ell$, and **d** $B^- \rightarrow D^{*+} \pi^- \ell^- \bar{\nu}_\ell$. The corresponding individual results are also shown

with a χ^2 of 15.6 for 43 degrees of freedom. The scale μ of the quantities in the kinematic scheme is 1 GeV.

The inclusive $\bar{B} \rightarrow X_c \ell^- \bar{\nu}_\ell$ branching fraction determined by this analysis is

$$\mathcal{B}(\bar{B} \rightarrow X_c \ell^- \bar{\nu}_\ell) = (10.65 \pm 0.16)\%. \quad (198)$$

Including the rate of charmless semileptonic decays (Sect. 5.4), $\mathcal{B}(\bar{B} \rightarrow X_u \ell^- \bar{\nu}_\ell) = (2.13 \pm 0.31) \times 10^{-3}$, we obtain the semileptonic branching fraction,

$$\mathcal{B}(\bar{B} \rightarrow X \ell^- \bar{\nu}_\ell) = (10.86 \pm 0.16)\%. \quad (199)$$

Table 74 Published and rescaled individual measurements and their averages for of the branching fraction $\mathcal{B}(B^- \rightarrow D_1^0 \ell^- \bar{\nu}_\ell) \times \mathcal{B}(D_1^0 \rightarrow D^{*+} \pi^-)$

Experiment	$\mathcal{B}(B^- \rightarrow D_1^0(D^{*+} \pi^-) \ell^- \bar{\nu}_\ell)[\%]$ (rescaled)	$\mathcal{B}(B^- \rightarrow D_1^0(D^{*+} \pi^-) \ell^- \bar{\nu}_\ell)[\%]$ (published)
ALEPH [497]	$0.437 \pm 0.085_{\text{stat}} \pm 0.056_{\text{syst}}$	$0.47 \pm 0.10_{\text{stat}} \pm 0.07_{\text{syst}}$
OPAL [498]	$0.570 \pm 0.210_{\text{stat}} \pm 0.101_{\text{syst}}$	$0.70 \pm 0.21_{\text{stat}} \pm 0.10_{\text{syst}}$
CLEO [499]	$0.347 \pm 0.085_{\text{stat}} \pm 0.056_{\text{syst}}$	$0.373 \pm 0.085_{\text{stat}} \pm 0.057_{\text{syst}}$
D0 [500]	$0.214 \pm 0.018_{\text{stat}} \pm 0.035_{\text{syst}}$	$0.219 \pm 0.018_{\text{stat}} \pm 0.035_{\text{syst}}$
Belle Tagged B^- [495]	$0.443 \pm 0.070_{\text{stat}} \pm 0.059_{\text{syst}}$	$0.42 \pm 0.07_{\text{stat}} \pm 0.07_{\text{syst}}$
Belle Tagged B^0 [495]	$0.612 \pm 0.200_{\text{stat}} \pm 0.077_{\text{syst}}$	$0.42 \pm 0.07_{\text{stat}} \pm 0.07_{\text{syst}}$
BABAR Tagged [501]	$0.274 \pm 0.030_{\text{stat}} \pm 0.029_{\text{syst}}$	$0.29 \pm 0.03_{\text{stat}} \pm 0.03_{\text{syst}}$
BABAR Untagged B^- [502]	$0.290 \pm 0.017_{\text{stat}} \pm 0.016_{\text{syst}}$	$0.30 \pm 0.02_{\text{stat}} \pm 0.02_{\text{syst}}$
BABAR Untagged B^0 [502]	$0.294 \pm 0.026_{\text{stat}} \pm 0.027_{\text{syst}}$	$0.30 \pm 0.02_{\text{stat}} \pm 0.02_{\text{syst}}$
Average	$0.281 \pm 0.010 \pm 0.015$	$\chi^2/\text{dof} = 12.7/8$ (CL = 11.7%)

Table 75 Published and rescaled individual measurements and their averages for $\mathcal{B}(B^- \rightarrow D_2^0 \ell^- \bar{\nu}_\ell) \times \mathcal{B}(D_2^0 \rightarrow D^{*+} \pi^-)$

Experiment	$\mathcal{B}(B^- \rightarrow D_2^0(D^{*+} \pi^-) \ell^- \bar{\nu}_\ell)[\%]$ (rescaled)	$\mathcal{B}(B^- \rightarrow D_2^0(D^{*+} \pi^-) \ell^- \bar{\nu}_\ell)[\%]$ (published)
CLEO [499]	$0.055 \pm 0.066_{\text{stat}} \pm 0.011_{\text{syst}}$	$0.059 \pm 0.066_{\text{stat}} \pm 0.011_{\text{syst}}$
D0 [500]	$0.086 \pm 0.018_{\text{stat}} \pm 0.020_{\text{syst}}$	$0.088 \pm 0.018_{\text{stat}} \pm 0.020_{\text{syst}}$
Belle [495]	$0.190 \pm 0.060_{\text{stat}} \pm 0.025_{\text{syst}}$	$0.18 \pm 0.06_{\text{stat}} \pm 0.03_{\text{syst}}$
BABAR tagged [501]	$0.075 \pm 0.013_{\text{stat}} \pm 0.009_{\text{syst}}$	$0.078 \pm 0.013_{\text{stat}} \pm 0.010_{\text{syst}}$
BABAR untagged B^- [502]	$0.087 \pm 0.009_{\text{stat}} \pm 0.007_{\text{syst}}$	$0.087 \pm 0.013_{\text{stat}} \pm 0.007_{\text{syst}}$
BABAR untagged B^0 [502]	$0.065 \pm 0.010_{\text{stat}} \pm 0.004_{\text{syst}}$	$0.087 \pm 0.013_{\text{stat}} \pm 0.007_{\text{syst}}$
Average	$0.077 \pm 0.006 \pm 0.004$	$\chi^2/\text{dof} = 5.3/5$ (CL = 37.7%)

Table 76 Published and rescaled individual measurements and their averages for $\mathcal{B}(B^- \rightarrow D_1^{\prime 0} \ell^- \bar{\nu}_\ell) \times \mathcal{B}(D_1^{\prime 0} \rightarrow D^{*+} \pi^-)$

Experiment	$\mathcal{B}(B^- \rightarrow D_1^{\prime 0}(D^{*+} \pi^-) \ell^- \bar{\nu}_\ell)[\%]$ (rescaled)	$\mathcal{B}(B^- \rightarrow D_1^{\prime 0}(D^{*+} \pi^-) \ell^- \bar{\nu}_\ell)[\%]$ (published)
DELPHI [503]	$0.71 \pm 0.17_{\text{stat}} \pm 0.18_{\text{syst}}$	$0.83 \pm 0.17_{\text{stat}} \pm 0.18_{\text{syst}}$
Belle [495]	$-0.03 \pm 0.06_{\text{stat}} \pm 0.07_{\text{syst}}$	$-0.03 \pm 0.06_{\text{stat}} \pm 0.07_{\text{syst}}$
BABAR [501]	$0.26 \pm 0.04_{\text{stat}} \pm 0.04_{\text{syst}}$	$0.27 \pm 0.04_{\text{stat}} \pm 0.05_{\text{syst}}$
Average	$0.13 \pm 0.03 \pm 0.02$	$\chi^2/\text{dof} = 18./2$ (CL = 0.0001%)

Table 77 Published and rescaled individual measurements and their averages for $\mathcal{B}(B^- \rightarrow D_0^{*0} \ell^- \bar{\nu}_\ell) \times \mathcal{B}(D_0^{*0} \rightarrow D^+ \pi^-)$

Experiment	$\mathcal{B}(B^- \rightarrow D_0^{*0}(D^+ \pi^-) \ell^- \bar{\nu}_\ell)[\%]$ (rescaled)	$\mathcal{B}(B^- \rightarrow D_0^{*0}(D^+ \pi^-) \ell^- \bar{\nu}_\ell)[\%]$ (published)
Belle Tagged B^- [495]	$0.25 \pm 0.04_{\text{stat}} \pm 0.06_{\text{syst}}$	$0.24 \pm 0.04_{\text{stat}} \pm 0.06_{\text{syst}}$
Belle Tagged B^0 [495]	$0.23 \pm 0.08_{\text{stat}} \pm 0.06_{\text{syst}}$	$0.24 \pm 0.04_{\text{stat}} \pm 0.06_{\text{syst}}$
BABAR Tagged [501]	$0.31 \pm 0.04_{\text{stat}} \pm 0.05_{\text{syst}}$	$0.26 \pm 0.05_{\text{stat}} \pm 0.04_{\text{syst}}$
Average	$0.28 \pm 0.03 \pm 0.04$	$\chi^2/\text{dof} = 0.49/2$ (CL = 78.0%)

5.2.3 Analysis in the 1S scheme

The fit relies on the same set of moment measurements and the calculations of the spectral moments described in Ref. [508]. The theoretical uncertainties are estimated as explained in Ref. [521]. Only trivial theory correlations, i.e. between the same moment at the same threshold are included in the analysis. The fit determines $|V_{cb}|$ and the six non-perturbative parameters mentioned above.

The detailed result of the fit using the $B \rightarrow X_S \gamma$ constraint is given in Table 80. The result in terms of the main parameters is

$$|V_{cb}| = (41.98 \pm 0.45) \times 10^{-3}, \tag{200}$$

$$m_b^{1S} = 4.691 \pm 0.037 \text{ GeV}, \tag{201}$$

$$\lambda_1 = -0.362 \pm 0.067 \text{ GeV}^2, \tag{202}$$

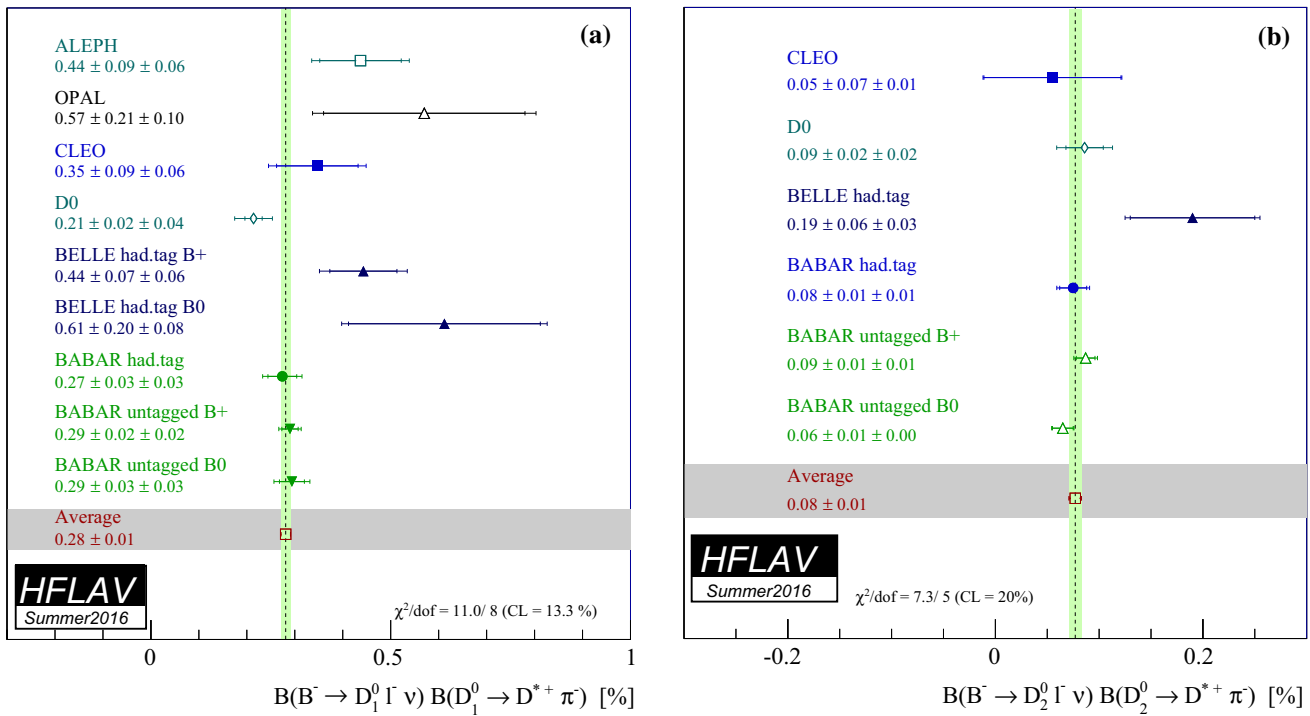


Fig. 54 Rescaled individual measurements and their averages for **a** $\mathcal{B}(B^- \rightarrow D_1^0 \ell^- \bar{\nu}_\ell) \times \mathcal{B}(D_1^0 \rightarrow D^{*+} \pi^-)$ and **b** $\mathcal{B}(B^- \rightarrow D_2^0 \ell^- \bar{\nu}_\ell) \times \mathcal{B}(D_2^0 \rightarrow D^{*+} \pi^-)$

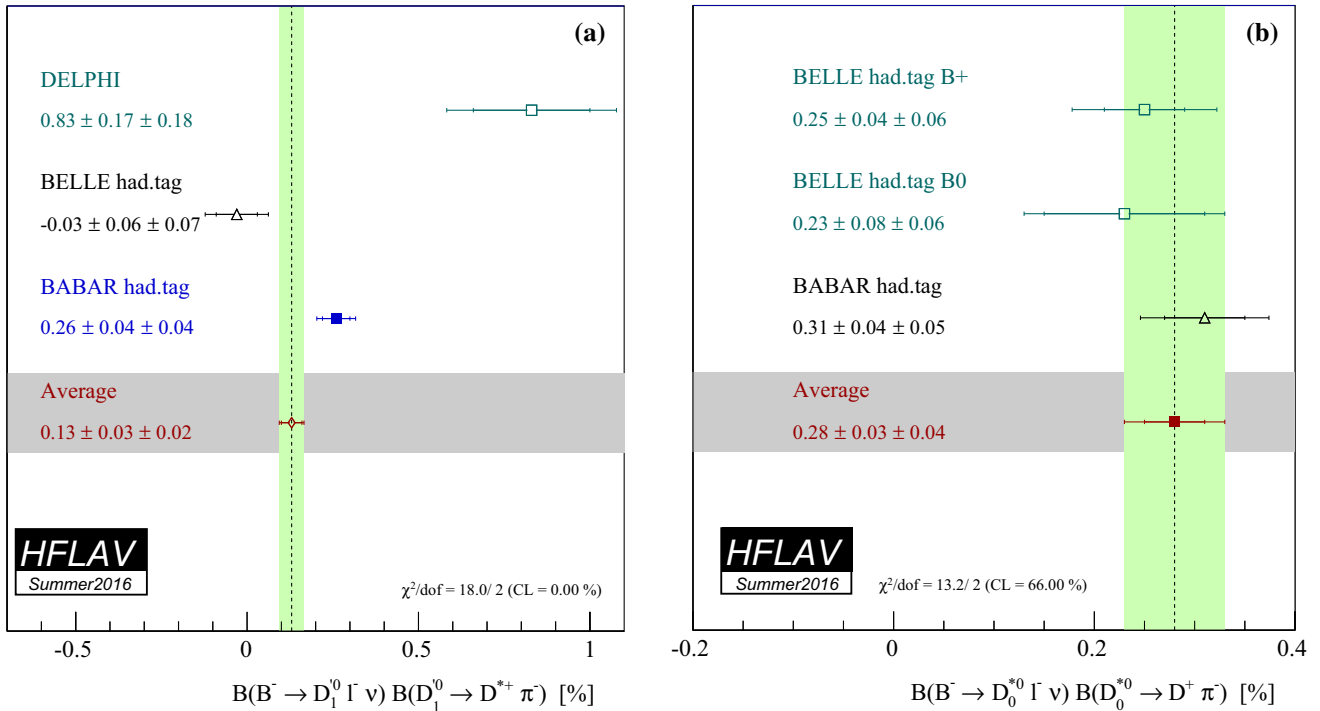


Fig. 55 Rescaled individual measurements and their averages for **a** $\mathcal{B}(B^- \rightarrow D_1^{*0} \ell^- \bar{\nu}_\ell) \times \mathcal{B}(D_1^{*0} \rightarrow D^{*+} \pi^-)$ and **b** $\mathcal{B}(B^- \rightarrow D_0^{*0} \ell^- \bar{\nu}_\ell) \times \mathcal{B}(D_0^{*0} \rightarrow D^+ \pi^-)$

with a χ^2 of 23.0 for 59 degrees of freedom. We find a good agreement in the central values of $|V_{cb}|$ between the kinetic and 1S scheme analyses. No conclusion should, however,

been drawn regarding the uncertainties in $|V_{cb}|$ as the two approaches are not equivalent in the number of higher-order corrections included.

Table 78 Experimental inputs used in the global analysis of $\bar{B} \rightarrow X_c \ell^- \bar{\nu}_\ell$. n is the order of the moment, c is the threshold value of the lepton momentum in GeV. In total, there are 23 measurements from BABAR, 15 measurements from Belle and 12 from other experiments

Experiment	Hadron moments (M_X^n)	Lepton moments (E_ℓ^n)
BABAR	$n = 2, c = 0.9, 1.1, 1.3, 1.5$ $n = 4, c = 0.8, 1.0, 1.2, 1.4$ $n = 6, c = 0.9, 1.3$ [509]	$n = 0, c = 0.6, 1.2, 1.5$ $n = 1, c = 0.6, 0.8, 1.0, 1.2, 1.5$ $n = 2, c = 0.6, 1.0, 1.5$ $n = 3, c = 0.8, 1.2$ [509,510]
Belle	$n = 2, c = 0.7, 1.1, 1.3, 1.5$ $n = 4, c = 0.7, 0.9, 1.3$ [511]	$n = 0, c = 0.6, 1.4$ $n = 1, c = 1.0, 1.4$ $n = 2, c = 0.6, 1.4$ $n = 3, c = 0.8, 1.2$ [512]
CDF	$n = 2, c = 0.7$ $n = 4, c = 0.7$ [513]	
CLEO	$n = 2, c = 1.0, 1.5$ $n = 4, c = 1.0, 1.5$ [514]	
DELPHI	$n = 2, c = 0.0$ $n = 4, c = 0.0$ $n = 6, c = 0.0$ [503]	$n = 1, c = 0.0$ $n = 2, c = 0.0$ $n = 3, c = 0.0$ [503]

Table 79 Fit result in the kinetic scheme, using a precise c -quark mass constraint. The error matrix of the fit contains experimental and theoretical contributions. In the lower part of the table, the correlation matrix of the parameters is given. The scale μ of the quantities in the kinematic scheme is 1 GeV

	$ V_{cb} (10^{-3})$	$m_b^{\text{kin}} (\text{GeV})$	$m_c^{\overline{\text{MS}}} (\text{GeV})$	$\mu_\pi^2 (\text{GeV}^2)$	$\rho_D^3 (\text{GeV}^3)$	$\mu_G^2 (\text{GeV}^2)$	$\rho_{LS}^3 (\text{GeV}^3)$
Value	42.19	4.554	0.987	0.464	0.169	0.333	-0.153
Error	0.78	0.018	0.015	0.076	0.043	0.053	0.096
$ V_{cb} $	1.000	-0.257	-0.078	0.354	0.289	-0.080	-0.051
m_b^{kin}		1.000	0.769	-0.054	0.097	0.360	-0.087
$m_c^{\overline{\text{MS}}}$			1.000	-0.021	0.027	0.059	-0.013
μ_π^2				1.000	0.732	0.012	0.020
ρ_D^3					1.000	-0.173	-0.123
μ_G^2						1.000	0.066
ρ_{LS}^3							1.000

5.3 Exclusive CKM-suppressed decays

In this section, we give results on exclusive charmless semileptonic branching fractions and the determination of $|V_{ub}|$ based on $B \rightarrow \pi l \nu$ decays. The measurements are based on two different event selections: tagged events, in which the second B meson in the event is fully (or partially) reconstructed, and untagged events, for which the momentum of the undetected neutrino is inferred from measurements of the total momentum sum of the detected particles and the knowledge of the initial state. The LHCb experiment recently reported a direct measurement of $|V_{ub}|/|V_{cb}|$ [522] reconstructing the $\Lambda_b^0 \rightarrow p \mu \nu$ decays and normalizing the branching fraction to the $\Lambda_b^0 \rightarrow \Lambda_c^+ (\rightarrow p K \pi) \mu \nu$ decays. We show a combination of $|V_{ub}| - |V_{cb}|$ using the LHCb constraint on $|V_{ub}|/|V_{cb}|$, the exclusive determination

of $|V_{ub}|$ from $B \rightarrow \pi l \nu$ and $|V_{cb}|$ from both $B \rightarrow D^* l \nu$ and $B \rightarrow D l \nu$. We also present branching fraction averages for $B^0 \rightarrow \rho \ell^+ \nu$, $B^+ \rightarrow \omega \ell^+ \nu$, $B^+ \rightarrow \eta \ell^+ \nu$ and $B^+ \rightarrow \eta' \ell^+ \nu$.

5.3.1 $B \rightarrow \pi l \nu$ branching fraction and q^2 spectrum

Currently, the four most precise measurements of the differential $B \rightarrow \pi l \nu$ decay rate as a function of the four-momentum transfer squared, q^2 , from BABAR and Belle [523–526] are used to obtain an average q^2 spectrum and an average for the total branching fraction. The measurements are presented in Fig. 58. From the two untagged BABAR analyses [525, 526], the combined results for $B^0 \rightarrow \pi^- \ell^+ \nu$ and $B^+ \rightarrow \pi^0 \ell^+ \nu$ decays based on isospin symmetry are used. The hadronic-tag analysis

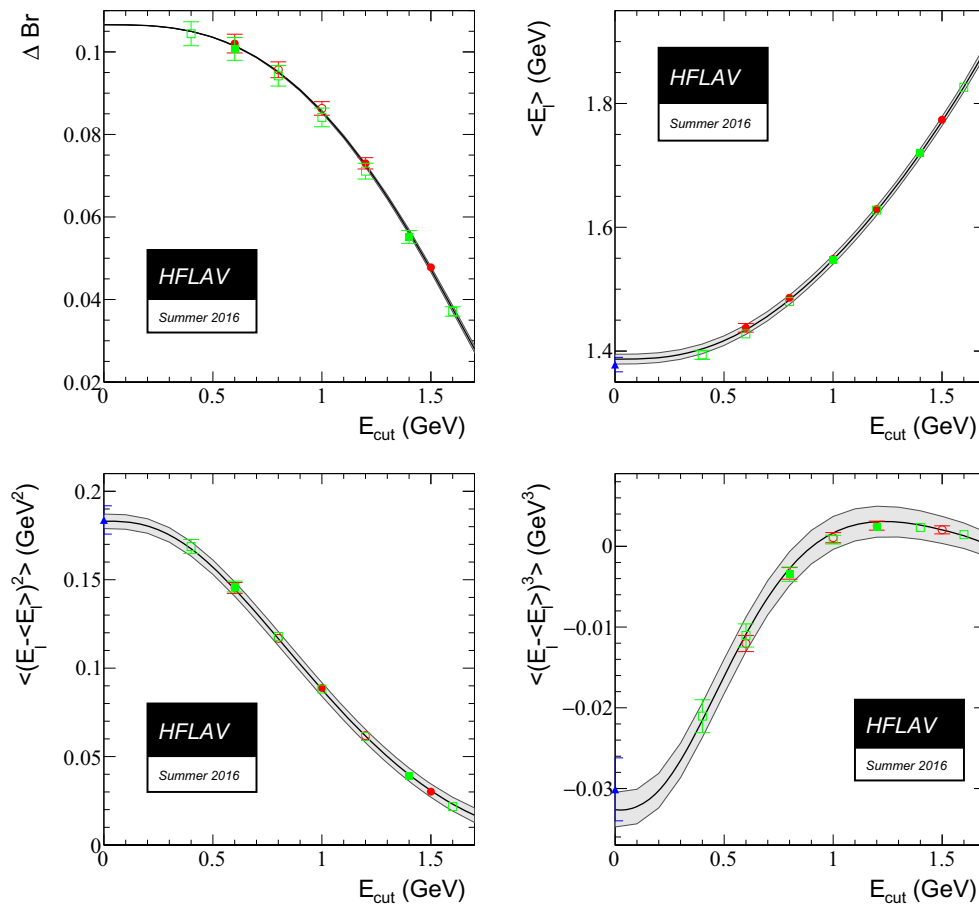


Fig. 56 Fit to the inclusive partial semileptonic branching ratios and to the lepton energy moments in the kinetic mass scheme. In all plots, the grey band is the theory prediction with total theory error. BABAR data

are shown by circles, Belle by squares and other experiments (DELPHI, CDF, CLEO) by triangles. Filled symbols mean that the point was used in the fit. Open symbols are measurements that were not used in the fit

by Belle [524] provides results for $B^0 \rightarrow \pi^- \ell^+ \nu$ and $B^+ \rightarrow \pi^0 \ell^+ \nu$ separately, but not for the combination of both channels. In the untagged analysis by Belle [523], only $B^0 \rightarrow \pi^- \ell^+ \nu$ decays were measured. The experimental measurements use different binnings in q^2 , but have matching bin edges, which allows them to be easily combined.

To arrive at an average q^2 spectrum, a binned maximum-likelihood fit to determine the average partial branching fraction in each q^2 interval is performed differentiating between common and individual uncertainties and correlations for the various measurements. Shared sources of systematic uncertainty of all measurements are included in the likelihood as nuisance parameters constrained using standard normal distributions. The most important shared sources of uncertainty are due to continuum subtraction, branching fractions, the number of B -meson pairs (only correlated among measurement by the same experiment), tracking efficiency (only correlated among measurements by the same experiment), uncertainties from modelling the $b \rightarrow u \ell \bar{\nu}_\ell$ contamination,

modelling of final state radiation, and contamination from $b \rightarrow c \ell \bar{\nu}_\ell$ decays.

The averaged q^2 spectrum is shown in Fig. 58. The probability of the average is computed as the χ^2 probability quantifying the agreement between the input spectra and the averaged spectrum and amounts to 6%. The partial branching fractions and the full covariance matrix obtained from the likelihood fit are given in Tables 81 and 82. The average for the total $B^0 \rightarrow \pi^- \ell^+ \nu_\ell$ branching fraction is obtained by summing up the partial branching fractions:

$$\mathcal{B}(B^0 \rightarrow \pi^- \ell^+ \nu_\ell) = (1.50 \pm 0.02_{\text{stat}} \pm 0.06_{\text{sys}}) \times 10^{-4}. \tag{203}$$

5.3.2 $|V_{ub}|$ from $B \rightarrow \pi l \nu$

The $|V_{ub}|$ average can be determined from the averaged q^2 spectrum in combination with a prediction for the normalization of the $B \rightarrow \pi$ form factor. The differential decay rate for light leptons (e, μ) is given by

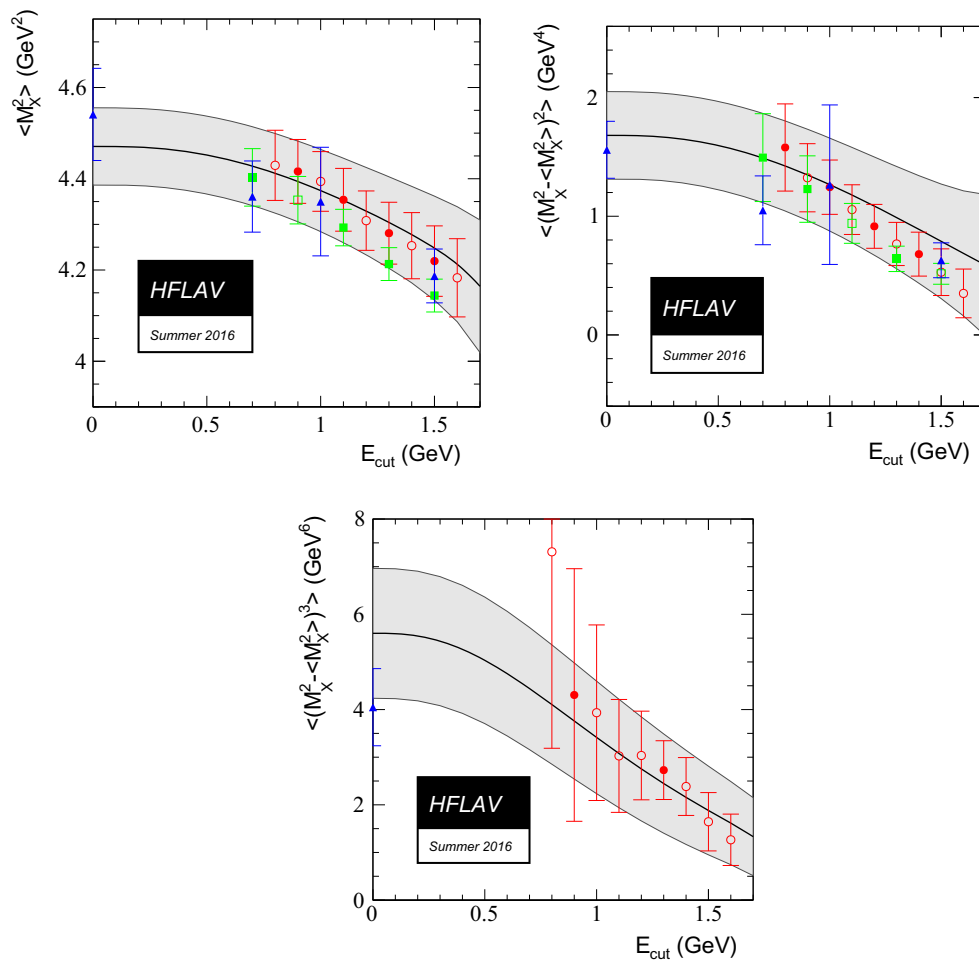


Fig. 57 Same as Fig. 56 for the fit to the hadronic mass moments in the kinetic mass scheme

Table 80 Fit result in the 1S scheme, using $B \rightarrow X_s \gamma$ moments as a constraint. In the lower part of the table, the correlation matrix of the parameters is given

	m_b^{1S} (GeV)	λ_1 (GeV ²)	ρ_1 (GeV ³)	τ_1 (GeV ³)	τ_2 (GeV ³)	τ_3 (GeV ³)	$ V_{cb} $ (10^{-3})
Value	4.691	-0.362	0.043	0.161	-0.017	0.213	41.98
Error	0.037	0.067	0.048	0.122	0.062	0.102	0.45
m_b^{1S}	1.000	0.434	0.213	-0.058	-0.629	-0.019	-0.215
λ_1		1.000	-0.467	-0.602	-0.239	-0.547	-0.403
ρ_1			1.000	0.129	-0.624	0.494	0.286
τ_1				1.000	0.062	-0.148	0.194
τ_2					1.000	-0.009	-0.145
τ_3						1.000	0.376
$ V_{cb} $							1.000

$$\Delta\Gamma = \Delta\Gamma(q_{\text{low}}^2, q_{\text{high}}^2) = \int_{q_{\text{low}}^2}^{q_{\text{high}}^2} dq^2 \left[\frac{8|\vec{p}_\pi|}{3} \frac{G_F^2 |V_{ub}|^2 q^2}{256 \pi^3 m_B^2} H_0^2(q^2) \right], \quad (204)$$

where G_F is Fermi’s constant, $|\vec{p}_\pi|$ is the absolute four-momentum of the final state π (a function of q^2), m_B the B^0 -meson mass, and $H_0(q^2)$ the only non-zero helicity amplitude. The helicity amplitude is a function of the form factor f_+ ,

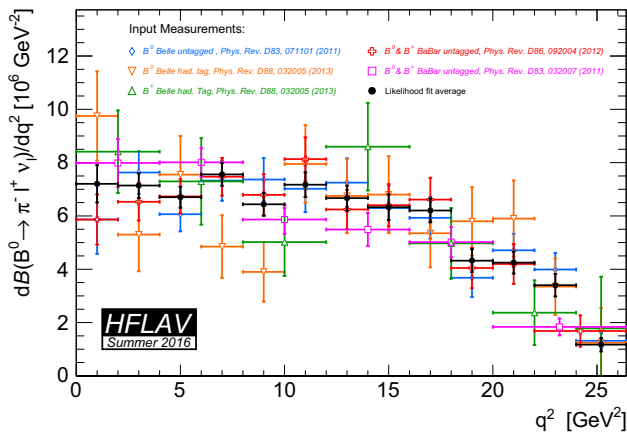


Fig. 58 The $B \rightarrow \pi \ell \nu$ q^2 spectrum measurements and the average spectrum obtained from the likelihood combination (shown in black)

$$H_0 = \frac{2m_B |\vec{p}_\pi|}{\sqrt{q^2}} f_+(q^2). \tag{205}$$

The form factor f_+ can be calculated with non-perturbative methods, but its general form can be constrained by the differential $B \rightarrow \pi \ell \nu$ spectrum. Here, we parametrize the form factor using the BCL parametrization [527].

The decay rate is proportional to $|V_{ub}|^2 |f_+(q^2)|^2$. Thus to extract $|V_{ub}|$ one needs to determine $f_+(q^2)$ (at least at one value of q^2). In order to enhance the precision, a binned χ^2 fit is performed using a χ^2 function of the form

$$\chi^2 = \left(\vec{\mathcal{B}} - \Delta \vec{\Gamma} \tau \right)^T C^{-1} \left(\vec{\mathcal{B}} - \Delta \vec{\Gamma} \tau \right) + \chi_{\text{LQCD}}^2 + \chi_{\text{LCSR}}^2 \tag{206}$$

Table 81 Partial $B^0 \rightarrow \pi^- \ell^+ \nu_\ell$ branching fractions per GeV^2 for the input measurements and the average obtained from the likelihood fit. The uncertainties are the combined statistical and systematic uncertainties

Δq^2 (GeV^2)	$\Delta \mathcal{B}(B^0 \rightarrow \pi^- \ell^+ \nu_\ell) / \Delta q^2$ [10^{-7}]					
	Belle untagged (B^0)	Belle tagged (B^0)	Belle tagged (B^+)	BABAR untagged ($B^{0,+}$, 12 bins)	BABAR untagged ($B^{0,+}$, 6 bins)	Average
0–2	58.7 ± 12.9	97.5 ± 16.7	84.1 ± 15.5	58.7 ± 9.4	79.9 ± 9.1	72.0 ± 7.0
2–4	76.3 ± 8.0	53.0 ± 13.8		65.3 ± 7.1		71.4 ± 4.6
4–6	60.6 ± 6.4	75.5 ± 14.5	73.0 ± 16.2	67.3 ± 6.4	80.1 ± 5.3	67.0 ± 3.9
6–8	73.3 ± 7.6	48.5 ± 11.8		74.7 ± 7.1		75.6 ± 4.3
8–10	73.7 ± 8.1	39.0 ± 11.2	50.2 ± 12.8	67.9 ± 7.8	58.7 ± 5.5	64.4 ± 4.3
10–12	70.2 ± 8.8	79.5 ± 14.6		81.3 ± 8.2		71.7 ± 4.6
12–14	72.5 ± 9.1	67.5 ± 13.9	86.0 ± 16.4	62.4 ± 7.4	54.9 ± 6.2	66.7 ± 4.7
14–16	63.0 ± 8.4	68.0 ± 14.4		64.0 ± 7.9		63.3 ± 4.8
16–18	59.3 ± 7.8	53.5 ± 12.8	49.7 ± 13.3	66.1 ± 8.2	50.2 ± 5.7	62.0 ± 4.4
18–20	36.8 ± 7.2	58.0 ± 12.8		40.5 ± 7.6		43.2 ± 4.3
20–22	47.1 ± 6.2	59.0 ± 14.3	23.7 ± 12.1	42.0 ± 7.5	18.4 ± 3.2	42.5 ± 4.1
22–24	39.9 ± 6.2	33.5 ± 10.6		16.8 ± 5.9		34.0 ± 4.2
24–26.4	13.2 ± 2.9	12.4 ± 13.0	17.8 ± 19.4			11.7 ± 2.6

with C denoting the covariance matrix given in Table 82, $\vec{\mathcal{B}}$ the vector of averaged branching fractions and $\Delta \vec{\Gamma} \tau$ the product of the vector of theoretical predictions of the partial decay rates and the B^0 -meson lifetime. The form factor normalization is included in the fit by the two extra terms in Eq. (206): χ_{LQCD} uses the latest FLAG lattice average [222] from two state-of-the-art unquenched lattice QCD calculations [528, 529]. The resulting constraints are quoted directly in terms of the coefficients b_j of the BCL parametrization and enter Eq. (206) as

$$\chi_{\text{LQCD}}^2 = \left(\vec{b} - \vec{b}_{\text{LQCD}} \right)^T C_{\text{LQCD}}^{-1} \left(\vec{b} - \vec{b}_{\text{LQCD}} \right), \tag{207}$$

with \vec{b} the vector containing the free parameters of the χ^2 fit constraining the form factor, \vec{b}_{LQCD} the averaged values from Ref. [222], and C_{LQCD} their covariance matrix. Additional information about the form factor can be obtained from light-cone sum rule calculations. The state-of-the-art calculation includes up to two-loop contributions [530]. It is included in Eq. (206) via

$$\chi_{\text{LQCR}}^2 = \left(f_+^{\text{LCSR}} - f_+(q^2 = 0; \vec{b}) \right)^2 / \sigma_{f_+}^2. \tag{208}$$

The $|V_{ub}|$ average is obtained for two versions: the first combines the data with the LQCD constraints and the second additionally includes the information from the LCSR calculation. The resulting values for $|V_{ub}|$ are

Table 82 Covariance matrix of the averaged partial branching fractions per GeV^2 in units of 10^{-14}

Δq^2 (GeV^2)	0-2	2-4	4-6	6-8	8-10	10-12	12-14	14-16	16-18	18-20	20-22	22-24	24-26.4
0-2	49.091	1.164	8.461	7.996	7.755	9.484	7.604	9.680	8.868	7.677	7.374	7.717	2.877
2-4		21.487	-0.0971	7.155	4.411	5.413	4.531	4.768	4.410	3.442	3.597	3.388	1.430
4-6			15.489	-0.563	5.818	4.449	4.392	4.157	4.024	3.185	3.169	3.013	1.343
6-8				18.2	2.377	7.889	6.014	5.938	5.429	4.096	3.781	3.863	1.428
8-10					18.124	1.540	7.496	5.224	5.441	4.197	3.848	4.094	1.673
10-12						21.340	4.213	7.696	6.493	5.170	4.686	4.888	1.950
12-14							21.875	0.719	6.144	3.846	3.939	3.922	1.500
14-16								23.040	5.219	6.123	4.045	4.681	1.807
16-18									19.798	1.662	4.362	4.140	1.690
18-20										18.0629	2.621	3.957	1.438
20-22											16.990	1.670	1.127
22-24												17.774	-0.293
24-26.4													6.516

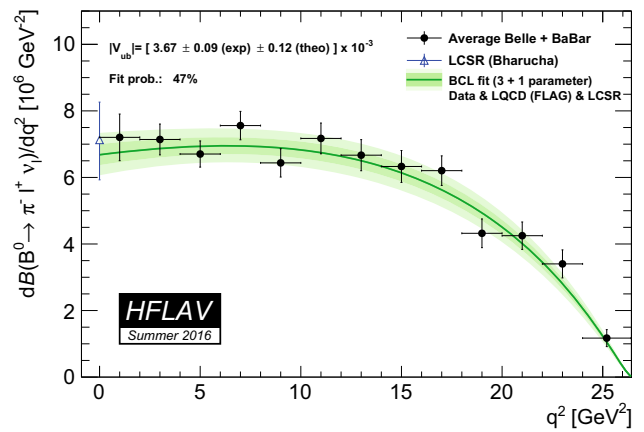


Fig. 59 Fit of the BCL parametrization to the averaged q^2 spectrum from BABAR and Belle and the LQCD and LCSR calculations. The error bands represent the 1σ (dark green) and 2σ (light green) uncertainties of the fitted spectrum

Table 83 Best fit values and uncertainties for the combined fit to data, LQCD and LCSR results

Parameter	Value
$ V_{ub} $	$(3.67 \pm 0.15) \times 10^{-3}$
b_0	0.418 ± 0.012
b_1	-0.399 ± 0.033
b_2	-0.578 ± 0.130

$$|V_{ub}| = \left(3.70 \pm 0.10 \text{ (exp)} \pm 0.12 \text{ (theo)} \right) \times 10^{-3} \text{ (data + LQCD)}, \tag{209}$$

$$|V_{ub}| = \left(3.67 \pm 0.09 \text{ (exp)} \pm 0.12 \text{ (theo)} \right) \times 10^{-3} \text{ (data + LQCD + LCSR)}, \tag{210}$$

for the first and second fit version, respectively. The result of the fit including both LQCD and LCSR is shown in Fig. 59. The χ^2 probability of the fit is 47%. We quote the result of the fit including both LQCD and LCSR calculations as our average for $|V_{ub}|$. The best fit values for $|V_{ub}|$ and the BCL parameters and their covariance matrix are given in Tables 83 and 84.

5.3.3 Combined extraction of $|V_{ub}|$ and $|V_{cb}|$

The LHCb experiment reported the first observation of the CKM suppressed decay $\Lambda_b^0 \rightarrow p\mu\nu$ [522] and the measurement of the ratio of partial branching fractions at high q^2 for $\Lambda_b^0 \rightarrow p\mu\nu$ and $\Lambda_b^0 \rightarrow \Lambda_c^+ (\rightarrow pK\pi)\mu\nu$ decays

Table 84 Covariance matrix for the combined fit to data, LQCD and LCSR results

Parameter	$ V_{ub} $	b_0	b_1	b_2
$ V_{ub} $	2.064×10^{-8}	-1.321×10^{-6}	-1.881×10^{-6}	7.454×10^{-6}
b_0		1.390×10^{-4}	8.074×10^{-5}	-8.953×10^{-4}
b_1			1.053×10^{-3}	-2.879×10^{-3}
b_2				1.673×10^{-2}

$$R = \frac{\mathcal{B}(\Lambda_b^0 \rightarrow p\mu\nu)_{q^2>15 \text{ GeV}^2}}{\mathcal{B}(\Lambda_b^0 \rightarrow \Lambda_c^+\mu\nu)_{q^2>7 \text{ GeV}^2}} = (1.00 \pm 0.04 \pm 0.08) \times 10^{-2}. \tag{211}$$

The ratio R is proportional to $(|V_{ub}|/|V_{cb}|)^2$ and sensitive to the form factors of $\Lambda_b^0 \rightarrow p$ and $\Lambda_b^0 \rightarrow \Lambda_c^+$ transitions that have to be computed with non-perturbative methods, like lattice QCD. The uncertainty on $\mathcal{B}(\Lambda_c^+ \rightarrow pK\pi)$ is the largest source of systematic uncertainties on R . Using the recent HFLAV average $\mathcal{B}(\Lambda_c^+ \rightarrow pK\pi) = (6.46 \pm 0.24)\%$ reported in Table 296, which includes the recent BESIII measurements [531], the rescaled value for R is

$$R = (0.95 \pm 0.04 \pm 0.07) \times 10^{-2} \tag{212}$$

With the precise lattice QCD prediction [532] of the form factors in the experimentally interesting q^2 region considered, results in

$$\frac{|V_{ub}|}{|V_{cb}|} = 0.080 \pm 0.004_{Exp.} \pm 0.004_{F.F.} \tag{213}$$

where the first uncertainty is the total experimental error and the second one is due to the knowledge of the form factors. A combined fit for $|V_{ub}|$ and $|V_{cb}|$ that includes the constraint from LHCb, and the determination of $|V_{ub}|$ and $|V_{cb}|$ from exclusive B meson decays, results in

$$|V_{ub}| = (3.50 \pm 0.13) \times 10^{-3} \tag{214}$$

$$|V_{cb}| = (39.13 \pm 0.59) \times 10^{-3} \tag{215}$$

$$\rho(|V_{ub}|, |V_{cb}|) = 0.14 \tag{216}$$

where the uncertainties are considered uncorrelated. The χ^2 of the fit is 4.4 for 2 d.o.f corresponding to a $P(\chi^2)$ of 11.0%. The fit result is shown in Fig. 60, where both the $\Delta\chi^2$ and the two-dimensional 68% C.L. contours are indicated. The $|V_{ub}|/|V_{cb}|$ value extracted from R is more compatible with the exclusive determinations of $|V_{ub}|$. Another recent calculation, by Faustov and Galkin [533], based on a relativistic quark model, gives a value of $|V_{ub}|/|V_{cb}|$ closer to the inclusive determinations.

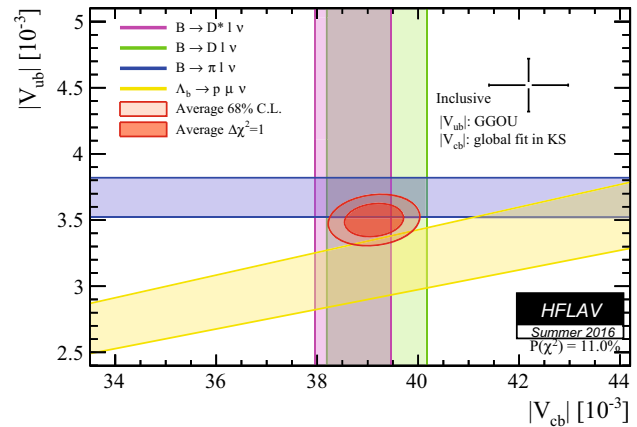


Fig. 60 $|V_{ub}|/|V_{cb}|$ combined average including the LHCb measurement of $|V_{ub}|/|V_{cb}|$, the exclusive $|V_{ub}|$ measurement from $B \rightarrow \pi l \nu$, and $|V_{cb}|$ measurements from both $B \rightarrow D^* \ell \nu$ and $B \rightarrow D \ell \nu$. The point with the error bars corresponds to the inclusive $|V_{cb}|$ from the kinetic scheme Sect. 5.2.2, and the inclusive $|V_{ub}|$ from GGOU calculation Sect. 5.4.3

Table 85 Summary of exclusive determinations of $B^0 \rightarrow \rho \ell^+ \nu$. The errors quoted correspond to statistical and systematic uncertainties, respectively

	$\mathcal{B} [10^{-4}]$
CLEO (untagged) ρ^+ [536]	$2.77 \pm 0.41 \pm 0.52$
CLEO (untagged) ρ^+ [537]	$2.93 \pm 0.37 \pm 0.37$
Belle (hadronic tag) ρ^+ [524]	$3.22 \pm 0.27 \pm 0.24$
Belle (hadronic tag) ρ^0 [524]	$3.39 \pm 0.18 \pm 0.18$
Belle (semileptonic tag) ρ^+ [538]	$2.24 \pm 0.54 \pm 0.31$
Belle (semileptonic tag) ρ^0 [538]	$2.50 \pm 0.43 \pm 0.33$
BABAR (untagged) ρ^+ [525]	$1.96 \pm 0.21 \pm 0.38$
BABAR (untagged) ρ^0 [525]	$1.86 \pm 0.19 \pm 0.32$
Average	$2.94 \pm 0.09 \pm 0.17$

5.3.4 Other exclusive charmless semileptonic B decays

We report the branching fraction average for $B^0 \rightarrow \rho \ell^+ \nu$, $B^+ \rightarrow \omega \ell^+ \nu$, $B^+ \rightarrow \eta \ell^+ \nu$ and $B^+ \rightarrow \eta' \ell^+ \nu$ decays. The measurements and their averages are listed in Tables 85, 86, 87, 88, and presented in Figs. 61 and 62.

Table 86 Summary of exclusive determinations of $B^+ \rightarrow \omega \ell^+ \nu$. The errors quoted correspond to statistical and systematic uncertainties, respectively

	$\mathcal{B} [10^{-4}]$
Belle (untagged) [539]	$1.30 \pm 0.40 \pm 0.36$
BABAR (loose ν reco.) [526]	$1.19 \pm 0.16 \pm 0.09$
BABAR (untagged) [540]	$1.21 \pm 0.14 \pm 0.08$
Belle (hadronic tag) [524]	$1.07 \pm 0.16 \pm 0.07$
BABAR (semileptonic tag) [541]	$1.35 \pm 0.21 \pm 0.11$
Average	$1.19 \pm 0.08 \pm 0.06$

Table 87 Summary of exclusive determinations of $B^+ \rightarrow \eta \ell^+ \nu$. The errors quoted correspond to statistical and systematic uncertainties, respectively

	$\mathcal{B} [10^{-4}]$
CLEO [542]	$0.45 \pm 0.23 \pm 0.11$
BABAR (untagged) [543]	$0.31 \pm 0.06 \pm 0.08$
BABAR (semileptonic tag) [544]	$0.64 \pm 0.20 \pm 0.04$
BABAR (loose ν -reco.) [526]	$0.38 \pm 0.05 \pm 0.05$
Average	$0.38 \pm 0.04 \pm 0.04$

In the $B^0 \rightarrow \rho^- \ell^+ \nu$ average, both the $B^0 \rightarrow \rho^- \ell^+ \nu$ and $B^+ \rightarrow \rho^0 \ell^+ \nu$ decays are used, where the $B^+ \rightarrow \rho^0 \ell^+ \nu$ are rescaled by $2\tau_{B^0}/\tau_{B^+}$ assuming the isospin symmetry. For $B^+ \rightarrow \omega \ell^+ \nu$ and $B^+ \rightarrow \eta \ell^+ \nu$ decays, the agreement between the different measurements is good. $B^+ \rightarrow \eta' \ell^+ \nu$ shows a discrepancy between the old CLEO measurement and the BABAR untagged analysis, but the statistical uncertainties of the CLEO measurement are large. The $B^0 \rightarrow \rho \ell^+ \nu$ results, instead, show significant differences, in particular the BABAR untagged analysis gives a branching fraction significantly lower (by about 2σ) that the Belle measurement based on the hadronic-tag. A possible reason for such discrepancy could be the broad nature of the ρ resonance that makes the control of the background under the ρ mass peak more difficult in the untagged analysis than in the hadronic-tag analysis.

We do not report $|V_{ub}|$ for these exclusive charmless decays, because the form factor calculations have not yet reached the precision achieved for $B \rightarrow \pi \ell \nu$ decays. Unquenched lattice QCD calculations of the form factors are not available for these decays, but LCSR calculations exist for all these decay modes. The most recent of these calculations for the $B \rightarrow \rho \ell \nu$ and $B \rightarrow \omega \ell \nu$ decays are reported in Refs. [534, 535].

5.4 Inclusive CKM-suppressed decays

Measurements of $B \rightarrow X_u \ell^+ \nu$ decays are very challenging because of the fifty times larger rates Cabibbo-

Table 88 Summary of exclusive determinations of $B^+ \rightarrow \eta' \ell^+ \nu$. The errors quoted correspond to statistical and systematic uncertainties, respectively

	$\mathcal{B} [10^{-4}]$
CLEO [542]	$2.71 \pm 0.80 \pm 0.56$
BABAR (semileptonic tag) [544]	$0.04 \pm 0.22 \pm 0.04,$ $(<0.47 \text{ @ } 90\% C.L.)$
BABAR (untagged) [526]	$0.24 \pm 0.08 \pm 0.03$
Average	$0.23 \pm 0.08 \pm 0.03$

favoured $B \rightarrow X_c \ell^+ \nu$ decays. Cuts designed to suppress this dominant background severely complicate the perturbative QCD calculations required to extract $|V_{ub}|$. For strict phase space limitations, parameterizations of the so-called shape functions are required to describe the unmeasured regions of the phase space. In this update, we use several theoretical calculations to extract $|V_{ub}|$ and do not advocate the use of one method over another. The authors of the different calculations have provided codes to compute the partial rates in limited regions of phase space covered by the measurements. Latest results by Belle [545] and BABAR [546] explore large portions of phase space, with a consequent reduction of the theoretical uncertainties.

In the averages, the systematic errors associated with the modeling of $B \rightarrow X_c \ell^+ \nu \ell$ and $B \rightarrow X_u \ell^+ \nu \ell$ decays and the theoretical uncertainties are taken as fully correlated among all measurements. Reconstruction-related uncertainties are taken as fully correlated within a given experiment. Measurements of partial branching fractions for $B \rightarrow X_u \ell^+ \nu \ell$ transitions from $\Upsilon(4S)$ decays, together with the corresponding selected region, are given in Table 89. The signal yields for all the measurements shown in Table 89 are not rescaled to common input values of the B meson lifetime (see Sect. 3) and the semileptonic width [327]. We use all results published by BABAR in Ref. [546], since the statistical correlations are given. To make use of the theoretical calculations of Ref. [547], we restrict the kinematic range of the invariant mass of the hadronic system, M_X , and the square of the invariant mass of the lepton pair, q^2 . This reduces the size of the data sample significantly, but also the theoretical uncertainty, as stated by the authors [547]. The dependence of the quoted error on the measured value for each source of uncertainty is taken into account in the calculation of the averages.

It has been first suggested by Neubert [548] and later detailed by Leibovich, Low, and Rothstein (LLR) [549] and Lange, Neubert and Paz (LNP) [550], that the uncertainty of the leading shape functions can be eliminated by comparing inclusive rates for $B \rightarrow X_u \ell^+ \nu \ell$ decays with the inclusive photon spectrum in $B \rightarrow X_s \gamma$, based on the assumption that

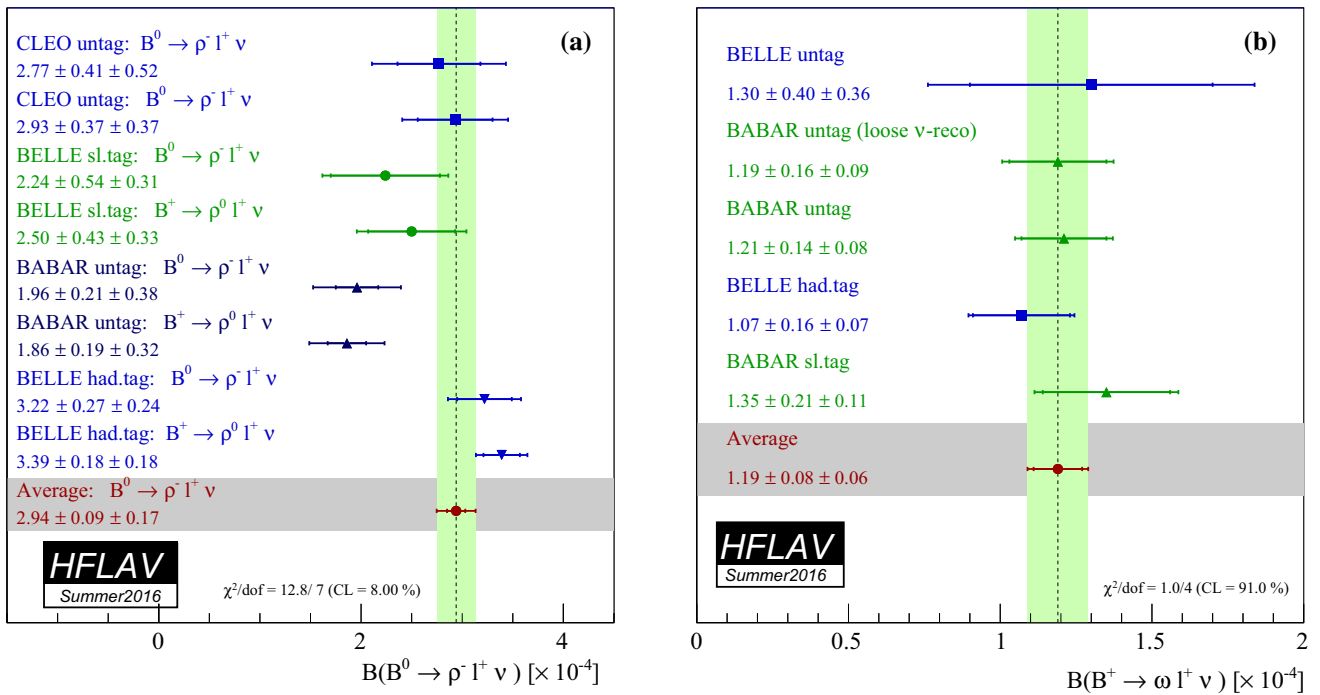


Fig. 61 **a** Summary of exclusive determinations of $B(B^0 \rightarrow \rho^- \ell^+ \nu)$ and their average. Measurements of $B^+ \rightarrow \rho^0 \ell^+ \nu$ branching fractions have been multiplied by $2\tau_{B^0}/\tau_{B^+}$ in accordance with isospin symmetry. **b** Summary of exclusive determinations of $B^+ \rightarrow \omega \ell^+ \nu$ and their average

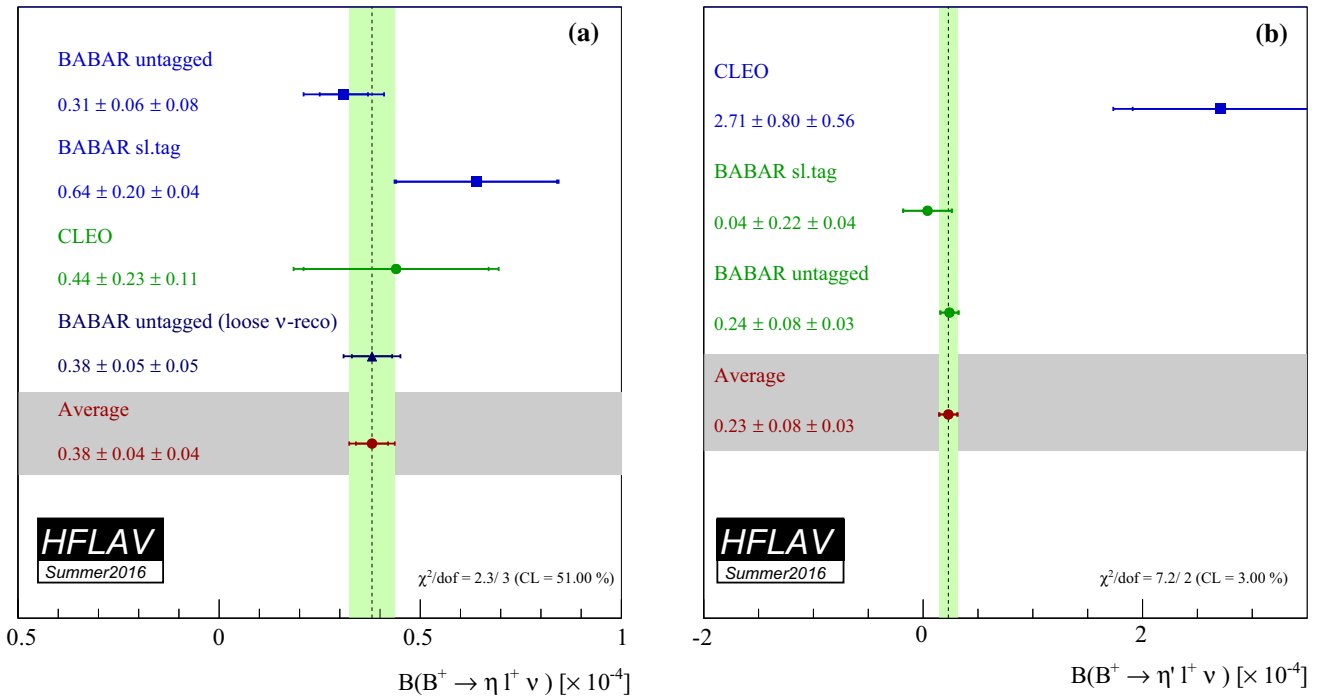


Fig. 62 **a** Summary of exclusive determinations of $B(B^+ \rightarrow \eta \ell^+ \nu)$ and their average. **b** Summary of exclusive determinations of $B(B^+ \rightarrow \eta' \ell^+ \nu)$ and their average

the shape functions for transitions to light quarks, u or s , are the same at first order. However, shape function uncertainties are only eliminated at the leading order and they still

enter via the signal models used for the determination of efficiency.

Table 89 Summary of measurements of partial branching fractions for $B \rightarrow X_u \ell^+ \nu_\ell$ decays. The errors quoted on $\Delta\mathcal{B}$ correspond to statistical and systematic uncertainties. E_e is the electron energy in the B rest frame, p^* the lepton momentum in the B frame and m_X is the invariant

mass of the hadronic system. The light-cone momentum P_+ is defined in the B rest frame as $P_+ = E_X - |\mathbf{p}_X|$. The s_h^{\max} variable is described in Refs. [552,553]

Measurement	Accepted region	$\Delta\mathcal{B}$ [10^{-4}]	Notes
CLEO [554]	$E_e > 2.1$ GeV	$3.3 \pm 0.2 \pm 0.7$	
BABAR [553]	$E_e > 2.0$ GeV, $s_h^{\max} < 3.5$ GeV ²	$4.4 \pm 0.4 \pm 0.4$	
BABAR [555]	$E_e > 2.0$ GeV	$5.7 \pm 0.4 \pm 0.5$	
Belle [556]	$E_e > 1.9$ GeV	$8.5 \pm 0.4 \pm 1.5$	
BABAR [546]	$M_X < 1.7$ GeV/ c^2 , $q^2 > 8$ GeV ² / c^4	$6.9 \pm 0.6 \pm 0.4$	
Belle [557]	$M_X < 1.7$ GeV/ c^2 , $q^2 > 8$ GeV ² / c^4	$7.4 \pm 0.9 \pm 1.3$	
Belle [558]	$M_X < 1.7$ GeV/ c^2 , $q^2 > 8$ GeV ² / c^4	$8.5 \pm 0.9 \pm 1.0$	Used only in BLL average
BABAR [546]	$P_+ < 0.66$ GeV	$9.9 \pm 0.9 \pm 0.8$	
BABAR [546]	$M_X < 1.7$ GeV/ c^2	$11.6 \pm 1.0 \pm 0.8$	
BABAR [546]	$M_X < 1.55$ GeV/ c^2	$10.9 \pm 0.8 \pm 0.6$	
Belle [545]	(M_X, q^2) fit, $p_\ell^* > 1$ GeV/ c	$19.6 \pm 1.7 \pm 1.6$	
BABAR [546]	(M_X, q^2) fit, $p_\ell^* > 1$ GeV/ c	$18.2 \pm 1.3 \pm 1.5$	
BABAR [546]	$p_\ell^* > 1.3$ GeV/ c	$15.5 \pm 1.3 \pm 1.4$	

In the following, the different theoretical methods and the resulting averages are described. A recent BABAR measurement of the inclusive electron spectrum [551] was released at the time of this writing and could not be included in the averages.

5.4.1 BLNP

Bosch, Lange, Neubert and Paz (BLNP) [559–562] provide theoretical expressions for the triple differential decay rate for $B \rightarrow X_u \ell^+ \nu_\ell$ events, incorporating all known contributions, whilst smoothly interpolating between the “shape-function region” of large hadronic energy and small invariant mass, and the “OPE region” in which all hadronic kinematical variables scale with the b -quark mass. BLNP assign uncertainties to the b -quark mass, which enters through the leading shape function, to sub-leading shape function forms, to possible weak annihilation contribution, and to matching scales. The BLNP calculation uses the shape function renormalization scheme; the heavy quark parameters determined from the global fit in the kinetic scheme, described in Sect. 5.2.2, were therefore translated into the shape function scheme by using a prescription by Neubert [563,564]. The resulting parameters are $m_b(\text{SF}) = (4.582 \pm 0.023 \pm 0.018)$ GeV, $\mu_\pi^2(\text{SF}) = (0.202 \pm 0.089_{-0.040}^{+0.020})$ GeV/ c^2 , where the second uncertainty is due to the scheme translation. The extracted values of $|V_{ub}|$ for each measurement along with their average are given in Table 90 and illustrated in Fig. 63a. The total uncertainty is ${}_{-6.0}^{+5.8}\%$ and is due to: statistics (${}_{-2.1}^{+2.1}\%$), detector effects (${}_{-1.8}^{+1.7}\%$), $B \rightarrow X_c \ell^+ \nu_\ell$ model (${}_{-1.2}^{+1.2}\%$), $B \rightarrow X_u \ell^+ \nu_\ell$ model

(${}_{-1.7}^{+1.8}\%$), heavy quark parameters (${}_{-2.6}^{+2.6}\%$), SF functional form (${}_{-0.3}^{+0.2}\%$), sub-leading shape functions (${}_{-0.7}^{+0.6}\%$), BLNP theory: matching scales μ, μ_i, μ_h (${}_{-3.7}^{+3.8}\%$), and weak annihilation (${}_{-1.4}^{+0.0}\%$). The error assigned to the matching scales is the source of the largest uncertainty, while the uncertainty due to HQE parameters (b -quark mass and μ_π^2) is second. The uncertainty due to weak annihilation has been assumed to be asymmetric, i.e. it only tends to decrease $|V_{ub}|$.

5.4.2 DGE

Andersen and Gardi (Dressed Gluon Exponentiation, DGE) [565] provide a framework where the on-shell b -quark calculation, converted into hadronic variables, is directly used as an approximation to the meson decay spectrum without the use of a leading-power non-perturbative function (or, in other words, a shape function). The on-shell mass of the b -quark within the B -meson (m_b) is required as input. The DGE calculation uses the \overline{MS} renormalization scheme. The heavy quark parameters determined from the global fit in the kinetic scheme, described in Sect. 5.2.2, were therefore translated into the \overline{MS} scheme by using a calculation by Gardi, giving $m_b(\overline{MS}) = (4.188 \pm 0.043)$ GeV. The extracted values of $|V_{ub}|$ for each measurement along with their average are given in Table 90 and illustrated in Fig. 63b. The total error is ${}_{-4.8}^{+4.8}\%$, whose breakdown is: statistics (${}_{-1.9}^{+1.9}\%$), detector effects (${}_{-1.7}^{+1.7}\%$), $B \rightarrow X_c \ell^+ \nu_\ell$ model (${}_{-1.3}^{+1.3}\%$), $B \rightarrow X_u \ell^+ \nu_\ell$ model (${}_{-1.7}^{+2.1}\%$), strong coupling α_s (${}_{-0.5}^{+0.5}\%$), m_b (${}_{-2.9}^{+3.2}\%$), weak annihilation (${}_{-1.8}^{+0.0}\%$),

Table 90 Summary of input parameters used by the different theory calculations, corresponding inclusive determinations of $|V_{ub}|$ and their average. The errors quoted on $|V_{ub}|$ correspond to experimental and theoretical uncertainties, respectively

	BLNP	DGE	GGOU	ADFR	BLL
Input parameters					
Scheme	SF	\overline{MS}	Kinetic	\overline{MS}	1S
Refs.	[563,564]	Ref. [565]	See Sect. 5.2.2	Ref. [566]	Ref. [547]
m_b (GeV)	4.582 ± 0.026	4.188 ± 0.043	4.554 ± 0.018	4.188 ± 0.043	4.704 ± 0.029
μ_π^2 (GeV ²)	$0.145^{+0.091}_{-0.097}$	–	0.414 ± 0.078	–	–
Ref.	$ V_{ub} $ values [10^{-3}]				
CLEO E_e [554]	$4.22 \pm 0.49^{+0.29}_{-0.34}$	$3.86 \pm 0.45^{+0.25}_{-0.27}$	$4.23 \pm 0.49^{+0.22}_{-0.31}$	$3.42 \pm 0.40^{+0.17}_{-0.17}$	–
Belle M_X, q^2 [557]	$4.51 \pm 0.47^{+0.27}_{-0.29}$	$4.43 \pm 0.47^{+0.19}_{-0.21}$	$4.52 \pm 0.48^{+0.25}_{-0.28}$	$3.93 \pm 0.41^{+0.18}_{-0.17}$	$4.68 \pm 0.49^{+0.30}_{-0.30}$
Belle E_e [556]	$4.93 \pm 0.46^{+0.26}_{-0.29}$	$4.82 \pm 0.45^{+0.23}_{-0.23}$	$4.95 \pm 0.46^{+0.16}_{-0.21}$	$4.48 \pm 0.42^{+0.20}_{-0.20}$	–
BABARE e [555]	$4.52 \pm 0.26^{+0.26}_{-0.30}$	$4.30 \pm 0.24^{+0.23}_{-0.25}$	$4.52 \pm 0.26^{+0.17}_{-0.24}$	$3.93 \pm 0.22^{+0.20}_{-0.20}$	–
BABAR E_e, s_h^{\max} [553]	$4.71 \pm 0.32^{+0.33}_{-0.38}$	$4.35 \pm 0.29^{+0.28}_{-0.30}$	–	$3.81 \pm 0.19^{+0.19}_{-0.18}$	–
Belle $p_\ell^*, (M_X, q^2)$ fit [545]	$4.50 \pm 0.27^{+0.20}_{-0.22}$	$4.62 \pm 0.28^{+0.13}_{-0.13}$	$4.62 \pm 0.28^{+0.09}_{-0.10}$	$4.50 \pm 0.30^{+0.20}_{-0.20}$	–
BABAR M_X [546]	$4.24 \pm 0.19^{+0.25}_{-0.25}$	$4.47 \pm 0.20^{+0.19}_{-0.24}$	$4.30 \pm 0.20^{+0.20}_{-0.21}$	$3.83 \pm 0.18^{+0.20}_{-0.19}$	–
BABAR M_X [546]	$4.03 \pm 0.22^{+0.22}_{-0.22}$	$4.22 \pm 0.23^{+0.21}_{-0.27}$	$4.10 \pm 0.23^{+0.16}_{-0.17}$	$3.75 \pm 0.21^{+0.18}_{-0.18}$	–
BABAR M_X, q^2 [546]	$4.32 \pm 0.23^{+0.26}_{-0.28}$	$4.24 \pm 0.22^{+0.18}_{-0.21}$	$4.33 \pm 0.23^{+0.24}_{-0.27}$	$3.75 \pm 0.20^{+0.17}_{-0.17}$	$4.50 \pm 0.24^{+0.29}_{-0.29}$
BABAR P_+ [546]	$4.09 \pm 0.25^{+0.25}_{-0.25}$	$4.17 \pm 0.25^{+0.28}_{-0.37}$	$4.25 \pm 0.26^{+0.26}_{-0.27}$	$3.57 \pm 0.22^{+0.19}_{-0.18}$	–
BABAR $p_\ell^*, (M_X, q^2)$ fit [546]	$4.33 \pm 0.24^{+0.19}_{-0.21}$	$4.45 \pm 0.24^{+0.12}_{-0.13}$	$4.44 \pm 0.24^{+0.09}_{-0.10}$	$4.33 \pm 0.24^{+0.19}_{-0.19}$	–
BABAR p_ℓ^* [546]	$4.34 \pm 0.27^{+0.20}_{-0.21}$	$4.43 \pm 0.27^{+0.13}_{-0.13}$	$4.43 \pm 0.27^{+0.09}_{-0.11}$	$4.28 \pm 0.27^{+0.19}_{-0.19}$	–
Belle M_X, q^2 [558]	–	–	–	–	$5.01 \pm 0.39^{+0.32}_{-0.32}$
Average	$4.44 \pm 0.15^{+0.21}_{-0.22}$	$4.52 \pm 0.16^{+0.15}_{-0.16}$	$4.52 \pm 0.15^{+0.11}_{-0.14}$	$4.08 \pm 0.13^{+0.18}_{-0.12}$	$4.62 \pm 0.20^{+0.29}_{-0.29}$

matching scales in DGE ($^{+0.5}_{-0.4}\%$). The largest contribution to the total error is due to the effect of the uncertainty on m_b . The uncertainty due to weak annihilation has been assumed to be asymmetric, i.e. it only tends to decrease $|V_{ub}|$.

5.4.3 GGOU

Gambino, Giordano, Ossola and Uraltsev (GGOU) [567] compute the triple differential decay rates of $B \rightarrow X_u \ell^+ \nu_\ell$, including all perturbative and non-perturbative effects through $O(\alpha_s^2 \beta_0)$ and $O(1/m_b^3)$. The Fermi motion is parameterized in terms of a single light-cone function for each structure function and for any value of q^2 , accounting for all subleading effects. The calculations are performed in the kinetic scheme, a framework characterized by a Wilsonian treatment with a hard cutoff $\mu \sim 1$ GeV. GGOU have not included calculations for the “ (E_e, s_h^{\max}) ” analysis [553]. The heavy quark parameters determined from the global fit in the kinetic scheme, described in Sect. 5.2.2, are used as inputs: $m_b^{kin} = (4.554 \pm 0.018)$ GeV, $\mu_\pi^2 = (0.464 \pm 0.076)$ GeV/ c^2 . The extracted values of $|V_{ub}|$ for each measurement along with their average are given in Table 90 and illustrated in Fig. 64a. The total error

is $^{+4.2}_{-4.6}\%$ whose breakdown is: statistics ($^{+2.0}_{-2.0}\%$), detector effects ($^{+1.7}_{-1.7}\%$), $B \rightarrow X_c \ell^+ \nu_\ell$ model ($^{+1.3}_{-1.3}\%$), $B \rightarrow X_u \ell^+ \nu_\ell$ model ($^{+1.8}_{-1.8}\%$), α_s , m_b and other non-perturbative parameters ($^{+1.4}_{-1.4}\%$), higher order perturbative and non-perturbative corrections ($^{+1.5}_{-1.5}\%$), modelling of the q^2 tail ($^{+1.2}_{-1.2}\%$), weak annihilations matrix element ($^{+0.0}_{-1.9}\%$), functional form of the distribution functions ($^{+0.2}_{-0.2}\%$). The leading uncertainties on $|V_{ub}|$ are both from theory, and are due to perturbative and non-perturbative parameters and the modelling of the q^2 tail. The uncertainty due to weak annihilation has been assumed to be asymmetric, i.e. it only tends to decrease $|V_{ub}|$.

5.4.4 ADFR

Aglietti, Di Lodovico, Ferrera and Ricciardi (ADFR) [568] use an approach to extract $|V_{ub}|$, that makes use of the ratio of the $B \rightarrow X_c \ell^+ \nu_\ell$ and $B \rightarrow X_u \ell^+ \nu_\ell$ widths. The normalized triple differential decay rate for $B \rightarrow X_u \ell^+ \nu_\ell$ [566,569–571] is calculated with a model based on (i) soft-gluon resummation to next-to-next-leading order and (ii) an effective QCD coupling without Landau pole. This coupling is constructed by means of an extrapola-

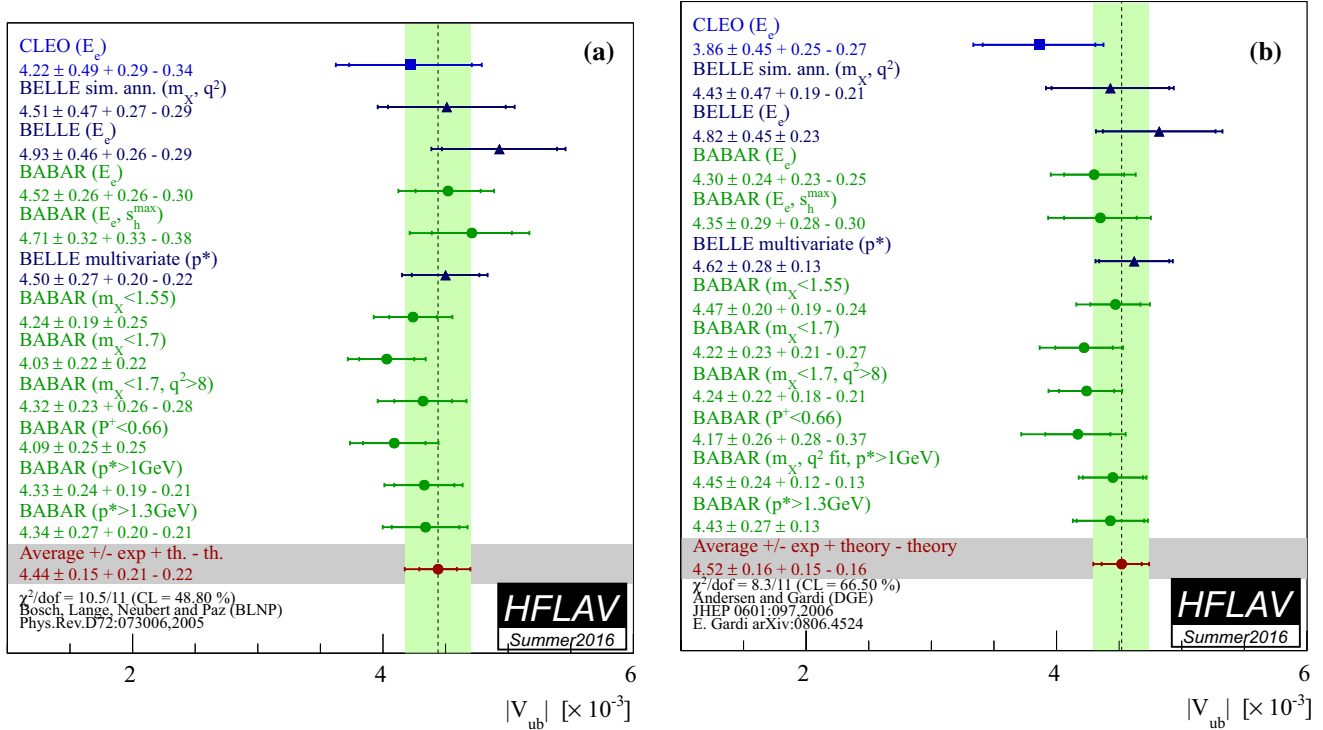


Fig. 63 Measurements of $|V_{ub}|$ from inclusive semileptonic decays and their average based on the BLNP (a) and DGE (b) prescription. The labels indicate the variables and selections used to define the signal regions in the different analyses

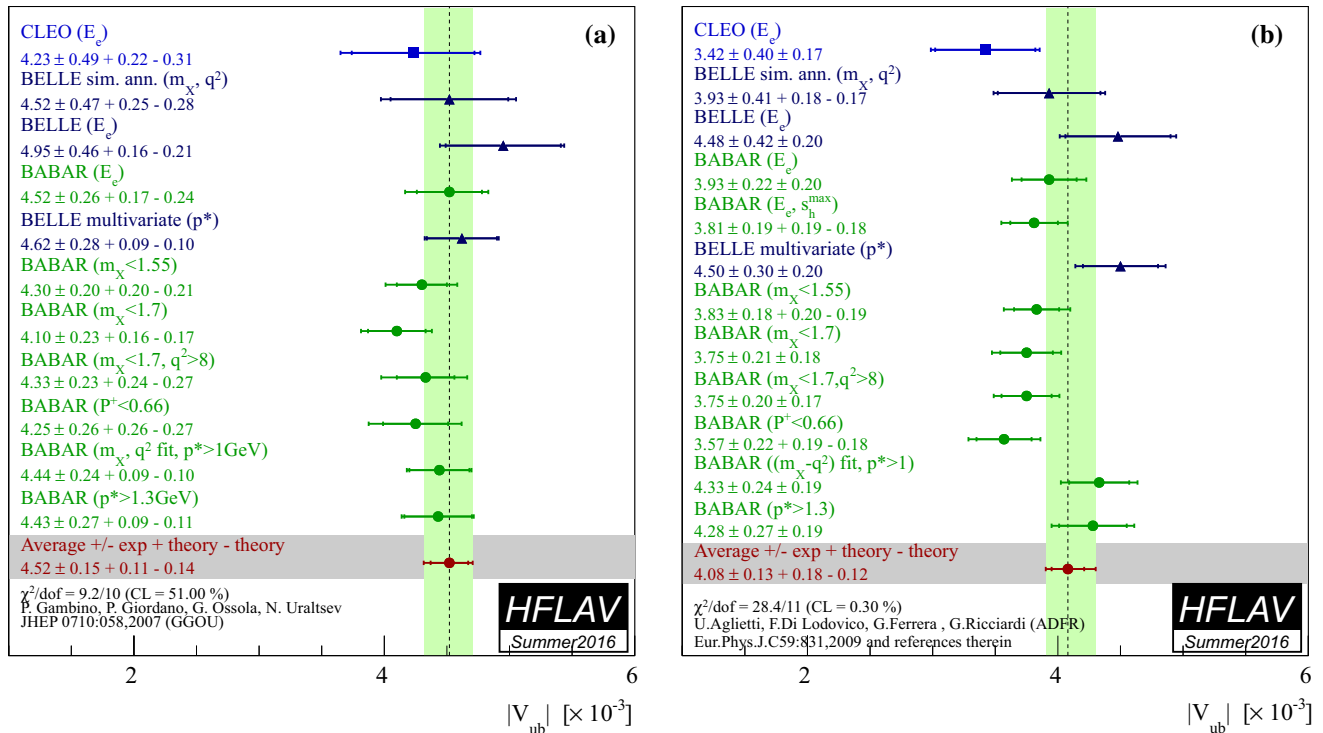


Fig. 64 Measurements of $|V_{ub}|$ from inclusive semileptonic decays and their average based on the GGOU (a) and ADFR (b) prescription. The labels indicate the variables and selections used to define the signal regions in the different analyses

tion to low energy of the high-energy behaviour of the standard coupling. More technically, an analyticity principle is used. The lower cut on the electron energy for the endpoint analyses is 2.3 GeV [566]. The ADFR calculation uses the \overline{MS} renormalization scheme; the heavy quark parameters determined from the global fit in the kinetic scheme, described in Sect. 5.2.2, were therefore translated into the \overline{MS} scheme by using a calculation by Gardi, giving $m_b(\overline{MS}) = (4.188 \pm 0.043)$ GeV. The extracted values of $|V_{ub}|$ for each measurement along with their average are given in Table 90 and illustrated in Fig. 64b. The total error is $^{+5.5\%}_{-5.5\%}$ whose breakdown is: statistics ($^{+1.9\%}_{-1.9\%}$), detector effects ($^{+1.7\%}_{-1.7\%}$), $B \rightarrow X_c \ell^+ \nu_\ell$ model ($^{+1.3\%}_{-1.3\%}$), $B \rightarrow X_u \ell^+ \nu_\ell$ model ($^{+1.3\%}_{-1.3\%}$), α_s ($^{+1.1\%}_{-1.0\%}$), $|V_{cb}|$ ($^{+1.9\%}_{-1.9\%}$), m_b ($^{+0.7\%}_{-0.7\%}$), m_c ($^{+1.3\%}_{-1.3\%}$), semileptonic branching fraction ($^{+0.8\%}_{-0.7\%}$), theory model ($^{+3.6\%}_{-3.6\%}$). The leading uncertainty is due to the theory model.

5.4.5 BLL

Bauer, Ligeti, and Luke (BLL) [547] give a HQET-based prescription that advocates combined cuts on the dilepton invariant mass, q^2 , and hadronic mass, m_X , to minimise the overall uncertainty on $|V_{ub}|$. In their reckoning a cut on m_X only, although most efficient at preserving phase space ($\sim 80\%$), makes the calculation of the partial rate untenable due to uncalculable corrections to the b -quark distribution function or shape function. These corrections are suppressed if events in the low q^2 region are removed. The cut combination used in measurements is $M_X < 1.7$ GeV/ c^2 and $q^2 > 8$ GeV $^2/c^4$. The extracted values of $|V_{ub}|$ for each measurement along with their average are given in Table 90 and illustrated in Fig. 65. The total error is $^{+7.7\%}_{-7.7\%}$ whose breakdown is: statistics ($^{+3.3\%}_{-3.3\%}$), detector effects ($^{+3.0\%}_{-3.0\%}$), $B \rightarrow X_c \ell^+ \nu_\ell$ model ($^{+1.6\%}_{-1.6\%}$), $B \rightarrow X_u \ell^+ \nu_\ell$ model ($^{+1.1\%}_{-1.1\%}$), spectral fraction (m_b) ($^{+3.0\%}_{-3.0\%}$), perturbative approach: strong coupling α_s ($^{+3.0\%}_{-3.0\%}$), residual shape function ($^{+2.5\%}_{-2.5\%}$), third order terms in the OPE ($^{+4.0\%}_{-4.0\%}$). The leading uncertainties, both from theory, are due to residual shape function effects and third order terms in the OPE expansion. The leading experimental uncertainty is due to statistics.

5.4.6 Summary

The averages presented in several different frameworks are presented in Table 91. In summary, we recognize that the experimental and theoretical uncertainties play out differently between the schemes and the theoretical assumptions for the theory calculations are different. Therefore, it is difficult to perform an average between the various determina-

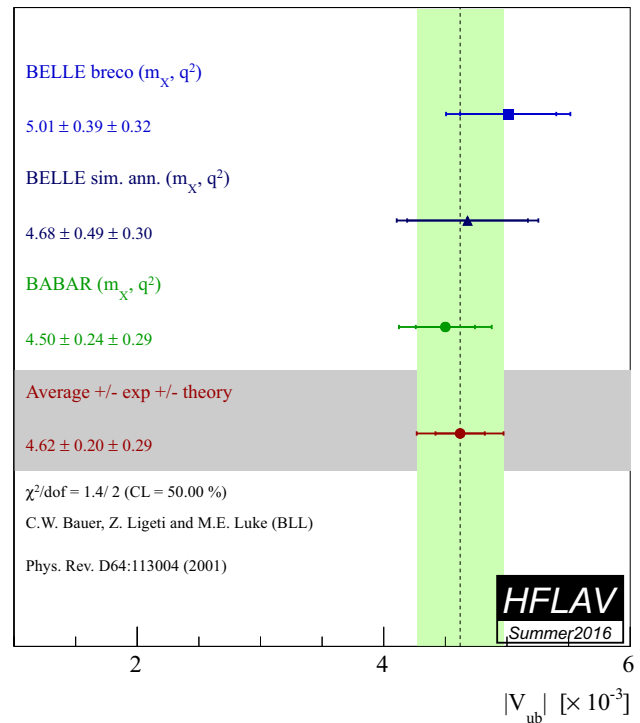


Fig. 65 Measurements of $|V_{ub}|$ from inclusive semileptonic decays and their average in the BLL prescription

Table 91 Summary of inclusive determinations of $|V_{ub}|$. The errors quoted on $|V_{ub}|$ correspond to experimental and theoretical uncertainties

Framework	$ V_{ub} $ (10^{-3})
BLNP	$4.44 \pm 0.15^{+0.21}_{-0.22}$
DGE	$4.52 \pm 0.16^{+0.15}_{-0.16}$
GGOU	$4.52 \pm 0.15^{+0.11}_{-0.14}$
ADFR	$4.08 \pm 0.13^{+0.18}_{-0.12}$
BLL (m_X/q^2 only)	$4.62 \pm 0.20 \pm 0.29$

tions of $|V_{ub}|$. Since the methodology is similar to that used to determine the inclusive $|V_{cb}|$ average, we choose to quote as reference value the average determined by the GGOU calculation, which gives $|V_{ub}| = (4.52 \pm 0.15^{+0.11}_{-0.14}) \times 10^{-3}$.

5.5 $B \rightarrow D^{(*)} \tau \nu_\tau$ decays

In the SM the semileptonic decay are tree level processes which proceed via coupling to the W^\pm boson. These couplings are assumed to be universal for all leptons and are well understood theoretically, (see Sects. 5.1, 5.2). This universality has been tested in purely leptonic and semileptonic B meson decays involving a τ lepton, which might be sensitive to a hypothetical charged Higgs boson or other non-SM processes.

Table 92 Measurements of $\mathcal{R}(D^*)$ and $\mathcal{R}(D)$, their correlations and the combined average

Experiment	$\mathcal{R}(D^*)$	$\mathcal{R}(D)$	ρ
BABAR [574,575]	$0.332 \pm 0.024_{\text{stat}} \pm 0.018_{\text{sys}}$	$0.440 \pm 0.058_{\text{stat}} \pm 0.042_{\text{sys}}$	-0.27
Belle [582]	$0.293 \pm 0.038_{\text{stat}} \pm 0.015_{\text{sys}}$	$0.375 \pm 0.064_{\text{stat}} \pm 0.026_{\text{sys}}$	-0.49
LHCb [583]	$0.336 \pm 0.027_{\text{stat}} \pm 0.030_{\text{sys}}$		
Belle [584]	$0.302 \pm 0.030_{\text{stat}} \pm 0.011_{\text{sys}}$		
Belle [585]	$0.270 \pm 0.035_{\text{stat}}^{+0.028}_{-0.025_{\text{sys}}}$		
Average	$0.310 \pm 0.015 \pm 0.008$	$0.403 \pm 0.040 \pm 0.024$	-0.23

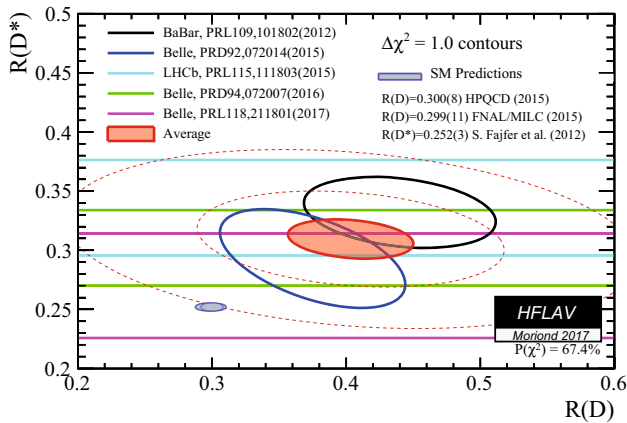


Fig. 66 Measurement of $\mathcal{R}(D)$ and $\mathcal{R}(D^*)$ and their average compared with the prediction for $\mathcal{R}(D^*)$ [577] and $\mathcal{R}(D)$ [494,573]. The dashed ellipses corresponds to the 2 and 4 σ contours

Compared to $B^+ \rightarrow \tau \nu_\tau$, the $B \rightarrow D^{(*)} \tau \nu_\tau$ decay has advantages: the branching fraction is relatively high, because it is not Cabibbo-suppressed, and it is a three-body decay allowing access to many observables besides the branching fraction, such as $D^{(*)}$ momentum, q^2 distributions, and measurements of the D^* and τ polarisations (see Ref. [572] and references therein for recent calculations).

Experiments have measured two ratios of branching fractions defined as

$$\mathcal{R}(D) = \frac{\mathcal{B}(B \rightarrow D \tau \nu_\tau)}{\mathcal{B}(B \rightarrow D \ell \nu_\ell)}, \tag{217}$$

$$\mathcal{R}(D^*) = \frac{\mathcal{B}(B \rightarrow D^* \tau \nu_\tau)}{\mathcal{B}(B \rightarrow D^* \ell \nu_\ell)} \tag{218}$$

where ℓ refers either to electron or μ . These ratios are independent of $|V_{cb}|$ and to a large extent, also of the $B \rightarrow D^{(*)}$ form factors. As a consequences the SM predictions for these ratios are quite precise:

- $\mathcal{R}(D) = 0.300 \pm 0.008$, which is an average obtained by FLAG [222] by combining the most recent lattice calculations of the $B \rightarrow D \ell \nu$ form factors [494,573];

- $\mathcal{R}(D^*) = 0.252 \pm 0.003$, which is a prediction, [574, 575] that updates recent QCD calculations [576,577] based on the recent $B \rightarrow D^*$ measurements from the B-Factories.

Recently, in Ref. [578] Bigi and Gambino re-analysed the recent experimental results and theoretical calculation of $B \rightarrow D \ell \nu$ obtaining $\mathcal{R}(D) = 0.299 \pm 0.003$, compatible with the predictions reported above but with a total error reduced by a factor three.

From the experimental side, in the case of the leptonic τ decay, the ratios $\mathcal{R}(D^{(*)})$ can be directly measured, and many systematic uncertainties cancel in the measurement. The $B^0 \rightarrow D^{*+} \tau \nu_\tau$ decay was first observed by Belle [579] performing an “inclusive” reconstruction, which is based on the reconstruction of the B_{tag} from all the particles of the events, other than the $D^{(*)}$ and the lepton candidate, without looking for any specific B_{tag} decay chain. Since then, both BABAR and Belle have published improved measurements and have found evidence for the $B \rightarrow D \tau \nu_\tau$ decays [580,581].

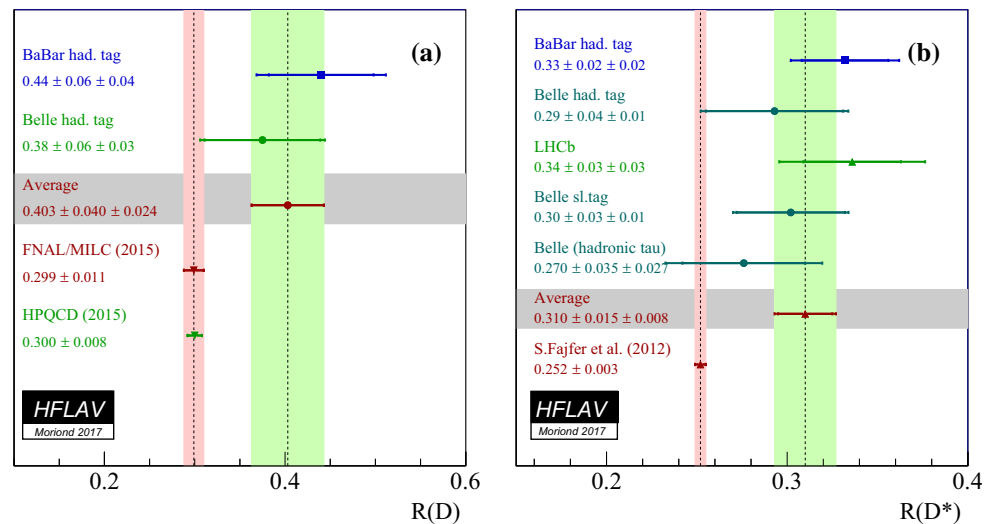
The most powerful way to study these decays at the B-Factories exploits the hadronic B_{tag} . Using the full dataset and an improved B_{tag} selection, BABAR measured [574]:

$$\begin{aligned} \mathcal{R}(D) &= 0.440 \pm 0.058 \pm 0.042, \\ \mathcal{R}(D^*) &= 0.332 \pm 0.024 \pm 0.018 \end{aligned} \tag{219}$$

where decays to both e^\pm and μ^\pm were summed and B^0 and B^- were combined in a isospin-constrained fit. The fact that the BABAR result exceeded SM predictions by 3.4σ , raised considerable interest.

Belle published various measurements using different techniques, and LHCb also joined the effort with a measurement of $R(D^*)$. The most important sources of systematic uncertainties correlated for the different measurement is due to the $B \rightarrow D^{**}$ background components that are difficult to disentangle from the signal. In the average the systematic uncertainties due to the $B \rightarrow D^{**}$ composition and kinematics are considered fully correlated among the measurements.

Fig. 67 **a** Measurement of $\mathcal{R}(D)$ and **b** $\mathcal{R}(D^*)$. The average is the projection of the average obtained from the combined fit



The results of the individual measurements, their averages and correlations are presented in Table 92 and Fig. 66. The combined results, projected separately on $\mathcal{R}(D)$ and $\mathcal{R}(D^*)$, are reported in Fig. 67a, b respectively.

The averaged $\mathcal{R}(D)$ and $\mathcal{R}(D^*)$ exceed the SM predictions by 2.2σ and 3.4σ respectively. Considering the $\mathcal{R}(D)$ and $\mathcal{R}(D^*)$ total correlation of -0.23 , the difference with respect to the SM is about 3.9σ , the combined $\chi^2 = 18.83$ for 2 degrees of freedom corresponds to a p -value of 8.3×10^{-5} , assuming Gaussian error distributions.

6 Decays of b -hadrons into open or hidden charm hadrons

Ground state B mesons and b baryons dominantly decay to particles containing a charm quark via the $b \rightarrow c$ quark transition. In this section, measurements of such decays to hadronic final states are considered; semileptonic decay modes, which are usually used to determine the strength of the $b \rightarrow c$ transition as quantified in the magnitude of the CKM matrix element $|V_{cb}|$, are discussed in Sect. 5. Some B meson decays to open or hidden charm hadrons that are fundamental for the measurements of CP -violation phases – like $\phi_s^{c\bar{c}s}$ (Sect. 3), $\beta \equiv \phi_1$ and $\gamma \equiv \phi_3$ (Sect. 4) – are discussed elsewhere in this report. Similarly, the use of $b \rightarrow c$ decay modes for the determination of important properties of b -hadrons, like their masses or (absolute, relative or effective) lifetimes, is discussed in Sect. 3. The properties of certain b hadron decays to open or hidden charm hadrons, such as small Q values and similar topologies for different modes,

allow the minimization of systematic uncertainties in these measurements.

The fact that decays to final states containing open or hidden charm hadrons dominate the b -hadron widths makes them a very important part of the experimental programme in heavy flavor physics. Understanding the rate of charm production in b -hadron decays is crucial to validate the HQE that underpins much of the theoretical framework for b physics (see, for example, Ref. [586] for a review). Moreover, such decays are often used as normalization modes for measurements of rarer decays. In addition, they are the dominant background in many analyses. To model accurately such backgrounds with simulated data, it is essential to have precise knowledge of the contributing decay modes. In particular, with the expected increase in the data samples at LHCb and Belle II, the enhanced statistical sensitivity has to be matched by low systematic uncertainties due to knowledge of the dominant b -hadron decay modes. For multibody decays, knowledge of the distribution of decays across the phase-space (e.g., the Dalitz plot density for three-body decays or the polarization amplitudes for vector-vector final states) is required in addition to the total branching fraction.

The large yields of $b \rightarrow c$ decays to multibody final states make them ideal to study the spectroscopy of both open and hidden charm hadrons. In particular, they have been used to both discover, and measure the properties of, exotic particles such as the $X(3872)$ [587,588], $Z(4430)^+$ [589,590] and $P_c(4450)^+$ [591] states. The large yields available similarly make decays involving $b \rightarrow c$ transitions very useful to study baryon-antibaryon pair production.

In addition to the dominant b -hadron decays to final states containing charmed hadrons, there are several decays in this category that are expected to be highly suppressed in the Standard Model. These are of interest to probe particular decay topologies (e.g., the $B^- \rightarrow D_s^- \phi$ decay, which is dominated by the annihilation diagram) and thereby constrain effects in other hadronic decays or to search for new physics. There are also other decays involving $b \rightarrow c$ transitions, such as $\bar{B}^0 \rightarrow D_s^- \pi^+$, that are mediated by the W emission involving the $|V_{ub}|$ CKM matrix element. Finally, some $b \rightarrow c$ decays involving lepton flavour or number violation are extremely suppressed in the Standard Model, and therefore provide highly sensitive null tests.

In this section, we give an exhaustive list of measured branching ratios of decay modes to hadrons containing charm quarks. The averaging procedure follows the methodology described in Sect. 2. Where available, correlations between measurements are taken into account. If an insignificant measurement and a limit for the same parameter are provided the former is taken so that it can be included in averages. The confidence level of an average is quoted if it is below 1%. We provide averages of the polarization amplitudes of B meson decays to vector-vector states, but we do not currently provide detailed averages of quantities obtained from Dalitz plot analyses, due to the complications arising from the dependence on the model used.

The results are presented in subsections organized according to the type of decaying bottom hadron: \bar{B}^0 (Sect. 6.1), B^- (Sect. 6.2), \bar{B}^0/B^- admixture (Sect. 6.3), \bar{B}_s^0 (Sect. 6.4), B_c^- (Sect. 6.5), b baryons (Sect. 6.6). For each subsection the measurements are arranged according to the final state into the following groups: a single charmed meson, two charmed mesons, a charmonium state, a charm baryon, or other states, like for example the $X(3872)$ meson. The individual measurements and averages are shown as numerical values in tables followed by a graphical representation of the averages. The symbol \mathcal{B} is used for branching ratios, f for production fractions (see Sect. 3), and σ for cross sections. The decay amplitudes for longitudinal, parallel, and perpendicular transverse polarization in pseudoscalar to vector-vector decays are denoted \mathcal{A}_0 , \mathcal{A}_\parallel , and \mathcal{A}_\perp , respectively, and the definitions $\delta_\parallel =$

$\arg(\mathcal{A}_\parallel/\mathcal{A}_0)$ and $\delta_\perp = \arg(\mathcal{A}_\perp/\mathcal{A}_0)$ are used for their relative phases. The inclusion of charge conjugate modes is always implied.

Following the approach used by the PDG [327], for decays that involve neutral kaons we mainly quote results in terms of final states including either a K^0 or \bar{K}^0 meson (instead of a K_S^0 or K_L^0). In some cases where the decay is not flavour-specific and the final state is not self-conjugate, the inclusion of the conjugate final state neutral kaon is implied – in fact, the flavour of the neutral kaon is never determined experimentally, and so the specification as K^0 or \bar{K}^0 simply follows the quark model expectation for the dominant decay. An exception occurs for some B_s^0 decays, specifically those to CP eigenstates, where the width difference between the mass eigenstates (see Sect. 3) means that the measured branching fraction, integrated over decay time, is specific to the studied final state [592]. Therefore it is appropriate to quote the branching fraction for, e.g., $\bar{B}_s^0 \rightarrow J/\psi K_S^0$ instead of $\bar{B}_s^0 \rightarrow J/\psi \bar{K}^0$.

Several measurements assume $\Gamma(\Upsilon(4S) \rightarrow B^+ B^-) = \Gamma(\Upsilon(4S) \rightarrow B^0 \bar{B}^0)$. While there is no evidence for isospin violation in $\Upsilon(4S)$ decays, deviations from this assumptions can be of the order of a few percent, see Sect. 3.1.1 and Ref. [593]. As the effect is negligible for many averages, we do not apply a correction or additional systematic uncertainty, but we point out that it can be relevant for averages with a percent level uncertainty.

6.1 Decays of \bar{B}^0 mesons

Measurements of \bar{B}^0 decays to charmed hadrons are summarized in Sects. 6.1.1–6.1.5.

6.1.1 Decays to a single open charm meson

Averages of \bar{B}^0 decays to a single open charm meson are shown in Tables 93, 94, 95, 96, 97, 98, 99, 100, 101, 102, 103, 104, 105 and Figs. 68, 69, 70, 71, 72, 73, 74, 75, 76, 77, 78, 79, 80. In this section D^{**} refers to the sum of all the non-strange charm meson states with masses in the range 2.2–2.8 GeV/ c^2 .

Table 93 Decays to a $D^{(*)}$ meson and one or more pions I [10^{-3}]

Parameter	Measurements	Average
$\mathcal{B}(\bar{B}^0 \rightarrow D^+\pi^-)$	BABAR [594]: $2.55 \pm 0.05 \pm 0.16$	2.65 ± 0.15
	BABAR [595]: $3.03 \pm 0.23 \pm 0.23$	
$\mathcal{B}(\bar{B}^0 \rightarrow D^*(2010)^+\pi^-)$	BABAR [594]: $2.79 \pm 0.08 \pm 0.17$	2.84 ± 0.16
	BABAR [595]: $2.99 \pm 0.23 \pm 0.24$	
$\mathcal{B}(\bar{B}^0 \rightarrow D^*(2010)^+\pi^-\pi^+\pi^-)$	Belle [596]: $6.81 \pm 0.23 \pm 0.72$	7.19 ± 0.30
	BABAR [597]: $7.26 \pm 0.11 \pm 0.31$	
$\mathcal{B}(\bar{B}^0 \rightarrow D^*(2007)^0\pi^-\pi^+\pi^-\pi^+)$	Belle [596]: $2.60 \pm 0.47 \pm 0.37$	2.60 ± 0.60
$\mathcal{B}(\bar{B}^0 \rightarrow D^*(2010)^+\pi^-\pi^+\pi^-\pi^+\pi^-)$	Belle [596]: $4.72 \pm 0.59 \pm 0.71$	4.72 ± 0.92
$\mathcal{B}(\bar{B}^0 \rightarrow D^*(2010)^+\omega(782)\pi^-)$	Belle [598]: $2.31 \pm 0.11 \pm 0.14$	2.41 ± 0.16
	BABAR [599]: $2.88 \pm 0.21 \pm 0.31$	

Table 94 Decays to a $D^{(*)}$ meson and one or more pions II [10^{-4}]

Parameter	Measurements	Average
$\mathcal{B}(\bar{B}^0 \rightarrow D^0\pi^0)$	Belle [600]: $2.25 \pm 0.14 \pm 0.35$	2.62 ± 0.15
	BABAR [601]: $2.69 \pm 0.09 \pm 0.13$	
$\mathcal{B}(\bar{B}^0 \rightarrow D^*(2007)^0\pi^0)$	Belle [600]: $1.39 \pm 0.18 \pm 0.26$	2.23 ± 0.22 CL = $0.2^0/_{00}$
	BABAR [601]: $3.05 \pm 0.14 \pm 0.28$	
$\mathcal{B}(\bar{B}^0 \rightarrow D^0\pi^+\pi^-)$	LHCb [602]: $8.46 \pm 0.14 \pm 0.49$	8.42 ± 0.49
	Belle [603]: $8.0 \pm 0.6 \pm 1.5$	8.42 ± 0.49
$\mathcal{B}(\bar{B}^0 \rightarrow D^*(2007)^0\pi^+\pi^-)$	Belle [603]: $6.2 \pm 1.2 \pm 1.8$	6.2 ± 2.2

Table 95 Decays to a $D^{(*)0}$ meson and a light meson [10^{-4}]

Parameter	Measurements	Average
$\mathcal{B}(\bar{B}^0 \rightarrow D^0\rho(770)^0)$	Belle [603]: $2.9 \pm 1.0 \pm 0.4$	2.9 ± 1.1
$\mathcal{B}(\bar{B}^0 \rightarrow D^*(2007)^0\rho(770)^0)$	Belle [603]: <5.1	<5.1
$\mathcal{B}(\bar{B}^0 \rightarrow D^0\eta)$	Belle [600]: $1.77 \pm 0.16 \pm 0.21$	2.36 ± 0.13
	BABAR [601]: $2.53 \pm 0.09 \pm 0.11$	
$\mathcal{B}(\bar{B}^0 \rightarrow D^*(2007)^0\eta)$	Belle [600]: $1.40 \pm 0.28 \pm 0.26$	2.26 ± 0.22 CL = $5.8^0/_{00}$
	BABAR [601]: $2.69 \pm 0.14 \pm 0.23$	
$\mathcal{B}(\bar{B}^0 \rightarrow D^0\eta'(958))$	Belle [604]: $1.14 \pm 0.20^{+0.10}_{-0.13}$	1.38 ± 0.12
	BABAR [601]: $1.48 \pm 0.13 \pm 0.07$	
$\mathcal{B}(\bar{B}^0 \rightarrow D^*(2007)^0\eta'(958))$	Belle [604]: $1.21 \pm 0.34 \pm 0.22$	1.40 ± 0.22
	BABAR [601]: $1.48 \pm 0.22 \pm 0.13$	
$\mathcal{B}(\bar{B}^0 \rightarrow D^0\omega(782))$	LHCb [602]: $2.81 \pm 0.72^{+0.30}_{-0.33}$	2.54 ± 0.16
	Belle [600]: $2.37 \pm 0.23 \pm 0.28$	
	BABAR [601]: $2.57 \pm 0.11 \pm 0.14$	
$\mathcal{B}(\bar{B}^0 \rightarrow D^*(2007)^0\omega(782))$	Belle [600]: $2.29 \pm 0.39 \pm 0.40$	3.64 ± 0.35 CL = $1.8^0/_{00}$
	BABAR [601]: $4.55 \pm 0.24 \pm 0.39$	$1.61^{+0.22}_{-0.21}$
$\mathcal{B}(\bar{B}^0 \rightarrow D^0f_2(1270))$	LHCb [602]: $1.61 \pm 0.11^{+0.19}_{-0.18}$	

Table 96 Decays to a $D^{(*)+}$ meson and one or more kaons [10^{-3}]

Parameter	Measurements	Average
$\mathcal{B}(\bar{B}^0 \rightarrow D^+ K^-)$	LHCb [47]: $0.220 \pm 0.003 \pm 0.013$ Belle [605]: $0.204 \pm 0.045 \pm 0.034$	0.219 ± 0.013
$\mathcal{B}(\bar{B}^0 \rightarrow D^*(2010)^+ K^-)$	Belle [605]: $0.204 \pm 0.041 \pm 0.023$	0.204 ± 0.047
$\mathcal{B}(\bar{B}^0 \rightarrow D^+ K^*(892)^-)$	BABAR [606]: $0.46 \pm 0.06 \pm 0.05$	0.46 ± 0.08
$\mathcal{B}(\bar{B}^0 \rightarrow D^*(2010)^+ K^*(892)^-)$	BABAR [606]: $0.32 \pm 0.06 \pm 0.03$	0.32 ± 0.07
$\mathcal{B}(\bar{B}^0 \rightarrow D^+ K^0 \pi^-)$	BABAR [606]: $0.49 \pm 0.07 \pm 0.05$	0.49 ± 0.09
$\mathcal{B}(\bar{B}^0 \rightarrow D^*(2010)^+ K^0 \pi^-)$	BABAR [606]: $0.30 \pm 0.07 \pm 0.03$	0.30 ± 0.08
$\mathcal{B}(\bar{B}^0 \rightarrow D^+ K^- K^0)$	Belle [607]: <0.31	<0.31
$\mathcal{B}(\bar{B}^0 \rightarrow D^*(2010)^+ K^- K^0)$	Belle [607]: <0.47	<0.47
$\mathcal{B}(\bar{B}^0 \rightarrow D^+ K^- K^*(892)^0)$	Belle [607]: $0.88 \pm 0.11 \pm 0.15$	0.88 ± 0.19
$\mathcal{B}(\bar{B}^0 \rightarrow D^*(2010)^+ K^- K^*(892)^0)$	Belle [607]: $1.29 \pm 0.22 \pm 0.25$	1.29 ± 0.33

Table 97 Decays to a $D^{(*)0}$ meson and a kaon [10^{-4}]

Parameter	Measurements	Average
$\mathcal{B}(\bar{B}^0 \rightarrow D^0 \bar{K}^0)$	Belle [608]: $0.50^{+0.13}_{-0.12} \pm 0.06$ BABAR [609]: $0.53 \pm 0.07 \pm 0.03$	0.52 ± 0.07
$\mathcal{B}(\bar{B}^0 \rightarrow D^*(2007)^0 \bar{K}^0)$	Belle [608]: <0.66 BABAR [609]: $0.36 \pm 0.12 \pm 0.03$	0.36 ± 0.12
$\mathcal{B}(\bar{B}^0 \rightarrow D^0 K^- \pi^+)$	BABAR [610]: $0.88 \pm 0.15 \pm 0.09$	0.88 ± 0.17
$\mathcal{B}(\bar{B}^0 \rightarrow D^0 \bar{K}^*(892)^0)$	Belle [608]: $0.48^{+0.11}_{-0.10} \pm 0.05$ BABAR [609]: $0.40 \pm 0.07 \pm 0.03$	0.42 ± 0.06
$\mathcal{B}(\bar{B}^0 \rightarrow D^0 \bar{K}^*(892)^0) \times \mathcal{B}(\bar{K}^*(892)^0 \rightarrow K^- \pi^+)$	BABAR [610]: $0.38 \pm 0.06 \pm 0.04$	0.38 ± 0.07
$\mathcal{B}(\bar{B}^0 \rightarrow D^*(2007)^0 \bar{K}^*(892)^0)$	Belle [608]: <0.69	<0.69
$\mathcal{B}(\bar{B}^0 \rightarrow \bar{D}^*(2007)^0 \bar{K}^*(892)^0)$	Belle [608]: <0.40	<0.40
$\mathcal{B}(\bar{B}^0 \rightarrow \bar{D}^0 K^- \pi^+)$	BABAR [610]: <0.19	<0.19
$\mathcal{B}(\bar{B}^0 \rightarrow \bar{D}^0 \bar{K}^*(892)^0)$	Belle [608]: <0.18 BABAR [609]: $0.00 \pm 0.05 \pm 0.03$	0.00 ± 0.06

Table 98 Decays to a $D_s^{(*)}$ meson [10^{-4}]

Parameter	Measurements	Average
$\mathcal{B}(\bar{B}^0 \rightarrow D_s^- \pi^+)$	Belle [611]: $0.199 \pm 0.026 \pm 0.018$ BABAR [612]: $0.25 \pm 0.04 \pm 0.02$	0.216 ± 0.026
$\mathcal{B}(\bar{B}^0 \rightarrow D_s^{*-} \pi^+)$	Belle [613]: $0.175 \pm 0.034 \pm 0.020$ BABAR [612]: $0.26^{+0.05}_{-0.04} \pm 0.02$	0.207 ± 0.032
$\mathcal{B}(\bar{B}^0 \rightarrow D_s^- \rho(770)^+)$	BABAR [612]: $0.11^{+0.09}_{-0.08} \pm 0.03$	$0.11^{+0.09}_{-0.09}$
$\mathcal{B}(\bar{B}^0 \rightarrow D_s^{*-} \rho(770)^+)$	BABAR [612]: $0.41^{+0.13}_{-0.12} \pm 0.04$	$0.41^{+0.14}_{-0.13}$
$\mathcal{B}(\bar{B}^0 \rightarrow D_s^- a_0(980)^+)$	BABAR [614]: $0.06^{+0.14}_{-0.11} \pm 0.01$	$0.06^{+0.14}_{-0.11}$
$\mathcal{B}(\bar{B}^0 \rightarrow D_s^{*-} a_0(980)^+)$	BABAR [614]: $0.14^{+0.21}_{-0.16} \pm 0.03$	$0.14^{+0.21}_{-0.16}$
$\mathcal{B}(\bar{B}^0 \rightarrow D_s^- a_2(1320)^+)$	BABAR [614]: $0.64^{+1.04}_{-0.57} \pm 0.15$	$0.64^{+1.05}_{-0.59}$
$\mathcal{B}(\bar{B}^0 \rightarrow D_s^{*-} a_2(1320)^+)$	BABAR [614]: <2.0	<2.0
$\mathcal{B}(\bar{B}^0 \rightarrow D_s^+ K^-)$	Belle [611]: $0.191 \pm 0.024 \pm 0.017$ BABAR [612]: $0.29 \pm 0.04 \pm 0.02$	0.221 ± 0.025
$\mathcal{B}(\bar{B}^0 \rightarrow D_s^{*+} K^-)$	Belle [613]: $0.202 \pm 0.033 \pm 0.022$ BABAR [612]: $0.24 \pm 0.04 \pm 0.02$	0.219 ± 0.031
$\mathcal{B}(\bar{B}^0 \rightarrow D_s^+ K^*(892)^-)$	BABAR [612]: $0.35^{+0.10}_{-0.09} \pm 0.04$	$0.35^{+0.11}_{-0.10}$
$\mathcal{B}(\bar{B}^0 \rightarrow D_s^{*+} K^*(892)^-)$	BABAR [612]: $0.32^{+0.14}_{-0.12} \pm 0.04$	$0.32^{+0.15}_{-0.13}$
$\mathcal{B}(\bar{B}^0 \rightarrow D_s^+ K_S^0 \pi^-)$	BABAR [615]: $0.55 \pm 0.13 \pm 0.10$	0.55 ± 0.17
$\mathcal{B}(\bar{B}^0 \rightarrow D_s^{*+} K^0 \pi^-)$	BABAR [615]: <0.55	<0.55

Table 99 Relative decay rates I

Parameter	Measurements	Average
$\mathcal{B}(\bar{B}^0 \rightarrow D^0 \rho(770)^0) / \mathcal{B}(\bar{B}^0 \rightarrow D^0 \omega(782))$	Belle [603]: 1.6 ± 0.8	1.6 ± 0.8
$\mathcal{B}(\bar{B}^0 \rightarrow D^+ \pi^+ \pi^- \pi^-) / \mathcal{B}(\bar{B}^0 \rightarrow D^+ \pi^-)$	LHCb [616]: $2.38 \pm 0.11 \pm 0.21$	2.38 ± 0.24
$\mathcal{B}(\bar{B}^0 \rightarrow D^*(2010)^+ \pi^-) / \mathcal{B}(\bar{B}^0 \rightarrow D^+ \pi^-)$	BABAR [595]: $0.99 \pm 0.11 \pm 0.08$	0.99 ± 0.14
$\mathcal{B}(\bar{B}^0 \rightarrow D^{*+} \pi^-) / \mathcal{B}(\bar{B}^0 \rightarrow D^+ \pi^-)$	BABAR [595]: $0.77 \pm 0.22 \pm 0.29$	0.77 ± 0.36
$\mathcal{B}(\bar{B}^0 \rightarrow D_s^+ K^- \pi^+ \pi^-) / \mathcal{B}(\bar{B}_s^0 \rightarrow D_s^+ K^- \pi^+ \pi^-)$	LHCb [617]: $0.54 \pm 0.07 \pm 0.07$	0.54 ± 0.10

Table 100 Relative decay rates II

Parameter	Measurements	Average
$\mathcal{B}(\bar{B}^0 \rightarrow D^0 K^- \pi^+) / \mathcal{B}(\bar{B}^0 \rightarrow D^0 \pi^- \pi^+)$	LHCb [618]: $0.106 \pm 0.007 \pm 0.008$	0.106 ± 0.011
$\mathcal{B}(\bar{B}^0 \rightarrow \bar{D}^0 K^- K^+) / \mathcal{B}(\bar{B}^0 \rightarrow \bar{D}^0 \pi^- \pi^+)$	LHCb [619]: $0.056 \pm 0.110 \pm 0.007$	0.056 ± 0.110
$\mathcal{B}(\bar{B}^0 \rightarrow D^+ K^-) / \mathcal{B}(\bar{B}^0 \rightarrow D^+ \pi^-)$	LHCb [47]: $0.0822 \pm 0.0011 \pm 0.0025$ Belle [605]: $0.068 \pm 0.015 \pm 0.007$	0.0818 ± 0.0027
$\mathcal{B}(\bar{B}^0 \rightarrow D^+ K^- \pi^+ \pi^-) / \mathcal{B}(\bar{B}^0 \rightarrow D^+ \pi^+ \pi^- \pi^-)$	LHCb [620]: $0.059 \pm 0.011 \pm 0.005$	0.059 ± 0.012
$\mathcal{B}(\bar{B}^0 \rightarrow D^*(2010)^+ K^-) / \mathcal{B}(\bar{B}^0 \rightarrow D^*(2010)^+ \pi^-)$	Belle [605]: $0.074 \pm 0.015 \pm 0.006$ BABAR [610]: $0.0776 \pm 0.0034 \pm 0.0029$	0.0773 ± 0.0043
$\mathcal{B}(\bar{B}^0 \rightarrow D_s^+ K^-) / \mathcal{B}(\bar{B}^0 \rightarrow D^+ \pi^-)$	LHCb [621]: $0.0129 \pm 0.0005 \pm 0.0008$	0.0129 ± 0.0009

Table 101 Absolute product decay rates to excited D mesons I [10^{-4}]

Parameter	Measurements	Average
$\mathcal{B}(\bar{B}^0 \rightarrow D_1(2420)^+ \pi^-) \times \mathcal{B}(D_1(2420)^+ \rightarrow D^+ \pi^- \pi^+)$	Belle [622]: $0.89 \pm 0.15^{+0.17}_{-0.31}$	$0.89^{+0.23}_{-0.34}$
$\mathcal{B}(\bar{B}^0 \rightarrow D_1^0(H)\omega(782)) \times \mathcal{B}(D_1^0(H) \rightarrow D^*(2010)^+ \pi^-)$	BABAR [599]: $4.1 \pm 1.2 \pm 1.1$	4.1 ± 1.6

Table 102 Absolute product decay rates to excited D mesons II [10^{-5}]

Parameter	Measurements	Average
$\mathcal{B}(\bar{B}^0 \rightarrow D_1(2420)^+ \pi^-) \times \mathcal{B}(D_1(2420)^+ \rightarrow D^*(2010)^+ \pi^- \pi^+)$	Belle [622]: <3.3	<3.3
$\mathcal{B}(\bar{B}^0 \rightarrow D_2^*(2460)^+ \pi^-) \times \mathcal{B}(D_2^*(2460)^+ \rightarrow D^*(2010)^+ \pi^- \pi^+)$	Belle [622]: <2.4	<2.4
$\mathcal{B}(\bar{B}^0 \rightarrow D_2^*(2460)^+ K^-) \times \mathcal{B}(D_2^*(2460)^+ \rightarrow D^0 \pi^+)$	BABAR [610]: $1.83 \pm 0.40 \pm 0.31$	1.83 ± 0.51
$\mathcal{B}(\bar{B}^0 \rightarrow D_{sJ}(2460)^- \pi^+) \times \mathcal{B}(D_{sJ}(2460)^- \rightarrow D_s^- \gamma)$	Belle [623]: <0.40	<0.40
$\mathcal{B}(\bar{B}^0 \rightarrow D_{sJ}^+(2460) K^-) \times \mathcal{B}(D_{sJ}^+(2460) \rightarrow D_s^+ \gamma)$	Belle [623]: <0.94	<0.94
$\mathcal{B}(\bar{B}^0 \rightarrow D_{sJ}^*(2317)^- \pi^+) \times \mathcal{B}(D_{sJ}^*(2317)^- \rightarrow D_s^- \pi^0)$	Belle [623]: <2.5	<2.5
$\mathcal{B}(\bar{B}^0 \rightarrow D_{sJ}^*(2317)^+ K^-) \times \mathcal{B}(D_{sJ}^*(2317)^+ \rightarrow D_s^+ \pi^0)$	Belle [623]: $5.3^{+1.5}_{-1.3} \pm 1.6$	$5.3^{+2.2}_{-2.0}$

Table 103 Absolute and relative decay rates to excited D mesons [10^{-2}]

Parameter	Measurements	Average
$\mathcal{B}(\bar{B}^0 \rightarrow D^{*+} \pi^-)$	BABAR [595]: $0.234 \pm 0.065 \pm 0.088$	0.234 ± 0.109
$[\mathcal{B}(\bar{B}^0 \rightarrow D_1^+ \pi^-) \times \mathcal{B}(D_1^+ \rightarrow D^+ \pi^+ \pi^-)] / \mathcal{B}(\bar{B}^0 \rightarrow D^+ \pi^+ \pi^- \pi^-)$	LHCb [616]: $2.1 \pm 0.5^{+0.3}_{-0.5}$	$2.1^{+0.6}_{-0.7}$

Table 104 Baryonic decays I [10^{-4}]

Parameter	Measurements	Average
$\mathcal{B}(\bar{B}^0 \rightarrow D^+ p \bar{p} \pi^-)$	BABAR [624]: $3.32 \pm 0.10 \pm 0.29$	3.32 ± 0.31
$\mathcal{B}(\bar{B}^0 \rightarrow D^*(2010)^+ p \bar{p} \pi^-)$	BABAR [624]: $4.55 \pm 0.16 \pm 0.39$	4.55 ± 0.42
$\mathcal{B}(\bar{B}^0 \rightarrow D^0 p \bar{p} \pi^- \pi^+)$	BABAR [624]: $2.99 \pm 0.21 \pm 0.45$	2.99 ± 0.50
$\mathcal{B}(\bar{B}^0 \rightarrow D^*(2007)^0 p \bar{p} \pi^- \pi^+)$	BABAR [624]: $1.91 \pm 0.36 \pm 0.29$	1.91 ± 0.46

Table 105 Baryonic decays II [10^{-5}]

Parameter	Measurements	Average
$\mathcal{B}(\bar{B}^0 \rightarrow D^0 p \bar{p})$	Belle [625]: $11.8 \pm 1.5 \pm 1.6$ BABAR [624]: $10.2 \pm 0.4 \pm 0.6$	10.4 ± 0.7
$\mathcal{B}(\bar{B}^0 \rightarrow D^*(2007)^0 p \bar{p})$	Belle [625]: $12.0^{+3.3}_{-2.9} \pm 2.1$ BABAR [624]: $9.7 \pm 0.7 \pm 0.9$	9.9 ± 1.1
$\mathcal{B}(\bar{B}^0 \rightarrow D_s^+ \Lambda \bar{p})$	Belle [626]: $2.9 \pm 0.7 \pm 0.6$	2.9 ± 0.9
$\mathcal{B}(\bar{B}^0 \rightarrow D^0 \Lambda^0 \bar{\Lambda}^0)$	Belle [627]: $1.05^{+0.57}_{-0.44} \pm 0.14$ BABAR [628]: $0.98^{+0.29}_{-0.26} \pm 0.19$	1.00 ± 0.28
$\mathcal{B}(\bar{B}^0 \rightarrow D^0 \Sigma^0 \bar{\Lambda} + \bar{B}^0 \rightarrow D^0 \Lambda \bar{\Sigma}^0)$	BABAR [628]: $1.5^{+0.9}_{-0.8} \pm 0.3$	$1.5^{+0.9}_{-0.9}$
$\mathcal{B}(\bar{B}^0 \rightarrow D^+ \Lambda \bar{p})$	Belle [629]: $3.36 \pm 0.63 \pm 0.44$	3.36 ± 0.77
$\mathcal{B}(\bar{B}^0 \rightarrow D^{*+} \Lambda \bar{p})$	Belle [629]: $2.51 \pm 0.26 \pm 0.35$	2.51 ± 0.44

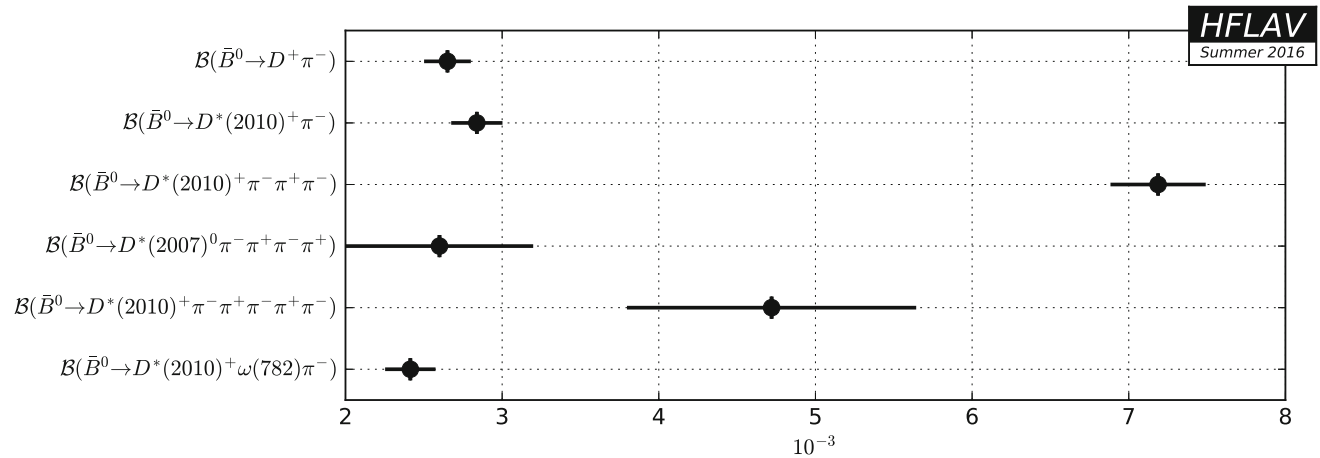


Fig. 68 Summary of the averages from Table 93

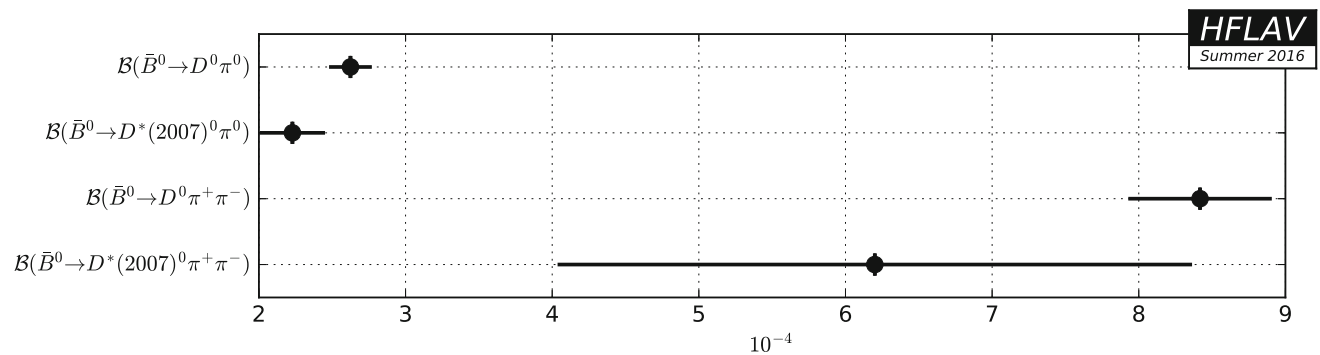


Fig. 69 Summary of the averages from Table 94

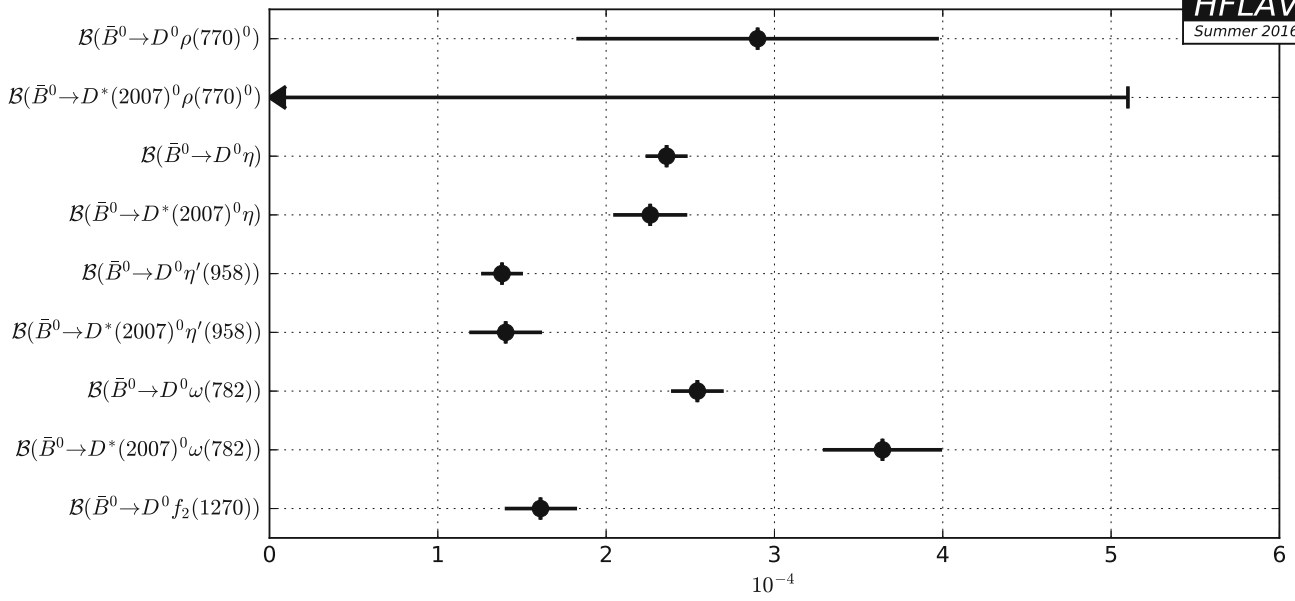


Fig. 70 Summary of the averages from Table 95

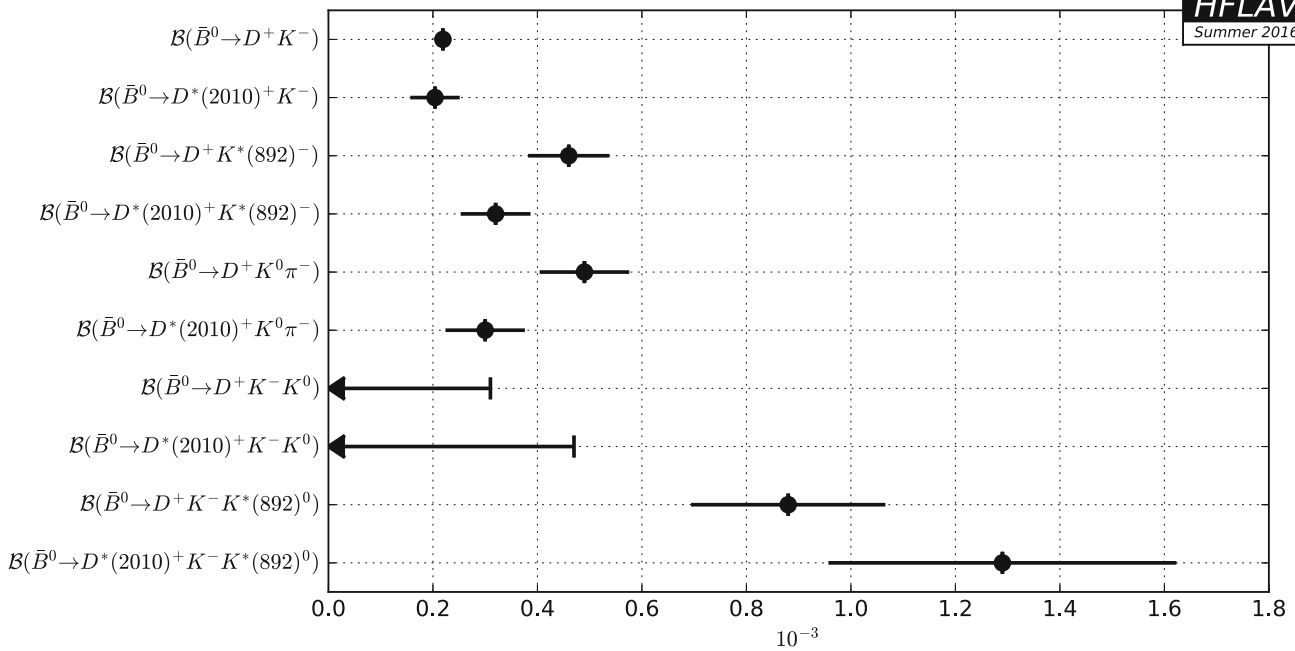


Fig. 71 Summary of the averages from Table 96

HFLAV
Summer 2016

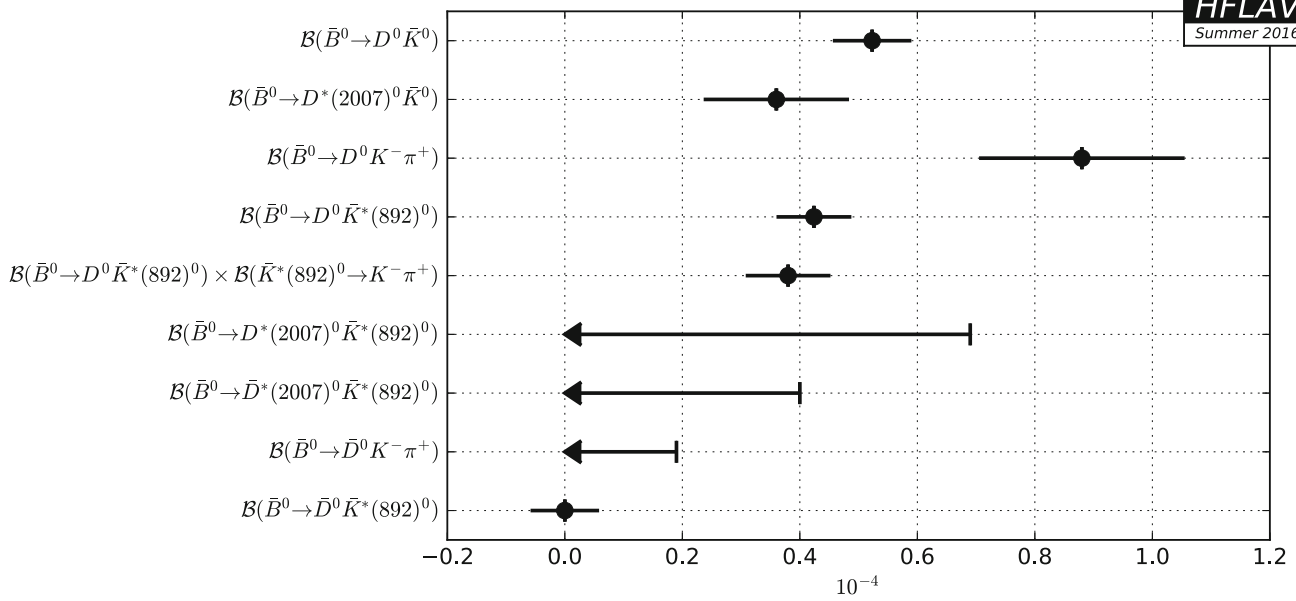


Fig. 72 Summary of the averages from Table 97

HFLAV
Summer 2016

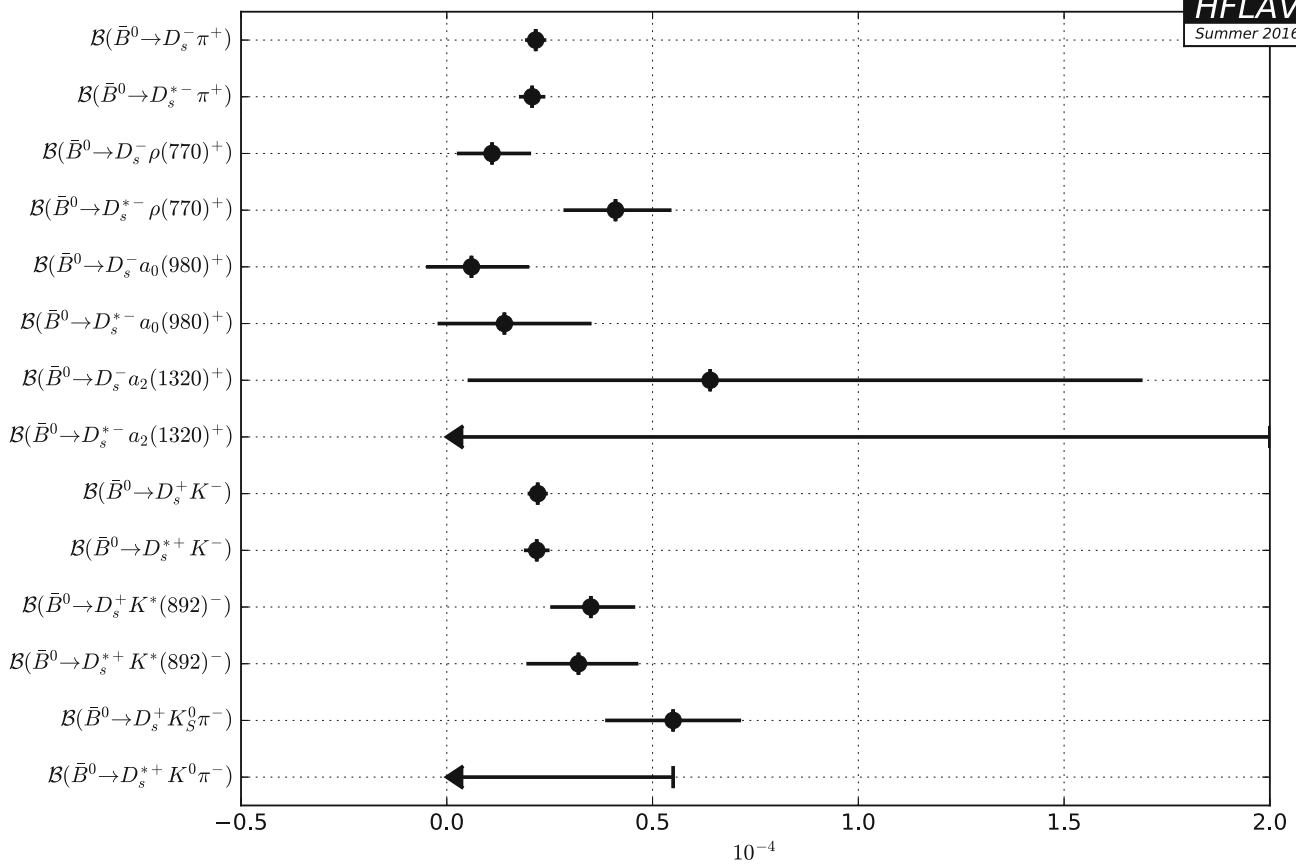


Fig. 73 Summary of the averages from Table 98

HFLAV
Summer 2016

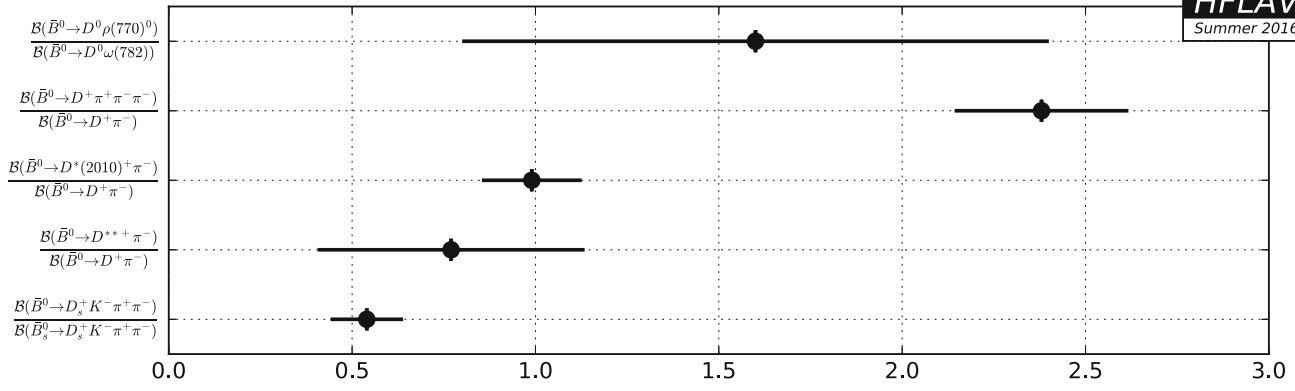


Fig. 74 Summary of the averages from Table 99

HFLAV
Summer 2016

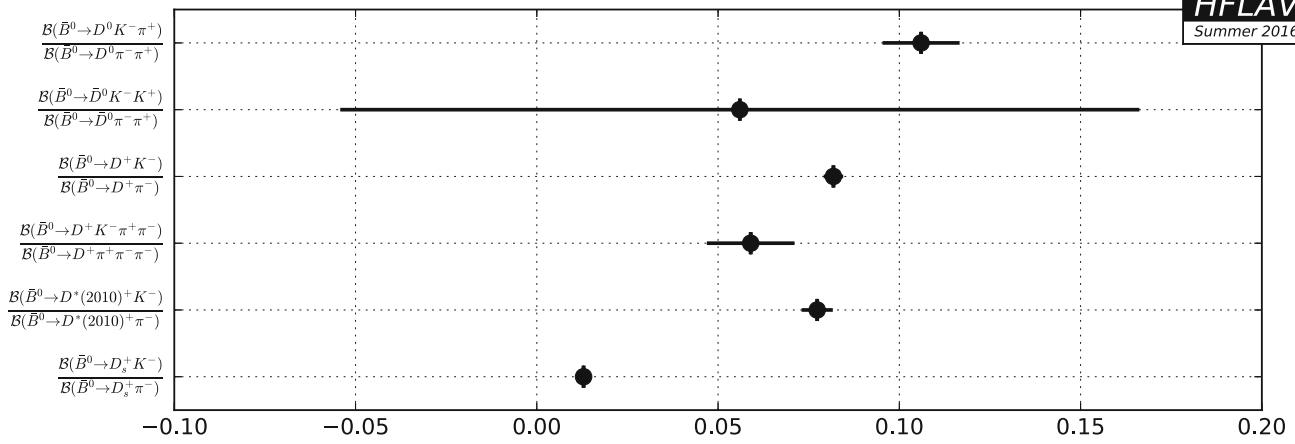


Fig. 75 Summary of the averages from Table 100

HFLAV
Summer 2016

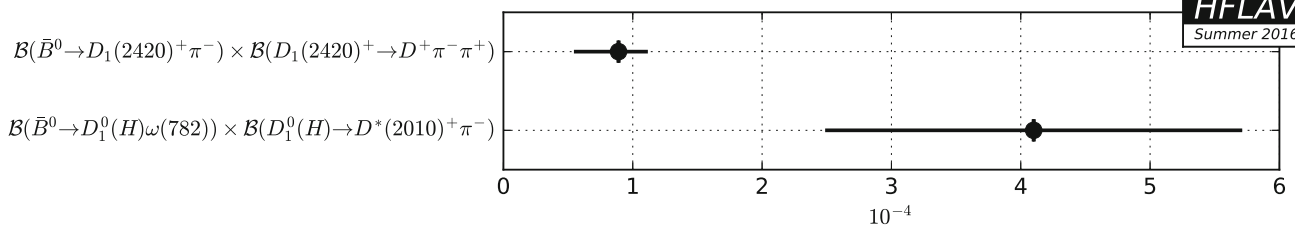


Fig. 76 Summary of the averages from Table 101

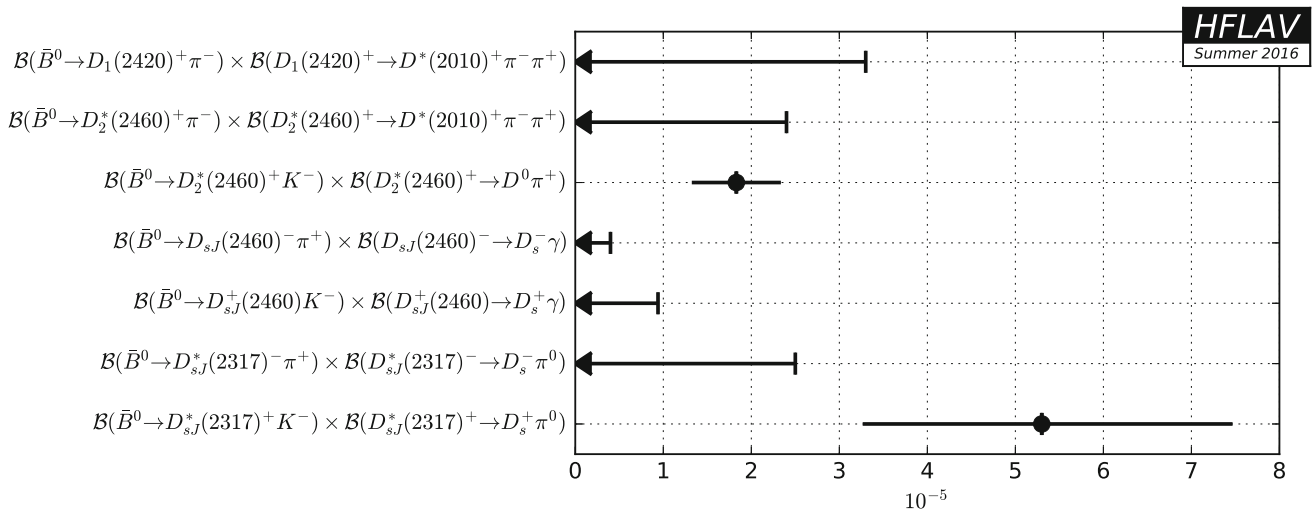


Fig. 77 Summary of the averages from Table 102

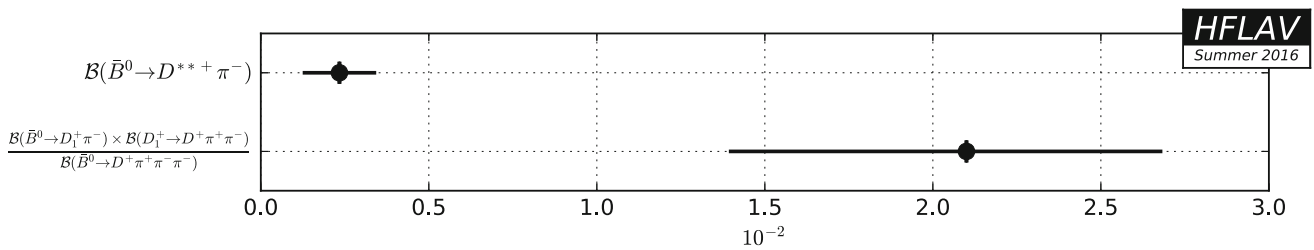


Fig. 78 Summary of the averages from Table 103

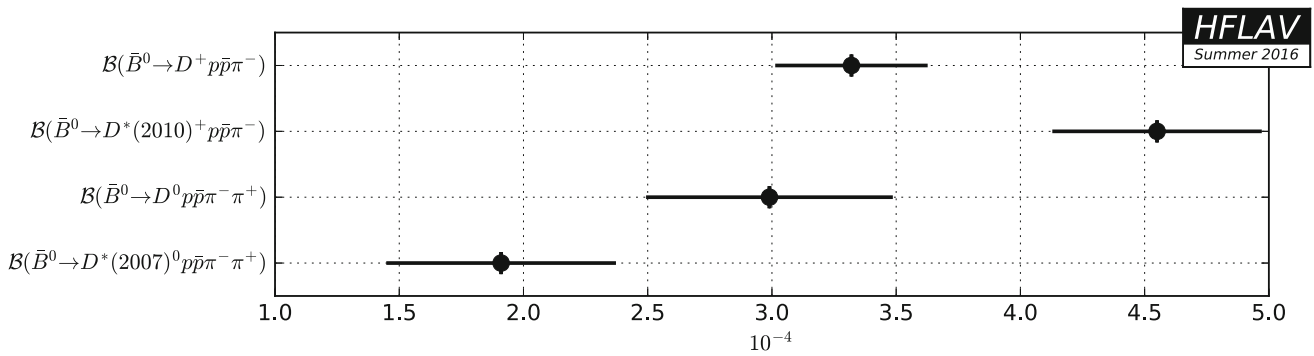


Fig. 79 Summary of the averages from Table 104

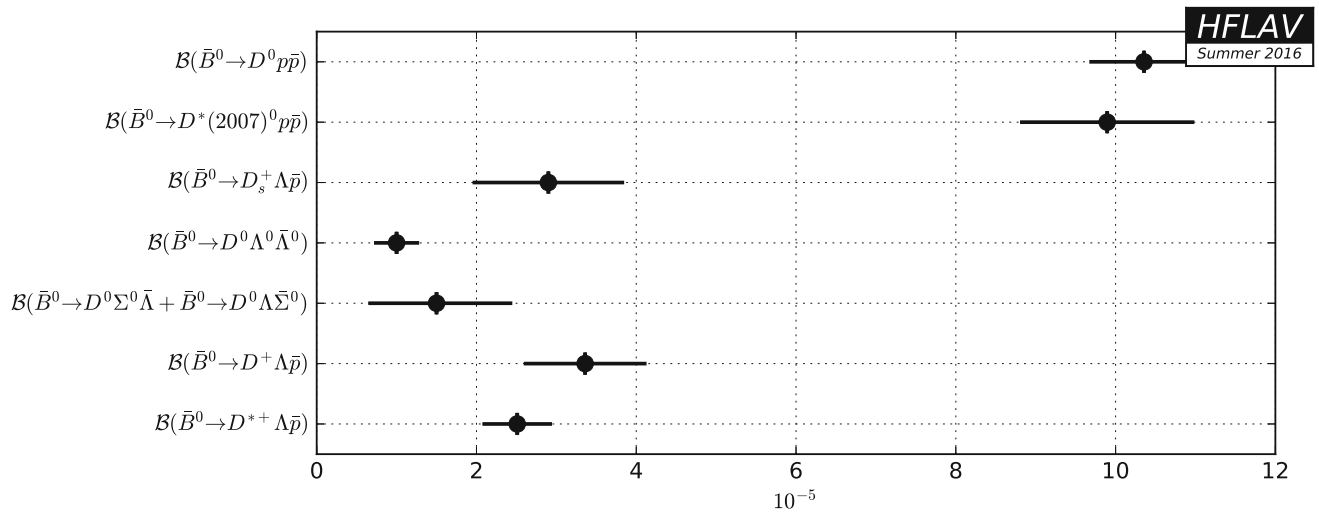


Fig. 80 Summary of the averages from Table 105

6.1.2 Decays to two open charm mesons

Averages of \bar{B}^0 decays to two open charm mesons are shown in Tables 106, 107, 108, 109, 110, 111, 112, 113, 114, 115 and Figs. 81, 82, 83, 84, 85, 86, 87, 88, 89.

Table 106 Decays to $D^{(*)+} D^{(*)-}$ [10^{-3}]

Parameter	Measurements	Average
$\mathcal{B}(\bar{B}^0 \rightarrow D^+ D^-)$	Belle [287]: $0.212 \pm 0.016 \pm 0.018$ BABAR [630]: $0.28 \pm 0.04 \pm 0.05$	0.220 ± 0.023
$\mathcal{B}(\bar{B}^0 \rightarrow D^*(2010)^- D^+)$	Belle [287]: $0.614 \pm 0.029 \pm 0.050$ BABAR [630]: $0.57 \pm 0.07 \pm 0.07$	0.603 ± 0.050
$\mathcal{B}(\bar{B}^0 \rightarrow D^*(2010)^- D^*(2010)^+)$	Belle [352]: $0.782 \pm 0.038 \pm 0.060$ BABAR [630]: $0.81 \pm 0.06 \pm 0.10$	0.790 ± 0.061
$\mathcal{B}(\bar{B}^0 \rightarrow D^0 \bar{D}^0)$	Belle [631]: <0.043 BABAR [630]: <0.06	<0.043
$\mathcal{B}(\bar{B}^0 \rightarrow D^0 \bar{D}^*(2007)^0)$	BABAR [630]: <0.29	<0.29
$\mathcal{B}(\bar{B}^0 \rightarrow D^*(2007)^0 \bar{D}^*(2007)^0)$	BABAR [630]: <0.09	<0.09

Table 107 Decays to two D mesons and a kaon I [10^{-3}]

Parameter	Measurements	Average
$\mathcal{B}(\bar{B}^0 \rightarrow D^*(2010)^+ D^- \bar{K}^0)$	BABAR [632]: $6.41 \pm 0.36 \pm 0.39$	6.41 ± 0.53
$\mathcal{B}(\bar{B}^0 \rightarrow D^*(2010)^- D^*(2010)^+ \bar{K}^0)$	BABAR [632]: $8.26 \pm 0.43 \pm 0.67$	8.26 ± 0.80
$\mathcal{B}(\bar{B}^0 \rightarrow D^*(2010)^+ D^*(2010)^- K_S^0)$	Belle [266]: $3.4 \pm 0.4 \pm 0.7$ BABAR [265]: $4.4 \pm 0.4 \pm 0.7$	3.9 ± 0.6
$\mathcal{B}(\bar{B}^0 \rightarrow D^*(2010)^+ \bar{D}^0 K^-)$	BABAR [632]: $2.47 \pm 0.10 \pm 0.18$	2.47 ± 0.21
$\mathcal{B}(\bar{B}^0 \rightarrow D^+ \bar{D}^*(2007)^0 K^-)$	BABAR [632]: $3.46 \pm 0.18 \pm 0.37$	3.46 ± 0.41
$\mathcal{B}(\bar{B}^0 \rightarrow D^*(2010)^+ \bar{D}^*(2007)^0 K^-)$	BABAR [632]: $10.6 \pm 0.3 \pm 0.9$	10.6 ± 0.9
$\mathcal{B}(\bar{B}^0 \rightarrow D^0 \bar{D}^*(2007)^0 \bar{K}^0)$	BABAR [632]: $1.08 \pm 0.32 \pm 0.36$	1.08 ± 0.48
$\mathcal{B}(\bar{B}^0 \rightarrow D^*(2007)^0 \bar{D}^*(2007)^0 \bar{K}^0)$	BABAR [632]: $2.40 \pm 0.55 \pm 0.67$	2.40 ± 0.87

Table 108 Decays to two D mesons and a kaon II [10^{-4}]

Parameter	Measurements	Average
$\mathcal{B}(\bar{B}^0 \rightarrow D^+ D^- \bar{K}^0)$	BABAR [632]: $7.5 \pm 1.2 \pm 1.2$	7.5 ± 1.7
$\mathcal{B}(\bar{B}^0 \rightarrow D^+ \bar{D}^0 K^-)$	BABAR [632]: $10.7 \pm 0.7 \pm 0.9$	10.7 ± 1.1
$\mathcal{B}(\bar{B}^0 \rightarrow D^0 \bar{D}^0 \bar{K}^0)$	BABAR [632]: $2.7 \pm 1.0 \pm 0.5$	2.7 ± 1.1
$\mathcal{B}(\bar{B}^0 \rightarrow D^0 \bar{D}^0 \pi^0 \bar{K}^0)$	Belle [633]: $1.73 \pm 0.70^{+0.31}_{-0.53}$	$1.73^{+0.77}_{-0.88}$

Table 109 Decays to $D_s^{(*)-} D^{(*)+}$ I [10^{-3}]

Parameter	Measurements	Average
$\mathcal{B}(\bar{B}^0 \rightarrow D_s^- D^+)$	Belle [634]: $7.5 \pm 0.2 \pm 1.1$ BABAR [635]: $9.0 \pm 1.8 \pm 1.4$	7.8 ± 1.0
$\mathcal{B}(\bar{B}^0 \rightarrow D_s^- D^*(2010)^+)$	BABAR [635]: $5.7 \pm 1.6 \pm 0.9$ BABAR [636]: $10.3 \pm 1.4 \pm 2.9$	6.8 ± 1.6
$\mathcal{B}(\bar{B}^0 \rightarrow D_s^{*-} D^*(2010)^+)$	BABAR [635]: $16.5 \pm 2.3 \pm 1.9$ BABAR [637]: $18.8 \pm 0.9 \pm 1.7$ BABAR [636]: $19.7 \pm 1.5 \pm 5.7$	18.1 ± 1.6
$\mathcal{B}(\bar{B}^0 \rightarrow D_s^{*-} D^+)$	BABAR [635]: $6.7 \pm 2.0 \pm 1.1$	6.7 ± 2.3

Table 110 Decays to $D_s^{(*)-} D^{(*)+}$ II [10^{-4}]

Parameter	Measurements	Average
$\mathcal{B}(\bar{B}^0 \rightarrow D_s^- D^+) \times \mathcal{B}(D_s^- \rightarrow \phi(1020)\pi^-)$	BABAR [635]: $2.67 \pm 0.61 \pm 0.47$	2.67 ± 0.77
$\mathcal{B}(\bar{B}^0 \rightarrow D_s^- D^*(2010)^+) \times \mathcal{B}(D_s^- \rightarrow \phi(1020)\pi^-)$	BABAR [635]: $5.11 \pm 0.94 \pm 0.72$	5.11 ± 1.18
$\mathcal{B}(\bar{B}^0 \rightarrow D_s^{*-} D^+) \times \mathcal{B}(D_s^- \rightarrow \phi(1020)\pi^-)$	BABAR [635]: $4.14 \pm 1.19 \pm 0.94$	4.14 ± 1.52
$\mathcal{B}(\bar{B}^0 \rightarrow D_s^{*-} D^*(2010)^+) \times \mathcal{B}(D_s^- \rightarrow \phi(1020)\pi^-)$	BABAR [635]: $12.2 \pm 2.2 \pm 2.2$	12.2 ± 3.1

Table 111 Decays to $D_s^{(*)+} D_s^{(*)-}$ [10^{-3}]

Parameter	Measurements	Average
$\mathcal{B}(\bar{B}^0 \rightarrow D_s^- D_s^+)$	Belle [634]: <0.036 BABAR [638]: <0.10	<0.036
$\mathcal{B}(\bar{B}^0 \rightarrow D_s^- D_s^{*+})$	BABAR [638]: <0.13	<0.13
$\mathcal{B}(\bar{B}^0 \rightarrow D_s^{*+} D_s^{*-})$	BABAR [638]: <0.24	<0.24

Table 112 Relative decay rates [10^{-3}]

Parameter	Measurements	Average
$\mathcal{B}(\bar{B}^0 \rightarrow D^0 \bar{D}^0) / \mathcal{B}(\bar{B}^- \rightarrow D^0 \bar{D}_s^-)$	LHCb [639]: $1.4 \pm 0.6 \pm 0.2$	1.4 ± 0.6

Table 113 Absolute decay rates to excited D_s mesons [10^{-3}]

Parameter	Measurements	Average
$\mathcal{B}(\bar{B}^0 \rightarrow D_{sJ}(2460)^- D^+)$	BABAR [635]: $2.6 \pm 1.5 \pm 0.7$	2.6 ± 1.7
$\mathcal{B}(\bar{B}^0 \rightarrow D_{sJ}(2460)^- D^*(2010)^+)$	BABAR [635]: $8.8 \pm 2.0 \pm 1.4$	8.8 ± 2.4
$\mathcal{B}(\bar{B}^0 \rightarrow D_{s1}(2536)^- D^*(2010)^+)$	BABAR [265]: $92 \pm 24 \pm 1$	92 ± 24

Table 114 Product decay rates to excited D_s mesons I [10^{-3}]

Parameter	Measurements	Average
$\mathcal{B}(\bar{B}^0 \rightarrow D^+ D_{sJ}(2460)^-) \times \mathcal{B}(D_{sJ}(2460)^- \rightarrow D_s^- \gamma)$	Belle [640]: $0.82^{+0.22}_{-0.19} \pm 0.25$ BABAR [641]: $0.8 \pm 0.2^{+0.3}_{-0.2}$	0.81 ± 0.23
$\mathcal{B}(\bar{B}^0 \rightarrow D^+ D_{sJ}(2460)^-) \times \mathcal{B}(D_{sJ}(2460)^- \rightarrow D_s^{*-} \pi^0)$	Belle [640]: $2.27^{+0.73}_{-0.62} \pm 0.68$ BABAR [641]: $2.8 \pm 0.8^{+1.1}_{-0.8}$	2.47 ± 0.76
$\mathcal{B}(\bar{B}^0 \rightarrow D_{sJ}(2460)^- D^*(2010)^+) \times \mathcal{B}(D_{sJ}(2460)^- \rightarrow D_s^{*-} \pi^0)$	BABAR [641]: $5.5 \pm 1.2^{+2.1}_{-1.6}$	$5.5^{+2.5}_{-2.0}$
$\mathcal{B}(\bar{B}^0 \rightarrow D_{sJ}(2460)^- D^*(2010)^+) \times \mathcal{B}(D_{sJ}(2460)^- \rightarrow D_s^- \gamma)$	BABAR [641]: $2.3 \pm 0.3^{+0.9}_{-0.6}$	$2.3^{+0.9}_{-0.7}$
$\mathcal{B}(\bar{B}^0 \rightarrow D_{sJ}^*(2317)^- D^*(2010)^+) \times \mathcal{B}(D_{sJ}^*(2317)^- \rightarrow D_s^- \pi^0)$	BABAR [641]: $1.5 \pm 0.4^{+0.5}_{-0.4}$	$1.5^{+0.7}_{-0.5}$
$\mathcal{B}(\bar{B}^0 \rightarrow D^+ D_{sJ}^*(2317)^-) \times \mathcal{B}(D_{sJ}^*(2317)^- \rightarrow D_s^- \pi^0)$	Belle [642]: $1.02^{+0.13}_{-0.12} \pm 0.11$ BABAR [641]: $1.8 \pm 0.4^{+0.7}_{-0.5}$	1.03 ± 0.16
$\mathcal{B}(\bar{B}^0 \rightarrow D^+ D_{sJ}^*(2317)^-) \times \mathcal{B}(D_{sJ}^*(2317)^- \rightarrow D_s^{*-} \gamma)$	Belle [640]: <0.95	<0.95

Table 115 Product decay rates to excited D_s mesons II [10^{-4}]

Parameter	Measurements	Average
$\mathcal{B}(\bar{B}^0 \rightarrow D_{s1}(2536)^- D^+) \times \mathcal{B}(D_{s1}(2536)^- \rightarrow D^*(2010)^- \bar{K}^0)$	BABAR [643]: $2.61 \pm 1.03 \pm 0.31$	2.61 ± 1.08
$\mathcal{B}(\bar{B}^0 \rightarrow D_{s1}(2536)^- D^+) \times \mathcal{B}(D_{s1}(2536)^- \rightarrow K^- \bar{D}^*(2007)^0)$	BABAR [643]: $1.71 \pm 0.48 \pm 0.32$	1.71 ± 0.58
$\mathcal{B}(\bar{B}^0 \rightarrow D_{s1}(2536)^- D^*(2010)^+) \times \mathcal{B}(D_{s1}(2536)^- \rightarrow D^*(2010)^- \bar{K}^0)$	BABAR [643]: $5.00 \pm 1.51 \pm 0.67$	5.00 ± 1.65
$\mathcal{B}(\bar{B}^0 \rightarrow D_{s1}(2536)^- D^*(2010)^+) \times \mathcal{B}(D_{s1}(2536)^- \rightarrow \bar{D}^*(2007)^0 K^+)$	BABAR [643]: $3.32 \pm 0.88 \pm 0.66$	3.32 ± 1.10
$\mathcal{B}(\bar{B}^0 \rightarrow D_{s1}(2536)^+ D^-) \times \mathcal{B}(D_{s1}(2536)^+ \rightarrow D^*(2007)^0 K^+ + D^*(2010)^+ K^0)$	Belle [644]: $2.75 \pm 0.62 \pm 0.36$	2.75 ± 0.72
$\mathcal{B}(\bar{B}^0 \rightarrow D_{s1}(2536)^+ D^*(2010)^-) \times \mathcal{B}(D_{s1}(2536)^+ \rightarrow D^*(2007)^0 K^+ + D^*(2010)^+ K^0)$	Belle [644]: $5.01 \pm 1.21 \pm 0.70$	5.01 ± 1.40
$\mathcal{B}(\bar{B}^0 \rightarrow D_{s1}(2536)^+ D^*(2010)^-) \times \mathcal{B}(D_{s1}(2536)^+ \rightarrow D^*(2010)^+ K_S^0)$	Belle [266]: <6.0	<6.0
$\mathcal{B}(\bar{B}^0 \rightarrow D^+ D_{sJ}(2460)^-) \times \mathcal{B}(D_{sJ}(2460)^- \rightarrow D_s^- \pi^+ \pi^-)$	Belle [640]: <2.0	<2.0
$\mathcal{B}(\bar{B}^0 \rightarrow D^+ D_{sJ}(2460)^-) \times \mathcal{B}(D_{sJ}(2460)^- \rightarrow D_s^- \pi^0)$	Belle [640]: <3.6	<3.6
$\mathcal{B}(\bar{B}^0 \rightarrow D^+ D_{sJ}(2460)^-) \times \mathcal{B}(D_{sJ}(2460)^- \rightarrow D_s^{*-} \gamma)$	Belle [640]: <6.0	<6.0

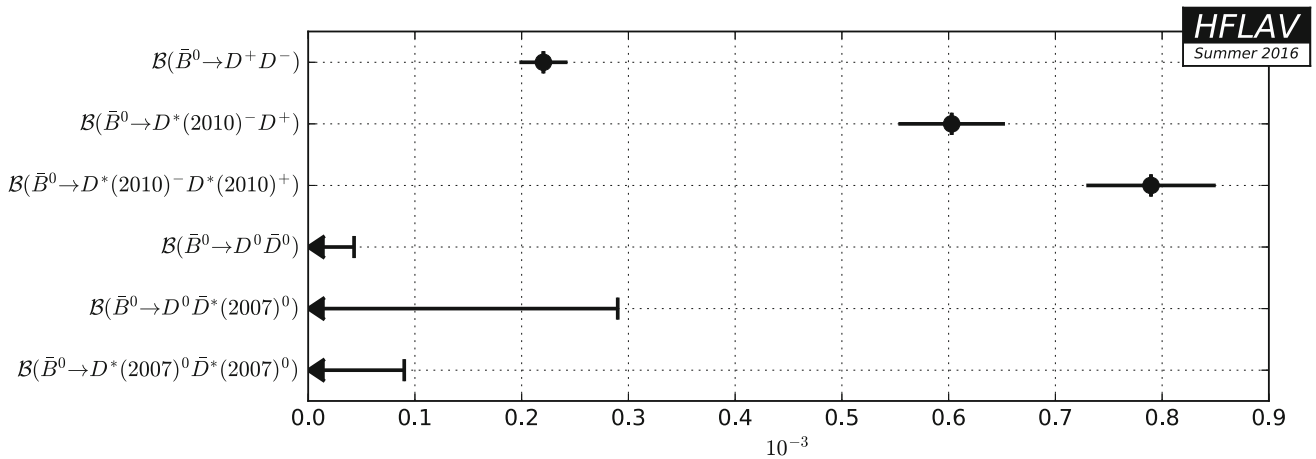


Fig. 81 Summary of the averages from Table 106

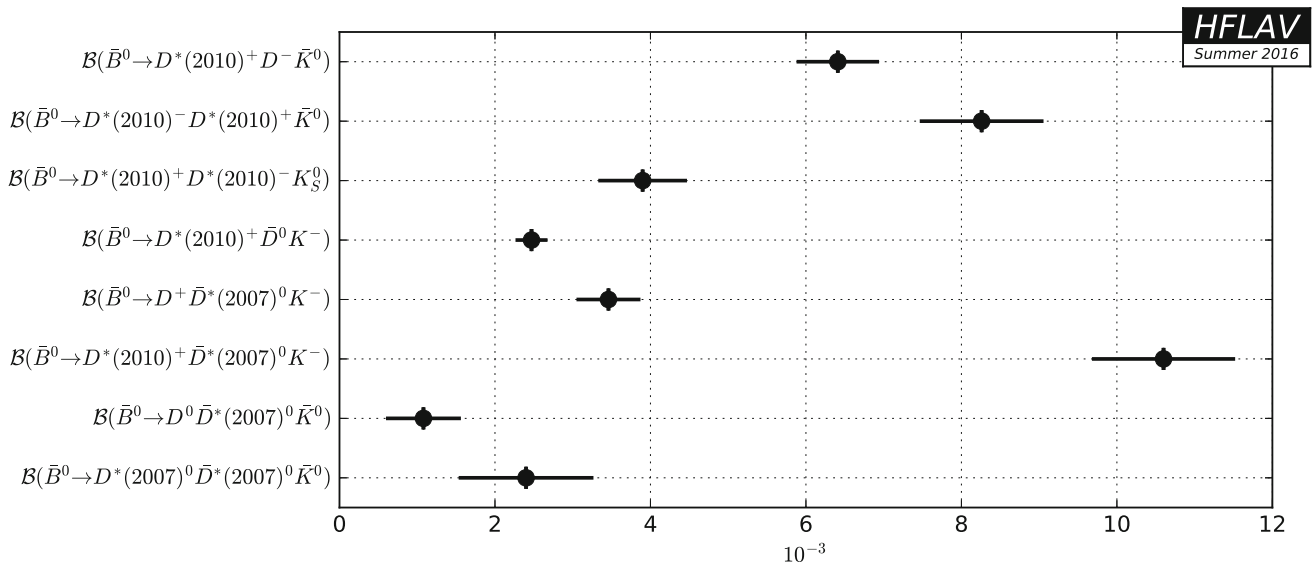


Fig. 82 Summary of the averages from Table 107

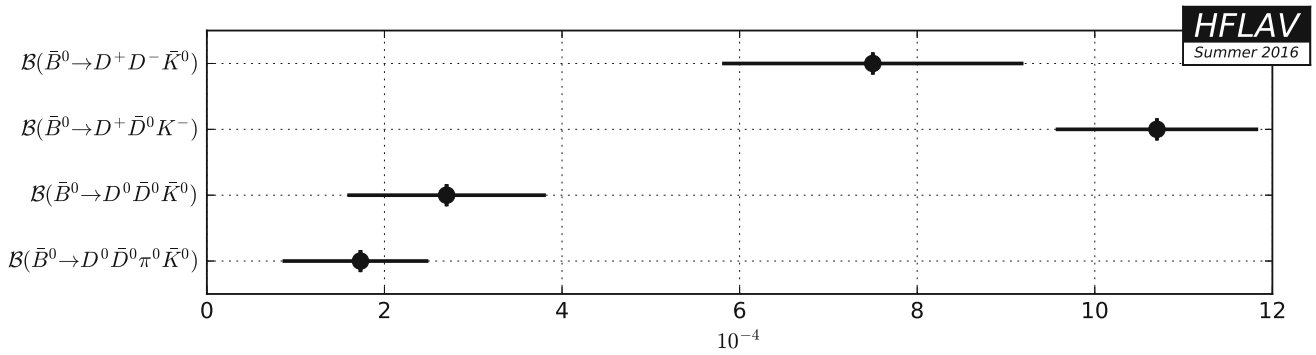


Fig. 83 Summary of the averages from Table 108

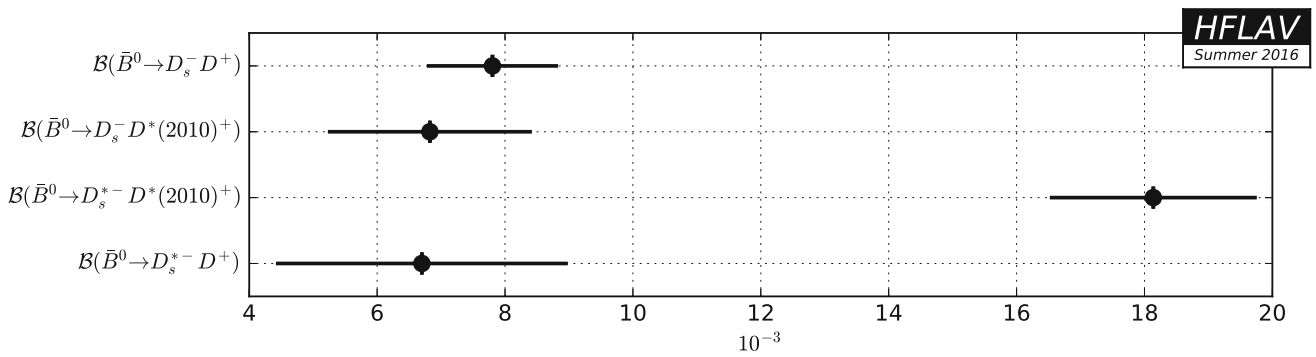


Fig. 84 Summary of the averages from Table 109

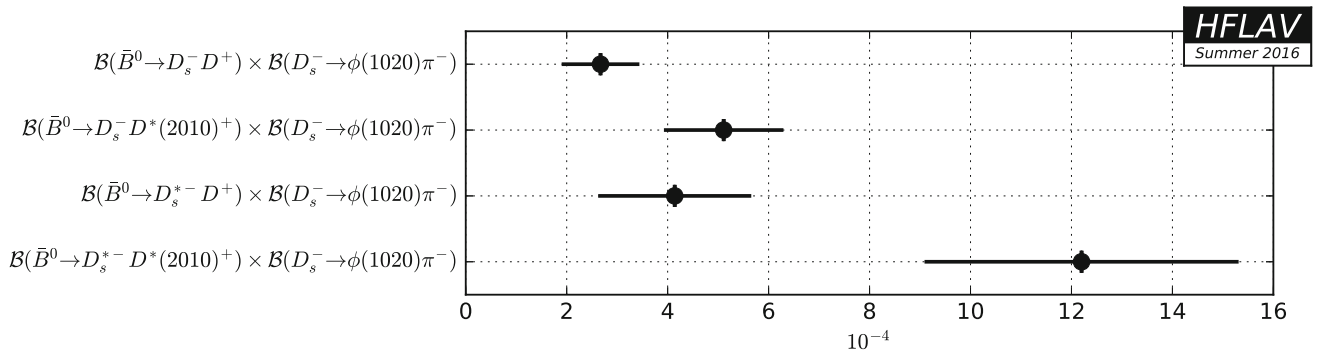


Fig. 85 Summary of the averages from Table 110

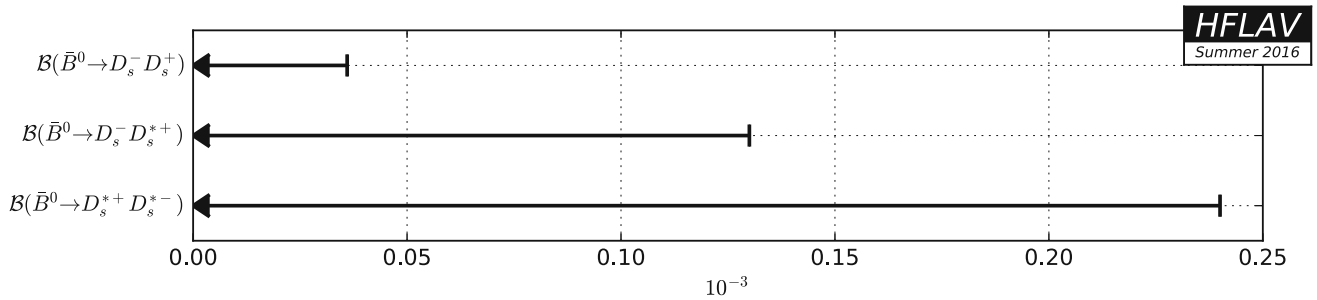


Fig. 86 Summary of the averages from Table 111

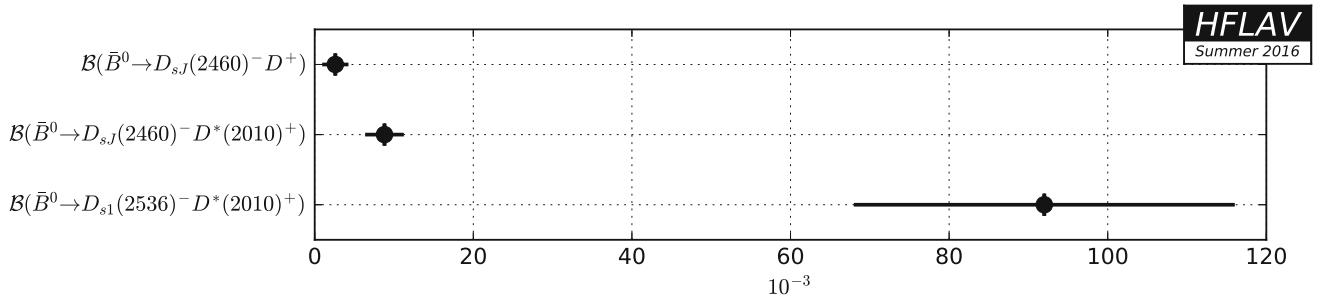


Fig. 87 Summary of the averages from Table 113

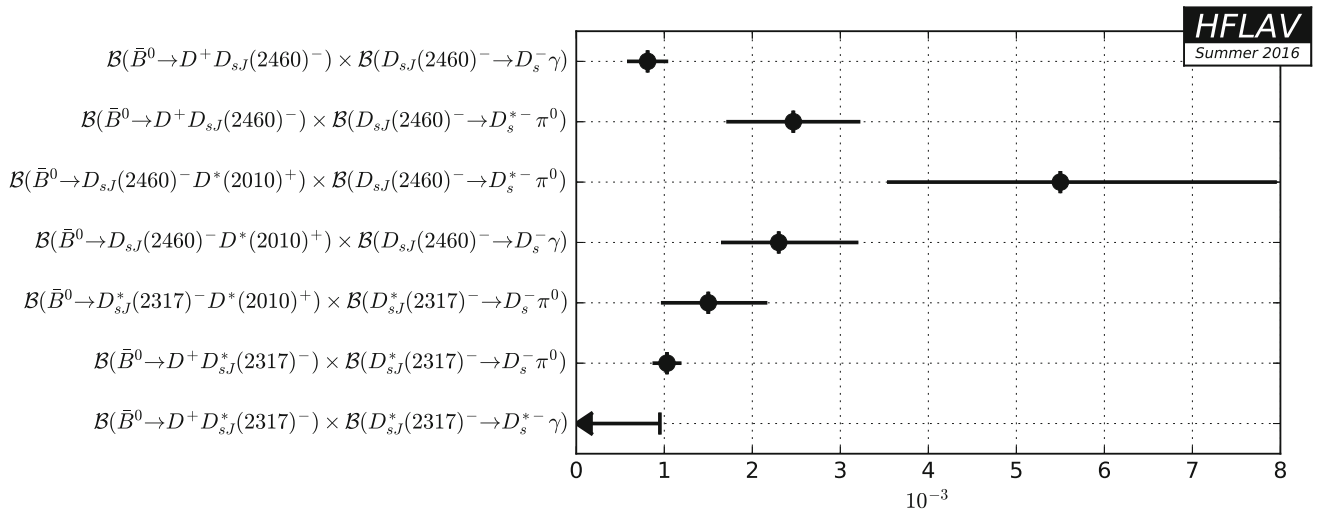


Fig. 88 Summary of the averages from Table 114

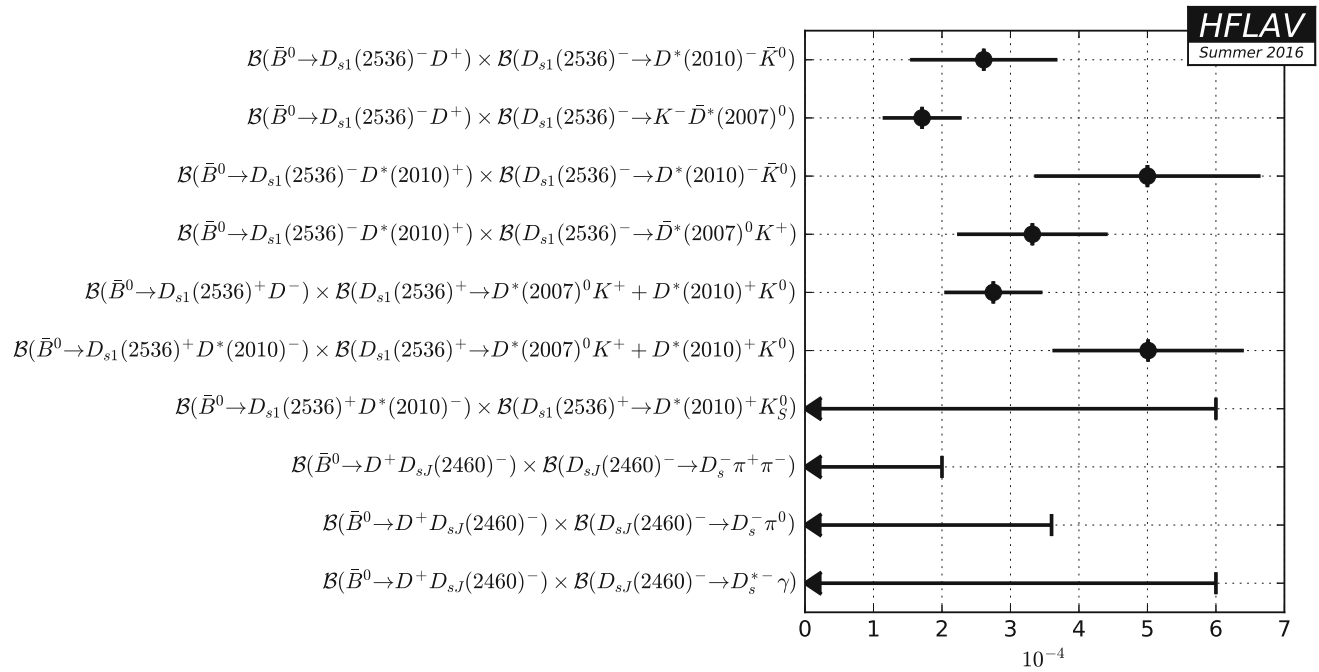


Fig. 89 Summary of the averages from Table 115

6.1.3 Decays to charmonium states

Averages of \bar{B}^0 decays to charmonium states are shown in Tables 116, 117, 118, 119, 120, 121, 122, 123, 124 and Figs. 90, 91, 92, 93, 94, 95, 96, 97, 98.

Table 116 Decays to J/ψ and one kaon [10^{-3}]

Parameter	Measurements	Average
$\mathcal{B}(\bar{B}^0 \rightarrow J/\psi \bar{K}^0)$	CDF [645]: $1.15 \pm 0.23 \pm 0.17$ Belle [646]: $0.79 \pm 0.04 \pm 0.09$ BABAR [10]: $0.869 \pm 0.022 \pm 0.030$	0.863 ± 0.035
$\mathcal{B}(\bar{B}^0 \rightarrow J/\psi K^- \pi^+)$	Belle [647]: $1.15 \pm 0.01 \pm 0.05$	1.15 ± 0.05
$\mathcal{B}(\bar{B}^0 \rightarrow J/\psi \bar{K}^*(892)^0)$	CDF [648]: $1.74 \pm 0.20 \pm 0.18$ Belle [647]: $1.19 \pm 0.01 \pm 0.08$ BABAR [10]: $1.309 \pm 0.026 \pm 0.077$	1.270 ± 0.056
$\mathcal{B}(\bar{B}^0 \rightarrow J/\psi \bar{K}^0 \pi^+ \pi^-)$	LHCb [649]: $0.430 \pm 0.030 \pm 0.037$ CDF [650]: $1.03 \pm 0.33 \pm 0.15$	0.440 ± 0.047
$\mathcal{B}(\bar{B}^0 \rightarrow J/\psi \bar{K}^0 \rho(770)^0)$	CDF [650]: $0.54 \pm 0.29 \pm 0.09$	0.54 ± 0.30
$\mathcal{B}(\bar{B}^0 \rightarrow J/\psi K^*(892)^- \pi^+)$	CDF [650]: $0.77 \pm 0.41 \pm 0.13$	0.77 ± 0.43
$\mathcal{B}(\bar{B}^0 \rightarrow J/\psi \omega(782) \bar{K}^0)$	BABAR [651]: $0.23 \pm 0.03 \pm 0.03$	0.23 ± 0.04
$\mathcal{B}(\bar{B}^0 \rightarrow J/\psi \phi(1020) \bar{K}^0)$	BABAR [652]: $0.102 \pm 0.038 \pm 0.010$	0.102 ± 0.039
$\mathcal{B}(\bar{B}^0 \rightarrow J/\psi \bar{K}_1^0(1270))$	Belle [653]: $1.30 \pm 0.34 \pm 0.31$	1.30 ± 0.46
$\mathcal{B}(\bar{B}^0 \rightarrow J/\psi \eta K_S^0)$	Belle [654]: $0.0522 \pm 0.0078 \pm 0.0049$ BABAR [655]: $0.084 \pm 0.026 \pm 0.027$	0.0540 ± 0.0089
$\mathcal{B}(\bar{B}^0 \rightarrow J/\psi \bar{K}^*(892)^0 \pi^+ \pi^-)$	CDF [650]: $0.66 \pm 0.19 \pm 0.11$	0.66 ± 0.22

Table 117 Decays to charmonium other than J/ψ and one kaon I [10^{-3}]

Parameter	Measurements	Average
$\mathcal{B}(\bar{B}^0 \rightarrow \psi(2S)\bar{K}^0)$	Belle [646]: 0.67 ± 0.11	0.655 ± 0.066
$\mathcal{B}(\bar{B}^0 \rightarrow \psi(2S)\bar{K}^*(892)^0)$	BABAR [10]: $0.646 \pm 0.065 \pm 0.051$ CDF [648]: $0.90 \pm 0.22 \pm 0.09$ BABAR [10]: $0.649 \pm 0.059 \pm 0.097$	0.696 ± 0.103
$\mathcal{B}(\bar{B}^0 \rightarrow \psi(2S)K^0)$	LHCb [649]: $0.47 \pm 0.07 \pm 0.07$	0.47 ± 0.10
$\mathcal{B}(\bar{B}^0 \rightarrow K^*(892)^0\psi(2S))$	Belle [656]: $0.552^{+0.035+0.053}_{-0.032-0.058}$	$0.552^{+0.064}_{-0.066}$
$\mathcal{B}(\bar{B}^0 \rightarrow \psi(2S)K^0) \times \mathcal{B}(\psi(2S) \rightarrow \chi_{c1}\gamma)$	Belle [657]: $0.68 \pm 0.10 \pm 0.07$	0.68 ± 0.12
$\mathcal{B}(\bar{B}^0 \rightarrow \psi(2S)K^0) \times \mathcal{B}(\psi(2S) \rightarrow \chi_{c2}\gamma)$	Belle [657]: $0.47 \pm 0.16 \pm 0.08$	0.47 ± 0.18
$\mathcal{B}(\bar{B}^0 \rightarrow \chi_{c0}\bar{K}^0)$	BABAR [658]: <1.24	<1.24
$\mathcal{B}(\bar{B}^0 \rightarrow \chi_{c0}\bar{K}^*(892)^0)$	BABAR [658]: <0.77 BABAR [659]: $0.17 \pm 0.03 \pm 0.02$	0.17 ± 0.04
$\mathcal{B}(\bar{B}^0 \rightarrow \chi_{c1}\bar{K}^0)$	Belle [660]: $0.378^{+0.017}_{-0.016} \pm 0.033$ BABAR [661]: $0.42 \pm 0.03 \pm 0.03$	0.396 ± 0.028
$\mathcal{B}(\bar{B}^0 \rightarrow \chi_{c1}K^-\pi^+)$	Belle [662]: $0.497 \pm 0.012 \pm 0.028$ BABAR [663]: $0.511 \pm 0.014 \pm 0.058$	0.500 ± 0.027
$\mathcal{B}(\bar{B}^0 \rightarrow \chi_{c1}\bar{K}^*(892)^0)$	Belle [664]: $0.31 \pm 0.03 \pm 0.07$ BABAR [661]: $0.25 \pm 0.02 \pm 0.02$	0.26 ± 0.03
$\mathcal{B}(\bar{B}^0 \rightarrow \chi_{c1}K^-\pi^+\pi^0)$	Belle [662]: $0.352 \pm 0.052 \pm 0.024$	0.352 ± 0.057
$\mathcal{B}(\bar{B}^0 \rightarrow \chi_{c1}\bar{K}^0\pi^+\pi^-)$	Belle [662]: $0.316 \pm 0.035 \pm 0.032$	0.316 ± 0.047
$\mathcal{B}(\bar{B}^0 \rightarrow \eta_c\bar{K}^0)$	Belle [665]: $1.23 \pm 0.23^{+0.40}_{-0.41}$ BABAR [666]: $0.64^{+0.22+0.28}_{-0.20-0.16}$ BABAR [667]: $1.14 \pm 0.15 \pm 0.34$	0.85 ± 0.24
$\mathcal{B}(\bar{B}^0 \rightarrow \eta_c\bar{K}^*(892)^0)$	Belle [665]: $1.62 \pm 0.32^{+0.55}_{-0.60}$ BABAR [668]: $0.57 \pm 0.06 \pm 0.09$ BABAR [666]: $0.80^{+0.21+0.37}_{-0.19-0.23}$	0.61 ± 0.10
$\mathcal{B}(\bar{B}^0 \rightarrow \eta_c(2S)\bar{K}^*(892)^0)$	BABAR [668]: <0.39	<0.39
$\mathcal{B}(\bar{B}^0 \rightarrow h_c(1P)\bar{K}^*(892)^0) \times \mathcal{B}(h_c(1P) \rightarrow \eta_c\gamma)$	BABAR [668]: <0.22	<0.22

Table 118 Decays to charmonium other than J/ψ and one kaon II [10^{-4}]

Parameter	Measurements	Average
$\mathcal{B}(\bar{B}^0 \rightarrow \psi(3770)\bar{K}^0) \times \mathcal{B}(\psi(3770) \rightarrow D^0\bar{D}^0)$	BABAR [643]: <1.23	<1.23
$\mathcal{B}(\bar{B}^0 \rightarrow \psi(3770)\bar{K}^0) \times \mathcal{B}(\psi(3770) \rightarrow D^+D^-)$	BABAR [643]: <1.88	<1.88
$\mathcal{B}(\bar{B}^0 \rightarrow \chi_{c2}\bar{K}^0)$	Belle [660]: <0.15 BABAR [661]: $0.15 \pm 0.09 \pm 0.03$	0.15 ± 0.09
$\mathcal{B}(\bar{B}^0 \rightarrow \chi_{c2}\bar{K}^*(892)^0)$	BABAR [661]: $0.66 \pm 0.18 \pm 0.05$	0.66 ± 0.19
$\mathcal{B}(\bar{B}^0 \rightarrow \chi_{c2}K^-\pi^+)$	Belle [662]: $0.72 \pm 0.09 \pm 0.05$	0.72 ± 0.10

Table 119 Decays to charmonium and light mesons I [10^{-5}]

Parameter	Measurements	Average
$\mathcal{B}(\bar{B}^0 \rightarrow J/\psi\pi^0)$	Belle [646]: $2.3 \pm 0.5 \pm 0.2$ BABAR [353]: $1.69 \pm 0.14 \pm 0.07$	1.74 ± 0.15
$\mathcal{B}(\bar{B}^0 \rightarrow J/\psi\pi^+\pi^-)$	BABAR [669]: <1.2	<1.2
$\mathcal{B}(\bar{B}^0 \rightarrow J/\psi\rho(770)^0)$	BABAR [669]: $2.7 \pm 0.3 \pm 0.2$	2.7 ± 0.4
$\mathcal{B}(\bar{B}^0 \rightarrow J/\psi\eta)$	Belle [670]: $1.23^{+0.18}_{-0.17} \pm 0.07$ BABAR [652]: <2.7	$1.23^{+0.19}_{-0.18}$
$\mathcal{B}(\bar{B}^0 \rightarrow J/\psi\eta'(958))$	Belle [670]: <0.74 BABAR [652]: <6.3	<0.74
$\mathcal{B}(\bar{B}^0 \rightarrow J/\psi f_2(1270))$	BABAR [669]: <0.46	<0.46
$\mathcal{B}(\bar{B}^0 \rightarrow J/\psi f_1(1285))$	LHCb [671]: $0.837 \pm 0.195^{+0.079}_{-0.075}$	$0.837^{+0.210}_{-0.209}$
$\mathcal{B}(\bar{B}^0 \rightarrow J/\psi K^0 K^\pm \pi^\mp)$	LHCb [649]: <2.1	<2.1
$\mathcal{B}(\bar{B}^0 \rightarrow J/\psi K^0 K^+ K^-)$	LHCb [649]: $2.02 \pm 0.43 \pm 0.19$	2.02 ± 0.47
$\mathcal{B}(\bar{B}^0 \rightarrow \chi_{c1}\pi^0)$	Belle [672]: $1.12 \pm 0.25 \pm 0.12$	1.12 ± 0.28

Table 120 Decays to charmonium and light mesons II [10^{-5}]

Parameter	Measurements	Average
$\mathcal{B}(\bar{B}^0 \rightarrow J/\psi a_0(980)) \times \mathcal{B}(a_0(980) \rightarrow K^+ K^-)$	LHCb [673]: <0.090	<0.090
$\mathcal{B}(\bar{B}^0 \rightarrow J/\psi f_0(980)) \times \mathcal{B}(f_0(980) \rightarrow \pi^+ \pi^-)$	LHCb [674]: <0.11	<0.11
$\mathcal{B}(\bar{B}^0 \rightarrow J/\psi f_1(1285)) \times \mathcal{B}(f_1(1285) \rightarrow \pi^+ \pi^- \pi^+ \pi^-)$	LHCb [671]: $0.0921 \pm 0.0214 \pm 0.0064$	0.0921 ± 0.0223
$\mathcal{B}(\bar{B}^0 \rightarrow J/\psi K^+ K^-)$	LHCb [673]: $0.253 \pm 0.031 \pm 0.019$	0.253 ± 0.036
$\mathcal{B}(\bar{B}^0 \rightarrow J/\psi\phi(1020))$	LHCb [673]: <0.019 Belle [675]: <0.094 BABAR [652]: <0.9	<0.019

Table 121 Decays to J/ψ and photons, baryons, or heavy mesons [10^{-5}]

Parameter	Measurements	Average
$\mathcal{B}(\bar{B}^0 \rightarrow J/\psi\gamma)$	LHCb [676]: <0.15 BABAR [677]: <0.16	<0.15
$\mathcal{B}(\bar{B}^0 \rightarrow J/\psi\bar{p}p)$	LHCb [678]: <0.052 Belle [679]: <0.083 BABAR [680]: <0.19	<0.052
$\mathcal{B}(\bar{B}^0 \rightarrow J/\psi D^0)$	Belle [681]: <2.0 BABAR [682]: <1.3	<1.3

Table 122 Relative decay rates I

Parameter	Measurements	Average
$\mathcal{B}(\bar{B}^0 \rightarrow J/\psi \bar{K}_1^0(1270))/\mathcal{B}(B^- \rightarrow J/\psi K^-)$	Belle [653]: $1.30 \pm 0.34 \pm 0.28$	1.30 ± 0.44
$\mathcal{B}(\bar{B}^0 \rightarrow J/\psi \bar{K}^*(892)^0)/\mathcal{B}(\bar{B}^0 \rightarrow J/\psi \bar{K}^0)$	CDF [683]: $1.39 \pm 0.36 \pm 0.10$	
	BABAR [10]: $1.51 \pm 0.05 \pm 0.08$	1.50 ± 0.09
$\mathcal{B}(\bar{B}^0 \rightarrow J/\psi \omega(782))/\mathcal{B}(\bar{B}^0 \rightarrow J/\psi \rho)$	LHCb [684]: $0.89 \pm 0.19^{+0.07}_{-0.13}$	$0.89^{+0.20}_{-0.23}$
$\mathcal{B}(\bar{B}^0 \rightarrow J/\psi \omega(782)\bar{K}^0)/\mathcal{B}(B^- \rightarrow J/\psi \omega(782)K^-)$	BABAR [651]: $0.7 \pm 0.1 \pm 0.1$	0.7 ± 0.1
$\mathcal{B}(\bar{B}^0 \rightarrow J/\psi K_S^0 \pi^- \pi^+)/\mathcal{B}(\bar{B}^0 \rightarrow J/\psi K_S^0)$	LHCb [649]: $0.493 \pm 0.034 \pm 0.027$	0.493 ± 0.043
$[\mathcal{B}(\bar{B}^0 \rightarrow \psi(2S)K_S^0) \times \mathcal{B}(\psi(2S) \rightarrow J/\psi \pi^- \pi^+)]/\mathcal{B}(\bar{B}^0 \rightarrow J/\psi K_S^0)$	LHCb [649]: $0.183 \pm 0.027 \pm 0.015$	0.183 ± 0.031
$\mathcal{B}(\bar{B}^0 \rightarrow \psi(2S)\bar{K}^*(892)^0)/\mathcal{B}(\bar{B}^0 \rightarrow \psi(2S)\bar{K}^0)$	BABAR [10]: $1.00 \pm 0.14 \pm 0.09$	1.00 ± 0.17
$\mathcal{B}(\bar{B}^0 \rightarrow \psi(2S)K(892)^{*0})/\mathcal{B}(\bar{B}^0 \rightarrow J/\psi K(892)^{*0})$	LHCb [685]: $0.476 \pm 0.014 \pm 0.016$	0.476 ± 0.021
$\mathcal{B}\bar{B}^0 \rightarrow \psi(2S)\pi^+\pi^-/\mathcal{B}\bar{B}^0 \rightarrow J/\psi \pi^+\pi^-$	LHCb [686]: $0.56 \pm 0.07 \pm 0.05$	0.56 ± 0.09
$\mathcal{B}(\bar{B}^0 \rightarrow \eta_c \bar{K}^0)/\mathcal{B}(B^- \rightarrow \eta_c K^-)$	BABAR [667]: $0.87 \pm 0.13 \pm 0.07$	0.87 ± 0.15
$\mathcal{B}(\bar{B}^0 \rightarrow \eta_c \bar{K}^0)/\mathcal{B}(\bar{B}^0 \rightarrow J/\psi \bar{K}^0)$	BABAR [667]: $1.34 \pm 0.19 \pm 0.40$	1.34 ± 0.44
$\mathcal{B}(\bar{B}^0 \rightarrow \eta_c \bar{K}^*(892)^0)/\mathcal{B}(B^- \rightarrow \eta_c K^-)$	BABAR [668]: $0.62 \pm 0.06 \pm 0.05$	0.62 ± 0.08
$\mathcal{B}(\bar{B}^0 \rightarrow \eta_c \bar{K}^*(892)^0)/\mathcal{B}(\bar{B}^0 \rightarrow \eta_c \bar{K}^0)$	Belle [665]: $1.33 \pm 0.36^{+0.24}_{-0.33}$	$1.33^{+0.43}_{-0.49}$
$\mathcal{B}(\bar{B}^0 \rightarrow \chi_{c1} K^- \pi^+)/\mathcal{B}(\bar{B}^0 \rightarrow J/\psi K^- \pi^+)$	BABAR [663]: $0.474 \pm 0.013 \pm 0.054$	0.474 ± 0.056
$\mathcal{B}(\bar{B}^0 \rightarrow \chi_{c1} \bar{K}^*(892)^0)/\mathcal{B}(\bar{B}^0 \rightarrow \chi_{c1} \bar{K}^0)$	BABAR [10]: $0.72 \pm 0.11 \pm 0.12$	0.72 ± 0.16
$[\mathcal{B}(\bar{B}^0 \rightarrow h_c(1P)\bar{K}^*(892)^0) \times \mathcal{B}(h_c(1P) \rightarrow \eta_c \gamma)]/\mathcal{B}(B^- \rightarrow \eta_c K^-)$	BABAR [668]: <0.236	<0.236

Table 123 Relative decay rates II

Parameter	Measurements	Average
$\mathcal{B}(\bar{B}^0 \rightarrow J/\psi \eta)/\mathcal{B}(\bar{B}_s^0 \rightarrow J/\psi \eta)$	LHCb [687]: $0.0185 \pm 0.0061 \pm 0.0014$	0.0185 ± 0.0063
$\mathcal{B}(\bar{B}^0 \rightarrow J/\psi \eta')/\mathcal{B}(\bar{B}_s^0 \rightarrow J/\psi \eta')$	LHCb [687]: $0.0228 \pm 0.0065 \pm 0.0016$	0.0228 ± 0.0067
$\mathcal{B}(\bar{B}^0 \rightarrow J/\psi K_S^0 K^\pm \pi^\mp)/\mathcal{B}(\bar{B}^0 \rightarrow J/\psi K_S^0 \pi^+ \pi^-)$	LHCb [649]: <0.048	<0.048
$\mathcal{B}(\bar{B}^0 \rightarrow J/\psi K_S^0 K^+ K^-)/\mathcal{B}(\bar{B}^0 \rightarrow J/\psi K_S^0 \pi^+ \pi^-)$	LHCb [649]: $0.047 \pm 0.010 \pm 0.004$	0.047 ± 0.011

Table 124 Polarization fractions

Parameter	Measurements	Average
$ \mathcal{A}_0 ^2(B^0 \rightarrow J/\psi \bar{K}^*(892)^0)/ \mathcal{A}_0 ^2(\bar{B}^0 \rightarrow J/\psi \bar{K}^*(892)^0)$	BABAR [688]: <0.32	<0.32
$ \mathcal{A}_0 ^2(\bar{B}^0 \rightarrow J/\psi K^*(892)^0)/ \mathcal{A}_0 ^2(B^0 \rightarrow J/\psi K^*(892)^0)$	BABAR [688]: <0.26	<0.26

HFLAV
Summer 2016

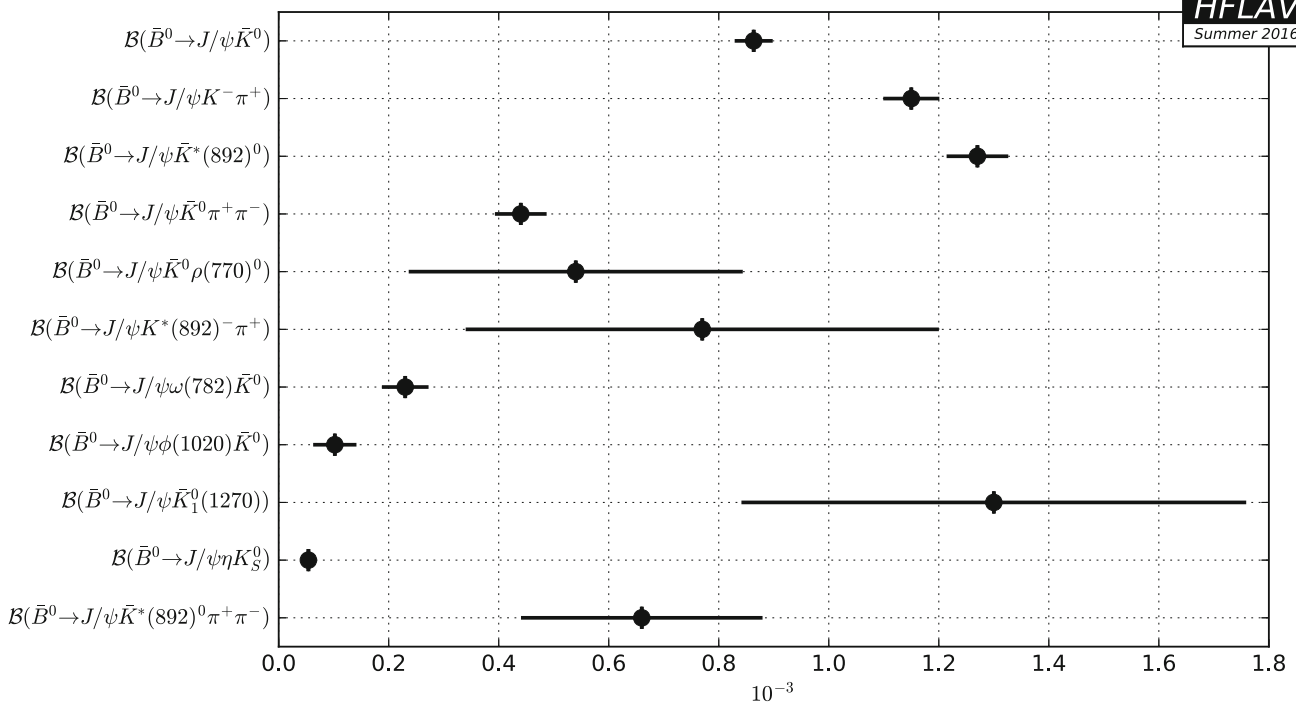


Fig. 90 Summary of the averages from Table 116

HFLAV
Summer 2016

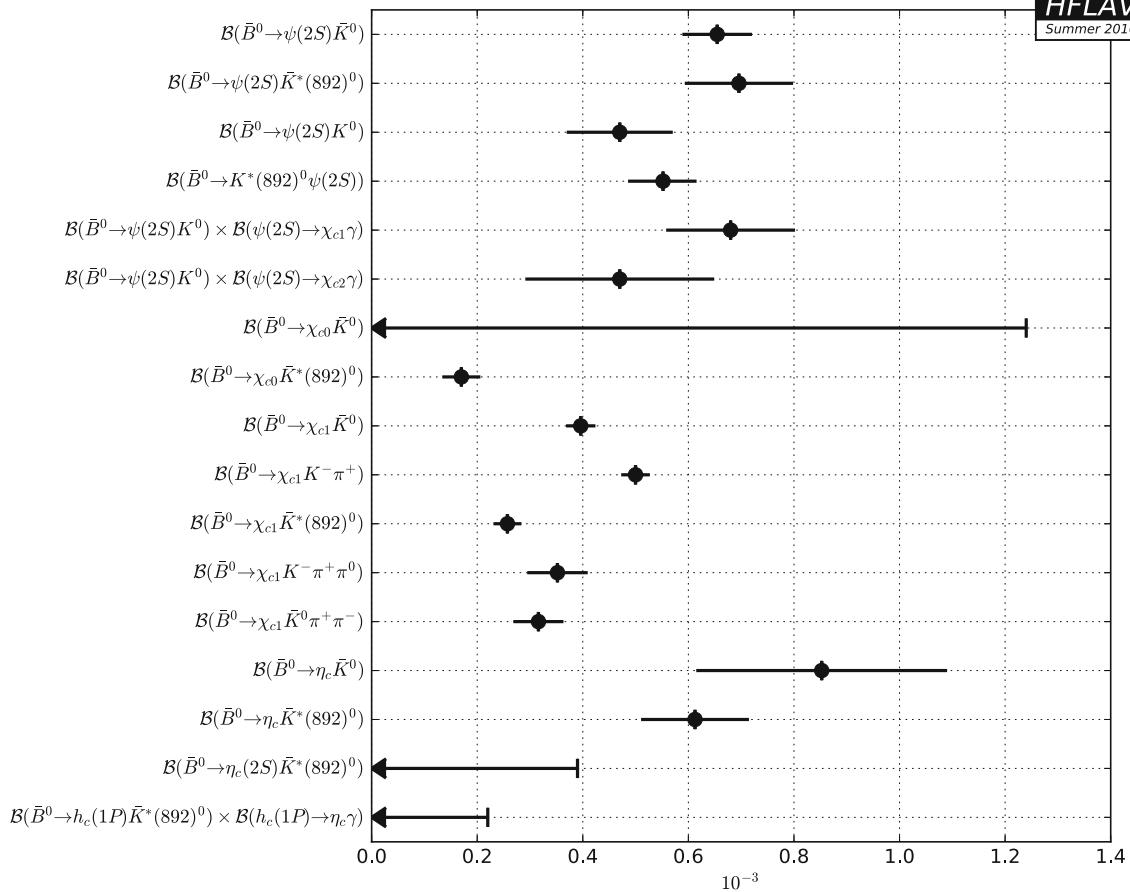


Fig. 91 Summary of the averages from Table 117

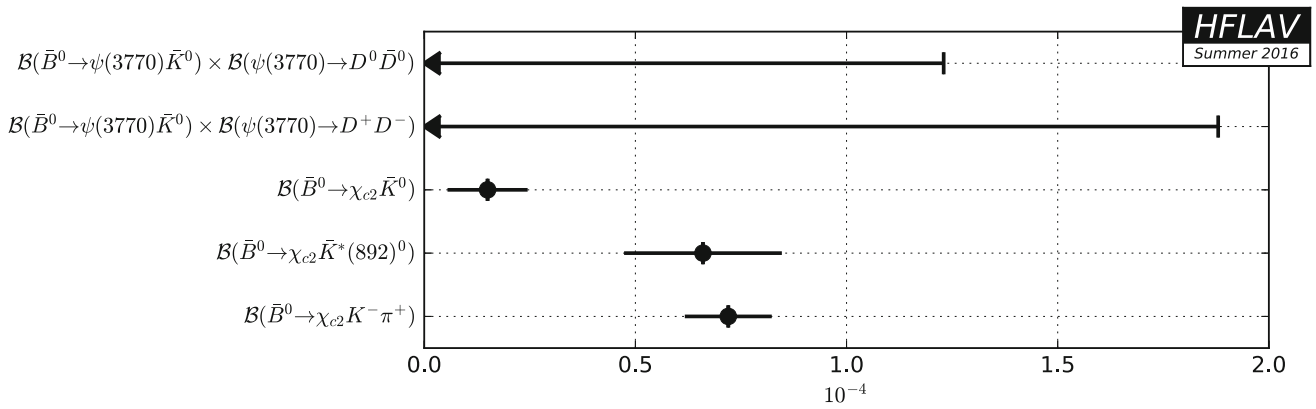


Fig. 92 Summary of the averages from Table 118

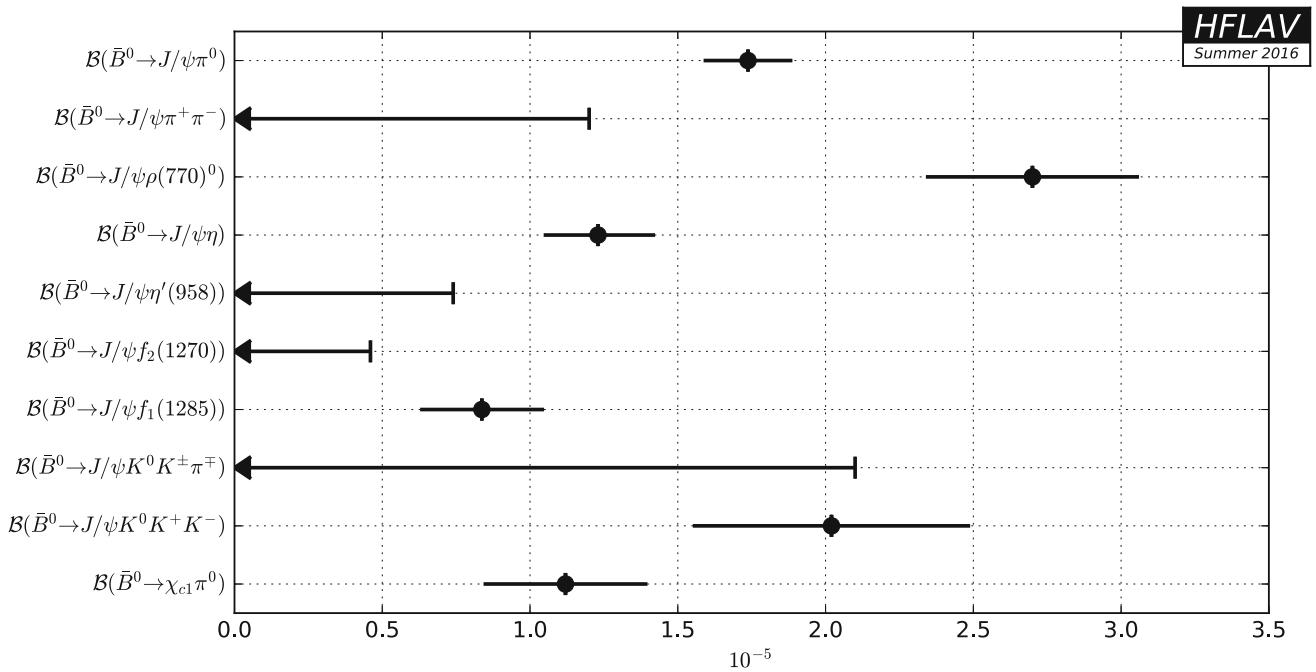


Fig. 93 Summary of the averages from Table 119

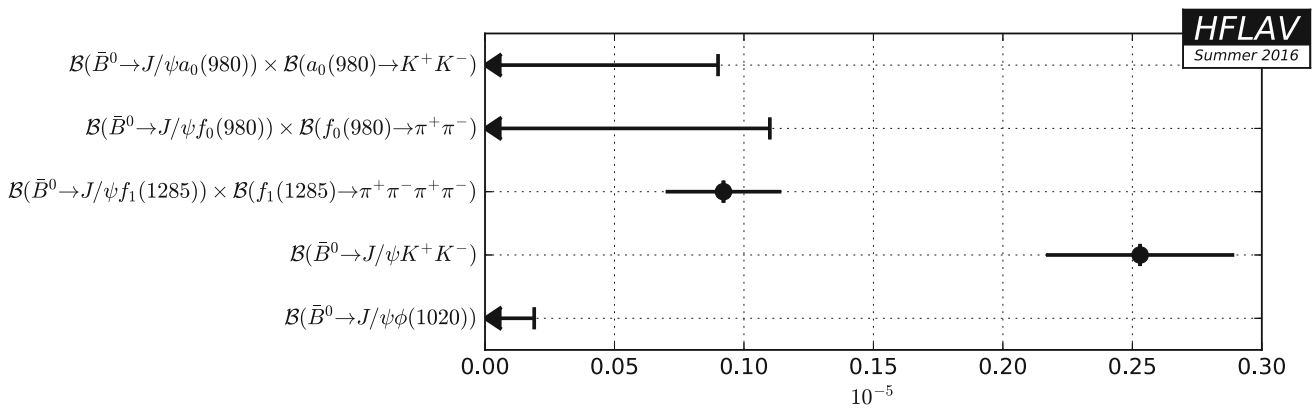


Fig. 94 Summary of the averages from Table 120

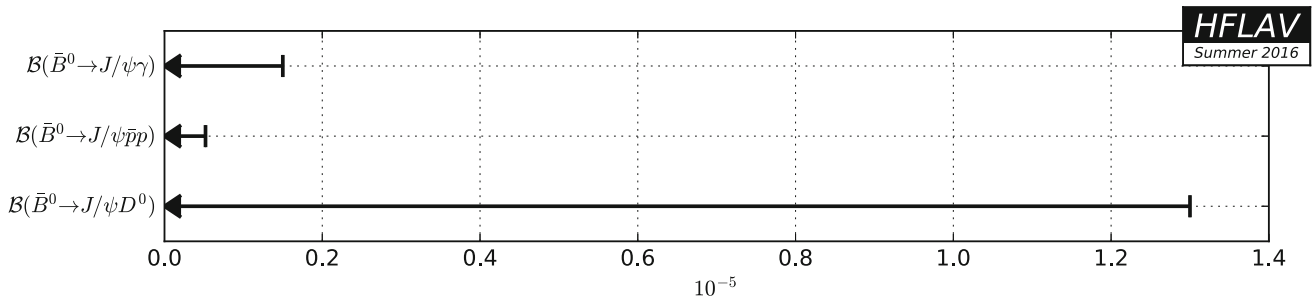


Fig. 95 Summary of the averages from Table 121

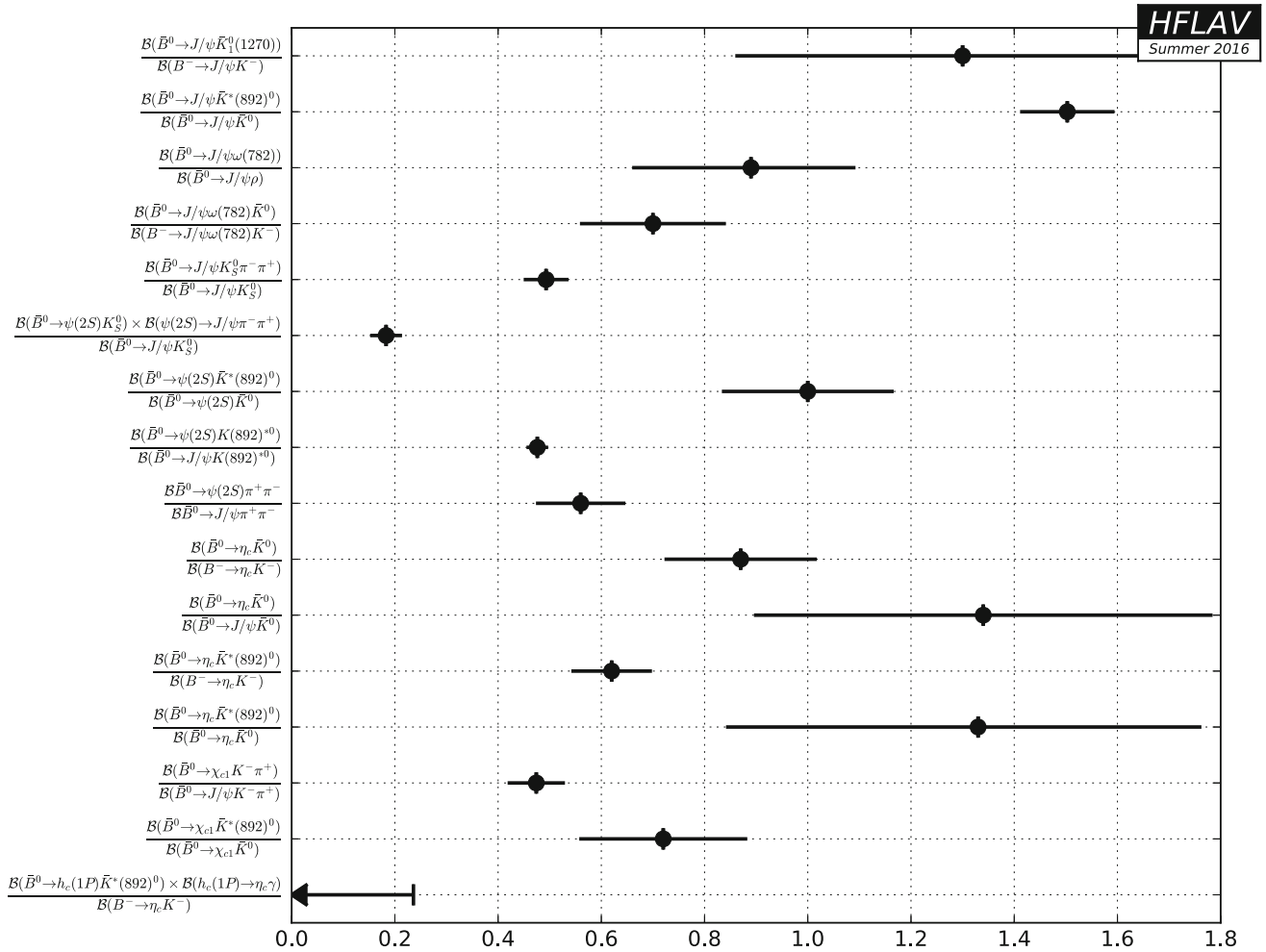


Fig. 96 Summary of the averages from Table 122

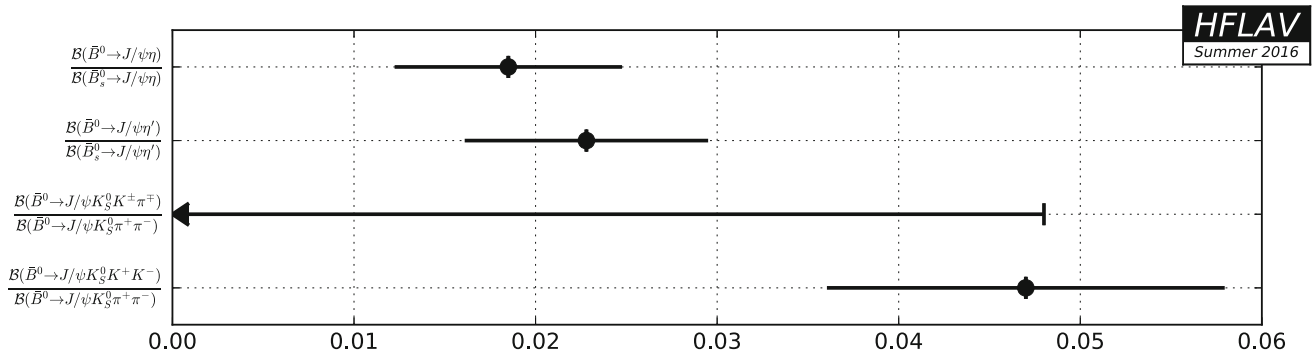


Fig. 97 Summary of the averages from Table 123

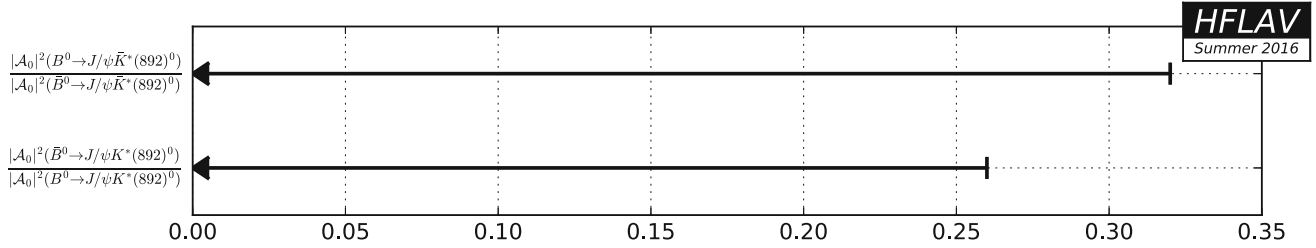


Fig. 98 Summary of the averages from Table 124

6.1.4 Decays to charm baryons

Averages of \bar{B}^0 decays to charm baryons are shown in Tables 125, 126, 127, 128 and Figs. 99, 100, 101.

Table 125 Absolute decay rates to charm baryons I [10^{-4}]

Parameter	Measurements	Average
$\mathcal{B}(\bar{B}^0 \rightarrow \Lambda_c^+ \bar{p} \pi^0)$	BABAR [689]: $1.94 \pm 0.17 \pm 0.52$	1.94 ± 0.55
$\mathcal{B}(\bar{B}^0 \rightarrow \Lambda_c^+ \bar{p} \pi^+ \pi^-)$	Belle [690]: $11.0^{+1.2}_{-1.2} \pm 3.5$ BABAR [691]: $12.3 \pm 0.5 \pm 3.3$	11.9 ± 3.2
$\mathcal{B}(\bar{B}^0 \rightarrow \Sigma_c^{++} \bar{p} \pi^-)$	Belle [692]: $2.1 \pm 0.2 \pm 0.6$ BABAR [691]: $2.13 \pm 0.10 \pm 0.56$	2.12 ± 0.55
$\mathcal{B}(\bar{B}^0 \rightarrow \Sigma_c^{*++} \bar{p} \pi^-)$	Belle [692]: $1.2 \pm 0.1 \pm 0.4$ BABAR [691]: $1.15 \pm 0.10 \pm 0.30$	1.16 ± 0.32
$\mathcal{B}(\bar{B}^0 \rightarrow \Sigma_c^0 \bar{p} \pi^+)$	Belle [692]: $1.4 \pm 0.2 \pm 0.4$ BABAR [691]: $0.91 \pm 0.07 \pm 0.24$	0.77 ± 0.23
$\mathcal{B}(\bar{B}^0 \rightarrow \Lambda_c^+ \Lambda_c^- \bar{K}^0)$	Belle [693]: $7.9^{+2.9}_{-2.3} \pm 4.3$ BABAR [694]: $3.8 \pm 3.1 \pm 2.1$	4.8 ± 3.5
$\mathcal{B}(\bar{B}^0 \rightarrow \Lambda_c^+ \bar{p} \pi^+ \pi^-_{\text{non-}\Sigma_c})$	BABAR [691]: $7.9 \pm 0.4 \pm 2.0$	7.9 ± 2.1

Table 126 Absolute decay rates to charm baryons II [10^{-5}]

Parameter	Measurements	Average
$\mathcal{B}(\bar{B}^0 \rightarrow \Lambda_c^+ \bar{p} K^+ K^-)$	BABAR [695]: $2.5 \pm 0.4 \pm 0.6$	2.5 ± 0.7
$\mathcal{B}(\bar{B}^0 \rightarrow \Lambda_c^+ \bar{p} \phi(1020))$	BABAR [695]: <1.2	<1.2
$\mathcal{B}(\bar{B}^0 \rightarrow \Sigma_c^{*0} \bar{p} \pi^+)$	Belle [692]: <3.3 BABAR [691]: $2.2 \pm 0.7 \pm 0.6$	2.2 ± 0.9
$\mathcal{B}(\bar{B}^0 \rightarrow \Lambda_c^+ \bar{p})$	Belle [696]: $2.19^{+0.56}_{-0.49} \pm 0.65$ BABAR [697]: $1.89 \pm 0.21 \pm 0.49$	1.90 ± 0.54
$\mathcal{B}(\bar{B}^0 \rightarrow \Lambda_c^+ \bar{p} \bar{K}^*(892)^0)$	BABAR [698]: $1.60 \pm 0.61 \pm 0.44$	1.60 ± 0.75
$\mathcal{B}(\bar{B}^0 \rightarrow \Sigma_c^{++} \bar{p} K^-)$	BABAR [698]: $1.11 \pm 0.30 \pm 0.30$	1.11 ± 0.43
$\mathcal{B}(\bar{B}^0 \rightarrow \Xi_c^+ \Lambda_c^-) \times \mathcal{B}(\Xi_c^+ \rightarrow \Xi^- \pi^+ \pi^+)$	Belle [699]: $9.3^{+3.7}_{-2.8} \pm 3.1$ BABAR [694]: $1.5 \pm 1.1 \pm 0.4$	1.7 ± 1.2
$\mathcal{B}(\bar{B}^0 \rightarrow \Lambda_c^+ \Lambda_c^-)$	Belle [700]: <5.7	<5.7
$\mathcal{B}(\bar{B}^0 \rightarrow \Lambda_c^+ \bar{\Lambda} K^-)$	BABAR [701]: $3.8 \pm 0.8 \pm 1.0$	3.8 ± 1.3
$\mathcal{B}(\bar{B}^0 \rightarrow \Lambda_c^+ \bar{p} K^- \pi^+)$	BABAR [698]: $4.33 \pm 0.82 \pm 1.18$	4.33 ± 1.43

Table 127 Absolute decay rates to charm baryons III [10^{-6}]

Parameter	Measurements	Average
$\mathcal{B}(\bar{B}^0 \rightarrow \Sigma_c^+ \bar{p}) \times \mathcal{B}(\Lambda_c^+ \rightarrow p K^- \pi^+)$	BABAR [689]: <1.5	<1.5
$\mathcal{B}(\bar{B}^0 \rightarrow \Lambda_c^+ \bar{p} p \bar{p}) \times \mathcal{B}(\Lambda_c^+ \rightarrow p K^- \pi^+)$	BABAR [702]: <0.14	<0.14

Table 128 Relative decay rates to charm baryons [10^{-3}]

Parameter	Measurements	Average
$\mathcal{B}(\bar{B}^0 \rightarrow \Lambda_c^- \Lambda_c^+) / \mathcal{B}(\bar{B}^0 \rightarrow D^+ D_s^-)$	LHCb [703]: <2	<2

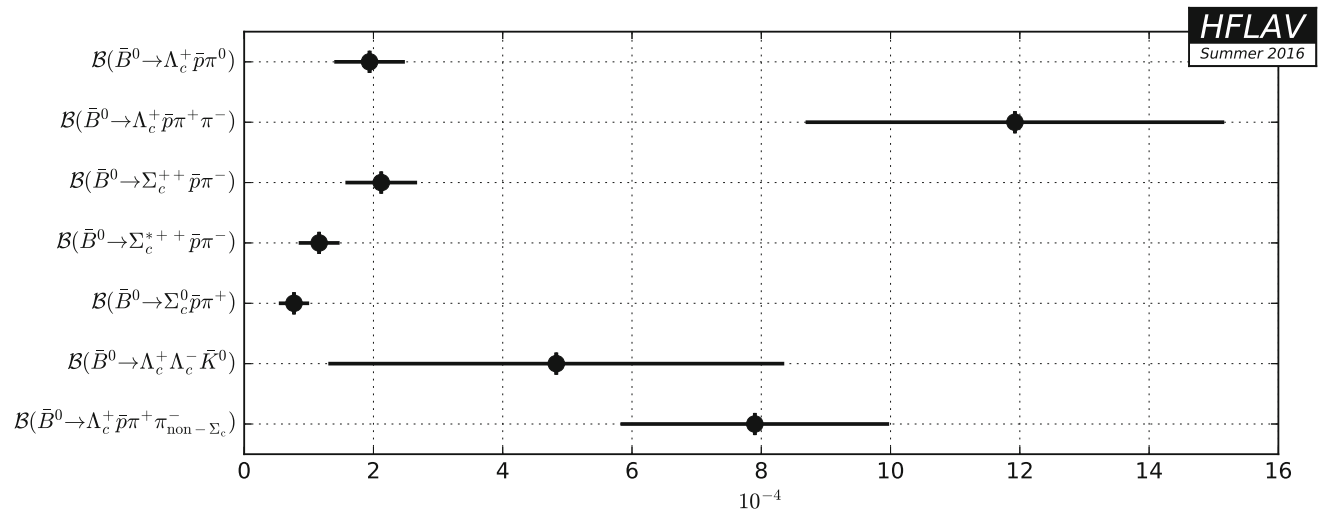


Fig. 99 Summary of the averages from Table 125

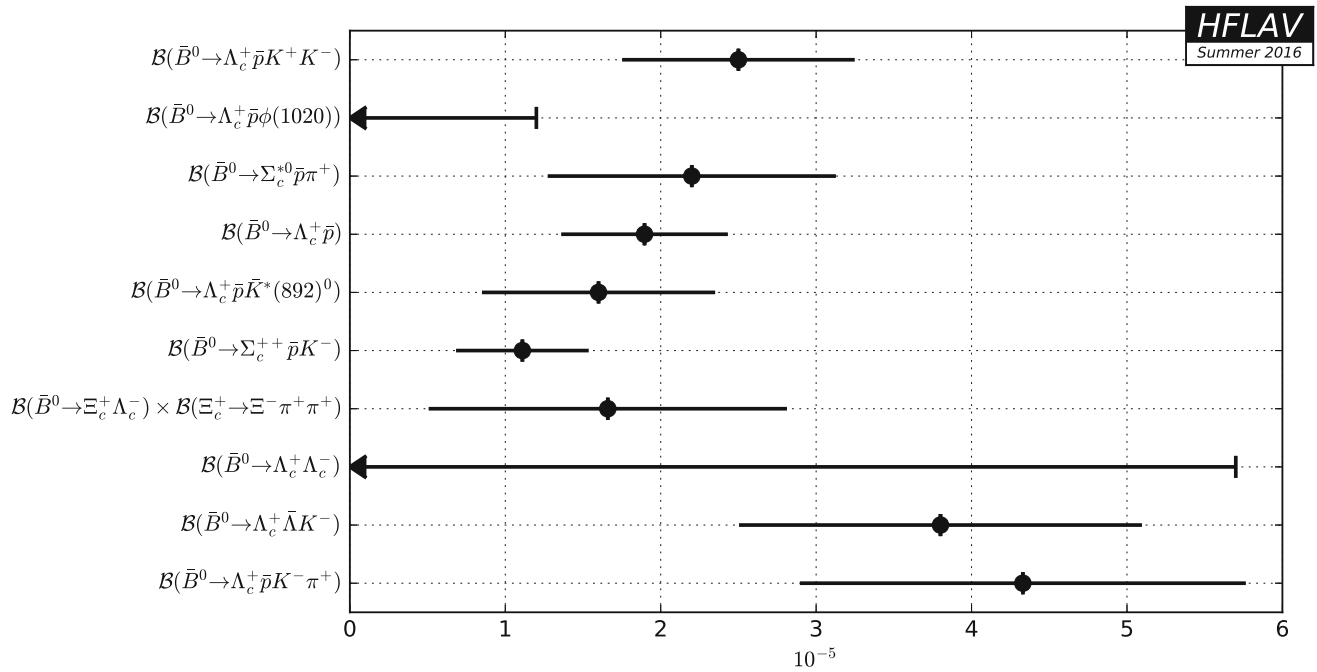


Fig. 100 Summary of the averages from Table 126

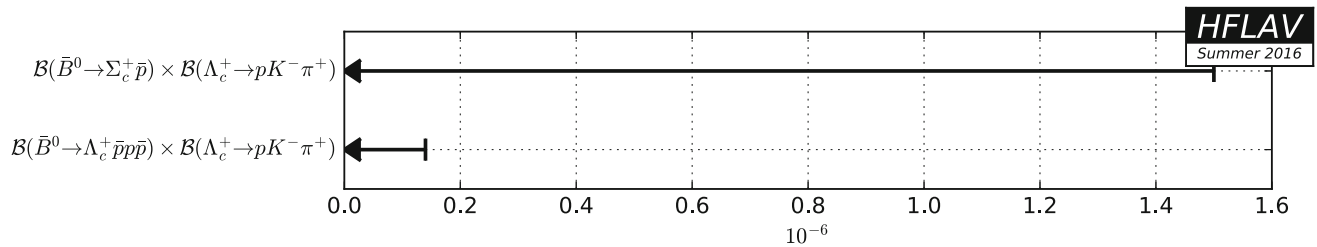


Fig. 101 Summary of the averages from Table 127

6.1.5 Decays to other (XYZ) states

Averages of \bar{B}^0 decays to other (XYZ) states are shown in Tables 129, 130, 131, 132, 133, 134 and Figs. 102, 103, 104, 105.

Table 129 Decays to X(3872) [10⁻⁵]

Parameter	Measurements	Average
$\mathcal{B}(\bar{B}^0 \rightarrow X(3872) \bar{K}^0) \times \mathcal{B}(X(3872) \rightarrow J/\psi \pi^+ \pi^-)$	BABAR [704]: $0.35 \pm 0.19 \pm 0.04$	0.35 ± 0.19
$\mathcal{B}(\bar{B}^0 \rightarrow X(3872) \bar{K}^0) \times \mathcal{B}(X(3872) \rightarrow J/\psi \omega(782))$	BABAR [651]: $0.6 \pm 0.3 \pm 0.1$	0.6 ± 0.3
$\mathcal{B}(\bar{B}^0 \rightarrow X(3872) \bar{K}^0) \times \mathcal{B}(X(3872) \rightarrow J/\psi \gamma)$	Belle [660]: $0.24^{+0.13}_{-0.14} \pm 0.07$ BABAR [661]: $0.26 \pm 0.18 \pm 0.02$	0.25 ± 0.12
$\mathcal{B}(\bar{B}^0 \rightarrow X(3872) \bar{K}^*(892)^0) \times \mathcal{B}(X(3872) \rightarrow J/\psi \gamma)$	BABAR [661]: $0.07 \pm 0.14 \pm 0.01$	0.07 ± 0.14
$\mathcal{B}(\bar{B}^0 \rightarrow X(3872) \bar{K}^0) \times \mathcal{B}(X(3872) \rightarrow \psi(2S) \gamma)$	Belle [660]: $0.662^{+0.130}_{-0.140} \pm 0.070$ BABAR [661]: $1.14 \pm 0.55 \pm 0.10$	0.695 ± 0.147
$\mathcal{B}(\bar{B}^0 \rightarrow X(3872) \bar{K}^*(892)^0) \times \mathcal{B}(X(3872) \rightarrow \psi(2S) \gamma)$	BABAR [661]: $-0.13 \pm 0.31 \pm 0.03$	-0.13 ± 0.31
$\mathcal{B}(\bar{B}^0 \rightarrow X(3872) K^0) \times \mathcal{B}(X(3872) \rightarrow \chi_{c1} \gamma)$	Belle [657]: < 0.96	< 0.96
$\mathcal{B}(\bar{B}^0 \rightarrow X(3872) K^0) \times \mathcal{B}(X(3872) \rightarrow \chi_{c2} \gamma)$	Belle [657]: < 1.22	< 1.22

Table 130 Decays to $X(3872)$ with $X(3872) \rightarrow D\bar{D}$ [10^{-4}]

Parameter	Measurements	Average
$\mathcal{B}(\bar{B}^0 \rightarrow X(3872)\bar{K}^0) \times \mathcal{B}(X(3872) \rightarrow \bar{D}^*(2007)^0 D^0)$	BABAR [643]: <4.37	<4.37

Table 131 Decays to neutral states other than $X(3872)$ [10^{-4}]

Parameter	Measurements	Average
$\mathcal{B}(\bar{B}^0 \rightarrow X(3823)K^0) \times \mathcal{B}(X(3823) \rightarrow \chi_{c1}\gamma)$	Belle [657]: <0.099	<0.099
$\mathcal{B}(\bar{B}^0 \rightarrow X(3823)K^0) \times \mathcal{B}(X(3823) \rightarrow \chi_{c2}\gamma)$	Belle [657]: <0.228	<0.228
$\mathcal{B}(\bar{B}^0 \rightarrow Y(3940)\bar{K}^0) \times \mathcal{B}(Y(3940) \rightarrow J/\psi\omega(782))$	BABAR [651]: $0.21 \pm 0.09 \pm 0.03$	0.21 ± 0.09
$\mathcal{B}(\bar{B}^0 \rightarrow Z_1(4050)K^-) \times \mathcal{B}(Z_1(4050) \rightarrow \chi_{c1}\pi^+)$	Belle [705]: $0.30^{+0.15+0.37}_{-0.08-0.16}$ BABAR [663]: <0.18	$0.30^{+0.40}_{-0.18}$
$\mathcal{B}(\bar{B}^0 \rightarrow Z_2(4250)K^-) \times \mathcal{B}(Z_2(4250) \rightarrow \chi_{c1}\pi^+)$	Belle [705]: $0.40^{+0.23+1.97}_{-0.09-0.05}$ BABAR [663]: <0.47	$0.40^{+1.98}_{-0.10}$

Table 132 Decays to charged states I [10^{-4}]

Parameter	Measurements	Average
$\mathcal{B}(\bar{B}^0 \rightarrow X(3872)^+K^-)$	BABAR [706]: <5.0	<5.0

Table 133 Decays to charged states II [10^{-5}]

Parameter	Measurements	Average
$\mathcal{B}(\bar{B}^0 \rightarrow X(3872)^+K^-) \times \mathcal{B}(X(3872)^+ \rightarrow J/\psi\pi^+\pi^0)$	BABAR [707]: <0.54	<0.54
$\mathcal{B}(\bar{B}^0 \rightarrow Z(4430)^+K^-) \times \mathcal{B}(Z(4430)^+ \rightarrow J/\psi\pi^+)$	Belle [647]: $0.54^{+0.40+0.11}_{-0.10-0.09}$ BABAR [708]: $-1.2 \pm 0.4 \pm 0.0$	$-0.11 \pm 0.24 \text{ CL} = 0.6^{0/}_{00}$
$\mathcal{B}(\bar{B}^0 \rightarrow Z(4430)^+K^-) \times \mathcal{B}(Z(4430)^+ \rightarrow \psi(2S)\pi^+)$	Belle [656]: $3.2^{+1.8+5.3}_{-0.9-1.6}$ BABAR [708]: $1.9 \pm 0.8 \pm 0.0$	1.9 ± 0.8
$\mathcal{B}(\bar{B}^0 \rightarrow Z_c(3900)^+K^-) \times \mathcal{B}(Z_c(3900)^+ \rightarrow J/\psi\pi^+)$	Belle [647]: <0.09	<0.09
$\mathcal{B}(\bar{B}^0 \rightarrow Z_c(4200)^+K^-) \times \mathcal{B}(Z_c(4200)^+ \rightarrow J/\psi\pi^+)$	Belle [647]: $2.2^{+0.7+1.1}_{-0.5-0.6}$	$2.2^{+1.3}_{-0.8}$

Table 134 Relative decay rates

Parameter	Measurements	Average
$\mathcal{B}(\bar{B}^0 \rightarrow X(3872)\bar{K}^0)/\mathcal{B}(B^- \rightarrow X(3872)K^-)$	BABAR [651]: $1.0^{+0.8+0.1}_{-0.6-0.2}$ BABAR [704]: $0.41 \pm 0.24 \pm 0.05$	0.47 ± 0.23
$\mathcal{B}(\bar{B}^0 \rightarrow Y(3940)\bar{K}^0)/\mathcal{B}(B^- \rightarrow Y(3940)K^-)$	BABAR [651]: $0.7^{+0.4}_{-0.3} \pm 0.1$	$0.7^{+0.4}_{-0.3}$

HFLAV
Summer 2016

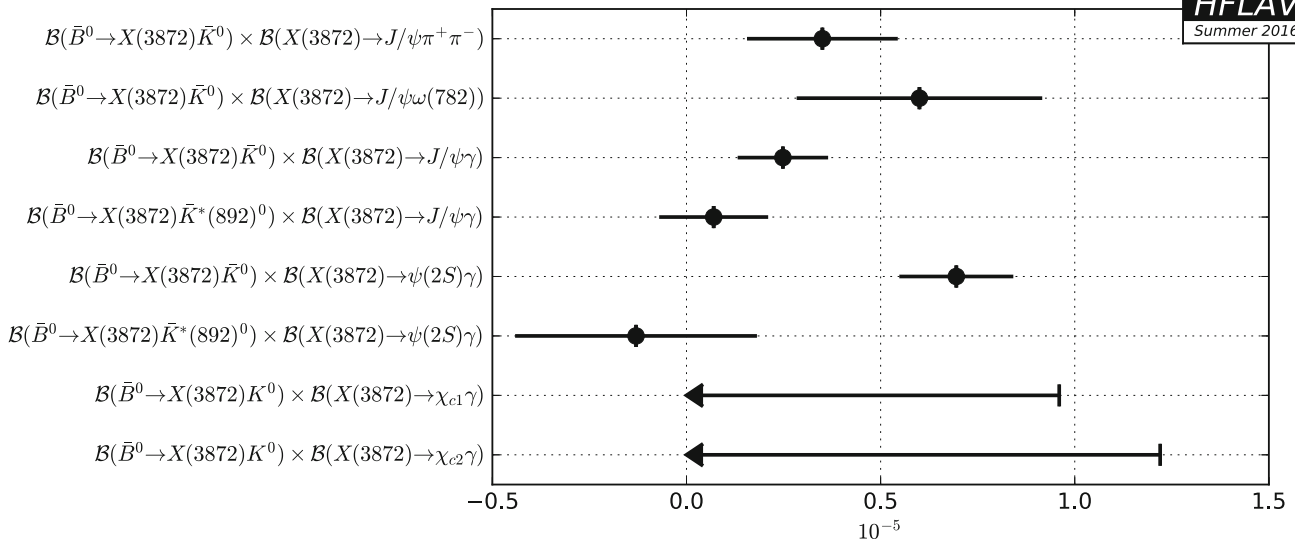


Fig. 102 Summary of the averages from Table 129

HFLAV
Summer 2016

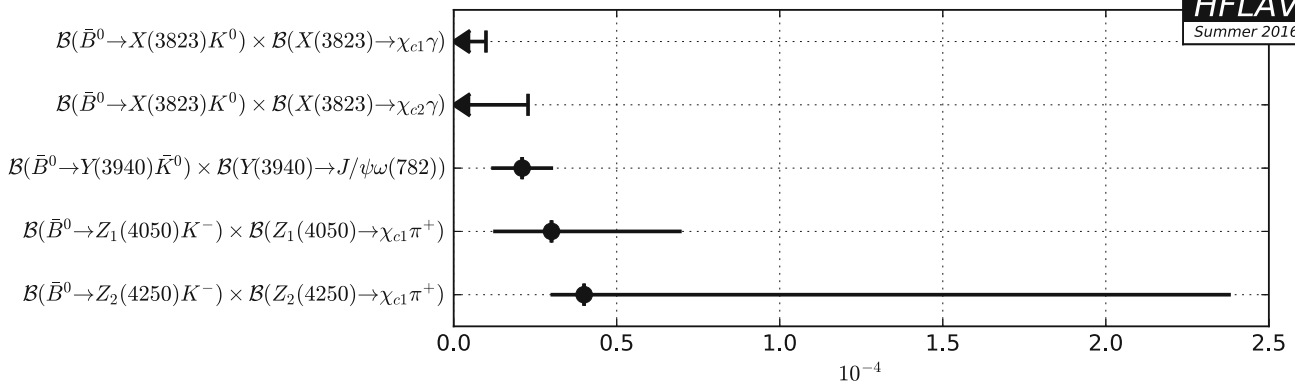


Fig. 103 Summary of the averages from Table 131

HFLAV
Summer 2016

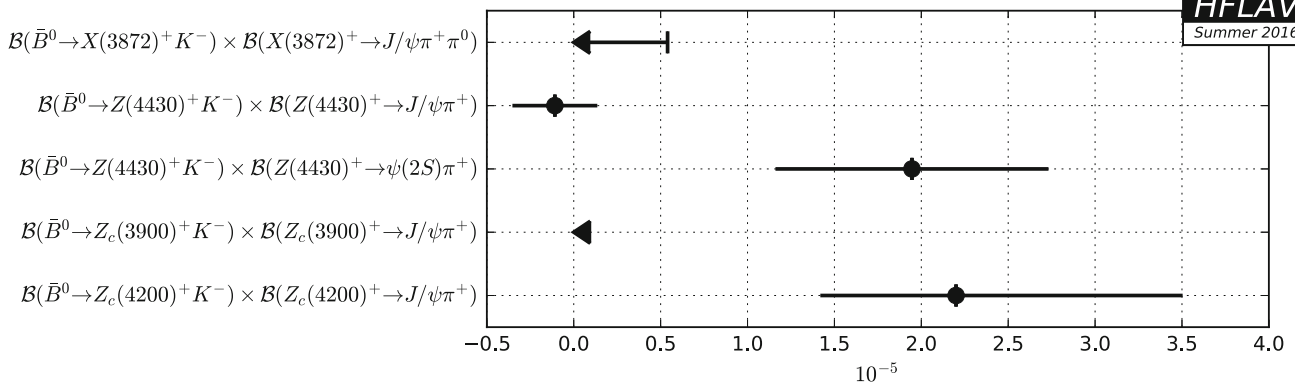


Fig. 104 Summary of the averages from Table 133

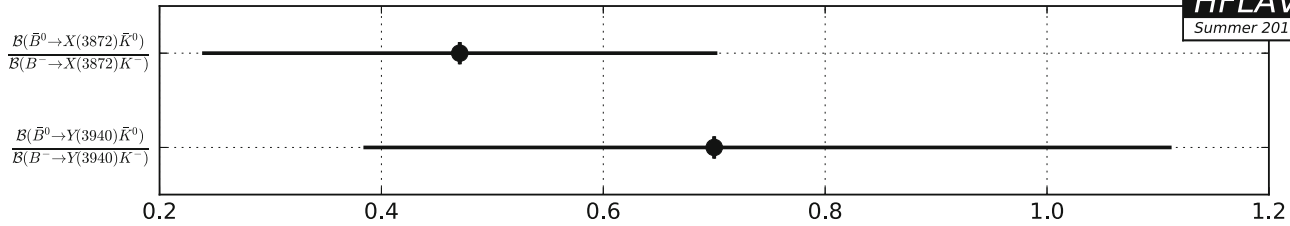


Fig. 105 Summary of the averages from Table 134

6.2 Decays of B^- mesons

Measurements of B^- decays to charmed hadrons are summarized in Sects. 6.2.1–6.2.5.

6.2.1 Decays to a single open charm meson

Averages of B^- decays to a single open charm meson are shown in Tables 135, 136, 137, 138, 139, 140, 141, 142, 143, 144, 145, 146, 147, 148, 149 and Figs. 106, 107, 108, 109, 110, 111, 112, 113, 114, 115, 116, 117, 118, 119. In this section D^{**} refers to the sum of all the non-strange charm meson states with masses in the range 2.2–2.8 GeV/ c^2 .

Table 135 Decays to a $D^{(*)}$ meson and one or more pions [10^{-2}]

Parameter	Measurements	Average
$\mathcal{B}(B^- \rightarrow D^*(2010)^-\pi^0)$	Belle [709]: <0.00036	<0.00036
$\mathcal{B}(B^- \rightarrow D^0\pi^-)$	BABAR [594]: $0.490 \pm 0.007 \pm 0.022$	
	BABAR [595]: $0.449 \pm 0.021 \pm 0.023$	0.475 ± 0.019
$\mathcal{B}(B^- \rightarrow D^*(2007)^0\pi^-)$	BABAR [594]: $0.552 \pm 0.017 \pm 0.042$	
	BABAR [595]: $0.513 \pm 0.022 \pm 0.028$	0.528 ± 0.028
$\mathcal{B}(B^- \rightarrow D^+\pi^-\pi^-)$	Belle [710]: $0.102 \pm 0.004 \pm 0.015$	
	BABAR [711]: $0.108 \pm 0.003 \pm 0.005$	0.107 ± 0.005
$\mathcal{B}(B^- \rightarrow D^*(2010)^+\pi^-\pi^-)$	Belle [710]: $0.125 \pm 0.008 \pm 0.022$	
	BABAR [712]: $0.122 \pm 0.005 \pm 0.018$	0.123 ± 0.015
$\mathcal{B}(B^- \rightarrow D^*(2007)^0\pi^-\pi^+\pi^-)$	Belle [596]: $1.055 \pm 0.047 \pm 0.129$	1.055 ± 0.137
$\mathcal{B}(B^- \rightarrow D^*(2010)^+\pi^-\pi^+\pi^-)$	Belle [596]: $0.256 \pm 0.026 \pm 0.033$	0.256 ± 0.042
$\mathcal{B}(B^- \rightarrow D^*(2007)^0\pi^-\pi^+\pi^+\pi^-)$	Belle [596]: $0.567 \pm 0.091 \pm 0.085$	0.567 ± 0.125

Table 136 Decays to a $D^{(*)0}$ meson and one or more kaons [10^{-3}]

Parameter	Measurements	Average
$\mathcal{B}(B^- \rightarrow D^0K^-)$	Belle [713]: $0.383 \pm 0.025 \pm 0.037$	0.383 ± 0.045
$\mathcal{B}(B^- \rightarrow D^*(2007)^0K^-)$	Belle [605]: $0.359 \pm 0.087 \pm 0.051$	0.359 ± 0.101
$\mathcal{B}(B^- \rightarrow D^0K^-K^0)$	Belle [607]: $0.55 \pm 0.14 \pm 0.08$	0.55 ± 0.16
$\mathcal{B}(B^- \rightarrow D^*(2007)^0K^-K^0)$	Belle [607]: <1.06	<1.06
$\mathcal{B}(B^- \rightarrow D^0K^-K^*(892)^0)$	Belle [607]: $0.75 \pm 0.13 \pm 0.11$	0.75 ± 0.17
$\mathcal{B}(B^- \rightarrow D^*(2007)^0K^-K^*(892)^0)$	Belle [607]: $1.53 \pm 0.31 \pm 0.29$	1.53 ± 0.42
$\mathcal{B}(B^- \rightarrow D^0K^*(892)^-)$	BABAR [714]: $0.529 \pm 0.030 \pm 0.034$	0.529 ± 0.045
$\mathcal{B}(B^- \rightarrow D^*(2007)^0K^*(892)^-)$	BABAR [715]: $0.83 \pm 0.11 \pm 0.10$	0.83 ± 0.15
$\mathcal{B}(B^- \rightarrow D^+K^-\pi^-)$	LHCb [716]: $0.0731 \pm 0.0019 \pm 0.0045$	0.0731 ± 0.0049

Table 137 Decays to a $D^{(*)-}$ meson and a neutral kaon or a kaon and a pion [10^{-6}]

Parameter	Measurements	Average
$\mathcal{B}(B^- \rightarrow D^- \bar{K}^0)$	BABAR [717]: $-3.8^{+2.2+1.2}_{-1.8-1.6}$	$-3.8^{+2.5}_{-2.4}$
$\mathcal{B}(B^- \rightarrow D^- \bar{K}^*(892)^0)$	BABAR [717]: $-5.3^{+2.3+1.4}_{-2.0-1.8}$	$-5.3^{+2.7}_{-2.7}$
$\mathcal{B}(B^- \rightarrow D^- K^- \pi^+)$	LHCb [718]: $5.31 \pm 0.90 \pm 0.59$	5.31 ± 1.08
$\mathcal{B}(B^- \rightarrow D^*(2010)^- \bar{K}^0)$	BABAR [719]: <9	<9

Table 138 Relative decay rates to D^0 mesons I

Parameter	Measurements	Average
$\mathcal{B}(B^- \rightarrow D^0 \pi^-) / \mathcal{B}(\bar{B}^0 \rightarrow D^+ \pi^-)$	CDF [720]: $1.97 \pm 0.10 \pm 0.21$	1.97 ± 0.23
$\mathcal{B}(B^- \rightarrow D^0 \pi^+ \pi^- \pi^-) / \mathcal{B}(B^- \rightarrow D^0 \pi^-)$	LHCb [616]: $1.27 \pm 0.06 \pm 0.11$	1.27 ± 0.13

Table 139 Relative decay rates to D^0 mesons II [10^{-2}]

Parameter	Measurements	Average
$\mathcal{B}(B^- \rightarrow \bar{D}^0 K^-) / \mathcal{B}(B^- \rightarrow D^0 K^-)$	Belle [721]: <19	<19
$\mathcal{B}(B^- \rightarrow D^0 K^-) / \mathcal{B}(B^- \rightarrow D^0 \pi^-)$	LHCb [436]: $7.79 \pm 0.06 \pm 0.19$ Belle [721]: $6.77 \pm 0.23 \pm 0.30$ Belle [713]: $7.7 \pm 0.5 \pm 0.6$ BABAR [722]: $8.31 \pm 0.35 \pm 0.20$	7.69 ± 0.16
$\mathcal{B}(B^- \rightarrow D^0 K^- \pi^+ \pi^-) / \mathcal{B}(B^- \rightarrow D^0 \pi^+ \pi^- \pi^-)$	LHCb [620]: $9.4 \pm 1.3 \pm 0.9$	9.4 ± 1.6

Table 140 Absolute decay rates to excited D mesons [10^{-3}]

Parameter	Measurements	Average
$\mathcal{B}(B^- \rightarrow D^{*0} \pi^-)$	BABAR [595]: $5.50 \pm 0.52 \pm 1.04$	5.50 ± 1.16

Table 141 Absolute product decay rates to excited D mesons I [10^{-3}]

Parameter	Measurements	Average
$\mathcal{B}(B^- \rightarrow D_1^0(2420) \pi^-) \times \mathcal{B}(D_1^0(2420) \rightarrow D^*(2010)^+ \pi^-)$	Belle [710]: $0.68 \pm 0.07 \pm 0.13$ BABAR [712]: $0.59 \pm 0.03 \pm 0.11$	0.62 ± 0.09
$\mathcal{B}(B^- \rightarrow D_1^0(2420) \pi^-) \times \mathcal{B}(D_1^0(2420) \rightarrow D^0 \pi^- \pi^+)$	Belle [622]: $0.185 \pm 0.029^{+0.035}_{-0.058}$	$0.185^{+0.045}_{-0.065}$
$\mathcal{B}(B^- \rightarrow D_0^{*0} \pi^-) \times \mathcal{B}(D_0^{*0} \rightarrow D^+ \pi^-)$	Belle [710]: $0.61 \pm 0.06 \pm 0.18$ BABAR [711]: $0.68 \pm 0.03 \pm 0.20$	0.63 ± 0.19
$\mathcal{B}(B^- \rightarrow D_1^0(H) \pi^-) \times \mathcal{B}(D_1^0(H) \rightarrow D^*(2010)^+ \pi^-)$	Belle [710]: $0.50 \pm 0.04 \pm 0.11$	0.50 ± 0.11
$\mathcal{B}(B^- \rightarrow D_2^{*0}(2460) \pi^-) \times \mathcal{B}(D_2^{*0}(2460) \rightarrow D^*(2010)^+ \pi^-)$	Belle [710]: $0.18 \pm 0.03 \pm 0.04$ BABAR [712]: $0.18 \pm 0.03 \pm 0.05$	0.18 ± 0.04
$\mathcal{B}(B^- \rightarrow D_2^{*0}(2460) \pi^-) \times \mathcal{B}(D_2^{*0}(2460) \rightarrow D^+ \pi^-)$	Belle [710]: $0.34 \pm 0.03 \pm 0.07$ BABAR [711]: $0.35 \pm 0.02 \pm 0.04$	0.35 ± 0.05

Table 142 Absolute product decay rates to excited D mesons II [10^{-5}]

Parameter	Measurements	Average
$\mathcal{B}(B^- \rightarrow D_1^0(2420) \pi^-) \times \mathcal{B}(D_1^0(2420) \rightarrow D^*(2007)^0 \pi^- \pi^+)$	Belle [622]: <0.6	<0.6
$\mathcal{B}(B^- \rightarrow D_2^{*0}(2460) \pi^-) \times \mathcal{B}(D_2^{*0}(2460) \rightarrow D^*(2007)^0 \pi^- \pi^+)$	Belle [622]: <2.2	<2.2

Table 143 Relative decay rates to excited D mesons

Parameter	Measurements	Average
$\mathcal{B}(B^- \rightarrow D^*(2007)^0 \pi^-) / \mathcal{B}(B^- \rightarrow D^0 \pi^-)$	BABAR [595]: $1.14 \pm 0.07 \pm 0.04$	1.14 ± 0.08
$\mathcal{B}(B^- \rightarrow D^{*0} \pi^-) / \mathcal{B}(B^- \rightarrow D^0 \pi^-)$	BABAR [595]: $1.22 \pm 0.13 \pm 0.23$	1.22 ± 0.26
$\mathcal{B}(B^- \rightarrow D_2^{*0}(2460) \pi^-) / \mathcal{B}(B^- \rightarrow D_1^0(2420) \pi^-)$	BABAR [712]: $0.80 \pm 0.07 \pm 0.16$	0.80 ± 0.17
$\mathcal{B}(B^- \rightarrow D^*(2007)^0 K^-) / \mathcal{B}(B^- \rightarrow D^*(2007)^0 \pi^-)$	Belle [605]: $0.078 \pm 0.019 \pm 0.009$ BABAR [723]: $0.0813 \pm 0.0040^{+0.0042}_{-0.0031}$	0.0811 ± 0.0053

Table 144 Relative product decay rates to excited D mesons

Parameter	Measurements	Average
$[\mathcal{B}(B^- \rightarrow D_1^0 \pi^-) \times \mathcal{B}(D_1^0 \rightarrow D^0 \pi^+ \pi^-)] / \mathcal{B}(B^- \rightarrow D^0 \pi^+ \pi^- \pi^-)$	LHCb [616]: $0.040 \pm 0.007 \pm 0.005$	0.040 ± 0.009
$[\mathcal{B}(B^- \rightarrow D_1^{*0} \pi^-) \times \mathcal{B}(D_1^{*0} \rightarrow D^{*+} \pi^-)] / \mathcal{B}(B^- \rightarrow D^0 \pi^+ \pi^- \pi^-)$	LHCb [616]: $0.093 \pm 0.016 \pm 0.009$	0.093 ± 0.018
$[\mathcal{B}(B^- \rightarrow D_1^{*0} \pi^-) \times \mathcal{B}(D_1^{*0} \rightarrow D^0 \pi^+ \pi^-)] / \mathcal{B}(B^- \rightarrow D^0 \pi^+ \pi^- \pi^-)$	LHCb [616]: $0.103 \pm 0.015 \pm 0.009$	0.103 ± 0.017
$[\mathcal{B}(B^- \rightarrow D_2^{*0} \pi^-) \times \mathcal{B}(D_2^{*0} \rightarrow D^{*+} \pi^-)] / \mathcal{B}(B^- \rightarrow D^0 \pi^+ \pi^- \pi^-)$	LHCb [616]: $0.039 \pm 0.012 \pm 0.004$	0.039 ± 0.013
$[\mathcal{B}(B^- \rightarrow D_2^{*0} \pi^-) \times \mathcal{B}(D_2^{*0} \rightarrow D^0 \pi^+ \pi^-)] / \mathcal{B}(B^- \rightarrow D^0 \pi^+ \pi^- \pi^-)$	LHCb [616]: $0.040 \pm 0.010 \pm 0.004$	0.040 ± 0.011
$[\mathcal{B}(B^- \rightarrow D_2^{*+} \pi^-) \times \mathcal{B}(D_2^{*+} \rightarrow D^0 \pi^- \pi^+)] / \mathcal{B}(B^- \rightarrow D^0 \pi^+ \pi^- \pi^-)$	LHCb [616]: $0.014 \pm 0.006 \pm 0.002$	0.014 ± 0.006

Table 145 Decays to $D_s^{(*)}$ mesons I [10^{-4}]

Parameter	Measurements	Average
$\mathcal{B}(B^- \rightarrow D_s^+ K^- \pi^-)$	Belle [724]: $1.94^{+0.09+0.26}_{-0.08-0.26}$ BABAR [615]: $2.02 \pm 0.13 \pm 0.38$	1.97 ± 0.23
$\mathcal{B}(B^- \rightarrow D_s^{*+} K^- \pi^-)$	Belle [724]: $1.47^{+0.15+0.23}_{-0.14-0.23}$ BABAR [615]: $1.67 \pm 0.16 \pm 0.35$	1.54 ± 0.22

Table 146 Decays to $D_s^{(*)}$ mesons I [10^{-5}]

Parameter	Measurements	Average
$\mathcal{B}(B^- \rightarrow D_s^+ K^- K^-)$	BABAR [615]: $1.1 \pm 0.4 \pm 0.2$	1.1 ± 0.4
$\mathcal{B}(B^- \rightarrow D_s^{*+} K^- K^-)$	BABAR [615]: <1.5	<1.5
$\mathcal{B}(B^- \rightarrow D_s^- \pi^0)$	BABAR [725]: $1.5^{+0.5}_{-0.4} \pm 0.2$	$1.5^{+0.5}_{-0.5}$
$\mathcal{B}(B^- \rightarrow D_s^- \phi(1020))$	LHCb [726]: $0.187^{+0.125}_{-0.073} \pm 0.037$ BABAR [727]: <0.19	$0.187^{+0.130}_{-0.082}$
$\mathcal{B}(B^- \rightarrow D_s^{*-} \phi(1020))$	BABAR [727]: <1.2	<1.2

Table 147 Baryonic decays I [10^{-4}]

Parameter	Measurements	Average
$\mathcal{B}(B^- \rightarrow D^0 p \bar{p} \pi^-)$	BABAR [624]: $3.72 \pm 0.11 \pm 0.25$	3.72 ± 0.27
$\mathcal{B}(B^- \rightarrow D^*(2007)^0 p \bar{p} \pi^-)$	BABAR [624]: $3.73 \pm 0.17 \pm 0.27$	3.73 ± 0.32
$\mathcal{B}(B^- \rightarrow D^+ p \bar{p} \pi^- \pi^-)$	BABAR [624]: $1.66 \pm 0.13 \pm 0.27$	1.66 ± 0.30
$\mathcal{B}(B^- \rightarrow D^*(2010)^+ p \bar{p} \pi^- \pi^-)$	BABAR [624]: $1.86 \pm 0.16 \pm 0.19$	1.86 ± 0.25

Table 148 Baryonic decays II [10^{-5}]

Parameter	Measurements	Average
$\mathcal{B}(B^- \rightarrow D^0 \Lambda \bar{p})$	Belle [728]: $1.43^{+0.28}_{-0.25} \pm 0.18$	$1.43^{+0.33}_{-0.31}$
$\mathcal{B}(B^- \rightarrow D^*(2007)^0 \Lambda \bar{p})$	Belle [728]: <4.8	<4.8
$\mathcal{B}(B^- \rightarrow D^- p \bar{p})$	Belle [625]: <1.5	<1.5
$\mathcal{B}(B^- \rightarrow D^*(2010)^- p \bar{p})$	Belle [625]: <1.5	<1.5

Table 149 Lepton number violating decays [10^{-6}]

Parameter	Measurements	Average
$\mathcal{B}(B^- \rightarrow D^- e^+ e^+)$	Belle [729]: <2.6	<2.6
$\mathcal{B}(B^- \rightarrow D^- e^+ \mu^+)$	Belle [729]: <1.8	<1.8
$\mathcal{B}(B^- \rightarrow D^- \mu^+ \mu^+)$	Belle [729]: <1.0	<1.0

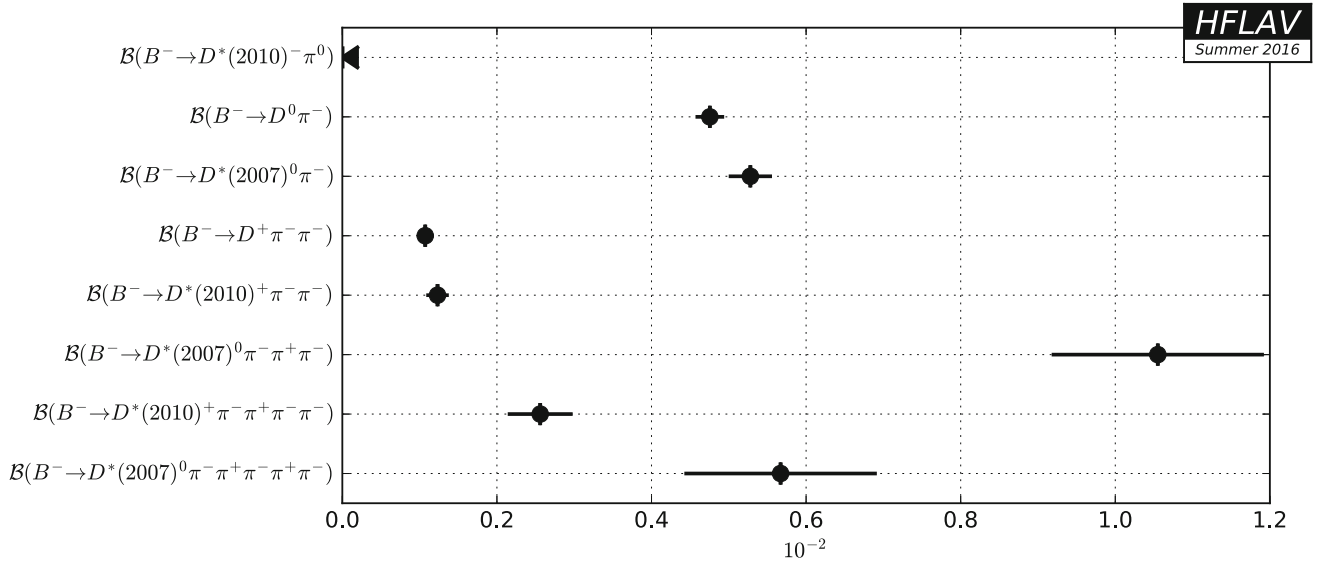


Fig. 106 Summary of the averages from Table 135

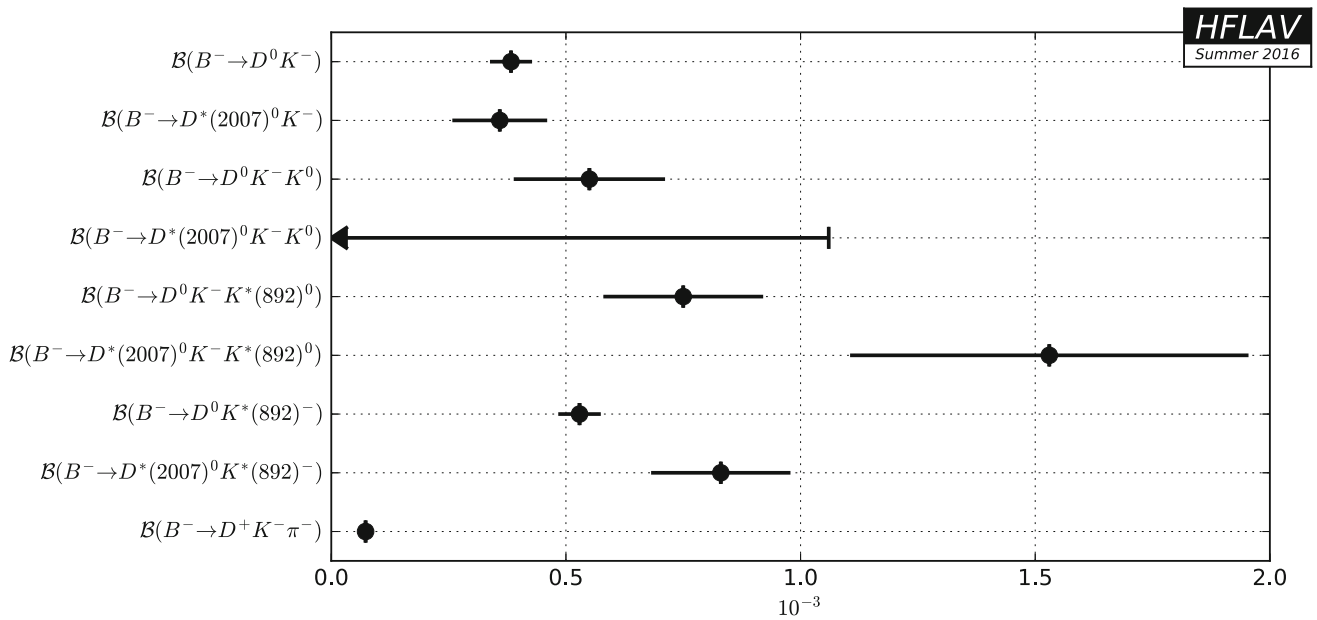


Fig. 107 Summary of the averages from Table 136

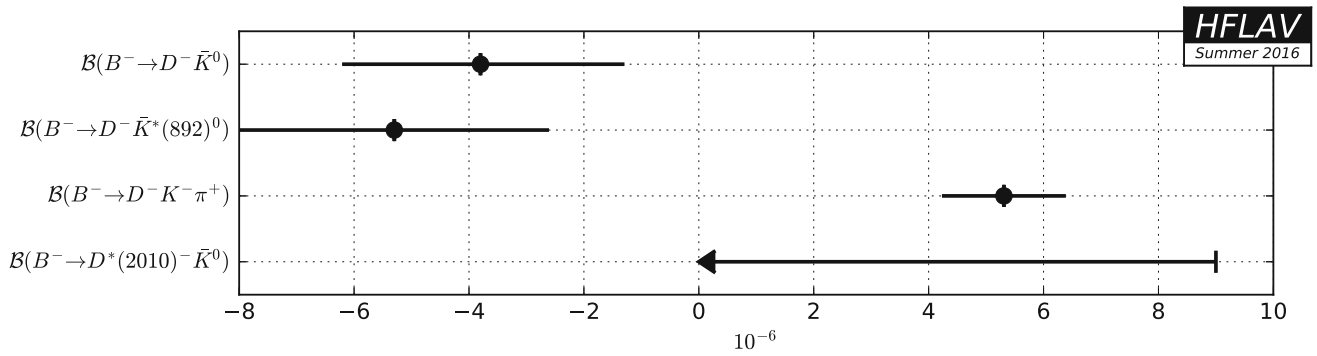


Fig. 108 Summary of the averages from Table 137

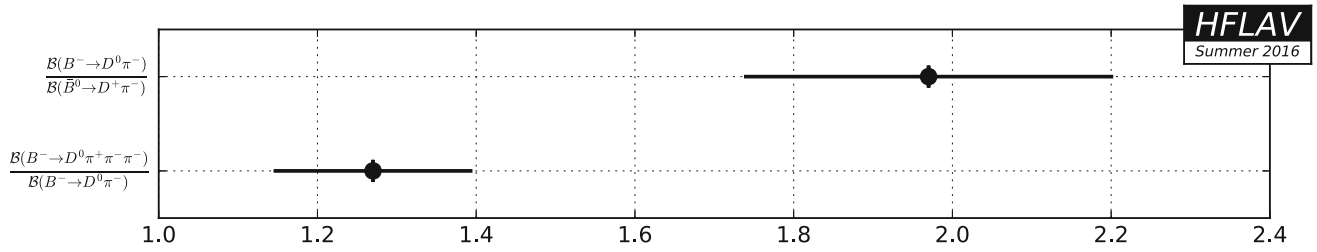


Fig. 109 Summary of the averages from Table 138

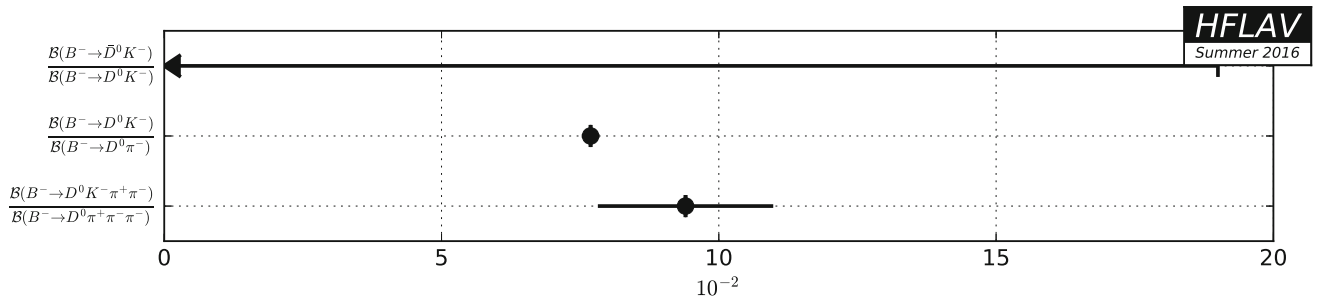


Fig. 110 Summary of the averages from Table 139

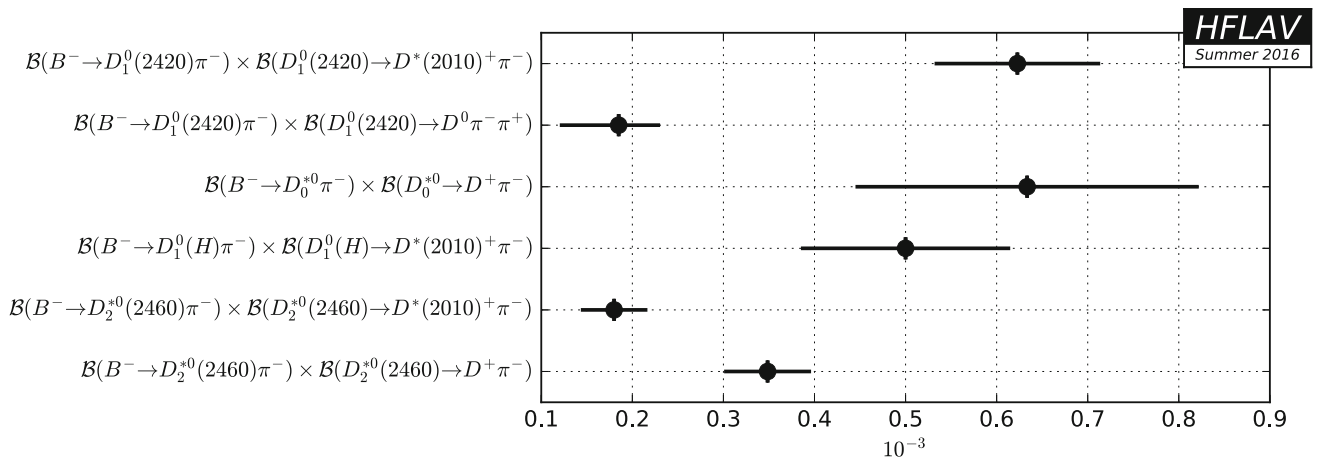


Fig. 111 Summary of the averages from Table 141

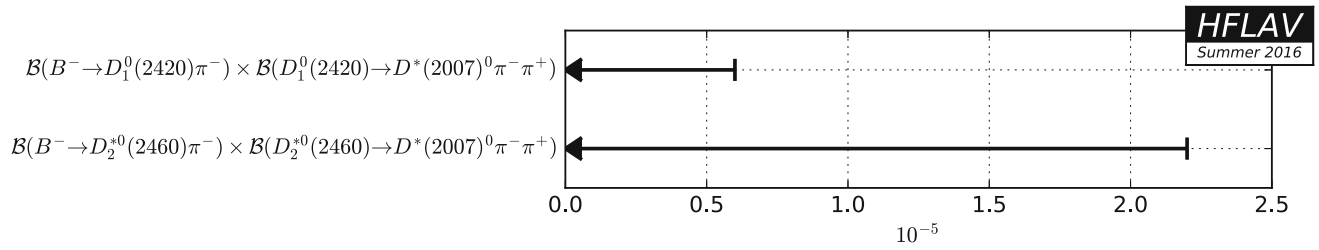


Fig. 112 Summary of the averages from Table 142

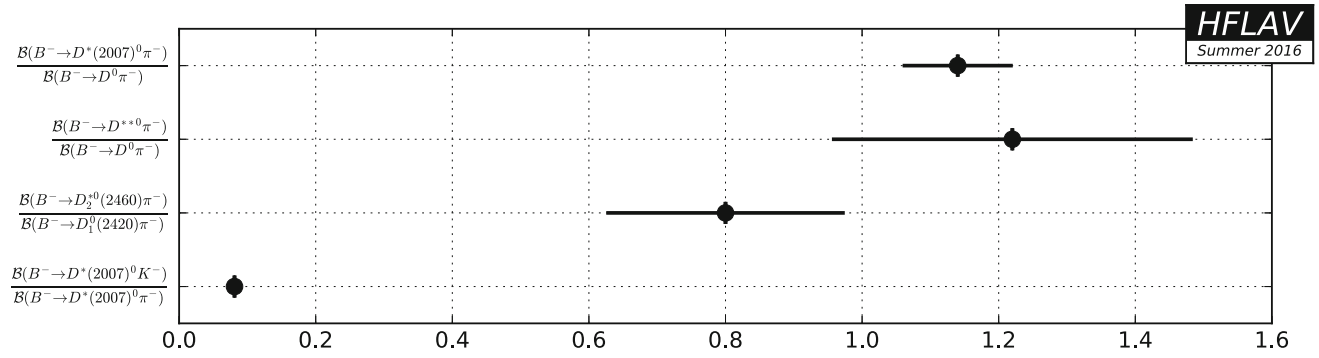


Fig. 113 Summary of the averages from Table 143

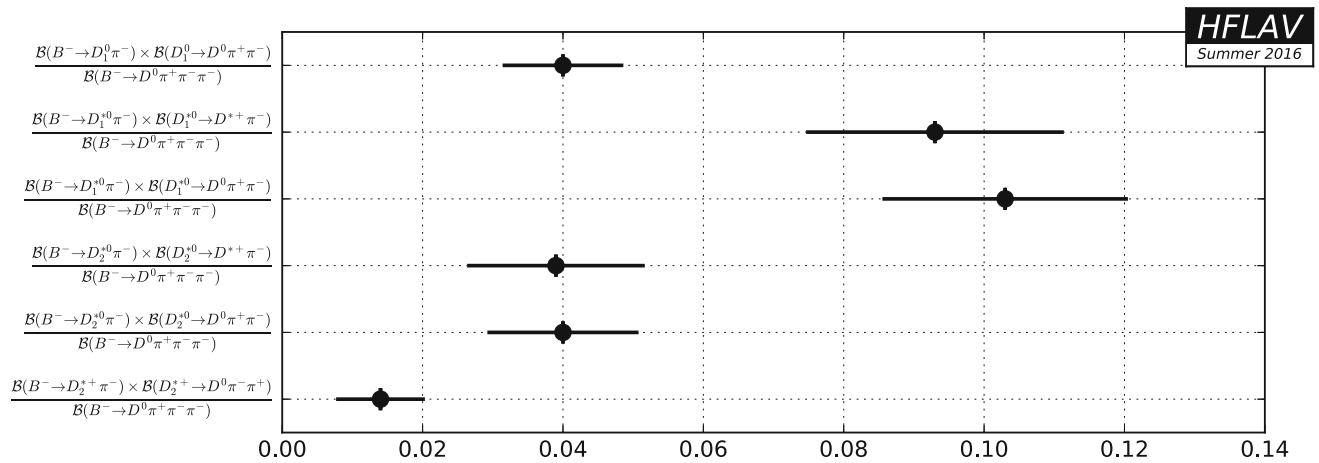


Fig. 114 Summary of the averages from Table 144

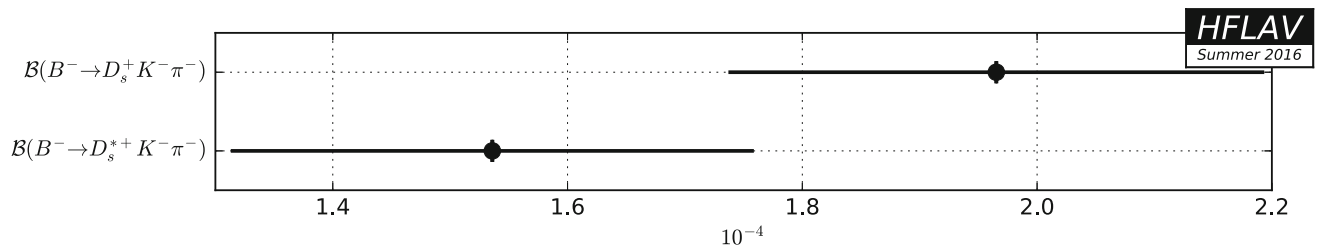


Fig. 115 Summary of the averages from Table 145

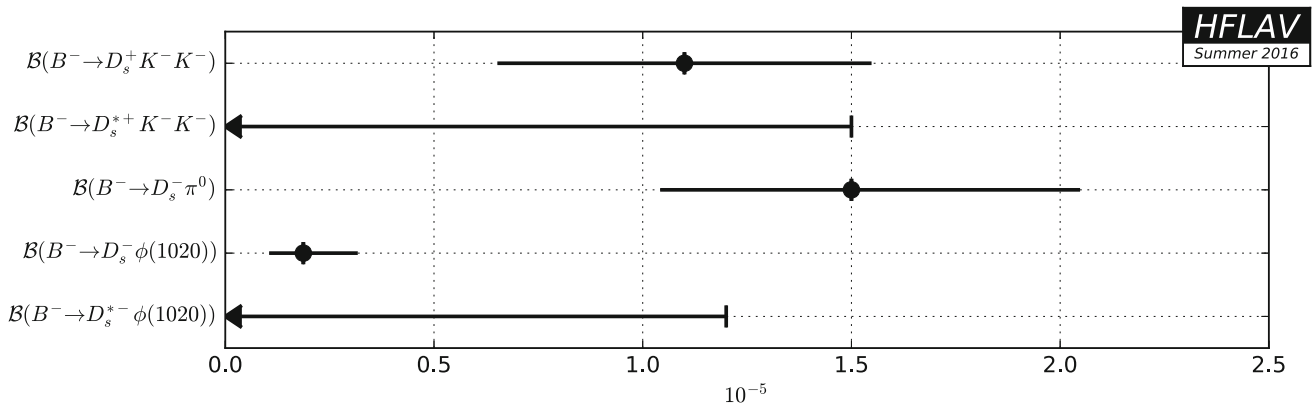


Fig. 116 Summary of the averages from Table 146

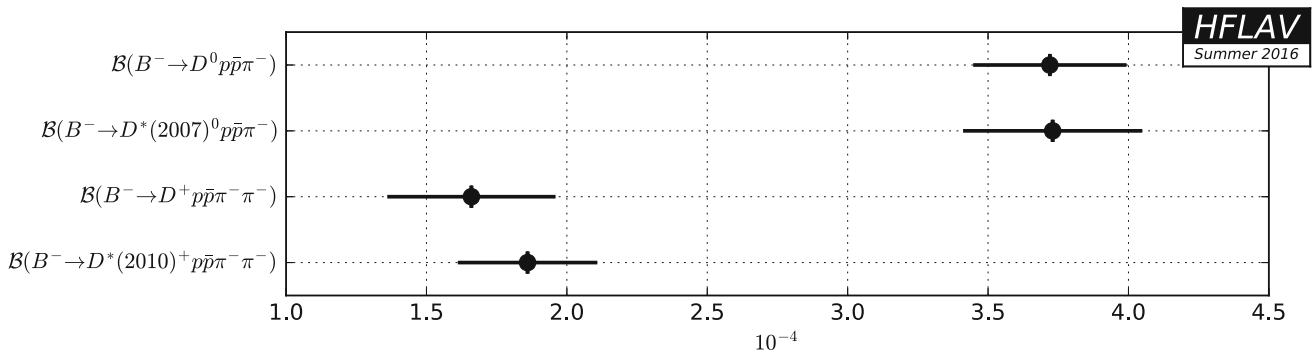


Fig. 117 Summary of the averages from Table 147

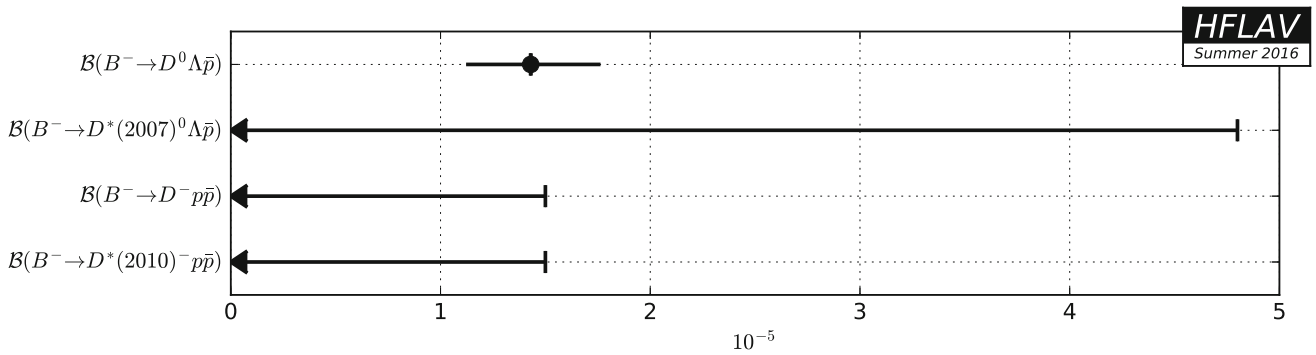


Fig. 118 Summary of the averages from Table 148

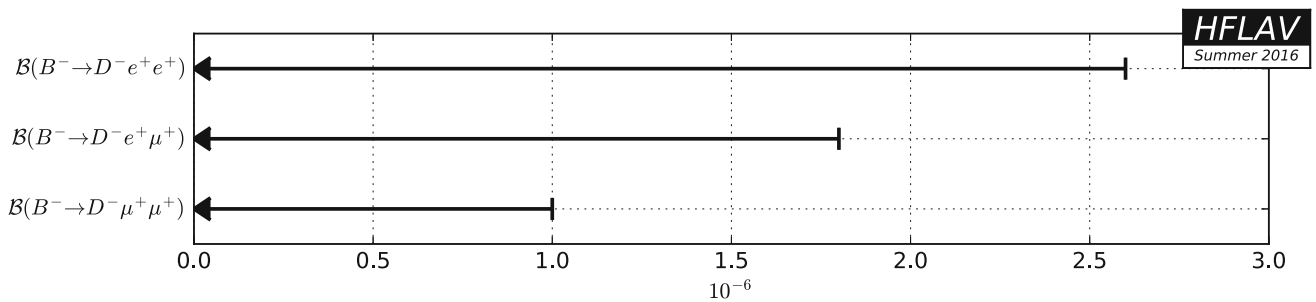


Fig. 119 Summary of the averages from Table 149

6.2.2 Decays to two open charm mesons

Averages of B^- decays to two open charm mesons are shown in Tables 150, 151, 152, 153, 154, 155, 156, 157, 158 and Figs. 120, 121, 122, 123, 124, 125, 126, 127.

Table 150 Decays to $D^{(*)-} D^{(*)0}$ [10^{-3}]

Parameter	Measurements	Average
$\mathcal{B}(B^- \rightarrow D^- D^0)$	Belle [631]: $0.385 \pm 0.031 \pm 0.038$ BABAR [630]: $0.38 \pm 0.06 \pm 0.05$	0.384 ± 0.042
$\mathcal{B}(B^- \rightarrow D^{*0} D^-)$	BABAR [630]: $0.63 \pm 0.14 \pm 0.10$	0.63 ± 0.17
$\mathcal{B}(B^- \rightarrow D_s^- D^0)$	Belle [730]: $0.459 \pm 0.072 \pm 0.056$ BABAR [630]: $0.36 \pm 0.05 \pm 0.04$	0.385 ± 0.046
$\mathcal{B}(B^- \rightarrow D^*(2007)^0 D^*(2010)^-)$	BABAR [630]: $0.81 \pm 0.12 \pm 0.12$	0.81 ± 0.17

Table 151 Decays to two D mesons and a kaon I [10^{-2}]

Parameter	Measurements	Average
$\mathcal{B}(B^- \rightarrow D^*(2007)^0 \bar{D}^0 K^-)$	BABAR [632]: $0.226 \pm 0.016 \pm 0.017$	0.226 ± 0.023
$\mathcal{B}(B^- \rightarrow D^0 \bar{D}^*(2007)^0 K^-)$	BABAR [632]: $0.632 \pm 0.019 \pm 0.045$	0.632 ± 0.049
$\mathcal{B}(B^- \rightarrow \bar{D}^*(2007)^0 D^*(2007)^0 K^-)$	BABAR [632]: $1.123 \pm 0.036 \pm 0.126$	1.123 ± 0.131
$\mathcal{B}(B^- \rightarrow D^*(2007)^0 D^- \bar{K}^0)$	BABAR [632]: $0.206 \pm 0.038 \pm 0.030$	0.206 ± 0.048
$\mathcal{B}(B^- \rightarrow D^0 D^*(2010)^- \bar{K}^0)$	BABAR [632]: $0.381 \pm 0.031 \pm 0.023$	0.381 ± 0.039
$\mathcal{B}(B^- \rightarrow D^*(2007)^0 D^*(2010)^- \bar{K}^0)$	BABAR [632]: $0.917 \pm 0.083 \pm 0.090$	0.917 ± 0.122

Table 152 Decays to two D mesons and a kaon II [10^{-3}]

Parameter	Measurements	Average
$\mathcal{B}(B^- \rightarrow D^0 \bar{D}^0 K^-)$	Belle [731]: $2.22 \pm 0.22^{+0.26}_{-0.24}$ BABAR [632]: $1.31 \pm 0.07 \pm 0.12$	1.44 ± 0.13
$\mathcal{B}(B^- \rightarrow D^0 \bar{D}^0 \pi^0 K^-)$	Belle [633]: $0.107 \pm 0.031^{+0.019}_{-0.033}$	$0.107^{+0.036}_{-0.045}$
$\mathcal{B}(B^- \rightarrow D^+ D^- K^-)$	Belle [732]: <0.90 BABAR [632]: $0.22 \pm 0.05 \pm 0.05$	0.22 ± 0.07
$\mathcal{B}(B^- \rightarrow D^*(2010)^+ D^- K^-)$	BABAR [632]: $0.60 \pm 0.10 \pm 0.08$	0.60 ± 0.13
$\mathcal{B}(B^- \rightarrow D^+ D^*(2010)^- K^-)$	BABAR [632]: $0.63 \pm 0.09 \pm 0.06$	0.63 ± 0.11
$\mathcal{B}(B^- \rightarrow D^*(2010)^- D^*(2010)^+ K^-)$	BABAR [632]: $1.32 \pm 0.13 \pm 0.12$	1.32 ± 0.18
$\mathcal{B}(B^- \rightarrow D^0 D^- \bar{K}^0)$	BABAR [632]: $1.55 \pm 0.17 \pm 0.13$	1.55 ± 0.21

Table 153 Decays to $D_s^{(*)-} D^{(*)+}$ [10^{-2}]

Parameter	Measurements	Average
$\mathcal{B}(B^- \rightarrow D_s^- D^0)$	BABAR [635]: $1.33 \pm 0.18 \pm 0.32$	1.33 ± 0.37
$\mathcal{B}(B^- \rightarrow D_s^- D^*(2007)^0)$	BABAR [635]: $1.21 \pm 0.23 \pm 0.20$	1.21 ± 0.30
$\mathcal{B}(B^- \rightarrow D_s^{*-} D^0)$	BABAR [635]: $0.93 \pm 0.18 \pm 0.19$	0.93 ± 0.26
$\mathcal{B}(B^- \rightarrow D_s^{*-} D^*(2007)^0)$	BABAR [635]: $1.70 \pm 0.26 \pm 0.24$	1.70 ± 0.35

Table 154 Product decays rates to $D_s^{(*)-} D^{(*)+}$ [10^{-4}]

Parameter	Measurements	Average
$\mathcal{B}(B^- \rightarrow D_s^- D^0) \times \mathcal{B}(D_s^- \rightarrow \phi(1020)\pi^-)$	BABAR [635]: $4.00 \pm 0.61 \pm 0.61$	4.00 ± 0.86
$\mathcal{B}(B^- \rightarrow D_s^- D^*(2007)^0) \times \mathcal{B}(D_s^- \rightarrow \phi(1020)\pi^-)$	BABAR [635]: $2.95 \pm 0.65 \pm 0.36$	2.95 ± 0.74
$\mathcal{B}(B^- \rightarrow D_s^{*-} D^0) \times \mathcal{B}(D_s^- \rightarrow \phi(1020)\pi^-)$	BABAR [635]: $3.13 \pm 1.19 \pm 0.58$	3.13 ± 1.32
$\mathcal{B}(B^- \rightarrow D_s^{*-} D^*(2007)^0) \times \mathcal{B}(D_s^- \rightarrow \phi(1020)\pi^-)$	BABAR [635]: $8.57 \pm 1.48 \pm 1.12$	8.57 ± 1.86

Table 155 Relative decay rates

Parameter	Measurements	Average
$\mathcal{B}(B^- \rightarrow D_s^- D^0) / \mathcal{B}(\bar{B}^0 \rightarrow D_s^+ D^-)$	LHCb [639]: $1.22 \pm 0.02 \pm 0.07$	1.22 ± 0.07

Table 156 Absolute decays rates to excited D_s mesons [10^{-3}]

Parameter	Measurements	Average
$\mathcal{B}(B^- \rightarrow D_{sJ}(2460)^- D^0)$	BABAR [635]: $4.3 \pm 1.6 \pm 1.3$	4.3 ± 2.1
$\mathcal{B}(B^- \rightarrow D_{sJ}(2460)^- D^*(2007)^0)$	BABAR [635]: $11.2 \pm 2.6 \pm 2.0$	11.2 ± 3.3

Table 157 Product decays rates to excited D_s mesons I [10^{-3}]

Parameter	Measurements	Average
$\mathcal{B}(B^- \rightarrow D^0 D_{sJ}(2460)^-) \times \mathcal{B}(D_{sJ}(2460)^- \rightarrow D_s^{*-} \pi^0)$	Belle [640]: $1.19^{+0.61}_{-0.49} \pm 0.36$ BABAR [641]: $2.7 \pm 0.7^{+1.0}_{-0.8}$	1.56 ± 0.57
$\mathcal{B}(B^- \rightarrow D_{sJ}(2460)^- D^*(2007)^0) \times \mathcal{B}(D_{sJ}(2460)^- \rightarrow D_s^- \gamma)$	BABAR [641]: $1.4 \pm 0.4^{+0.6}_{-0.4}$	$1.4^{+0.7}_{-0.6}$
$\mathcal{B}(B^- \rightarrow D_{sJ}(2460)^- D^*(2007)^0) \times \mathcal{B}(D_{sJ}(2460)^- \rightarrow D_s^{*-} \pi^0)$	BABAR [641]: $7.6 \pm 1.7^{+3.2}_{-2.4}$	$7.6^{+3.6}_{-2.9}$

Table 158 Product decays rates to excited D_s mesons II [10^{-3}]

Parameter	Measurements	Average
$\mathcal{B}(B^- \rightarrow D^0 D_{sJ}^*(2317)^-) \times \mathcal{B}(D_{sJ}^*(2317)^- \rightarrow D_s^- \pi^0)$	Belle [642]: $0.80^{+0.13}_{-0.12} \pm 0.12$ BABAR [641]: $1.0 \pm 0.3^{+0.4}_{-0.2}$	0.82 ± 0.17
$\mathcal{B}(B^- \rightarrow D^0 D_{sJ}^*(2317)^-) \times \mathcal{B}(D_{sJ}^*(2317)^- \rightarrow D_s^{*-} \gamma)$	Belle [640]: <0.76	<0.76
$\mathcal{B}(B^- \rightarrow D_{sJ}^*(2317)^- D^*(2007)^0) \times \mathcal{B}(D_{sJ}^*(2317)^- \rightarrow D_s^- \pi^0)$	BABAR [641]: $0.9 \pm 0.6^{+0.4}_{-0.3}$	$0.9^{+0.7}_{-0.7}$
$\mathcal{B}(B^- \rightarrow D^0 D_{sJ}(2460)^-) \times \mathcal{B}(D_{sJ}(2460)^- \rightarrow D_s^- \gamma)$	Belle [640]: $0.56^{+0.16}_{-0.15} \pm 0.17$ BABAR [641]: $0.6 \pm 0.2^{+0.2}_{-0.1}$	0.58 ± 0.18
$\mathcal{B}(B^- \rightarrow D^0 D_{sJ}(2460)^-) \times \mathcal{B}(D_{sJ}(2460)^- \rightarrow D_s^{*-} \gamma)$	Belle [640]: <0.98	<0.98
$\mathcal{B}(B^- \rightarrow D^0 D_{sJ}(2460)^-) \times \mathcal{B}(D_{sJ}(2460)^- \rightarrow D_s^- \pi^0)$	Belle [640]: <0.27	<0.27
$\mathcal{B}(B^- \rightarrow D^0 D_{sJ}(2460)^-) \times \mathcal{B}(D_{sJ}(2460)^- \rightarrow D_s^- \pi^+ \pi^-)$	Belle [640]: <0.22	<0.22
$\mathcal{B}(B^+ \rightarrow D_{s1}(2536)^+ \bar{D}^0) \times \mathcal{B}(D_{s1}(2536)^+ \rightarrow D^*(2007)^0 K^+ + D^*(2010)^+ K^0)$	Belle [644]: $0.397 \pm 0.085 \pm 0.056$	0.397 ± 0.102
$\mathcal{B}(B^- \rightarrow D_{s1}(2536)^- D^0) \times \mathcal{B}(D_{s1}(2536)^- \rightarrow \bar{D}^*(2007)^0 K^-)$	BABAR [643]: $0.216 \pm 0.052 \pm 0.045$	0.216 ± 0.069
$\mathcal{B}(B^- \rightarrow D_{s1}(2536)^- D^0) \times \mathcal{B}(D_{s1}(2536)^- \rightarrow D^*(2010)^- \bar{K}^0)$	BABAR [643]: $0.230 \pm 0.098 \pm 0.043$	0.230 ± 0.107
$\mathcal{B}(B^- \rightarrow D_{s1}(2536)^- \bar{D}^*(2007)^0) \times \mathcal{B}(D_{s1}(2536)^- \rightarrow \bar{D}^*(2007)^0 K^-)$	BABAR [643]: $0.546 \pm 0.117 \pm 0.104$	0.546 ± 0.157
$\mathcal{B}(B^- \rightarrow D_{s1}(2536)^- D^*(2007)^0) \times \mathcal{B}(D_{s1}(2536)^- \rightarrow D^*(2010)^- \bar{K}^0)$	BABAR [643]: <1.069	<1.069

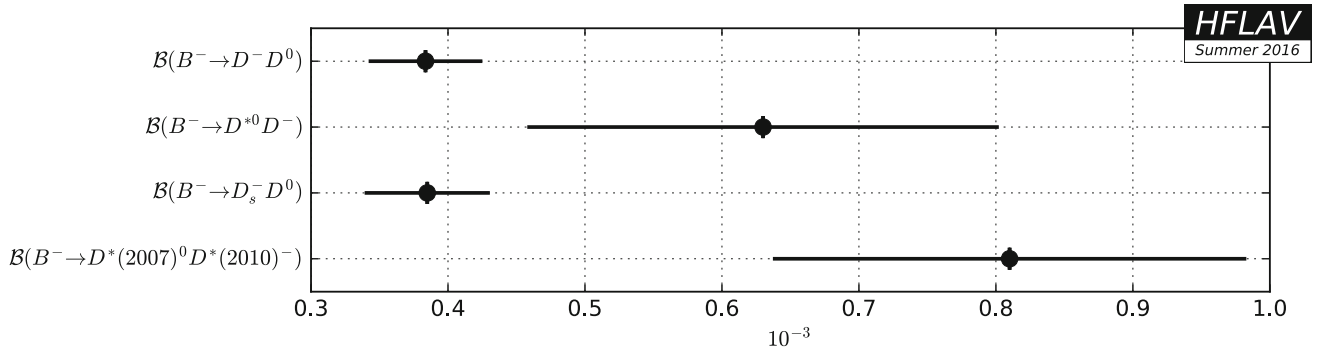


Fig. 120 Summary of the averages from Table 150

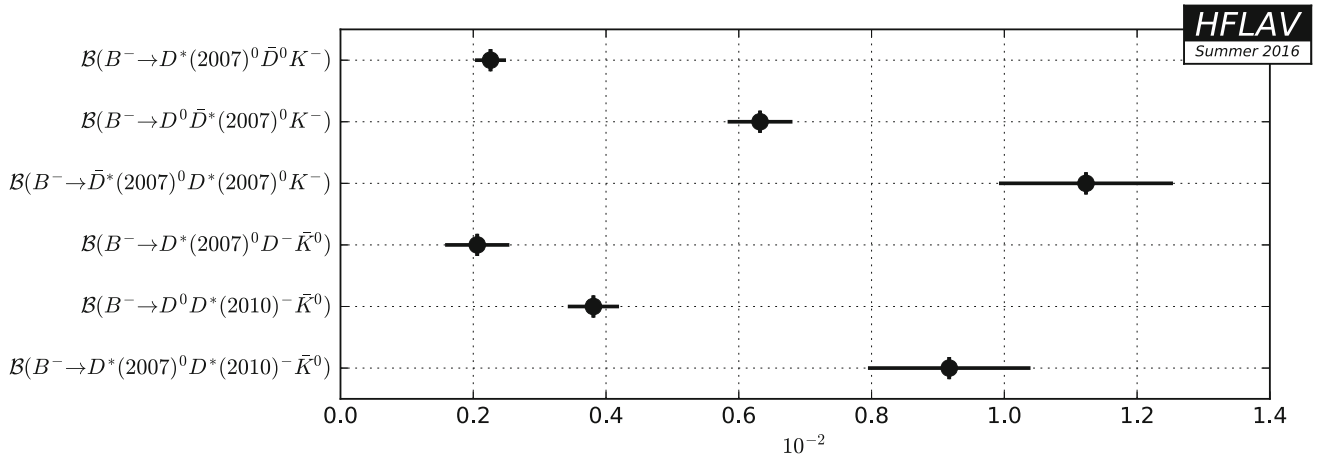


Fig. 121 Summary of the averages from Table 151

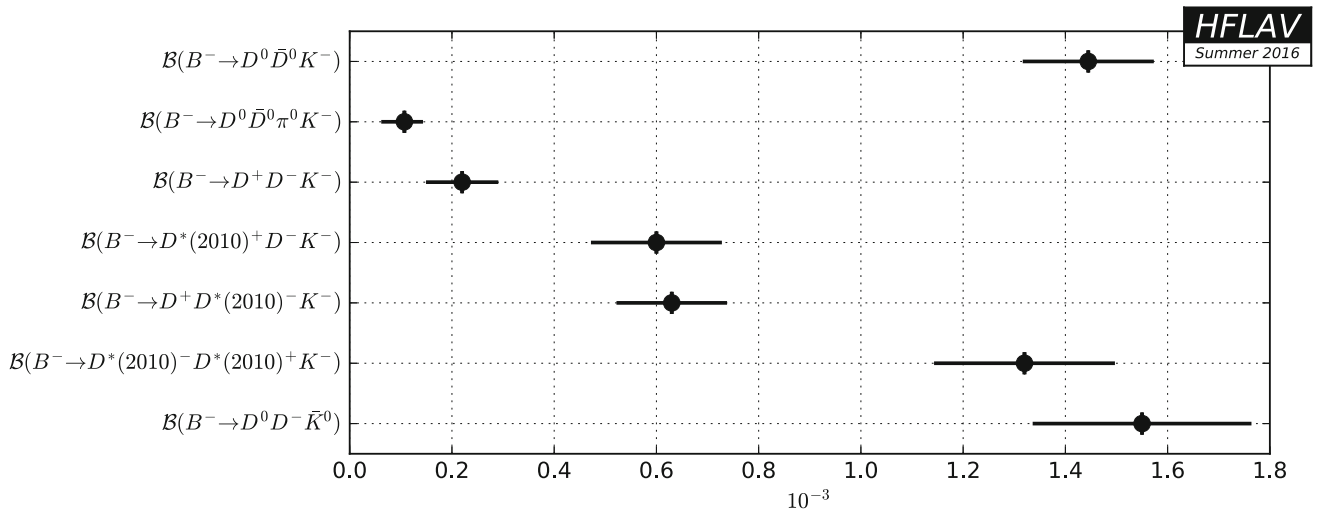


Fig. 122 Summary of the averages from Table 152